

5101-286
Flat-Plate
Solar Array Project

DOE/JPL-1012-124
Distribution Category UC-63b

Progress Report 26

for the Period July 1985 to April 1986

and Proceedings of the
26th Project Integration Meeting

(NASA-CR-179926) PROCEEDINGS OF THE 26TH
PROJECT INTEGRATION MEETING Progress
Report, Jul. 1985 - Apr. 1986 (Jet
Propulsion Lab.) 697 p CSCI 10A

N87-16390
THRU
N87-16444
Unclas
G3/44 42909

Prepared for
U.S. Department of Energy
Through an Agreement with
National Aeronautics and Space Administration
by
Jet Propulsion Laboratory
California Institute of Technology
Pasadena, California

JPL Publication 86-23

5101-286
Flat-Plate
Solar Array Project

DOE/JPL-1012-124
Distribution Category UC-63b

Progress Report 26

for the Period July 1985 to April 1986

and Proceedings of the
26th Project Integration Meeting

Prepared for
U.S. Department of Energy
Through an Agreement with
National Aeronautics and Space Administration
by
Jet Propulsion Laboratory
California Institute of Technology
Pasadena, California

JPL Publication 86-23

Prepared by the Jet Propulsion Laboratory, California Institute of Technology, for the U.S. Department of Energy through an agreement with the National Aeronautics and Space Administration.

The JPL Flat-Plate Solar Array Project is sponsored by the U.S. Department of Energy and is part of the National Photovoltaics Program to initiate a major effort toward the development of cost-competitive solar arrays.

This report was prepared as an account of work sponsored by an agency of the United States Government. Neither the United States Government nor any agency thereof, nor any of their employees, makes any warranty, express or implied, or assumes any legal liability or responsibility for the accuracy, completeness, or usefulness of any information, apparatus, product, or process disclosed, or represents that its use would not infringe privately owned rights.

Reference herein to any specific commercial product, process, or service by trade name, trademark, manufacturer, or otherwise, does not necessarily constitute or imply its endorsement, recommendation, or favoring by the United States Government or any agency thereof. The views and opinions of authors expressed herein do not necessarily state or reflect those of the United States Government or any agency thereof.

This document reports on work done under NASA Task RE-152, Amendment 419, DOE/NASA IAA No. DE-A101-85CE89008.

ABSTRACT

This report describes progress made by the Flat-Plate Solar Array (FSA) Project during the period July 1985 to April 1986. It includes reports on silicon sheet growth and characterization, silicon material, process development, high-efficiency cells, environmental isolation, engineering sciences, and reliability physics. It also includes technical and plenary presentations made at the 26th Project Integration Meeting (PIM) held at Pasadena, California, on April 29-30 and May 1, 1986.

This 26th and final PIM was divided into three specific areas: (1) April 29 consisted of an overview of the progress and the significance of the results of 11 years of progress to the PV manufacturers, users, and community; (2) April 30 provided detailed summaries of the progress of the FSA contractors and in-house work since the 25th PIM; and (3) May 1 offered an opportunity for industry and users to explain their continuing participation in the manufacture and use of crystalline-silicon photovoltaics.

NOMENCLATURE

AC	alternating current
AE	acoustic emission
AM	air mass (e.g., AM1 = unit air mass)
AMOCO	American Oil Company
AR	antireflective
ARAPS	Angular Resolved Auger Parameter Spectroscopy
ASEC	Applied Solar Energy Corp.
a-Si	amorphous silicon
ASLBIC	Absolute spectral light-beam induced current
ASME	American Society of Mechanical Engineers
ASTM	American Society for Testing and Materials
BA	butyl acrylate
B-E-T	Brunauer-Emmet-Teller
BIS	Bremstrahlung Isochromate Spectroscopy
BOS	balance of system (non-array elements of a PV system)
BP	British Petroleum
BPU	basic processing units
BSC	back-surface contact
BSF	back-surface field
BSR	back-surface reflector
Caltech	California Institute of Technology
CEC	Commission of European Communities
CER	controlled-environment reactor
CIV	Corona Inception Voltage
CML	constant melt level
CORECT	Committee on Renewable Energy Commerce and Trade

COSMIC	Computer Software Management Information Center
CPVC	chlorinated polyvinyl chloride
c-Si	single-crystal silicon
CSTR	continuous-flow, stirred reactor
CV	capacitance voltage
CVD	chemical vapor deposition
CVT	chemical vapor transport
CY	calendar year
Cz	Czochralski (classical silicon crystal growth method)
DAS	data acquisition system
DC	direct current
DCS	dichlorosilane
DI	deionized
DLTS	deep-level transient spectroscopy
DOD	U.S. Department of Defense
DOE	U.S. Department of Energy
DSC	differential scanning calorimetry
DT	double torsion
DTM	dendrite thickness monitor
DW	dendritic web
EBIC	electron-beam-induced current
EDAX, EDX	electron-dispersive analysis of x-rays
EDS	energy-dispersive spectroscopy
EFG	edge-defined film-fed growth (silicon-ribbon growth method)
EMA	ethylene methyl acrylate
EMC	Energy Materials Corp.
EPDM	ethylene-propylene-diene monomer

EPR	electron paramagnetic resonance
EPRI	Electric Power Research Institute
EPSDU	experimental process system development unit
ESP	edge-supported pulling (silicon-sheet production process)
ESR	edge-stabilized ribbon
ESR	Electron Spin Resonance
EVA	ethylene vinyl acetate
FA	failure analysis
FAST	fixed abrasive slicing technique
FBR	fluidized-bed reactor
FEP	fluorinated ethylene propylene (Teflon FEP DuPont)
FF	fill factor
FPUP	Federal Photovoltaics Utilization Program
FSA	Flat-Plate Solar Array Project
FSR	free-space reactor
FTIR	Fourier transform infrared
FZ	float-zone (silicon sheet growth method)
GC	gas chromatography
GFCI	ground-fault circuit interruptor
h	heat transfer coefficient; hour(s)
HALS	hindered amine light stabilizer
HEM	heat-exchange method (silicon-crystal ingot-growth method)
ICB	ion cluster beam
ID	inside diameter
IEEE	Institute of Electrical and Electronics Engineers, Inc.
IES	Institute of Environmental Sciences
IIT	Illinois Institute of Technology

IITRI	IIT Research Institute
IPEG	Improved Price Estimation Guidelines
IR	infrared
ISES	International Solar Energy Society
ITO	indium-tin oxide
I-V	current-voltage
JPL	Jet Propulsion Laboratory
JRC	Joint Research Centre
LAPSS	Large-Area Pulsed Solar Simulator
LASS	low-angle silicon sheet growth method
LBIC	light-beam-induced current
LCP	Lifetime Cost and Performance
LED	light emitting diode
LPCVD	low-pressure chemical vapor deposition
LPE	liquid-phase epitaxy
LVDT	linear voltage displacement transducer
MBE	molecular-beam epitaxy
MBOE	million barrels of oil equivalent
MEPSDU	module experimental process system development unit
mgSi	metallurgical silicon
MINP	metal insulator, n-p
MIS	metal-insulator semiconductor (cell configuration)
MLB	modulated light beam
MOD	metallo-organic deposition
MOS	metal oxide semiconductor
MSEC	Mobil Solar Energy Corp.
m-Si	microcrystalline silicon

NASA	National Aeronautics and Space Administration
NBS	National Bureau of Standards
NEC	National Electrical Code
NMA	non-mass analyzed
NOC	nominal operating conditions
NOCT	nominal operating cell temperature
OFHC	oxygen-free hard copper
O&M	operation and maintenance
OPTAR	Outdoor Photothermal Aging Reactor
PA&I	Project Analysis and Integration Area (of FSA)
PC	personal computer
PC	power conditioner
PC	printed circuit
PCS	power-conditioning system
PC/TS	Performance Criteria/Test Standards (SERI)
PDU	process development unit
PE	polyethylene
PEBA	pulsed electron beam annealing
PECVD	plasma-enhanced chemical vapor deposition
P/FR	problem/failure report
PG&E	Pacific Gas & Electric
PIM	Project Integration Meeting
P_{\max}	maximum power
PMMA	polymethyl methacrylate
PMR	Progress Management Report
PnBA	poly-n-butyl acrylate
PRC	Photovoltaics Review Committee

PU	polyurethane
PV	photovoltaic(s)
PVB	polyvinyl butyral
PVC	polyvinyl chloride
PVD	physical vapor deposition
PVUSA	Photovoltaics for Utility Service Applications
R&D	research and development
RBS	Rutherford back-scattering
RES	Residential Experiment Station
RF	radio frequency
RH	relative humidity
RSID	Reference Spectral Irradiance Distribution
RTP	rapid thermal processing
RTV	room-temperature vulcanized
SAMICS	Solar Array Manufacturing Industry Costing Standards
SAMIS	Standard Assembly-Line Manufacturing Industry Simulation
SAMPEG	Standard Assembly-Line Manufacturing Price-Estimation Guidelines
SCAP1D	Solar-Cell Analysis Program in One Dimension
SCLS	solar-cell laser scanner
SEAL	Scanning Electron Analysis Laboratories
SEEMA	Solar-Cell Efficiency Estimation Methodology and Analysis
SEM	scanning electron microscope
SERI	Solar Energy Research Institute
SIMRAND	<u>SIM</u> ulation of <u>R</u> esearch <u>ANd</u> <u>D</u> evelopment Projects
SIMS	secondary ion mass spectroscopy
SINDA	Systems Improved Numerical Differencing Analyzer
SMUD	Sacramento (California) Municipal Utility District

SOC	standard operating conditions (module performance)
SOLMET	solar radiation surface meteorological observations
SRH	Schockley-Reed-Hall
STC	silicon tetrachloride
STC	solar-cell transistor
STC	standard test conditions
SUNYA	State University of New York at Albany
TCM	transparent conducting material
TCO	transparent conducting oxide
TCS	trichlorosilane
TEM	transmission electron microscope
TGA	thermogravimetric analysis
TMY	typical meteorological year
TREI	Texas Research and Engineering Institute
TTU	Texas Technology University
UCC	Union Carbide Corp.
UCLA	University of California, Los Angeles
UCP	ubiquitous crystallization process
UL	Underwriters Laboratories, Inc.
UV	ultraviolet
VFE	vertical floating emitter
VTE	vertical thermal element
XPS	x-ray photoemission spectroscopy

DEFINITION OF SYMBOLS

I_{sc}	short-circuit current
$I-V$	current-voltage
J_{sc}	short-circuit current density
k	equilibrium constant
L_D	minority carrier diffusion length
P	power
P_{max}	maximum power
S	incident solar energy density
T	temperature
U	superficial velocity
U_{mf}	minimum fluidization velocity
V_{oc}	open-circuit voltage
y	molecular percent silane
η	Greek letter eta: efficiency
σ_{xx}	Greek letter sigma: lateral stress
σ_{yy}	Greek letter sigma: longitudinal stress
Ω	Greek letter omega: resistance in ohms

PRECEDING PAGE BLANK NOT FILMED

METRIC CONVERSION FACTORS

Approximate Conversions from Metric Measures			
Symbol	When You Know	Multiply by	To Find
LENGTH			
mm	millimeters	0.04	inches
cm	centimeters	0.4	inches
m	meters	3.3	feet
m	meters	1.1	yards
km	kilometers	0.6	miles
AREA			
cm ²	square centimeters	0.16	square inches
m ²	square meters	1.2	square yards
km ²	square kilometers	0.4	square miles
ha	hectares (10,000 m ²)	2.5	acres
MASS (weight)			
g	grams	0.035	ounces
kg	kilograms	2.2	pounds
t	tonnes (1000 kg)	1.1	short tons
VOLUME			
ml	milliliters	0.03	fluid ounces
l	liters	2.1	pints
l	liters	1.06	quarts
l	liters	0.26	gallons
m ³	cubic meters	35	cubic feet
m ³	cubic meters	1.3	cubic yards
TEMPERATURE (exact)			
°C	Celsius temperature	9/5 (then add 32)	Fahrenheit temperature

1	2	3	4	5	6	7	8	9	10	11	12	13	14	15	16	17	18	19	20	21	22	23
1	2	3	4	5	6	7	8	9	10	11	12	13	14	15	16	17	18	19	20	21	22	23
1	2	3	4	5	6	7	8	9	10	11	12	13	14	15	16	17	18	19	20	21	22	23
1	2	3	4	5	6	7	8	9	10	11	12	13	14	15	16	17	18	19	20	21	22	23
1	2	3	4	5	6	7	8	9	10	11	12	13	14	15	16	17	18	19	20	21	22	23
1	2	3	4	5	6	7	8	9	10	11	12	13	14	15	16	17	18	19	20	21	22	23
1	2	3	4	5	6	7	8	9	10	11	12	13	14	15	16	17	18	19	20	21	22	23
1	2	3	4	5	6	7	8	9	10	11	12	13	14	15	16	17	18	19	20	21	22	23
1	2	3	4	5	6	7	8	9	10	11	12	13	14	15	16	17	18	19	20	21	22	23
1	2	3	4	5	6	7	8	9	10	11	12	13	14	15	16	17	18	19	20	21	22	23
1	2	3	4	5	6	7	8	9	10	11	12	13	14	15	16	17	18	19	20	21	22	23
1	2	3	4	5	6	7	8	9	10	11	12	13	14	15	16	17	18	19	20	21	22	23
1	2	3	4	5	6	7	8	9	10	11	12	13	14	15	16	17	18	19	20	21	22	23
1	2	3	4	5	6	7	8	9	10	11	12	13	14	15	16	17	18	19	20	21	22	23
1	2	3	4	5	6	7	8	9	10	11	12	13	14	15	16	17	18	19	20	21	22	23
1	2	3	4	5	6	7	8	9	10	11	12	13	14	15	16	17	18	19	20	21	22	23
1	2	3	4	5	6	7	8	9	10	11	12	13	14	15	16	17	18	19	20	21	22	23
1	2	3	4	5	6	7	8	9	10	11	12	13	14	15	16	17	18	19	20	21	22	23
1	2	3	4	5	6	7	8	9	10	11	12	13	14	15	16	17	18	19	20	21	22	23
1	2	3	4	5	6	7	8	9	10	11	12	13	14	15	16	17	18	19	20	21	22	23
1	2	3	4	5	6	7	8	9	10	11	12	13	14	15	16	17	18	19	20	21	22	23
1	2	3	4	5	6	7	8	9	10	11	12	13	14	15	16	17	18	19	20	21	22	23
1	2	3	4	5	6	7	8	9	10	11	12	13	14	15	16	17	18	19	20	21	22	23
1	2	3	4	5	6	7	8	9	10	11	12	13	14	15	16	17	18	19	20	21	22	23
1	2	3	4	5	6	7	8	9	10	11	12	13	14	15	16	17	18	19	20	21	22	23
1	2	3	4	5	6	7	8	9	10	11	12	13	14	15	16	17	18	19	20	21	22	23
1	2	3	4	5	6	7	8	9	10	11	12	13	14	15	16	17	18	19	20	21	22	23
1	2	3	4	5	6	7	8	9	10	11	12	13	14	15	16	17	18	19	20	21	22	23
1	2	3	4	5	6	7	8	9	10	11	12	13	14	15	16	17	18	19	20	21	22	23
1	2	3	4	5	6	7	8	9	10	11	12	13	14	15	16	17	18	19	20	21	22	23
1	2	3	4	5	6	7	8	9	10	11	12	13	14	15	16	17	18	19	20	21	22	23
1	2	3	4	5	6	7	8	9	10	11	12	13	14	15	16	17	18	19	20	21	22	23
1	2	3	4	5	6	7	8	9	10	11	12	13	14	15	16	17	18	19	20	21	22	23
1	2	3	4	5	6	7	8	9	10	11	12	13	14	15	16	17	18	19	20	21	22	23
1	2	3	4	5	6	7	8	9	10	11	12	13	14	15	16	17	18	19	20	21	22	23
1	2	3	4	5	6	7	8	9	10	11	12	13	14	15	16	17	18	19	20	21	22	23
1	2	3	4	5	6	7	8	9	10	11	12	13	14	15	16	17	18	19	20	21	22	23
1	2	3	4	5	6	7	8	9	10	11	12	13	14	15	16	17	18	19	20	21	22	23
1	2	3	4	5	6	7	8	9	10	11	12	13	14	15	16	17	18	19	20	21	22	23
1	2	3	4	5	6	7	8	9	10	11	12	13	14	15	16	17	18	19	20	21	22	23
1	2	3	4	5	6	7	8	9	10	11	12	13	14	15	16	17	18	19	20	21	22	23
1	2	3	4	5	6	7	8	9	10	11	12	13	14	15	16	17	18	19	20	21	22	23
1	2	3	4	5	6	7	8	9	10	11	12	13	14	15	16	17	18	19	20	21	22	23
1	2	3	4	5	6	7	8	9	10	11	12	13	14	15	16	17	18	19	20	21	22	23
1	2	3	4	5	6	7	8	9	10	11	12	13	14	15	16	17	18	19	20	21	22	23
1	2	3	4	5	6	7	8	9	10	11	12	13	14	15	16	17	18	19	20	21	22	23
1	2	3	4	5	6	7	8	9	10	11	12	13	14	15	16	17	18	19	20	21	22	23
1	2	3	4	5	6	7	8	9	10	11	12	13	14	15	16	17	18	19	20	21	22	23
1	2	3	4	5	6	7	8	9	10	11	12	13	14	15	16	17	18	19	20	21	22	23
1	2	3	4	5	6	7	8	9	10	11	12	13	14	15	16	17	18	19	20	21	22	23
1	2	3	4	5	6	7	8	9	10	11	12	13	14	15	16	17	18	19	20	21	22	23
1	2	3	4	5	6	7	8	9	10	11	12	13	14	15	16	17	18	19	20	21	22	23
1	2	3	4	5	6	7	8	9	10	11	12	13	14	15	16	17	18	19	20	21	22	23
1	2	3	4	5	6	7	8	9	10	11	12	13	14	15	16	17	18	19	20	21	22	23
1	2	3	4	5	6	7	8	9	10	11	12	13	14	15	16	17	18	19	20	21	22	23
1	2	3	4	5	6	7	8	9	10	11	12	13	14	15	16	17	18	19	20	21	22	23
1	2	3	4	5	6	7	8	9	10	11	12	13	14	15	16	17	18	19	20	21	22	23
1	2	3	4	5	6	7	8	9	10	11	12	13	14	15	16	17	18	19	20	21	22	23
1	2	3	4	5	6	7	8	9	10	11	12	13	14	15	16	17	18	19	20	21	22	23
1	2	3	4	5	6	7	8	9	10	11	12	13	14	15	16	17	18	19	20	21	22	23
1	2	3	4	5	6	7	8	9	10	11	12	13	14	15	16	17	18	19	20	21	22	23
1	2	3	4	5	6	7	8	9	10	11	12	13	14	15	16	17	18	19	20	21	22	23
1	2	3	4	5	6	7	8	9	10	11	12	13	14	15	16	17</						

CONTENTS

PROGRESS REPORT

PROJECT SUMMARY	3
AREA REPORTS	11
Advanced Materials and Devices Research Area	11
Silicon Materials Task and Advanced Silicon Sheet Task	11
Device Research Task (Processing and High-Efficiency Solar Cells)	25
Project Analysis and Integration Area	37
Reliability and Engineering Sciences Area	41

PROCEEDINGS OF THE 26TH PROJECT INTEGRATION MEETING

INTRODUCTION	67
AGENDA	69
PLENARY SESSIONS	73
Summary	73
Introduction to Proceedings (W. Callaghan, Jet Propulsion Laboratory)	83
DOE Comments (M. Prince, U.S. Department of Energy)	85
The Jet Propulsion Laboratory Low-Cost Solar Array Project: 1974-1986 (P. Maycock, Photovoltaic Energy Systems, Inc.)	91
Historical Overview, Accomplishments, and Value of the FSA Project: Industry (R. Little, Spire Corp.)	97
Silicon Material Task Review (J. Lorenz, Consultant)	107
Technical Progress in Silicon Sheet Growth Under DOE/JPL FSA Program: 1975-1986 (J. Kalejs, Mobil Solar Energy Corp.)	117
A Review of High-Efficiency Silicon Solar Cells (A. Rohatgi, Georgia Institute of Technology)	129

PLENARY SESSIONS (Cont'd)

Process Research and Development (D. Bickler, Jet Propulsion Laboratory)	139
JPL Encapsulation Task (P. Willis, Springborn Laboratories, Inc.)	145
Crystalline-Silicon Photovoltaics Summary Module Design and Reliability (R. Ross, Jr., Jet Propulsion Laboratory)	157
Module Evaluation (C. Gay, ARCO Solar, Inc.)	165
Project Analysis and Integration Economic Analyses Summary (H. Macomber, Consultant)	167
Panel: Recommendations for Crystalline-Silicon in DOE's 5-Year Photovoltaic Research Plan	
J. Day, Strategies Unlimited	177
G. Smith, U.S. Navy	179
K. Firor, Pacific Gas and Electric	181
E. Ralph, Hughes Aircraft	185
K. Koliwad, Jet Propulsion Laboratory	189
C. Rose, Westinghouse Electric Corp.	191
E. Daniels, Solarex Corp.	193

TECHNICAL SESSIONS	199
------------------------------	-----

CELL TECHNOLOGY

ADVANCED SILICON SHEET (A. Morrison, Chairman)	199
Report on the Fourth Stress/Strain Workshop (M. Leipold, Jet Propulsion Laboratory)	201
Silicon Dendritic Web Growth (R. Hopkins, Westinghouse Electric Corp.)	203
JPL Web Team (D. Bickler, Jet Propulsion Laboratory)	223
Stress and Efficiency Studies in Edge-Defined Film- Fed Growth (J. Kalejs, Mobil Solar Energy Corp.) . . .	229

TECHNICAL SESSIONS (Cont'd)

High-Purity Silicon Crystal Growth Investigations (T. Ciszek, Solar Energy Research Institute)	241
Analysis of Silicon Stress/Strain Relationships (O. Dillon, University of Kentucky)	255
Silicon Stress/Strain Activities at JPL (C. Chen, . Jet Propulsion Laboratory)	285
Creep of Web Ribbons (S. Hyland and D. Ast, Cornell University)	297
Surface Property Modification of Semiconductors by Fluid Absorption (S. Danyluk, University of Illinois at Chicago)	307
Czochralski Crystal Growth: Modeling Study (M. Dudukovic, P. Ramachandran, R. Srivastava, and D. Dorsey, Chemical Reaction Engineering Lab, Dept. of Chemical Engineering, Washington University)	319
HIGH-EFFICIENCY SOLAR CELLS (P. Alexander, Chairman)	329
Optimization Methods and Silicon Solar Cell Numerical Models (K. Girardini, University of California, Los Angeles)	331
Novel Measurement Techniques (Development and Analysis of Silicon Solar Cells Near 20% Efficiency) (M. Wolf and M. Newhouse, University of Pennsylvania)	345
Measurement of Minority Carrier Lifetime, Mobility and Diffusion Length in Heavily Doped Silicon (S. Swirhun and R. Swanson, Stanford University)	357
Point Contact Silicon Solar Cells (R. Swanson, Stanford University)	367
SiN _x Passivation of Silicon Surfaces (L. Olsen, University of Washington)	375
Development of High-Efficiency Solar Cells on Silicon Web (D. Meier, Westinghouse Research and Development Center)	383
PROCESSING (B. Gallagher, Chairman)	401
Amorphous Diffusion Barriers (E. Kolawa, F. So, and M-A. Nicolet, California Institute of Technology)	403

TECHNICAL SESSIONS (Cont'd)

Metallo-Organic Decomposition Film Development (J. Parker, Electrink, Inc.)	409
Ink-Jet Printing of Silver Metallization for Photovoltaics (R. Vest, Purdue University)	419
Laser-Assisted Solar Cell Metallization Processing (D. Meier, Westinghouse Electric Corp., Research and Development Center)	437
Process Research of Non-Czochralski Silicon Material (R. Campbell, Westinghouse Electric Corp., Advanced Energy Systems Division)	451
Rapid Thermal Processing of Czochralski Silicon Substrates: Defects, Denuded Zones, and Minority Carrier Lifetime (G. Rozgonyi, D. Yang, Y. Cao, and Z. Radzimski, North Carolina State University)	461
Use of Low-Energy Hydrogen Ion Implants in High-Efficiency Crystalline-Silicon Solar Cells (S. Fonash, R. Singh, and H. Mu, Pennsylvania State University)	473
Low-Pressure, Chemical Vapor Deposition Polysilicon (B. Gallagher and G. Crotty, Jet Propulsion Laboratory)	483

MODULE AND RELIABILITY TECHNOLOGY

MODULE TECHNOLOGY

(M. Smokler, Chairman)	489
Accuracy and Long-Term Stability of Amorphous-Silicon Measurements (R. Mueller, Jet Propulsion Laboratory)	491
Long-Term Stability of Amorphous-Silicon Modules (R. Ross, Jr., Jet Propulsion Laboratory)	497
Solar Cell Reliability Testing (J. Lathrop, Solar Cell Destruction Lab, Clemson University)	505
Long-Term Module Testing at Wyle Laboratories (D. Otth, Jet Propulsion Laboratory)	519
Module Encapsulation Technology (P. Willis, Springborn Laboratories)	525
Commercial Module Test Program (M. Smokler, Jet Propulsion Laboratory)	549

TECHNICAL SESSIONS (Cont'd)

High-Efficiency Module Design (M. Spitzer, Spire Corp.)	557
Measuring Research Progress in Photovoltaics (B. Jackson and P. McGuire, Jet Propulsion Laboratory).	567
RELIABILITY PHYSICS	
(E. Cuddihy, Chairman)	577
Mechanistic Studies of Photothermal Aging (R. Liang, Jet Propulsion Laboratory)	581
UV-T-RH Combined Environmental Testing (C. Gonzalez, Jet Propulsion Laboratory)	591
Computer Modeling of Photodegradation (J. Guillet, University of Toronto)	599
Chemical Bonding Technology (E. Plueddemann, Dow Corning Corp.)	615
Anticorrosion Studies (J. Boerio, University of Cincinnati)	621
Electrochemical Aging Effects in Photovoltaic Modules (G. Mon, Jet Propulsion Laboratory)	629
Leakage-Current Properties of Encapsulants (L. Wen, Jet Propulsion Laboratory)	647
Water Permeation and Electrical Properties of Pottants, Backings, and Pottant/Backing Composites (J. Orehtsky, Wilkes College)	659
SILICON MATERIALS	
(R. Lutwack, Chairman)	677
Review of the Workshop on Low-Cost Polysilicon for Terrestrial Photovoltaic Solar Cell Applications (R. Lutwack, Jet Propulsion Laboratory)	679
Polycrystalline Silicon Research and Development (S. Iya, Union Carbide Corp.)	687
PHOTOGRAPHS FROM PREVIOUS PROJECT INTEGRATION MEETINGS	694

PROGRESS REPORT

ORIGINAL P E T S
OF POOR Q ALITY

Project Summary

INTRODUCTION

This report describes the activities of the Flate-Plate Solar Array (FSA) Project from May 1985 through April 1986, including the 26th FSA Project Integration Meeting (PIM), held April 29-30 and May 1, 1986.

The FSA Project at the Jet Propulsion Laboratory (JPL), sponsored by the U.S. Department of Energy (DOE), has the responsibility for advancing solar array technology while encouraging industry to reduce the price of arrays to a level at which photovoltaic (PV) electric power systems will be competitive with more conventional power sources. This responsibility has included developing the technology for producing low-cost, long-life PV modules and arrays. More than 100 organizations have participated in FSA-sponsored research and development (R&D) of low-cost solar module manufacturing and mass-production technology, the transfer of this technology to industry for commercialization, and the development and testing of advanced prototype modules and arrays. Economic analyses were used to select, for sponsorship, those R&D efforts most likely to result in significant cost reductions. The following is an account of the progress that has been made during the reporting period.

SUMMARY OF PROGRESS

Experimental test runs of a fluidized-bed reactor (FBR) at the Union Carbide Corp. (UCC) experimental process system development unit (EPSDU) at Washougal, Washington, continue to demonstrate the practicality of converting silane to silicon. The 6-in.-diameter FBR was equipped with a high-purity quartz liner to prevent metallic impurity contamination of the silicon product from the FBR walls during operation. Three test runs were conducted in a re-designed reactor, each run lasting between 54 to 72 h. Operating conditions were smooth and steady, and conversion of silane to silicon was complete. Excellent potential for achieving silicon with semiconductor-grade purity was demonstrated. Analysis indicated that much of the impurities were from the silicon seed particles. Thus further work is required in high-purity seed preparation.

A useful analytical model for evaluation of FBR operating parameters and for sealing up reactors was completed by Washington University at St. Louis.

The FSA funding of polysilicon processes was completed with a FSA-sponsored research forum, "Low-Cost Polysilicon for Terrestrial Photovoltaic Solar Cell Applications," held in October 1985. More than 70 attendees from around the world participated in the descriptions and discussions of new polysilicon processes (including those developed under FSA Project sponsorship), of polysilicon process economics, and of the polysilicon market for the semiconductor and PV industries.

A well-planned, comprehensive, long-term multi-organization research effort on defining growth-induced stresses in silicon ribbons and evaluating the quality of the resultant ribbon, initiated early in 1983, is making good progress, from both analytical and experimental approaches. Mathematical

PROJECT SUMMARY

models have been created that predict more accurately stress and strain history during the silicon growth process and the residual stresses in the silicon ribbons. These models are an advance from previous ones because they take into account the growth history of the ribbon and the material's non-linearity and creep behavior. Relevant ribbon-temperature data and boundary conditions are obtained experimentally from various growth equipment and are used to refine and confirm the theoretical analyses. Thus, researchers are evaluating various grower geometric configurations and ribbon temperature distributions, allowing them to identify critical trade-offs in ribbon-growth equipment.

During this reporting period, significant progress was made at the University of Kentucky in the following areas:

- (1) Elevated-temperature tensile tests on Czochralski (Cz) and dendritic web ribbon material.
- (2) Dislocation mapping, including preferred slip orientations, dislocation mobility, and dislocation multiplication.
- (3) Stress/strain analysis, through use of the Sumino-Haasen dislocation model.

The final report was written on silicon crystal growth parameter effects on minority-carrier lifetimes in bulk silicon as studied at the Solar Energy Research Institute (SERI) by the use of high-purity, float-zone (FZ) techniques. Progress leading to higher-efficiency solar cells was made in understanding lifetime degradation mechanisms, effects of dopants, and in the characterization of lifetime-related crystallographic defects.

Mathematical models describing the Cz crystal growth process were developed by Washington University at St. Louis. A simple model correctly portrays the more detailed conduction-dominated model and is, therefore, suitable for computer control of the growth process.

Studies of edge-defined film-fed growth (EFG) silicon ribbon at Mobil Solar Energy Corp. stress analysis with increased creep rates, beyond the "high-creep" condition modeled previously, show that significant changes in residual stress arise from the imposed transverse isotherm variations.

At Westinghouse Electric Corp., a dendritic-web crystal 1.2 m long was grown at a maximum area growth rate of $10 \text{ cm}^2/\text{min}$. The goal was $13 \text{ cm}^2/\text{min}$ in June 1985, and $16 \text{ cm}^2/\text{min}$ in December 1985. A record throughput of $47,000 \text{ cm}^2$ (defined as ribbon area grown in a single furnace in 7 days) was established for replenished growth. The length of the longest ribbon with the use of melt replenishment was increased to 17 m, for a replenishment rate between 90 and 100% of that required for constant melt level.

Refinement of the web thermal stress model permitted calculations of the temperature and stress distributions in ribbon from the melting point (growth interface) to room temperature. Elastic buckling studies indicate that interface stresses and those caused by final cooldown do not currently limit area growth rate.

PROJECT SUMMARY

Simultaneous web grower operations were accomplished for both the closed-loop melt replenishment and temperature control systems, and the closed-loop heater coil position and temperature control systems under conditions of constant melt level. The maximum period for continuous growth under conditions of closed-loop control of heater coil position and melt temperature for constant melt level was 5.5 h.

An FSA stress/strain workshop was held in March 1985. Several technical conclusions were reached. The use of elastic approximations is appropriate in that strains are small (except for calculations of residual stress). Mechanical property measurements will be confined to the low-strain regime (a very difficult region in which to make measurements). Calculations of ribbon-dislocation distribution qualitatively agree with experimental observation. Observed dislocation densities are generally lower than calculated. Critical maximum values of ribbon width and pull speed may exist that are only slightly greater than those presently being achieved.

A high-speed, high-temperature cutting facility was constructed at the University of Chicago to cut silicon at a precise feed rate, depth of cut, and fluid environment. The surface morphology and debris size analysis are being used to indicate the deformation mode. The modification of silicon surface properties by various fluids is being studied.

Across-the-board progress has been made by the organizations (mainly universities) that are participating in higher-efficiency, crystalline-silicon, solar-cell research. These efforts are directed toward the characterization of various silicon-sheet materials, material-device property interaction investigations, measurement techniques, and process research.

The work at the University of California, Los Angeles (UCLA), on development of an optimization algorithm for use with numerical silicon solar cell models is almost complete. By coupling an optimization algorithm with a solar cell model, it is possible to simultaneously vary design variables such as impurity concentrations, front-junction depth, back-junction depth, and cell thickness to maximize the predicted cell efficiency.

A final report has been written explaining the efforts at the University of Pennsylvania to identify, develop, and analyze useful techniques for measuring bulk recombination rates, surface recombination rates, and surface recombination velocities in all regions of high-efficiency silicon solar cells. Recent work has addressed the areas of refinement and automation of the previously developed DC measurement, "absolute spectral light-beam-induced current" (ASLBIC), and the theoretical evaluation of dynamic measurements in complex device structures.

Experimental work on p- and n-type heavily doped layers at Stanford University has been essentially completed. This work has, for the first time, given reliable data of minority carrier diffusivities in both p- and n-type heavily doped silicon, covering a broad range of doping concentrations from 10^{15} to 10^{20} cm^{-3} . One of the key results is that the minority carrier diffusivities are higher by a factor of 2 in silicon as compared to majority carrier diffusivities.

PROJECT SUMMARY

At the University of Florida, results are reported of the first direct measurement of the minority electron transit time in a p-type (Si:B) transparent, heavily doped silicon layer. The value was obtained by a high-frequency conductance method. A new method has been developed and illustrated that significantly improves the accuracy of lifetime (τ) determined by voltage transients. This method requires only pressure contacts, and thus may be used to determine τ after key processing steps in manufacturing.

The work at the University of Washington on experimental techniques for passivating silicon surfaces is almost complete. The approach consisted of:

- (1) Characterization of silicon surfaces of homogeneously doped substrates.
- (2) Surface characterization of high-efficiency n^+/p and p^+/n silicon cells.
- (3) Determination of dominant current-loss mechanisms in high-efficiency cells.
- (4) Physical characterization of interfaces.

Special emphasis was placed on studies of interfaces between silicon and SiN_x deposited by plasma-enhanced chemical vapor deposition (PECVD).

Performance results of the floating emitter cells, designed by C.T. Sah Associates and fabricated by Applied Solar Energy Corp. (ASEC), were not good. It was not resolved whether the floating emitter design is a viable high-efficiency solar cell design, as the effects of the processing problems on the overall cell performance was not determined.

Using dendritic web material, Westinghouse fabricated cells with a double-layer antireflective (AR) coating and an aluminum back-surface reflector (BSR). An efficiency of 16.0% was measured by JPL. Westinghouse continues work toward the goal of making 18% efficient cells from web material.

A successful, simultaneous front and back junction formation process using liquid dopants was achieved at Westinghouse using a flash diffusion (heat lamp) technique. It was determined that to produce the highest quality cells, an annealing cycle should follow the diffusion process to anneal quenched-in defects. An Interim Price Estimated Guidelines (IPEG) cost analysis indicated that a cost reduction of 25 to 35% could be achieved.

Studies at the Pennsylvania State University established that low-energy hydrogen ion implants can result in hydrogen-caused effects in all three regions of a solar cell (namely, emitter, space charge region, and base). In web, Cz, and FZ material, low-energy hydrogen ion implantation can reduce the surface recombination velocity. Hydrogen implants also were found to passivate space charge region recombination centers. In web cells, hydrogen implants also were found to passivate the base region.

PROJECT SUMMARY

In exploring the fundamental interaction of hydrogen with impurities in silicon, it was found that H^+ implants can passivate the deep levels resulting from fast diffusing metal impurities (Au and Cr), probably by gettering. Implanted hydrogen can neutralize boron acceptors in silicon and can alter the diffusion properties on ion-implanted boron in silicon.

Amorphous W-Zr and W-N alloys have been investigated as diffusion barriers for silicon sheet metallization schemes at the California Institute of Technology (Caltech). The thermal stability of the electrical characteristics of shallow n^+p junctions was significantly improved by incorporating W-N layers in the contact schemes. It also was shown that deposition parameters have important influences on the performance of W-N thin films as diffusion barriers.

Oxygen- and carbon-related defects in silicon were studied by the State University of New York at Albany, especially as related to high-efficiency silicon solar cells, and including gettering of deleterious impurities. Coordinated experimental and theoretical studies of process-induced defects were carried out. The first kinetics model, which fits all the thermal donor formation data, has been developed.

The manufacture and evaluation of selected metallo-organic solution for use in solar cell metallization were investigated by Electrink, Inc. The mixed metallo-organic solutions provided the hoped-for performance improvements.

Based on the most recent Westinghouse process descriptions available for the production of modules with dendritic web solar cells, new cost estimates were prepared. The Solar Array Manufacturing Industry Costing Standards (SAMICS) computer program price FOB estimate was \$1.02/ W_p (1985 dollars) for 13.7% efficient modules manufactured in a 25-MW/year production facility.

An updated estimate of Cz module production cost was prepared using state-of-the-art processing technology. Estimated production costs for a 25 MW factory resulted in a FOB price of \$1.45/ W_p (1985 dollars), assuming a module efficiency of 13.5%.

The Standard Assembly-Line Manufacturing Industry Simulation (SAMIS) computer model has been completely converted to run on the IBM PC/XT (or compatible system). The implementation includes three modes of operation: SAMIS, Standard Assembly-Line Manufacturing Price-Estimation Guideline (SAMPEG), and IPEG.

Three Simulation of Research And Development (SIMRAND) documents have been published by JPL. One describes theory and application, and the other two describe computer programs. The three documents and the computer code have been submitted to the Computer Software Management Information Center (COSMIC).

An October 1985 JPL paper concluded that Cz technology essentially meets the Cherry Hill goals. The original FSA Project goals were essentially those that originated at the Cherry Hill Conference in 1973. Because current program goals are much more demanding than the original goals, further technology development efforts will be required if they are to be met. Further reductions in wafer costs were identified as the principal technical barrier to the technology reaching current National PV Program goals.

PROJECT SUMMARY

Through cooperative relationships with ARCO Solar, Chronar, Solarex, and Sovonics, amorphous-silicon (a-Si) submodules have been obtained and included in the various testing activities at JPL and at Clemson University. A series of experiments and efforts have been performed at JPL and are continuing on a-Si modules which include:

- (1) Hot-spot performance.
- (2) Electrochemical corrosion mechanisms and corrosion rates.
- (3) Failure analysis techniques and capabilities which have been modified and developed for thin-film modules.
- (4) Failure analysis of existing commercial a-Si module deficiencies.

At Clemson, a-Si devices are now being subjected to a variety of environmental stress tests similar to those used for reliability attribute evaluation of crystalline-silicon-type cells during the past several years.

Research has continued at Clemson University on performing tests that will lead to identification of degradation mechanisms in thin-film cells. Work has been completed on developing stress-testing procedures, specifically for a-Si cells. Much of the effort went into developing a measurement system for accelerated testing of a-Si cells with a repeatability of 1%.

A major portion of the amorphous-cell hot-spot testing at JPL was summarized in a paper, titled Hot-Spot Durability Testing of Amorphous-Silicon Cells and Modules, October 1985.

Electrochemical corrosion research at JPL focuses on corrosion mechanisms to which both crystalline and a-Si modules may be subjected in central station applications, on the determination of corrosion rates, and on the ascertainment of means of corrosion passivation. Corrosion mechanisms and rates have been previously determined and reported and, therefore, the present objective is to study the details of the corrosion processes and to develop passivation design strategies.

The determination of humidity degradation rates and the identification of key electrochemical failure mechanisms continued for generic module designs based upon temperature/humidity testing cycles and including amorphous, EFG ribbon, dendritic web ribbon, and Cz-type modules.

Field tests initiated in June through August 1985 resulted in significant power degradation for all modules on several a-Si submodules with samples short-circuited, open-circuited, or under Nener-diode loads, simulating maximum power loading. This led to a new series of accelerated field tests.

A variety of types of failures and deficiencies, as would be expected for any new product, are being uncovered in the testing of these modules. JPL is performing failure analyses and is in constant communication with the manufacturers regarding the specific problems and possible solutions for each manufacturer's product. The close working arrangements are similar to those developed during the past decade on crystalline-silicon modules.

PROJECT SUMMARY

Basic module technology needs that are unique to a-Si modules are being formulated as a result of test results, failure analysis, and encapsulation studies. Both superstrate and substrate module designs and the technologies appropriate for each concept are being studied.

For a substrate design, a transparent top-cover plastic film is needed with an adhesive lower layer for bonding to indium-tin oxide (ITO), or other electrically conductive transparent material. If it is found that ultraviolet (UV) affects a-Si solar cells, then the outer cover plastic film would have to be UV-screened, up to the limit of the offending wavelengths. If UV-screening is not needed for a-Si protection, the most viable top cover candidate is Teflon FEP-C (Du Pont), in combination with a virtually weatherable acrylic adhesive. Extensive testing of teflon FEP-C is continuing. One of the key material challenges seems related to bonding the adhesive to ITO, or its equivalent.

A model of autocatalytic photooxidation has been proposed. Photo-oxidation initially takes place at a slow rate while generating degraded products. These products will, in turn, catalyze further photooxidation reactions resulting in a drastic increase in the rate of subsequent degradation.

It is recognized that water, besides accelerating corrosion reactions within PV modules, catalyzes a host of other degradative phenomena such as delaminations, reduction of mechanical strength, enhancement of electrical breakdown probability, etc. A fundamental study being performed is the measurement of water sorption by PV encapsulants.

A report has been published by JPL, titled The Aging Correlation (RH + t): Relative Humidity (%) + Temperature (°C), by E. F. Cuddihy, dated January 15, 1986. This report describes the aging correlation between corrosion lifetime and relative humidity RH (%) and temperature t (°C) in relation to a better understanding of the fundamental mechanisms of degradation and aging.

A comprehensive report, Chemical Bonding Technology: Direct Investigation of Interfacial Bonds, by J.L. Koenig, et al., was published in January 1986.

An organosilane primer for bonding EVA to glass, that had been previously developed by Dr. Plueddemann of Dow Corning, has achieved enormous industrial acceptance. Experimental testing has found that this primer acts to significantly reduce the quantities of water absorbed at the interface between glass and EVA, which is an important factor related to limiting module leakage current and in the reduction of corrosion. An experimental prototype of a more hydrophobic coupling agent (primer) has been completed at Dow Corning.

Dr. J. Boerio, University of Cincinnati, is continuing studies to determine if organosilane coupling agents can function as anti-corrosion agents for the aluminum metallization used on crystalline-silicon solar cells. He has experimentally been able to chemically monitor the interface between EVA and an aluminized back surface of solar cells. Evidence is accumulating that a self-priming EVA with a coupling agent accomplishes both structural bonding to glass, and also corrosion protection for the solar cell's aluminized back surface.

PROJECT SUMMARY

A report by E. Cuddihy of JPL, titled A Concept for the Intrinsic Dielectric Strength of Electrical Insulation Materials, was published on April 15, 1985. Based on the theories in the report, an experimental capability to measure the intrinsic DC dielectric strength property has been established at Springborn Laboratories and can now be monitored as a function of aging.

Previously, back surface materials have been identified that raised the fire resistance of glass superstrate PV modules to Class A and B levels. During the latest tests, problems were identified with the edge-seal systems.

Achievement of the 15% efficient PV module goal has been demonstrated. Spire Corp. has delivered a full-size module that JPL measurements show to have 15.2% efficiency at standard conditions [100 mW per square centimeter irradiance, ASTM 892-82 (global) irradiance spectrum, and 25°C cell temperature]. Encapsulated cell efficiency is 16.9%. The cells were manufactured from a FZ-grown silicon ingot. Spire has produced similar efficiency cells from a Cz-grown silicon ingot, indicating that the 15% goal is achievable with the more readily available Cz material.

Additional meetings confirmed the success of the American-European round-robin of measurements of reference solar cells. JPL also authored the American Society for Testing and Materials (ASTM) subcommittee draft Document 130, "Standard Method for the Calibration of Nonconcentrator Terrestrial Photovoltaic Primary Reference Cells Under Direct Irradiance."

Area Reports

ADVANCED MATERIALS AND DEVICES RESEARCH AREA

Silicon Materials Research Task and Advanced Silicon Sheet Task

INTRODUCTION

The objectives of the Silicon Materials Task and the Advanced Silicon Sheet Task are:

- (1) To identify the critical technical barriers to low-cost silicon purification and sheet growth that must be overcome to produce a PV cell substrate material at a price consistent with FSA Project objectives.
- (2) To overcome these barriers by performing and supporting appropriate R&D.

Present solar-cell technology is based mainly on the use of silicon wafers obtained by inner-diameter slicing of Czochralski-grown ingots from Siemens reactor produced semiconductor-grade silicon. This method of producing single-crystal silicon wafers is tailored to the production of semiconductor devices rather than solar cells. The small market now offered by present solar-cell users does not justify the industrial development of high-volume silicon production techniques that would result in low-cost PV electrical energy.

It is important to develop alternative low-cost processes for producing refined silicon and sheet material suitable for long-life, high-efficiency solar PV energy conversion. To meet FSA objectives, research must be performed to overcome barriers to the successful realization of the most promising processes for producing large quantities of pure silicon and large areas of crystallized silicon at a low cost. The form of the refined silicon must be suitable for use in sheet-growth processes. The sheet, in turn, must be suitable for direct incorporation into automated industrial schemes to produce solar arrays.

AREA REPORTS

Silane can be purified relatively easily and, because of its high reactivity, can be more readily decomposed or reduced to form silicon than can trichlorosilane (TCS), the material of choice in use today in the conventional silicon production process. Thus, silicon purification involving deposition of silicon from silane is being pursued.

AREA REPORTS

Because of its potential for further reduction in the cost of silicon, research also is being conducted on a process that offers promise for making less-pure, solar-cell-grade silicon by refinement of metallurgical-grade silicon (mgSi).

Growth of crystalline silicon material in a geometry that does not require cutting to achieve proper thickness is an obvious way to eliminate costly post-production processing and material waste. Growth techniques such as EFG, dendritic-web growth (Web), low-angle silicon sheet (LASS), and edge-supported pulling (ESP) are candidates for such solar cell material. Problems generic to all sheet growth technologies are being addressed in the program. Special emphasis is placed on the dendritic web process because it seems to have the highest probability of successfully achieving the program goals for silicon sheet material.

SUMMARY OF PROGRESS

Silicon Materials Task

Semiconductor-Grade Silicon Refinement Process

Silicon Refinement Using Silane (Union Carbide Corp.)

The objective of the UCC program is to solve the critical problem of silane (SiH_4) pyrolysis in FBRs to produce semiconductor-grade silicon for PV applications. The production of ultra-pure SiH_4 by the process developed through this contract has already been demonstrated in a 100-MT/year pilot plant. The SiH_4 -to-silicon conversion reactor in this plant is a modified Siemens reactor (built by Komatsu Electrical Materials, Inc.), that does not have the potential to achieve the DOE low-cost goal for polysilicon.

The UCC program was completed on April 30, 1986. Contamination of the polysilicon product was the major problem that was addressed in this FSA Progress Report 26 period.

Early in the period, the reactor was redesigned, primarily to reduce its length to accommodate commercially available quartz-liner tubes without the need of joining two tubes to fit the original reactor length. Use of a single tube would prevent the cracking caused by misalignment of the two joined sections. The original, 110-in. length of the reactor was shortened to 84 in. Other changes included use of a stainless steel bellows to maintain sealing at the liner ends and use of a distributor plate consisting of a perforated stainless-steel plate fitted with screens in the holes. The performance of the distributor plate will approximate that of the well-qualified JPL design.

To complete the test program, three tests using quartz liners were made, ranging in duration from 54 to 72 h, and one test using a polysilicon liner, of 48-h duration. The new reactor operated well, with no liner breakage during operation. The 72-h test successfully accomplished a key contractual requirement.

In these tests, the feed concentration of SiH_4 in hydrogen was nominally in the 20 to 30% range, although higher SiH_4 concentrations up to 60%

AREA REPORTS

were tested for short durations. Operating conditions were smooth and steady, and conversion of SiH_4 to silicon was complete. Seed particles of approximately 300- μm mean diameter were grown to product particles of more than 1000- μm diameter.

Spark-source mass spectrometry as well as neutron activation were used to analyze seed and product. Excellent potential for achieving semiconductor-grade purity was demonstrated. Analytical results indicated a significant portion of the impurity content of the product is from the seed. Further work, therefore, is required in the area of high-purity seed preparation.

The final report on the contract is being prepared.

Chemical Vapor Transport Process for Purifying Metallurgical-Grade Silicon (Solar Energy Research Institute)

This program is concerned with investigation of a chemical vapor transport process in which HCl is reacted with $\text{Cu}_3\text{Si}:\text{Si}$ material (the silicon being metallurgical grade) to generate a mixture of chlorosilanes (mostly trichlorosilane). The chlorosilanes then are transported in the gaseous state and the silicon they contain is deposited by pyrolysis on a filament kept at elevated temperature, about 1050°C. The study was completed. Purification steps included:

- (1) Slagging during the electrode fabrication process to getter magnesium, calcium, barium, aluminum, manganese, and sulfur.
- (2) Selective reaction and transport because of differential diffusion rates of the elements in the alloy.
- (3) Removal of elements such as boron, titanium, molybdenum, and zirconium as chlorides by condensation on the cold walls and reactor base plate.

The maximum growth rate for deposition of the refined silicon, about 1.9 g/h, occurred for a chlorine/hydrogen ratio of 0.3 at 1100°C. The product is typically n-type with a resistivity range of 0.1 to 1 ohm-cm. It can be fabricated into cells having a 9.6% conversion efficiency without anti-reflectant coatings (baseline cells also were 9.6% efficient).

Silicon Particle Growth Research (California Institute of Technology)

The objectives of this research are to describe theoretically the growth of silicon particles from SiH_4 in a free-space reactor and to determine experimentally the conditions for maximum particle growth. This effort ended January 31, 1986.

Prior to this reporting period, the phenomenon of runaway nucleation was studied. This phenomenon involves a 10^4 -fold increase in silicon particle concentration when the SiH_4 concentration is increased from 3 to 3.4%. In the present period, experimental conditions were demonstrated that will avoid runaway nucleation. The growth of a small number of seed particles to

AREA REPORTS

supermicron size was demonstrated by controlling the rate of gas-phase reactions in a way that favored vapor diffusion to existing particles as compared to homogeneous nucleation.

Modeling of Silane Pyrolysis in Fluidized-Bed Reactors (Washington University at St. Louis)

This program is aimed at developing a model to describe the production of silicon by pyrolysis of SiH_4 in FBRs. The model will be useful for the interpretation of experimental data, for the determination of the ranges of operating parameters for maximum throughput and yield, and for providing a basis for design of scaled-up reactors for pilot plants.

The technical effort was completed and the final report published. In this program, two models were developed to treat the system in which chemical vapor deposition on silicon seed particles and gas-phase nucleation reactions to form fine particles occur simultaneously. A population balance was used to describe the size distribution of the fine particles. Growth of the seed particles was attributed to chemical vapor deposition and the capture of the fine particles on the surface of the seed particles. In the JPL FBR, good agreement was obtained between model predictions and experimental data for particle growth rate, silane conversion efficiency, and amount of fine particles formed. Effects of uncertainties in the kinetic and hydrodynamic parameters on the model predictions were discussed. Both distributor plate design and good contact between the solid phase and the silane play an important role in decreasing fine-particle formation.

Research on Pyrolysis in Fluidized-Bed Reactors (Jet Propulsion Laboratory)

The objective of this effort is to obtain a fundamental understanding of the pyrolysis of SiH_4 and the deposition of silicon in FBRs. The final report on this research was issued.

Experimental results obtained in the program indicated that more than 90% of the total silicon fed into the reactor as silane is deposited on the FBR bed particles and the remaining silicon becomes elutriated fines. The mechanism of silicon deposition from the pyrolysis of silane is described by a six-path process. Excellent purity of silicon product was obtained when a quartz liner was employed in the FBR.

Workshop

An FSA-sponsored workshop titled, "Low-Cost Polysilicon for Terrestrial Photovoltaic Solar Cell Applications," was held October 28-30, 1985, at Las Vegas, Nevada. There were more than 70 attendees, including representatives from Japan, Taiwan, Federal Republic of Germany, Canada, India, Norway, and Brazil. The workshop provided a forum for descriptions and discussions of new polysilicon processes (including those developed under FSA Project sponsorship), of polysilicon process economics, and of the polysilicon market for the semiconductor and PV industries.

AREA REPORTS

SUMMARY OF PROGRESS

Advanced Silicon Sheet Task
Shaped-Sheet Technology

Stress and Efficiency Studies in EFG Silicon (Mobil Solar Energy Corp.)

The goals of this program are:

- (1) To define low-stress configurations for silicon sheet growth that will maximize solar cell efficiency and at the same time lead to increased throughput rates.
- (2) To investigate causes of deficiency in performance of solar cells fabricated from low-resistivity silicon.

Stress analysis with increased creep rates, beyond the "high-creep" condition modeled previously, shows that significant changes in residual stress arise from the imposed transverse isotherm variations. These changes are essentially independent of the detailed shape of the transverse isotherm profile. Stress reduction is predicted only for the case where the sheet edge is cooled relative to the center.

Modeling was carried out on the influence of end effects on residual stress distributions in finite-size blanks. "Shear flow" stress distribution, used in calculation of residual stresses from laser interferometric measurements of blank curvatures under four-point bending, was obtained. Redistributed stresses were related to stress distributions in semi-infinite sheet from which the blanks were assumed to be cut.

Electron-beam-induced current (EBIC) characterization of diffusion length of float-zone silicon (that was heat treated and stressed at 1000°C) shows that larger variations in diffusion length with dislocation density are observed against background diffusion lengths. These were of the order of 100 μm than found in samples correspondingly treated at about 1200°C. A relationship between diffusion length and dislocation density was obtained for these samples.

No correlation of changes in defect density with gallium concentration levels was found in either oxygen-lean or oxygen-rich EFG material.

An apparatus was designed, constructed, and checked out to measure stress relaxation at high temperatures using four-point bending.

An extension to this contract, covering technical effort to June 30, was put into effect on April 24. The work will consist of three tasks:

- (1) Modeling studies of the effects of stress to allow correlation of theoretical results with results of experimental stress testing.
- (2) Four-point bending tests on silicon to study stress relaxation at high temperature, especially in the range of 800 to 1200°C, using the new apparatus.

AREA REPORTS

- (3) Analysis of experimental results of the stress relaxation tests to obtain an improved estimate of the creep law that can be used in modeling silicon behavior.

Dendritic-Web Ribbon Growth (Westinghouse Electric Corp.)

Westinghouse is conducting a 3-year program, which started early in CY 1984, on the development of the growth of silicon dendritic-web ribbon, and on the fabrication of high-efficiency solar cells made from this material. The purpose is to improve this dendritic-web technology and to demonstrate capabilities that are consistent with utility requirements. The CY 1985 ribbon-growth contract objectives included demonstration by mid-June of uninterruptedly, growing 2 m or more of ribbon at an area growth rate of at least $13 \text{ cm}^2/\text{min}$ under conditions of constant melt level (CML). A mid-December 1985 objective was to demonstrate an area growth rate of at least $16 \text{ cm}^2/\text{min}$ for the same conditions. The CY 1986 area growth rate objective is to demonstrate the rate required to meet DOE PV program goals, as indicated by an updated Westinghouse economic analysis.

The above CY 1985 area growth-rate objectives were not met. Improvements in this and other parameters, however, were achieved in this report period. For ribbon lengths of a meter or more, the maximum area growth rate achieved in the augmented program was increased to $10 \text{ cm}^2/\text{min}$ (for a 1.2-m-long crystal from the previous maximum of $8 \text{ cm}^2/\text{min}$). The length of the longest ribbon grown with the use of melt replenishment was increased to 17 m, for a replenishment rate between 90 and 100% of that required for constant melt level. The previous value for length of ribbon grown was 7.4 m, for a replenishment rate of only about 50%. Maximum ribbon width was increased to 6.9 cm from the previous value of 6.7 cm.

Maximum ribbon width for growth restart after a termination was increased to 6 cm from a previous value of 4.9 cm. A technique also was developed for initiating growth from "ribbon seed" (pieces of cut ribbon), and growth was initiated from such seed at a maximum width of 4.5 cm. Both of these techniques are important because their use would save considerable time required to grow ribbon to wide widths (typical widening rates are around 1 cm/h).

A record was set for throughput (defined as ribbon area grown in a single furnace in a week's time, 7 days) for replenished growth. The throughput was raised to $47,000 \text{ cm}^2$ from its previous record value of $27,000 \text{ cm}^2$.

Considerable progress was made toward automated closed-loop control of the ribbon growth process. In July 1985, the first demonstrations of closed-loop furnace-temperature control were successfully made. The control system employed the dendrite thickness monitor, which performs simultaneous, non-contact sensing of the thicknesses of the two dendrites of a growing crystal and compares these thicknesses with a reference value. In one 5-h test, a ribbon of 5.5 m length was grown without operator intervention. The test was terminated intentionally for manual melt replenishment. In these initial tests, with the heater coil being stationary, the average dendrite thickness

AREA REPORTS

was controlled. In the November/December period, simultaneous operations were accomplished for both the closed-loop melt replenishment and temperature control systems, and the closed-loop heater coil position and temperature control systems under conditions of constant melt level (achieved by manual replenishment). The control system for heater coil position allows control of the thickness of both dendrites to the proper values, rather than control of the average thickness. The maximum period for continuous growth under conditions of closed-loop control of heater coil position and melt temperature for constant melt level was 5.5 h. More than 60 h of accumulated run time were conducted with various combinations of closed-loop control functions.

Refinement of the thermal stress model permitted calculations of the temperature and stress distributions in ribbon from the melting point (growth interface) to room temperature. Elastic buckling studies indicate that interface stresses and those caused by final cooldown do not currently limit area growth rate. Application of a Penning-Jordan-type plastic flow analysis produced good agreement between calculated residual stresses and those measured on actual ribbons. New lower-stress designs based on these analyses gave improved ribbon growth, including the record width of 6.9 cm.

An extension of the contract to Westinghouse, covering the calendar year (CY) 1986 effort on development of the ribbon growth process, was put into effect on February 21, 1986.

Silicon Sheet Supporting Studies

Modification of Silicon Surface Properties by Fluid Absorption (University of Illinois at Chicago)

In this program, the modification of silicon surface properties by various fluids is being studied, and residual stress in silicon sheet is being measured by laser interferometry.

High-temperature indentation damage in silicon was evaluated by using a recently completed high-temperature indentation fixture. Radial crack length, as a function of indentation temperature, was measured over the range from 25 to 300°C. Indentations were made in (100) p-type and (100) n-type Cz silicon. The data indicate that crack length remains constant from 100 to 250°C. This plateau is expected to have a significant influence on sawing, since elevated temperatures are expected because of the sliding contact. The data also indicate that the crack lengths for p-type silicon typically are smaller than for n-type silicon.

A high-speed, high-temperature cutting facility was constructed to cut silicon at a precise feed rate, depth of cut, and fluid environment. The surface morphology and debris size analysis are being used to indicate the deformation mode. For cuts made in air, the average debris size decreases from 1.7 to 1.0 μm when the temperature is raised from room temperature to 100°C. At room temperature, the average debris size increases from 1.7 to 5.6 μm for cuts made in air and ethanol, respectively. The surface morphology of the groove also varies with fluid and temperature. For deionized water and ethanol, as temperature is increased from room temperature to 100°C, the ploughed regions broaden by a factor of two.

AREA REPORTS

The damage formed during scratching and/or indentation was modeled by dislocations propagating in the space charge field of the silicon. The surface of the silicon was described by a limited number of surface sites that may interact with fluids or adsorbates. Because surface sites are limited, they may not sustain the surface charge necessary for equilibrium, and the extent of the space charge region may vary with the surface site density and energy as well as the electrochemical potential.

The Debye length that may be calculated by this model is therefore related to the damage zone (generated by indentation), since dislocations must propagate in the space charge field.

Efforts continued on measuring residual stress in silicon sheet materials using shadow moiré and laser interferometry. Residual stress distributions were determined for EFG and dendritic web ribbon samples. The results consistently indicated that for both sheet materials, the edges of the sheet are in compression while the center region is in tension. The EFG samples have a consistently higher residual stress of 5 to 10 MPa as compared with the dendritic web material stress of 0.5 MPa.

Analysis of Stress/Strain Relationships (University of Kentucky)

This program is aimed at developing stress/strain models for silicon sheet growth processes and evaluating the relationship between silicon growth structure and stress/strain.

Significant progress was made in the following areas:

- (1) Elevated-temperature tensile tests on Cz and dendritic web ribbon material.
- (2) Dislocation mapping, including preferred slip orientations, dislocation mobility, and dislocation multiplication.
- (3) Stress/strain analysis, through use of the Sumino-Haasen dislocation model.

Several tensile tests of Cz silicon samples were conducted at 800 to 1000°C. The data are close to those obtained by K. Sumino. Elevated-temperature tensile testing has been difficult. Some furnace sealing problems were solved, and now a vacuum of 10^{-6} torr can be achieved. Molybdenum test grips are used in a 1% hydrogen-in-argon gas mixture. Specimens tested have had several crystallographic orientations, and different slip systems can be identified after the test is complete. Stress/strain curves were produced. Preliminary initial yield data (strain rate of 4×10^{-4} to $13 \times 10^{-4} \text{ s}^{-1}$) for 800, 900, and 1000°C are approximately 29, 20, and 10 MPa, respectively.

Successful tensile tests on Westinghouse web samples were carried out at 1100 and 1150°C. Reproducibility of test results at 1100°C and 10^{-4} s^{-1} strain rate seemed very good. Flow stress values are comparable with Cz data. Cz samples were used to study effects of laser-cut edges. Significant differences in stress/strain behavior were noted for polished versus unpolished edges.

AREA REPORTS

Studies began on the behavior of a single dislocation moving in the stress field associated with a Westinghouse ribbon thermal profile. This activity complements both University of Kentucky continuum calculations and Westinghouse's activity. These studies involve 3-cm-wide ribbon with only half the ribbon considered. Dislocations introduced at two different positions on the growth interface both end up at the ribbon centerline. Calculations were made using single-dislocation considerations (no interactions of any kind) and only motion in glide was considered.

In the area of dislocation mapping, dislocations are "inserted" analytically at the ribbon melt interface at various positions across the ribbon width. Subsequent motion of each dislocation is tracked as it moves through the thermal stress field. Evaluation of analytical results to date indicates significant dislocation motion and multiplication occur within the first 0.5 cm of the 3-cm-wide ribbon melt interface.

Efforts are just beginning in the area of experimental microstructural observations correlated with stress/buckling phenomena.

In the stress/strain activity, analyses were carried out of thermal stresses associated with a Westinghouse temperature profile, $T(x) = 1292 + 120e^{-5x} - 86.5x$. Most of the large growth stresses are near the growth interface for this profile. The final dislocation value is $3 \times 10^3/\text{cm}^2$ near the center, and $1.1 \times 10^3/\text{cm}^2$ near the outside edge. The first five buckling modes also were predicted and graphically documented. A critical buckling thickness of 158 μm was calculated for a 6 x 12 cm piece of ribbon.

Residual stresses, developed in a ribbon grown with a newer temperature profile, $T(x) = 1372 + 40e^{-5x} - 99.83x$, were calculated. Low residual stress values were obtained that were relatively consistent with Westinghouse splitwidth residual stress measurements. During this period, the maximum (critical) width to which ribbon could be grown in the Westinghouse thermal profile (given above in this paragraph) also was calculated with zero starting dislocation ($N_0 = 0$). A critical width is predicted of above 6 cm. As the starting dislocation density increases, the critical width decreases. For example, for $N_0 = 30/\text{cm}^2$ the critical width is predicted to be about 3.5 cm.

Based on work performed in this program, a paper titled, "Thermal Stresses and Buckling of Elastic Plates with Reinforced Edges," was presented at the Southeastern Conference on Theoretical Applied Mechanics held in Columbia, North Carolina, in April 1986.

Analysis of High-Speed Growth of Silicon Sheets in Inclined-Meniscus Configurations (Massachusetts Institute of Technology)

Work continued to identify the parameters and operating conditions for high-speed growth of thin silicon sheet. The thermal-capillary model and finite-element analysis were used to describe the growth of thin silicon sheets both with planar and with deformed melt-solid interfaces. Dependence of crystal thickness upon pull speed was computed, and the thickness was found to decrease with increasing pull speed. Because the inclined meniscus further

AREA REPORTS

reduces the thickness, it consequently limits the pull speed. The melt-solid interface remained flat with a deflection of 6 to 7% over the range of pull speeds. The higher melt-solid interface deflection encountered with dendritic web ribbon growth cannot be explained by low-axial temperature gradient.

Because of the roll-off in Project funding, the contract to the Massachusetts Institute of Technology is being terminated.

Optimization of Silicon Crystals for High-Efficiency Solar Cells (Solar Energy Research Institute)

This program was completed on March 31, 1986. Silicon crystal growth parameter effects on minority-carrier lifetime were investigated using high-purity FZ techniques. The goals of the work were:

- (1) To optimize dopants and minority carrier lifetime in FZ material for high-efficiency solar cell applications.
- (2) To improve understanding of life-time degradation mechanisms (point defects, impurities, thermal history, etc.).
- (3) To characterize lifetime-related crystallographic defects in silicon crystals by x-ray topography.

Float zoning of high-purity, dislocation-free silicon was conducted both as a tool to study minority-carrier lifetime dependence on various growth parameters, and also as a means of growing long-lifetime, heavily-doped, p-type silicon for use in solar cells. Lifetime values of 303 μ s for 0.46 ohm-cm resistivity silicon and 214 μ s for 0.36 ohm-cm resistivity silicon were achieved when gallium was used as the p-type dopant in [100] crystals. Dislocation-free crystals doped with boron, aluminum, indium, and gallium over a range of resistivities also were grown to establish correlations between lifetime and resistivity with dopant species as a parameter. The effect of crystal cooling rate on lifetime was determined in the range 50 to 600°C/min. The lifetime decreased with increasing cooling rate for both dislocation-free and dislocated crystals. The presence of dislocations, however, had a much more dominant effect in degrading lifetime than did cooling rate.

Calculation techniques and pertinent property data were developed for a comparison of vacuum and gas ambients as they affect impurity concentration profiles in float-zoned and cold-crucible-grown crystals. Graphical impurity profiles were obtained for various segregation and evaporation coefficients in the general case and also for the specific impurities in silicon of aluminum, antimony, arsenic, boron, copper, gallium, gold, indium, iron, manganese, and phosphorus. Results indicated that multiple pre-passes in vacuum prior to the crystal growth pass were helpful in reducing the content of most metallic impurities to negligible levels.

X-ray topography was used to examine both dislocations and lattice-plane curvature in silicon ribbons grown by various methods, and to look at micro-defects in dislocation-free silicon crystals. Improvements also were made in lifetime measurement of heavily-doped silicon.

AREA REPORTS

The draft final report on this program was written and reviewed by cognizant JPL personnel. The final report is being published.

Crystal Growth Modeling Studies (Washington University at St. Louis)

The purpose of this study is to develop a mathematical model describing the Cz crystal growth process. The model is intended to serve as a basis for predicting the important process parameters such as pulling rate and interface shape, to provide strategies for growth of large-diameter crystals, and to lead to improved process control algorithms.

A conduction-dominated model was developed, suitable for predicting the temperature distribution in the crystal and for calculating the melt-crystal interface shape for an assumed melt temperature profile and heat transfer coefficient. A simple model then was developed that correlates the pulling rate and the interface shape as a function of major operating parameters, such as crystal radius and crucible temperature. This simple model correctly portrays the more detailed conduction-dominated model and is therefore suitable for computer control of the growth process.

An analytical study was made of the use of a cooling jet of argon to control the crystallization in the Cz process. This would increase the ingot growth rate and to improve the crystal quality. The effect of jet cooling on the interface shape and pulling rate is significant, and the crystal diameter tends to be more stable in the rapid-cooling environment of the jet.

A study was performed of stress effects for Cz growth. Stresses can be calculated by finite-element analysis, and the effect of growth interface shape on stresses was determined.

Because of the roll-off in Project funding, the contract to Washington University at St. Louis is being terminated. As a result, a stress study to determine the effects of localized high-thermal gradients induced by jet cooling will not be completed.

Electrical, Structural, and Chemical Characterization of Silicon Sheet Material (Cornell University)

The objective of this program is to investigate the physical structure and the chemical nature of defects in silicon sheet material.

The high-temperature deformation of silicon dendritic web ribbon is being studied to obtain accurate creep data for modeling stress relaxation in this silicon material.

Four-point bending at 1000°C was carried out at Mobil Solar Energy Corp. Testing revealed a unique two-stage deformation behavior for dendritic web ribbon that is very different from either single-crystal silicon (either FZ or Cz) or from polycrystalline material (such as EFG silicon). A dendritic web sample subjected to a load initially showed a high creep rate, but after about 1 min the creep rate decreased to almost zero. Then, another period of rapid creep commenced, followed by a period of slow creep. This sequence repeated

AREA REPORTS

itself one more time before the test was ended and confirmed results that had been obtained previously by Cornell. Two samples from the same ribbon, loaded under identical conditions, showed strain bursts at the identical strains, indicating that this behavior is related to crystal morphology and conceivably linked to the presence of two planes in the ribbon.

Preliminary analysis of the data obtained at 1000°C by four-point bending of dendritic web ribbons yielded a value for creep strain rate, $\dot{\epsilon}$, of $8.81 \times 10^{-8} \sigma^3 \text{ s}^{-1}$, where σ is the stress in MPa. This result is in good agreement with the data measured for Cz and dendritic web materials by the University of Kentucky.

Oxygen measurements by Fourier transform infrared (FTIR) spectroscopy reveal a very high oxygen content of about 20 ppma (near the solubility limit) for dendritic web silicon. In addition, a shoulder on the 9- μm infrared (IR) absorption peak of interstitial oxygen in silicon in many of the samples has been variously linked to SiO_2 in the form of coesite at the cores of dislocations, and to complexes of silicon, O, and vacancies absorbing in this IR region. Appearance or lack of this shoulder has not been correlated to the growth configuration, or any other known sample parameter.

Width of the absorption peak associated with interstitial oxygen in silicon is wider in the dendritic web silicon (about 35 to 45 cm^{-1}) than in Cz silicon (about 33 cm^{-1}). A wider absorption peak is generally thought to be related to stress in the specimen, but no quantitative analysis of this effect has been carried out. In two samples with a known amount of stress, the sample with the higher stress had a wider absorption peak than the sample with the lower stress.

Width of the IR absorption peak decreased by annealing a high-stress sample at 850°C for 24 h. This phenomenon was not observed with a low-stress sample.

Materials Properties Modification (Jet Propulsion Laboratory)

Effort was focused on developing a constitutive equation for the behavior of silicon deformation at high temperatures and to obtain improved model predictions for stable ribbon growth. A large variation exists in the constitutive equations and parameters used by different investigators to describe plastic deformation and buckling of ribbon at high temperature. Consequently, correlation of their results is difficult. For example, using results from Mobil Solar Energy's experiments on high-temperature creep response of several Cz and FZ silicon samples by four-point bending, an attempt was made to evaluate the creep data by using equations for primary and secondary creep. The results, however, indicated no correlation between the Mobil-based data and published information.

Several important equations were discussed and evaluated in the FSA-sponsored stress/strain workshop held at the University of Kentucky on March 18-19, 1986. An equation used by most investigators, including K. Sumino of Japan, is recommended as a standard constitutive equation for high-temperature deformation of single-crystal silicon. Values from the literature for the parameters in this constitutive equation were compiled. Efforts continue to define and refine the constitutive equation.

AREA REPORTS

In the effort on measurement of high-temperature properties of silicon sheet, Cz tensile samples tested at 1000°C to 4% total strain were characterized by x-ray transmission topography. Several microstructural features were noted:

- (1) Extensive structure was generated in a nonhomogeneous manner throughout the reduced-gage section of the sample.
- (2) Structure was generated from stress concentration sites at both the extensometer pinholes and the loading pinholes.
- (3) Greater plastic deformation around sample holes were observed for [220] topographs than for [422] topographs.

Because of these problems, a new test sample configuration and processing procedures were developed. Ultrasonic machining of the test samples of either Cz or dendritic web material is now possible as compared to the previously used microgrit blasting technique. With appropriate protective coatings on the silicon sheet faces, the as-cut samples are planar-etched only on the edges to remove damage induced by the ultrasonic cutting. All sample configuration tolerances have been significantly tightened. In addition, the ratio of tab to active gage cross-sectional area has been increased from 2:1 to 5:1 for old versus new sample designs.

The testing equipment, used for tensile tests, is being calibrated after addition of a high-vacuum capability to the elevated-temperature furnace.

A systematic study was conducted involving measuring the structural and electrical characteristics of low- and high-stress Westinghouse dendritic web ribbon as a function of annealing temperature in the range of 450 to 1050°C. The lower-stress ribbon had residual stresses ranging from 1.0 to 9.5 Mdyn/cm² while the residual stresses for the higher-stress material were measured to be between 38 and 40 Mdyn/cm². Results indicate the minority carrier lifetime of web ribbon can be improved with annealing. Magnitude of improvement in the lifetime depends on annealing temperature and residual stress of the material. Material with lower residual stress improved by an order of magnitude, while the higher-stress material improved by a factor of six. The peak in the lifetime improvement for the higher stress material occurred at a lower annealing temperature than for low-stress ribbon. In both cases, the peak lifetime was at a temperature lower than the usual processing temperature for n⁺-p junction formation. This implies that devices should be processed at a temperature lower than the one standardly used, to optimize fully the performance of solar cells.

Workshop

A workshop at the University of Kentucky, Lexington, Kentucky on March 18 and 19 was organized and sponsored by the FSA Advanced Silicon Sheet Task to review progress relating to control of stress and strain during silicon ribbon growth. About 20 people attended including contractors, JPL participants, and other PV program representatives.

AREA REPORTS

The presented results indicated considerable progress in understanding the stress and strain problem from both an analytical and experimental approach. Specifically, several technical conclusions were reached. The use of elastic approximations is appropriate in that strains are small (except for calculations of residual stress). Mechanical property measurements will be confined to the low-strain regime (a very difficult region in which to make measurements). Calculations of ribbon-dislocation distribution qualitatively agree with experimental observation. Observed dislocation densities are generally lower than calculated. Critical maximum values of ribbon width and pull speed may exist that are only slightly greater than those presently being achieved.

Device Research Task (Processing and High-Efficiency Solar Cells)

INTRODUCTION

This task has been expanded since the last 25th PIM to include process research in addition to device research. The objective of this task is to assist the FSA Project in meeting its near- and long-term goals by identifying and implementing research in the areas of device physics, device structures, measurement techniques, material-device interactions, and cell processing.

The research efforts of this task are described and reflect the diversity of device research being conducted. All of the contracts being reported are either completed or near completion and culminate the device research efforts of the FSA Project.

SUMMARY OF PROGRESS

Optimization Methods and Silicon Solar Cell Numerical Models (University of California, Los Angeles)

The goal of this project is the development of an optimization algorithm for use with numerical silicon solar cell models. By coupling an optimization algorithm with a solar cell model, it is possible to simultaneously vary design variables such as impurity concentrations, front-junction depth, back-junction depth, and cell thickness to maximize the predicted cell efficiency.

An optimization algorithm was developed at UCLA and interfaced with the Solar Cell Analysis Program in One Dimension (SCAP1D). SCAP1D used finite difference methods to solve the differential equations which, along with several relations from the physics of semiconductors, describe mathematically the operation of a solar cell. A major obstacle was that the numerical methods used in SCAP1D required a significant amount of computer time, and during an optimization the model is called iteratively until the design variables converge to the values associated with the maximum efficiency. UCLA alleviated this problem by designing an optimization code specifically for use with numerically intensive simulations to reduce the number of times the efficiency had to be calculated to achieve convergence to the optimal solution. Adapting SCAP1D so that it could be called iteratively by the optimization code provided another means of reducing the central processing unit time required to complete an optimization. Instead of calculating the entire current-voltage (I-V) curve, as is usually done in SCAP1D, only the efficiency was calculated (maximum power voltage and current) and the solution from previous calculations was used to initiate the next solution.

Optimizations were run for a variety of substrate qualities and levels of front- and back-surface passivation. This was done to determine how these variables affect the optimized efficiency and the values of the optimized design variables. The sensitivity of efficiency to each of the design variables was investigated by changing one variable and reoptimizing the others.

AREA REPORTS

This effort is near completion, and the final work will be to include variables associated with the design of an AR coating in the optimization.

Carrier Transport and Recombination Parameters in Heavily Doped Silicon (Stanford University)

Experimental work on p- and n-type heavily doped layers has been essentially completed. This work has, for the first time, given reliable data of minority carrier diffusivities in both p- and n-type heavily doped silicon, covering a broad range of doping concentrations from 10^{15} to 10^{20} cm^{-3} .

One of the key results is that the minority carrier diffusivities are higher by a factor of 2 in silicon as compared to majority carrier diffusivities. The Stanford University work is written up in their Final Report 957159.

Development and Analysis of Silicon Solar Cells of Near 20% Efficiency (University of Pennsylvania)

The objective of this contract is to identify, develop, and analyze useful techniques for measuring bulk recombination rates, surface recombination rates, and surface recombination velocities in all regions of high-efficiency silicon solar cells. Recent work has addressed the areas of refinement and automation of the previously developed DC measurement "absolute spectral light-beam-induced current" (ASLBIC), and the theoretical evaluation of dynamic measurements in complex device structures.

To make ASLBIC measurements requires UV illumination, especially in "emitters" of high-efficiency solar cells of presently prevailing designs. To improve the ASLBIC measurement accuracy, the system was equipped with blocked interference filters selected to transmit on the various lines of the Hg light source for higher spectral purity. Intensity monitoring, and computer data acquisition and evaluation yielded repeatability of better than half of a percent. For the accurate determination of the absolute light levels, various photodiodes with traceable calibration were used, but systematic calibration differences of 3 to 5% at wavelengths about 400 nm, and greater below 400 nm, were not reconciled. Software was implemented to completely sample the parameter space of the unknown with numerous s, τ pairs. The results can be displayed 3-dimensionally showing the full extent of regions of good fit of the modeled to the experimental data. Also, software was written using the simplex minimization algorithm to find the best numerical fit.

A theoretical methodology was developed to analyze and compare the dynamic measurement techniques in existence. In this treatment, the true relaxation constants of the system were identified as sums of the inverse of the bulk lifetime and the eigenvalues of the region where the eigenvalues are a function of the region length, mobility, and boundary transport velocities. It is these relaxation constants that are most directly obtained from dynamic measurements. The relaxation constants were analyzed to determine the relationship to and influence by the complexities of the actual devices. For thin layers, it was

AREA REPORTS

shown that the eigenvalue term will be large relative to the bulk lifetime term and, hence, will dominate the response. A drift field, as is often present in emitter regions, adds a third term to the relaxation constant. A methodology was developed to calculate the relaxation constants of a compound region such as that present in a base region with a Hi-Lo junction.

This effort has been completed with submission of the Final Report.

SiN_x Passivation of Silicon Surfaces (University of Washington)

The primary objective of this program is to investigate experimental techniques for passivating silicon surfaces. The approach consists of: (1) characterization of silicon surfaces of homogeneously doped substrates, (2) surface characterization of high-efficiency n⁺/p and p⁺/n silicon cells, (3) determination of dominant current-loss mechanisms in high-efficiency cells, and (4) physical characterization of interfaces. Special emphasis is being placed on studies of interfaces between silicon and SiN_x deposited by plasma-enhanced PECVD.

Work has progressed on determining the effect of dopant concentration on surface state density. The approach to investigating this effect was to build metal-insulator semiconductor (MIS) structures and then take high-frequency capacitance voltage (CV) measurements on those structures to determine the interface state density at midgap (D_{ss}). The MIS structures were fabricated with insulator layers consisting of 700 Å of SiN_x and were characterized for both n- and p-type substrates. The resistivity of the n- and p-type material varied from 0.005 to 7 ohm-cm, and 0.01 to 7 ohm-cm, respectively.

When high-frequency CV measurements were performed on these structures to determine D_{ss} , it was found that the SiN_x/Si interfaces with as-deposited SiN_x exhibited values of D_{ss} larger for n-type substrates than for p-type substrates and that, after heat treatment, this difference became even more pronounced. Also, it was found that the D_{ss} for SiN_x/n-type silicon is essentially independent of dopant concentration while the D_{ss} for SiN_x/n-type silicon interface increases from 10^{12} to 10^{13} states cm⁻² eV⁻¹ as the phosphorus concentration increases from 10^{16} to 10^{18} atoms cm⁻³. These results suggest that SiN_x can passivate a p⁺/n cell more effectively than an n⁺/p cell.

This contract is near completion and the remaining effort will focus on verifying the passivation results with more testing. Working on special structures also will allow measurement of both surface recombination velocity and interface state density.

High-Efficiency Cell Floating Emitter Design (ASEC)

The ASEC effort during this report period was to fabricate several cell lots (including a final lot) of the floating emitter design by C. T. Sah Associates. Although the emitter design has several variations, only the back-surface contact (BSC) vertical-floating emitter (VFE) solar-cell transistor (SCT) design was fabricated.

AREA REPORTS

Performance results of the fabricated cells from initial lots were not good. Cell efficiencies of initial lots ranged from 1 to 11% with the majority of cells being under 7%. The V_{oc} 's were very good. More than 600 mV in many cases, and up to a maximum of 621 mV. However, the I_{sc} 's were not good and accounted for the overall poor cell performances. I_{sc} 's were in the 15 to 25 mA/cm² range, some as low as 2 to 3 mA/cm². By comparison, cell efficiencies of the final lot ranged from 11% to more than 15% for an average of 13.2%, with one-third of the cells measuring more than 14% efficient. V_{oc} 's ranged from 575 to 605 mV, similar to the previous lots. The best improvement was in the J_{sc} values of the final lot which measured between 35 to 45 mA/cm² for the 4 cm² cells as compared to 2 to 25 mA/cm² for J_{sc} 's of the previous lots. It is postulated that those changes from the previous lots to the final lot (that greatly improved current collection efficiency) included reducing the cell thickness from 8 to 4 mils, and increasing the bulk resistivity from <10 to 50 ohm-cm.

Some of the processing problems encountered in fabricating the floating emitter cells included mask alignments, oxide layers, induced during boron diffusion, nonuniformity of both the POCl₃ diffused layers, and the passivated SiO₂ layers. Some of these problems no doubt contributed to some of the poor performances of some cells. The issue that was not resolved was whether or not the floating emitter design is a viable solar cell design, as it was not determined what effect the processing problems had on the overall cell performance. The improvement in performance of the final lot of cells was encouraging and suggested that there might be a potential for the design to be a high-efficiency device. It was concluded, therefore, that the floating emitter design needs more work both in analysis and processing before its full potential as a high-efficiency device can be determined. The ASEC effort is described in their Final Report 957098, which is being completed.

High-Efficiency Solar Cells on Web (Westinghouse)

The major efforts of the Westinghouse contract are to identify carrier loss mechanisms, design high-efficiency cell structures with the aid of numerical models, and to process high-efficiency solar cell structures. The program goal is to produce an 18% efficient dendritic web cell.

Transmission electron microscopy (TEM), laser-beam-induced current (LBIC), and deep-level transient spectroscopy (DLTS) were analysis tools used to compare baseline high efficiency (~15%) with low-efficiency (~10%) web solar cells. The results of these analyses indicated that dislocations (and not twin planes) were the primary causes in limiting diffusion lengths (and, hence, cell efficiency).

It was found that the diffusion lengths and efficiencies of web cells could be improved by hydrogen implantations carried out with an energy of 1500 eV and a beam current density of 2 mA/cm² for 2 min. As an example, the diffusion length (19 μ m) and efficiency (8%, no AR) of a cell were improved respectively to 120 μ m and 10.3% (no AR) after hydrogen implantation. However, higher quality cells of more than 10% efficiency (no AR) showed little improvement after hydrogen implantation.

AREA REPORTS

A double-layer AR coating consisting of ZnS and MgF₂ was employed to enhance the short-circuit current by 51% and the efficiency by 55%. With this coating and an aluminum BSR, web cells with an efficiency of 16.0% (as measured by JPL) were fabricated.

Final work on this contract included the reduction of the dopant surface concentration and junction depth in the emitter using an arsenic diffusion, and the reduction of base resistivity in the web cell from 4 to 0.2 ohm-cm. With these improvements along with the hydrogen ion implantation, double-layer AR coating, oxide surface passivation, and aluminum BSR, the program goal of an 18% efficient cell may be achieved.

Laser-Assisted Metallization (Westinghouse)

The objective of this contract is to develop a laser-assisted metallization process in which the metal grid line pattern is written directly on the cell substrate, thereby precluding the use of photolithography. In its full implementation, there would be no vacuum processing, and a thick (~8 μ m) conductor would be electroplated onto the laser-deposited metal in order to carry the photocurrent without excessive ohmic losses.

During this report period, cells were fabricated using an argon ion laser with output power ranging from 1 to 8 W. Initial results (decomposing silver neodecanoate on base silicon) were unsuccessful because the decomposed film would not adhere to the silicon through the subsequent plating processes. To circumvent this problem, 1500 Å of Ti and 500 Å of Pd were first evaporated onto the silicon surface. Titanium provides adherence to the silicon while the palladium cap protects the titanium from oxidation. The silver neodecanoate solution was then spun on the palladium layer, and the grid lines were written with the laser. After rinsing the undecomposed film from the wafer, the grid lines were electroplated with silver. This silver film then acted as an etching mask to remove the palladium and titanium layers from the field.

Cells fabricated in this manner had efficiencies as high as 16.6% with normal fill factors (FFs). The laser processing did not degrade junction quality, bulk lifetime, series resistance, or shunt resistance. However, the necessity of incorporating layers deposited by evaporation detracted from the original goals of this technique.

Several experiments were conducted to incorporate the use of titanium organometallic inks to eliminate the evaporative step. Grid lines were written on spun-on Ti MOD films, which were hard baked at 400°C prior to spinning on the silver neodecanoate. After laser writing, the grid lines were sharp while the remainder of the film had a consistent TiO₂ AR coating. Although the grid lines survived the plating process, their adhesion was unacceptable.

Research on this Ti process was initiated [as well as those using metallo-organic solutions containing adhesion promoters (Bi) or metal ions which are able to form silicides (Ni and Pt)], but was stopped when the follow-on contract was terminated prematurely.

AREA REPORTS

Ink-Jet Printer System (Purdue University)

The objective of this contract is to develop a computer-controlled ink-jet printer that will print metal inks in a configured pattern on solar cells. The ink-jet printing system uses a modified Siemens print head with 12 nozzles, and a computer-controlled X-Y table upon which the cells to be metallized are mounted. Work since the last PIM has consisted of upgrading the hardware and conducting ink-jet printing studies to evaluate the entire printing system.

The most significant hardware improvement has been the incorporation of an IBM/AT computer to operate the ink-jet printer system. Prior to this, the ink-jet printer system was connected to the Purdue mainframe computer for operation. With acquisition of the IBM/AT computer, the ink-jet printer system is now an independent, standalone, operational system.

The ink-jet printing studies have uncovered a contact resistance problem. It was determined that a silicon oxide layer is formed between the silicon surface and the contacts (metal inks) when the printed ink is fired to remove organics. One approach to this problem is to find an additive for the metallo-organic ink that will form a conductive glass with the silicon oxides during the firing cycle. A second approach is to adjust the firing conditions to eliminate or reduce the formation of silicon oxides. Both approaches are being investigated. Solving the high-contact resistance problem is the last remaining problem to be solved on this contract. The ink-jet printer assembly has been exercised repeatedly and performs well.

Process Research of Non-Cz Silicon Material (Westinghouse)

The goals of the contract were: (1) to investigate simultaneous diffusion of liquid dopants for front and back junctions, (2) to investigate process control parameters, and (3) to perform a cost analysis of the simultaneous junction formation process.

The efforts on this contract end on a positive note. A successful, simultaneous junction formation process using liquid dopants was achieved using a flash diffusion (heat lamp) technique. Earlier attempts to simultaneously form junctions by thermal diffusion of liquid dopants were unsuccessful because of the cross-contamination of dopants on the front and back junctions. The flash diffusion process involves subjection of the web material to a high temperature, short-time heat pulse from tungsten-halogen flash lamps. Times of 5 to 15 s and temperatures of 1000 to 1150°C were investigated. It was determined that to produce the highest quality cells, an annealing cycle (nominal 800°C for 30 min) should follow the diffusion process to anneal quenched-in defects. Two ohm-cm n-base cells were fabricated with efficiencies greater than 15% (AM-1, 100 mW/cm²).

A cost analysis was conducted using IPEG methodology. The analysis indicated that a cost reduction of 25 to 35% could be achieved when comparing the flash diffusion process to the old sequential diffusion process.

AREA REPORTS

Rapid Thermal Processing Effects on Cz Silicon Substrates: Defects, Denuded Zones, and Minority Carrier Lifetime (North Carolina State University)

The main objectives of this study were to evaluate rapid thermal processing (RTP) as a viable procedure for: (1) Cz substrate modification using high temperature dissolution treatments, and (2) rapid junction activation following ion implantation. The idea behind the first treatment is to dissolve grown-in defects and nucleation sites for oxygen precipitation, while the second process would be done as quickly as possible, e.g., 10 s, to prevent any subsequent defect nucleation or lifetime degrading processes from occurring.

The experimental approach for substrate evaluation used preferential chemical etching and x-ray topography to delineate defects that are subsequently correlated with minority carrier lifetime which, in turn, is determined by a pulsed metal oxide semiconductor (MOS) test device. The x-ray delineation of grown-in defects were enhanced by a lithium decoration procedure performed at temperatures below 450°C, both prior to and after a high-temperature dissolution anneal. Experimental equipment installed and brought up to operational speed during the initial 8 months of this project include a computerized semiconductor measurement system, Model CSM/16, purchased from the Materials Development Corp., which measures both τ_g and τ_r via CV, C-t and C-T analyses, and a 15-kW rotating anode x-ray generator, Elliott Model GX-21, capable of either Lang or double-crystal x-ray topography on wafers up to 6 in. in diameter. Silicon wafers examined were as-grown, as well as furnace and RTP annealed with various combinations of 1200, 750, and 1050°C thermal cycles.

Results showed excellent correlation between process-induced defects and τ values for τ_g span a range from 100 to 1000 μm , while τ_r is generally a factor of 10 lower. RTP-induced slip dislocations were initially the main factor in obtaining low τ , but this has recently been corrected with an improved RTP process.

Diffusion Barriers (California Institute of Technology)

The objective of this effort is to investigate amorphous metal alloys as diffusion barriers in silicon metallization schemes. Amorphous W-Zr and W-N alloys have been investigated as diffusion barriers. It was shown that amorphous W-Zr films crystallize at 900°C, which is 200°C higher than for amorphous W-Ni films, but that the films nonetheless react with metallic overlayers at temperatures far below the crystallization temperature. Specifically, it was shown that failures in a Si/W-Zr/Al metallization were dominated by highly localized interactions. However, W-N alloys (crystallization temperature ~600°C) were applied successfully as diffusion barriers in contact structures with Al and Ag overlayers. The thermal stability of the electrical characteristics of shallow n⁺p junctions was significantly improved by incorporating W-N layers in the contact schemes. It also was shown that deposition parameters have important influences on the performance of W-N thin films as diffusion barriers.

AREA REPORTS

Use of Low-Energy Hydrogen Ion Implants in High-Efficiency Crystalline Silicon Solar Cells (Pennsylvania State University)

This program explored the use of low-energy hydrogen ion implants in the fabrication of high-efficiency crystalline silicon solar cells. The work established that low-energy hydrogen ion implants can result in hydrogen-caused effects in all three regions of a solar cell, viz, emitter, space charge region, and base. In web, Cz, and FZ material, low-energy hydrogen ion implantation can reduce the surface recombination velocity. Also in web, Cz, and FZ material, hydrogen implants were found to passivate space charge region recombination centers. In web cells, hydrogen implants were also found to passivate the base region. However, similar improvement was not seen for the base region of Cz or FZ cells. In the case of web material, hydrogen is believed to be able to diffuse into the base region where it can passivate structural defects present in web in the base.

In exploring the fundamental interaction of hydrogen with impurities in silicon, it was found (using DLTS) that H^+ implants can passivate the deep levels resulting from fast diffusing metal impurities (Au, Cr), but not those resulting from slow-diffusing metal impurities (Ti). This suggests that gettering, not some chemical interaction, may be the dominant "passivation" effect in hydrogen's rendering deep levels inactive. Other fundamental work substantiated the recent result of other groups that hydrogen (in this case, implanted hydrogen) can neutralize boron acceptors in silicon. Heating during H^+ implantation above $\sim 180^\circ\text{C}$ removes this neutralization phenomenon. It also was established that hydrogen implants can alter the diffusion properties of ion implanted boron in silicon; however, this was not found to be the case for ion implanted As.

Heavy Doping Effects in High-Efficiency Silicon Solar Cells (University of Florida)

The goal of this contract is to investigate theoretically and experimentally the effects of heavily doped crystalline and polycrystalline silicon upon the conversion efficiency of junction silicon solar cells.

The results are reported of the first direct measurement of the minority electron transit time in a p-type (Si:B) transparent heavily doped layer. The value was obtained by a high-frequency conductance method. From the transit time, values were determined for the minority electron diffusion coefficient D and mobility μ . The new results indicate that the position-averaged D and μ are smaller by a factor 7 than the corresponding majority carrier μ for a layer whose doping concentration ranged from $3 \times 10^{19} \text{ cm}^{-3}$ to 10^{20} cm^{-3} (Reference 1).

Studies were made of the temperature dependence of the emitter saturation current for bipolar devices by varying the surface recombination velocity at the heavily doped emitter surface. From this dependence, a value for the bandgap narrowing was derived that is in better agreement with other determinations than were previous results obtained from the temperature dependence measured on devices with ohmic contacts (Reference 2).

AREA REPORTS

Analytical solutions were developed for any degree of accuracy for minority-carrier transport in the passivated emitter layer of solar cells. The simplest of these, accurate to within 5% for most emitters, reveals the competing physical mechanisms in a way that benefits the informed and systematic design of solar cells (Reference 3).

A new method has been developed and illustrated that significantly improves the accuracy of lifetime (τ) determined by voltage transients. This method requires only pressure contacts, and thus may be used to determine τ after key processing steps in manufacturing (Reference 4).

Studies of Oxygen- and Carbon-Related Defects in High-Efficiency Silicon Solar Cells (State University of New York at Albany)

Oxygen- and carbon-related defects were studied in silicon, especially as related to high-efficiency silicon solar cells, including gettering of deleterious impurities. Surveys were made of process-induced defects, of lifetime measurement techniques, and of defect aggregates in general. Coordinated experimental and theoretical studies of process-induced defects were carried out. Studies indicate that the vacancy is the likely source of the anomalous oxygen diffusion (observed by Stavola, et al.) confirmed the identification of the (V·O₂) and the (V·O₂+O_i) center, and indicated that defect-enhanced diffusion (such as ion implantation or neutron transmission doping) can lead to thermal donors, and presumably other impurity complexes. A theory has been developed that describes the electrical behavior of the hierarchy of thermally induced double donors, including a core and an electronically repulsive oxygen-rich region. Identification has been made of the most likely core for the homogeneously nucleated oxygen precipitate as the "ylid," the saddle point for oxygen diffusion stabilized by the presence of two or more additional oxygens. It also was concluded that the precipitation strain energy can also cause the emission of an interstitial leaving as the core the (V·O₂) center; two of these emissions will create a (V₂·O₂) center, a recombination center, thereby destroying the donor. It also was concluded that the likeliest emitted interstitial is an unbonded silicon O molecule, which is also the likely interstitial involved in high-temperature and oxidation processes, and in supersaturated "excess" oxygen found in as-grown crystals. The first kinetics model which fits all the thermal donor formation data has been developed. Studies of the multioxygen diffusing defects are under way. Studies were made of the gettering of Fe at oxygen surfaces using Rutherford back scattering (RBS), and using electron paramagnetic response (EPR) have found the (Fe·V·O) center, the basic gettering defect.

Metallo-Organic Decomposition Inks (Electrink, Inc.)

This effort investigates the manufacture and evaluation of selected metallo-organic solutions and covers the details of the associated manufacturing processes. Technical support for the development of solution compositions also was used to optimize their use for metallization in PV cells.

AREA REPORTS

To date, solutions using four different metals and mixtures of solutions of three of these metals have been made. The primary metallization metal compound under investigation is silver neodecanoate. Other ink solutions being investigated include silver neodecanoate with small additions of bismuth or platinum 2-ethylhexanoate which serve to improve adhesion to substrates and resistance to solder leaching. These compounds were dissolved in benzene or xylene. Nickel 2-ethylhexanoate and nickel neodecanoate also were made. Metallo-organic compounds using gold, silicon, titanium, copper, tin, and lead are planned to determine metal film properties such as conductivity, adhesion, and solderability at low cost.

All of the processes used for the metallo-organic compounds were adapted from those developed at Purdue University under the direction of Dr. R. Vest. Interpretation of thermal analysis results has led to a better understanding of the formation as well as the decomposition reactions and, hence, to improvements in the process procedures. In the case of silver neodecanoate and the nickel compounds, it was determined that the reaction pH required careful control to ensure the yield and purity of the product.

The bismuth and platinum compounds tended to precipitate solids from solution on standing, although no solids appeared in bismuth solutions below 5% after several months. Platinum solutions greater than 5% have not been reliably made because of the formation of a black (decomposition product) precipitate.

Precipitates also occurred when small amounts of concentrated solutions of bismuth and/or platinum compounds were added to concentrated (>20%) xylene solutions of silver neodecanoate. Bismuth compound was added at under 0.5% while the platinum compound was less than 1.5% in the silver neodecanoate solution. The mixed metallo-organic solutions provided the hoped-for performance improvements.

Low-Pressure Chemical Vapor Deposition of Polycrystalline Silicon (Jet Propulsion Laboratory)

In the final attempt to reduce surface recombination at the front contacts, the use of a doped polysilicon layer has shown theoretical promise. The low-pressure chemical vapor deposition (LPCVD) system was modified to deposit polycrystalline silicon to allow the investigation to define the controlling process parameters and requirements for producing films for use as an integral portion of the solar cell contact system.

The film depositions used a conventional hot wall LPCVD reactor with a dual-stage Alcatel rotary pump. Both undoped and in-situ PH_3 -doped polysilicon deposition processes were developed and characterized. At the temperatures (610°C) and pressures (320 mTorr) used, the deposition rate of the undoped silane was $110 \text{ \AA}/\text{min}$. While at a $[\text{PH}_3]/[\text{SiH}_4]$ concentration of 2.5×10^{-2} , it dropped to $8.3 \text{ \AA}/\text{min}$.

Structures were fabricated using a $[\text{PH}_3]/[\text{SiH}_4]$ ratio of 2.5×10^{-2} . The preliminary data are shown below. The data of each run are the average of four devices.

AREA REPORTS

Run	V_{oc} , mV	I_{sc} , mA	Fill Factor	Efficiency (η)	Film Thickness (τ)	ρ_s
151-1	639.5	128.5	818	16.72	1.5 KÅ	70
151-2	638.5	127.5	812	16.52	30-40 Å	VL
151-3	645.3	125.0	811	16.36	400 Å	VL
151-4	637.2	132.8	807	17.08	150 Å	VL
151-5	650.6	130.0	811	17.15	1.0 KÅ	138
151-6	648.0	128.6	811	16.81	200 Å	VL
151-7	643.9	129.5	799	16.65	Control	

The data indicate that LPCVD films can form a viable contacting system and the high FFs show there are no series resistance problems.

REFERENCES

- (1) Neugroschel, A., Hwang, B.Y., and Park, J.S., IEEE Electr. Dev. Lett., EDL-7, p. 81, 1986.
- (2) Park, J.S., Neugroschel, A., and Lindholm, F.A., IEEE Trans. Electr. Dev., to be published.
- (3) Park, J.S., Neugroschel, A., and Lindholm, F.A., IEEE Trans. Electr. Dev., ED-33, p. 240, 1986.
- (4) Lindholm, F.A., et al., Plenary-Session Lecture, Photovoltaic Specialists Conf., Las Vegas, October 1985.

PROJECT ANALYSIS AND INTEGRATION AREA

INTRODUCTION

The objective of the Project Analysis and Integration Area (PA&I) is to support the planning, analysis, integration, and decision making activities of FSA. Accordingly, PA&I supports the Project by developing and documenting Project plans based, in part, on the technical and economic assessments performed by PA&I of the various technical options. Goals for module technical performance and costs, derived from National Photovoltaics Program goals, are established by PA&I for each of the major technical activities in the Project. Assessments of progress toward achievement of goals are made to guide decision making within the Project.

SUMMARY OF PROGRESS

Technology Update

Based on the most recent process descriptions made available for Westinghouse, new cost estimates were prepared for the production of dendritic web modules. The Solar Array Manufacturing Industry Costing Standards (SAMICS) computer program cost estimate was \$1.02/W_p (1985 dollars) for 13.7% efficient modules manufactured in a 25 MW/year production facility.

Sensitivity studies were carried out using Standard Assembly-Line Manufacturing Industry Simulation (SAMIS) to investigate the impact of technical developments within several areas of the dendritic web program. One finding was that continued research on the web growth process was necessary for the project to reach its objectives. Improved web growth rates are necessary if the technology is to be competitive with conventional energy sources. Another finding was that a new combined junction formation process resulted in cost savings in the area of cell processing. JPL-sponsored research to lower the cost of solar-grade silicon promises to further reduce the cost of this solar cell technology.

An updated estimate of Cz module production cost was prepared using state-of-the-art processing technology. Estimated production costs for a 25 MW factory were \$1.45/W_p (1985 dollars), assuming a module efficiency of 13.5%.

The status of crystal silicon PV technology was presented at the 26th PIM in April 1986. The presentation is summarized in the proceedings section of this document. The methodologies which have been developed by PA&I for assessing the status of the technology were also covered in the presentation. The methodologies discussed in the presentation were SAMIS, SIMRAND, and Lifetime Cost and Performance (LCP). Examples were given that showed how each methodology was used in assessing specific aspects of PV technologies. A handout was prepared for the meeting that summarized the capabilities of each of these models, illustrated their application in assessing PV technologies, and indicated the current status and availability of each model.

PRECEDING PAGE BLANK NOT FILMED

AREA REPORTS

Software Development

SAMIS

The SAMIS model has been completely converted to run on the IBM PC/XT (or compatible system). The implementation includes three modes of operation: SAMIS, Standard Assembly-Line Manufacturing Price - Estimation Guideline (SAMPEG), and Improved Price Estimation Guidelines (IPEG). The SAMIS mode provides the most detailed analysis of production costs. A hypothetical factory is "built" based on a detailed set of manufacturing process descriptions provided by the user. The cost of labor along with materials, building space, and utilities are taken from a supporting cost account catalog. A detailed financial model is applied to determine the annual costs of operation. An extensive set of output reports, including year-by-year financial reports for the company, are made available by SAMIS.

SAMPEG is a simplified version of SAMIS and is the usual way to run the program. SAMPEG runs in a few minutes, but the reports available are less detailed than SAMIS results. They consist of a summary cost estimate for the modeled company and each of its manufacturing processes.

IPEG is a linear approximation of the more detailed model of the firm constructed by SAMIS. Overhead factors are applied to direct input costs to arrive at total cost. IPEG is particularly useful for investigating the effects of changes in financial parameters on cost estimates prepared by more detailed SAMIS runs. Price estimates calculated with either IPEG or SAMPEG will approximate a SAMIS estimate.

Copies of the PC version of SAMIS and supporting documentation can be obtained through the Computer Software Management and Information Center (COSMIC) located in Athens, Georgia.

SIMRAND

Three JPL documents have been published: The SIMRAND Methodology: Theory and Application for the Simulation of Research and Development Projects, JPL 85-98; The SIMRAND I Computer Program: Simulation of Research and Development Projects, JPL 85-96; and The RANDOM Computer Program: A Linear Congruential Random Number Generator, JPL 85-97. The computer code and the three documents have been submitted to COSMIC (NASA's software dissemination center).

SIMulation of Research AND Development Projects (SIMRAND) is a decision making methodology for selecting the best course of action in the uncertain environment of R&D projects. SIMRAND makes it possible to model complex decisions involving a number of alternative paths. One or more points along each path can be described as random variables with a range of possible outcomes.

SIMRAND has been used successfully to compare the outlook for competing silicon solar cell technologies. SIMRAND has also been used to rank small solar thermal systems on the basis of cost, and to rank alternative designs for autonomous spacecraft at JPL.

AREA REPORTS

ADDITIONAL ACTIVITIES

Process Cost Estimation Using Basic Processing Units

Earlier studies of manufacturing processes for the production of advanced PV modules have been updated and expanded to reflect more recent technological developments. These basic processing units (BPUs) are manufacturing process descriptions and cost estimates that cover example processes likely to be used in the commercial production of PV modules. The BPUs are not an exhaustive set of all possible combinations of manufacturing equipment and processes, but provide a place to start when examining an immature or ill-defined manufacturing facility of the future.

BPUs provide a baseline understanding of the resources required by various manufacturing processes used in PV module production. Each BPU provides information on the equipment used by the process including estimates of the output rate, cost, and lifetime. Also, floor space, direct labor, and material and utility inputs to the process are described. Cost estimates included with each BPU can be summed to provide rough estimates of the cost of various production sequences for PV modules. In addition, the BPUs can be used as a source of information for engineering cost studies. The SAMIS Computer program, which is an engineering cost model, was used to prepare the production cost estimates for each BPU.

Cherry Hill Revisited

A paper was presented at the IEEE Photovoltaic Specialists Conference (held in Las Vegas, Nevada, October 21-25, 1985), tracing the beginning of the FSA Project as part of the emerging National Photovoltaics Program to the present. The paper covered many of the highlights of the Project as measured by progress toward the Program goals. The original goals for the DOE National Photovoltaics Program were established as an outcome of the Cherry Hill, New Jersey, Conference (in 1973) on Photovoltaic Conversion of Solar Energy for Terrestrial Applications. It was envisioned that a \$0.50/W_p price (1975 dollars), a 10% module level efficiency, and a 20-year lifetime were needed to be competitive with fossil-fuel generated, grid-supplied electricity. The paper reconstructs the details of the original goals and objectives for crystalline silicon technology and concludes with an economic comparison to the 1985 state-of-the-art Cz PV module technology.

The paper concluded that Cz technology essentially meets the Cherry Hill goals. Because current program goals are much more demanding than the original goals, further technology development efforts will be required if they are to be met. Further reductions in wafer costs were identified as the principal technical barrier to the technology reaching current national program goals.

RELIABILITY AND ENGINEERING SCIENCES AREA

Materials Research: Single Junction Thin Film

Thin-Film Module Reliability Task

1. Hot-Spot Endurance of Amorphous-Silicon Modules

Part of the reporting period was involved in the design and fabrication of a new test bench for the purpose of improving control of hot-spot test accuracy.

Testing of the response of ARCO a-Si cells to back biasing was completed when two additional cells in a previously tested module were subjected to a 100-h cyclic hot-spot test. The hot-spot temperature reached a marginally acceptable value and the cells suffered the usual amount of erosion. Aside from this, no other changes were noted. A test performed to determine the relationship of the temperature of test cells in the ARCO modules to the temperature of the glass superstrate indicated that the difference is only on the order of a few degrees and less than the other uncertainties involved in the testing.

The hot-spot testing of Chronar submodules was completed. With cells in back bias and currents equal to those expected in a module cell string, the hot-spot temperatures usually did not exceed 120°C. The 100-h cyclic hot-spot test was performed on two Chronar modules. The test current was initially set to the module short-circuit current, which was deemed the appropriate current for performing the test. It was difficult to find cells with a back-bias voltage high enough to provide a power dissipation leading to a significant hot-spot temperature. The cells in the Chronar module had a lower breakdown voltage than the cells in the previously tested submodules. Also, the cells in the module exhibited a downward drift in current as the test progressed. As a result of the above factors, the power dissipation obtained in the cells tested was not enough to produce a hot-spot problem.

Many cells in a Solarex test structure were tested. The response of the cells was similar to that of the cells in the ARCO submodule previously tested.

Cells in a Sovonics module were tested and found to be very sensitive to back biasing with one of the cells becoming shorted in the initial phases of testing. Otherwise, the second-quadrant responses obtained for the cells were similar to those obtained for the ARCO Solar amorphous cells, once the cells stabilized after exhibiting rapidly changing characteristics. The overall effect was the dichotomous behavior observed in previously tested ARCO cells. The initial voltage breakdown occurred at about 8 V, with current runaway, followed by a much lower shunt resistance upon subsequent back biasing than originally exhibited. The Sovonics cells exhibited an even greater lowering of the shunt resistance than the ARCO cells. One of the cells exhibited a very erratic behavior, starting out like a previously untested cell, but then changing suddenly to a lower shunt resistance. After additional power dissipation, it changed back to its initial second-quadrant curve. Two of the cells exhibited the low shunt resistance behavior characteristic of amorphous cells that have already been back biased. In these two cases, the back

PRECEDING PAGE BLANK NOT FILMED

AREA REPORTS

biasing occurred as the test was initiated. Apparently, the cells suffered from some transient voltage surge occurring at the onset of testing.

The rate of change of temperature with power dissipated ranged from about 6°C to about 18°C/W. These results are within the range of those obtained for the ARCO amorphous cells. The Sovonics modules have a short-circuit current of about 2.75 amps. In the high shunt resistance mode, that amount of current was enough to produce hot-spot temperatures exceeding 140°C in one of the cells tested. Another cell, however, had multiple hot-spots. During the period of testing, the dominant hot spot (one with highest temperature) alternated among the ones in existence until there were two at the same temperature. At this point, it took about 3 A of power dissipation to reach a temperature in excess of 140°C. Apparently, the hot spots were sharing the power dissipation evenly, requiring more total power dissipation to reach a given hot-spot temperature.

The only visible effect noted during the testing was a small blister around one of the hot spots. The hot-spot temperature of the cell did reach in excess of 170°C, at which point the test was terminated. The back-bias current was equivalent to the short-circuit current produced by a Sovonics module, and the voltage was equivalent to that of two series cells. Therefore, based on this result, the use of bypass diodes around every one or two cells seems rational.

A major portion of the amorphous-cell hot-spot testing was summarized in a paper, titled Hot-Spot Durability Testing of Amorphous-Silicon Cells and Modules, by C. Gonzalez and E. Jetter. It was presented at the 18th IEEE Photovoltaic Specialists Conference in Las Vegas, Nevada, in October 1985.

2. Electrochemical Corrosion of Amorphous-Silicon Modules

Electrochemical corrosion research focuses on corrosion mechanisms to which both crystalline and a-Si modules may be subjected in central station applications, on the determination of corrosion rates, and on the ascertainment of means of corrosion passification. Corrosion mechanisms and rates have been previously determined and reported, so the present objective is to study the details of the corrosion processes and to develop passification design strategies.

It has previously been determined that module leakage currents are responsible for observed electrochemical corrosion. An experiment called SVI has revealed the detailed nature of module leakage-current behavior. Encapsulants polyvinyl butyral (PVB) and ethylene vinyl acetate (EVA), sandwiched between symmetric cylindrical brass electrodes with guard rings, were mounted on glass and subjected to a broad range of controlled temperature/humidity environments. Bulk, surface, and interfacial electrical conductivities were frequently monitored. It was determined that surface currents are relatively small, and that the encapsulant/glass interfaces support the highest levels of leakage current.

In a related experiment called CHRNRI, Chronar-supplied, self-laminating, substrate films have been mounted to glass substrates upon which 200 Å Ti-Ag cylindrical electrodes with guard rings have been vapor deposited. The critical interfacial conductivities are presently being monitored for this amorphous-module-like sample configuration.

AREA REPORTS

In yet another experiment called BEMCOVSI, glass-mounted EVA sample is undergoing exposure to an 85°C/10% relative humidity (RH) environment while being exposed to 1 sun of UV radiation. During the initial 1000 h exposure period, interfacial, bulk, and surface currents have remained steady. The interfacial current is 10 times higher than the surface current while the bulk current is intermediate.

3. Solar Cell Reliability Testing

At Clemson University, research has continued on performing tests that will lead to identification of degradation mechanisms in thin-film cells. Work has been completed on developing stress-testing procedures, specifically for a-Si cells. Much of the effort went into developing a measurement system for accelerated testing of a-Si cells with a repeatability of 1%.

A variety of cells (including encapsulated and unencapsulated, and single-junction and tandem-junction) and several designs have been subjected to accelerated stress tests, in which the parameters are test time, temperature, illumination, and open- or short-circuiting. Most cell samples have been supplied by ARCO Solar, Inc., Chronar Corp., Solarex Corp., and Sovonics Solar Systems. From physical observation of cells that have degraded during these tests, it appears that irreversible degradation at elevated temperatures is the result of a solid-state reaction between aluminum and a-Si films.

4. Module Reliability Testing

The determination of humidity degradation rates and the identification of key electrochemical failure mechanisms continued for generic module designs based upon temperature/humidity testing cycles and data from solar radiation surface meteorological observations (SOLMET) weather tapes. Thirty-six modules, including amorphous, EFG ribbon, dendritic web ribbon, and Cz types, were under long-term exposure at 85°C/5% RH and 85°C/85% RH with 15 V and 250 V on selected samples for evaluating sensitivity to electrochemical degradation. Inspection periods of 10, 20, 45, 90, and 180 days were scheduled and included electrical (I-V curve) and visual performance data. Significant 40-day results included series resistance increases and power losses for shorted cell string a-Si modules in 85°C/85% RH over 85°C/5% RH environments and visual electrochemical degradation for print-Ag Cz cells in glass-EVA-Tedlar and glass-aliphatic polyurethane-glass module types exposed to 85°C/85% RH and a 250-V bias between shorted cell string and frame. This degradation, however, resulted in minor peak power losses of less than 5%. Further, the 40-day performance results for the Cz modules were consistent with goals established for 20-year field equivalent transmissivity and series resistance values obtained from previous testing. Consequently, the long-term tests were not continued beyond day 40.

Field tests initiated in June through August 1985 on several a-Si submodules with samples short-circuited, open-circuited or under Zener-diode loads, simulating maximum power loading, resulted in significant power degradation for all modules. This led to a new series of accelerated field tests to evaluate the effects of temperature and possible annealing while the submodules are under Zener-diode

AREA REPORTS

loads, simulating maximum power loading. Back-surface heaters to maintain a constant (24-h) temperature or cyclic a.m. (8:00 to 5:00 p.m. daily) temperature were installed on several samples and set at 70, 85, and 100°C levels. Visual inspection and electrical performance measurements were scheduled at 2, 4, 10, 20, 40, 80, and 160 days of exposure. To date, the cycled modules have completed 80 days of testing and I-V curve comparisons have shown progressive decreases in shunt resistance levels resulting in average peak power losses up to 26.8% for 80°C samples, and 39.7% for 100°C samples. The next scheduled inspection period is in June 1986 and may identify a further separation in results for the 85 and 100°C levels. The continuous heating samples have completed 40 days of exposure and are being compared with the cyclic sample results at 85 and 100°C levels. After 22 days, the 100°C module cracked severely during a rain shower and was removed from the test. Comparative data should be completed in May after the day 80 inspection period.

5. Thin-Film Module Development

Hughes Aircraft Company completed deliveries of 4 x 1 ft modules that consisted of an encapsulated and framed assembly of Chronar submodules. These modules were subjected to the standard Block V qualification tests to determine what further work was needed in increasing the reliability of a-Si modules. It was clear from the tests that further development should be performed at the submodule level to optimize the package design while obtaining the desired reliability. A contract, therefore, was undertaken with Chronar Corp. for a program of material selection, module design, module fabrication, and module test. As part of this effort, module assemblies of diverse types have been supplied to JPL for testing. These are being subjected to some of the standard qualification tests and to special field tests. Also, samples of module materials are being subjected to environmental stress tests and other studies.

Modules have also been obtained again from ARCO Solar, Inc., Solarex Corp., and Sovonics for special field tests, some standard qualification tests, and special stress tests and studies.

The problem of module development was also attacked by exploratory development of module encapsulant systems. The approach taken consisted of formulating concepts for thin-film encapsulation and generating an initial description of thin-film encapsulation construction elements. This route was patterned after the approach taken in 1977. Construction elements for crystalline-silicon solar cell modules were then generated, leading to the identification of EVA as an encapsulant.

For a thin-film glass superstrate design, the rear surface to be protected by encapsulation is considered to be aluminum. A key requirement, therefore, is to prevent aluminum corrosion. Thus, for the construction elements, the first layer against the aluminum is considered to be a chemical coupling agent. It may be based on organosilane chemistry that functions doubly as an anticorrosion agent and a chemical bonding agent. The next layer could be a pressure-sensitive adhesive to permit instant adhesion during manufacturing. This layer must later cross-link to work efficiently with the chemical coupling agent. The last layer is a mechanically durable back-cover plastic film, with the initial choice being fluorinated ethylene propylene (Teflon FEP Du Pont).

AREA REPORTS

As practiced in the thin-film manufacturing process, a final step is to heat the module at 100°C for a period of time specific to each manufacturer. This time is generally longer than 1 h. The cross-linking reaction required for the adhesive layer could be made to occur during this thermal process. The adhesive could also contain the coupling agent as a compounding ingredient. Thus, bonding to the aluminum and adhesive cross-linking could be accomplished simultaneously.

The above approach uses dry films and pressure-sensitive adhesives to satisfy the construction elements, but the same could be accomplished with liquid casting systems. These could be deposited, for example, by curtain coating, as part of an in-line total manufacturing operation. Initially, acrylic and EVA chemistries will be explored for pressure-sensitive adhesives, and urethane chemistries will be emphasized for the liquid systems.

For a substrate design, construction elements are viewed as being a transparent top cover plastic film, with an adhesive lower layer for bonding to ITO, or other electrically conductive transparent material. There is a current awareness that thin-film modules using a-Si apparently suffer a reduction in power output, which on speculation may be related in part to exposure to light. If true, it can be conjectured that UV light up to 360 nm may be involved, since these wavelengths can cause photodegradation of polysilanes. Thus, if it is ever found that UV affects a-Si, then the outer cover plastic film would have to be UV-screened, up to the limit of the offending wavelengths.

If UV-screening is not needed for a-Si protection, the most viable top cover candidate is Teflon FEP-C (Du Pont), in combination with a virtually weatherable acrylic adhesive. One of the key material challenges appears related to bonding the adhesive to ITO, or its equivalent.

From EVA weather stabilizer studies, the experimental aging of advanced EVA formulations with low-molecular-weight and high-molecular-weight hindered amine light stabilizers (HALS) is beginning to indicate that long-term EVA stabilization is better served with low-molecular-weight HALS. This family of compounds provides protection against UV-photooxidation. It is speculated that the low-molecular-weight HALS has greater mobility within the bulk EVA, and is thus able to diffuse more readily to EVA sites undergoing UV-photooxidation. The high-molecular-weight HALS, however, would diffuse more slowly, if at all, and this may limit its capability to respond to localized sites of EVA photooxidation. An initial reason for investigating high-molecular-weight HALS was to guard against the potential for physical loss by migration or evaporation, a concern with low-molecular-weight compounds. The current experimental trends suggest that an optimum molecular weight may be needed to maintain sufficient diffusion for protection, while minimizing the potential for diffusion-related physical losses.

In any event, the current commercial choices are Tinuvin-770 (a low-molecular-weight HALS), and Cyasorb UV-3346 (a high-molecular-weight HALS). The trend currently favors Tinuvin-770. There clearly is a need to develop an intermediate-molecular-weight HALS.

Aging of fully compounded and weather-stabilized EVA strongly suggests that this material may not need the additional protection of a UV-screening top cover film. The need for a UV-screening film was conceptualized early in

AREA REPORTS

the FSA program, but experimental evidence is suggesting otherwise. If true, this would permit the use of Teflon FEP-C as an outer cover film. This non-UV-screening film is known to be a naturally weatherable material.

The aging of test specimens of Teflon FEP-C over A-9918 EVA on the outdoor heating racks, and in the RS/4 UV acceleration chambers, was initiated this year. At this writing, the samples have been aged more than 4000 h, with no problems. This encouraging testing will continue as long as possible.

Addressing the problem of flammability, Springborn developed a curable and processable, 18-mil-thick, non-flammable, EVA lamination film to be used in replacement of the conventionally clear EVA film which is positioned behind the solar cells. Preliminary module testing at UL indicated no positive improvements, as well as no negatives. It is necessary to conduct more testing and to modify PV module designs to more efficiently utilize the features of this new material. Interestingly, this new material is promising as a nonflammable gasket material for PV modules, but this application has not yet been tested.

This new material has a very high oxygen rating value of nearly 48%. This is the percentage of oxygen required in an atmosphere in order for this material to just sustain a flame. The material cannot be ignited, even in a direct flame, in a normal atmosphere of 20% oxygen.

6. Reliability Prediction and Management

One of the activities under this task was the development of software for the prediction of power loss resulting from open circuits in an array field of a-Si modules. Debugging of the software was suspended at that point to attend to more pressing matters.

The major activity for this reporting period was the preparation and initiation of combined environmental tests in a Bemco oven containing a controlled temperature and humidity environment and an UV lamp. The initial phase consisted of the design and fabrication of test fixtures and measurement apparatuses in support of the environmental testing. The most notable of these is a fixture for obtaining a-Si-cell I-V curves in the JPL large-area pulsed solar simulator (LAPSS).

The Bemco oven is an air-interchange, heat-and-refrigeration unit with a temperature range of -40 to 175°C and varying humidity (10 to 100%). The oven has a 2000 W medium-pressure-mercury UV lamp capable of putting out one to two suns of UV radiation at a distance of 40 cm from the lamp.

Much of the activity in the early stages of the test was concerned with the shakedown of the system and the solution of a number of attendant problems occurring in the system. The UV-lamp cooling system was converted to all stainless steel as a result of deposits on the glass cooling jacket surrounding the lamp. Another problem, involving the oven microprocessor/controller, resulted in erratic control of the oven parameters after a power outage and subsequent reprogramming of the controller. After consultation with the manufacturer, modifications were made that resolved the problems.

AREA REPORTS

The following types of samples are being tested in the oven: 1.9 x 10.2 cm strips of module encapsulant and cover materials, 10.2 x 10.2 cm laminated Tedlar-EVA-glass coupons, 10.2 x 10.2 cm a-Si submodules (some with a Tedlar front cover), and other assorted samples.

Measurements of the UV radiation have been made using a photocell radiometer and chemical actinometers. The use of radiometers will be expanded over the initial limited use when the entire Bemco system is mated to a computer allowing frequent precise measurements to be made. The use of actinometers is being phased out. Spectral-radiometric measurements will be made with a monochromator.

Several sample physical parameters were measured during the first three months of testing, about 8 weeks of actual oven-running time. One of these, sample weight loss, is a measure of the loss of additives, absorbers, and screening agents. Losses of up to 1.35% were measured for the samples exposed in the Bemco. The combination of weight loss measurements and transmission measurements in the UV range (the latter is discussed below) imply the loss of UV screening agents. Several Tedlar samples were exposed in a dry oven (no UV) and a vacuum oven (no UV) for 500 h. The weight loss of the samples in the dry oven was approximately equal to the weight loss of similar samples in the Bemco oven for the same period of time, while the weight loss of the samples in the vacuum oven was greater. This implies that the mechanism for loss of the screening agents is related more to the thermal environment than to the UV radiation.

The sample transmission measurements at 400 nm showed gains from a few percent to 15%, with a loss in transmission becoming apparent at higher wavelengths. The change in transmission seems to have stabilized. The interpretation of these results is that the sample exposure time was long enough to result in loss of the UV screening agents, but not long enough to result in the loss in transmission that is expected to occur with time at 400 nm.

The "push test" developed at JPL, using a steel-ball push device, was used to test several laminated-Tedlar-front-cover samples. The device is used to depress the Tedlar through the application of a force through the steel-ball-tip (1/16 in. diameter). When this test was applied to the modules with a Tedlar front cover that had shown severe cracking when exposed at the Southwest Residential Experiment Station, the Tedlar cracked and revealed its embrittlement. When the test was performed on samples removed from the oven (7 weeks of exposure) no cracking developed and the materials appeared to retain their ductility. The cumulative exposure time in the oven by the end of the reporting period was not long enough to cause the deterioration noted in the field.

The I-V curves of the cells in a Chronar a-Si submodule were measured after 3 weeks of exposure. Two cells showed an increase in max-power. The rest showed a loss, with the average of all losses being 11%. The cells in an ARCO a-Si submodule were measured after 8 weeks of exposure and showed an average max-power loss of 19%.

AREA REPORTS

7. Module Failure Analysis

Failure analysis continued on four ARCO Solar Genesis modules. Each of the modules had a severely warped frame that was displaced from its original position about the edges of the module. The two cells on each module with a border on the module edge were found to have a large fraction of their surface areas shadowed by the distorted frame. The frames were removed, and the modules were reflashed at the LAPSS. Power on two of the modules was completely recovered, while power on the other two modules was only partially recovered, with about 10% power loss remaining.

A Hughes Aircraft Corp. PV module (S/N KPOH 06) was received on July 2 with a reported 47% power loss after 37 thermal cycles. It was found that only six of the 12 cell strings contributed to module power. This module consists of four Chronar amorphous submodules which are arranged in parallel. The reported 49% power loss, found by shadowing tests, was caused by the failure of six of the 12 strings to contribute any power. Further testing showed that the strings were intermittent, with any given string sometimes contributing power and sometimes not, even though the module had not been stressed thermally or mechanically at any time. It is found, however, that two of the strings consistently failed to contribute any power. Interior examination showed an open-circuit condition between the negative terminal column tie copper strip and the cell adjacent to it, for each of the two failed strings. For some strings, I_{sc} was found to decrease with increasing temperature, indicating an increasing series resistance as the temperature is increased. All evidence leads to the conclusion that the solder joints are defective that join the column tie copper strips to the adjacent cells.

Two submodules (KAOH-3 and KAOH-5) from Chronar were received at the failure analysis lab on August 8 with a reported open-circuit condition after environmental test (HF-10) at JPL. The module consists of 84 cells: 28 cells in series and three cells in parallel. Close examination by the curve-tracer indicates that more than one cell of each string was completely open. The locations of the reported open-circuit conditions have been determined. For each module, electrical continuity was observed between the column tie copper strips and adjacent cells. The sources of the open circuits were found to be across the cell interconnect regions within the thin-film layer. KAOH-3 was examined in detail, and it was found that nearly all cells examined exhibited highly resistive ohmic behavior (usually megohm range) across the transparent conductive oxide (TCO) scribe line. Energy-dispersive spectroscopy (EDS) of the inside surface of the two samples of the back side layer of paint showed an elemental distribution matching that of the complementary thin-film layer. To obtain the observed elemental distribution, the adhesion of the back side of the thin-film layer and the paint must have been strong enough to produce an uneven, yet clear fracture of the thin-film layer upon delamination or tangential strain of the paint.

Integrity of the cell string continuity was examined on one of the Chronar modules that has no back cover. Shunt resistance of the individual cells was compared with the pinhole density of the individual cells. Preliminary results indicate that the shunt resistance of an individual cell is closely related to the pinhole density.

AREA REPORTS

Close examination of the whisker signal of the solar cell laser scanner (SCLS) on a-Si modules has revealed that the signal is clearly modified, even though the modulation was small when it was processed by electric amplifying circuits. To analyze the whisker signal of the SCLS on an a-Si module, the risetime and decay time of the laser scanner light source measured by a fast risetime photodiode were compared with those of the response time of the a-Si thin-film modules (Sanyo 7703-2). The risetime of both the laser scanner light source and the response time of the a-Si module is 1.0 ms, and the decay time of the thin-film module is 20 times longer than the light source, which is of the same order as the risetime. This may mean that the carrier transit time of the device causes the whisker signal before the initial carriers reach equilibrium with the recombination and/or trap centers of which decay time is longer than the transit time.

Feasibility of on-line computer analysis of the SCLS data and the sun-u-later data was tested by connecting them to the analog-to-digital converter of the DECLAB-23 of the Digital MNC System. The plotting program of the display of the SCLS was found useful.

During this report period, a paper entitled "Effects of Excitation Intensity on the Photocurrent Image of Thin-Film Silicon Solar Modules," by Q. Kim, A. Shumka, and J. Trask, has been accepted to be published in Solar Cells in 1986.

Systems Research

Crystalline-Silicon Module Reliability Task

1. Water-Module Interaction Research

It is recognized that water, besides accelerating corrosion reactions within PV modules, catalyzes a host of other degradative phenomena such as delaminations, reduction of mechanical strength, enhancement of electrical breakdown probability, etc. The purpose of this research is to understand these interactions and to develop means to deal with them.

A fundamental study in this area is the measurement of water sorption by PV encapsulants. Sorption data are obtained using a Cahn Balance mounted above an environmental chamber within which the encapsulant specimen, suspended from one arm of the balance, is exposed to a controlled T/RH environment.

To address the question of how exposure to UV affects encapsulant sorption properties, Chronar-supplied substrate films mounted on Pyrex glass slides have been weighed. The sorption isotherms of some of these pristine samples will be determined with the Cahn Balance. The remaining samples have been mounted in the Bemco chamber for exposure at 85°C/10% RH to 1 UV sun. After a suitable period, the sorption isotherms of these UV-exposed samples will be obtained and the effect of photothermal exposure on EVA sorption characteristics determined.

Liquid water also contributes to module degradation. To ascertain the effects of the transition from a cool night to a warm day (dew formation), a specially prepared PVB sample was mounted to a heat exchanger that allowed sample heating and cooling independently of the controlled Bemco chamber

AREA REPORTS

ambient conditions. The sample was exposed to simulated day-night cycles so as to induce the formation of dew during the "night." With the onset of "day," large current transients were observed (specifically, for the surface current) that decayed to steady values as the "day" progressed. These large current spikes were not evident when there was no dew.

A hermetically sealed module should respond only to thermal, not humidity, changes in the environment. To test this supposition, a PVB sample was conditioned for 24 h in a vacuum at 40°C, then sealed and exposed to various humidity levels at both 40 and 85°C. Bulk and surface currents were observed to remain relatively steady. Leakage current response obeyed the usual Arrhenius temperature law.

Mini-modules mounted at the JPL outdoor test stand were observed to exhibit large current spikes during the transition from dewy dawn to warmer morning. Leakage current response of SVI samples, discussed above, and XTEST samples (encapsulated cell-frame module-like test coupons originally used to determine module electrochemical corrosion mechanisms and rates) were characterized in controlled steady laboratory environments. It was then decided to mount these samples in an outdoor environment and so characterize their response in a transient environment.

An ongoing analytical study of the experimental data parallels the experimental effort. Mathematical models of module behavior are continually being formulated and modified in accordance with the measurement data. In turn, the analysis provides direction for future experimentation.

2. Photothermal Stability Research

A model of autocatalytic photooxidation has been proposed. Photooxidation initially takes place at a slow rate while generating degraded products. These products will, in turn, catalyze further photooxidation reactions resulting in a drastic increase in the rate of subsequent degradation.

EVA samples have been aged at 120 and 135°C with varying UV intensities. Optical transmission changes were analyzed. The rate of loss of transmission which can be correlated to the formation of photooxidation products was monitored. These rates can be compared with those obtained during the initial stage of aging to validate the autocatalytic photooxidation model.

A program to study the failure of Tedlar/EVA/stainless steel modules was initiated. Cracking, observed outdoors in real time conditions, was simulated in accelerated testing. An experimental technique was developed to quantitatively assess the extent of degradation. Photothermal aging was carried out of freestanding Tedlar films at 6 suns, 85°C for up to 23 days. Stress-strain measurement of these samples showed no significant change in mechanical properties. This is in contrast to module testing results in which Tedlar film in a Tedlar/EVA encapsulated module showed signs of embrittlement after 21 days of photothermal aging at six suns and 85°C. Potential synergistic effects of Tedlar and EVA are being investigated.

AREA REPORTS

A report has been published by E. Cuddihy, entitled The Aging Correlation (RH + t): Relative Humidity (%) + Temperature (°C), JPL Publication 86-7, 5101-283, DOE/JPL-1012-121, dated January 15, 1986. This report discusses an aging correlation between corrosion lifetime and relative humidity RH (%) and temperature t (°C) in relation to activities supported by the FSA Project to better understand the fundamental mechanisms of degradation and aging.

University of Toronto researchers are continuing their work on computer modeling of photooxidation of polymers. They have modified their previously developed computer program for the simulation of the photooxidation and photostabilization of hydrocarbons to ANSI standard FORTRAN and a new interactive version has been developed. They also have included in the night-day cycles of their file-oriented simulation program the possibility of varying temperature during such cycles. This modification has greatly increased the accuracy in predicting what the actual time to failure (time required to break 5% of C-H bonds) in polyethylene and EVA.

3. Reliability-Durability of Bonding Materials

A comprehensive effort on chemical bonding has been completed with issuance of JPL Publication 866, 5101-284, DOE/JPL-1012-120, Chemical Bonding Technology: Direct Investigation of Interfacial Bonds, by J.L. Koenig, et al., dated January 1986.

Dr. Plueddemann of Dow Corning had previously developed a successful primer for bonding EVA to glass that carries the Springborn designation A-11861. This primer, based on organosilane chemistry, has achieved enormous industrial acceptance. Experimental testing has found that this primer acts to significantly reduce the quantities of water absorbed at the interface between glass and EVA, an important factor related to limiting module leakage current. Dr. Plueddemann therefore continues the development of experimental organosilane coupling agents that are even more highly hydrophobic, with the intent to further reduce the quantities of interfacially absorbed water. In turn, this would lead to improved resistance to electrical-leakage currents.

An experimental prototype of a more hydrophobic coupling agent (primer) has been completed at Dow Corning, and the designation of this experimental primer is X1-6121. Sample quantities have been sent to JPL and Springborn. JPL will measure leakage current, whereas Springborn will prepare test specimens of glass beads dispersed in EVA, with and without the new Dow Corning primer X1-6121. When prepared, the equilibrium absorbed water contents will be measured and compared with samples using the standard 11861 EVA/glass primer. This test is to determine if the new primer indeed acts to further reduce the absorption of interfacial water by PV modules.

The finding that organosilane coupling agents act to reduce interfacial water has significance for corrosion protection. Metallic corrosion usually requires the presence of liquid water, as one necessary requirement. The adhesion studies with primed EVA/glass specimens clearly demonstrated that organosilane coupling agents are enormously effective in reducing the accumulation of interfacial water. This suggests that organosilanes chemically reacted onto metallic surfaces may function as anti-corrosion agents, through the action of reducing or excluding liquid water at the

AREA REPORTS

metallic surface. Dr. J. Boerio, University of Cincinnati, is carrying out the studies to determine if organosilane coupling agents can function as anti-corrosion agents for the aluminum metallization employed on crystalline-silicon solar cells.

Dr. Boerio has experimentally been able to chemically monitor the interface between EVA and an aluminized back surface of solar cells. The successful technique is based on reflectance IR spectroscopy. In initial experiments, Boerio has successfully monitored aluminum corrosion when using unprimed samples of EVA on the solar cell back surface. Next, the aluminized back surface of the same commercial solar cell was primed with A-11861 primer, followed by overcoating with a laminated and cured layer of EVA. This work is in progress, but initial results show that no corrosion has formed after 1 week of immersion in boiling water. The aging is continuing, but already the evidence is accumulating that a self-priming EVA with A-11861 coupling agent accomplishes both structural bonding to glass, and also corrosion protection for the solar cell's aluminized back surface. There is great industrial interest in a self-priming EVA for these two functions.

4. Reliability-Durability of Electrical Insulation

A theory, developed at JPL, suggests that the fundamentally correct definition of the intrinsic dielectric strength property of electrical insulation material has been identified. This new theory has been published as a project report by E. Cuddihy, A Concept for the Intrinsic Dielectric Strength of Electrical Insulation Materials, JPL Publication 85-20, 5105-252, DOE/JPL-1012-105, dated April 15, 1985. It also has been submitted for formal publication in the Journal, IEEE Transactions on Electrical Insulation.

Based on these theories, an experimental capability to measure the intrinsic DC dielectric strength property has been established at Springborn Laboratories, and can now be monitored as a function of aging. For this purpose, the DC dielectric strength of A-9918 EVA is being monitored as a function of aging on the outdoor photothermal aging racks (OPTAR), which are being operated at 70, 90, and 105°C. The EVA is also being aged in UV-accelerated RS/4 chambers at 50°C and at 85°C. There are two RS/4 chambers being operated at 50°C, one with and one without a periodic water spray cycle. These are referred to as RS/4-dry and RS/4-wet. The unit operating at 85°C is dry. DC dielectric strength values have been measured at 2000 and 4000 h of aging in the RS/4 chambers, and at 2000 h on the outdoor racks. These data are summarized in Table 1.

The trend indicates a reduction in the DC dielectric strength with dry aging in the RS/4 chambers, and also outdoors on the heating racks. Wet RS/4 aging at 50°C, however, results in an increase in the DC dielectric strength. The speculation is that aging causes an increase in ionic species in the EVA which could reduce the DC dielectric strength, whereas the water spray cycle results in extraction of these ionic species. Thus, the DC dielectric strength increases for wet aging while it decreases for dry aging, or under conditions where ionic extraction does not occur. These aging experiments are continuing.

JPL has developed specialized test equipment that permits the direct, non-destructive, in situ measurement of selected electrical properties of

AREA REPORTS

Table 1. DC Dielectric Strength, Volts/mil

Sample	Aging Time, Hours		
	0	2000	4000
RS/4-Dry, 50°C	3500	3060	3240
RS/4-Dry, 85°C	3500	2100	1980
RS/4-Wet, 50°C	3500	3830	4120
OPTAR 70°C	3500	2850	--
OPTAR 90°C	3500	3140	--
OPTAR 105°C	3500	*	--
*Sample untestable.			

materials undergoing accelerated aging in environmental aging chambers. These measurements can be made on scheduled intervals without the need to remove the aging samples from the chambers. This equipment will enable automatic in situ measurement of partial discharge, the pulse height analysis measurements of specimens undergoing temperature/humidity exposure, and electrochemical leakage current. JPL also operates a Biddle high-voltage tester to measure the voltage breakdown characteristics of control and aged test specimens. This latter test is destructive in nature.

In preparation for electrical aging experiments at JPL, Chronar supplied six self-adhesive films which have been applied to aluminum substrate plates. Four samples each, of these polymer films, were prepared at JPL. One of the four samples of each type was used as a control, to first measure its set of non-destructive electrical properties, followed by the destructive measurement of its voltage breakdown level. Two of the remaining three samples of each type were placed in the environmental aging chamber in which a constant temperature/humidity/UV environment is being maintained. The remaining sample is being exposed outdoors at the JPL test facility.

Non-destructive measurements of corona inception voltage and pulse height analysis have been made on Chronar self-adhesive films mounted on aluminum substrates. This set of measurements were made after approximately 500 h of exposure to 1 UV sun and a chamber environment of 85°C/5% RH. Comparisons will be made with the original measurements on the control samples, and aging will be continued. These data will ultimately be analyzed to ascertain the effects of aging on parameters that assess propensity for an insulation to break down electrically. Similar data on the samples exposed to an outdoor environment at the JPL test stand will be obtained at the end of summer.

AREA REPORTS

5. Module Flammability Research

The research effort to develop the technology base required to construct fire-ratable PV modules using hydrocarbon encapsulants has resulted in the identification of several high-temperature, back-surface candidate materials capable of raising the fire resistance of modules to Class A and Class B levels.

During this reporting period, another series of Class A burning-brand tests was completed in October 1985. The focus of this test series was to evaluate several edge-seal systems and perform array-level flammability tests. The results indicated that very few edge-seal systems were able to pass the test with a Class A burning brand placed over the module's aluminum frame. In most of these cases, success was attributed to edge materials that were not consumed by the intense heat. Post-test analyses indicated that failure was caused by one of two mechanisms: complete loss of the edge material, or loss of edge-material structural properties because of heat. Both of these failures, resulting in loosening and separation of the back-surface material and glass from the aluminum channel, eventually led to flame penetration at or near the aluminum channel.

Array-level tests were conducted using two modules mounted above a UL standard Class A burning-brand-test deck to simulate a typical roof section. Although test results varied, the key factor was maintaining module back-surface integrity, at least to the extent that the roofing felt was not ignited. In these cases, the amount of damage to the roofing felt was minimal. The installation of fire-rated shingles, shakes, or rolled roofing (which for these tests was not used) would provide an additional margin of safety. Thus, special high-temperature edge-seal systems may only be necessary for integral-mount applications.

Dielectric and voltage breakdown tests were performed to understand why modules using HITCO 7628 have not been able to pass the JPL Block V high-pot test. Test results on both Solarex Corp. and ARCO Solar, Inc. modules indicated that the HITCO material may have a low dielectric withstand capability relative to other materials, such as Tedlar. Tests on samples of the HITCO 7628 material not integrated into a module verify results obtained at the module level. Leakage current in excess of 50 μ A occurs through the material below the minimum acceptance 1500 V level.

Samples of the HITCO 7628 material (coated on two sides) were bound to Kapton and to a TPX methylpentene polymer. Results of dielectric and voltage breakdown testing at the material level indicate that using either of these materials with the high-temperature, HITCO material is sufficient to provide voltage withstand in excess of JPL Block V requirements. At present, samples of Kapton and TPX methylpentene polymer, laminated to HITCO 7628, have been subjected to a chamber environment of 85C for 7 days and 85C/85% RH for 45 days. Inspection after the 52-day period of the Kapton samples showed no visible signs of delamination, while the TPX samples showed a slight curling. The samples were returned to the chamber and will be subjected to further high-pot testing in June.

AREA REPORTS

6. Crystalline-Silicon Module Development

The long sought goal of demonstrating 15% PV module efficiency has been realized. On the JPL High-Efficiency Module Contract with Spire Corp., Spire has delivered a module that JPL measurements show to have 15.2% efficiency at standard conditions [100 mW per sq cm irradiance, ASTM 892-82 (global) irradiance spectrum and 25°C cell temperature]. Encapsulated cell efficiency is 16.9%.

The module power output is 75.2 W. Dimensions are 91.2 x 54.2 cm and the packing factor is 0.901. The module contains 84 cells, each 53.0 sq cm in area. The cells are manufactured from float-zone-grown silicon ingot. Spire has produced similar cells manufactured from Cz-grown silicon ingot, indicating that the 15% goal is achievable with the more readily available Cz material.

The practicality of repeatable production of high-efficiency module cells was demonstrated during the manufacture of cells for the above module. For one batch of 25 cells, the yield was 100% and the average cell efficiency was 18.1%.

The cell design for the high-efficiency module was selected after a variety of designs had been manufactured and incorporated into mini-modules to measure module efficiency and normal operating cell temperature (NOCT). One type of cell, incorporating a BSR and a polished front surface, was shown to result in a module NOCT 4°C less (46°C) than was the case for cells without the BSR and with texture etched front surfaces. It had been hoped that the BSR approach would provide the higher efficiency (of the two approaches) at NOCT. Experiments indicated, however, that the efficiency of the latter cells could be made higher enough at any given temperature as to surpass the performance of the BSR cells at NOCT. The texture etched cells, therefore, were selected as the preferred design.

An advantage of the BSR approach is the expected longer life of the cells because of lower NOCT. It did not seem useful to investigate the economic trade-off because it was not possible to carry on the effort long enough to optimize both cell designs and obtain a reliable measure of the difference in their efficiencies.

7. Module Environmental Testing

The last program of Block V tests has been completed on commercial crystalline-silicon modules, involving module manufacturers from France, Italy, the United States, West Germany, and Japan. The only other tests performed were on a-Si modules. The results of environmental testing performed during the reporting period are shown in Table 2.

AREA REPORTS

Table 2. Block V Tests of Commercial Crystalline-Silicon Modules

Module Code	Quantity	Test	Results
D4	1	Hot spot	Some discoloration of interconnects and collectors. Two small cell cracks
J1	4	MI-10K	Cell string resistance increased for all modules for up, neutral plane, and downward forces. Unacceptable power loss of -11, -13, -15, and -36%, respectively
	6	Final hi-pot/continuity	Satisfactory
	1	Hot spot	Satisfactory
E2	2	T150	Discoloration of gridlines adjacent to frame
	6	Final hi-pot/continuity	Satisfactory
	1	Hot spot	Blistering of cells, burning of Tedlar
V2	4	T-50	One o.k., three electrical failures at -7, -7, and -23%
	2	HF-10	J-boxes yellowing
	1	T-150	J-box yellowing
	2	MI-10K	Three cracked cells, power satisfactory
	3	Final hi-pot/continuity	One failed hi-pot, continuity satisfactory
	1	Hot spot	Satisfactory
V3	4	T-50	Satisfactory
	3	HF-10	J-boxes yellowing, some cell discoloration
	1	T-150	Satisfactory

AREA REPORTS

Table 2. (Cont'd)

Module Code	Quantity	Test	Results
V4	3	MI-10K	Satisfactory
	4	Final hi-pot/ continuity	Satisfactory
	1	Hot spot	Satisfactory
	4	T-50	Satisfactory
	3	HF-10	J-boxes yellowing
	1	T-150	J-box yellowing
V5	3	MI-10K	Satisfactory
	4	Final hi-pot/ continuity	Satisfactory
	4	T-50	Satisfactory
	3	HF-10	J-boxes yellowing
	1	T-150	J-box yellowing
	3	MI-10K	Satisfactory
01	4	Final hi-pot/ continuity	Satisfactory
	4	HF-10	Minor warping of J-boxes
	4	MI-10K	Satisfactory
	2	T-150	Satisfactory
	4	MI-10K	Satisfactory
	7	Final hi-pot/ continuity	Satisfactory
	1	HS-100	Two of the tested cells have one blister each, burned encapsulant surrounding one interconnect

AREA REPORTS

Table 2. (Cont'd)

Module Code	Quantity	Test	Results
KA a-Si	2	HF-10	Electrical failures, major delamination back surface, one module
KP a-Si	2	HF-10	Electrical failures, increased delamination of cover glass and encapsulant
	1	T-150	Electrical failure, additional delamination of module glass and cover glass, tearing of Tedlar around J-box
	2	HF-10	Electrical failures, additional delamination of module glass and cover glass
OH	10	Hi-pot continuity	Six modules failed initial continuity test, in some cases at very high resistance
	6	T-50	Some cover glass delamination, Tedlar delaminating adjacent to frame edge
	2	T-150	One cracked cell, additional delamination of cover glass and Tedlar
	4	HF-10	Satisfactory
	4	MI-10K	Satisfactory
	6	Final hi-pot/ continuity	Satisfactory
	1	Hot spot	Satisfactory
UF	6	Hi-pot	Failed
	6	continuity	Satisfactory
UM	4	Hi-pot/ continuity	Satisfactory
W2	1	Hot spot	Satisfactory

AREA REPORTS

Table 2. (Cont'd)

Module Code	Quantity	Test	Results
R3	1	Hot spot	Satisfactory
S0 a-Si	1	Hail	Power satisfactory, module surface dimpled
Y a-Si	2	Hail	Power satisfactory, glass cracked in one module, probably because of a distorted frame

T-50	= 50 thermal cycles, -40 to +90°C.		
T-150	= 200 thermal cycles (150 plus original 50).		
HF-10	= 10 humidity/freeze cycles. 85°C/85% RH, then -40°C, 10 cycles (days).		
MI-10K	= Mechanical cycling, 50 lb/ft squared (2400 Pa) alternating, 10,000 cycles.		

Continuity = Electric current at twice the I_{sc} across joints in the metal frame for 2 min. Allowable voltage drop, 1 V.

8. Electrical Measurements Technology Development

Following the calibration of 18 reference cells at JPL and SERI as part of the Commission of European Communities (CEC) Round-Robin of measurements on reference cells, the data were sent to the CEC Joint Research Center (JRC), Ispra, Italy, on August 5, 1985. During September 9-11, 1985, M. Smokler and R. Mueller attended the Second Expert Meeting on the Collaborative Project on Solar Energy in Ispra, Italy, as the U.S. participants. This project is directed by the Summit Working Group on Technology, Growth, and Employment, and the operating agent is the CEC JRC in Ispra.

The meeting was held to discuss the results and methods of the participants in the CEC Round-Robin of measurements on reference cells. The other participating countries were the United Kingdom, France, Italy, West Germany, and Japan. Considerable interest was expressed in the JPL results obtained with the filtered LAPSS (a JPL development). The characteristics of this device were incorporated into the recommendations made by the meeting participants. The filtered LAPSS provided accurate measurements using a relatively

AREA REPORTS

unsophisticated method. The Round-Robin was considered to be successful in achieving its objectives. In spite of the wide variety of methods and equipment used by the participants, a first comparison of the results showed agreement to within $\pm 2\%$ for crystalline-silicon cells and $\pm 2.5\%$ for a-Si cells among the majority of the participants (JPL and SERI included).

R. Mueller attended two regular and two interim meetings of the ASTM E44.09 subcommittee on Photovoltaic Electric Power Systems and authored the subcommittee draft Document 130, "Standard Method for the Calibration of Non-concentrator Terrestrial Photovoltaic Primary Reference Cells Under Direct Irradiance." This document has been approved by subcommittee ballot and will soon be presented for a full E44 committee ballot. He also has been shepherding a proposed draft on a Standard Method for Measuring the NOCT of a PV Module. It has been well received, but it has been decided that the method must first be tried and proven at two or three more laboratories other than JPL before it could be accepted as a proposed ASTM draft document.

The British Petroleum (BP) Round-Robin of measurements on modules was completed in Europe during late 1985. The results were made available to JPL and there was concern about the JPL measurements apparently being too low. It was learned that JPL and the Europeans (BP and Ispra) were not using the same Reference Spectral Irradiance Distributions (RSID) when correcting the solar simulator measurements. When the module and reference cell measurements taken at JPL were corrected to the same RSIDs as were those taken by Ispra, the average difference is less than 1% for the reference cell calibrations and $\pm 2\%$ for the module power measurements. The comparison between JPL and BP reference cell calibrations remains not very good. The average difference remains at 2% with a high standard deviation of nearly 4%. These results were submitted to BP.

A paper, titled Air Mass 1.5 Global and Direct Solar Simulation and Secondary Reference Cell Calibration Using a Filtered Large Area Pulsed Solar Simulator, was presented at the 18th IEEE Photovoltaics Specialists Conference in Las Vegas, Nevada, on October 25, 1985.

Many measurements were made using the JPL filtered LAPSS to assist numerous vendors with the accuracy of their measurements. During this reporting period, the most significant support was that of performing electrical measurements on the Spire high-efficiency cells, mini-modules, and modules as they made improvements and finally achieved a module efficiency of over 15% when measured using the JPL global filtered LAPSS. Temperature coefficient measurements were also made on several types of a-Si modules. Testing the a-Si modules led to the discovery that it was necessary to make changes in the LAPSS program software to accommodate these devices. The testing procedure had to be changed, including eventual hardware modifications, to avoid stressing or damaging these devices because of voltages presented by the LAPSS data acquisition system during testing. It also was determined through computer analysis of the LAPSS global spectral irradiance distribution that it is a close match to the Air Mass Zero spectral irradiance distribution.

AREA REPORTS

9. Module Failure Analysis

A Solar Power Corp. module (Model G12-361CT, S/N 13197) reported intermittent loss in V_{OC} . This module consists of 36 crystalline cells in series. This intermittent failure was not verified. Metallic contamination and dendrite growth, however, was found on the insulating material between the contact pads on the terminal printed circuit (PC) board. This contamination is suggested as the cause for the reported failure.

A polysilicon module, VB2H-3013 (from Photowatt), was received at the failure analysis (FA) lab on August 27 with a reported 23% power loss after a T-50 test. The reported 23% power loss was found to be caused by four cracked cells. This is one of the four modules encapsulated with PVB/Tedlar system. No other encapsulant systems such as EVA/Tedlar, EVA/glass, or PVB/glass have failed in T-50. This failed module consists of 36 cells in series, with two shunt diodes for each 18-cell string. Laser scanning by the 5145Å Argon laser showed one broken cell, and laser scanning by the 6328Å He-Ne laser showed four broken cells at the first scan, indicating the current limited by the broken cell.

The second scan with the same He-Ne laser, however, showed two broken cells, indicating an intermittent problem of the two cells. The cracks on these cells intermittently isolated portions of the cell topside from the remainder of the cell string. When three of these cells were shorted across, module power increased to just 10% below the power of the module when it was received. The mechanism responsible for cracking the cells is not well understood. Three more PVB/Tedlar modules have been received at the Failure Analysis Lab. (S/N VB2H-3014 and S/N VB2H-3015 both underwent T-50, HF-10, and M/I testing and showed power losses of 7.0 and 1.6%, respectively. S/N VB2H-2955 underwent T-200 and showed a power loss of 10.4%).

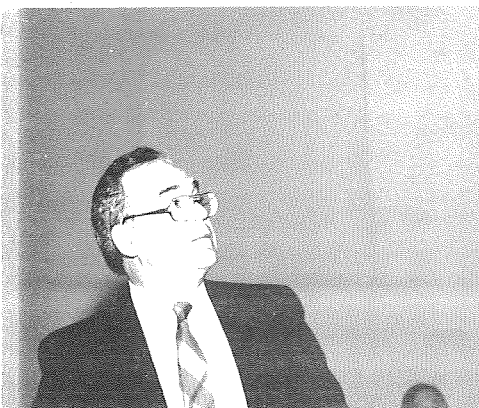
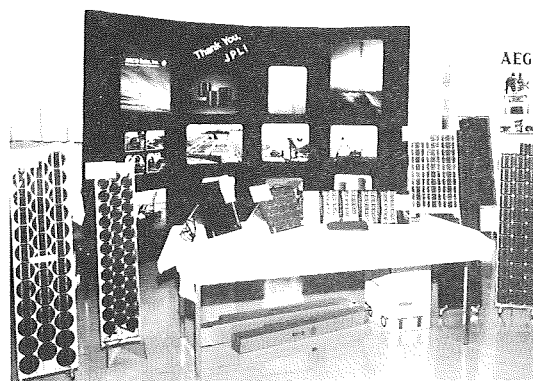
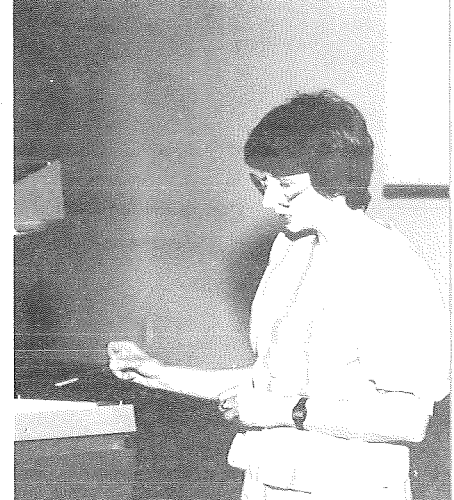
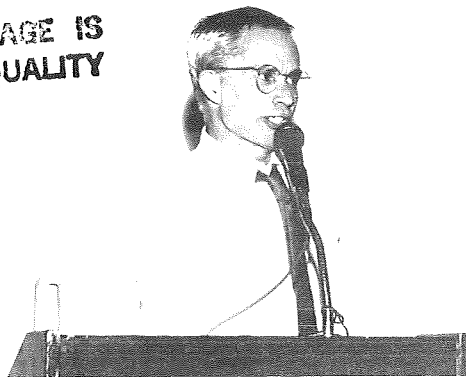
The laser scanner showed some cell cracking in all of these modules. Additional Photowatt modules that incorporate encapsulation systems other than PVB/Tedlar have been received at the FA lab. These include two modules each of PVB/glass, EVA/Tedlar, and EVA/glass. All of the modules have a test history similar to that for the PVB/Tedlar modules, but show very little degradation (<2.4%) in their electrical power. No cracking was observed when the PVB/glass, EVA/Tedlar, and EVA/glass modules were examined visually. Laser scanning of the modules did not show any cell cracking. The top side cover glass of the PVB/Tedlar and EVA/Tedlar modules was found to have a rough texture, whereas the top side cover glasses of the PVB/glass and EVA/glass modules were found to be smooth. The Tedlar back side of the PVB/Tedlar modules were found to wrinkle after environmental testing, but the Tedlar back side of the EVA/Tedlar modules was found to remain smooth after environmental testing. This suggests that the cause for cell cracking in the PVB/Tedlar module is related to thermal expansion of the PVB encapsulant.

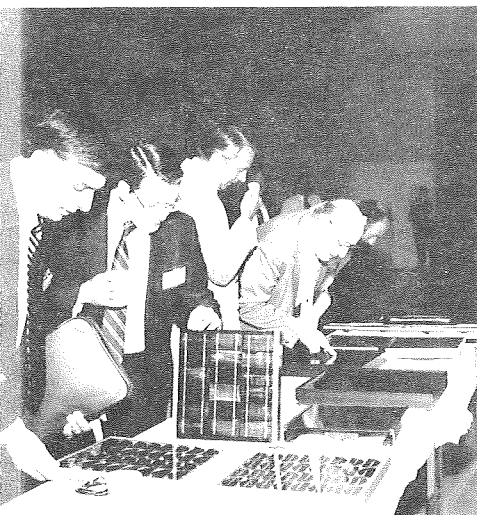
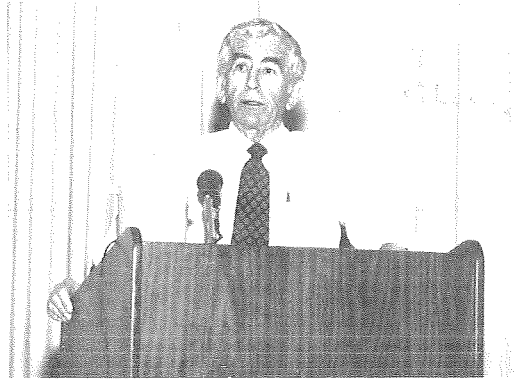
Analysis of the polycrystalline silicon module from Siemens (BJOH-2558) has been completed. A 34% power loss after 10 K cycles mechanical integrity test was reported. This module consists of 144 4-in. diameter circular cells: four in parallel, and 36 in series. Four shunt diodes were externally installed, each in parallel with four 9-cell strings. The solar cell laser

AREA REPORTS

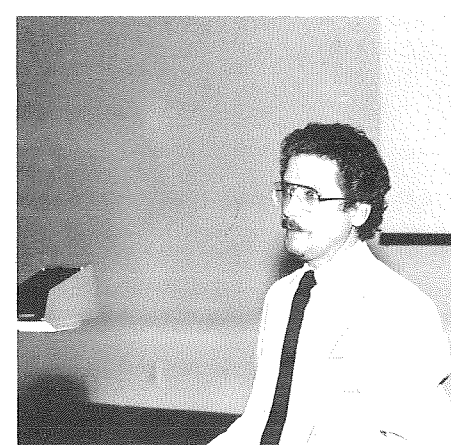
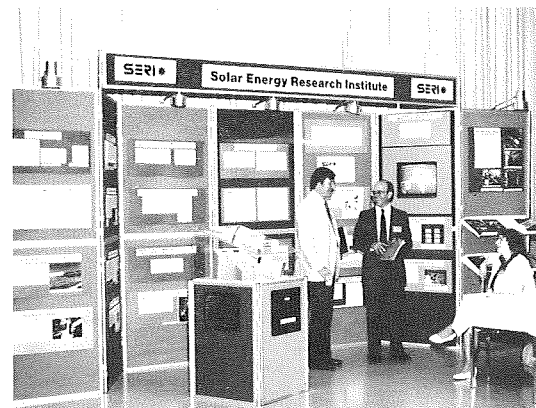
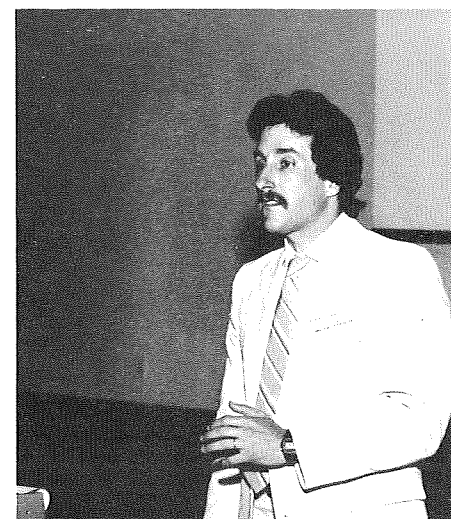
scanner indicates that one of the four 9-cell strings does not contribute any power to the output. Close examination of the I-V characteristics of the individual strings indicates that most of the output power of half of the module is generated by three strings out of eight. Dark I-V characteristics of the two submodules, each consisting of four parallel strings, did not show any clear differences between strings. Photocurrent images of the module were reexamined by a solar-cell laser scanner, using an argon laser with and without the shunt diodes. No clear differences between strings were observed for the images even at the highest laser-power level of the equipment. Intermittent characteristics of the module in the SCLS and light I-V curves were verified as being caused by a stress-sensitive discontinuity of the cell interconnects.

ORIGINAL PAGE IS
OF POOR QUALITY





ORIGINAL PAGE IS
OF POOR QUALITY



**PROCEEDINGS OF
THE 26th PROJECT
INTEGRATION
MEETING**

PROCEEDINGS

INTRODUCTION

The 26th and final Project Integration Meeting (PIM) of the Flat-Plate Solar Array (FSA) Project of the Jet Propulsion Laboratory was held at the Pasadena Center, Pasadena, California, on April 29 and 30, and May 1, 1986.

The thrust of this meeting was to summarize the Project's non-concentrating, crystalline-silicon, solar-cell research and development (R&D) activities of the past 11 years. This R&D has provided the majority of the technology base for today's crystalline-silicon, terrestrial photovoltaic module production, and has established a foundation of technology for tomorrow's higher-efficiency, lower-cost, and more reliable modules.

The meeting was divided into three specific areas of interest with each day devoted to one of these areas:

Day 1 (April 29) consisted of an overview of the progress and the significance of the results of the 11 years of Project activities, and a discussion of future needs and directions.

Day 2 (April 30) provided detailed technical summaries of the progress of FSA contractors and in-house work since the 25th PIM (June 19-20, 1985).

Day 3 (May 1, morning) provided an opportunity for industry and users to explain their continuing participation in the manufacture and use of crystalline-silicon photovoltaics.

A summary of each of these days is presented later in this document.

A final set of Project documentation is currently being prepared and will be distributed late this year, and will be available through the National Technical Information Service.

As this was the last PIM, and because this will be the final PIM Proceeding and Progress Report, the FSA Project would like to take this opportunity to thank all of the organizations and individuals who have participated in the Project during the last 11 years. It has been your continued dedication and contributions that have made the Project the success that it is. We salute you and wish you continued success in the future.

PRECEDING PAGE BLANK NOT FILMED

26th FLAT-PLATE SOLAR ARRAY (FSA)

PROJECT INTEGRATION MEETING (PIM)

AGENDA

ORIGINAL PAGE IS
OF POOR QUALITYApril 29 (Tuesday)

7:30 a.m. Registration (Lobby)

ONE-DAY OVERVIEW (Room C124)

8:30	Welcome and Announcements	W. Callaghan (JPL)	15 min
	DOE comments	M. Prince (DOE)	15 min
	Historical Overview, Accomplishments, and Value of the FSA Project		60 min
	Government	P. Maycock (PV Energy Systems)	
	Industry	R. Little (Spire Corp.)	
10:00	BREAK AND PARALLEL DOE MEETING		40 min
	A short (25 min) DOE briefing for the press and invitees who have never attended a PIM. DOE will give a brief overview of their National PV Program and introduce the key personnel from DOE, JPL, Sandia, and SERI. A question and answer period will follow.		
10:40	Crystalline-Silicon PV Summaries: Accomplishments, Lessons Learned, Potential and Continuing R&D Needs		
	Silicon Material	J. Lorenz (Consultant)	20 min
	Silicon Sheet	F. Wald (Mobil Solar Energy Corp.)	25 min
	Higher-Efficiency Cell Research	A. Rohatgi (Georgia Tech.)	20 min
	Processing R&D	D. Bickler (JPL)	20 min
12:05	LUNCH		
1:20	Summaries: Continuation		
	Encapsulation	P. Willis (Springborn Labs, Inc.)	20 min
	Module Design and Reliability	R. Ross (JPL)	25 min
	Module Evaluation	C. Gay (ARCO Solar, Inc.)	20 min
	Economic Analyses	H. Macomber (Consultant)	20 min
2:45	BREAK		
3:15	Panel: R. Annan, Chairman (DOE)		2 hours
	Recommendations for Crystalline- Silicon in DOE's 5-Year Photovoltaic Research Plan	J. Day (Strategies Unlimited) G. Smith (Naval Weapons Center) K. Firor (PG&E) G. Ralph (Hughes Aircraft) K. Koliwad (JPL) C. Rose (Westinghouse) E. Daniels (Solarex)	
5:15	Closing Remarks: FSA and DOE		20 min
5:35	Social Hour		

April 30 THREE PARALLEL TECHNICAL SESSIONS (see next page).May 1 INDUSTRY-USERS DAY (morning), agenda to be announced.

PRECEDING PAGE BLANK NOT FILMED

April 30 (Wednesday) (Room C124)

ADVANCED SILICON SHEET

A. Morrison, Chairman

8:00	Fourth Silicon Stress/Strain Workshop	M. Leipold (JPL)	10 min
8:10	Dendritic Web Ribbon	R. Hopkins (Westinghouse Electric Corp.)	35 min
8:45	JPL Web Team	D. Bickler (JPL)	20 min
9:05	Stress and Efficiency Studies in Edge-Defined Film-Fed Growth of Silicon Ribbons	J. Kalejs (Mobil Solar Energy Corp.)	20 min
9:25	Optimization of Silicon Crystals for High-Efficiency Solar Cells	T. Cizek (Solar Energy Research Institute)	20 min
9:45	BREAK		
10:05	Analysis of Stress/Strain Relationships in Sheet	O. Dillon (Univ. of Kentucky)	20 min
10:25	Sheet Stress/Strain Activities at JPL	B. Wada (JPL)	10 min
10:35	High-Temperature Testing of Silicon	T. O'Donnell (JPL)	10 min
10:45	Characterization of Silicon Sheet	S. Hyland (Cornell Univ.)	20 min
11:05	Silicon Sheet Surface Studies	S. Danyluk (Univ. of Illinois at Chicago)	20 min
11:25	Czochralski Crystal Growth Modeling Study	M. Dudukovic (Washington Univ., St. Louis)	20 min
11:45	LUNCH		75 min

HIGH-EFFICIENCY SOLAR CELLS

P. Alexander, Chairman

1:00	Optimization Methods and Solar Cell Numerical Models	S. Jacobsen (Univ. of California, L.A.)	15 min
1:15	Novel Measurement Techniques	M. Wolf (Univ. of Pennsylvania)	10 min
1:25	Measurement of Lifetime and Diffusion Length in Heavily Doped p-Type Silicon	R. Swanson (Stanford Univ.)	20 min
1:45	Surface Passivation (SiN_x)	L. Olsen (Univ. of Washington)	20 min
2:05	High-Efficiency Solar Cells on Web	D. Meier (Westinghouse Electric Corp.)	20 min

PROCESSING

B. Gallagher, Chairman

2:25	Diffusion Barriers	E. Kolawa (California Inst. of Technology)	20 min
2:45	BREAK		
3:05	MOD Film Development	J. Parker (Electrlink)	10 min
3:15	Ink-Jet Printer System	R. Vest (Purdue Univ.)	20 min
3:35	Laser-Assisted Cell Metallization	D. Meier (Westinghouse Electric Corp.)	20 min
3:55	Simultaneous Junction Formation Using Liquid Dopants	R. Campbell (Westinghouse Electric Corp.)	15 min
4:10	Rapid Thermal Processing (RTP) of Ion-Implanted Silicon	G. Rozgonyi (North Carolina State Univ.)	20 min
4:30	Hydrogen Ion Implantation	S. Fonash (Pennsylvania State Univ.)	20 min
4:50	Low-Pressure CVD of Polysilicon	B. Gallagher (JPL)	10 min

MODULE AND RELIABILITY TECHNOLOGY AGENDA

ORIGINAL PAGE IS
OF POOR QUALITYApril 30 (Wednesday) (Room C101-102)MODULE TECHNOLOGY

M. Smokler, Chairman

8:00	Accuracy and Long-Term Stability of Amorphous-Silicon Measurements	R. Mueller (JPL)	20 min
8:20	Long-Term Stability of Amorphous-Silicon Modules	R. Ross (JPL)	30 min
8:50	Reliability Testing of Thin-Film Cells	J. Lathrop (Clemson Univ.)	30 min
9:20	Long-Term Module Testing at Wyle Laboratory	D. Otth (JPL)	20 min
9:40	BREAK		
10:00	Module Encapsulation Technology	P. Willis (Springborn Laboratory)	30 min
10:30	Commercial Module Test Program	M. Smokler (JPL)	20 min
10:50	High-Efficiency Module Development	M. Spitzer (Spire Corp.)	20 min
11:10	Measuring Research Progress in Photovoltaics	B. Jackson (JPL)	30 min
11:40	LUNCH		

RELIABILITY PHYSICS

E. Cuddihy, Chairman

1:00	Mechanistic Studies of Photothermal Aging	R. Liang (JPL)	20 min
1:20	UV-T-RH Combined Environmental Testing	C. Gonzalez (JPL)	20 min
1:40	Computer Modeling of Photodegradation	J. Guillet (Univ. of Toronto)	20 min
2:00	Chemical Bonding Technology	E. Plueddemann (Dow Corning)	15 min
2:15	Anticorrosion Studies	J. Boerio (Univ. of Cincinnati)	15 min
2:30	BREAK		
2:50	Electrochemical Aging Effects in Modules	G. Mon (JPL)	30 min
3:20	Leakage-Current Properties of Encapsulants	A. Wen (JPL)	30 min
3:50	Water Permeation and Dielectric Properties	J. Orehtsky (Wilkes College)	30 min

SILICON MATERIALS

R. Lutwack, Chairman

April 30 (Wednesday) (Room C103)

1:00	Workshop Summary: Low-Cost Polysilicon for Terrestrial PV Solar Cell Applications	R. Lutwack (JPL)	20 min
1:20	Silane Process Research and Development	S. Iya (Union Carbide Corp.)	20 min

Plenary Sessions

SUMMARY

After welcoming participants to the 26th and final Project Integration Meeting (PIM), W.T. Callaghan, Manager of the Flat-Plate Solar Array (FSA) Project at the Jet Propulsion Laboratory (JPL), announced that, as requested by the U.S. Department of Energy (DOE), JPL plans to phase out FSA as of the end of September 1986. After that, in place of FSA, JPL will support the DOE National Photovoltaic Program in specific photovoltaic (PV) activities.

Since the FSA Project began in 1975, prices of PV modules have been reduced by a factor of 15, module efficiencies have increased by a factor of 3, and 10-year warranties now are available where there were none before. On the other hand, significant challenges face U.S. PV companies as foreign PV programs have increased and public interest has decreased because of reduced fossil-fuel energy prices and lessened interest in long-term energy planning.

Callaghan announced and displayed a long-term goal of the FSA Project: a 15.2%, AM 1.5, 75.2 W module (STC, global spectra). The module, developed by Spire Corp. under contract to FSA, represents the first, full-sized, 15% efficient, flat-plate, crystalline-silicon PV module ever made.

Morton Prince, who has been in the DOE National Photovoltaic Program Office throughout the life of the FSA Project, stated, "Many of the original objectives of the FSA Project have been accomplished and several objectives are close to meeting their goals. All of this was accomplished with less than 36% of the original budget, even without taking inflation into account. Part of this accomplishment is due to you in industry as you have been willing (rightfully so) to cost-share many of the more expensive items and I want to thank you for your contributions to our success."

Prince listed some key technology parameters for single-crystal silicon technology along with his beliefs as to what the status of these parameters was, is, and will be. Improvements still are possible with silicon, however, such as improved efficiencies and improved understanding of ribbon technology. He stated that DOE believes that these improvements are still worth pursuing and hopes to have JPL and others make these improvements.

Paul Maycock, Photovoltaic Energy Systems, Inc., presented an historical overview of the initiation and early events of national PV activities, including those of FSA. His viewpoints on major conclusions and results of the JPL/FSA activities are as follows:

Because of the DOE/JPL program, more than 2000 professionals devoted their careers to solving cost and performance problems in photovoltaics.

Virtually all of the technical feasibility and technical readiness goals were fully met by the JPL/DOE effort.

The shift in emphasis in 1981 from a balanced, well funded, research development test and evaluation PV program to an underfunded, high-risk research effort delayed the carefully planned transition from technology

PLENARY SESSIONS

readiness to commercial readiness. JPL was forced to cancel five key commercial readiness contracts involving silicon production, sheet production, ingot casting, and crystal film deposition.

Crystal-silicon photovoltaics is a truly remarkable energy product. It is uniquely reliable (30 years plus), highly efficient, environmentally benign, and can be manufactured with costs permitting fully economic photovoltaics to be used for U.S. peaking and intermediate power, and for stand-alone power in remote sites.

The DOE/JPL FSA Project is one of the more successful, cost effective, Government/university/industry, technology-development efforts in the history of U.S. Federal support of technology.

Maycock concluded with the statement that he was proud to have had a small role in management of the JPL/FSA Project and he joined the industry in saying, "Well done!"

Roger Little, of Spire Corp., presented an historical overview of the progress of photovoltaics as a function of oil price and DOE PV budgeting levels. He reviewed the state of the worldwide PV industry, the PV interests and activities of utilities, and the phases of evolution that a technology such as photovoltaics goes through on the way to commercialization. Although he has lengthened his estimate of the time it will take for photovoltaics to evolve from discovery to commercialization to an interval of from 50 to 80 years, Little's remarks were optimistic. He indicated that PV manufacturers must be patient because the markets for photovoltaics are coming, they are growing, and they are very real.

Overviews of national PV activities, and how the FSA Project fits into those efforts, were followed by eight summaries regarding specific technical efforts of the Project. These included accomplishments, lessons learned, and potential and continuing R&D needs.

In his review of the Silicon Material Task efforts, Jim Lorenz, consultant, stated that worldwide attention was attracted to the JPL/DOE Project because of the quality of the processes in the Task, which is a prime example of the proper use of Government funding of high-cost, high-risk R&D. The Task provided a technology base for a possible silane-to-silicon deposition process.

This Task resulted in the development and commercialization of a novel process for making silane and high-quality semiconductor-grade polycrystalline silicon [Union Carbide Corp. (UCC) silane-to-silicon process], and ensured adequate capacity in the United States for pure silane for the DOE/Solar Energy Research Institute (SERI) amorphous-silicon (a-Si) R&D program and for future production. The United States has a leadership role in the production and use of pure silane and pure polysilicon.

The UCC process has the potential to provide the most pure polysilicon for photovoltaics or semiconductor use. Silicon technologies of value to the worldwide electronics industry have been established and published.

PLENARY SESSIONS

Substituting for F. Wald, J. Kalejs, Mobil Solar Energy Corp., reviewed the technical progress made in the Silicon Sheet Growth Program during the 11 years of the DOE/JPL FSA Project. In 1976, when the Program began, there were nine proposed techniques to produce silicon ribbon. By 1980, this number had decreased to three techniques. At present, in 1986, only two of the techniques have survived to the start-up, pilot-plant stage in industry. These two are the edge-defined, film-fed growth (EFG) technique, developed by Mobil Solar Energy Corp. that produces closed shape polygons, and the WEB dendritic technique developed by Westinghouse Electric Corp. that produces single ribbons. Kalejs discussed both the status and future concerns of the EFG and WEB techniques.

Two other silicon-sheet growth techniques are available to industry: Low-Angle Silicon Sheet (LASS) developed by Energy Materials Corp. (EMC), and Edge-Stabilized Ribbon (ESR). Other silicon-sheet processes are being developed in France, Japan, and West Germany.

In his review of High-Efficiency Silicon Solar Cells, A. Rohatgi, Georgia Institute of Technology, reported that the first solar cells, fabricated in 1954, were only 6% efficient. By 1960, because of impetus for improvement from the U.S. space programs, solar cell efficiencies had climbed to 10 to 12%. In 1975, when the FSA Project began, space solar cell efficiencies had increased to 14 to 15%. Today, the Point-Contact Solar Cell, developed at Stanford University under a FSA contract, has an efficiency of 22.2%, close to the theoretical maximum efficiency of about 25%.

Rohatgi discussed various parameters that affect solar cell efficiency. It is not understood why solar cells produced from less expensive Czochralski (Cz) silicon are less efficient than cells fabricated from more expensive float-zone (FZ) silicon. Performance characteristics were presented of recently produced, high-efficient solar cells fabricated by Westinghouse Electric Corp., Spire Corp., University of New South Wales, and Stanford University.

Don Bickler, JPL, discussed the major processes involved in production of crystalline-silicon solar cells: surface preparation, junction formation, metallization, and assembly. The status of each of these processes, and the sequence in which these processes are applied, were described as they were in 1975, as they were in 1985, and what they may be in the future. Bickler pointed out that, from 1975 to 1985, progress in lowering the cost of solar cell processing has reached a plateau, that emphasis today is on improvement of cell efficiencies, and that any new cell designs proposed in the future will require development of new production processes and sequences.

P. Willis, Springborn Laboratories, Inc., presented a detailed summary of the diverse encapsulation materials and techniques that evolved to meet the cost-goals of the FSA Project. A "typical" solar cell now consists of low iron glass, two layers of ethylene vinyl acetate (EVA) polymers, a porous spacer, primers/adhesives, a back cover of Tedlar, and a gasket/seal for a volume cost of \$1.30/ft². This compares well with the Project's original goal of \$1.40/ft². Willis concluded that the FSA Project resulted in high-performance, cost-effective encapsulation systems for PV modules.

PLENARY SESSIONS

Evolution of the design and reliability of solar modules was described by R.G. Ross, Jr., JPL. Design requirements of modules involved 14 different considerations, including residential building and material electrical codes, wind-loading, hail-impact, and operating temperature levels, module flammability, and interfaces for both the array structure and the operation of the system.

Reliability research involved 11 diverse investigations including glass-fracture strength, soiling levels, electrochemical corrosion, and bypass-diode qualification tests. Based on these internationally recognized studies, and performance assessment and failure analyses, the FSA Project in its 11-year duration served to nurture the development of 45 different solar module designs from 15 PV manufacturers.

In his summary of solar module evolution, C. Gay of ARCO Solar, Inc. pointed out that although laboratory testing may yield acceptable results, the credibility of the usefulness of PV energy depends upon performance of modules in the field. The 6.5 MW Carissa Plain installation by ARCO has performed extremely well both in predicted delivery of electrical energy and in reliability. Warranty replacements of modules are running less than one module out of every 25,000 modules.

An economic-analysis summary of the manufacture of crystalline-silicon modules involving silicon ingot/sheet, growth, slicing, cell manufacture, and module assembly, was presented by H.L. Macomber, a consultant. Economic analyses provided:

- (1) Useful quantitative aspects for complex decision-making to the FSA Project.
- (2) Yardsticks for design and performance to industry.
- (3) Demonstration of how to evaluate and understand the worth of an R&D activity both to JPL and to other Government agencies and programs.

Macomber concluded that future R&D funds for PV energy must be provided by the Federal Government because the solar industry today does not reap enough profits from its present-day sales of PV equipment.

Following the morning presentation of eight summaries dealing with crystalline-silicon photovoltaics, a panel of seven participated in an afternoon session dealing with "Recommendations for Crystalline-Silicon in the DOE's Five-Year Photovoltaic Research Plan." Chairman of the panel was R. Annan of DOE.

In his introductory remarks, R. Annan pointed out a series of present-day paradoxes. Although a strong policy statement has been made for the pursuit of PV energy, the budgetary response has been poor. And, although a strong scientific and engineering partnership exists among PV industrial companies, universities, and the Federal Government, Federal funding remains below required levels. Photovoltaic technologies are strong, but the markets for PV products are weak. The development of PV energy is a long-term affair, but it is faced with short-term politics.

PLENARY SESSIONS

John Day, Strategies Unlimited, discussed the changes that have taken place in the PV industry during the 11-year period of the FSA Project. In 1975, when the Project began, 95% of the PV industry's cash flow came from the Federal Government, the Government was the only purchaser, and the industry was run by individualistic entrepreneurs operating under-financed small ventures. By contrast, today, the Federal Government provides only 25% of the industry's cash flow, there are commercial purchase besides the Government, and the industry now is run by planning teams operating in well-financed industrial companies.

As for the future, Day indicated that for the next 5 to 10 years, photovoltaics will continue to be used to generate power in remote locations. Beyond 10 years, there will be an increase in grid-connected PV applications. His recommendations for Government PV-policy for the next 5 years are:

- (1) Give assistance in the export of PV equipment.
- (2) Provide education about PV energy to electrical utilities.
- (3) Provide for long-term research efforts.

G. Smith, U.S. Navy, stated that the U.S. Department of Defense (DOD) is the largest single consumer of energy in the United States, annually using about 250 million barrels of oil equivalent (MBOE). Of this, 70% is provided by petroleum products. A renewable energy source such as photovoltaics, therefore, can play a major role in DOD energy-management objectives, specifically in programs aimed at petroleum substitution in shore facilities. The latter accounts for about 25% of DOD's total energy budget. Thus, DOD, potentially, can be a several billion dollar per year market for the PV industry.

Through the Federal Photovoltaics Utilization Program (FPUP), the DOD installed 218 diverse PV systems that ranged in size from a few watts to 56 kW. The Navy, which now serves as the lead service within DOD for PV-system activities, has identified 21,000 cost-effective applications for photovoltaics throughout the service.

In an effort to expand PV-use more aggressively throughout DOD, a tri-service Photovoltaics Review Committee (PRC) was formed in December 1985 with the following partial list of 5-year objectives:

- (1) To study ways of identifying potential PV applications within DOD.
- (2) To reduce overall costs of DOD PV-related products.
- (3) To transfer technical information about photovoltaics throughout the military.
- (4) To promote widespread application of PV systems in the three service branches.

PLENARY SESSIONS

Smith outlined six activities being considered by the PRC, one of which is sponsorship of a joint industry/DOD meeting at which there would be a free exchange of information on the PV needs of the various services. The DOD is a lead agency and an active participant of the Committee on Renewable Energy Commerce and Trade (CORECT).

Speaking as a representative of an electrical utility, K. Firor of Pacific Gas and Electric (PG&E) indicated that a utility must balance the benefits of photovoltaics (free fuel, modularity, minimal water use, short lead times, few moving parts, peak load match, minimal environmental impact, and political and social acceptance) against the obstacles to a utility's use of photovoltaics (high costs, fear of the unknown, unknown O&M costs, unknown O&M procedures, unknown reliability, unknown power quality, and unfamiliarity of the technology). She pointed out that just because R&D people know how to handle photovoltaics does not mean that a utility will build a solar power plant. She presented a diagram that detailed a realistic view of the many inputs required by a utility company's management before a decision can be made to build a PV power plant.

According to E.L. Ralph, Hughes Aircraft Company, there is no clear superiority among thin films, multi-bandgap cells, and crystalline silicon, if balance-of-system costs, reliability, and efficiency are considered. Crystalline-silicon technology, however, has several factors in its favor: a proven database, proven advances waiting to be incorporated into commercial production, and potential for considerable future advances.

Ralph feels that DOE support for the Crystalline-Silicon Program is dangerously low. His recommendations for the Program are:

- (1) Need for a production technology to lead to modules with 15% efficiency.
- (2) Need for a research program to lead to flat modules with 18% efficiency.
- (3) A research program with multi-bandgap (silicon-based) cells to yield flat modules with 25% efficiency.

Ralph presented a list of crystalline-silicon research needs that included the following:

- (1) Sheet growth: crystal quality, automatic growth, and high-throughput.
- (2) Minimization of surface losses: physical/chemical structures, surface properties, and methods.
- (3) Measurements: lifetimes, mobilities, and recombination at surfaces and interfaces.
- (4) Process development: attainment of low-cost processes compatible with high-efficiency.

PLENARY SESSIONS

K.M. Koliwad, JPL, stated that crystalline-silicon technology can meet the long-range objectives of the DOE PV Program. Future research should focus on the solution of fundamental problems to permit the production of high-quality silicon sheet, and on the advance of knowledge of basic mechanisms of charge-carrier losses to allow the production of large-area, high-efficiency solar cells on low-cost silicon sheet.

Koliwad recommended:

- (1) An emphasis of fundamental and generic research to benefit a large segment of the PV industry.
- (2) A balance among various technology options and a balance among industry, university, and Federal laboratories.
- (3) Development of a mechanism for longer-term support to universities.
- (4) Establishment of a formal procedure to transfer technology from research to applications.
- (5) Use of DOD and other support for leverage in related areas.

C. Rose, of Westinghouse Electric Corp., presented a summary of dendritic web technology. In December 1984, web growth was 9000 cm²/week/furnance with a module efficiency of 13%. By December 1985, web growth and module efficiency had increased to 47,000 cm²/week/furnance and 14%, respectively. Rose discussed research requirements for high-speed, silicon ribbon growth, requirements for silicon materials, and requirements for flat-plate collectors.

E.E. Daniels, Solarex Corp., summarized the accomplishments of the PV industrial community. With respect to the four silicon-technology options (single crystal, semicrystalline, amorphous, and ribbon), Daniels showed a diagram that depicted Cz and semicrystalline silicon accounting for 65 and 35%, respectively, of the PV market in 1984.

But, by 1991, the Daniels-diagram predicts a market made up of semicrystalline silicon (46%), amorphous silicon (38%), Cz silicon (6%), silicon ribbon (5%), and other silicon technologies (5%).

INDUSTRY-USERS DAY SUMMARIES

Following the plenary sessions of the first day, and the three parallel technical sessions of the second day, the third morning of the 26th PIM was devoted to a novel session called Industry-Users Day. Representatives from 14 diverse organizations presented brief, informal discussions of present-day activities in the evolving field of photovoltaics.

R. Johnson, Strategies Unlimited. In spite of present-day pessimism because of foreign competition, loss of tax benefits, and cutbacks, the future looks optimistic as markets for photovoltaics continue to grow. North America is the largest single consumer of PV power modules.

PLENARY SESSIONS

W. Breneman, Union Carbide Corporation. The Electronics Division of UCC now has a Polysilicon Department producing silicon from extremely pure silane in plants at Washougal and Moses Lake, Washington, with production being 100 and 2400 MT/year, respectively. A 3000 MT/year plant is planned, using fluidized-bed reactors (FBRs). As yet, no location for this plant has been selected.

A. Morrison, Kayex Corp.. Substituting for Dick Lane, Andy Morrison stated that Kayex Corp., a subsidiary of General Signal, prepares economically viable silicon by an advanced Cz technique.

D. Jewett, Energy Materials Corp.. Jewett revealed that EMC now has a low-angle silicon sheet process that operates with continuous replenishment and high-speed growth. The EMC process will be offered to industry with a pilot-plant capability within a year.

F. Schmid, Crystal Systems. Schmid expects that the 100 x 100 mm silicon wafers will be around for the next 10 years. The heat-exchange method (HEM) technique for the growth of silicon ingots needs more R&D to increase its throughput. Wafers are prepared from low-cost silicon by HEM ingot-growth and slicing of the ingots by the fixed abrasive slicing technique (FAST).

E. Sachs, A.D. Little Company. Sachs described 12 man-years of development of ESR at A.D. Little Company (ADL). Use of a single-ribbon, melt-replenished furnace, operated 100 h continuously (three-shift operation, 96% duty-cycle) to produce 62,000 cm² of silicon ribbon, yields silicon that is fabricated into solar cells with 12.7% efficiency.

K.V. Ravi, Mobil Solar Energy Program. Ravi described the EFG process for production of closed-shape, thin-shelled polygons of silicon ribbon. A photo was shown of a 20-ft-high nonagon of silicon and a hexagon with 4-in.-wide sides. Mobil believes that the EFG process is the only silicon-ribbon technology that will make photovoltaics economically feasible. The EFG-produced silicon ribbon routinely yields solar cells of 14% efficiency.

C. Rose, Westinghouse Electric Corp.. In 1980, Westinghouse transferred its dendritic web ribbon process from R&D to a pilot-plant installation. Cuts in funding by the Reagan Administration, however, threw the program into confusion. Recently, Westinghouse decided to change its pilot-plant line to a manufacturing mode to demonstrate the cost of the project. When those figures have been obtained, Westinghouse will make a decision whether to continue with the development of the process.

L. Kashar, Scanning Electron Analysis Laboratories. Kashar explained what instruments the Scanning Electron Analysis Laboratories (SEAL) had available to carry out microanalysis of PV cells. Such information can provide valuable data concerning the relationships between contaminants and cell performance.

C. Gay, ARCO Solar. Crystalline silicon has been the mainstay of PV-cell production, while R&D proceeds for thin-film cells. Although single-crystal PV cells now produce electricity for about \$5/W_p, they must get down to \$0.50/W_p to compete with coal and nuclear power plants.

PLENARY SESSIONS

J. Goldsmith, Solarex Corp.. Solarex, which is a wholly-owned subsidiary of American Oil Company (AMOCO), has a heavy investment in a-Si and thin films. More work is needed. Thus, the continuation of FSA-type projects is necessary for the development of a viable, U.S. national resource.

I. Shahryar, Solec International. Solec has become a specialty manufacturing house, turning out 10 to 12% efficient solar cells to fit a specific customer's desires.

M. Spitzer, Spire Corp.. Substituting for Roger Little, Mark Spitzer described Spire's worldwide activity in the development of automated equipment for the production of solar modules and ancillary solar equipment.

W. O'Neill, AEG. AEG, purchased by Mercedes-Benz and having links to Telefunken, has offices in 103 countries and operating solar systems in 55 countries. The company has 90 years experience in DC motors and DC appliances. AEG uses semi-crystalline silicon to fabricate pliable, flexible modules with glass encapsulant and stainless steel framing. Folding solar modules are made for military use. AEG also makes balance-of-system components: charge regulators, inverters, and charge controllers for hybrid installations (wind/PV and wind/PV/diesel). AEG, with offices in Somerville, New Jersey, and Phoenix, Arizona, can offer 100 kW solar arrays.

K. Firor, Pacific Gas & Electric. In an attempt to advance education about photovoltaics to utilities, PG&E now is involved in a project called Photovoltaics for Utility Service Applications (PVUSA). The PVUSA program consists of the installation of 10 MW capacity during a 10-year period at two different sites, each with different insulations. The program will proceed in two phases:

Phase 1 (1986 to 1990) will lead to an installation of 3.5 MW at each site. This will cost \$14.5 million, of which 37% will be provided by PG&E, DOE will provide 50%, and the Electric Power Research Institute (EPRI) will provide remaining 13%.

Phase 2 (1990 to 1994) will lead to an installation of a 1 MW, PG&E-designed plant at the insolation site, and a 0.5 MW, PG&E-designed plant at the direct insolation site. DOE will provide \$20 million and PG&E will provide \$14.5 million.

INTRODUCTION TO PROCEEDINGS

JET PROPULSION LABORATORY

W. T. Callaghan

W. T. Callaghan, Manager of the Flat-Plate Solar Array (FSA) Project, opened the 26th, and last, Project Integration Meeting (PIM) by welcoming the participants.

In his remarks, he reviewed the accomplishments made, the dedication shown by the many firms, universities, and persons who have been involved in the FSA Project. "Like so many long-term relationships in life, FSA is a difficult one to end. We can all be very proud of our role in helping to reduce prices by a factor of 15, we can point to module efficiency increases of a factor of 3, and we can cite 10-year warranties now where there were none before."

He also cited reduced fossil fuel energy prices, lessened public interest in long-term energy planning, and increased foreign photovoltaic (PV) programs as the challenges facing U.S. PV firms.

A long-term goal was accomplished by the FSA Project when Callaghan introduced the audience to the Spire Corp. 15.2% AM 1.5, 75.2 W module (STC, global spectra) that had just been tested by FSA. The module was developed under contract to FSA by Spire Corp. and represents the first, full-sized 15% flat-plate crystalline silicon PV module ever made.

In recognition of their contributions to the success of the FSA Project, Callaghan cited Mrs. Mary J. Phillips and Mr. Elmer Christensen from the FSA Project Office. In addition, commemorative plaques were presented to Mr. Robert Forney (JPL), Mr. John Goldsmith (Solarex Corp.), and Dr. Morton Prince, U.S. Department of Energy (DOE), for their invaluable contributions to the development of photovoltaic science.

PRECEDING PAGE BLANK NOT FILMED

C-2

DOE COMMENTS

U.S. DEPARTMENT OF ENERGY

M. Prince

TODAY IS AN EXCITING DAY FOR ME AND I BELIEVE FOR MANY INDIVIDUALS/ASSOCIATED WITH THE FSA PROJECT. MANY OF THE ORIGINAL OBJECTIVES OF THE PROJECT HAVE BEEN ACCOMPLISHED AND SEVERAL OBJECTIVES ARE CLOSE TO MEETING THEIR GOALS. ALL OF THIS WAS ACCOMPLISHED WITH MUCH LESS THAN 1/2 OF THE ORIGINALLY PLANNED BUDGET, ESPECIALLY WHEN ADJUSTED FOR THE INFLATION THAT WE HAVE HAD DURING THE PAST 11 YEARS.

I AM NOT EXACTLY SURE WHAT PAUL MAYCOCK AND ROGER LITTLE ARE GOING TO SAY. BUT I AM APOLOGIZING TO THEM NOW IF I PREEMPT THEM.

IN PREPARING MY COMMENTS, I WENT BACK TO SOME EARLY JPL DOCUMENTS TO SEE WHAT WAS ORIGINALLY PROPOSED AND HOW WELL THESE OBJECTIVES WERE MET. THE FIRST MEETING I ATTENDED WAS THE INDUSTRIAL BRIEFING OF FEBRUARY 5, 1975 WHICH KICKED-OFF THE LOW COST SILICON SOLAR ARRAY PROJECT WHICH EVENTUALLY EVOLVED INTO THE FLAT-PLATE SOLAR ARRAY PROJECT. THAT MEETING WAS HELD SIMULTANEOUSLY UP AT THE VON KARMAN AUDITORIUM AT JPL AND AT A NASA AUDITORIUM IN WASHINGTON USING A SECURED COMMUNICATION LINE.

MANY OF THE ORIGINAL PARTICIPANTS AND ATTENDEES OF THAT BRIEFING ARE HERE TODAY. I WOULD LIKE TO QUICKLY RUN THRU FOUR SLIDES ^{OFF} AT THAT BRIEFING.

PRECEDING PAGE BLANK NOT FILMED

PLENARY SESSIONS

SLIDE 1 SHOWS THE ORIGINAL ORGANIZATION OF THE PROJECT WITH THE FIVE TECHNICAL TASKS SUPPORTED WITH AN ANALYSIS AND INTEGRATION STAFF. ALL THE ORIGINAL MANAGERS EXCEPT RALPH LUTWACK HAVE GONE ON TO OTHER ACTIVITIES.

SLIDE 2, SHOWS THE ORIGINAL OBJECTIVE OF THE SI MATERIAL TASK OF \$35/KG FOR RAW-STOCK SI. TODAY IN 1975, \$ WE ARE WAY AHEAD AT THAT OBJECTIVE AND WITH THE UNION CARBIDE WORK ON THE FBR, WE EXPECT THAT WE WILL CUT THE COST SIGNIFICANTLY FURTHER IN THE NEAR FUTURE.

SLIDE 3 SHOWS THE ORIGINAL OBJECTIVES ~~AT~~^{OF} THE LARGE AREA SILICON SHEET TASK. ALTHOUGH WE HAVEN'T MADE THE PRODUCTION TYPE OBJECTIVES. WE HAVE REACHED THE HIGH EFFICIENCY MODULE GOAL WITH 13% AVAILABLE COMMERCIALY AND 15% MADE IN THE LABORATORY.

SLIDE 4 SHOWS THE OBJECTIVES AT THE MODULE ENCAPSULATION TASK. HERE WE HAVE ~~MEET~~ THE OBJECTIVE QUITE WELL.

THE AUTOMATED SOLAR ARRAY ASSEMBLY TASK AND THE LARGE SCALE PRODUCTION TASK ALSO HAD OBJECTIVES THAT WE COULD NOT MEET BECAUSE OF BUDGET LIMITATIONS AND CHANGES IN WHAT THE GOVERNMENT COULD DO FROM A PROGRAMMATIC POINT OF VIEW.

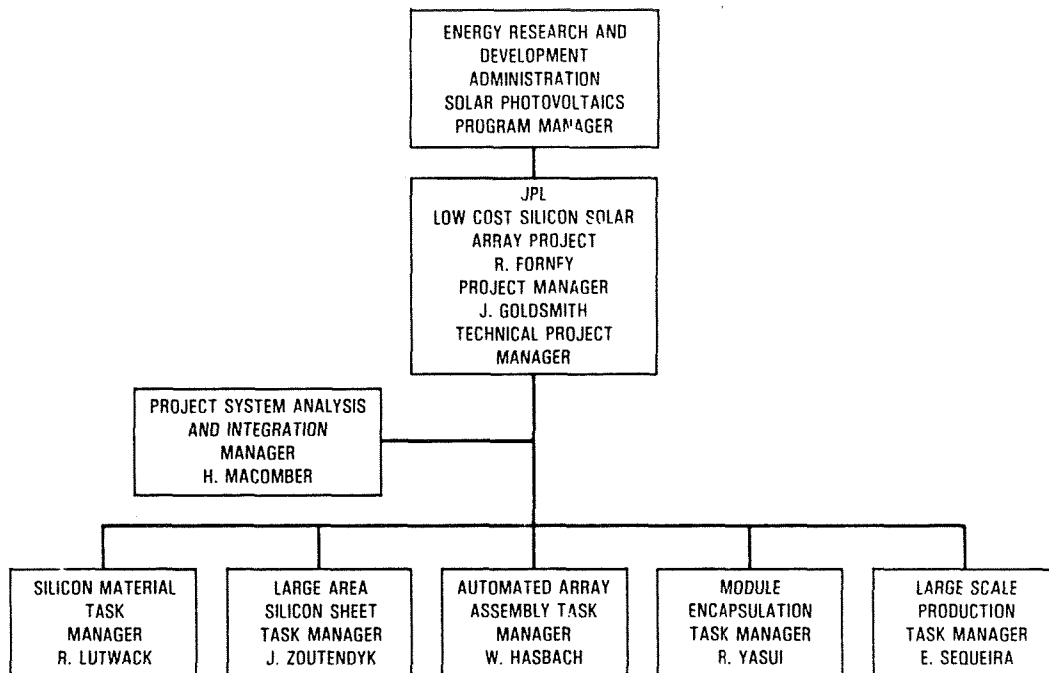
PLENARY SESSIONS

ABOUT A YEAR LATER WE HAD OUR FIRST PIM WITH ABOUT 20 CONTRACTORS IN MID-JANUARY 1976. AT THAT TIME WE HAD A FIRST OVERALL REVIEW AND SMALLER TASK MEETINGS. THAT MEETING SET THE EXCELLENT TONE FOR THE FUTURE INTEGRATION MEETINGS OF WHICH THIS IS THE LAST FOR THE FSA PROJECT.

ANOTHER EARLY SHEET THAT I FOUND INTERESTING IS THE ORIGINAL PROJECT BUDGET REQUIREMENTS OF OVER \$650M FOR TEN YEARS AND THE FIRST REVISION WHICH WAS MADE AFTER OUR FY 1976 BUDGET FIGURES CAME OUT. THIS EXTENDED THE PROJECT FROM 10 TO 12 YEARS AT ABOUT THE SAME OVERALL BUDGET LEVEL. IT IS INTERESTING TO NOTE THAT THE FSA PROJECT HAS SPENT \$228M THRU FEBRUARY OF THIS YEAR AND WILL PROBABLY COMPLETE ITS ACTIVITY WITH EXPENDITURES UNDER \$235M. THIS WILL BE LESS THAN 36% OF THE ORIGINAL BUDGET EVEN WITHOUT TAKING INFLATION INTO ACCOUNT. MANY OF THE EXPENSIVE ITEMS IN THE ORIGINAL PLAN SUCH AS THE PRODUCTION PILOT LINES AND THE MULTI-MEGAWATT BUYS WERE ELIMINATED FROM THE PROJECT. BUT IN SPITE OF THESE REDUCTIONS IN SCOPE, THE PROJECT HAS BEEN SUCCESSFUL FINANCIALLY AS WELL AS TECHNICALLY. PART OF THIS ACCOMPLISHMENT IS DUE TO YOU IN INDUSTRY AS YOU HAVE BEEN WILLING (RIGHTFULLY SO) TO COST-SHARE MANY OF THE MORE EXPENSIVE ITEMS AND I WANT TO THANK YOU FOR YOUR CONTRIBUTIONS TO OUR SUCCESS.

FINALLY SINCE TODAY WE WILL BE HEARING WHERE WE ARE COMING FROM, WHERE WE ARE, AND WHERE INDUSTRY IS GOING TO BE, I THOUGHT I WOULD PUT MY VIEWS BEFORE YOU. IN MY LAST SLIDE I HAVE LISTED SOME KEY TECHNOLOGY PARAMETERS FOR THE SINGLE CRYSTAL SILICON TECHNOLOGY WITH MY BELIEFS AS TO WHAT THE STATUS WAS, IS AND WILL BE. AS YOU SEE I BELIEVE THAT WE HAVE REACHED MOST OF THE ULTIMATE TECHNOLOGY END POINTS. HOWEVER, WE STILL HAVE SOME IMPROVEMENTS POSSIBLE WITH SILICON SUCH AS IMPROVED EFFICIENCIES AND IMPROVED UNDERSTANDING OF RIBBON TECHNOLOGY. WE AT DOE BELIEVE THESE ARE STILL WORTH PURSUING AND HOPE TO HAVE JPL WITH THEIR STRONG IN-HOUSE TECHNOLOGY GROUPS HELP US MAKE THESE IMPROVEMENTS.

Low Cost Silicon Solar Array Project
JPL PROJECT ORGANIZATION



Low Cost Silicon Solar Array Project
SILICON MATERIAL TASK
TASK OBJECTIVES

- **Production**
 - Establish process with high volume production capability
 - Demonstrate suitability for meeting 1985 goal equivalent to 500 MW of modules per year
- **Price**
 - Demonstrate energy use and economic effectiveness
 - Obtain production price of < \$35 per KG

Low Cost Silicon Solar Array Project

LARGE AREA SILICON SHEET TASK

- **Large area low cost silicon sheets**
(< \$ 1.60/sq ft)
- **Silicon sheets with high photovoltaic efficiency**
(> 10% terrestrial array efficiency)
- **Automated sheet production capability**
(> 50 million sq ft/yr)

Low Cost Silicon Solar Array Project

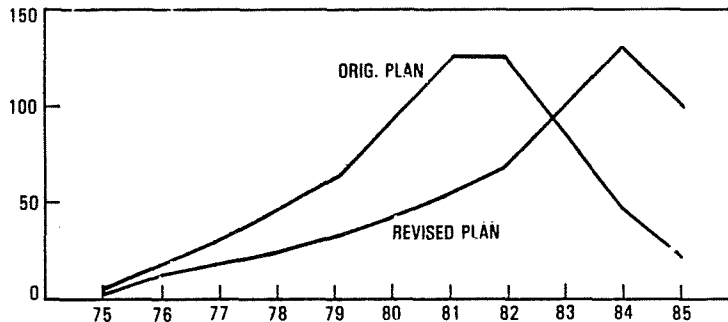
MODULE ENCAPSULATION TASK

- **Near Term Objective**
 - **Select the best candidate encapsulation material and process for integration into the automated array task by 1978**
- **Long range objective**
 - **Develop, test and qualify encapsulation materials and processes for arrays with a design operating lifetime greater than 20 yr**

Low-Cost Silicon Solar Array Project

CURRENT TEN-YEAR SUMMARY — OBLIGATIONS REVISED BUDGET COMPARISON

	75\$			77\$								
\$ MILLIONS FY	75	76	77	78	79	80	81	82	83	84	85	TOTAL
ORIG. PLAN	3.0	16.1	30.2	46.2	62.3	91.2	124.0	124.0	84.2	47.0	22.0	656.6
REVISED PLAN	3.0	12.4	18	24	32	42	54	68	100	130	100	586.9



* TRANSITION PERIOD FUNDS

Low-Cost Silicon Solar Array Project

JPL/FSA PROJECT ACCOMPLISHMENTS

- **General** — DOE (and ERDA) funded activities at JPL has made possible a nascent industry making terrestrial photovoltaic cells, modules and systems (\$ 200 M/year). The Project's findings has helped the U.S. semiconductor industry with technology development as well.

• **Specific Technology Developments**

Parameter	1975 Status	Present Status	Near-Future Status
Rawstock Material	\$80/Kilogram	\$40/Kilogram	\$20/Kilogram
Silicon Crystal Size	3" Diameter	6" Diameter	8" Diameter
Crystal Slicing	O.D. Saws	Multiple Wire, Multiple Band and Large I.D. Saws	Multiple Wire, Multiple Band and Large I.D. Saws
Ribbon Technology	EFG	EFG, Dendritic Web, ESP, RTR	EFG, Dendritic Web, ESP, RTR
Junction Formation	Two Diffusions	Simultaneous Diffusion, Ion Implantation Plus Anneal	Simultaneous Diffusion, Ion Implantation Plus Anneal
Contact Formation	Evaporation	Evaporation, Silk Screen Printing, Laser Deposition	Evaporation, Silk Screen Printing, Laser Deposition
Assembly of Cells	Hand Assembly	Automatic Stringing Equipment	Automatic Stringing Equipment

THE JET PROPULSION LABORATORY LOW-COST SOLAR ARRAY PROJECT 1974-1986

PHOTOVOLTAIC ENERGY SYSTEMS, INC.

P. D. Maycock

Historical Overview

The Lowcost Solar Array Project (LSA) had its origin in the JPL-organized Cherry Hill Conference on October 23-25, 1973. /1 Cherry Hill was dedicated to find paths for implementing all forms of solar energy. The Cherry Hill Conference heard a large number of invited papers on silicon and polysilicon from many persons still very active in PV. Gene Ralph presented a detailed development plan which actually had "milestones." Gene's road map (Fig 1) was a precursor to the JPL-LSA plan. We heard other papers at Cherry Hill. Dr. Joe Lindmayer, having just formed Solarex, gave a paper entitled "Silicon Cells." He said, "I believe that terrestrial cells could be produced now (1973) for \$10 per Watt peak and a panel completed for \$20 per Watt. It seems certain that the efficiency could be over 20 percent." We heard from C.G. Currin of Dow Corning and R.K. Riel of Westinghouse on dendritic web; Tom Surek, Bruce Chalmers, A.I. "Eddy" Mlavsky and G.H. Schwuttke on EFG ribbon. On polysilicon we heard from P.H. Fang, Ting L. Chu, P.A. Iles and Bernie Seraphin.

At this key conference, several National Science Foundation professionals were leaders in the PV discussions. When the Energy Research and Development Administration was formed in 1973, some of these NSF professionals were assigned to ERDA to set up the U.S. Photovoltaics Program. The NSF crew was Dr. Dick Blieden, Dr. Len Magid, Dr. Lloyd Herwig, Dr. Don Schueller and Doug Warschauer. Dick Blieden had charge of all the electric options and Len Magid was running PV. Len had negotiated and helped plan and fund the JPL program.

Another key national effort in establishing energy priorities was the Dixy Lee Ray Report - "The Nation's Energy Future" /2 which also scoped out the potential for PV.

Our good friend, Bob Forney, was the first manager of the LSA program and John Goldsmith was his technical director. John found greener pastures at Solarex and represents one of our most important results of the project - people. We trained - John and dozens others very well so they could join industry and become leaders in the private sector.

In this timeframe we had the origins of the precise milestones which guided the program. Mort Prince joined ERDA in July 1975 and took over the PV branch. I joined ERDA in August '75 and took over the PV division in 1977. Hank Marvin had joined us in August '75 to lead the solar division and despite some pressure from management, we issued the so-called "Marvin Plan." /3 The objectives of this plan were our "bible" for the entire program until the Reagan budget hit the street and we started high risk research. Table 1 shows the key objectives for the LSA Technology Development area of the Marvin Plan. Table 2 shows the planned funding for the entire PV program. The LSA project was primarily concerned with the technology development goals.

A key factor in the planning of the LSA program was the FEA Task Force Report Project Independence Blue Print issued November 1974. /4 Our PV team was

PLENARY SESSIONS

instrumental in writing Section VII. Some names pop out that are worth mentioning. The PV participants included Mickey Alpers, Dick Blieden, Gene Ralph, Ralph Luttwack, Sam Taylor, Lloyd Herwig, Dan Bernatowicz, Pete Bos, Bill Cherry, John Goldsmith (NASA Lewis), Pat Rahilly, Fred Bartels. Project Independence proposed an accelerated national effort which would by 1985 cause:

Peak Power Production - 1000MW
Average PV Array Cost - \$500/kW peak (the famous \$.50/W goal in 1975\$)
Total Installed Cost - \$900/kW peak
Number of PV Workers - 38,700

Obviously these were a bit optimistic, but the goals were the results of our best thinking at the time. The JPL, ERDA, DOE Photovoltaic goals were the result of a complicated consensus process by the best minds in government and industry.

JPL analyzed every step in the creation of a crystal silicon module in terms of material used, material cost, material properties; process used, cost and results. The major programs included: polysilicon production cost and properties; crystal silicon; slicing or area creation; cell formation; metallization; interconnection; packaging and testing. For every program element, a matrix of technical options was defined and funded. For example, in the polysilicon area, twelve chemical approaches to purifying silicon were funded. For every program element, detailed technical feasibility milestones were established. As technical feasibility was shown, technical readiness goals, and finally commercial readiness objectives were established. Table 3 shows the history of funding of the LSA project versus the planned budget. This funding plan and goals become the basis for the PVRD&D Act of 1978 which called for nearly \$2 billion of RDT&E and essentially institutionalized the goals of the Marvin Plan.

It is clear that the budgets imposed by President Reagan did not allow the plan to be implemented. I left DOE because adequate resources were not being offered in order to meet our commercial readiness goals. I felt by forming the Renewable Energy Institute, getting on the Boards of SEIA and ASEC and "working" the Hill to mark up Reagan's proposed \$20 million levels to \$50 million plus, that I could do more for PV than staying with a bankrupt policy.

Major Conclusions and Results of JPL/LSA

- The DOE/JPL program caused over 2000 professionals to devote their careers to solving cost and performance problems in PV.
- Virtually all of the technical feasibility and technical readiness goals were fully met by the JPL/DOE effort.
- The shift in emphasis in 1981 from a balanced, well funded RDT&E PV program to an underfunded, high risk research effort delayed the carefully planned transition from technology readiness to commercial readiness. JPL was forced to cancel five key commercial readiness contracts involving silicon production, sheet production, ingot casting and crystal film deposition.
- Crystal silicon PV is a truly remarkable energy product. It is uniquely reliable (30 year plus), high efficient, environmentally benign, that can be manufactured with costs permitting fully economic PV for the U.S. peaking and intermediate power and for stand alone power in remote sites.
- The DOE/JPL LSA project is one of the most successful, cost effective, government/university/industry technology development efforts in the history of U.S. federal support of technology.

I am proud to have had a small role in managing the JPL/LSA project and join the industry in saying well done!

PLENARY SESSIONS

References:

- 1 Workshop proceedings "Photovoltaic Conversion of Solar Energy for Terrestrial Applications, Vol I, Vol II, October 23-25, 1973, Cherry Hill, NJ, Organized by JPL; Sponsored by NSF RANN-NSF-RA-N-74-03.
- 2 "The Nation's Energy Future", Report to Richard M. Nixon, Submitted by Dr. Dixy Lee Ray, December 1, 1973, Washington 1281.
- 3 "Marvin Plan" - February 3, 1978, "National PV Program Plan" DOE/ET-0035(78).
- 4 Federal Energy Administration Project Independence Blue Print Final Task Force Report Solar Energy, Directed by NSF, November 1974.

Figure 1. Gene Ralph's Cherry Hill Road Map for PV-1973

MILESTONE SCHEDULE			
PARAMETER	TECHNOLOGY STATUS		
	PRESENT 1973	5 YEARS 1978	10 YEARS 1983
Cell Size (cm ²)	20	45 or Cont. Ribbon	Continuous Multi-Ribbon or sheet
Cell Efficiency (% AMO)	14	16	18
(% AMI)	16.5	19	21
Cell Cost (\$/watt AMI)	5	2.50	0.30
Power System Cost (\$/watt AMI)	20	5	<1
Production Rate (Mw/yr)	.09	6	200

Table 1. Objectives and Goals

Objectives and Goals

The overall objective of the photovoltaic program is to ensure that photovoltaic conversion systems play a significant role in the nation's energy supply by stimulating an industry capable of providing approximately 50 GWe of installed electricity generating capacity by the year 2000.

In order to achieve this overall objective, several time-phased program goals have been defined.

• Near Term:

- To achieve photovoltaic flat-plate module or concentrator array prices of \$2 per peak watt (1975 dollars) at an annual production rate of 20 peak megawatts in 1982. At this price level, energy costs should range from 100 to 200 mills/kwh.

• Mid Term:

- To achieve photovoltaic flat-plate module or concentrator array prices of \$0.50 per peak watt (in 1975 dollars), and an annual production rate of 500 peak megawatts in 1986. At this price level, energy costs should be in the range of 50 to 80 mills/kwh. Studies project that photovoltaic systems will begin to compete for both distributed and larger load-center utility-type applications and thereby open up significant markets for large-scale photovoltaic systems. This production level would permit the use of industrial-scale array production processes and would ensure the market availability of photovoltaic arrays as they become economic.

• Far Term:

- To achieve photovoltaic flat-plate module or concentrator array price goal of \$0.10 to \$0.30 per peak watt in 1990 (in 1975 dollars), and an annual production rate of 10-20 peak gigawatts in 2000. At this price range, energy costs should be in the range of 40 to 60 mills/kwh and be cost effective for utility applications. Such a level of annual photovoltaic capacity installation can ensure that photovoltaic conversion systems become a significant source in the Nation's energy supply.

Achievement of these goals can make photovoltaic systems economically competitive with other energy sources for dispersed on-site applications as well as for central power generation.

Since these goals are time specific it is assumed that program funding will follow that identified in Table 3. Significant departures in funding will affect the time of performance.

Table 2. Photovoltaic Funding
Performance Funding (B/A) Needed for Photovoltaic
Activities (\$ in Millions)

PROGRAM ACTIVITY	FY 77	FY 78	FY 79	FY 80	FY 81	FY 82	FY 83	FY 84	FY 85	FY 86	TOTAL 77-86
TECHNOLOGY DEVELOPMENT	33.7	36.0*	27.0	40.0	50.0	60.0	60.0	50.0	40.0	30.0	426.7
RESEARCH & ADVANCED DEVELOPMENT	6.2	8.7	13.5	20.0	25.0	30.0	30.0	35.0	35.0	25.0	228.4
SYSTEMS SUPPORT	7.0	9.0	9.7	10.0	10.0	8.0	8.0	6.0	6.0	4.0	77.7
QUALITY ASSURANCE	0.0	1.0	2.0	3.0	4.0	4.0	4.0	3.0	2.0	2.0	25.0
PROGRAM MANAGEMENT & ANALYSIS	2.0	2.3*	1.8	2.0	2.0	2.0	2.0	2.0	2.0	2.0	19.9
ST&A - FLAT PLATE	6.5	2.0	11.0	20.0	50.0	60.0	60.0	60.0	50.0	40.0	395.5
ST&A - CONCENTRATORS	0.0	5.0	11.0	20.0							
ST&A - FEDERAL PURCHASES	0.0	12.2*	20.0**	20.0**	40.0**	20.0**	0.0	0.0	0.0	0.0	112.2
TOTAL PROGRAM	55.4	76.2*	95.8	135.0	181.0	184.0	184.0	156.0	135.0	103.0	1285.4

*INCLUDES SUPPLEMENTAL FUNDS - \$19 million

**DEPENDS ON NEA PASSAGE

Table 3. Low-Cost Silicon Solar Array Project
Current 10-Year Summary

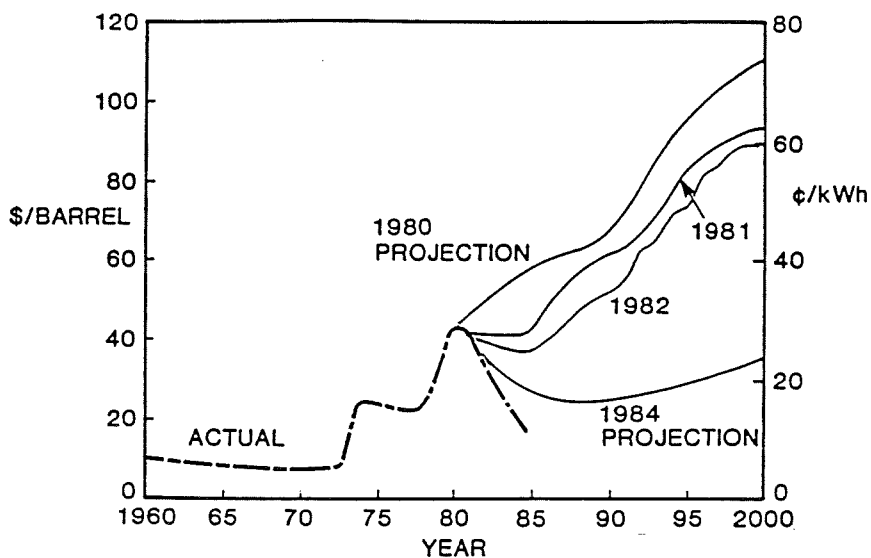
	75\$			77\$								
\$ MILLIONS FY	75	76	77	78	79	80	81	82	83	84	85	TOTAL
ORIG. PLAN	3.0	16.1 6.4*	30.2	46.2	62.3	91.2	124.0	124.0	84.2	47.0	22.0	656.6
REVISED PLAN	3.0	12.4 3.5*	18	24	32	42	54	68	100	130	100	586.9
ACTUAL	3.0	19	32	36	38	42	29	17	13.6	14	15	258.6

HISTORICAL OVERVIEW, ACCOMPLISHMENTS, AND VALUE OF THE FSA PROJECT: INDUSTRY

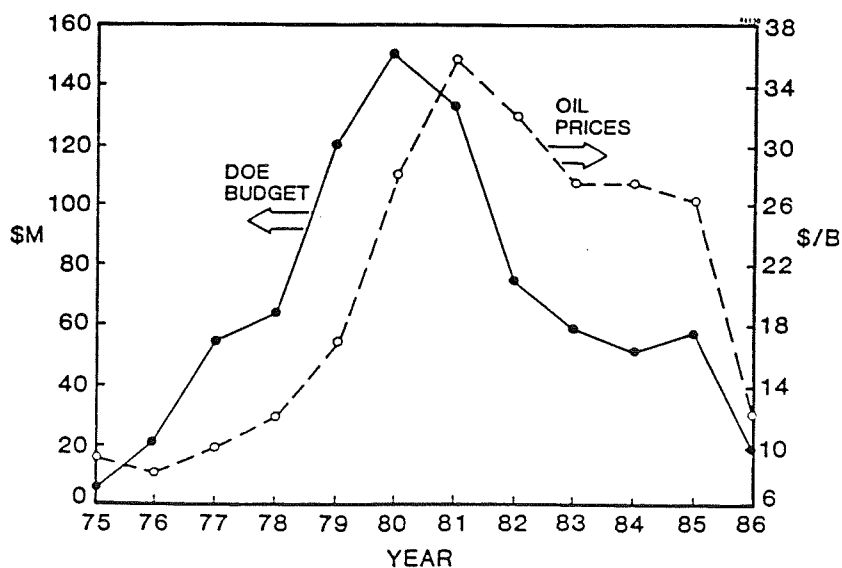
SPIRE CORPORATION

R. Little

Southern California Edison Data



DOE PV Budget Per Annum



PRECEDING PAGE BLANK NOT FILMED

United States

- ARCO SOLAR 4.9 MW
- SOLAREX 2.2 MW
- SOLAVOLT 0.5 MW
- SOLEC INTERNATIONAL 0.4 MW
- CHRONAR
- SOVONICS
- MOBIL SOLAR
- WESTINGHOUSE
- ENTECH

Europe

- PHOTOWATT (FRANCE) 1.0 MW
- AEG (WEST GERMANY) 0.8 MW
- PRAGMA (ITALY) 0.5 MW
- BP SOLAR (AUS, SPAIN, G.B.) 0.4 MW
- ANSALDO (ITALY)
- HELIOS (ITALY)
- SIEMENS (FRG)
- ISOFOTON (SPAIN)

Japan

- SANYO 3.9 MW
- FUJI 2.8 MW
- SHARP 0.5 MW
- KYOCERA
- HOXAN
- KANEKA
- NEC
- HITACHI
- KOMATSU
- MITSUBISHI
- TAIYO YUDEN

PLENARY SESSIONS

Developing World

- INDIA
- CHINA
- SAUDI ARABIA
- ALGERIA
- AUSTRALIA
- CANADA
- BRAZIL

Upside

- DOE
- OTA
- STATE
PROGRAMS
- UTILITIES
- DOD

Photovoltaics: More than an Energy Option

- UTILITY GROWTH
- BALANCE OF PAYMENTS
- FOREIGN RELIANCE
- WORLD STANDARD OF LIVING
- MILITARY STRONGER

PV Progress

- $\eta \sim 15\%$
- ENDURANCE > 20 YEARS
- LOW COST FEASIBLE

PLENARY SESSIONS

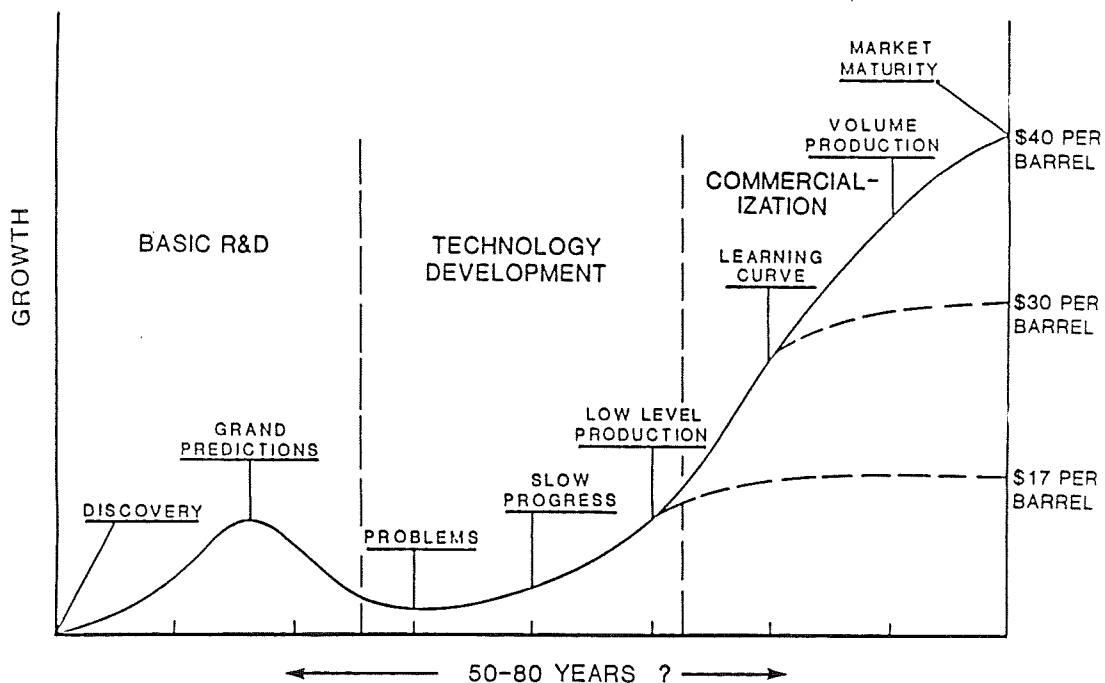
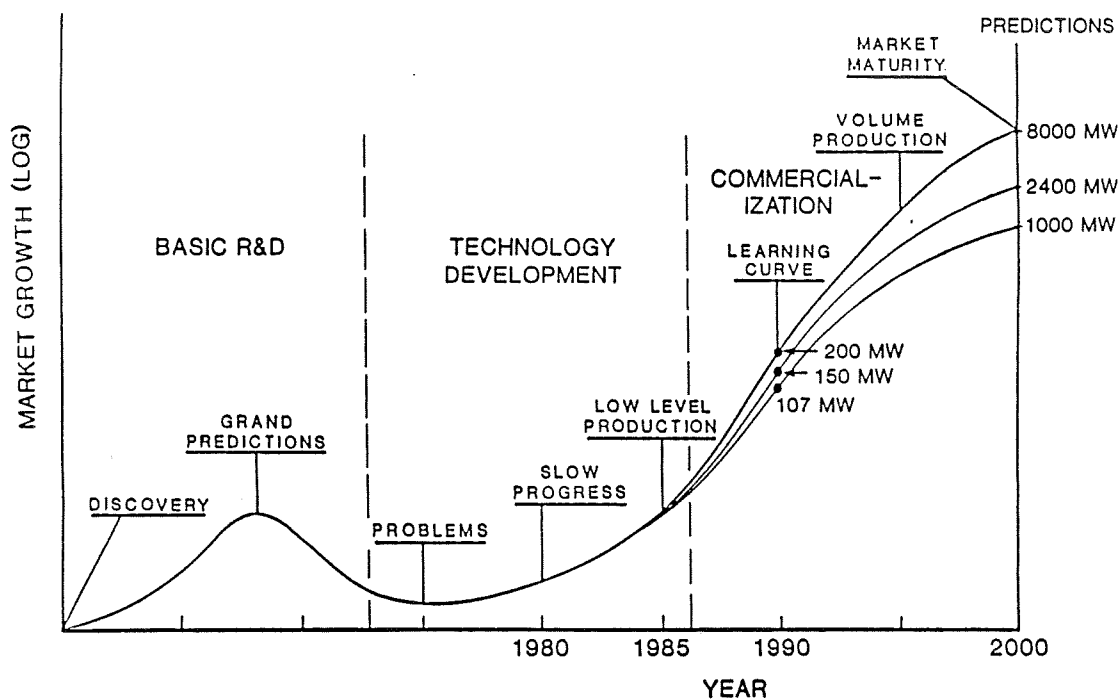
Utility Interest

- ALABAMA POWER
- ARIZONA PUBLIC SERVICE CO.
- AUSTIN MUNICIPAL POWER
- BOSTON EDISON
- CON. ED.
- EL PASO ELECTRIC
- EPRI
- FLORIDA P&L
- GEORGIA POWER
- NEW ENGLAND ELECTRIC
(MASS ELECTRIC)
- NEW YORK POWER AUTHORITY
- PG&E
- SAN DIEGO G&E
- SMUD
- SO. CAL. ED.
- TVA
- VIRGINIA ELECTRIC POWER

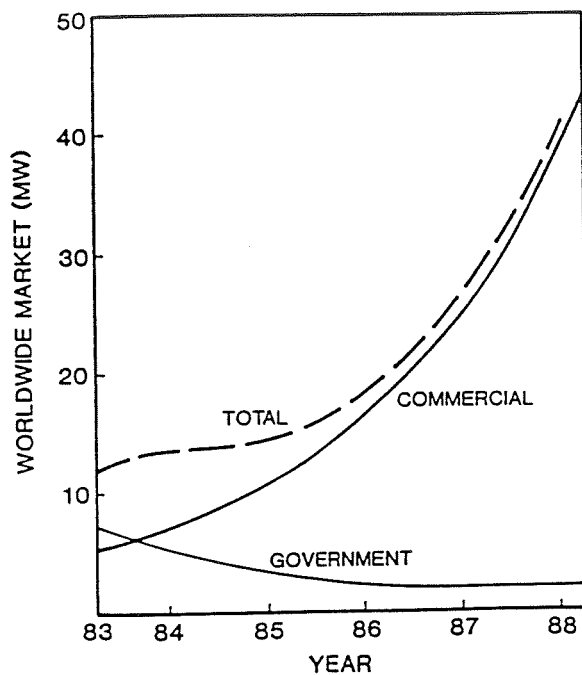
Utility Activities

- | | |
|----------------------|--------------------------------|
| ● PG&E | PVUSA |
| ● EPRI | CONCENTRATOR
MANUFACTURING |
| | THIN FILM RESEARCH
SUPPORT |
| | RIBBON |
| ● SO. CAL. ED. | THIN FILMS |
| | GaAs |
| ● AUSTIN | 300 kW |
| ● ALABAMA | MANUFACTURE
OF α -Si |
| ● NEES | GARDNER PROJECT |
| ● VIRGINIA | TEST PROGRAM |
| ● NUMEROUS UTILITIES | INSOLATION MONITORING |

PV Technology Commercialization



PV Market: Government Versus Commercial



Massachusetts

- MASS.PV CENTER
 - ASSIST INDUSTRY
 - TRAIN VISITORS
 - INFORMATION DISSEMINATION
- CENTER FOR EXCELLENCE
 - OPERATE NERES
 - DEFINING GOALS NOW
 - REMOTE APPLICATIONS STRESSED
 - INSULATION ISSUES
 - SANDIA ASSISTED
 - FUNDS IN JEOPARDY
- MASS.PUP PROGRAM

PLENARY SESSIONS

Massachusetts PUP

- \$1M
- MULTI-AGENCY
- APPLICATIONS
- COST EFFECTIVE
- CENTRALLY FUNDED
 - AGENCY ADMINISTERED

DOD — Marvroules

- MILITARY MUST BUY IF COMPETITIVE
- REPORT (Draft)
 - 200 SYSTEMS
 - 21,000 POTENTIAL APPLICATIONS
- TRI-SERVICE
 - NAVY LEAD
 - ADVISORY GROUP
- EDUCATION

DOE Involvement

- R&D PROGRAM
- SUPPORT TO OTHER AGENCIES
- DOD
- CORECT
- MANAGEMENT STRUCTURE
 - CONSOLIDATED

Office of Technology Assessment

PV

- GREATER FLEXIBILITY
 - MODULAR NATURE
 - LOWER INSTALLATION COST
 - SHORTER LEAD-TIMES
- CLEAN AND EFFICIENT
- ABUNDANT SOURCE ENERGY
- MAJOR CONTRIBUTIONS BY YEAR 2000
- DEMONSTRATED FEASIBILITY
- ECONOMIES OF SCALE WILL REDUCE COST

NEEDS

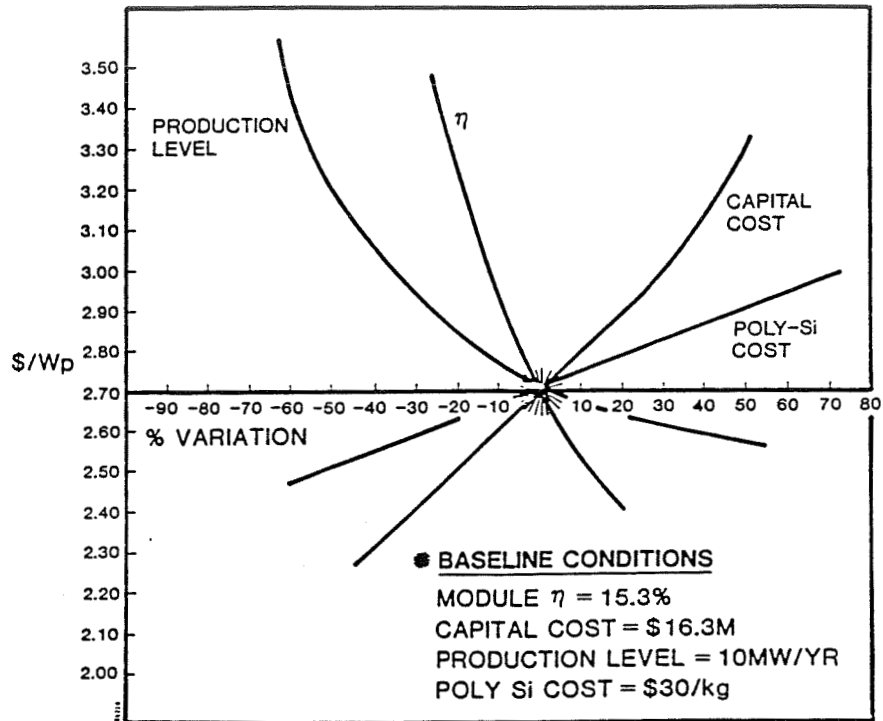
- FAVORABLE TAX TREATMENT IMPORTANT
- COOPERATION OF GOVT/IND/UTIL/LABS
- UTILITIES MUST HAVE FULL PURPA BENEFITS

SOURCE: Office of Science and Technology:
"New Electric Power Technologies"
July, 1985 OTA-E-246

"In a policy reversal, New Hampshire's largest utility says that it will buy electricity from small water, solar, wind and cogeneration power producers as an alternative to reviving plans to complete Unit 2 of the Seabrook nuclear power plant."

The Boston Globe - April 21, 1986

Sensitivity Analysis of Module Manufacturing Costs



Cost of Manufacture: EPRI

- 25 MW LEVEL
- X-Si: \$1.90/Wp
- α -Si MODULES: \$1.15/Wp
- CONCENTRATORS: \$1.40/Wp

ALL TECHNOLOGIES LOOK GOOD
WITH SCALE UP

SILICON MATERIAL TASK REVIEW

CONSULTANT

J. H. Lorenz

Introduction

1974/75 FLAT-PLATE SOLAR ARRAY PROJECT WAS FUNDED

IMPORTANT PART OF THE RENEWABLE ENERGY PLAN

SILICON WAS SELECTED AS IT WAS THE ONLY FIELD TESTED
PV MATERIAL

POLYSILICON, AS THE BASE MATERIAL FOR SEMICONDUCTORS, WAS
AVAILABLE, SO ALL FSA TASKS COULD BEGIN WORK

SEMICONDUCTOR POLYSILICON SOLD FOR \$60 - \$70 PER KILOGRAM
WITH IMPURITIES IN THE PARTS PER MILLION

SOLAR CELLS COULD BE MADE FROM "LESS PURE" SILICON
PROBLEM WAS TO DEFINE THIS TERM AND
DEVISE PROCESSES TO MAKE THE DESIRED SILICON

GOALS OF THE SILICON MATERIAL TASK WERE:

TO ESTABLISH SILICON MATERIAL PROCESSES WITH A PURITY
ADEQUATE FOR THE PV CELL REQUIREMENTS

WITH A MARKET PRICE OF \$10 PER KILOGRAM (1975 \$)

(\$19 IN 1985 \$)

SCALABLE TO 1000 TONS/YEAR PRODUCTION PLANTS

PRECEDING PAGE BLANK NOT FILMED

FSA Project: Silicon Material Task

OBJECTIVES:

TO EVALUATE TECHNOLOGIES, NEW AND OLD
TO DEVELOP THE MOST PROMISING TECHNOLOGIES
TO ESTABLISH PRACTICALITY OF THE PROCESSES TO MEET
PRODUCTION, ENERGY USE, AND ECONOMIC CRITERIA
TO DEVELOP AN INFORMATION BASE ON IMPURITIES IN
POLYSILICON AND TO DETERMINE THEIR EFFECTS ON
SOLAR CELL PERFORMANCE

APPROACH:

1. DETERMINE PROCESS FEASIBILITY

16 CONTRACTS WERE ISSUED: TO INDUSTRY, UNIVERSITIES AND
NON-PROFIT GROUPS TO WORK ON PROCESSES, IMPURITIES AND
SPECIFICATIONS -- ON A LABORATORY SCALE

2. MILESTONES WERE SET - FOR FORCED SELECTION OF THE PROCESSES

TO FUND THE MOST PROMISING THROUGH PROCESS DEVELOPMENT
TO DEMONSTRATE PRACTICALITY OF THE PROCESSES
TO MEET SCALE-UP, ENERGY USE AND ECONOMIC CRITERIA

3. ESTABLISH TECHNICAL READINESS OF THE INTEGRATED PROCESS

THROUGH YEAR LONG OPERATION OF A PILOT PLANT --
TO OBTAIN OPERATING DATA, OPTIMIZE DESIGN PARAMETERS,
CONFIRM PRODUCT PURITY

PLENARY SESSIONS

FSA Project: Silicon Material Task (Cont'd)

4. FUND SUPPORT PROGRAMS FOR THE TASK:

ON HYDROCHLORINATION OF SILICON

(FIRST STAGE OF UCC PROCESS)

DR. J. MUI AT MIT AND LATER HIS OWN COMPANY

DATA ON MATERIALS, CATALYSTS, RATES

ON ACADEMIC STUDIES OF SILICON AEROSOLS AND FLUIDIZED BED

MODELS AT JPL, CAL TECH AND WASHINGTON UNIVERSITY

TECHNICAL CONSULTANTS TO AID THE CONTRACTORS AND JPL

ON IMPURITY EFFECTS IN SILICON

PLENARY SESSIONS

Contractors for Process Development on Silicon

A. FOR SEMICONDUCTOR GRADE SILICON

HEMLOCK SEMICONDUCTOR CORP.	DICHLOROSILANE CVD
J C SCHUMACHER CO.	BROMOSILANE CVD/FB
UNION CARBIDE CORP.	SILANE PROCESS
JET PROPULSION LAB.	PYROLYZING SILANE

B. FOR SOLAR GRADE SILICON

AEROCHEM RESEARCH LABS.	SILANE/SILICON PLASMA JET
	Na/HALIDE FLAME IMPACTION REACTOR
BATTELLE COLUMBUS LABS.	Zn/SIL TET
DOW CORNING CORP.	DIRECT ARC FURNACE
MOTOROLA INC.	SiF ₂ TRANSPORT
SRI INTERNATIONAL INC	Na/SIL TET
TEXAS INSTRUMENTS INC.	CARBOTHEMIC REDUCTION SiO ₂
	ROTARY CHAMBER/TCS/FB
WESTINGHOUSE ELECTRIC CORP.	PLASMA ARC HEATER PROCESS NA/SIL TET

PLENARY SESSIONS

United States Polysilicon Production Capacity (Metric Tons)

	1983	1984	1985	1986	1987	1988	1990
1. Union Carbide Washougal Moses Lake	50 -	100 -	120 700	120 1200	120 1600	120 2400	120 2400
2. Hemlock (SEH, Mitsubishi)	1000	1200	1200	1400	1400	1400	2000
3. Ethyl Corp	1/86 \$45M	Houston			500	1000	1000
4. Monsanto	230	230	230	230	230	230	-
5. Motorola	100	100	100	100	100	-	-
6. Texas Ins.	350	350	350	350	-	-	-
7. Nippon Kokan	140	200	200	200	200	200	-

PILOT PLANTS

1. Great Lakes	-	-	-	20	20	20	1000
2. Schumacher Oceanside	-	-	-	40	40	1000	1000
3. Bunnington Rochester	-	-	-	-	-	-	1000

PLANNING

1. Alcan, Canada
2. Pasadena Group
3. ALCOA

PLENARY SESSIONS

Accomplishments for the Project

- o RESULTED IN THE DEVELOPMENT AND COMMERCIALIZATION OF A NOVEL PROCESS FOR MAKING SILANE AND HIGH QUALITY SEMICONDUCTOR GRADE POLYCRYSTALLINE SILICON
--THE UNION CARBIDE SILANE TO SILICON PROCESS
- o ATTRACTED WORLD WIDE ATTENTION TO THE JPL/DOE PROJECT--DUE TO THE QUALITY OF THE PROCESSES IN THE TASK
- o UCC PROCESS RECEIVED 12 NASA SPECIAL RECOGNITION AWARDS
CHIEF DESIGN ENGINEER (BILL BRENNEMAN) WAS HONORED WITH 1985 PIONEER AWARD OF THE AMERICAN INSTITUTE OF CHEMISTS
- o SILANE PART OF THE UCC PROCESS WAS COMPLETED THROUGH THE FEASIBILITY VERIFICATION IN A 100 TON PER YEAR PILOT PLANT
- o ASSURED ADEQUATE CAPACITY IN THE U. S. FOR PURE SILANE FOR THE DOE/SERI AMORPHOUS SILICON R & D PROGRAM AND FOR FUTURE PRODUCTION
- o PROVIDED A TECHNOLOGY BASE FOR POSSIBLE DEPOSITION PROCESSES -- EVEN THOUGH THE GOAL OF \$10/KG SILICON WAS NOT REALIZED: UCC & JPL ON FLUIDIZED BEDS;
CAL TECH ON FREE-SPACE DEPOSITION PARTICLE GROWTH
- o MADE THE DIRECTORS OF UCC TAKE NOTICE -- RESULTING IN THE COMMERCIALIZATION WITH A 1200 TON PER YEAR PLANT

PLENARY SESSIONS

Accomplishments for the Project (Cont'd)

- o CONFIRMED, WITH HEMLOCK'S WORK, THAT DICHLOROSILANE HAS SOME ADVANTAGES OVER TCS DEPOSITION
- o DEFINED THE EFFECTS OF IMPURITIES IN SILICON ON SOLAR CELL PERFORMANCE (WESTINGHOUSE AND MONSANTO)
- o PRESENTED THE RELATIVE ECONOMICS OF THE POTENTIALS OF THE SILICON PROCESSES, INCLUDING COMPARISON WITH THE TCS/CVD SEMICONDUCTOR PROCESS

PLENARY SESSIONS

Accomplishments for Electronics in General

- o HELPED PUT THE U. S. IN POSITION FOR A LEADERSHIP ROLE IN PURE POLYSILICON PRODUCTION

	POLYSILICON CAPACITIES	TONS PER YEAR
	<u>UNITED STATES</u>	<u>WORLD</u>
1976	950	1804
1986	3600 (1200)	E 3120 J 1200

- o CATALYZED THE INTEREST OF COMPANIES TO GET INTO SILICON
 - SCHUMACHER HAS A 40 TON PILOT PLANT
 - ETHYL CORP. HAS ANNOUNCED A PILOT PLANT BASED ON SILANE
 - FOUR OTHER COMPANIES IN U S ARE CONSIDERING POLYSILICON
- o CONFIRMED HIGH PRESSURE, HIGH TEMPERATURE CHEMICAL REACTIONS COULD BE ENGINEERED
- o DETAILED IN THE HEMLOCK CONTRACT A POSSIBLE IMPROVEMENT OF THE TCS/CVD PROCESS -- BY USING DICHLOROSILANE AND THE RECYCLING OF THE SIL TET (1ST STEP IN UCC PROCESS)
- o UCC PROCESS HAS THE POTENTIAL TO PROVIDE THE MOST PURE POLYSILICON FOR PV OR SEMICONDUCTOR USE
- o PROVIDED A PURE SOURCE OF SILANE FOR ALL USES AND ASSURED THE U. S. A LEADERSHIP ROLE IN SILANE
- o SPURRED CURRENT SILANE SUPPLIERS TO IMPROVE THEIR QUALITY FOR BOTH PV AND SEMICONDUCTOR USE

PLENARY SESSIONS

Yet to be Done

A. TO MEET THE GOAL

(GOVERNMENT FUNDING WILL BE NEEDED FOR THIS WORK)

FSA PROJECT DID NOT ACHIEVE ITS GOAL -- NOR DID THE MATERIALS TASK

TO ACHIEVE THE LOW COST SILICON, A LOW COST DEPOSITION PROCESS MUST BE FULLY DEVELOPED -- THE FLUIDIZED BED TECHNIQUE LOOKS PROMISING, BUT NEEDS ENGINEERING WORK ON MATERIAL OF CONSTRUCTION, OPTIMUM CONDITIONS FOR GROWTH AND DETERMINATION OF PRODUCT PURITY

THE FREE SPACE REACTOR DEPOSITION COULD BE LOWEST COST, IF THE PARTICLES COULD BE GROWN TO A LARGER SIZE.

B. TO EXPAND THE USE OF THE TECHNOLOGIES

(INDUSTRY WILL DO THIS WORK)

OTHER COMPANIES HAVE OR ARE LOOKING AT THE TECHNOLOGY IN THE FIELD OF ELECTRONICS

AVAILABILITY OF PURE SILANE IN LARGE VOLUMES WILL ENCOURAGE INVESTIGATION OF OTHER USES

INTEGRATION OF PARTS OF THESE PROCESSES INTO THE ELECTRONICS AREA HYDROGENATION, DICHLOROSILANE

PLENARY SESSIONS

Conclusions

- o PART OF THE OBJECTIVES OF THE MATERIAL TASK WERE ACHIEVED
- o TECHNOLOGY DATA BASES WERE ESTABLISHED FOR THE UNFINISHED DEPOSITION WORK
- o THE U S HAS ENHANCED THEIR LEADERSHIP IN POLYCRYSTALLINE SILICON
- o TECHNOLOGY OF VALUE TO THE WORLD-WIDE ELECTRONICS INDUSTRY HAS BEEN ESTABLISHED AND PUBLISHED
- o THE MATERIAL TASK IS A PRIME EXAMPLE OF THE PROPER USE OF GOVERNMENT FUNDING OF HIGH COST, HIGH RISK RESEARCH AND DEVELOPMENT

TECHNICAL PROGRESS IN SILICON SHEET GROWTH UNDER DOE/JPL FSA PROGRAM 1975-1986

MOBIL SOLAR ENERGY CORPORATION

J. P. Kalejs

Topics of Presentation

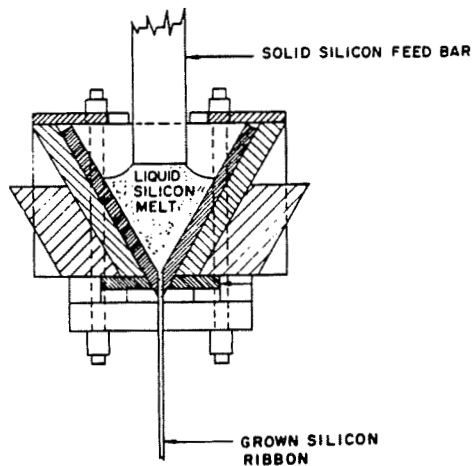
- SILICON SHEET TECHNOLOGIES - THEN AND NOW:
 - 1975-77: TECHNOLOGICAL FEASIBILITY STUDIES
 - 1978-80: PROCESS SELECTION
 - 1981-86: ECONOMIC FEASIBILITY DEMONSTRATIONS
- FUTURE POTENTIAL/R&D REQUIREMENTS

Sheet and Ingot Technologies Supported Under ERDA/FSA Programs 1976-1986

	1976	1980	1986
Sheet	EFG (Mobil Tyco)	EFG (Mobil Solar)	EFG (industry; full scale pilot plant)
	CAST (IBM)		
	Inverted Stepanov (RCA)		
	Web Dendritic (U. of S. Carolina)	WEB (Westinghouse, 1977)	WEB (industry; start-up pilot plant)
	RTR (Motorola)		
	SOC (Honeywell)	SOC (Honeywell)	
	CVD-Glass (Rockwell)		
	CVD-Si (GE)		
	Hot Forming (U. of Pennsylvania)		
		LASS (EMC, 1979) (SERI)	[Available to industry]
Ingots		Vacuum Die Casting (ARCO, 1979)	
		ESP (Ciszek, 1979) (SERI)	
		ESR (Sachs, 1979) (SERI)	[Available to industry]
	HEM (Crystal Systems)	HEM (Crystal Systems)	[Industry; material for sale]
		Advanced CZ (HAMCO/KAYEX, 1977)	[Industry; equipment for sale]
		" (Siltec, 1977)	
		" (Texas Instruments, 1977)	
		" (Varian, 1977)	
		Ingot Casting (UCP) (Semix, 1980)	[Industry]

Technical Progress/Results 1975-1977
Process Selection 1978-1980

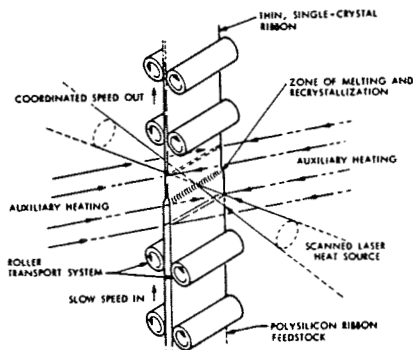
Inverted Stepanov



FEASIBILITY NOT DEMONSTRATED

- SUITABLE DIE MATERIAL NOT FOUND,
- PROCESS STABILITY NOT DEMONSTRATED

Ribbon-to-Ribbon (RTR)



ACCOMPLISHMENTS

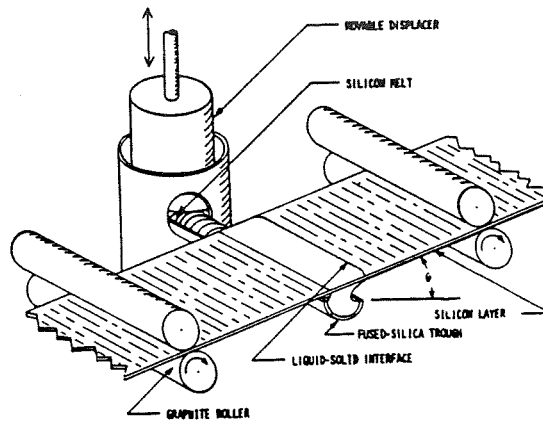
- CONTINUOUS GROWTH OF 5 CM WIDE RIBBON UP TO 25 CM LENGTH OF FEEDSTOCK DEMONSTRATED IN MULTIPLE RIBBON FORMAT UP TO 5-7 CM/MIN.

CONCERNS

- SUPPLY OF SUITABLE POLYRIBBON FEEDSTOCK,
- FEEDSTOCK WITH SUBSTRATE CONTAMINATION.

Silicon on Ceramic (SOC)

ORIGINAL PAGE IS
OF POOR QUALITY

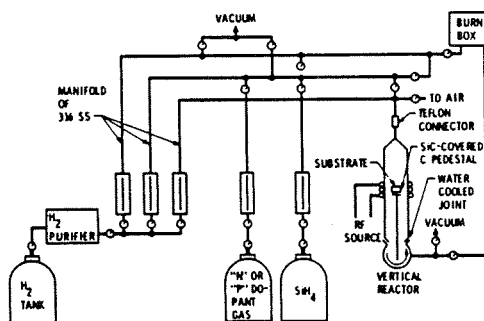


FEASIBILITY NOT DEMONSTRATED

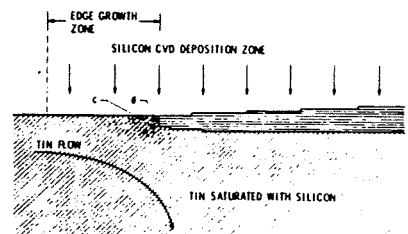
- SUBSTRATE MATERIAL CONTAMINATION NOT UNDER CONTROL.
- DIMENSIONAL CONTROL OVER LARGE AREAS (10 CM WIDE) AT HIGH SPEEDS (30 CM/MIN) A PROBLEM.
- HIGH SPEEDS OF 10-20 CM/MIN AND SMALL GRAINS MAY IMPAIR EFFICIENCY (USUALLY LESS THAN 10%).

Chemical Vapor Deposition (CVD)

GLASS SUBSTRATE



SI-SN SYSTEM

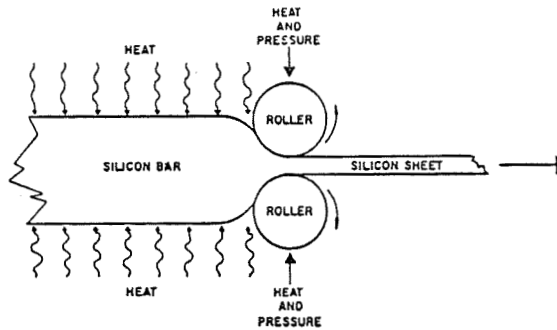


FEASIBILITY NOT DEMONSTRATED

- NO GEOMETRICAL CONTROL OF SHEET DIMENSIONS.
- GRAIN SIZE TOO SMALL, NUCLEATION UNCONTROLLED.

Hot Forming

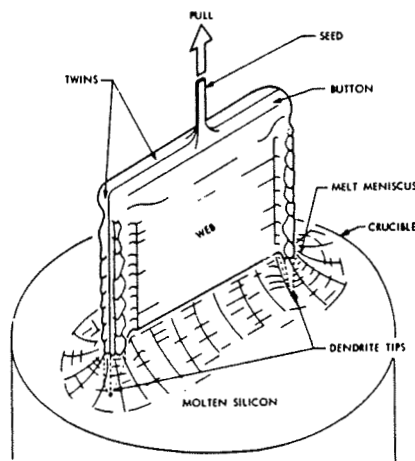
PROCESS: I. COMPRESSION OF POLYSILICON.
II. ANNEAL TO INCREASE GRAIN SIZE.



FEASIBILITY NOT DEMONSTRATED

- LARGE GRAIN RECRYSTALLIZATION TOO SLOW.
- CONTAMINATION EFFECTS UNDETERMINED.

WEB Dendritic (WEB)



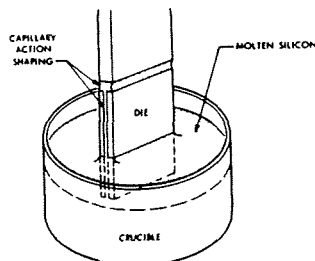
ACCOMPLISHMENTS

- CONTINUOUS GROWTH OF WEB OF 3 CM WIDTH, AT 1-2 CM/MIN AND 150 MICRON THICKNESS MADE ROUTINE IN SINGLE RIBBON FURNACES. MELT REPLENISHMENT DEMONSTRATED.
- MAXIMUM EFFICIENCIES OF 15%.

CONCERNS

- LONG TERM STABILITY/REPRODUCIBILITY.
- GROWTH SPEED/WIDTH (AREAL RATE) LIMITATIONS COMMON TO ALL VERTICAL SHEET GROWTH TECHNIQUES.

Edge-Defined Film-Fed Growth (EFG) Capillary Action Shaping Technique (CAST)



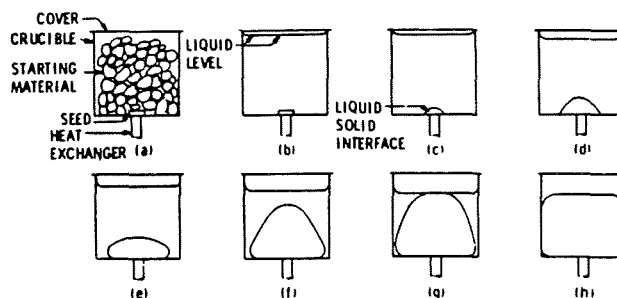
ACCOMPLISHMENTS (EFG)

- CONTINUOUS GROWTH OF UP TO 10 CM WIDE RIBBON UP TO 3 CM/MIN AND 250 MICRONS THICKNESS IN MULTIPLE (x4) MACHINE FORMAT/MELT REPLENISHMENT MADE ROUTINE.
- AVERAGE CELL EFFICIENCIES OF THE ORDER OF 9% (NO H₂ PASSIVATION).

CONCERNS

- MULTIPLE MACHINE COMPLEXITY, MATERIAL INHOMOGENEITY HAMPER ROUTINE OPERATION AND REPRODUCIBILITY.
- HIGH H_{EFF} EFG (CARTRIDGE CONCEPT) OPERATES CLOSE TO REGION OF THERMO-CAPILLARY INSTABILITY.
- DIE MATERIAL REACTIVITY.
- VERTICAL EFG LIMITED TO 2-3 CM/MIN GROWTH SPEED BY CREEP
 - AREAL RATE LIMITATION COMMON TO ALL VERTICAL SHEET GROWTH TECHNIQUES.

Heat Exchanger Method (HEM)



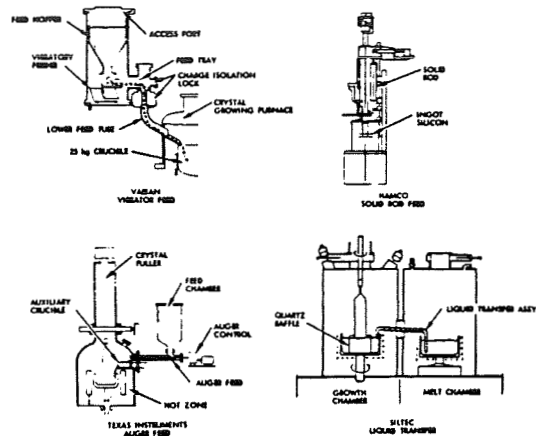
ACCOMPLISHMENTS

- LARGE SINGLE CRYSTAL INGOT (33 x 33 x 18 cm³, 45 KG) SOLIDIFICATION DEMONSTRATED AT 1.25 KG/HR.
- HIGH (90%) SINGLE CRYSTAL YIELD, HIGH (UP TO 15%) EFFICIENCIES.

CONCERNS

- IMPROVED SLICING TECHNIQUES WITH INCREASED SPEED, REDUCED KERF LOSS NOT AVAILABLE.
- HIGHER SINGLE CRYSTAL YIELDS (PERFECTION) OBTAINED AT SLOWEST SOLIDIFICATION RATES.

Continuous Czochralski



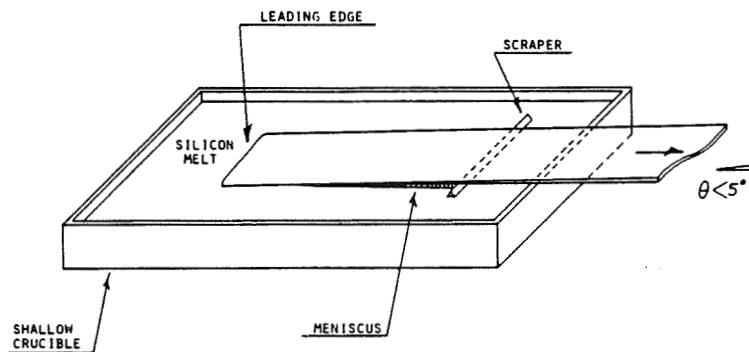
ACCOMPLISHMENTS

- MULTIPLE INGOT GROWTH ESTABLISHED (150 KG), UP TO 15 CM DIAMETER.

CONCERNS

- REDUCED YIELD DUE TO POLYCRYSTALLINITY.
- FEASIBILITY OF HIGH THROUGHPUT WAFERING.
- THROUGHPUT LIMITS IN RANGE 1.5 KG/HR.

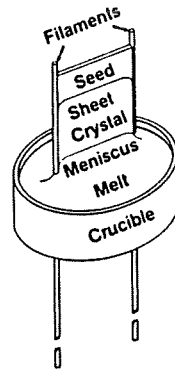
New Developments 1978-1981 Low-Angle Silicon Sheet (LASS)



FEASIBILITY NOT DEMONSTRATED

- GROWTH RATES OF 30-60 CM/MIN ACHIEVED FOR SHORT LENGTHS.
- THICKNESS/DENDRITE CONTROL PARAMETERS NOT ESTABLISHED.
- LONG TERM GROWTH STABILITY UNTESTED.

Edge Supported Pulling (ESP) Edge Stabilized Ribbon (ESR)



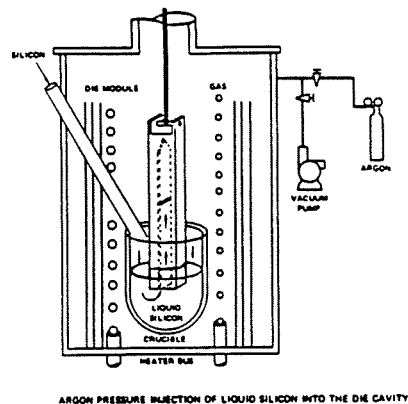
ACCOMPLISHMENTS

- PROCESS STABILITY/EDGE DEFINITION FOR RIBBON GROWTH ACHIEVED WITHOUT NEED OF DIE.

CONCERNS

- LONG TERM GROWTH REPRODUCIBILITY.
- IMPACT OF EDGE STABILIZERS ON QUALITY, YIELD.
- GROWTH SPEED/WIDTH (AREAL RATE) LIMITATIONS COMMON TO ALL VERTICAL SHEET TECHNIQUES.

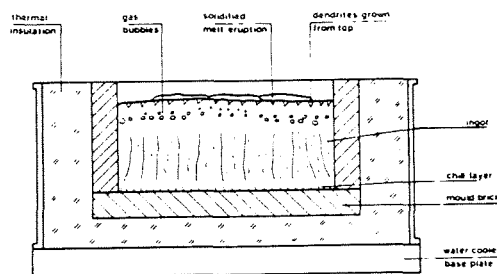
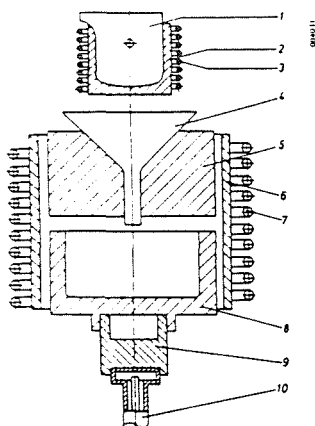
Vacuum Die Casting



FEASIBILITY NOT DEMONSTRATED

- MOLD CONSTRUCTION MATERIAL A PROBLEM.
- STRESS CONTROL PARAMETERS UNDETERMINED, GRAIN NUCLEATION NOT CONTROLLED.

SEMIX Ingot Casting (UCP)



(WACKER PROCESS ILLUSTRATIONS:
HELMREICH ET AL. 1980, 1982)

ACCOMPLISHMENTS

- SOLAR CELL EFFICIENCIES OF 13-14% OVER 100 CM² AREAS.
- 20 CM X 20 CM X 10 CM INGOTS.

CONCERNS

- THROUGHPUT LIMITATIONS DUE TO CONSTITUTIONAL SUPERCOOLING.
- MATERIAL INHOMOGENEITY (PROCESS YIELD).
- WAFERING RATE AND KERF LOSS FACTORS.

Silicon Sheet Technologies 1986 and Beyond

EFG

(CLOSED SHAPE POLYGONS)

WEB

(SINGLE RIBBON)

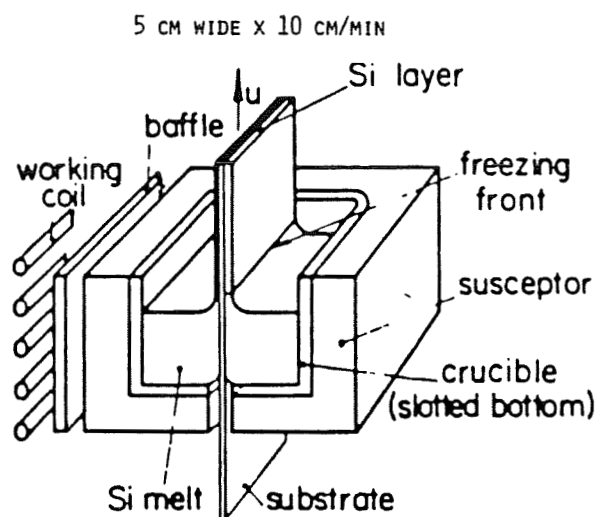
AND

INCLINED INTERFACE SHEET GROWTH

- LASS - EMC (USA)
- RAD - CGE (FRANCE)
- HSW - SIEMENS (W. GERMANY)
- RQ - TOHOKU (JAPAN)
- ARCO (USA)
- RAFT - WACKER (W. GERMANY)

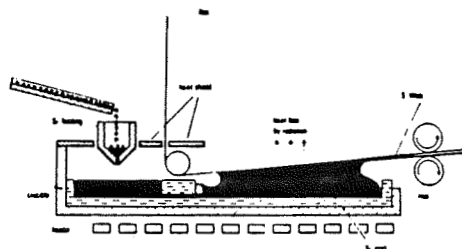
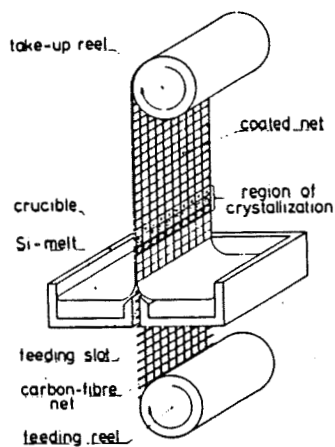
ALL SINGLE RIBBON TECHNIQUES

High Throughput Single Ribbon RAD (CGE)



High Throughput Single Ribbon HWS (Siemens)

6 CM WIDE X 100 CM/MIN



1986 Status/Future Potential
EFG
(Closed Shape Polygons)

- STATUS
- AREAL OUTPUT OF CURRENT NONAGON AT
(9) x (5 CM WIDE x 2.2 CM/MIN) = 100 CM²/MIN.
 - LARGE (~45 CM²) CELL EFFICIENCIES OF 13-15%.
 - BEST CELL (45 CM²) IS 15.1%.
- CONCERNS
- CUTTING/YIELD LIMITATIONS (MATERIAL STRENGTH).
 - IMPROVEMENTS IN PASSIVATION OF MICRODEFECTS.
 - PRODUCTIVITY LIMITATIONS DUE TO STRESS AND DIE MATERIAL DETERIORATION.

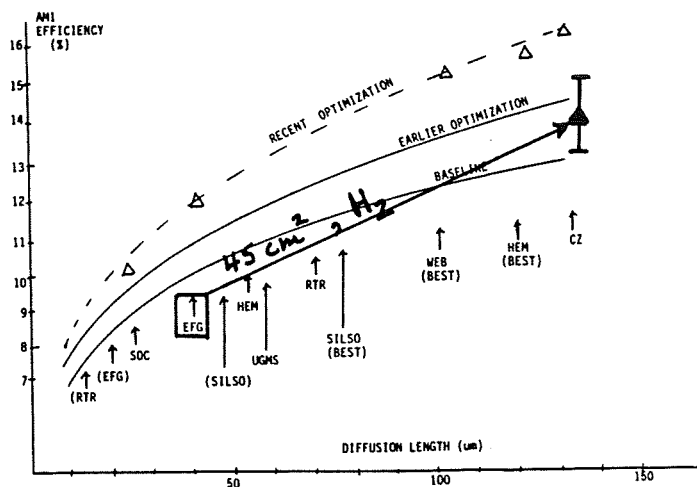
1986 Status/Future Potential (Cont'd)
WEB
(Single Ribbon)

- STATUS
- AREAL OUTPUT OF SINGLE CRYSTAL FURNACES AT
4 CM WIDE x 1.5 CM/MIN = 6 CM²/MIN (8.5 CM²/MIN BEST).
 - LARGE BATCH (~25 CM²) CELL EFFICIENCIES BEST AVERAGE 14%.
 - BEST CELL (4 CM²) 17.3%.
- CONCERNS
- AREAL OUTPUT LIMITATIONS MAY BE BELOW 10 CM²/MIN FOR
BEST (≥16%) CELLS.
 - LONG TERM GROWTH STABILITY.

Large-Area Silicon Sheet Task

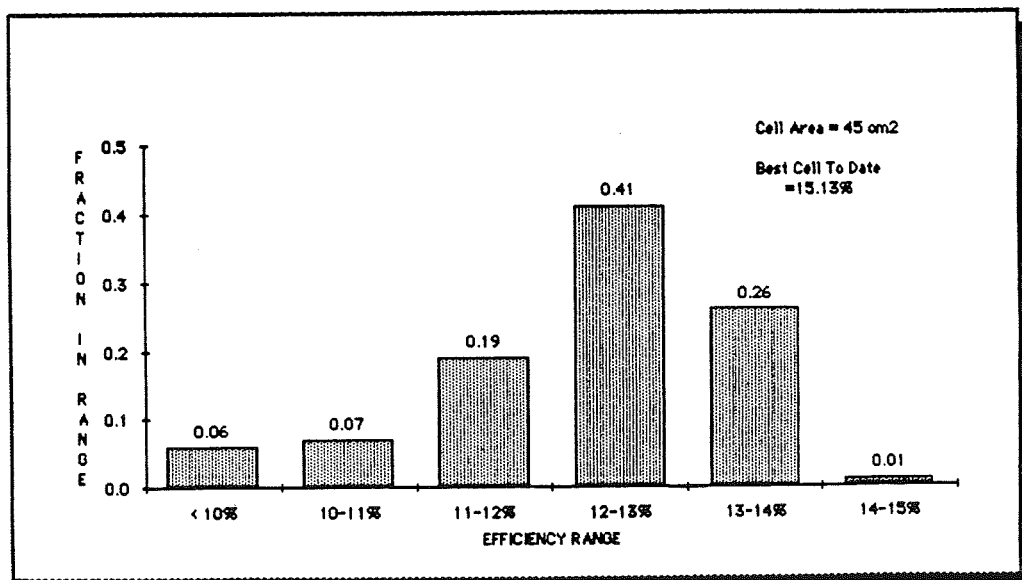
AM1 Efficiency vs Diffusion Length

FOR VARIOUS SILICON SHEETS,
BASELINE AND OPTIMIZED PROCESSING



ASEC - 16TH PIM, SEPTEMBER 1980

Current Cell Efficiency Distribution (Mean Value = 12.21%)



Key R&D Requirements to Meet Potential

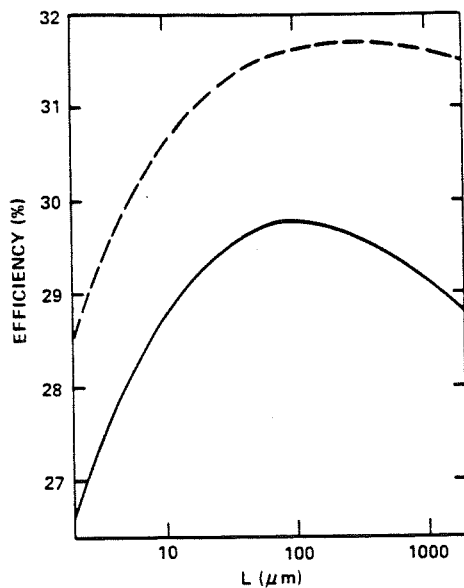
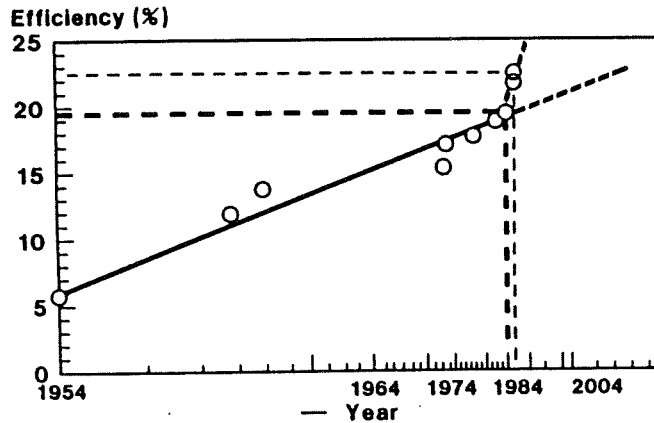
- UNDERSTANDING OF RECOMBINATION EFFECTS OF BASIC SILICON MICRODEFECTS AND PASSIVATION SCHEMES TO ACHIEVE 200-300 MICRON DIFFUSION LENGTHS CONSISTENTLY OVER LARGE AREAS.
- ACHIEVEMENT OF MEANS TO INCREASE HOMOGENEITY AND STRENGTH OF SILICON SHEET MATERIAL TO MAXIMIZE PROCESSING YIELDS.
- UNDERSTANDING OF INCLINED INTERFACE SOLIDIFICATION PROCESSES IN SPEED RANGE OF 5-100 CM/MIN
 - SINGLE RIBBON AREAL RATES UP TO 1000 CM²/MIN MAY BE POSSIBLE.

A REVIEW OF HIGH-EFFICIENCY SILICON SOLAR CELLS

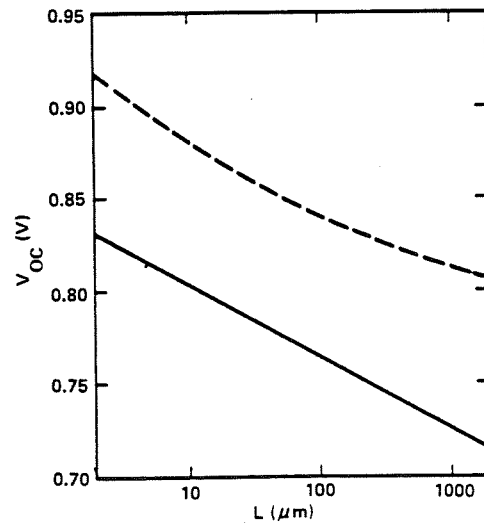
GEORGIA INSTITUTE OF TECHNOLOGY

A. Rohatgi

Historical Development of Silicon Solar Cells



Efficiency of silicon solar cells as a function of thickness for textured cells with back reflectors

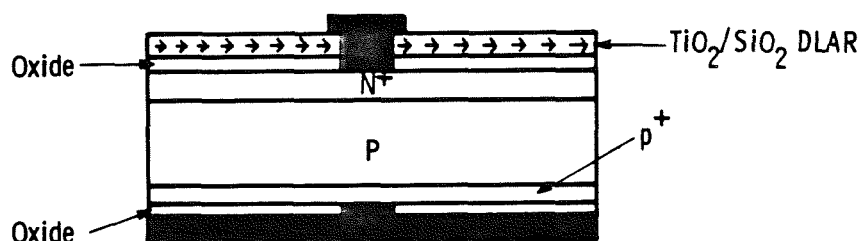


Open-circuit voltage as a function of cell thickness for radiative recombination only (dashed line) and for radiative, Auger and free carrier absorption (solid line).

Operating Parameters of Optimum (100 μ m) Silicon Solar Cell

V_{OC}	=	769 mV	710	740
I_{SC}	=	42.2 MA/cm ²	42.0	40.0
FF	=	0.890	0.84	0.85
$V_{MAX PWR}$	=	703 mV		
Efficiency	=	29.8%	25.0	25.1
		Theory	Practical	

Schematic Diagram of Westinghouse 18.3% Efficient Silicon Cell Design

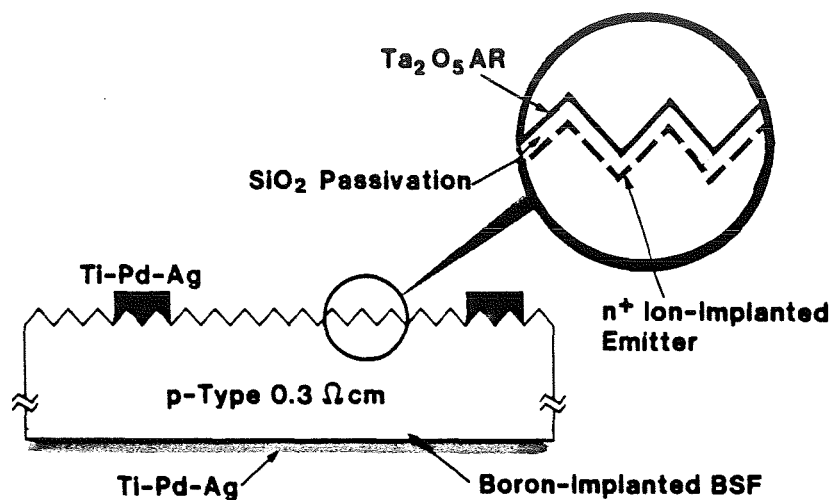


Effect of Oxide Passivation and Double-Layer AR Coating on 0.2 - 0.3 Ohm-cm Float-Zone Silicon Cells Fabricated by Conventional Metallization and Lithography

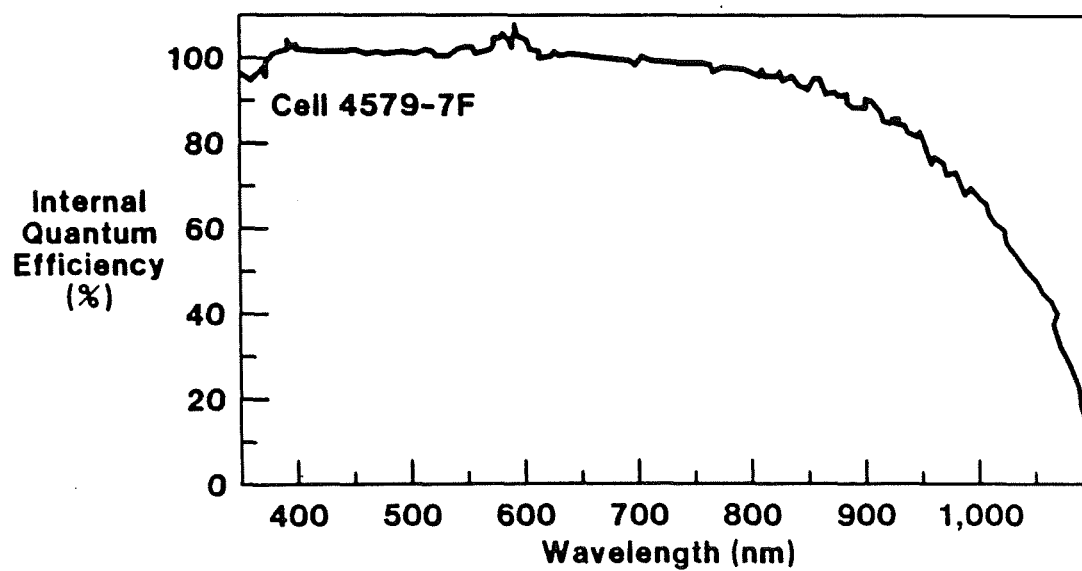
Cell ID	Short-Circuit Current J_{sc} mA/cm ²	Open-Circuit Voltage V_{oc} Volts	Fill Factor	Cell Efficiency %
<u>No Passivation and Single-Layer AR</u>				
Q-1	33.0	0.606	0.790	15.7
Q-2	33.0	0.607	0.790	15.8
Q-3	32.8	0.605	0.790	15.6
<u>Passivation and Single-Layer AR</u>				
14-1	34.0	0.621	0.800	16.9
14-2	34.0	0.620	0.809	17.0
14-9	34.1	0.620	0.805	17.1
<u>Passivation and Double-Layer AR</u>				
4-1	35.9	0.623	0.809	18.1
4-2	36.2	0.622	0.809	18.2
4-3	36.1	0.623	0.815	18.3

*AM1, 100 mW/cm² Illumination

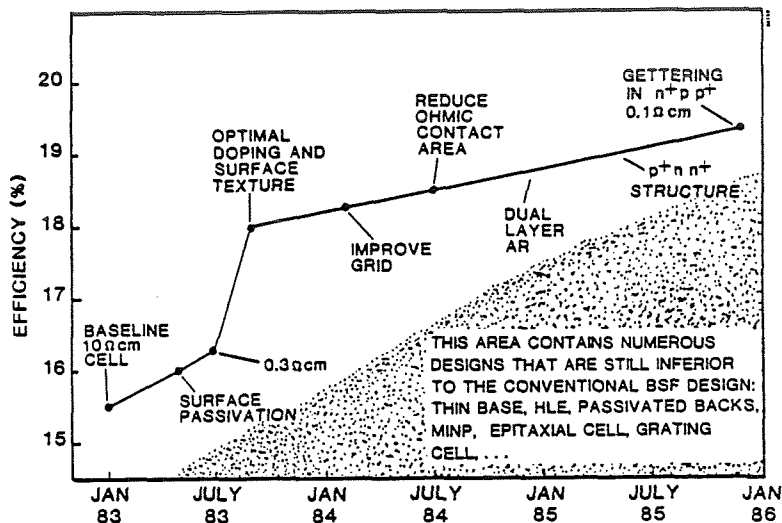
Spire Corporation's Approach to High-Efficiency Solar Cells



Internal Quantum Efficiency of Spire Corp. Cell

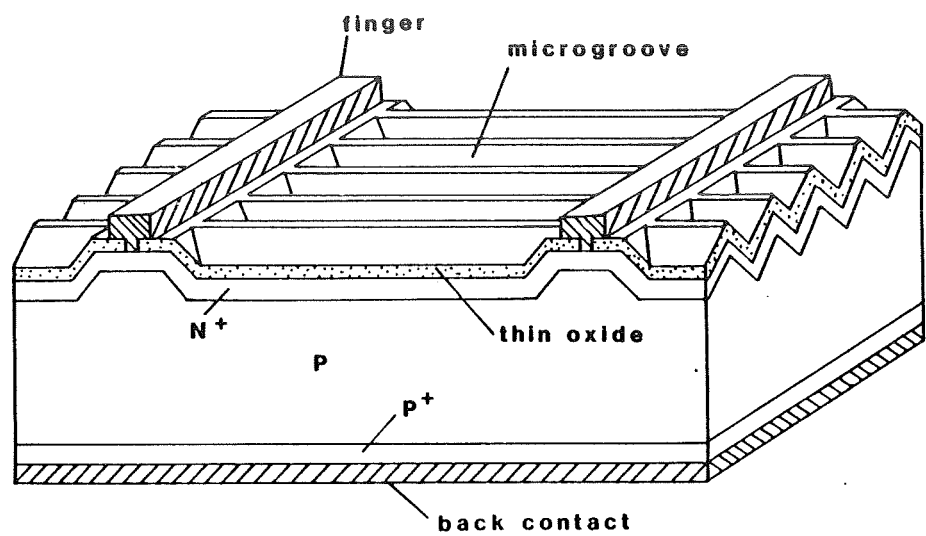


Spire Progress in Silicon Cell Design and Performance

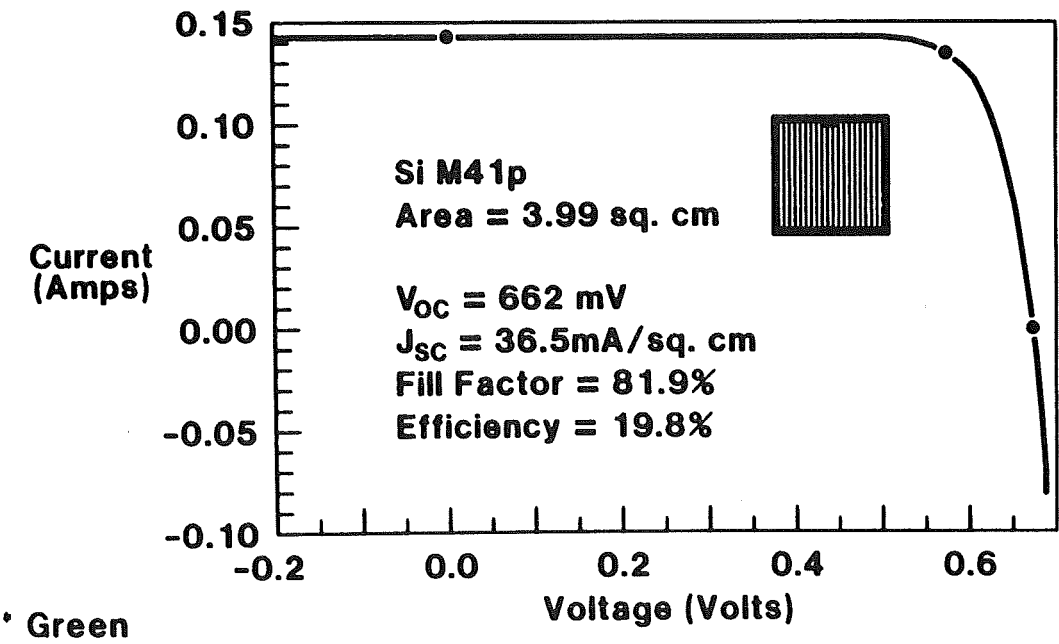


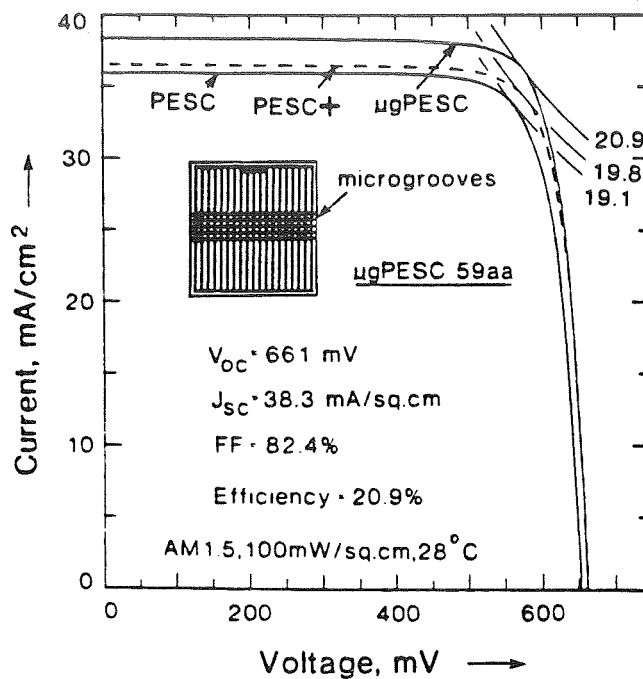
Lot: 4751
 Originator: LMG
 Date: 12/19/85
 Comment: Module Cells
 Resistivity: 1.50 Ω-cm
 Material: Si
 Thickness: 20 mils
 Surface: Tex
 AR Coat: TiO2
 Illumination: AM1.5 (100 mW/cm²)
 Temperature: 28 C
 Spire Corporation

Cell	Area (cm ²)	Voc (V)	Isc (A)	Jsc mA/cm ²	Pm (W)	Vm (V)	Im (A)	FF (%)	Eff. (%)
1	53.04	0.616	2.007	37.8	0.9639	0.498	1.934	78.0	18.2
2	53.04	0.615	2.020	38.1	0.9685	0.510	1.898	78.0	18.3
3	53.04	0.614	2.001	37.7	0.9686	0.511	1.895	78.9	18.3
4	53.04	0.608	1.964	37.0	0.9417	0.518	1.816	78.8	17.8
5	53.04	0.613	1.989	37.5	0.9702	0.521	1.862	79.6	18.3
6	53.04	0.612	1.987	37.5	0.9553	0.504	1.895	78.6	18.0
7	53.04	0.613	1.988	37.5	0.9656	0.504	1.915	79.3	18.2
8	53.04	0.608	1.948	36.7	0.9477	0.510	1.857	80.0	17.9
9	53.04	0.612	1.979	37.3	0.9625	0.519	1.856	79.5	18.1
10	53.04	0.615	2.002	37.7	0.9804	0.509	1.928	79.7	18.5
11	53.04	0.614	1.999	37.7	0.9787	0.519	1.885	79.7	18.5
12	53.04	0.606	1.934	36.5	0.9036	0.494	1.831	77.0	17.0
13	53.04	0.613	1.992	37.5	0.9730	0.509	1.912	79.6	18.3
14	53.04	0.610	1.962	37.0	0.9411	0.508	1.851	78.6	17.7
15	53.04	0.612	1.963	37.0	0.9531	0.510	1.868	79.3	18.0
16	53.04	0.610	1.961	37.0	0.9575	0.521	1.836	80.0	18.1
17	53.04	0.610	1.962	37.0	0.9554	0.524	1.824	79.8	18.0
18	53.04	0.613	1.972	37.2	0.9710	0.509	1.906	80.3	18.3
19	53.04	0.611	1.974	37.2	0.9625	0.507	1.900	79.8	18.1
20	53.04	0.611	1.971	37.2	0.9475	0.507	1.870	78.7	17.9
21	53.04	0.614	1.988	37.5	0.9699	0.514	1.888	79.4	18.3
22	53.04	0.607	1.944	36.6	0.9356	0.518	1.806	79.3	17.6
23	53.04	0.612	1.981	37.3	0.9613	0.511	1.880	79.2	18.1
24	53.04	0.613	1.991	37.5	0.9593	0.506	1.895	78.6	18.1
25	53.04	0.614	1.997	37.7	0.9755	0.520	1.877	79.6	18.4
mean		0.612	1.979	37.3	0.9588	0.511	1.875	79.2	18.1
std dev		0.002	0.021	0.4	0.0165	0.007	0.034	0.8	0.3
Delete:		12.							
mean		0.612	1.981	37.3	0.9611	0.512	1.877	79.3	18.1
std dev		0.002	0.019	0.4	0.0121	0.007	0.034	0.6	0.2



Output Current-Voltage Characteristics of an Improved PESC Cell Fabricated on a 0.2 Ω cm Substrate



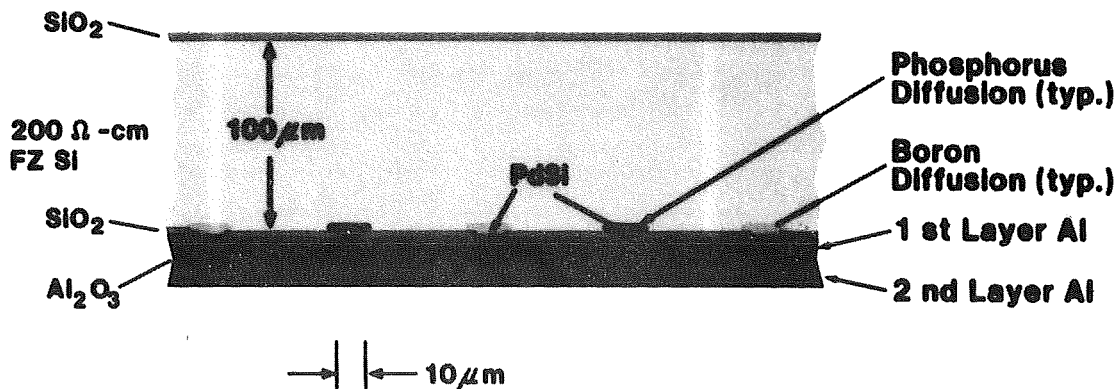


Output characteristics of a high efficiency microgrooved PESC solar cell measured under standard terrestrial test conditions (AM1.5, 100 mW/cm², 28°C) compared to those of previous generations of nongrooved PESC cells calibrated by the Solar Energy Research Institute (SERI), Colorado. The inset shows the contact design for the cell.

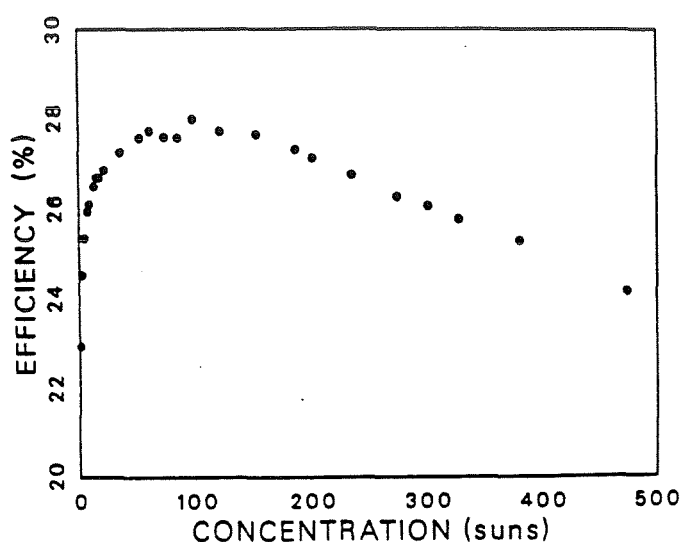
Green, Appl. Phys. Lett., Vol. 48, No. 3, 20 January 1986.

Stanford University Approach to High-Efficiency Solar Cells

Structure of the Point-Contact-Cell



Stanford Point Contact Cell FT11-3B



ONE SUN: $V_{OC} = 682 \text{ mV}$, $J_{SC} = 41.5 \text{ mA/cm}^2$,
 $FF = 0.785$, $EFF. = 22.2\%$

Evolution of High-Efficiency Silicon Solar Cell Performance Over
Recent Years as Measured by the Solar Energy Research Institute
(AM 1.5, 100 mW/cm^2 , 28°C)

Date	Cell Description ^a	V_{oc} (mV)	j_{sc} (mA cm^{-2})	FF (%)	η (%)
May 1983	ASEC	620	34.8	79.3	17.1
Aug. 1983	Westinghouse (4 Ωcm)	600	36.2	79.3	17.2
Sept. 1983	UNSW MINP (0.2 Ωcm)	641	35.5	82.2	18.7
Sept. 1983	SPIRE textured (0.2 Ωcm)	622	36.1	80.1	18.0
Dec. 1983	UNSW PESC (0.2 Ωcm)	653	36.0	81.1	19.1
May 1984	Westinghouse DLAR (0.1 – 0.2 Ωcm)	627	36.0	80.0	18.1
Feb. 1985	Westinghouse (0.3 Ωcm)	623	36.1	81.5	18.3
May 1985	UNSW PESC (0.25 Ωcm)	649	37.0	82.2	19.8
May 1985	UNSW PESC (0.2 Ωcm)	662	36.5	81.9	19.8
Oct. 1985	SPIRE textured (0.3 $\Omega\text{-cm n-type}$)	635	36.3	81.6	18.8
Jan. 1986	UNSW microgrooved PESC (0.1 Ωcm)	654	37.0	82.9	20.1
	UNSW microgrooved PESC (0.2 Ωcm)	661	38.3	82.4	20.9
April 1986	Stanford University (Point contact cell 500 $\Omega\text{-cm}$)	682	41.5	78.5	22.2

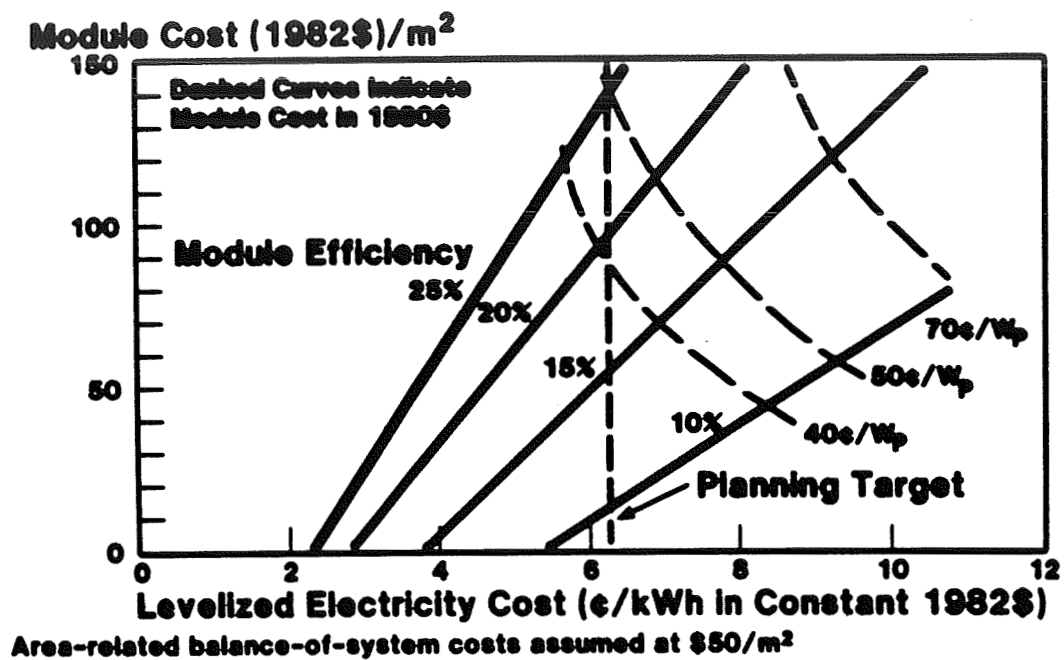
Silicon Material/Processing Research

- **More Sensitive And Better Methods To Detect And Identify Lifetime Limiting Traps In Silicon**
- **Role Of Carbon And Oxygen Content On Defect Formation And On Cell Performance**
- **Role Of Dopants And Their Interactions With Defects And Impurities**
- **Process Induced Defects**
- **Gettering, Defect Passivation Or Defect Elimination During Crystal Growth And Processing**

Measurements/Modeling Issues

- **Considerable Amount Of Ambiguity And Assumptions Are Involved In Modeling And Device Design**
- **All Parameters In Actual Device Are Not Known Accurately Enough To Do Precise Modeling; S , ΔV_G , T_A , N_{xj} , L**
- **Concern About The Values Of Minority Carrier Mobility And Diffusivity At High Doping Concentrations**
- **Need For Innovative Cell Design**

Flat-Plate PV Module Cost as a Function of Levelized Electricity Cost



ORIGINAL PAGE IS
OF POOR QUALITY

PROCESS RESEARCH AND DEVELOPMENT

JET PROPULSION LABORATORY

D. B. Bickler

Processing Overview

- 1975 to 1985 progress in low cost processing has reached a plateau
- Current emphasis upon high efficiency
- New cell designs; will need process development

Major Processing Categories

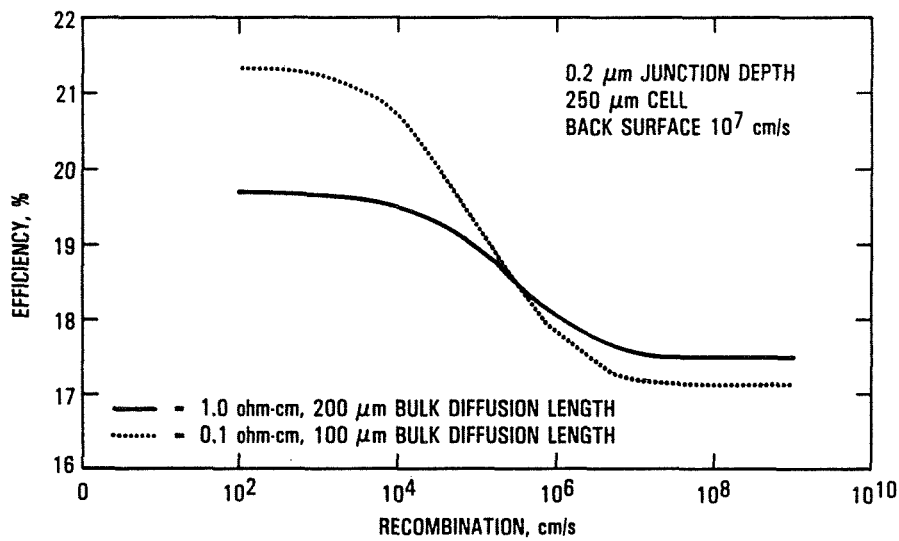
- **Surface preparation:** Damage removal etch
Passivation
A-R coat
BSR
- **Junction formation:** Diffusion
BSF
Edge isolation
- **Metallization:** Front and back
- **Assembly:** Cell interconnection
Encapsulation
Framing
Cable wiring
- **Sequences:** Relationships when combining individual processes

PRECEDING PAGE BLANK NOT FILMED

Surface Preparation

1975	1985	Future
Acid etch	Hydroxide etch	Hydroxide, then acid Etch
Polymer anti-reflection (A/R)	Texture with polymer or dielectric A/R	A/R matched to passivation
\$1.22/W	\$0.20/W	\$0.10 to \$1.00/W

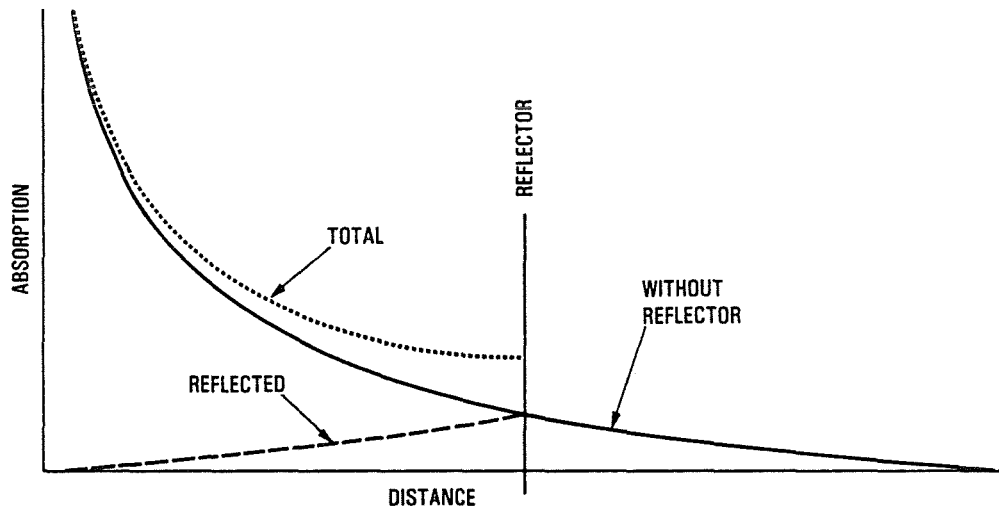
Efficiency Versus Front Surface Recombination Velocity*



When the front surface recombination velocity is brought below 10^5 cm/s, lower resistivity (0.1 Ω -cm) material outperforms 1.0 Ω -cm material even when the bulk diffusion length is less

*From E.I.H. Lin

Back Surface Reflector (BSR)



The use of a BSR is better than a cell of twice the thickness because the reflected photons are absorbed nearer to the junction. This means that bulk material with lesser bulk diffusion length can be utilized efficiently.

Junction Formation

1975	1985	Future
0.4 μm junction	0.3 μm	0.2 μm
Ohmic back	BSF	BSR*
\$0.43/W	\$0.28/W	\$0.15 to \$1.00/W

* Not a junction process; requires surface passivation.

Metallization

1975	1985	Future
Mask and Ni plate	Screen print Ag	Laser writing plate up
Solder dip		
Full back	Aluminum back with solderable pads	Gridded back
\$1.00/W	\$0.30/W	\$0.10 to \$0.20/W

Assembly

1975	1985	Future
CZ	CZ	Ribbon
PF = .6	PF = .8	PF = .9
Interconnectors	Redundant ribbons	Redundant ribbons
Soldered	Soldered	Welded
Potted in polymer	Bonded to glass	Bonded to glass
Metal back mount	Frame mounted	Framed in field
\$5.28/W	\$0.80/W	\$0.05 to \$1.00/W

Sequences

1975	1985	Future
Acid etch	Texture	Acid etch
Diffuse	Diffuse	Oxidize
Etch	BSF	Mask front
A-R coat	Clean	Etch
Mask	Mask	Diffuse
Etch	Edge etch	Mask front
Plate	Print back	Etch back and edge
Clamp mask	Print grid	Etch front
Edge etch	Fire	Passivate front and back
Solder dip	A-R coat	Align and mask front and back
Clean flux	Test	Etch
Test		Metallize front and back
		BSR
Hand solder interconnect	Ribbon solder	Test
Clean flux	Clean flux	Weld
Prime glass	Bond glass	Bond glass
Pot	Frame	Frame
Frame	Test	Test
Test		
\$30.00/W*	\$5.00/W*	\$2.00 to \$10.00/W
*With yield and profit.		

JPL ENCAPSULATION TASK

SPRINGBORN LABORATORIES, INC.

P. Willis

JPL Encapsulation Task (Inception: 1975)

- OVERALL GOAL:
- PRODUCTION OF ELECTRICAL POWER FROM PHOTOVOLTAICS COMPETITIVE WITH COMMERCIAL POWER SOURCES
 - TARGET: \$0.70 PER PEAK WATT (1980 DOLLARS)

WHY ENCAPSULATION?

- MECHANICAL SUPPORT — PREVENT CELL BREAKAGE
- THERMAL CONDUCTION — DISSIPATE HEAT
- ENVIRONMENTAL PROTECTION — PREVENT CORROSION
- PACKAGING / HANDLING — TRANSPORTATION AND FIELD DEPLOYMENT OF MODULES

Performance Requirements

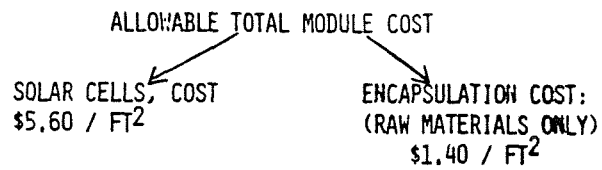
- SERVICE LIFE 30 YEARS
- LIGHT TRANSMISSION TO SOLAR CELLS >90% OF INCIDENT
- LOSS IN MODULE POWER AFTER 30 YEARS <10% OF INITIAL
- PROCESSING AND FABRICATION AUTOMATED
- STRUCTURAL PERFORMANCE NO FAILURES (INCLUDING HANDLING AND WEATHERING)

-
- MUST CONFORM TO COST GOALS

PRECEDING PAGE BLANK NOT FILMED

Encapsulation Cost Goals

$$\bullet \quad \$ 0.70/W_{PK} \times 10 W/FT^2 = \underline{\underline{\$7.00 / FT^2}}$$



	% OF MODULE COST	\$/M ²	\$/FT ²
ENCAPSULATION SYSTEM	20	14	1.40*

* 1980 \$

- COST NOW SERVED AS DRIVER FOR SELECTION OF MATERIALS
- NEED TO REDEFINE ENCAPSULATION REQUIREMENTS
 - WHAT COMPONENTS ARE NEEDED ?
 - WHAT MUST MATERIALS DO ?
- DOES ENCAPSULATION PACKAGE MEET BOTH COST AND PERFORMANCE REQUIREMENTS ?

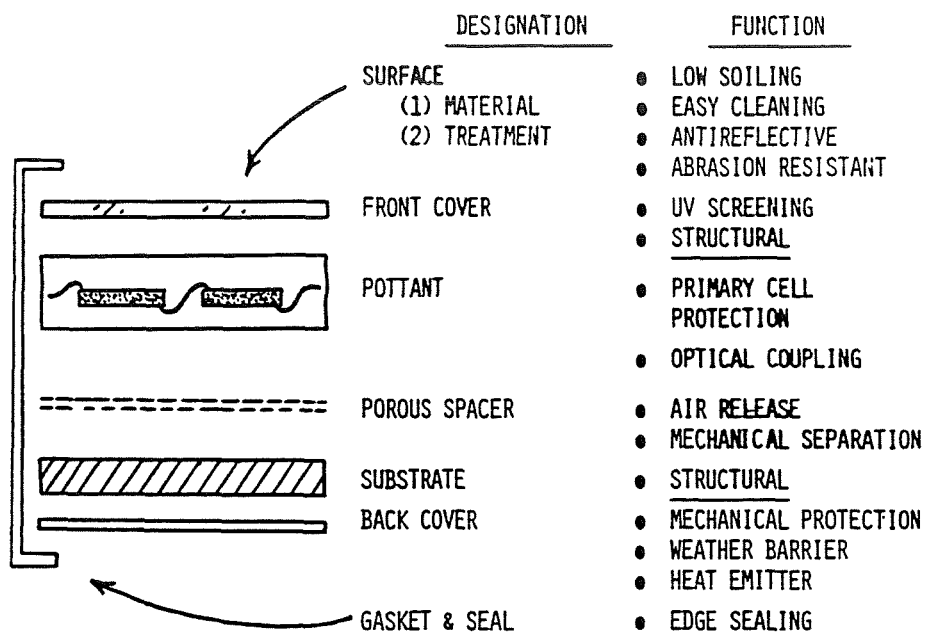
Early Encapsulation Systems

TWO SCHOOLS OF THOUGHT:

- A. POURABLE SYRUPS
- B. DRY FILM LAMINATION

<u>APPROACHES</u>	
<u>COMPONENTS</u>	<u>DEFICIENCIES</u>
<ul style="list-style-type: none"> • SILICONE LIQUIDS VERY HIGH COST (\$12 / LB) (CASTING SYRUP) • URETHANE LIQUIDS (CASTING SYRUP) 	<ul style="list-style-type: none"> MIXING AND PUMPING UNPREDICTABLE ADHESION LONG CURE TIMES BUBBLE ENTRAPMENT MOISTURE SENSITIVE YELLOWING WITH AGE
<ul style="list-style-type: none"> • POLYVINYL BUTYRAL (PVB) (LAMINATION FILM) 	<ul style="list-style-type: none"> SPECIALIZED STORAGE DIFFICULT PROCESS - AUTOCLAVE LONG LAMINATION TIMES MODERATE COST
<ul style="list-style-type: none"> • SUBSTRATES: FIBERGLASS, ALUMINUM 	<ul style="list-style-type: none"> HIGH THERMAL EXPANSIONS HIGH MOISTURE EXPANSION HIGH COST
<ul style="list-style-type: none"> • INDUSTRIAL PROCESSING 	<ul style="list-style-type: none"> NOT CONSIDERED AT THIS TIME
<hr/> <ul style="list-style-type: none"> • OVERALL PERFORMANCE QUESTIONABLE ? • MAJOR OBJECTION: CANNOT MEET FSA COST GOALS 	

Module Construction Elements



- ADHESIVES AND PRIMERS WHERE REQUIRED

- NOTE: TWO DESIGNS - SUBSTRATE OR SUPERSTRATE
ONLY ONE STRUCTURAL COMPONENT

MODULE FABRICATION TECHNIQUES

- (1) SHEET LAMINATION METHOD
- (2) LIQUID CASTING METHOD

- GOAL : IDENTIFY COST-EFFECTIVE MATERIALS AND PROCESSES

Pottant Development

- POTTANT IS THE HEART OF THE ENCSPSULATION PACKAGE - RECEIVED GREATEST EMPHASIS
- REQUIREMENTS:
 - OPTICAL TRANSPARENCY
 - LOW MELTING POINT
 - ELECTRICAL INSULATION
 - RUBBERY (LOW MODULUS)
 - NO CELL BREAKAGE !
 - RESISTANT TO FLOW IN SERVICE
 - SUITABLE FOR AUTOMATED PRODUCTION (HIGH VOLUME)
 - COST EFFECTIVE
- THESE PROPERTIES FOUND IN TRANSPARENT "ELASTOMERS"
- PROBLEM - LOW COST POLYMERS MAY HAVE DEFICIENCIES:
 - HEAT (OXIDATION) SENSITIVITY
 - LIGHT (ULTRAVIOLET) SENSITIVITY
 - WATER (HYDROLYSIS) SENSITIVITY
- ALL TRANSPARENT "ELASTOMERS" SURVEYED TO SELECT COMPOUND WITH DESIRED PROPERTIES AND ABILITY TO BE STABILIZED WITH ADDITIVES - IMPART ENVIRONMENTAL STABILITY

Current Candidates

	<u>COST</u>
A. LAMINATION FILMS:	
ETHYLENE VINYL ACETATE (EVA)	\$ 0.95/ LB
ETHYLENE METHYL ACRYLATE (EMA)	\$ 0.95/ LB
B. CASTING LIQUIDS:	
POLY N-BUTYL ACRYLATE (BA)	\$ 1.00/ LB
ALIPHATIC POLYURETHANE (PU)	\$ 3.00/ LB

Development of EVA Pottant

EVA BEST OVERALL CHOICE:

ETHYLENE VINYL ACETATE POLYMERS (EVA)

ADVANTAGES

MANY GRADES AVAILABLE
OXIDATION (HEAT) STABLE
HYDROLYSIS (WATER) STABLE
WIDE RANGE OF VISCOSITY
EASY TO PROCESS
LOW COST
GOOD ADHESIVE PROPERTIES

DEFICIENCIES

THERMOPLASTIC (NO CREEP
RESISTANCE)
ULTRAVIOLET SENSITIVE

-
- MODULE FABRICATION GRADE DEVELOPED DESIGNATION: EVA A9918
 - CONTAINS CURING AGENTS AND STABILIZERS
 - DEFICIENCIES SUCCESSFULLY CORRECTED

Properties/Benefits EVA A-9918

- NO COLD STORAGE REQUIRED
- HIGH TRANSPARENCY
- DIMENSIONAL STABILITY
- GOOD FLOW AND VOLUMETRIC FILL
- FAST CURE (\$0.10 /FT² IN VOLUME)
- EASY LAMINATION (MODULE PROCESSING)
- EXCELLENT ENVIRONMENTAL STABILITY
- LOW COST
- PRODUCED AS ROLLS OF FILM

Other Candidate Encapsulation Materials

STRUCTURAL COMPONENTS:

SUPERSTRATE : LOAD-BEARING TOP SURFACE

- TEMPERED LOW-IRON FLOAT GLASS 1/8" THICK \$0.75 /FT²

SUBSTRATES: LOAD-BEARING UNDER SURFACE

- COLD ROLLED MILD STEEL, 28 GA. \$0.26 /FT²
- WOOD HARDBOARDS, 1/8" THICK \$0.14 /FT²

(NOTE: THESE MATERIALS REQUIRE ADDITIONAL TREATMENT FOR ENVIRONMENTAL STABILITY)

POROUS SPACER: VACUUM EVACUATION, MECHANICAL SPACING
AND ELECTRICAL ISOLATION

- CRANEGLAS 230 NON-WOVEN GLASS MAT \$0.02 /FT²

OUTER COVERS: MECHANICAL PROTECTION, SOIL RESISTANT,
UV SCREENING

- ACRYLAR X-22417 (3M CORP.) \$0.07 /FT²
- TEDLAR 100B630UT (DU PONT) \$0.10 /FT²
- TEDLAR 400B620SE (DU PONT) \$0.30 /FT²
- FEP FILM , 2 MIL THICK \$0.20 /FT²

(NON-SCREENING, OUTSTANDING WEATHERABILITY
HIGH TRANSPARENCY, OPTICAL COUPLING)

- * ALL PRICES ARE FOR VOLUME PRODUCTION

Other Candidate Encapsulation Materials (Cont'd)

BACK COVER FILMS: MECHANICAL PROTECTION, ELECTRICAL ISOLATION, AND HEAT REFLECTION

- TEDLAR 150BS30WH (DU PONT) \$ 0.13 /FT²
- TEDLAR 200BL20WH (DU PONT) \$ 0.16 /FT²
- SCOTCHPAR 20CP WHITE (3M) \$ 0.12 /FT²
- KORAD 63000 WHITE (XCEL CORP) \$ 0.09 /FT²

GASKETS & SEALANTS : EDGE PROTECTION

- EPDM GASKET (E-633, PAWLING RUBBER CO) *
- BUTYL TAPE (5354, 3M CORP) *
- OTHERS -----

* VARIES WITH PERIMETER

ADHESIVES / PRIMERS:

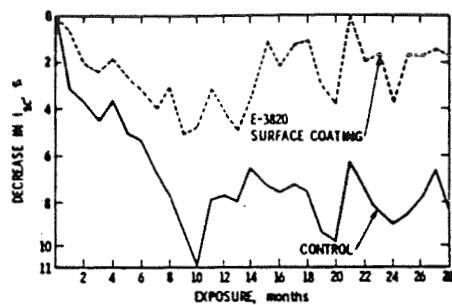
- PRIMERS IDENTIFIED FOR ALMOST ALL INTERFACES
- HIGH DURABILITY AND LOW COST (~ \$0.02 /FT²)
- SELF - PRIMING GRADE OF EVA DEVELOPED

EVA Bond Strengths, Pound/Inch of Width

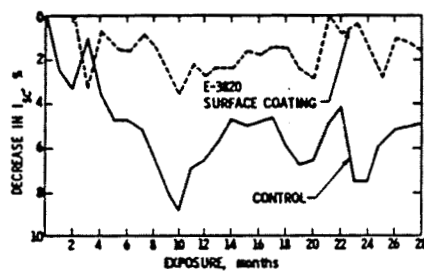
<u>MATERIALS</u>	<u>CONTROL</u>	<u>2 WK IMMERSION</u>	<u>2 HR BOILING WATER</u>
SUNADEX GLASS	34.8	30.0	32.3
WINDOW GLASS	39.6	37.9	27.1
WINDOW GLASS (SELF-PRIMING EVA)	35.4	41.9	COHESIVE

Anti-Soiling Treatments

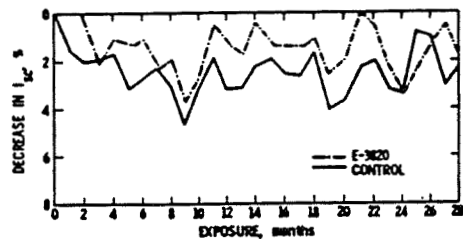
SURFACE: ACRYLAR IMPROVEMENT 3.9%



SURFACE: TEDLAR IMPROVEMENT 3.8%



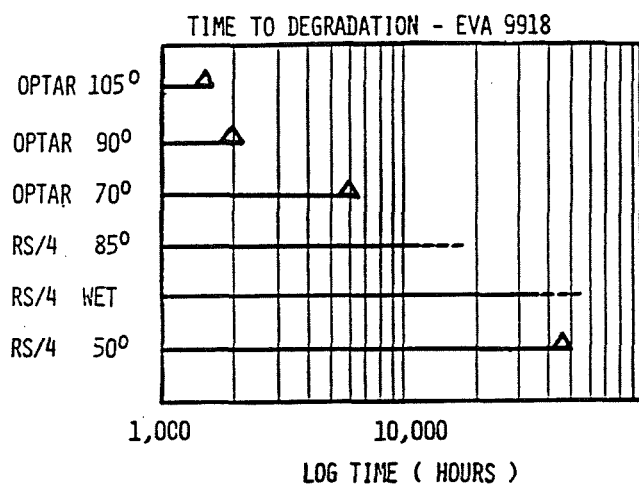
SURFACE: GLASS IMPROVEMENT 1%



Aging and Lifetime Predictions

- HOW LONG WILL MODULES LAST ?
- NEW ACCELERATED AGING TECHNIQUE DEVELOPED:
OUTDOOR PHOTOTHERMAL REACTOR (OPTAR)
- COMBINES NATURAL LIGHT AND HEAT

Severity Index

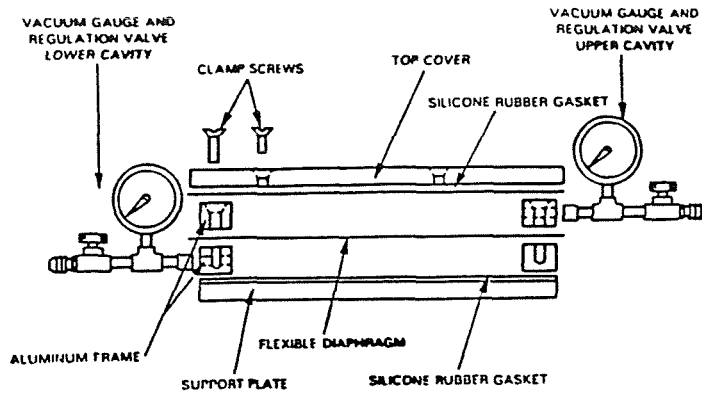


- OPTARS MOST EFFICIENT AGING TECHNIQUE
- MODULES HAVE VERY HIGH ENDURANCE
NO EFFECT: 20,000 HRS - 70°C / SUNLIGHT
LITTLE EFFECT: 20,000 HRS - 90°C / SUNLIGHT
STRONG EFFECT: 20,000 HRS - 105°C / SUNLIGHT
- DEGRADED MODULES SHOW NO POWER LOSS
- ENCAPSULATION SYSTEM WORKS WELL
LIFE PROGNOSIS : GOOD !

Module Fabrication

ORIGINAL PAGE IS
OF POOR QUALITY

• VACUUM LAMINATION - METHOD OF CHOICE



- RELATIVELY SIMPLE EQUIPMENT
- DRY FILMS - NO LIQUIDS
- ALL COMPONENTS ASSEMBLED IN ONE STEP
- FAST CYCLE TIMES
- AUTOMATION / HIGH VOLUME POSSIBLE
- COST EFFECTIVE

-
- LAMINATORS ~~COMM~~ERCIALLY AVAILABLE
(SPIRE CORPORATION)

Current Status

HOW CLOSE DID WE COME ?

<u>"TYPICAL" MODULE</u>	<u>VOLUME COST, \$/FT²</u>
LOW IRON GLASS	0.75
EVA (TWO LAYERS)	0.20
POROUS SPACER	0.02
PRIMERS / ADHESIVES	0.02
BACK COVER (TEDLAR)	0.16
GASKET / SEAL (EST.)	0.15
	<u>\$ 1.30 / FT²</u>

- MAJOR ENCAPSULATION COMPONENTS DEVELOPED/
IDENTIFIED AND COMMERCIALY AVAILABLE
- EVA POTTANT FILM - WIDE INDUSTRIAL ACCEPTANCE
- VIABLE MANUFACTURING PROCESS IDENTIFIED
- FIELD PERFORMANCE - VERY PROMISING

Remaining Efforts

- LIFETIME ANALYSIS : DEVELOP AND VERIFY
PREDICTIVE AGING METHODS

Summary

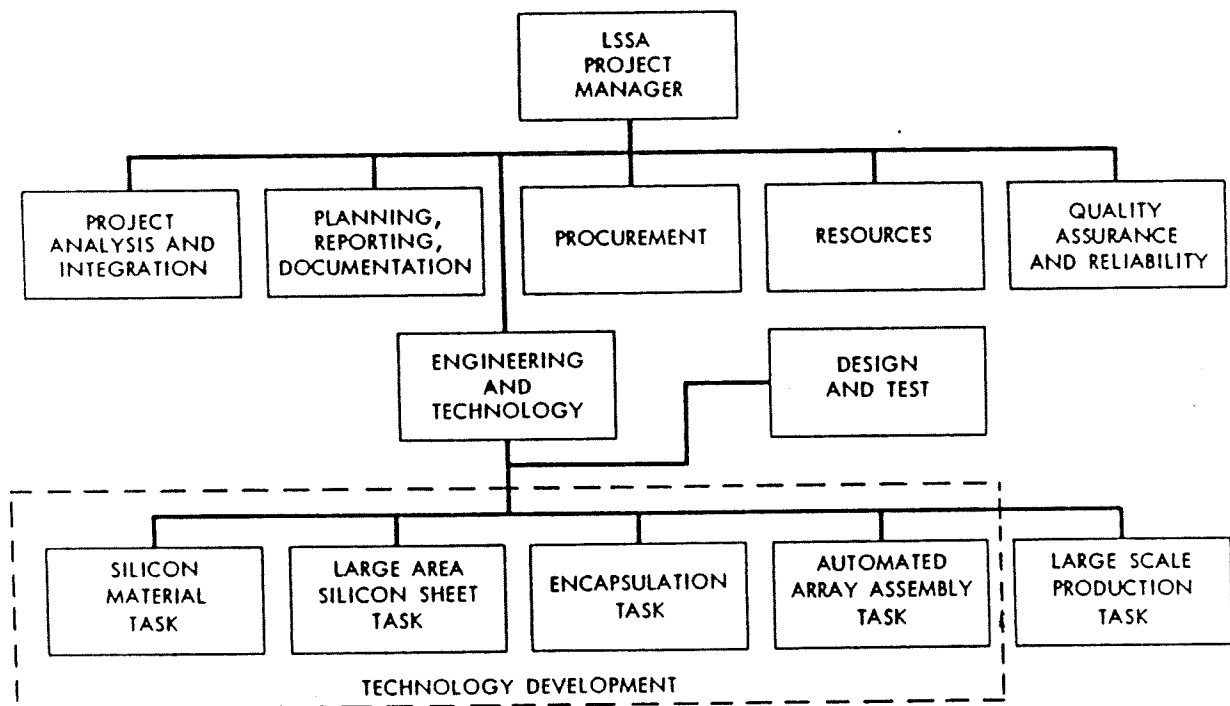
FSA PROGRAM HAS RESULTED IN HIGH
PERFORMANCE COST-EFFECTIVE ENCAP-
SULATION SYSTEMS FOR PHOTOVOLTAIC
MODULES

CRYSTALLINE-SILICON PHOTOVOLTAICS SUMMARY MODULE DESIGN AND RELIABILITY

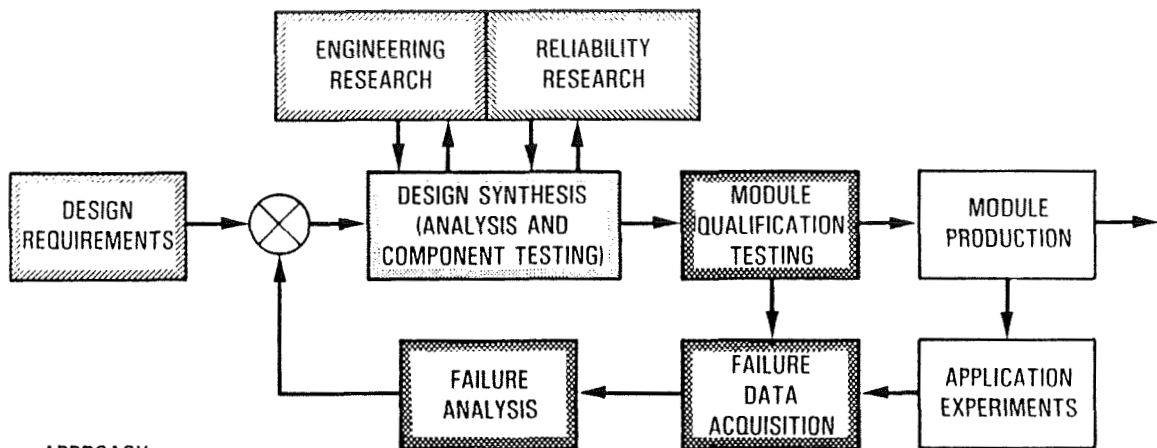
JET PROPULSION LABORATORY

R. G. Ross, Jr.

Low-Cost Silicon Solar Array Project 1975 Organization Chart



Reliability and Engineering Sciences Functional Organization (Closed-Loop Process)



APPROACH

- Derive requirements
- Synthesize designs
- Evaluate designs using laboratory and field tests
- Acquire and feed back performance data
- Develop improved technologies
- Use feedback and technology to improve designs

Design Requirement Generation

- **Objective**
 - Focus the development of low-cost long-life module technology toward commercial needs of future large-scale PV applications
- **Approach**
 - Define and develop module and array design requirements for future large-scale applications using private-sector experts and JPL in-house skills
 - Performance
 - Safety
 - Reliability
 - System (Array) Integration
 - Develop near-term versions of the requirements to serve as specifications for procurement of modules for testing and application experiments
 - Iterate the requirements with results fed back from testing experience

Module Design and Test Specifications

- JPL Crystalline-Si module design requirements have achieved international recognition and use
- Block I: 5-342 First Generation Oct 75
- Block II: 5-342-1B Second Generation Dec 76
- Block III: 5-342-1C Second Generation Update May 77
- PRDA 38: 5101-65 Intermediate Load Center Oct 77
- Block IV: 5101-16A ILC (Third Generation) Nov 78
 5101-83 Residential (Third Generation) Nov 78
- Block V: 5101-161 ILC Applications Feb 81
 5101-162 Residential Feb 81

Design Requirements Accomplishments

- Definitive requirements developed in following areas:
 - Residential building codes (Burt Hill)
 - Utility design practices (Bechtel)
 - National electrical codes (UL)
 - Module safety (UL)
 - Product liability (Carnegie Mellon)
 - Wind loading levels (Boeing/CSU)
 - Array wiring safety (UL)
 - Module flammability (UL)
 - Hail impact levels (JPL)
 - Operating temperature levels (JPL)
 - Module reliability (JPL)
 - Array circuit design practices (JPL)
 - Array structural interfaces (Bechtel, Burt Hill, JPL)
 - System operational interfaces (JPL)

Design Requirements
Current Status and Future Needs

- Most module requirements for large-scale applications are in place for both C-Si and thin-film modules
 - Building code implications understood
 - National Electrical Code (Article 690) in place
 - Module safety requirements (UL 1703) in place
 - Operating temperature levels understood
 - Fire-resistance requirements in place
 - Array/system interface issues understood
 - Wind loading levels understood
 - Hail impact levels determined
 - JPL C-Si module design requirements internationally recognized
- Problem: Transferring the extensive existing technology base to new entries
- Problem: Crystalline-Si module specifications are not sufficient for thin-film modules

Engineering Sciences and Reliability Research

- Objective
 - Develop the engineering technology base required to achieve low-cost, efficient, and safe modules for large-scale applications
 - Develop the technology base required for reliable 30-year life modules
- Approach
 - Identify technology shortfalls through continuous feedback of results from design reviews, qualification tests, field application experiments, and laboratory investigations
 - Draw upon industry experts and JPL in-house experience to develop the generic technology advances required

Engineering Sciences Accomplishments

- Comprehensive design and construction technology base defined in following areas:
 - Electrical circuit analysis tools (JPL)
 - Module thermal design and test methods (JPL)
 - Module safety design practices (UL)
 - Electrical connection means (AMP, Motorola, Cannon)
 - Fire-resistant module construction practices (JPL, HITCO, Gila River)
 - Bypass diode integration practices (JPL, GE)
 - Array structural designs
 - Residential (Burt Hill, AIA, JPL)
 - Central station (Bechtel, JPL)
 - Array safety system designs (UL)
 - Array/power-conditioner interface characterization (JPL)

Reliability Research Accomplishments

- Definitive technology bases generated for:
 - Glass fracture strength (JPL)
 - Hail impact damage and probability (JPL)
 - Interconnect fatigue (JPL)
 - Soiling levels (JPL)
 - Cell fracture strength (JPL)
 - Hot-spot heating analysis and test methods (JPL)
- Substantial technology generated for:
 - Electrochemical corrosion analysis and test methods (JPL)
 - Bypass diode qualification test methods (JPL)
- Important technology generated for:
 - Electrical breakdown parameter dependencies (JPL, Bechtel, Hughes)
 - Corrosion resistance of C-Si and T-F cells (JPL, Clemson)
 - Module reliability synergisms (JPL, Wyle)

Engineering Sciences and Reliability
Current Status and Future Needs

- Most engineering technologies are in place for both C-Si and thin-film modules
 - Structural/thermal design approaches and methods
 - Safety design practices
 - Circuit design approaches and analysis methods
 - System interfacing techniques
- Most technologies are in place for 30-year-life crystalline-Si modules. Exceptions include:
 - Long-term aging of electrical insulation systems
 - Long-term photothermal aging of rear surface films
 - Long-term corrosion of cell metallizations
 - Long-term stability of bonded interfaces
- Significant technology advances required to achieve 30-year-life thin-film modules

Module Development

- Objective
 - Facilitate the transfer of DOE sponsored technology developments into PV manufacturers and their products
 - Define and quantify design deficiencies as an important management tool to focus government and industry R&D efforts at key problems and to assess program performance against its goals
- Approach
 - Prepare module specifications reflecting future application requirements and encouraging state-of-the-art technology
 - Contract with private industry for module design and fabrication
 - Conduct detailed evaluation, test and failure analysis of delivered modules
 - Iterate design, design reviews, manufacture and tests until successful module qualification

Module Development Accomplishments

- Nurtured the development of 45 module designs within 15 PV manufacturers over a 10-year period
- Maintained R&D focus on critical-path problems by providing an internationally recognized assessment of PV module electrical performance and reliability
 - Developed unique facilities and techniques for performance assessment and failure analysis
 - Performed qualification tests on over 150 different module designs
 - Block I through Block V
 - DOE application experiments
 - Commercial (U.S. and foreign)
 - Conducted 435 major failure analyses involving 1200 reported design deficiencies

MODULE EVALUATION

ARCO Solar, Inc.

C. Gay

- Customer Is Key
 - Education
 - Experience
 - Confidence
- Relationship Between Laboratory Testing and Real World — Credibility
 - Predictable Energy Delivery
 - Carrisa Plains Within 3% Over 1 Year
 - Predictable Reliability
 - Less Than 1 Warranty Replacement Per 25,000 Modules (Over 500,000 Large Modules in the Field)

PRECEDING PAGE BLANK NOT FILMED

PROJECT ANALYSIS AND INTEGRATION ECONOMIC ANALYSES SUMMARY

CONSULTANT

H. L. Macomber

40236

Overview

- INTRODUCTION
- START-UP
- MID-TERM AND BEYOND
- OBSERVATIONS

Introduction

- LOOK AT PA & I
 - Economic Analysis Plus For Crystalline Silicon PV
 - Accomplishments, Lessons Learned, Potential and Continuing R&D Needs
- LOOK INSIDE
 - Business Investment Decision Analysis Well Developed and Practised in Industry
 - New to Government Led Programs
- LOOK FROM OUTSIDE
 - Effects on Industry, Effects on Gov't Programs

PRECEDING PAGE BLANK NOT FILMED

PA&I Start-Up

- WHY
 - System Motivated
 - Achieve Proposed Objectives
- HOW
 - Planning, Modeling, Analysis, Liaison
- WHAT
 - Task Efforts; Project/Program Objectives & Goals;
Industry Technology, Market & Economic Information
- WHO
 - Early Players at JPL, ERDA, Other Labs & Industry

Materials from Early Presentations: 1975-1976

LOW COST SILICON SOLAR ARRAY PROJECT SYSTEMS ANALYSIS AND INTEGRATION

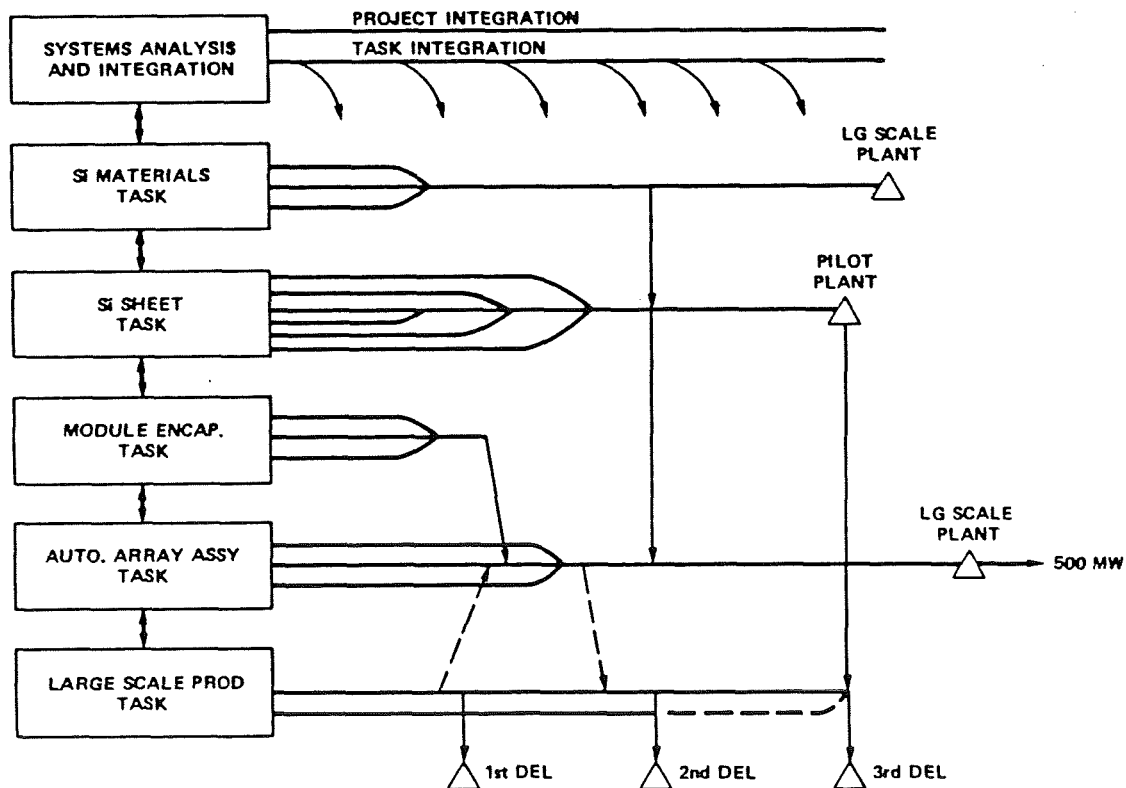
H. L. Macomber

1975

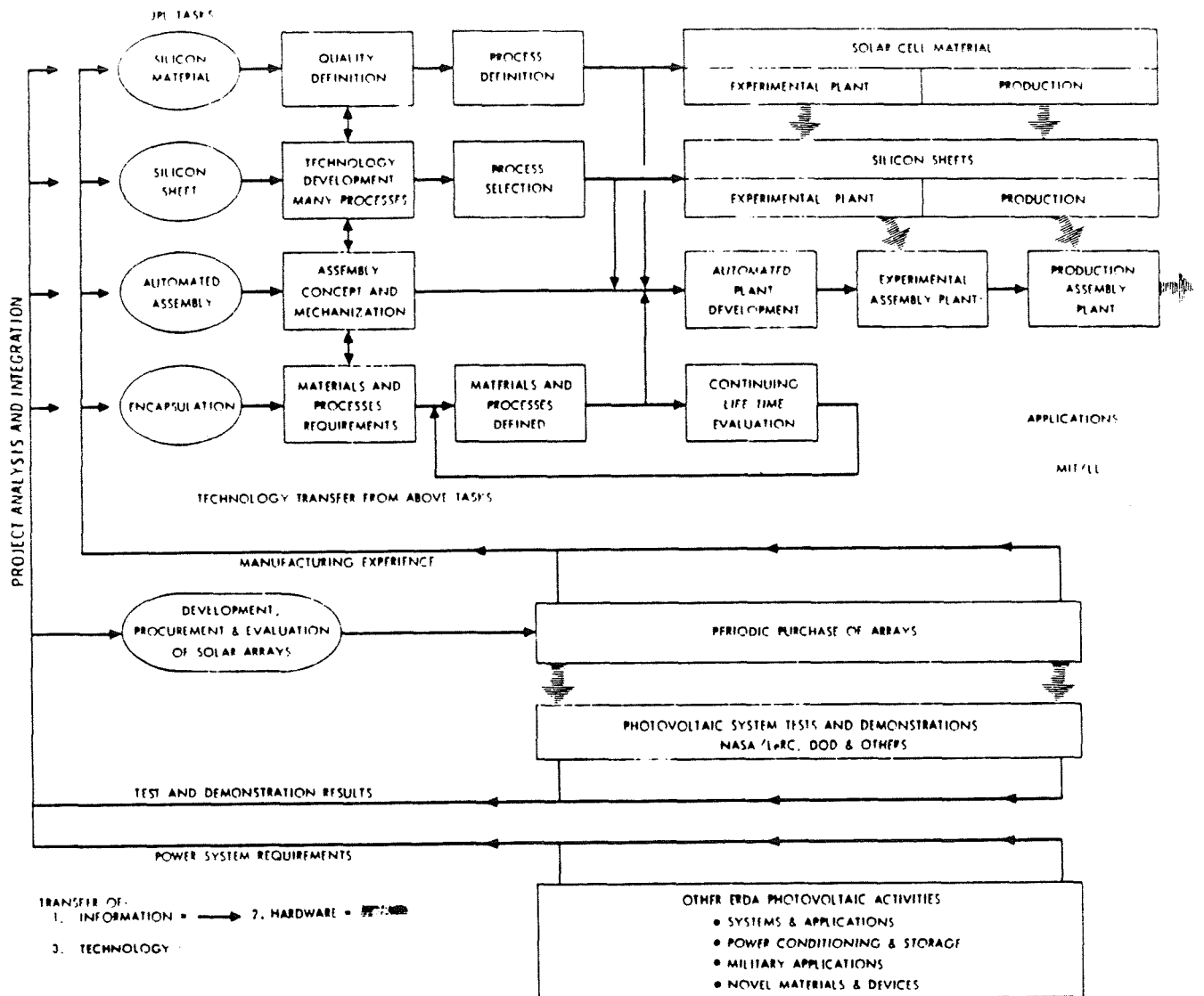
Systems Analysis and Integration: Objectives

- DEVELOP AND PROVIDE THE PROJECT INFORMATION REQUIRED FOR ASSESSING THE PROBABILITY OF ACHIEVING THE PROJECT GOALS
- PROVIDE PROJECT RECOMMENDATIONS FOR MAXIMIZING THE PROBABILITY OF ACHIEVING THE PROJECT GOALS
- PROVIDE THE NECESSARY SYSTEMS ANALYSIS, SYSTEM ENGINEERING AND DESIGN, AND SYSTEM TEST SUPPORT FOR ASSURING THE INTEGRATION OF PROJECT TASKS TO ACHIEVE THE PROJECT GOALS
- PROVIDE PROJECT SUPPORT FOR INTEGRATING THE PROJECT WITH ERDA PV PROGRAM

Task Process



Functional Relationships Within the Project and Between the Project and ERDA



Mid-Term and Beyond

• MODELS — PARTIAL LIST OF EARLY EFFORTS

- **USES:** "Utility-owned Solar Electric System"
- **SAMIS:** "Solar Array Manufacturing Industry Simulation"
- **SAMICS:** "Solar Array Manufacturing Industry Costing Standards"
- **IPEG:** "Improved Price Estimation Guidelines"
- **PAG:** "Price Allocation Guidelines"
- **PADEM:** "Project Alternative Design Evaluation Model"
- **LCP:** "Lifetime Cost and Performance"
- **ESA:** "Energy Systems Economic Analysis"
- ***SIMRAND:** "SIMulations of Research And Development"
- ***SAMPEG:** (Simplified Version of SAMIS)

* After HLM Tenure

• PLANS — PARTIAL LIST OF EARLY EFFORTS

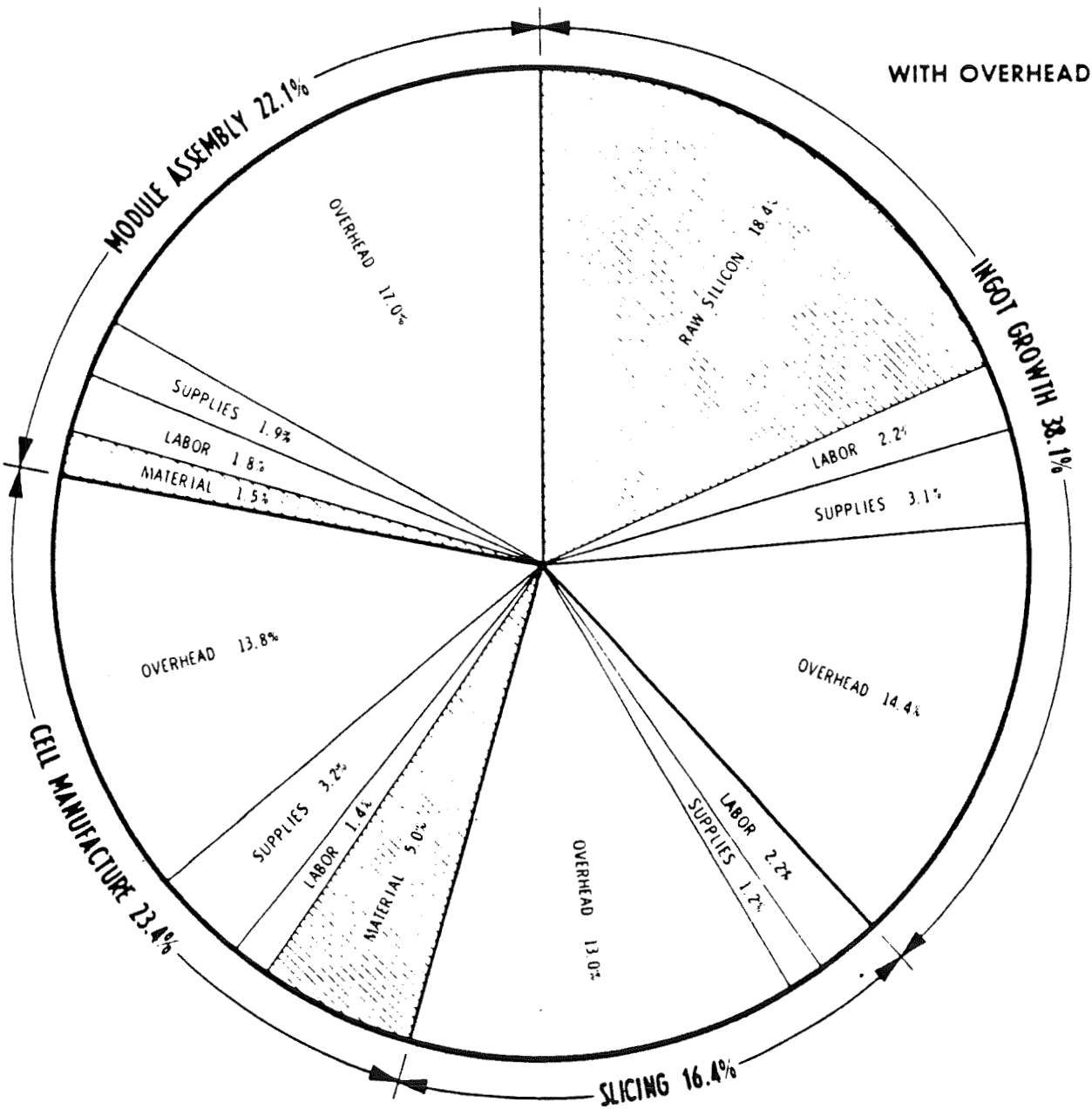
- **LSSA (FSA) Interface Activity Plan** 11/75
- **PV Systems Planning Group – Interim Systems Development Plan** 9/76
- **PV Planning Group – Draft Study Report (PV Strategy Inputs)** 7/77
- **PV Program Multi-year Plan** 10/78
- **Technical Readiness, 1982 Plan** 9/79
- **Annual Project Plans**

• ANALYSIS — SELECTED EARLY WORKS

- **Industry Growth Rate Studies**
- **Learning (Experience) Curve Assessments**
- **Pricing Studies**
- **Cost Allocation Studies**
- **Efficiency vs Cost Trade-Offs — A Workshop**
- **SERI Venture Analysis Inputs**

Some Early Analyses: 1975-1976

Present State-of-the-Art Major Manufacturing Cost Estimates

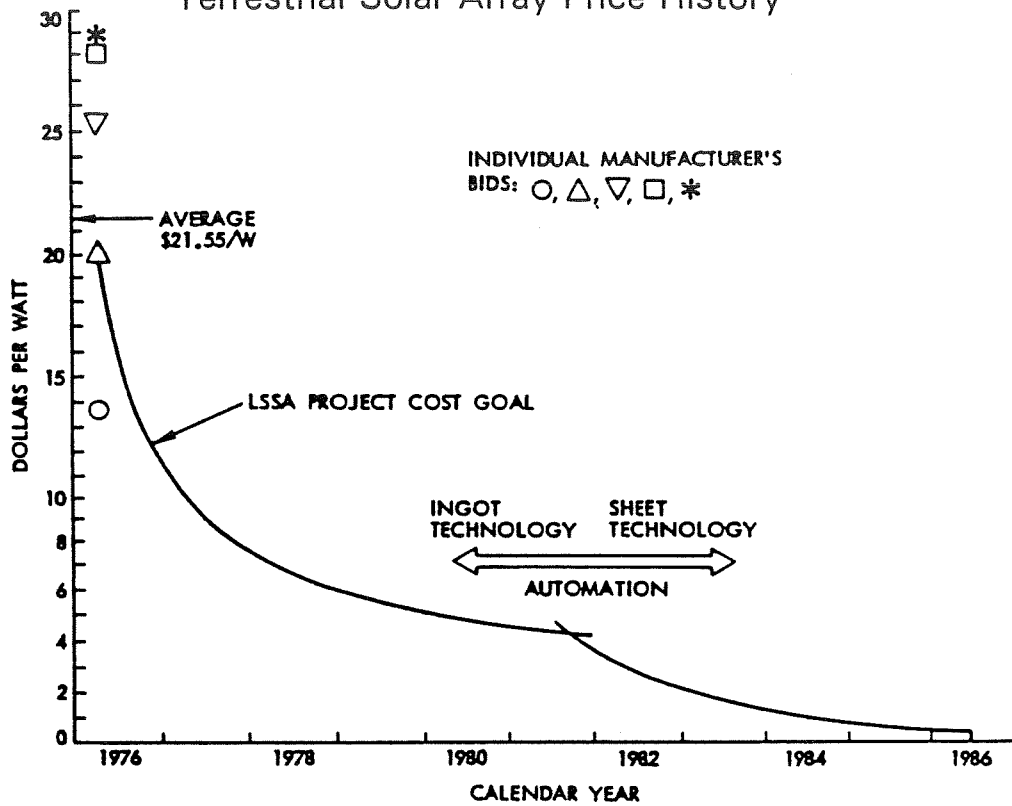


BASED ON SAMIS* COMPUTER PROGRAM (ID3)

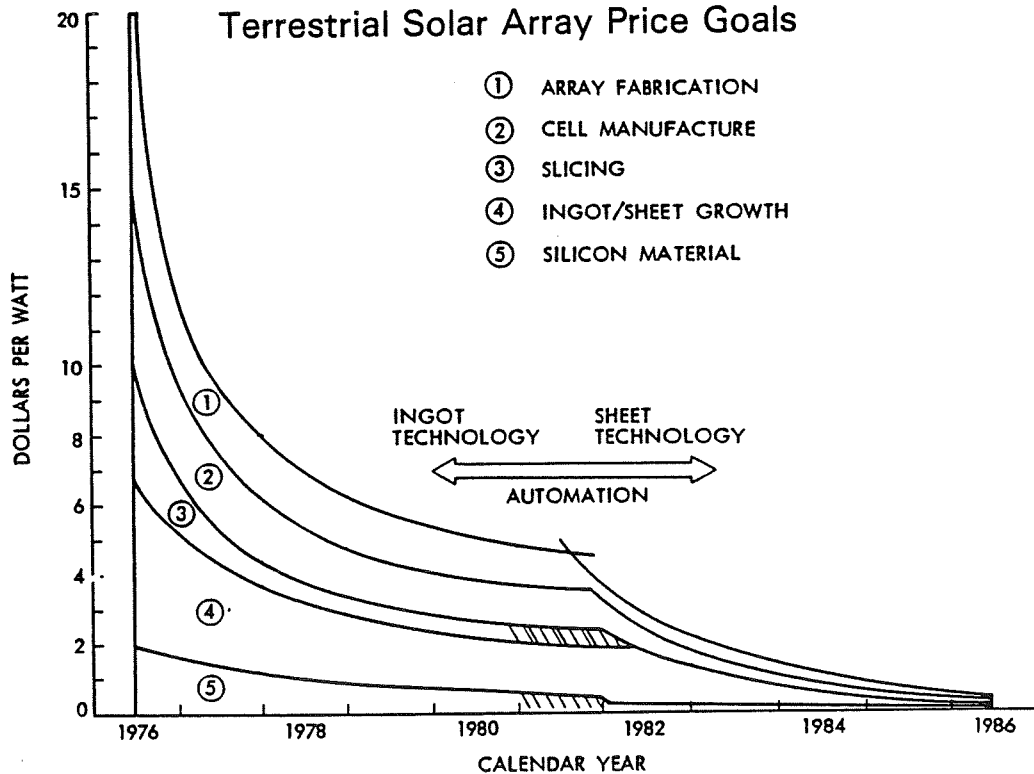
* SOLAR ARRAY MANUFACTURING INDUSTRY SIMULATION

ORIGINAL PAGE IS
OF POOR QUALITY

Terrestrial Solar Array Price History








Terrestrial Solar Array Price Goals



Project Cost Goal Allocations (all costs in 1975 dollars)

ORIGINAL PAGE IS
OF POOR QUALITY

		CALENDAR YEAR					
		1976	1978	1980	1982	1984	1986
SILICON MATERIAL							
Silicon Material	Semiconductor Grade  Solar Grade						
	\$/kg	60	50	40	15	10	7
	\$/w	1.9	1.1	0.65	0.09	0.05	0.03
INGOT/SHEET GROWTH							
Processing Value Added - \$/w	Czochralski Ingots  Large Area Sheet						
		4.8	2.1	1.6	1.9	0.52	0.14
Wafer Material - \$/w		6.7	3.2	2.2	2.0	0.57	0.17
INGOT SLICING							
Processing Value Added - \$/w		3.7	0.6	0.5	0.01	0	0
Wafers - \$/w		10.4	3.8	2.7	2.0	0.57	0.17
CELL MANUFACTURE							
Materials Added (Contacts, etc.) - \$/w	Silver  Commercial Conductor						
		0.8	0.4	0.35	0.20	0.08	0.07
Processing Value Added - \$/w	Mostly Manual  Automated						
		4.3	1.2	0.85	0.25	0.09	0.06
Cells - \$/w		15.5	5.4	3.9	2.45	0.72	0.30
ARRAY FABRICATION							
Materials Added (Encapsulation, Framing, etc.) - \$/w		0.5	0.5	0.3	0.10	0.08	0.08
Processing Value Added - \$/w	Mostly Manual  Automated						
		4.0	1.1	0.8	0.45	0.18	0.12
ARRAY PRICE GOALS - \$/w		20	7	5	3	1	0.50
Silicon material in final product		27%	30%	38%	78%	87%	91%
Total processing value added		84%	71%	75%	87%	73%	64%
Watts/kg of silicon material		32	47	62	162	187	203
Cell efficiency (AM1)		11%	11.5%	12%	12.5%	13%	13.5%
Cell thickness - mils		15	12	12	10	10	10

Mid-Term and Beyond (Cont'd)

- LIAISON — SELECTED ACTIVITIES
 - PIMS
 - Industry Reviews: Models, Inputs, Allocations, and Assessments
 - Technology Transfer of SAMIS/SAMICS/IPEG
 - Intertask/Interproject Coordination Support
 - Conference Presentations

Observations

- RESULTS
 - Many Products Developed —
Models, Plans, and Assessments
 - Provided Project/Program Strategy Inputs
- VALUE
 - To Project/Program — Useful Quantitative
Inputs to Complex Decision Making
 - To Industry — Provided Yardsticks,
But Value Mixed Since NOT Company Specific
 - To JPL and Other Government Programs —
Demonstrated Application of a Key Element
to Any Program: How To Evaluate and Understand
the Worth of an R&D Activity

More Observations

- THE FUTURE
 - For Program — Models/Techniques Available,
Culture Remains — But Who is the Practitioner
and How Does the Analytical Technology Continue
to be Improved to Better Reflect Real World
- For Industry — Models/Techniques Available*,
But, Small Firms Usually Lack Resources to
Implement and Big Companies Usually Have Own
Ways to Conduct Investment Decision Analyses.

*Software and Documentation Available from COSMIC:
The Computer Software Management Information Center, Suite 112
Barrow Hall, University of Georgia, Athens, Georgia 30602.

PANEL: RECOMMENDATIONS FOR CRYSTALLINE-SILICON IN DOE'S 5-YEAR PHOTOVOLTAIC RESEARCH PLAN

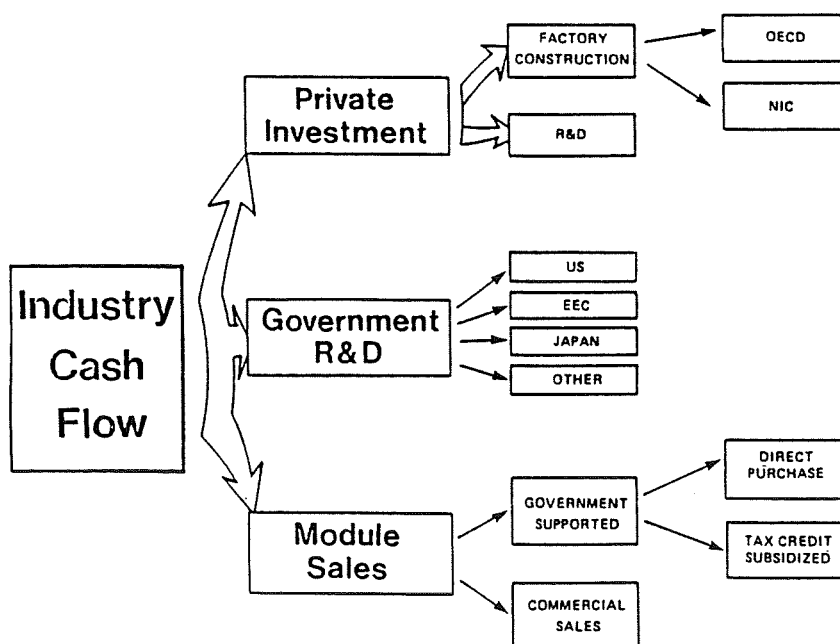
STRATEGIES UNLIMITED

J. Day

Industry Perspective on Change

- o INDUSTRY CASH FLOW
- o CHANGE IN
 - Government Influence
 - the Market
 - the nature of the business
 - the people
 - the companies
- o Where is the future?
- o Changing Government Policy

Industry Cash Flow



PLENARY SESSIONS

Change

	1976	1985
Government Influence	95% of Cash Flow	25% of Cash Flow
Market	Sell to the Government	Sell to the Commercial Market
Nature Of Business	Entrepreneurial	Controlled, deliberately Planned Organizations
The People	Individualists	Team Players
The Companies	Small Ventures Under financed	Industrial Companies well financed

Where is the Future?

o Next 5-10 years ---	Remote Power
o Beyond 10 years ---	Grid Connected

Government Policy Recommendations

Next 5 Years	---	Export Assistance
	---	Utility Education
	---	Long Term Research

C-3

PANEL: RECOMMENDATIONS FOR CRYSTALLINE-SILICON IN DOE'S 5-YEAR PHOTOVOLTAIC RESEARCH PLAN

U.S. NAVY

G. Smith

Activities by the Department of Defense Photovoltaic Review Committee

The Department of Defense (DoD) is the largest single consumer of energy in the U.S., using approximately 250 million barrels of oil equivalent (MBOE) annually. Currently, upwards of 70 percent of the DoD energy requirement is met by petroleum-based products. While DoD expenditures for fuel have dropped \$1 billion per fiscal year since 1983, assured supplies of petroleum to meet future energy needs remains a predominant issue. Recent world events relating to the availability of petroleum fuels, stability of supplies, and volatility of fuel costs have made the issue of effective energy management a high priority within DoD. In particular, DoD has initiated programs to: ensure that petroleum supplies are available to sustain peacetime and combat operations (e.g., through the Defense Fuel Supply Center); improve the energy efficiency of the operating forces and the shore establishment; and substitute more plentiful energy sources for petroleum.

Conservation and renewable energy technologies (e.g., photovoltaics, wind, geothermal, biomass, active/passive solar, etc.) can play a major role in contributing to DoD energy management objectives, particularly in programs aimed at petroleum substitution in shore facilities. These facilities account for approximately 25 percent of the total energy budget for DoD. In 1985 in particular, facilities accounted for \$3 billion of the \$11 billion dollar energy budget.

One of the most promising alternative technologies for use by the military is photovoltaics (PV) -- a technology that directly converts sunlight to electricity. The advantages to PV are that it is fuel free, simple to operate and maintain, modular in nature, and environmentally benign. Furthermore, in remote areas without access to grid-connected power, this technology has been shown to be cost-competitive with conventional energy alternatives, such as diesel - and kerosene-engine generators.

DoD has had substantial experience with PV, primarily through joint activities with the U.S. Department of Energy's (DOE) Federal Photovoltaics Utilization Program (FPUP). FPUP was designed to increase PV awareness and experience in federal agencies through the design, procurement, installation, and operation of PV systems at their facilities. Through FPUP, more than 3,000 systems were installed at 26 federal agencies. DoD was one of the principal agency participants in this program, accounting for approximately 25 percent of FPUP funds, or \$5.8 million. This funding contributed to the installation of 218 PV systems that spanned a wide variety of applications and ranged in size from a few watts to 56 kW. PV proved to be particularly viable power source in remote areas that required reliable energy supplies, and were difficult to reach for system refueling, operation and maintenance.

Currently, the Navy serves as the lead service within DoD for photovoltaic system activities, and is the principal agent responsible for the transfer of technology from PV research and development efforts to the user community. Based on a recent survey completed by the Navy, more than 21,000 cost-effective applications for PV were identified throughout this service branch.

In an effort to more aggressively expand PV use throughout DoD, a tri-service group was formed in December 1985. Formally titled the Photovoltaics Review Committee, this group was given a five-year charter to achieve the following objectives: study different methods of identifying potential applications within DoD; reduce overall costs of DoD PV-related products; transfer technical information about PV throughout the military; and promote widespread application of these systems in the three service branches. The Photovoltaics Review Committee comprises energy officials from each of the three services.

A number of factors combine to demonstrate the timeliness and need for the PV Review Committee to support the development and use of PV throughout DoD.

The price of oil has decreased resulting in diminished interest in conservation and renewable technologies, despite indicators by many individuals in the public and private sectors that this price decline is only a short-term fluctuation.

The pressure from the Gramm-Rudman-Hollings budget bill has made new project initiation extremely difficult.

There is a reluctance on the part of military decision-makers to propose projects that have high up-front capital costs, such as photovoltaics.

The expiration of federal tax credits has dealt an economic blow to the photovoltaics industry at a time when it has matured and provides quality products and services.

There has been a turnover in the decision-making echelons throughout each of the services, which has resulted in a cadre of professionals who are uninformed about photovoltaics.

Thus, there is a strong need to encourage the continued use of PV technology which promises to provide a proven, reliable, and cost-effective electricity source for a variety of DoD applications.

The Photovoltaics review Committee is considering a number of activities which it will be pursuing over the next year. These include:

Developing a Five-Year Plan to identify PV-related initiatives to be undertaken by the Committee over the period 1987 to 1991.

Developing an educational videotape to encourage the use of PV systems at the field level.

Producing a brochure on PV for DoD applications which would serve as a companion document to the videotape.

Preparing a PV design and applications handbook for base commanders.

Sponsoring a joint industry/DoD meeting in which there would be a free exchange of information on the PV needs of the various services.

Securing engineering analysis and technical support and assistance to conduct activities required by the Committee.

A number of potential benefits are to be realized by the success of the DoD PV Review Committee. Specifically, DoD would obtain cost-effective, reliable energy alternatives for meeting facility energy needs and reduce requirements for petroleum-based fuels, particularly imports. The PV industry would increase sales to the military, a potential high-volume buyer of PV over the next few years, and thus move closer to its goal of mass production and lower prices. DOE, by assisting in the development of these activities, would increase the awareness among the military of the merits of PV, and thus help industry to increase sales of this technology. These activities contribute to DOE initiatives as lead agency for the Committee on Renewable Energy Commerce and Trade (CORECT), a federal interagency working group formed to enhance commerce in U.S. renewable energy products and related services. The DoD serves as an active participant in the CORECT.

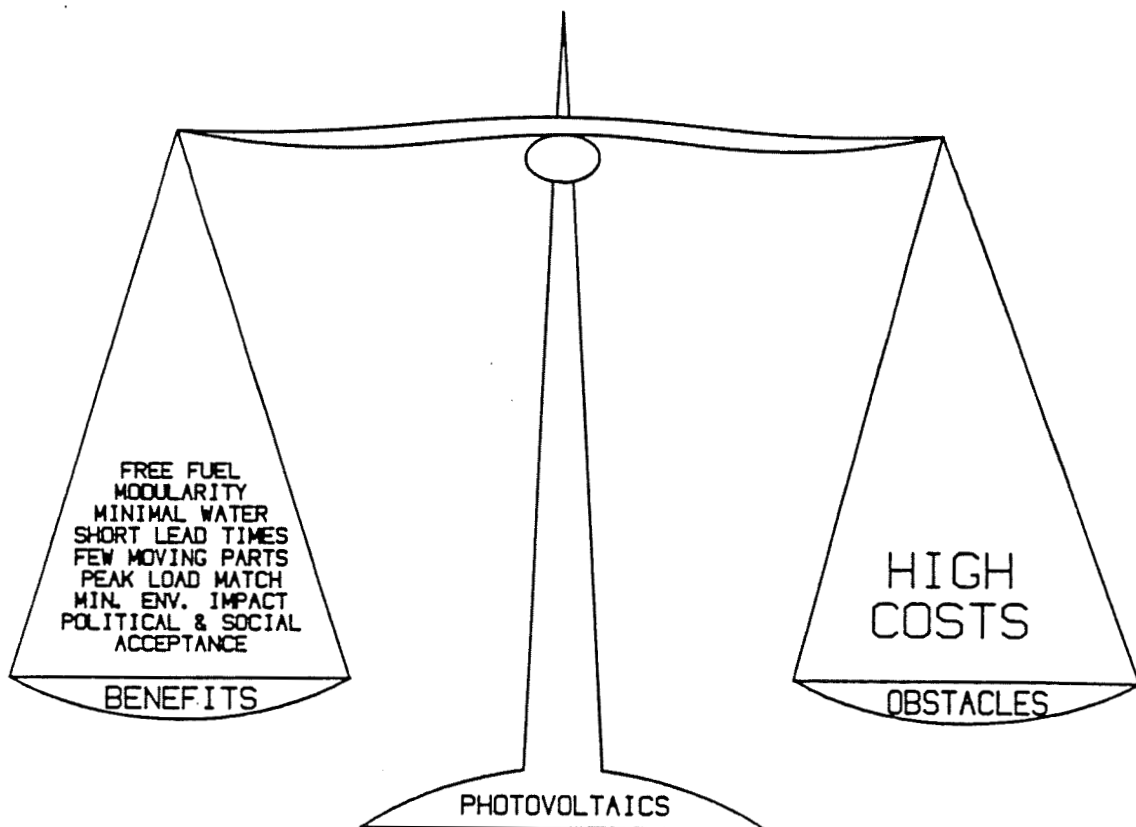
PANEL: RECOMMENDATIONS FOR CRYSTALLINE-SILICON IN DOE'S 5-YEAR PHOTOVOLTAIC RESEARCH PLAN

PACIFIC GAS AND ELECTRIC

K. Firor

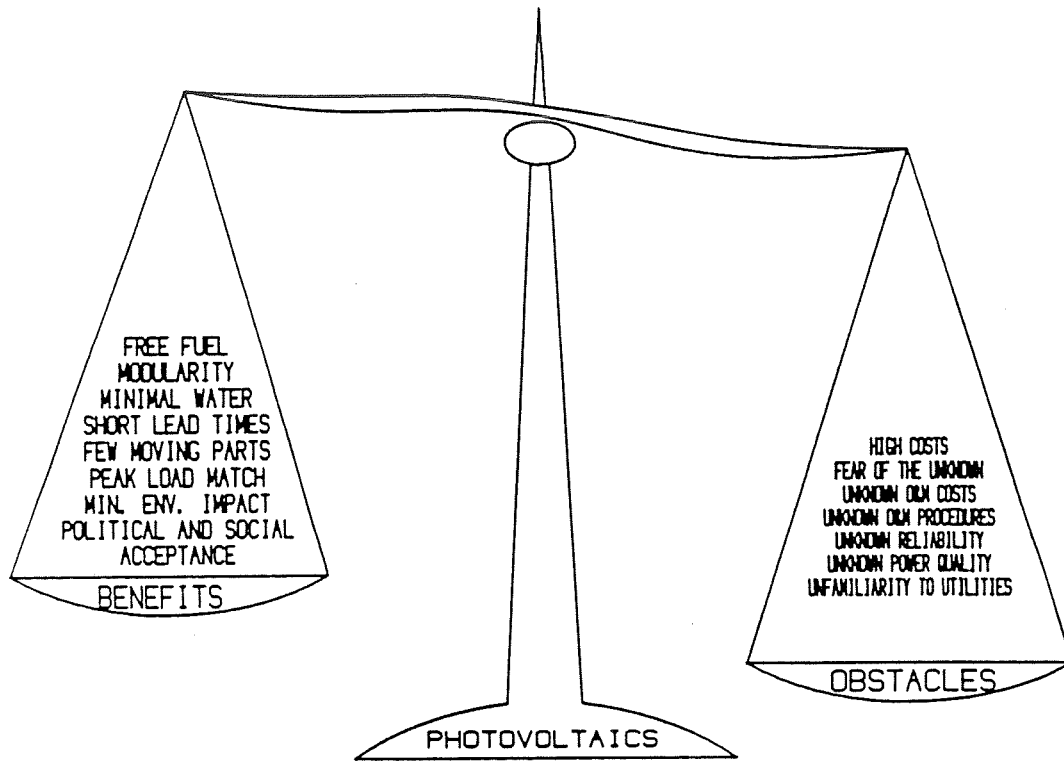
Utility Industry Familiarization with Photovoltaics

In the view of the technical community, high costs
are the major obstacle to commercialization of
photovoltaics.

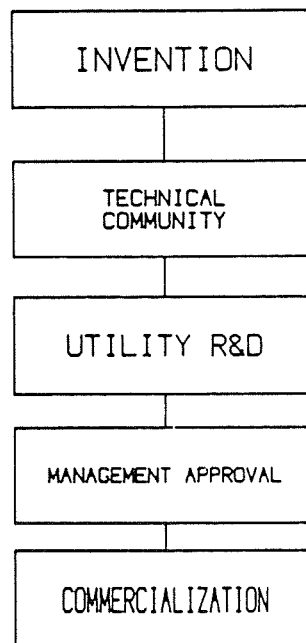


PLENARY SESSIONS

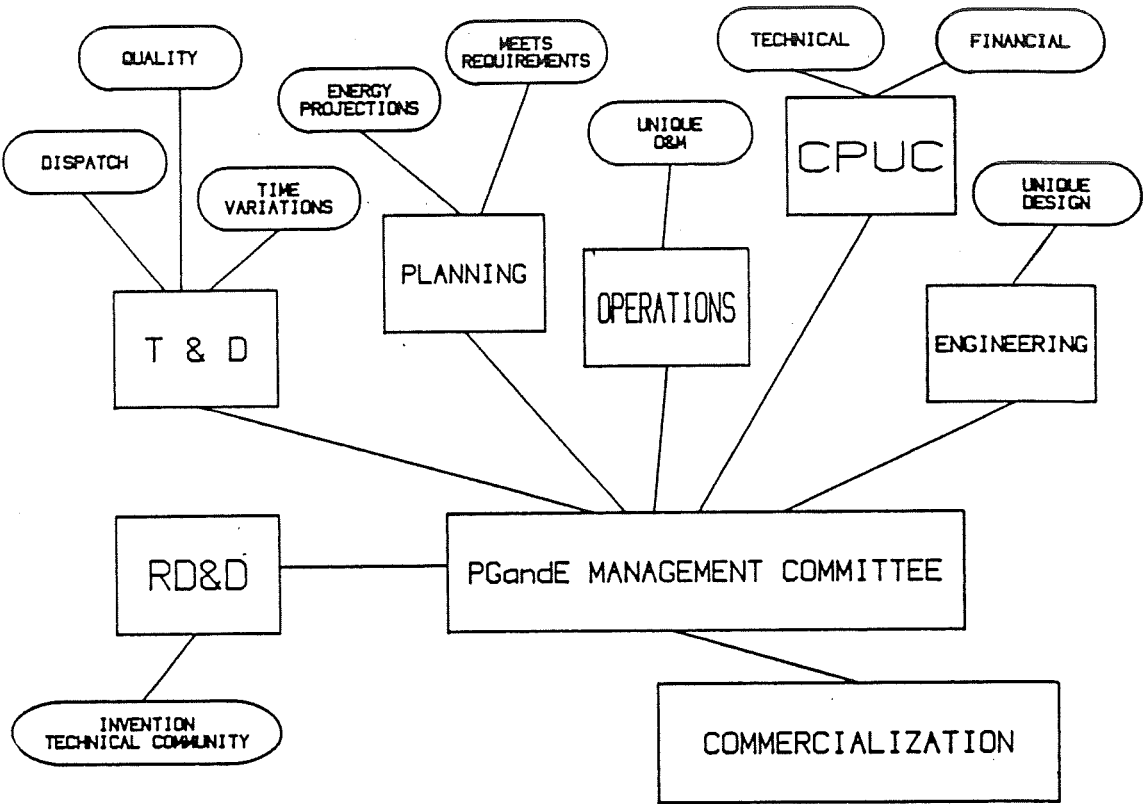
From the perspective of a utility company, many unknowns accompany high costs in the list of obstacles.



Many people believe that utility companies will make the decision to build PV power plants based on input from EPRI or their own research group.



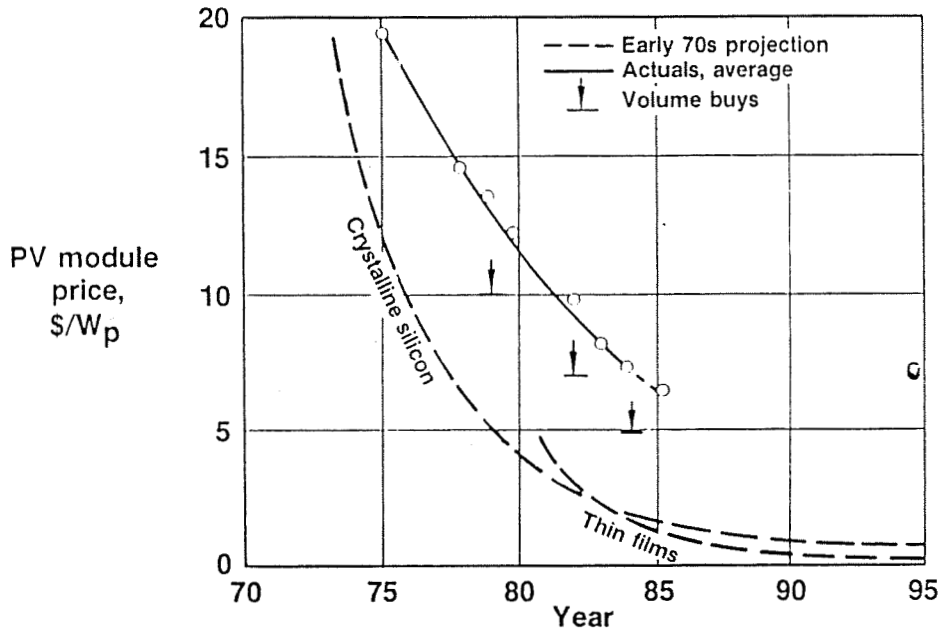
A more realistic view shows the many inputs required by a utility company's management before the decision to build PV power plants can be made.



PANEL: RECOMMENDATIONS FOR CRYSTALLINE-SILICON IN DOE'S 5-YEAR PHOTOVOLTAIC RESEARCH PLAN

HUGHES AIRCRAFT

E. L. Ralph



Market Factors

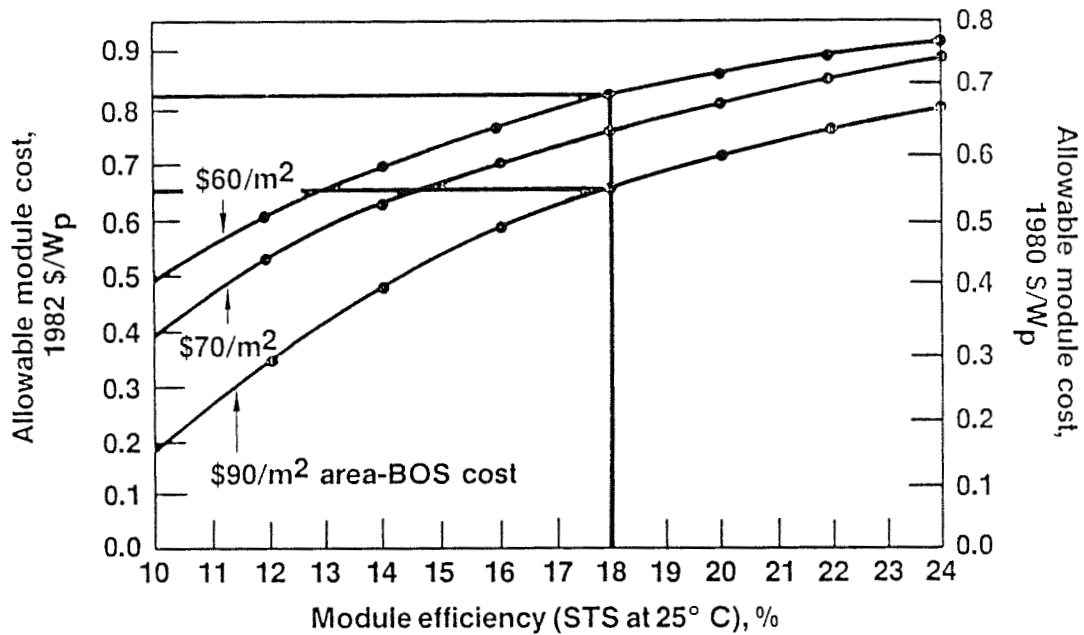
- Markets needed at various price levels
- Cost reduction comes in steps
- Profits needed to finance research and development
- New technology plus new capital reduce costs
- New markets penetrated with lower costs
- Sound pricing and management needed
- Specialty markets exist
- Utilities need and like PV systems

PRECEDING PAGE BLANK NOT FILMED

Future Expectations (Terrestrial)

- Silicon cell efficiency of 20%
- Silicon cell array efficiency of 18%
- Sheet grown silicon arrays of 17%, and \$1/Wp
- Amorphous silicon modules of 9% and $< \$1/\text{Wp}$
- Tandem α -silicon cells of $> 12\% \eta$
- Competitive CuInSe_2 and CdTe cells

Module Costs Versus Efficiency
(15¢/kWh 30-Year Levelized Energy Costs)



PV Program Assessment

- NO CLEAR SUPERIORITY BETWEEN:
THIN FILMS, MULTIBAND GAP CELLS, CRYSTALLINE Si
(WHEN BOS COSTS, RELIABILITY, AND η CONSIDERED)
- CRYSTALLINE SILICON CELL TECHNOLOGY HAS IN ITS FAVOR:
A PROVEN DATA BASE
PROVEN ADVANCES NOT YET INCORPORATED INTO PRODUCTION
CONSIDERABLE FUTURE ADVANCES AVAILABLE
- LAST YEAR JAPAN (NEDO) ESTABLISHED A POWERFUL XTAL Si PROGRAM
GOALS: 18% CELL & 15% MODULES BY 1988
BY 1990 PV ENERGY COST AT \$.50/KWH - DIESEL COMPETITIVE
- DOE CRYSTALLINE SILICON PROGRAM DANGEROUSLY LOW

Program Recommendations: Crystalline Silicon

GOALS: PRODUCTION TECHNOLOGY LEADING TO 15% MODULES
RESEARCH LEADING TO 18% FLAT MODULES
RESEARCH LEADING TO 25% FLAT MODULES, MULTIBAND GAP (Si BASE)

RESEARCH NEEDS:

- SHEET GROWTH :
CRYSTAL QUALITY, HI THROUGHPUT SHEET, AUTOMATIC GROWTH
- MINIMIZE CELL SURFACE LOSSES :
PHYSICAL/CHEMICAL STRUCTURES, SURFACE PROPERTIES, METHODS
- MEASUREMENTS :
RECOMBINATION AT SURFACES AND INTERFACES, LIFETIMES, MOBILITIES
- PROCESS DEVELOPMENT :
LOW COST, COMPATIBLE WITH HIGH EFFICIENCY GOALS

PANEL: RECOMMENDATIONS FOR CRYSTALLINE-SILICON IN DOE'S 5-YEAR PHOTOVOLTAIC RESEARCH PLAN

JET PROPULSION LABORATORY

K. M. Koliwad

Future Crystalline Silicon Research

- CRYSTALLINE SILICON TECHNOLOGY CAN MEET THE LONG-RANGE OBJECTIVES OF DOE PV PROGRAM
- FUTURE RESEARCH SHOULD FOCUS ON
 - SOLVING FUNDAMENTAL PROBLEMS TO ENABLE THE PRODUCTION OF HIGH QUALITY SILICON SHEET
 - ADVANCING THE KNOWLEDGE OF BASIC MECHANISMS OF CHARGE CARRIER LOSSES LEADING TO LARGE AREA HIGH EFFICIENCY SOLAR CELLS ON LOW-COST SILICON SHEET

Recommendations

- ° EMPHASIZE FUNDAMENTAL AND GENERIC RESEARCH THAT CAN BENEFIT A LARGE SEGMENT OF THE INDUSTRY
- ° KEEP A BALANCE BETWEEN THE VARIOUS TECHNOLOGY OPTIONS
- ° KEEP A BALANCE BETWEEN INDUSTRY, UNIVERSITY AND FEDERAL LABORATORIES
- ° DEVELOP A MECHANISM FOR LONGER TERM SUPPORT TO UNIVERSITIES
- ° AS YOU EMPHASIZE RESEARCH, THE TECHNOLOGY TRANSFER PROCESS BECOMES A CRITICAL ACTIVITY. THE PROGRAM SHOULD ESTABLISH A FORMAL PROCESS FOR DOING THAT.
- ° LEVERAGE DOD AND OTHER SUPPORT IN RELATED AREAS

PRECEDING PAGE BLANK NOT FILMED

PANEL: RECOMMENDATIONS FOR CRYSTALLINE-SILICON IN DOE'S 5-YEAR PHOTOVOLTAIC RESEARCH PLAN

WESTINGHOUSE ELECTRIC CORPORATION

C. Rose

Dendritic Web Technology Progress and Long-Range Requirements

<u>Date</u>	<u>Web Growth (cm²/Week/Furnace)</u>	<u>Module Efficiency (%)</u>
December 1984	9,000	13%
December 1985	47,000	14%
December 1986	100,000	14.5%
December 1987	150,000	15%

Advanced Silicon Sheet Requirements General Research in High-Speed Ribbon Growth

- Detailed Analysis of Plastic Flow and Deformation to Optimize Growth Speed
- Control of Thermal Stress Induced Ribbon Buckling to Produce > 10 cm Wide Ribbons
- On-Line Crystal Quality Assessment
- Improved Replenishment/Growth Region Isolation in Molten Silicon
- Refinements in Closed Loop Growth Controls in Ribbon Furnaces
- Removal of Web Strips During Continuous Growth

PRECEDING PAGE BLANK NOT FILMED

Silicon Materials Requirements

- Material Capable of Continuous Feed
- Small Particles, Semiconductor Grade
- Cost < \$30/kg

Flat-Plate Collector Requirements

"15% Modules from a \$90/m² Process"

- Cell Efficiency/Material Characteristics Correlation
- High Throughput Simultaneous Junction Formation
- Multilayered AR Coating
- Back Surface Grid
- Lower Cost Metallization System
- Low Cost Ribbon Cassette Designs
- Automated Material Handling Devices

PANEL: RECOMMENDATIONS FOR CRYSTALLINE-SILICON IN DOE'S 5-YEAR PHOTOVOLTAIC RESEARCH PLAN

SOLAREX CORPORATION

E. E. Daniels

Crystalline Technology Development Focus

- **Silicon**
- **Wafer Fabrication**
- **Cell Processing**
- **Product Assembly**
- **Arraying**
- **Systems Integration**

The Crystalline Photovoltaic Industry Today

- **Established Reliability**
- **Dramatic Improvement in Performance**
- **Significant Price Reductions**
- **Growing Commercial Acceptance**

Vertical Integration

- o SILICON PRODUCTION
- o CRYSTALLIZATION
- o WAFERING
- o CELL PRODUCTION
- o MODULE ASSEMBLY

SYSTEM DESIGN, ASSEMBLY, INSTALLATION

Photovoltaic Advantages

- O ENVIRONMENTAL BENIGN
- O MAINTENANCE FREE
- O ECONOMIC UNIT SIZE
- O EASILY INSTALLED
- O SHORT LEAD TIMES
- O VERY LOW OPERATING COSTS
- O PROVEN RELIABILITY

Accomplishments of the Photovoltaic Community

- **Research & Development**
 - **Established Sound Technology Base**
- **Industry**
 - **Utilization of Sound Technology Base**
 - **Establish Sound Business Base**

Crystalline Industry Focus

- **User Awareness**
- **User Acceptance**

Technology

OPTIONS

- O SINGLE CRYSTAL
- O SEMICRYSTALLINE
- O RIBBON
- O AMORPHOUS

The Future: Technology

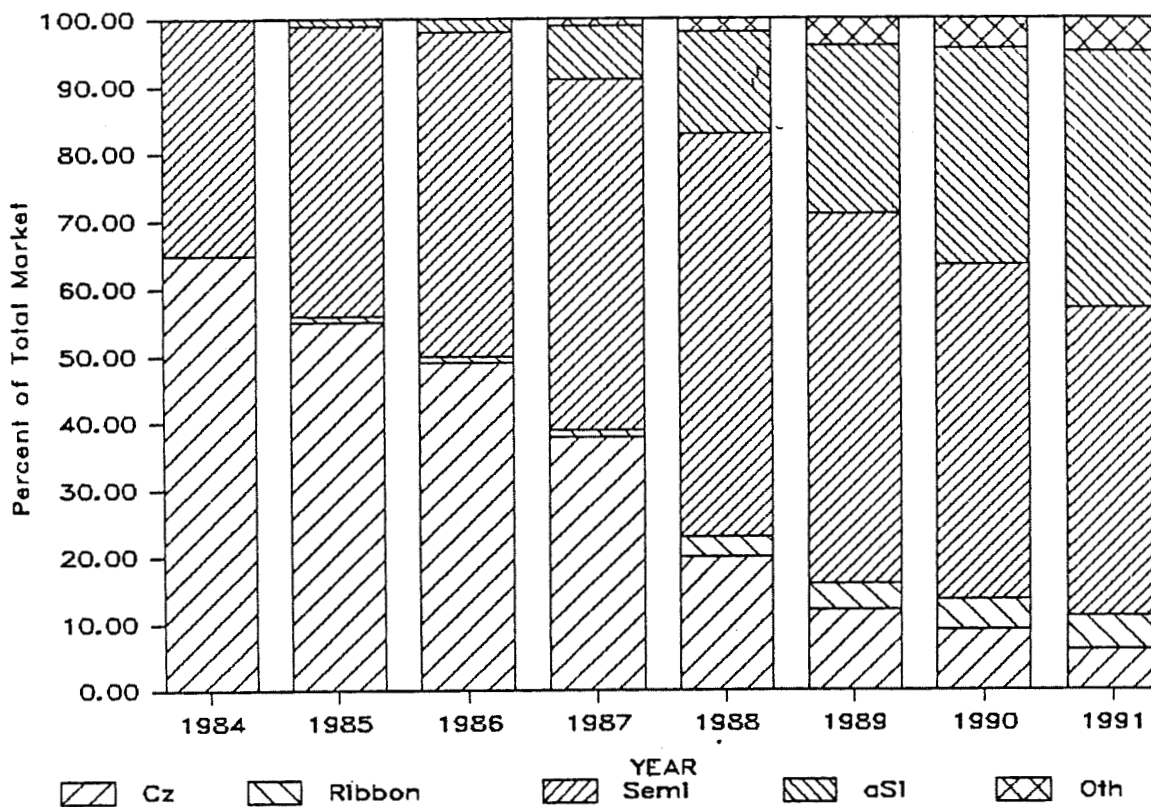
Crystalline Technology

- Semicrystalline (Poly) Product for Next 5-10 Years
- 8 - Major Manufacturers Have Introduced this Technology Since 1981

Sheet Technology

- May Actually Be Polycrystalline
- Needs to Prove Reliability

World Photovoltaics Market (Technology as a Percent of Market)



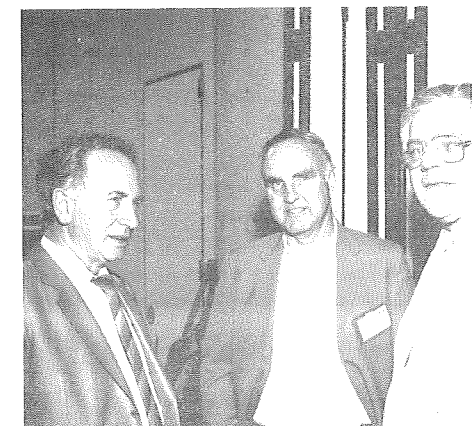
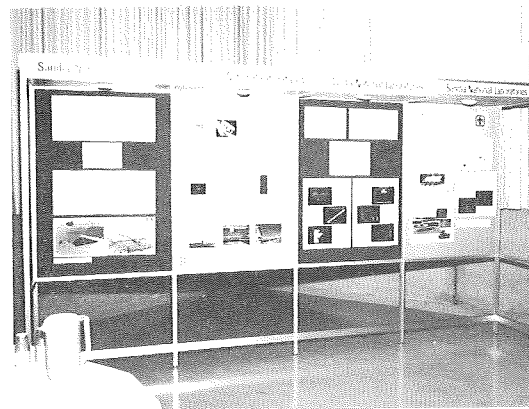
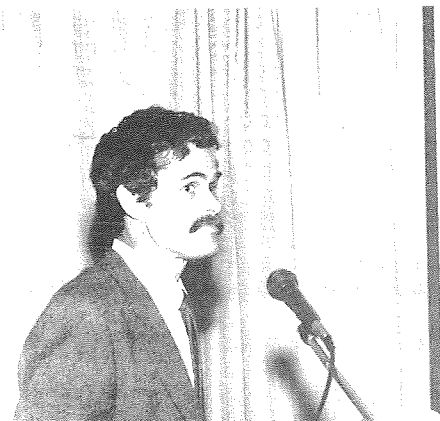
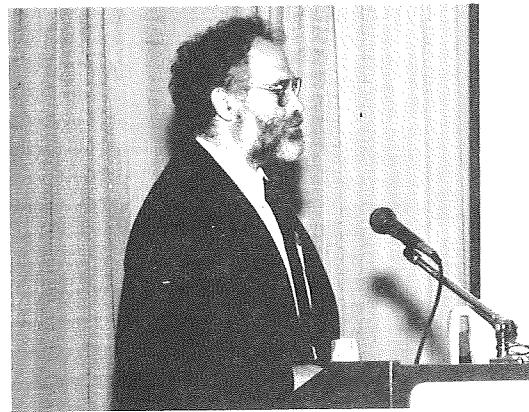
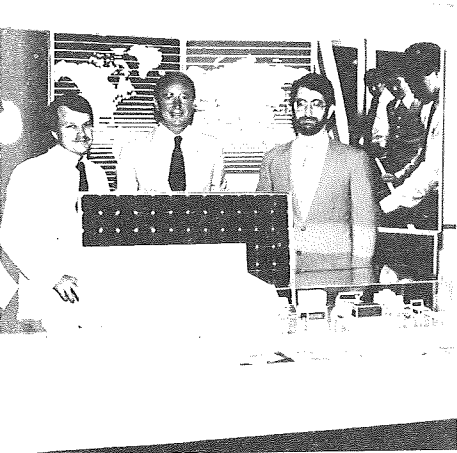
The Future: Industry Needs

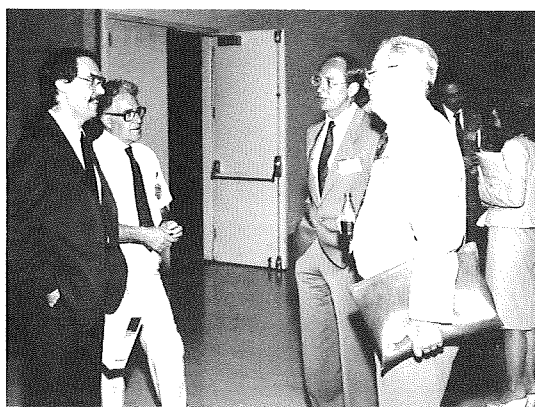
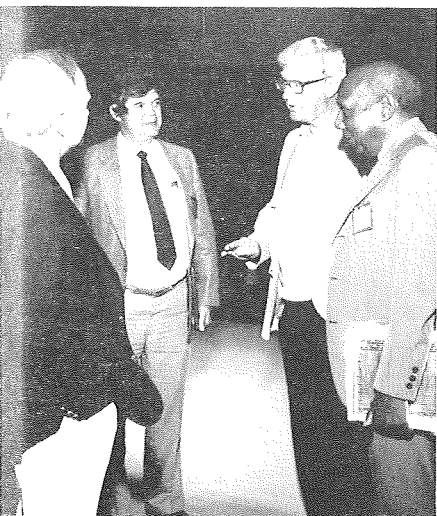
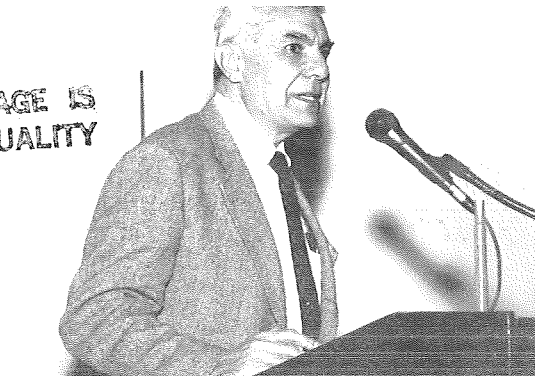
Viable Business Base Development

- **Education**
 - **Appropriate Demonstration Projects**
- **Internationally Recognized Test Sequence**
- **Internationally Accepted Product Rating System**
- **Financing Support**



ORIGINAL PAGE IS
OF POOR QUALITY





TECHNICAL SESSIONS

Cell Technology

ADVANCED SILICON SHEET

Andrew D. Morrison, Chairman

Eleven presentations were made at this session covering research on silicon-shaped sheet technology.

JPL reported on the FSA-sponsored Fourth Silicon Stress/Strain Workshop held March 18 and 19, 1986, at the University of Kentucky, Lexington, Kentucky. The purpose of this Workshop was to review, coordinate, and assess the progress in understanding and controlling stress and strain during the crystal growth of silicon ribbon.

Westinghouse Electric Corp. reviewed progress in its program to develop the technology of the dendritic web ribbon process. Thermal stress analysis, automated closed-loop control of ribbon growth, and increased ribbon area growth rates were subjects receiving emphasis.

JPL reported on its Web Team activities which are directed toward identifying and attacking problem areas in the growth of dendritic web ribbon, to complement the program at Westinghouse Electric Corp.

Mobil Solar Energy Corp. reviewed progress in its stress and efficiency studies of edge-defined film-fed growth (EFG) material. Effort was concentrated on the definition of conditions that will reduce stress, on quantifying dislocation electrical activity and limits on solar cell efficiency, and on studying the effects of dopants on EFG characteristics.

The Solar Energy Research Institute (SERI) described the work on silicon for high-efficiency solar cells. Topics that were discussed included the contributions made by evaporation and segregation to impurity profiles of float-zone (FZ) crystals, study of the effects of some crystal growth parameters on minority-carrier lifetimes, and defect investigations by x-ray topography.

The University of Kentucky presented results of its work on stress/strain relationships in silicon ribbon. Calculations of stress fields, dislocation densities, and buckling were made; uniaxial tensile tests were made on silicon at 1150°C; and dislocation motion studies were performed.

JPL described in-house work on silicon stress/strain, including the study of fracture mechanics, and on the high-temperature test program in which the low-strain response of silicon sheet materials above 1000°C is being measured and new high-temperature material property data are being determined.

Cornell University reported on their results in the study of high-temperature deformation of dendritic web ribbon, and in the work on measuring oxygen in the material.

ADVANCED SILICON SHEET

The University of Illinois at Chicago discussed their program which is aimed at developing an understanding of the basic mechanisms of deformation during the lubricated cutting of silicon, and at developing a nondestructive measurement technique for residual stresses in silicon sheet.

Washington University at St. Louis reported on their modeling study of Czochralski (Cz) crystal growth.

REPORT ON THE FOURTH STRESS STRAIN/WORKSHOP

JET PROPULSION LABORATORY

M. H. Leipold

Purpose

- TO REVIEW, COORDINATE AND ASSESS THE PROGRESS IN UNDERSTANDING AND CONTROLLING STRESS AND STRAIN DURING THE CRYSTAL GROWTH OF SILICON RIBBON

Location

- HOSTED BY THE UNIVERSITY OF KENTUCKY AT LEXINGTON, KY
ON MAR 18-19, 1986

Content

- 12 TECHNICAL PRESENTATIONS BY CONTRACTOR, JPL STAFF AND GUEST SPEAKERS. MEETING ATTENDANCE WAS 25

Technical Background

- NUMEROUS 'LIMITS' TO RIBBON GROWTH RATE EXIST
 - REJECTION OF HEAT OF FUSION
 - MACRO STRESS - ELASTIC OR PLASTIC BUCKLING STRUCTURE
 - MICRO STRESS - INTERNAL DISLOCATION

Technical Progress

- COMPUTER ANALYSIS OF STRESS AS A FUNCTION OF TEMPERATURE PROFILE
 - CREEP RELAXATION STILL IN QUESTION
- MACRO-DEFORMATION BECOMING TRACTABLE
 - ELASTIC BUCKLING REDUCED WITH BETTER PROFILES
 - PLASTIC BUCKLING SENSITIVE TO DATA FOR HIGH TEMPERATURE MECHANICAL PROPERTIES OF Si
 - SUMINO DATA VERY USEFUL
 - TESTS IN PROGRESS
- MICRO-DEFORMATION SHOWS PROGRESS
 - COMPUTER MODELS NOW DESCRIBE DISLOCATION, MULTIPLICATION & MOTION
 - BETTER DATA NEED
 - NUMBER OF DISLOCATION SOURCES IS INDETERMINANT

Technical Prognosis

- BETTER UNDERSTANDING OF PROCESS IS YIELDING SOME IMPROVEMENTS
- EXISTENCE OF FINITE 'SPEED LIMITS' IS LIKELY
- VARIOUS APPROACHES TO CONTROLLING STRESS EXIST
 - SOLID SOLUTION HARDENING
 - CONTROLLED TEMPERATURE PROFILES ACROSS WIDTH
 - CRYSTAL FRONT NOT PERPENDICULAR TO RIBBON
 - CONTROL OF STRAIN DISTRIBUTION
- PERFORMANCE WINDOW STILL AVAILABLE

SILICON DENDRITIC WEB GROWTH

WESTINGHOUSE ELECTRIC CORPORATION

R. Hopkins

Silicon Dendritic Web Development

Recent Highlights

- Area Rate $10 \text{ cm}^2/\text{min}$, $> 1 \text{ m}$ Length
- Maximum Web Width 7 cm; 6 cm Wide Web Frequently Grown
- 17 m Long Web Grown with Continuous Replenishment
- Closed Loop Control System Successfully Demonstrated
- Growth Initiation from "Web Seeds" Up to 4.5 cm Wide
- Doubled Maximum Weekly Single Web Furnace Output to $47,000 \text{ cm}^2$

Overview of Web Growth Studies

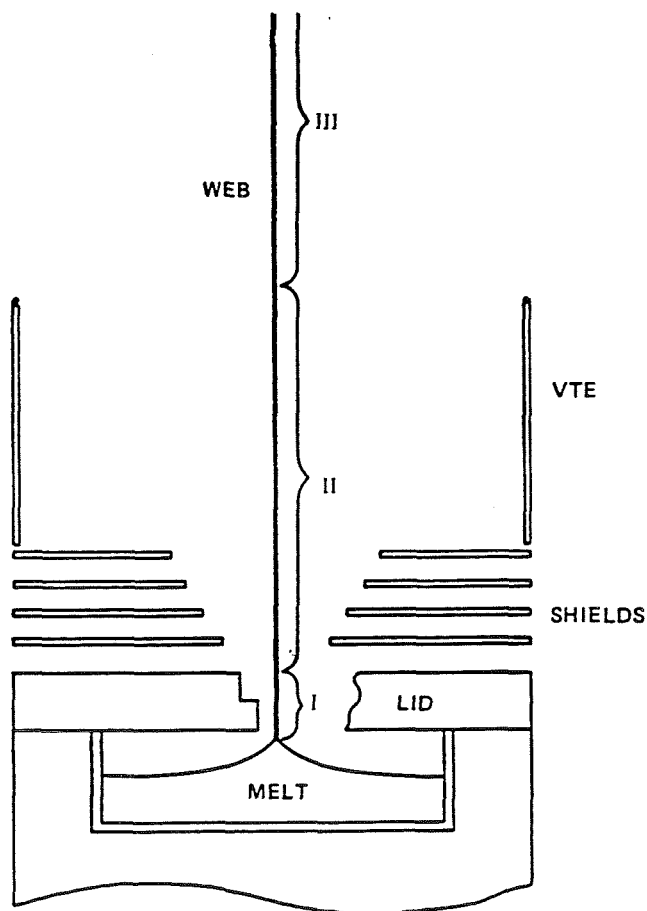
- Area Rate Development
 - Thermal Stress Effects:
 - Elastic Buckling
 - Plastic Deformation
 - (R. G. Seidensticker, J. P. McHugh, J. Spitznagel, S. Y. Lien, R. Hundal, R. Spreccase)
- Closed Loop Control of Web Growth
 - (J. Easoz, P. Piotrowski, C. S. Duncan, F. Przywarty, E. L. Kochka)
- Summary

Silicon Dendritic Web Development Modeling Studies

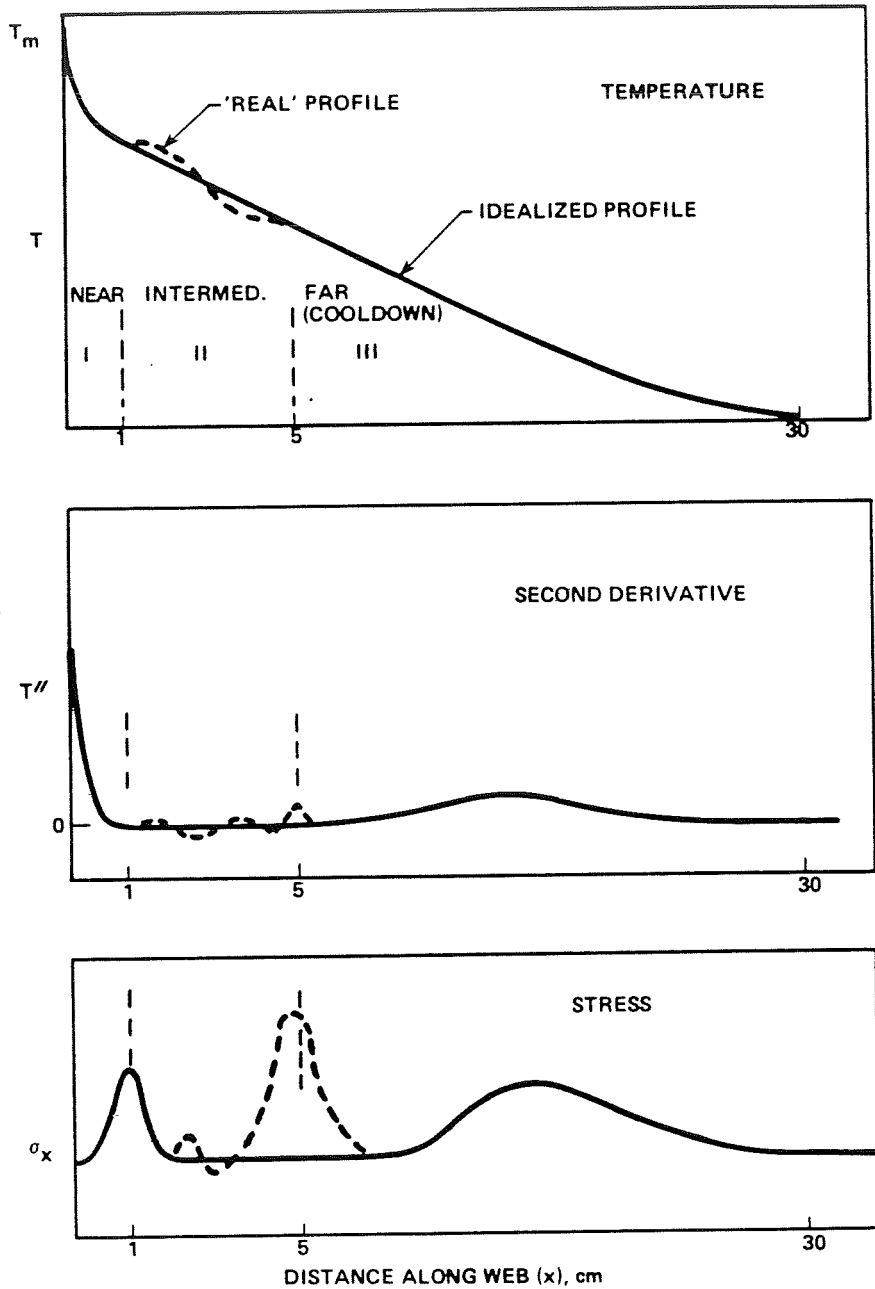
Elastic Deformation

- Model Full Cooling Curve to Analyze Buckling
- Area Rate Currently Not Limited by Interface or Cooldown Stresses
- Intermediate Stress Must be Controlled in Real Systems
- Intermediate Stress
 - Can Trigger Mixed Buckling Mode
 - Direct Cause of Buckles
 - Can Interact to Cause Plastic Flow
- Webs can Grow Continuously in Quasi-Stable Buckled Form

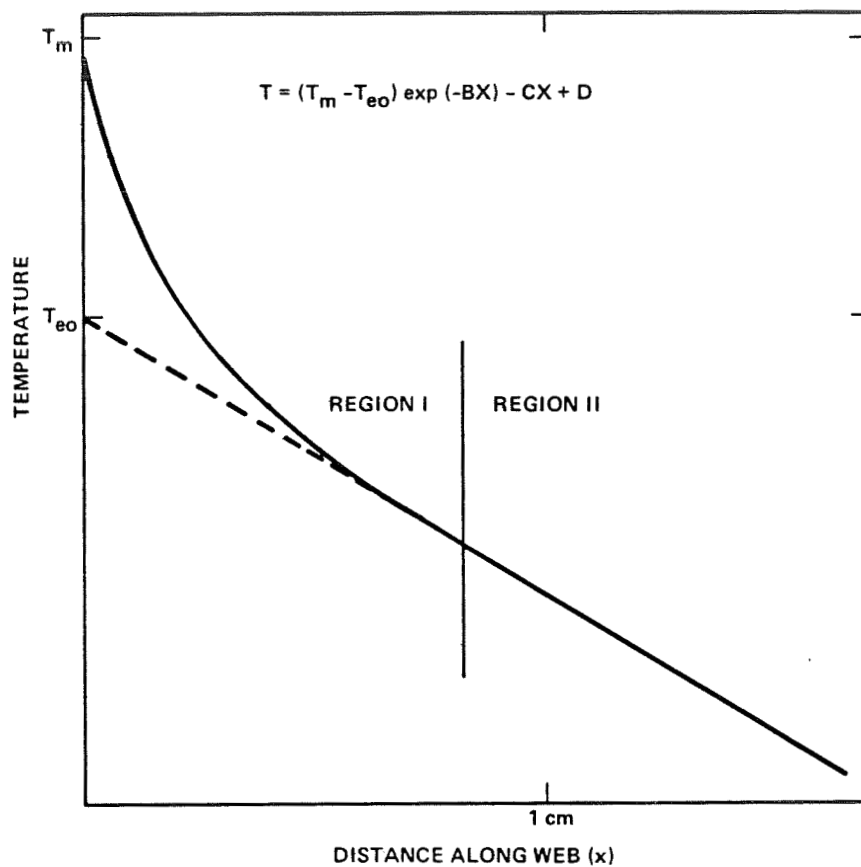
Thermal Stress Regions in Silicon Web



Web Axial Temperature and Stress Distributions



Interface Temperature Distribution (Exponential-Linear)

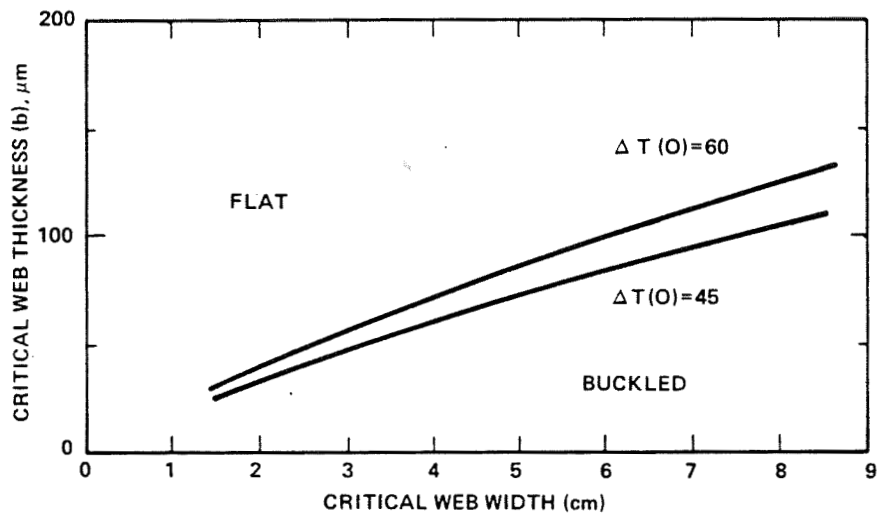


Near Stress Summary

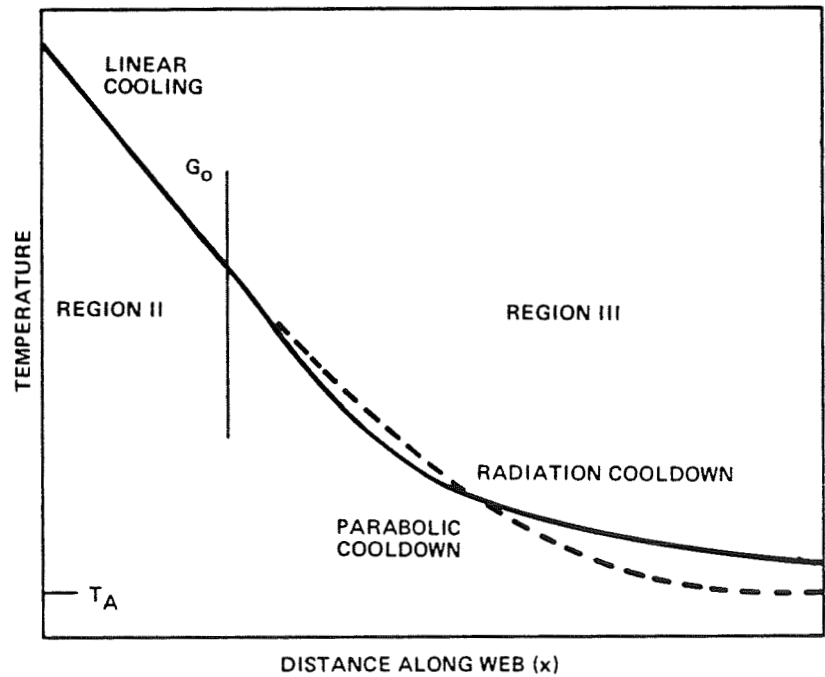
Critical Buckling Thickness And Width Are Related By:

$$b=1.72 (\Delta T)^{.63}W^{.82}$$

$$\Delta T=(T_m-T_{eo})$$



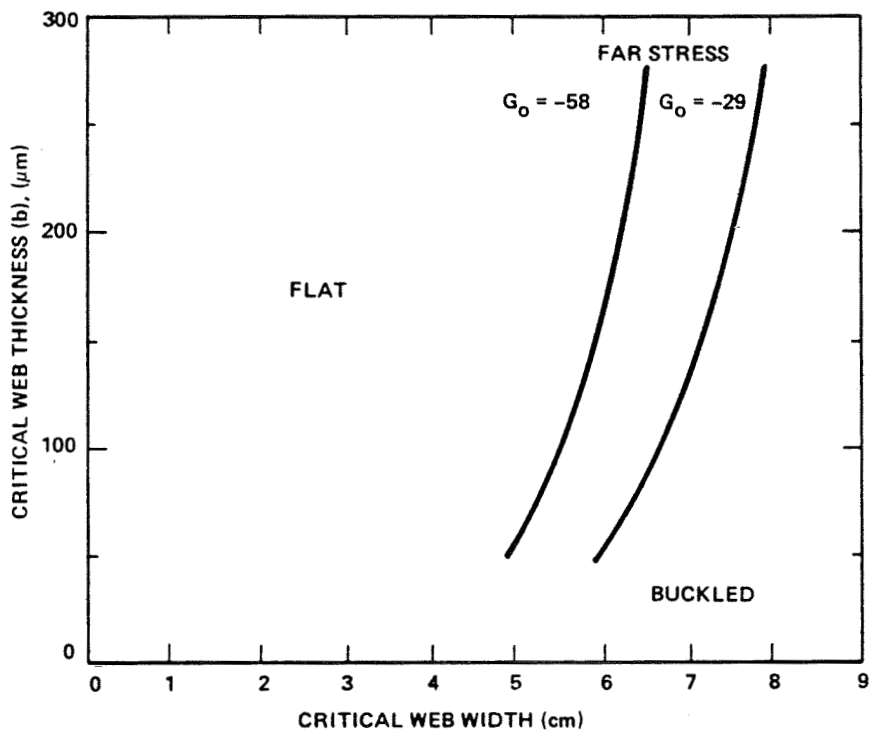
Cooldown Temperature Curves



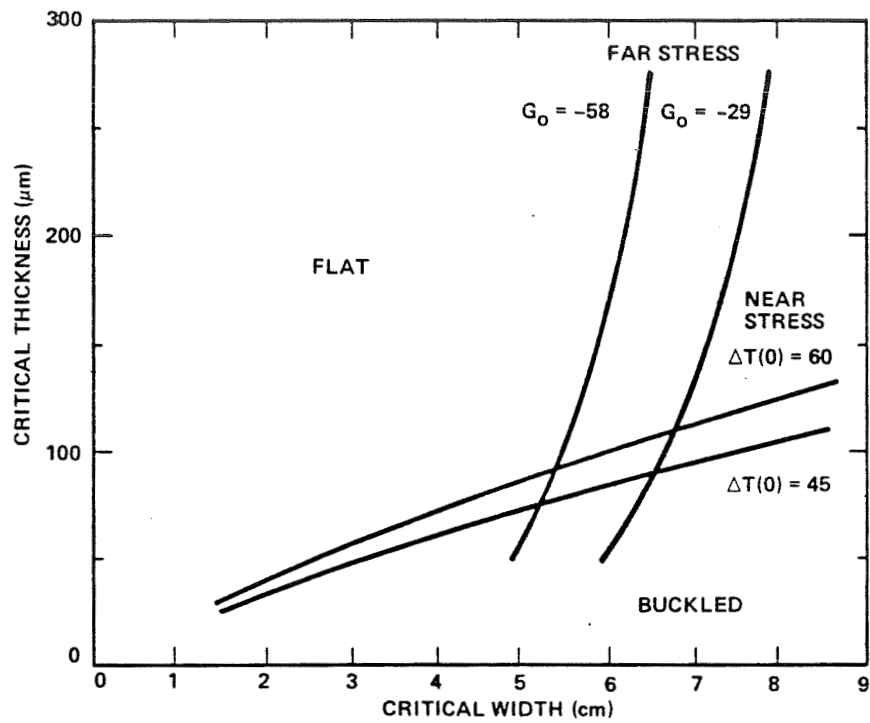
Far (Cooldown) Stress Summary

Critical Buckling Thickness And Width Are Related By:

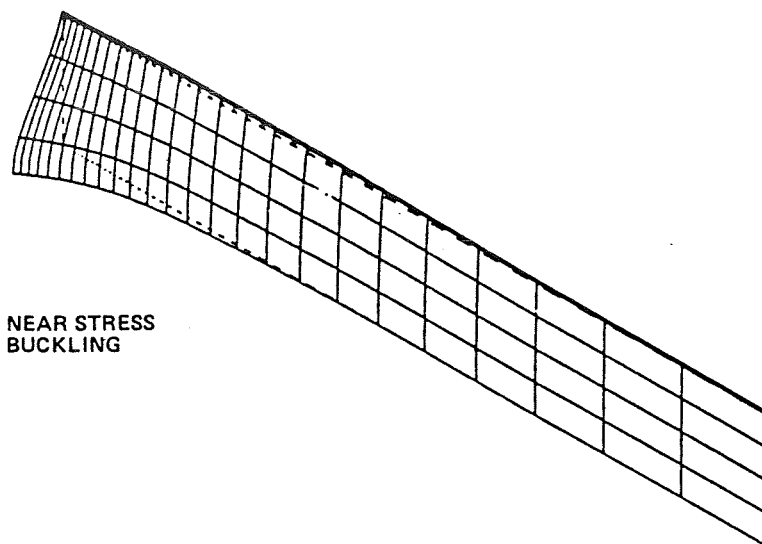
$$b \cong \text{Const. } G_o W^{3.8}$$



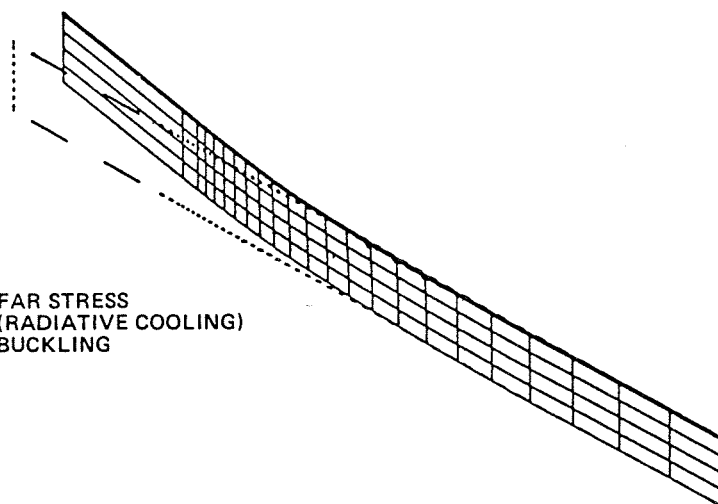
Parametric Variation of Critical Buckling Width and Thickness



Buckled Web Shapes

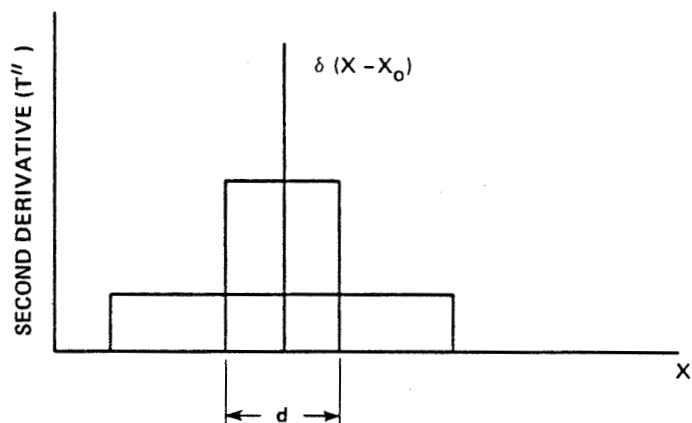
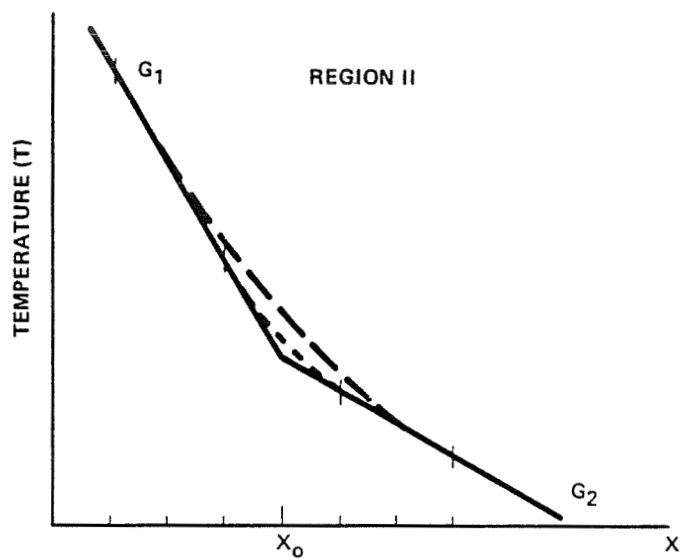


NEAR STRESS
BUCKLING

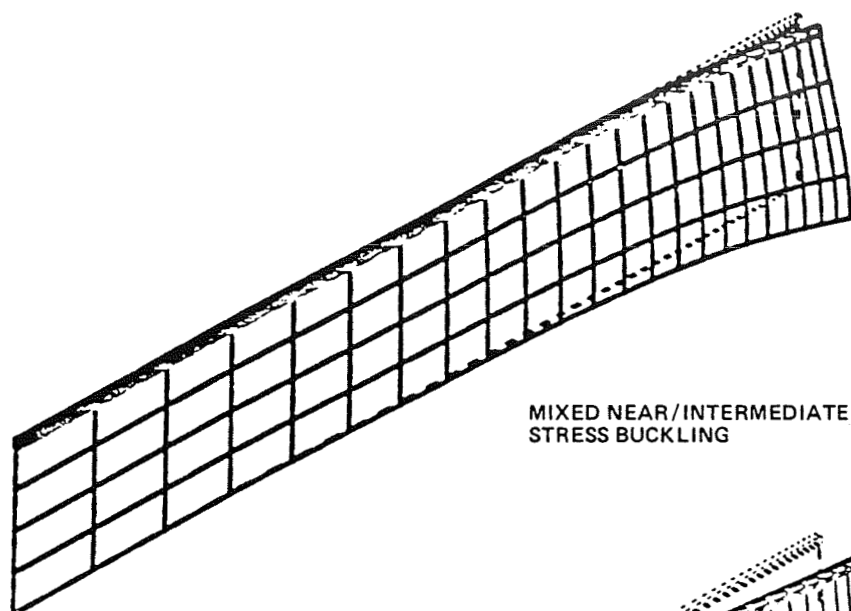


FAR STRESS
(RADIATIVE COOLING)
BUCKLING

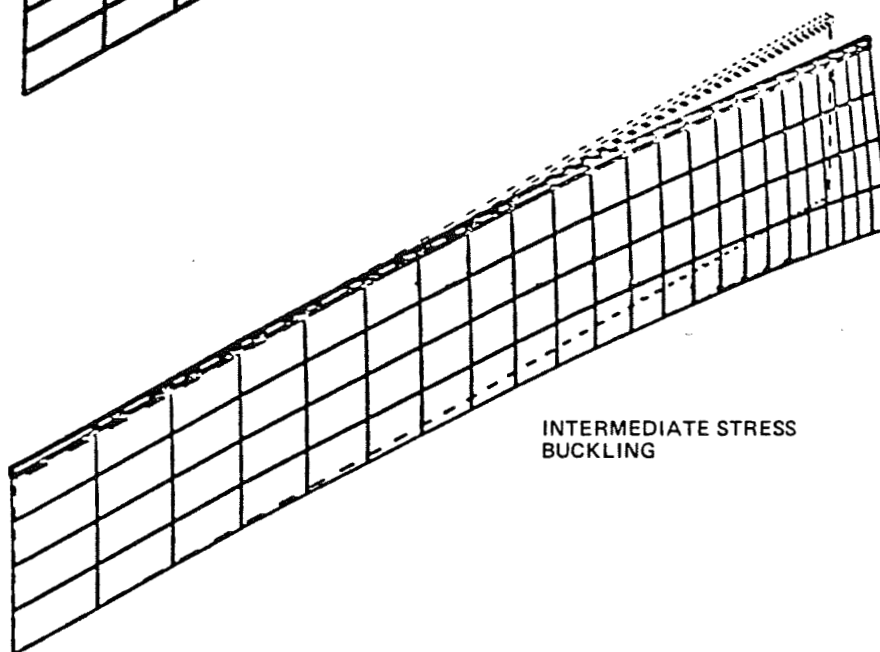
Change in Second Derivative with Bend Transition
in Web Temperature Profile



Buckled Web Shapes

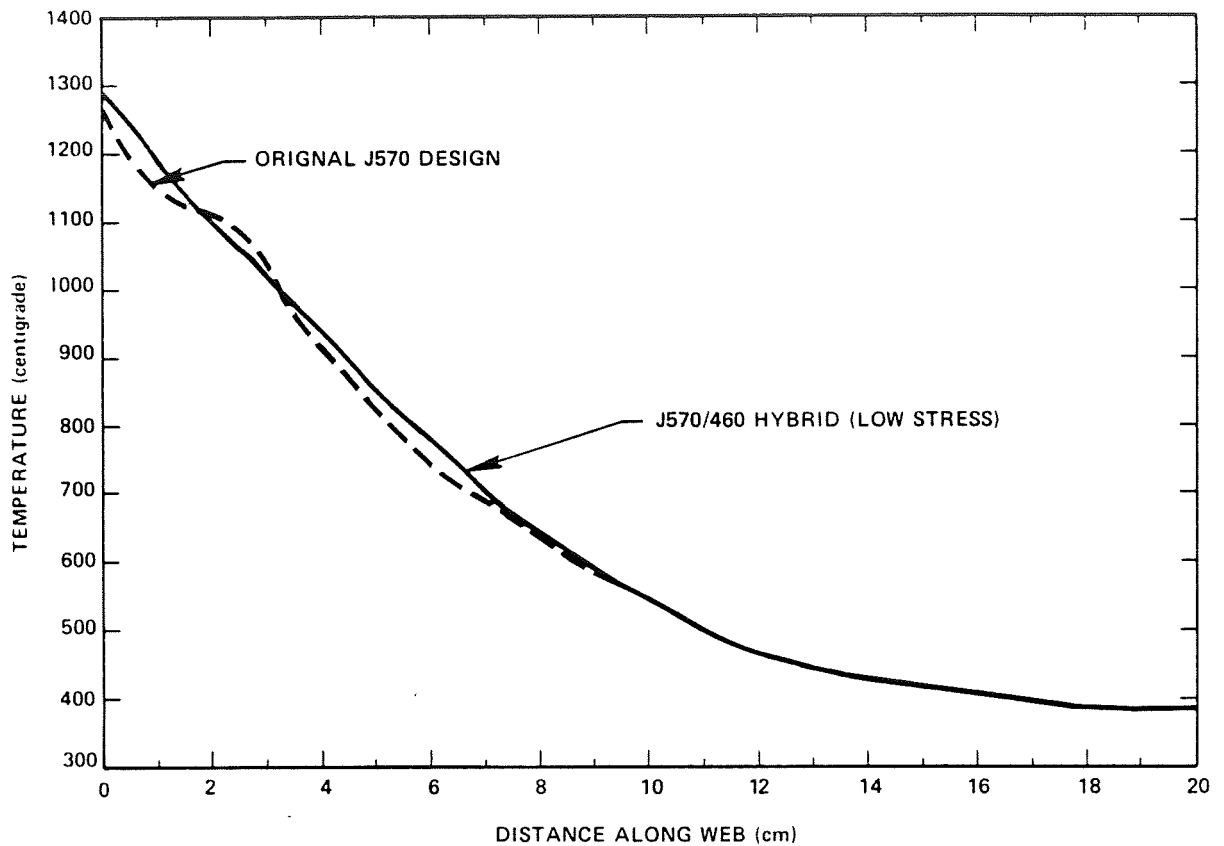


MIXED NEAR/INTERMEDIATE
STRESS BUCKLING



INTERMEDIATE STRESS
BUCKLING

Improved Linearity in Measured Axial Temperature Profiles

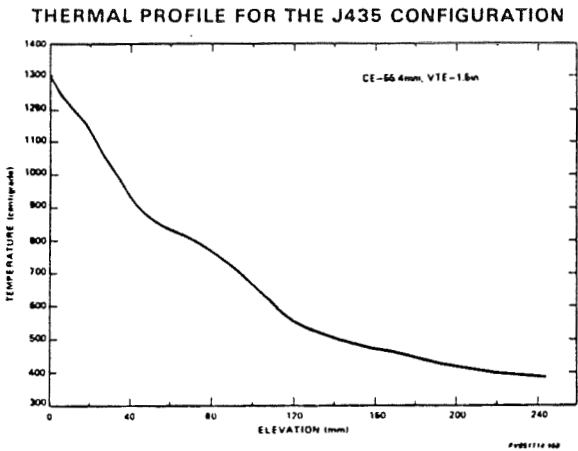


Silicon Dendritic Web Development Modeling Studies

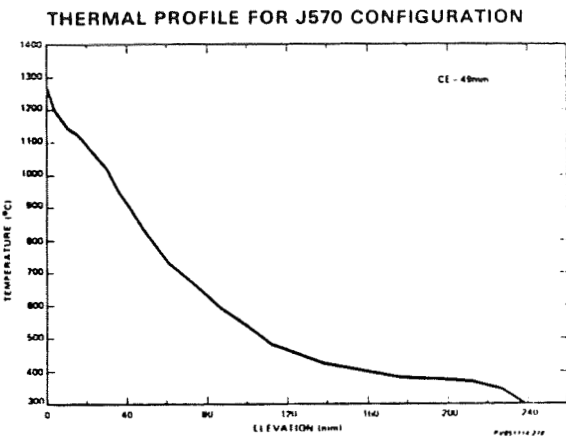
Plastic Deformation

- Penning/Jordan Type Model Developed/Applied to Web
- Predict Defect Distributions in Web
- Residual Stress Estimations in Qualitative Agreement with Experiment
- Residual Stress can Promote/Reduce Buckling
- Plastic Flow Geometry Specific; Controllable by Design

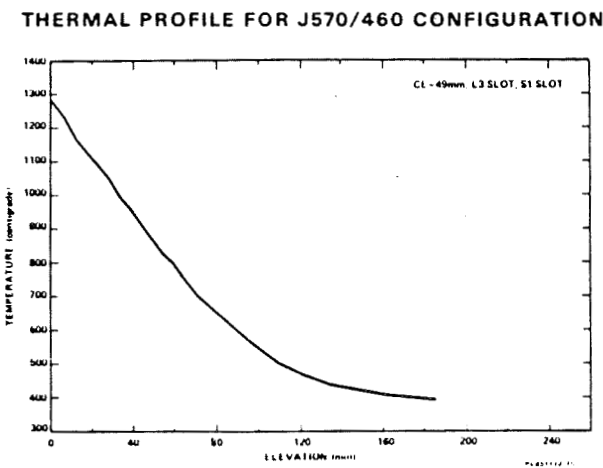
Axial Temperature Profiles Resulting in Widely Different Residual Stress States



High Positive
Residual Stress

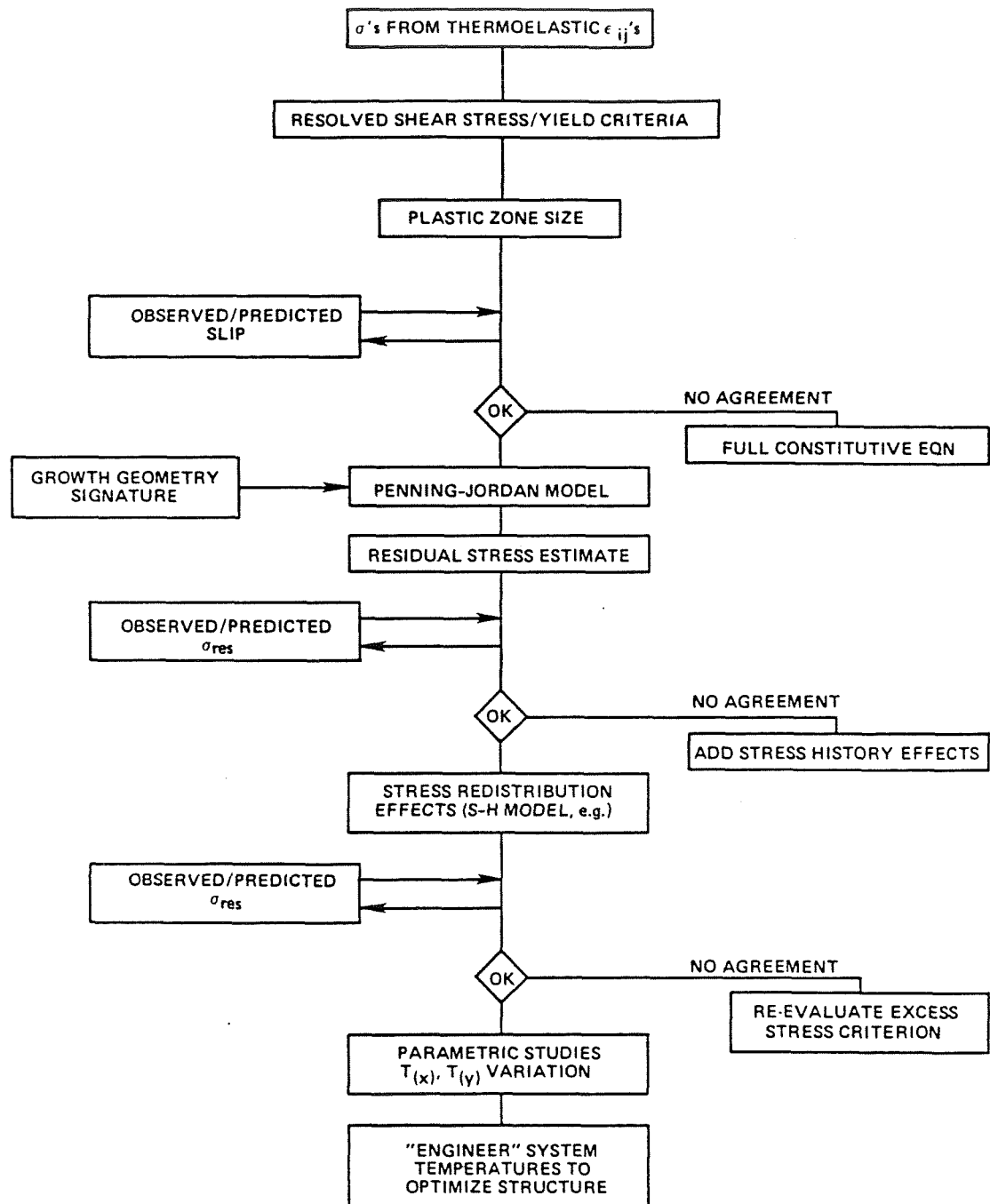


High Negative
Residual Stress

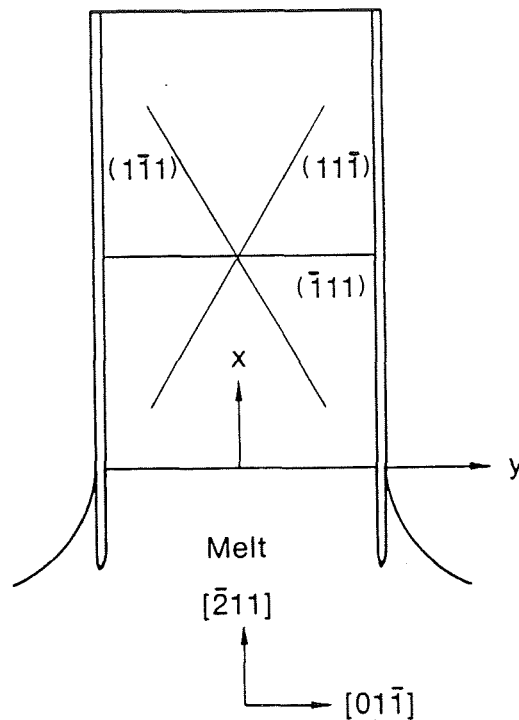


Low (Negative) Residual Stress

Web Plasticity Analysis



Web Slip Geometry



Plasticity: Penning/Jordan Model

1. Distortions from Thermal Stresses Mostly Elastic
2. Stress Redistribution Effects Small
 - Can Predict Slip Patterns
3. Dislocation Density Proportional to Resolved Shear Stress

$$\rho_a \propto \sum_{x=0}^{x=L} (\tau_a - \tau_y) \Delta x ; y = \text{Const}$$

4. Shear Strain Proportional to ρ_a

$$\dot{\epsilon}_a \propto \rho_a \cdot b \cdot v$$

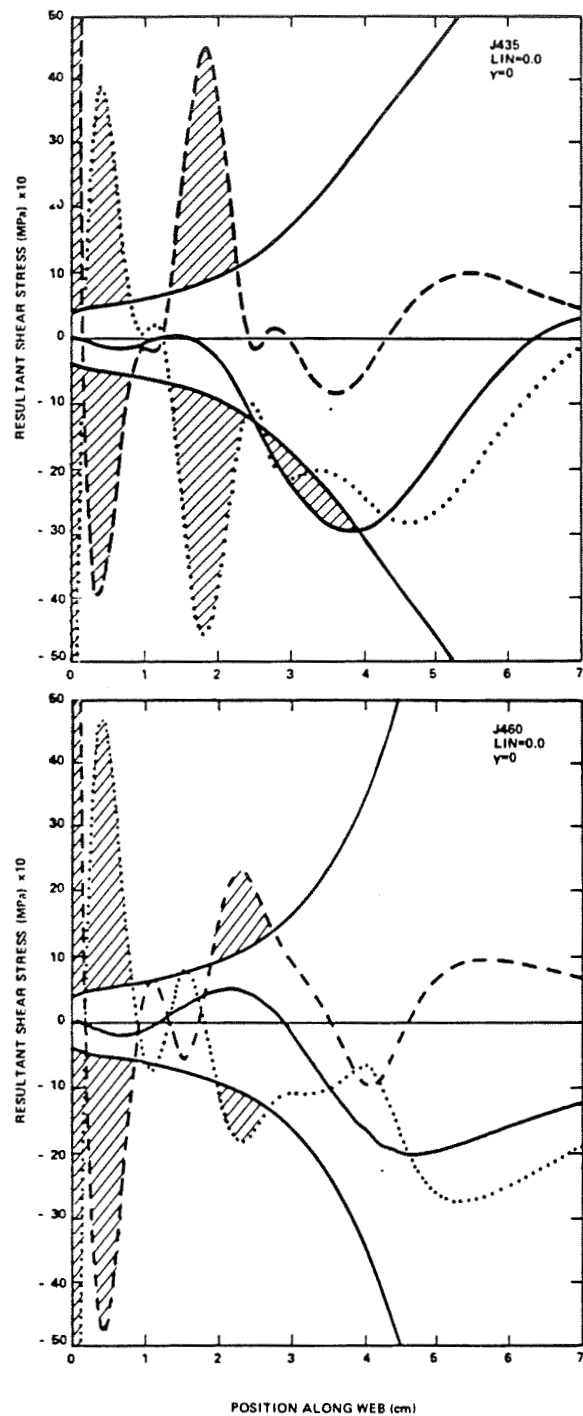
$$v = f(\tau_a, T)$$

$$\epsilon_a \propto \sum_{x=0}^{x=L} (\tau_a - \tau_y) v \Delta x$$

5. Residual Stress Determined By Net "Plastic" Shear Strain

$$\Delta \sigma_x \propto \sum_a \epsilon_a$$

Resultant Shear Stress Along Web for Various Slip Systems



J435 (5334)

J460

Comparison of Calculated "Excess Stress" from
Model and Measured Residual Stress*

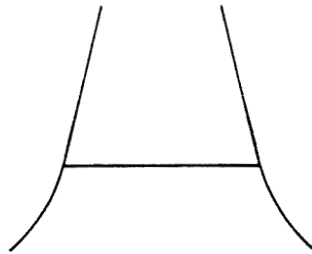
<u>Configuration</u>	<u>Theory at Growth Temp.</u>	<u>Theory T = 300°K</u>	<u>$\Delta \sigma_x$ (Meas) Mdynes/cm²</u>
J435 (5334)	-36.1	+36.1	20-30
J460	+5.6	-5.6	0 \pm 10

*Not Corrected for Dislocation Velocity Differences

Closed Loop Control Status

- Successful Demonstration of Coupled Coil and Temperature Controls
 - 35% Increase in Crystal Length with Controls
 - Average Dendrite Controlled to $\pm 50 \mu\text{m}$ Control Specification
 - Maximum Controlled Run Length 5.5 Hours (τ System ~ 3 min)
- Experimental Prototype In Place; Operational Data Being Collected

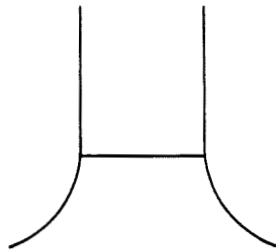
Response of Diameter to Velocity or Temperature Change



Increasing Diameter

$$T < T_{\text{Growth}}$$

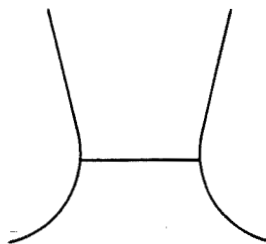
or $V < V_{\text{Growth}}$



Constant Diameter

$$T = T_{\text{Growth}}$$

$V = V_{\text{Growth}}$

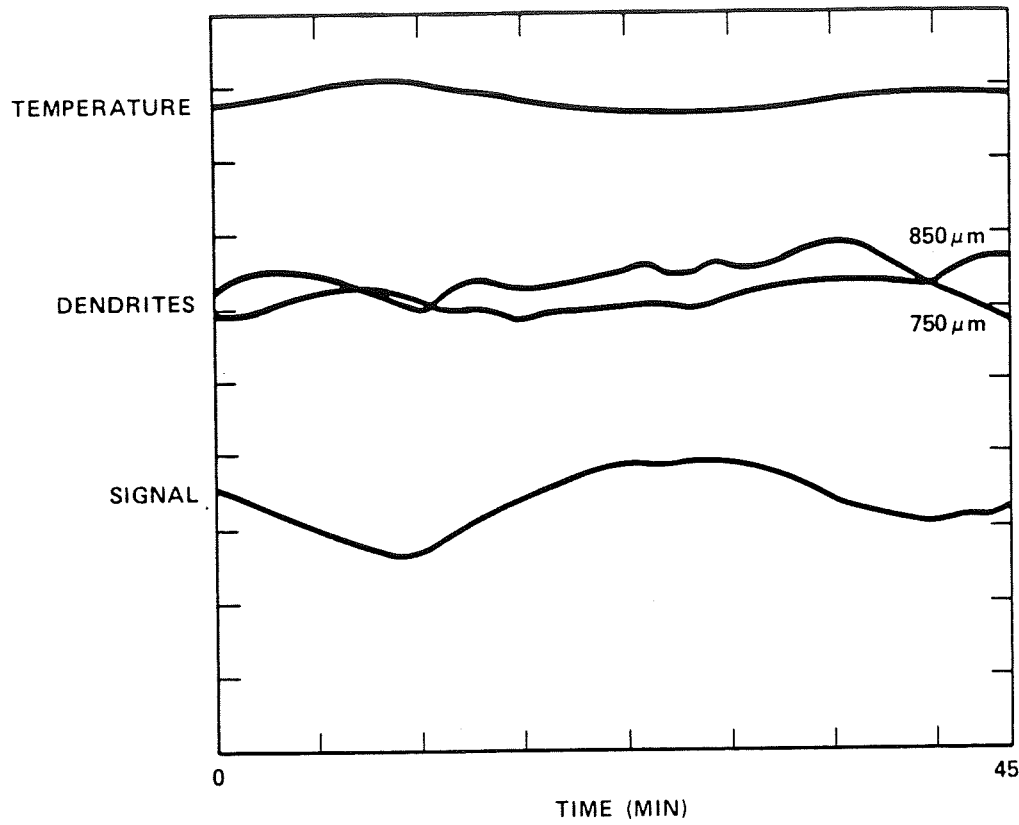


Decreasing Diameter

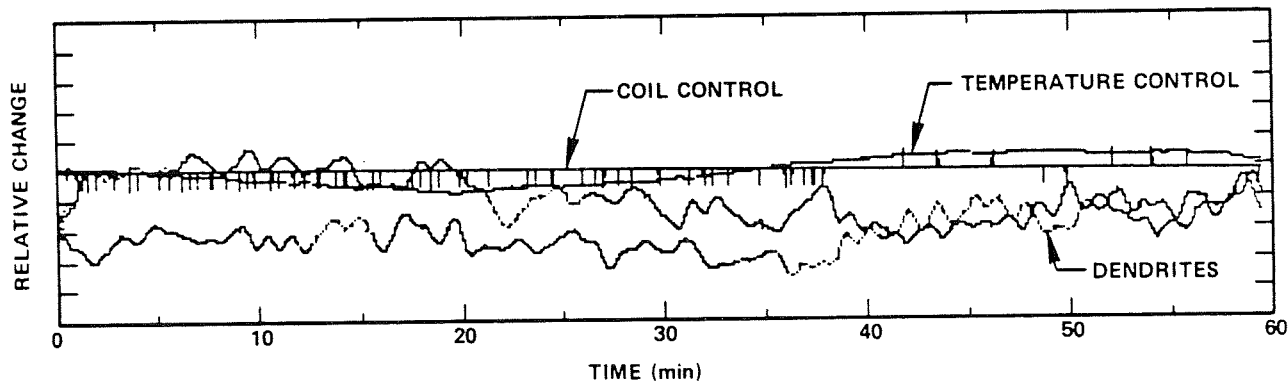
$$T > T_{\text{Growth}}$$

or $V > V_{\text{Growth}}$

Sample Data from Controlled Growth Run
(Control Point = 825)



Coil Positioning Control



Silicon Dendritic Web Development

Status and Future Activities

- Key Elastic Stress Generation Mechanisms Identified
 - Analytic Focus: Intermediate Stress
Interaction of Near/
Intermediate Stress
 - Experiment Focus: Linearization of
Intermediate Profile
Smooth Cooldown Curve
- General Features of Plastic Flow Appear Predictable
 - Analytic Studies: Refine Flow Model
Parametric Studies
Analyze Elastic/Plastic
Interactions
 - Experiment: Correlation of Observed
Defects/Stress with Model
Engineer Lid Temperature
Profile to Control
Deformation
- Closed Loop Web Growth System Functional
 - Refine Electronics
 - Simplify Hardware and Software
 - Develop Operational Experience to Achieve
Routine Behavior

JPL WEB TEAM

JET PROPULSION LABORATORY

D. B. Bickler

Web Team

- **Background**

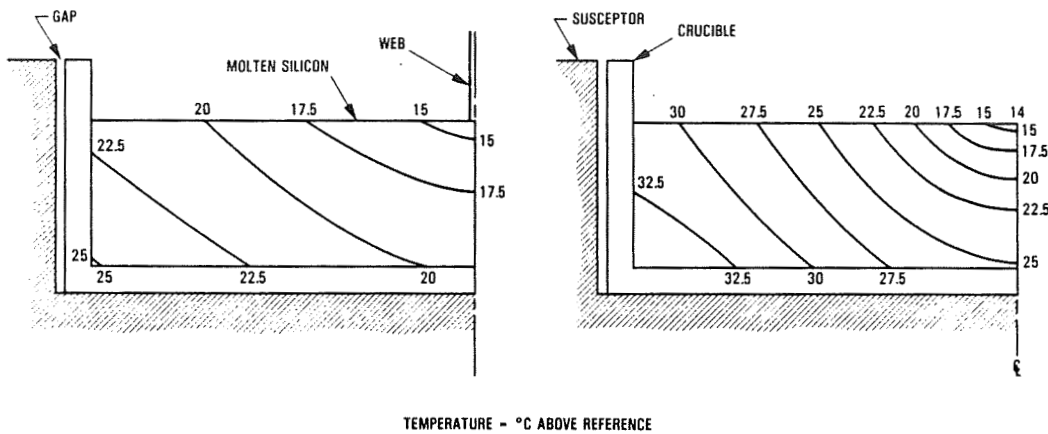
- DOE Five-Year Research Plan goals significantly lowered the FSA \$/m² allowable for modules while raising efficiency requirements
- Silicon sheet costs have not kept pace with reductions in other areas of module fabrication
- Dendritic web viewed as most probable sheet option to meet both \$/m² and efficiency requirements
- Area throughput rate limiting factor for years in dendritic web economics

- | | |
|-------------------------------|--|
| • May 1983: | DOE issues Five-Year Research Plan |
| • June 1984: | JPL reviews ribbon situation and decides to broaden research base in dendritic web |
| • September 1984: | Web Team formed to take independent analytical and experimental look at web

Purchase order placed with Westinghouse for fabrication and delivery of a web growth system |
| • November 1984: | JPL internal review of proposed Web Team activities |
| • December-January 1984-1985: | Two JPL operators trained at Westinghouse |
| • January 1985: | Facilities for growth system tested by exercising test bed furnace |
| • February 1985: | Growth system received at JPL |
| • April 1985: | Major external review of Web Team activities. First web grown at JPL |

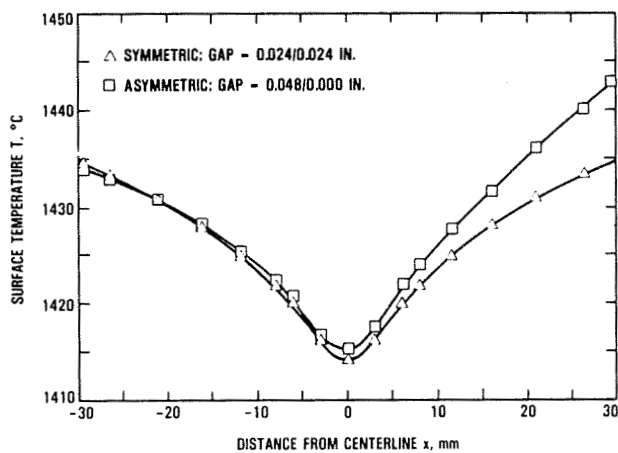
PRECEDING PAGE BLANK NOT FILMED

Computed Isotherms With and Without the Growing Web



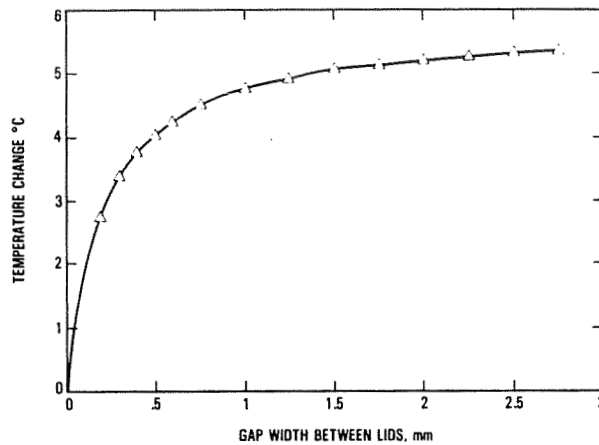
Thermal modeling was done using the "SINDA" program to investigate the effects of varying key parameters

Crucible-to-Susceptor Gap Effect on Surface Temperature



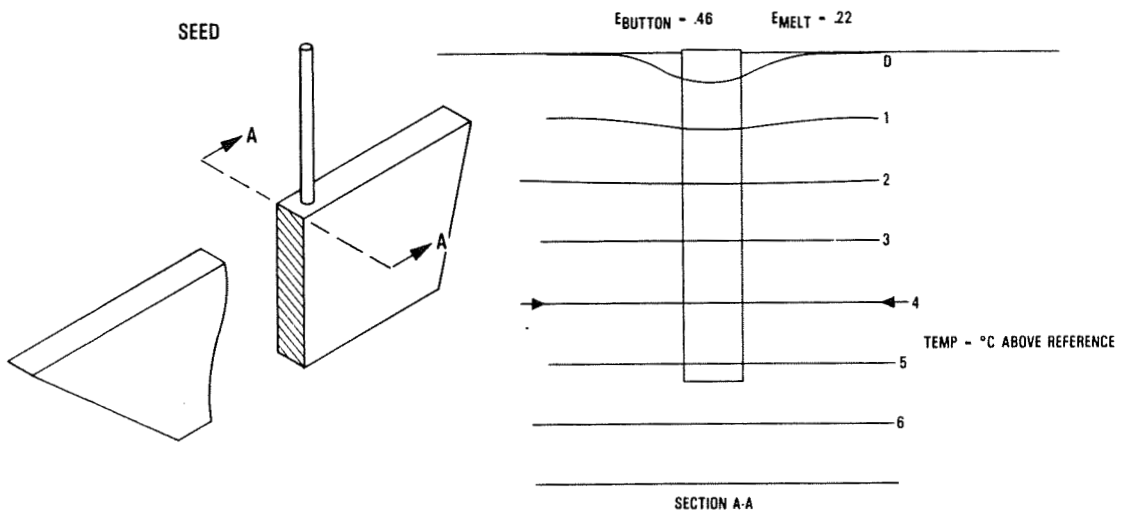
Differential thermal expansion causes a varying gap between the crucible sides and the susceptor. Beyond 0.021 in., gap increase causes insignificant change in heat transfer

Melt Surface Temperature Change as a Function of Lid Gap



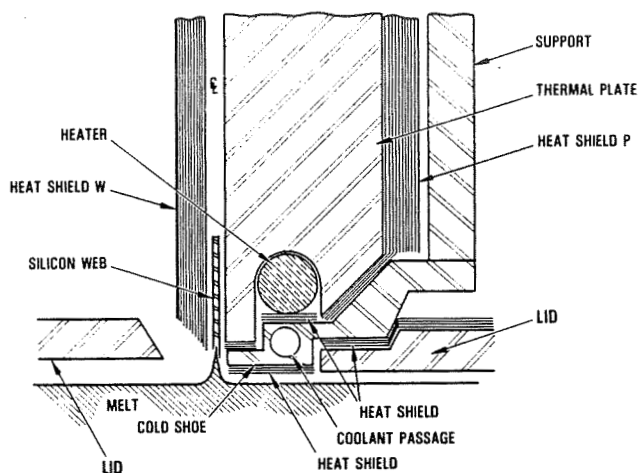
Thermal warping of the molybdenum lids causes a change in heat transfer from the surface of the molten silicon. A 0.5 mm variation in lid gap may cause as much as 4°C change in melt surface temperature

Button Growth



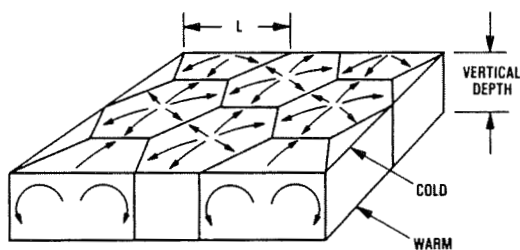
The solid to liquid interface cannot be an isotherm (i.e., the freezing point). A simplified computer run gives a 5°C difference over actual button dimensions.

Cold Shoe



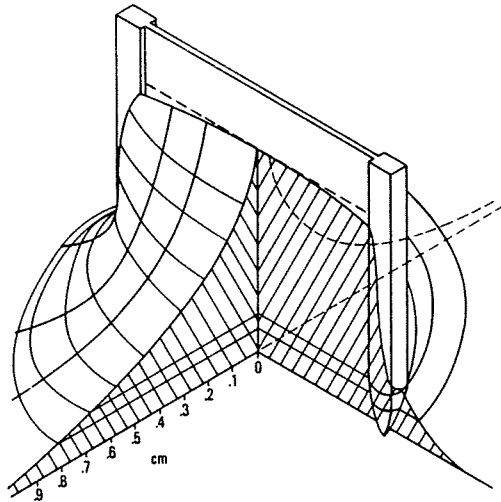
A "cold shoe" design was analyzed for the feasibility of high heat transfer rates from the growing web. Analysis showed need for severe gradients in shoe as well as sensitivity to small dimensional changes. SiO contamination expected to be a major problem

Benard Cells



Vertical temperature gradients (from thermal analysis) indicate convection (Benard cells) in molten silicon causes instability at melt depths used

Meniscus Geometry

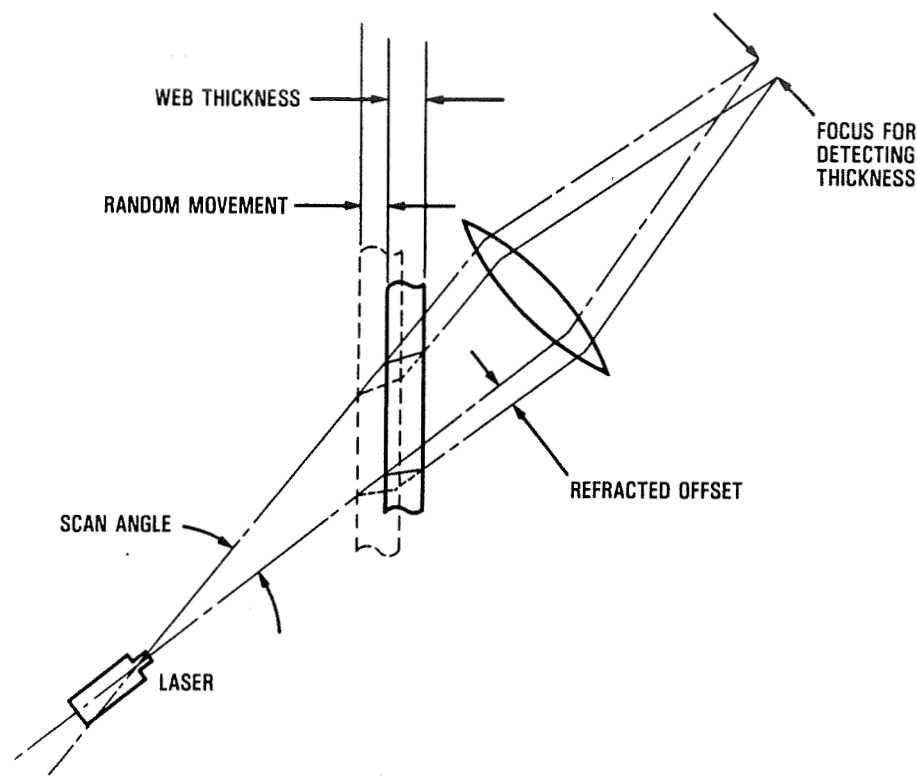


Meniscus shape is dictated by surface tension of the molten silicon. The meniscus is higher on the web where a cylindrical curvature exists. The end meniscus is pulled lower by the convex horizontal curvature component

Radio Frequency Studies

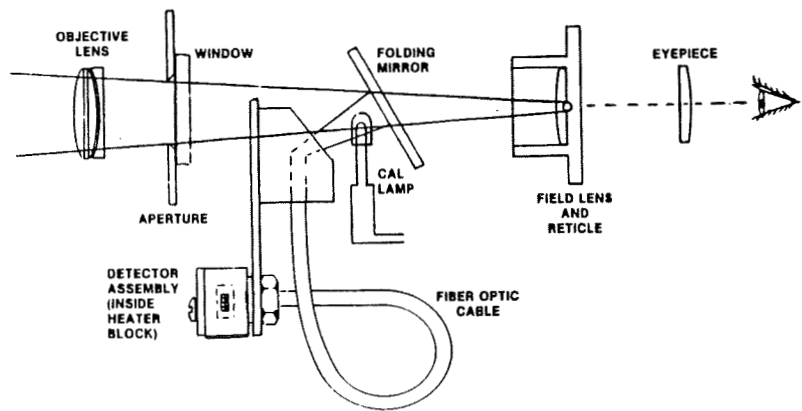
- **Objective**
 - **Devise means for determining radio frequency coupling with furnace elements**
- **Results**
 - **Mathematical methods are too complex, require simplifying assumptions which dominate results**
 - **Relatively simple probe, 25 turns 0.250 in. diameter with semi-rigid coaxial shaft**
 - **Without susceptor, inside field about twice that outside of coil**
 - **Susceptor with shields absorbs over 99.3% of the energy**
 - **No measurable field in vicinity of web**

Scanning Thickness Detector



Sensing Head Optical System

Section 7 — MAINTENANCE & FIELD SERVICE



STRESS AND EFFICIENCY STUDIES IN EDGE-DEFINED FILM-FED GROWTH

MOBIL SOLAR ENERGY CORPORATION

J. Kalejs

TECHNOLOGY ADVANCED MATERIALS RESEARCH TASK	REPORT DATE APRIL 30, 1986
APPROACH STRESS AND EFFICIENCY STUDIES IN EFG CONTRACTOR MOBIL SOLAR ENERGY CORPORATION, CONTRACT NUMBER 956312	STATUS: <ul style="list-style-type: none"> ● STRESS ANALYSIS SHOWS POTENTIAL FOR REDUCING SHEET STRESS AT LOWER GROWTH SPEEDS (≤ 2 CM/MIN FOR EFG) EXISTS: <ul style="list-style-type: none"> - WHEN SHEET EDGES ARE COOLER THAN CENTERLINE, - REDUCTIONS SENSITIVE TO CREEP BELOW 1200°C, ● QUANTITATIVE RELATIONSHIPS ESTABLISHED BETWEEN L AND N_d FOR FZ SILICON STRESSED ABOVE 900°C: <ul style="list-style-type: none"> - $L \sim N_d^{-1/4}$, - POINT DEFECT CONTRIBUTIONS TO DEGRADATION DEFINED, ● DOPANTS IN EFG MATERIAL SHOWN TO INFLUENCE DISLOCATION ACTIVITY, POINT DEFECT RECOMBINATION,
GOALS <ul style="list-style-type: none"> ● TO DEFINE MINIMUM STRESS CONFIGURATION FOR SILICON SHEET GROWTH, ● TO QUANTIFY DISLOCATION ELECTRICAL ACTIVITY AND LIMITS ON CELL EFFICIENCY, ● TO STUDY BULK LIFETIME DEGRADATION DUE TO INCREASE IN DOPING LEVELS, 	

Topics of Presentation

- BRIEF SUMMARY OF WORK 1982-86,
- DEVELOPMENTS SINCE 25TH PIM,

Stress Studies, 1982-1986: Accomplishments

- DEVELOPED FINITE ELEMENT ANALYSIS FOR CALCULATING RESIDUAL STRESS WITH PLASTIC DEFORMATION IN HIGH SPEED SHEET GROWTH (WITH PROF. J. HUTCHINSON, HARVARD U.).
- VERIFIED QUANTITATIVE FINITE ELEMENT MODEL FOR EFG CONTROL VARIABLE RELATIONSHIPS/TEMPERATURE PROFILE CALCULATIONS (WITH PROF. R.A. BROWN, MIT).
- DEVELOPED RESIDUAL STRESS MEASUREMENT TECHNIQUE FOR EFG MATERIAL USING SHADOW MOIRE INTERFEROMETRY (WITH PROF. S. DANYLUK, U. OF ILLINOIS AT CHICAGO).
- TRANSIENT CREEP INVESTIGATED IN SILICON FOR 800-1400°C IN STRAIN (10^{-3}) AND STRAIN RATE (10^{-4} s^{-1}) REGIMES OF SHEET GROWTH.

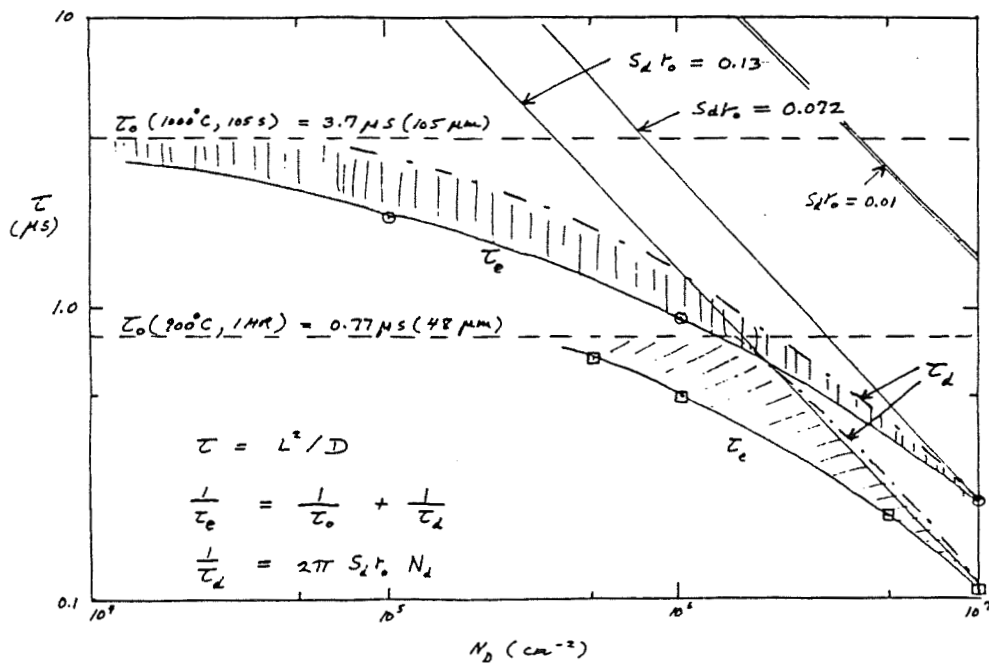
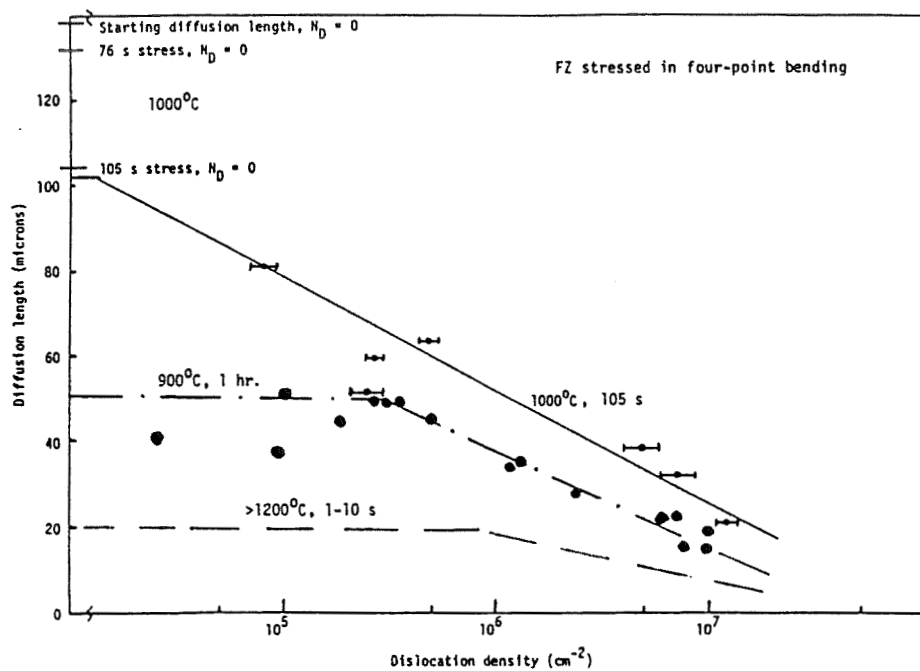
Defect Electrical Activity Studies, 1984-1986: Accomplishments

- DEVELOPED QUANTITATIVE MINORITY CARRIER DIFFUSION LENGTH MEASUREMENTS FOR DISLOCATED, INHOMOGENEOUS MATERIAL USING EBIC.
- OBTAINED QUANTITATIVE DATA ON DOPANT (B, GA) INFLUENCE ON DEFECT DENSITIES AND ELECTRICAL ACTIVITY IN EFG MATERIAL.

Dislocation Electrical Activity

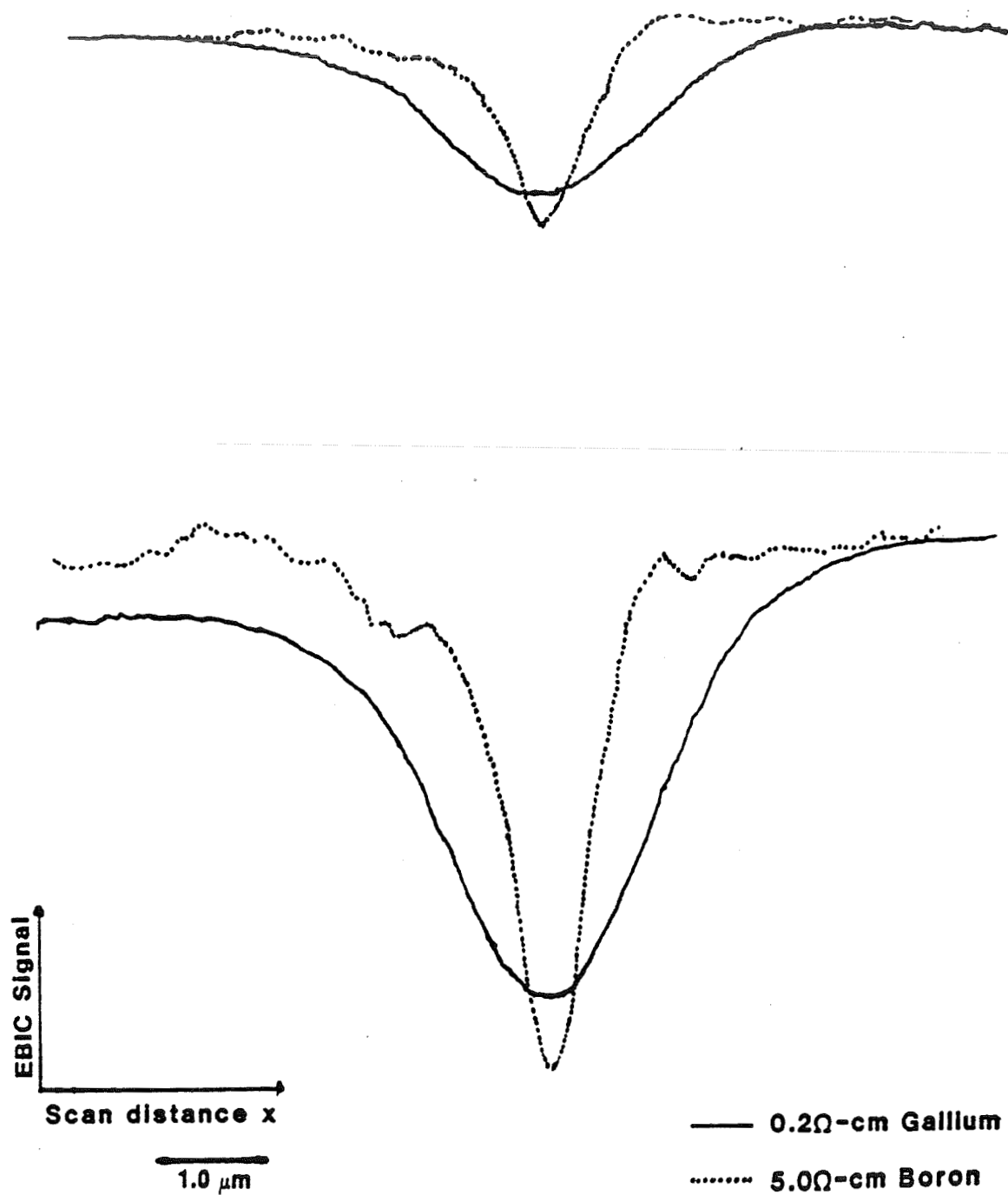
- L vs. N_d RELATIONSHIPS ESTABLISHED FOR FZ SILICON STRESSED IN TEMPERATURE RANGE 900-1400°C
 - MICRODEFECT RECOMBINATION LIMITS IN $N_d \leq 10^4 \text{ cm}^{-2}$ REGIONS.
 - DISLOCATION EFFECTS GIVE $L \sim N_d^{-1/4}$ ABOVE N_d THRESHOLD THAT DEPENDS ON MICRODEFECT RECOMBINATION LEVEL.
- CONTRAST TO AS-GROWN DISLOCATION ACTIVITY FOR WHICH $L \sim N_d^{-1/2}$ ($\tau \sim N_d^{-1}$).

Diffusion Length Dependence on Heat Treatment and Dislocation Density

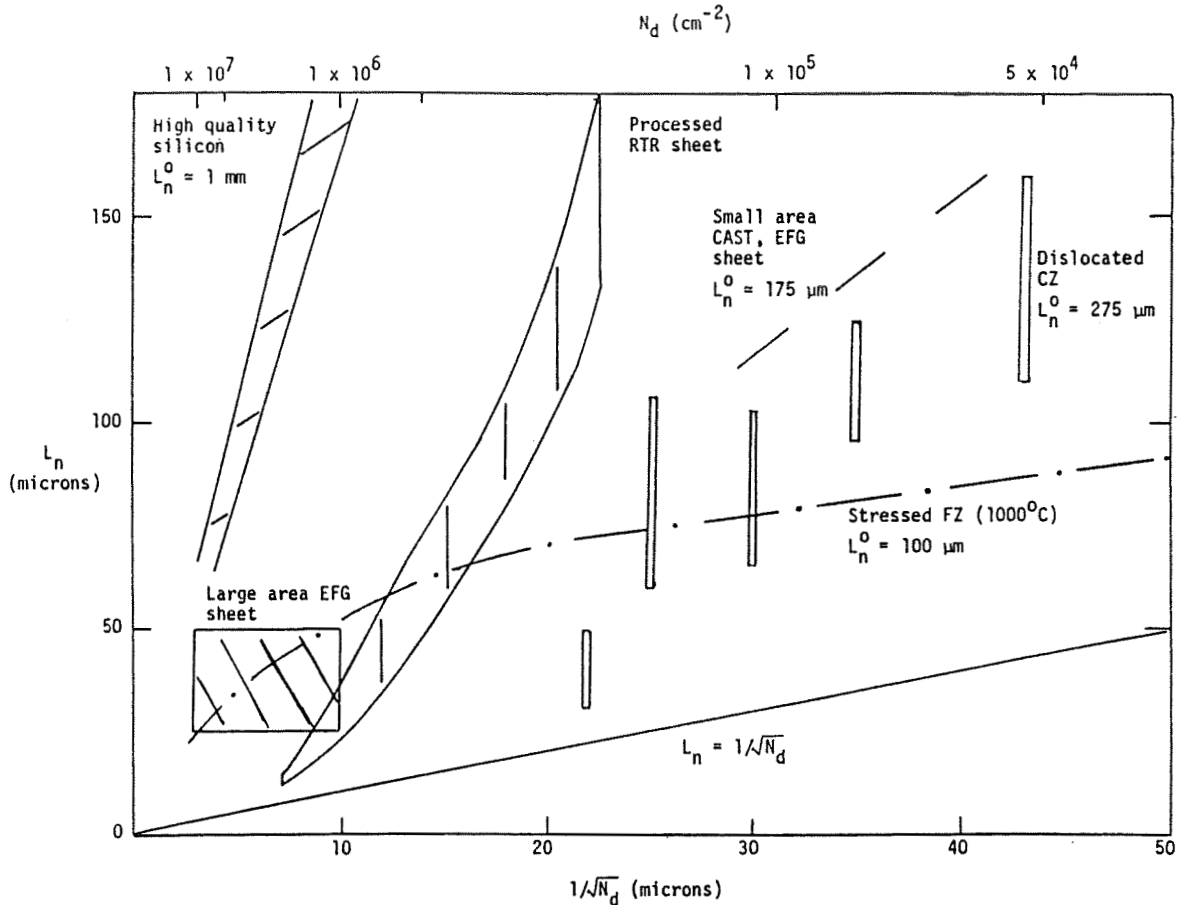


ORIGINAL PAGE IS
 OF POOR QUALITY

EBIC Line Scans of Dislocations in High and Low Resistivity
EFG Silicon Ribbon



ORIGINAL PAGE IS
OF POOR QUALITY



Dislocation Versus Point Defect Limitations on Lifetime

- RESULTS SUGGEST ELECTRICAL ACTIVITY OF GROWN-IN DISLOCATIONS DIFFERS FROM CREEP-RELATED DISLOCATIONS.
- $L \sim N_d^{-1/4}$ ($\tau \sim N_d^{-1/2}$) DEPENDENCE MAY BE RELATED TO DISLOCATION "DEBRIS" OR TOTAL AREA SWEEPED OUT BY DISLOCATIONS, REQUIRES POINT DEFECT-DISLOCATION INTERACTION DYNAMICS TO BE INCLUDED.
- L IS NOT EQUAL TO MEAN DISLOCATION SEPARATION $\ell = N_d^{-1/2}$ FOR ANY SITUATION, INDICATING ONLY SMALL FRACTION OF CORE SITES ARE ACTIVE.

Future Directions for Electrical Activity Studies

DEVELOPMENT OF PASSIVATION SCHEMES FOR DEFECTS AND
PROCESSING/PASSIVATION OPTIMIZATION CRUCIAL TO
VIABILITY OF CURRENT SHEET MATERIAL FOR LOW-COST
PHOTOVOLTAIC INDUSTRY.

CURRENT EFG STATUS:

L: 100-200 MICRONS
 η : 13-15% (45 cm² AREAS)

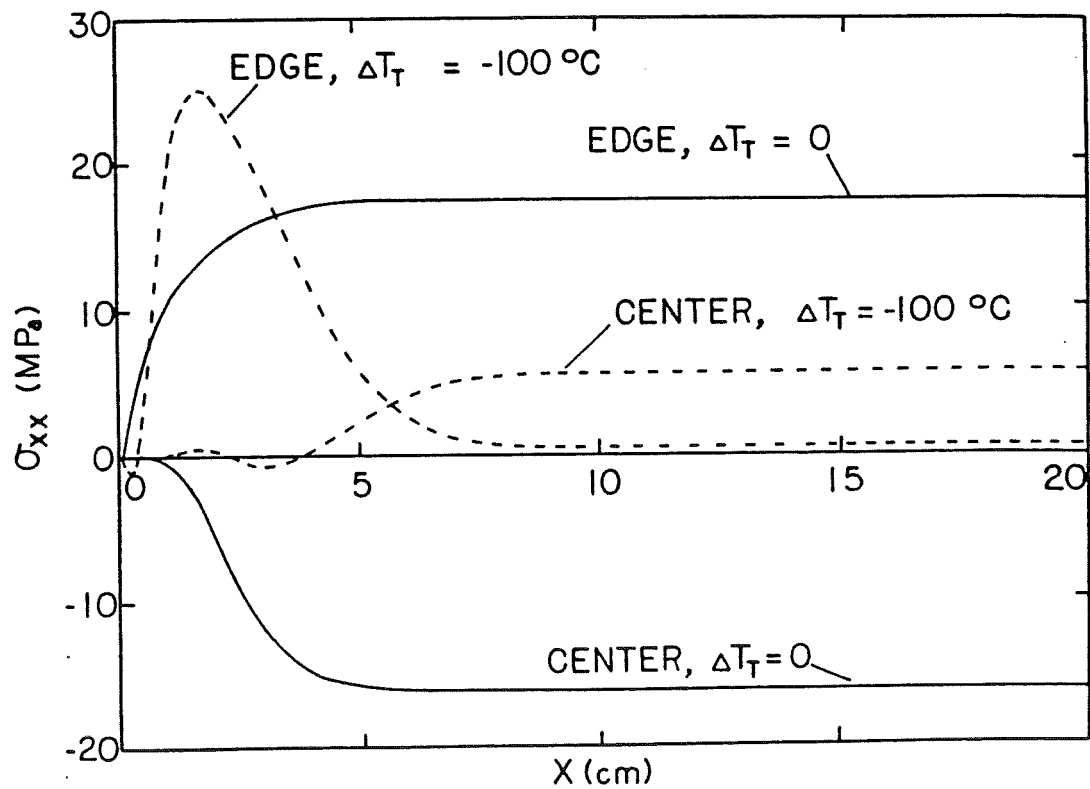
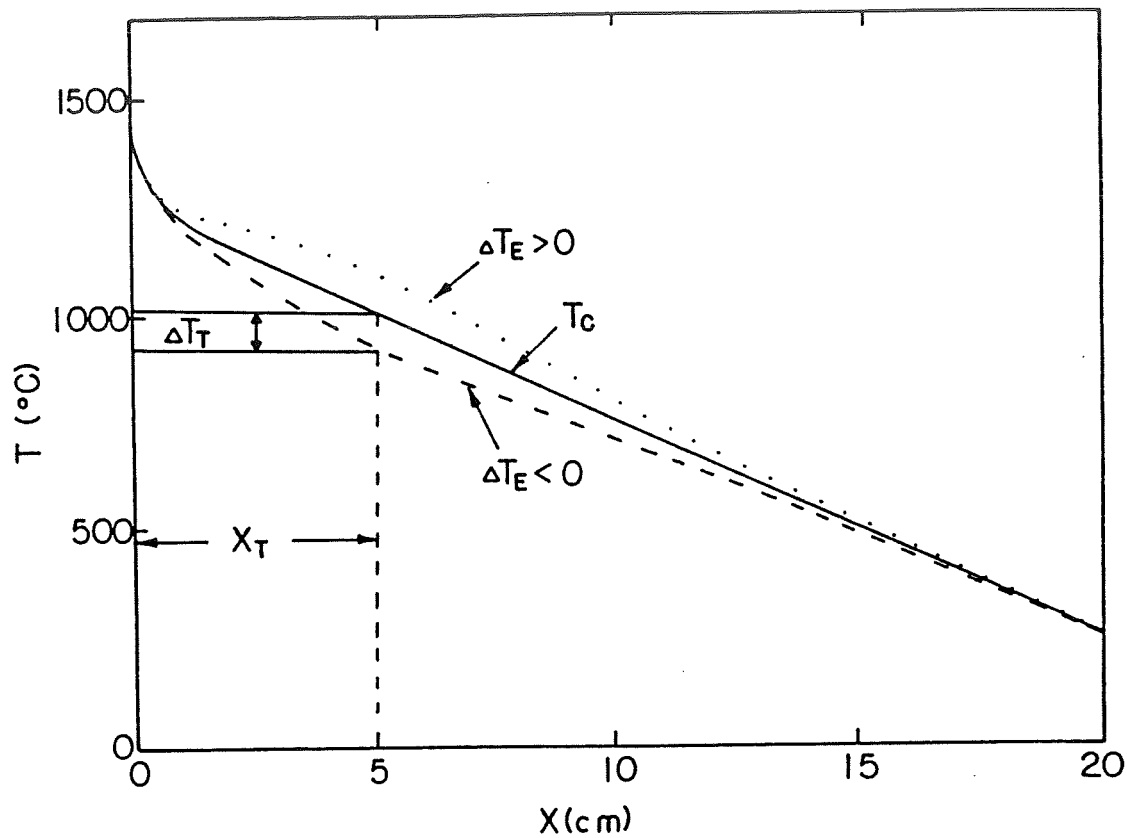
FUTURE REQUIREMENTS:

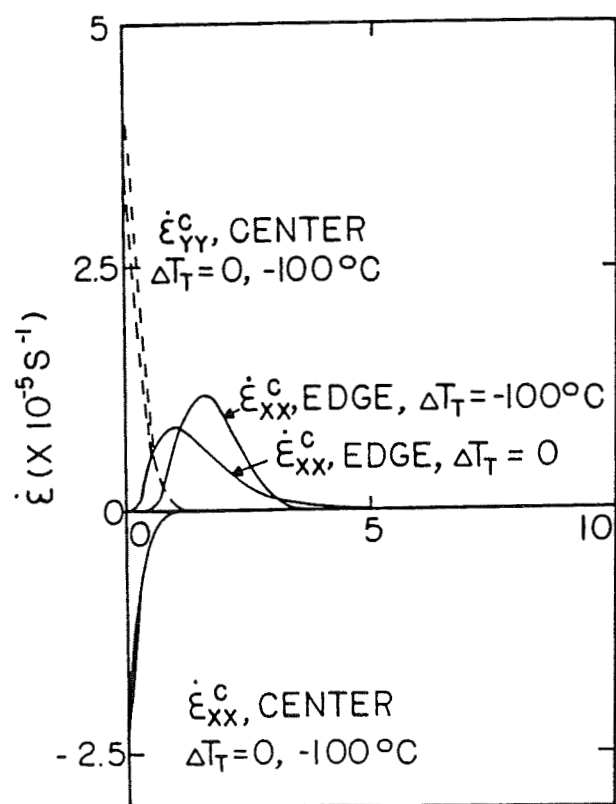
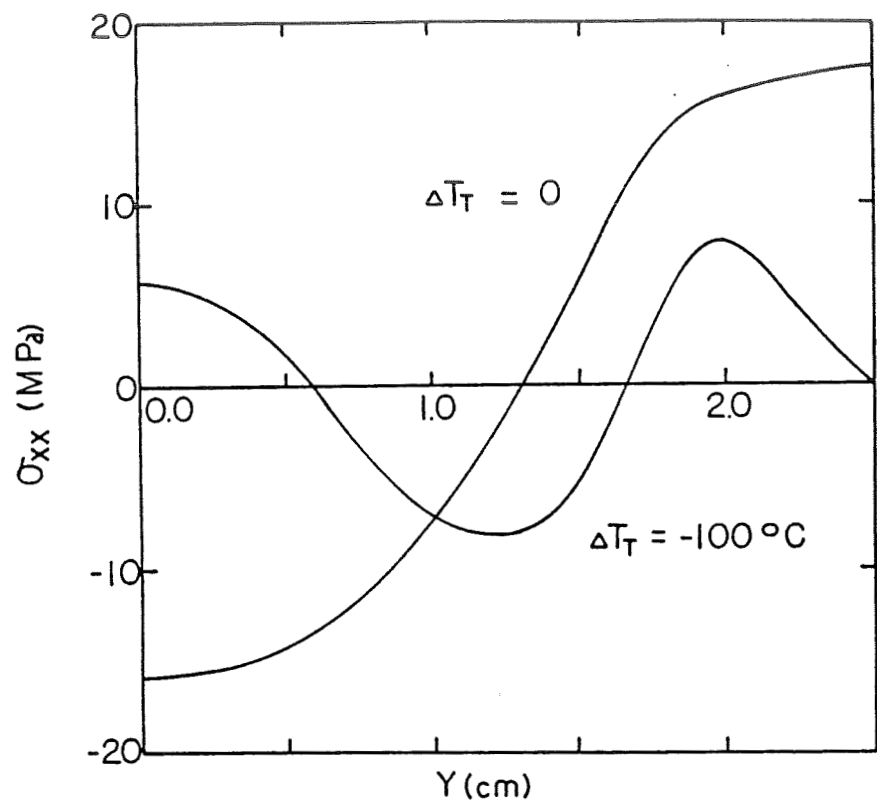
L: 200-300 MICRONS
 η : $\geq 16\%$

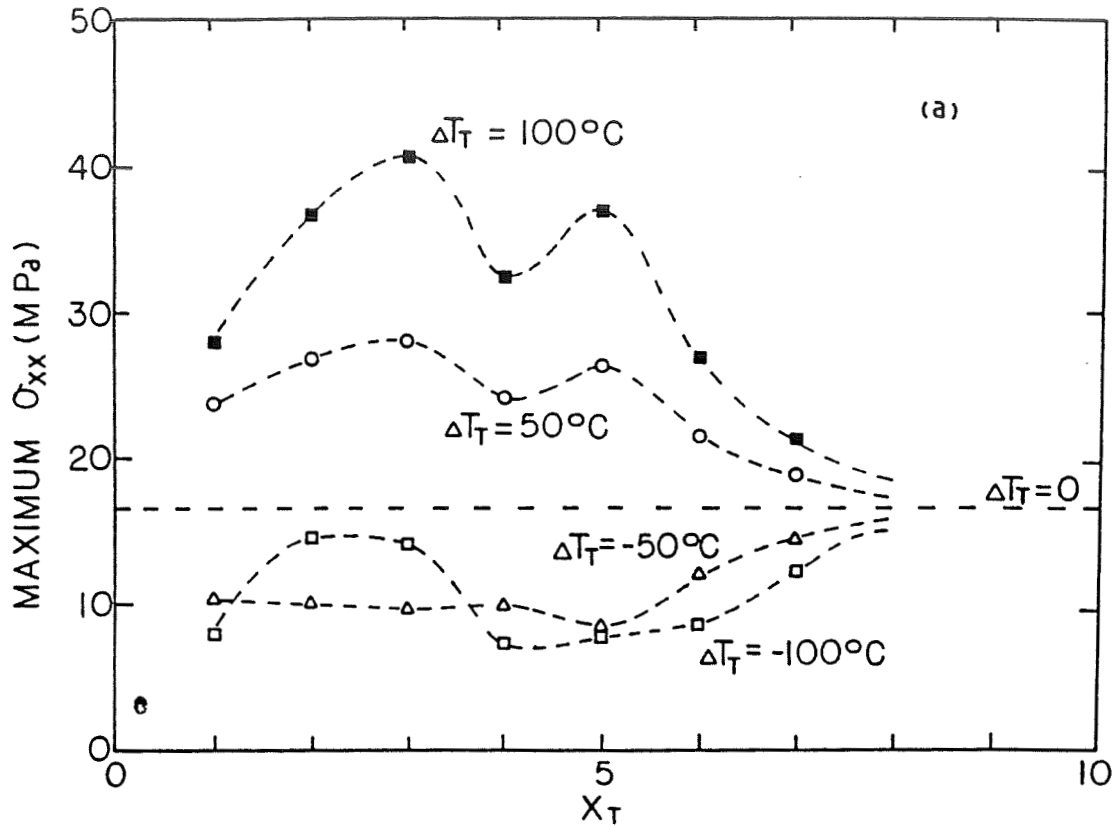
FUNDAMENTAL NEED IS FOR DEVELOPMENT OF MODELS FOR
AND IDENTIFICATION OF RELATIVE CONTRIBUTIONS OF
POINT DEFECTS AND DISLOCATIONS TO LIFETIME
LIMITATIONS, PARTICULARLY IN LOW RESISTIVITY SILICON.

- FINITE ELEMENT MODELING OF EFFECTS OF TRANSVERSE ISOTHERM
NONUNIFORMITY ON STRESS
 - P. MATAGA, J. HUTCHINSON (HARVARD U.).
- STRESS REDISTRIBUTION IN FINITE SIZE BLANKS
 - L. BUCCIARELLI (MIT).
- STRESS RELAXATION MEASUREMENT IN SILICON BETWEEN
800°C AND 1200°C
 - PLANS FOR EXPERIMENTS.

ADVANCED SILICON SHEET







Transverse Isotherm Effects: Conclusions

- NONUNIFORMITY LEADS TO HIGHER MAXIMUM STRESS IN THE SHEET
 - INCREASES TENDENCY FOR BUCKLING,
 - INCREASES DEFECT DENSITY,
 - ONLY EDGE COOLING REDUCES RESIDUAL STRESS,
- SIGNIFICANT COMPENSATION FOR HIGH AXIAL TEMPERATURE PROFILE NONUNIFORMITY CANNOT BE PRODUCED FOR MODERATE ($100\text{--}300^\circ\text{C}$) EDGE COOLING,
- RESIDUAL STRESS DISTRIBUTION IS FUNDAMENTALLY ALTERED
 - POSSIBLE THERE ARE TEMPERATURE DISTRIBUTIONS WHICH REDUCE STRESS TO ZERO,
 - CREEP BEHAVIOR BETWEEN 800°C AND 1200°C NEEDS TO BE STUDIED,

Coordination of Frame and Stress Components Sign Convention

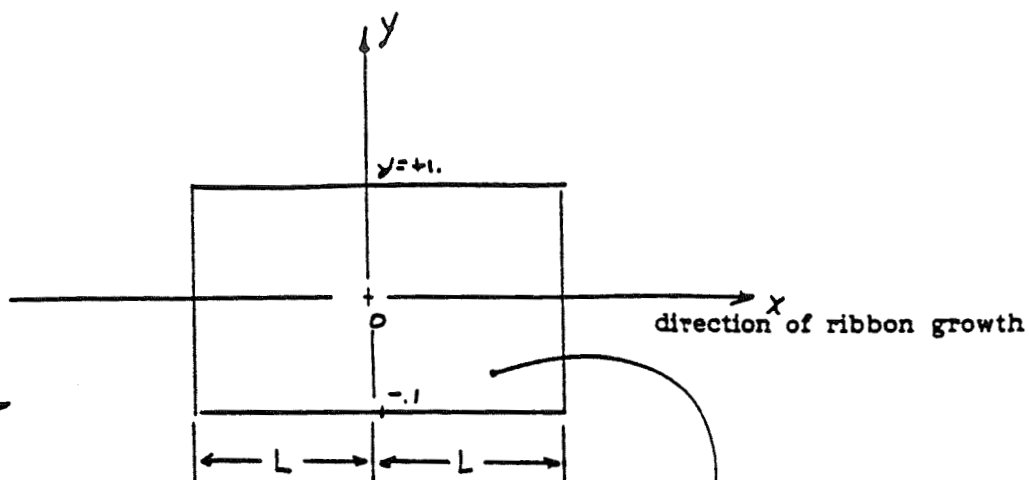
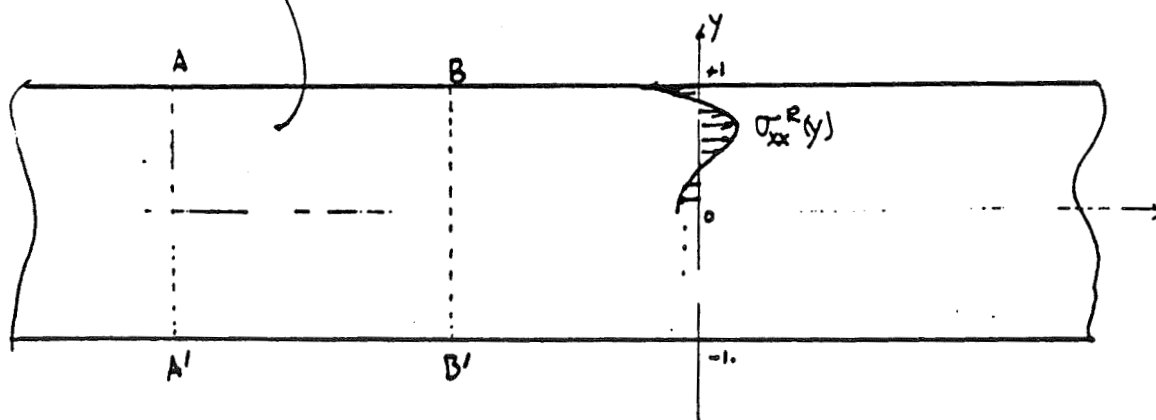
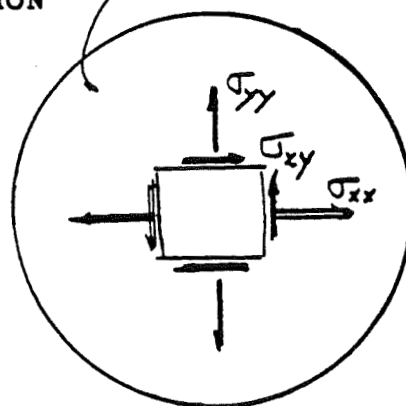


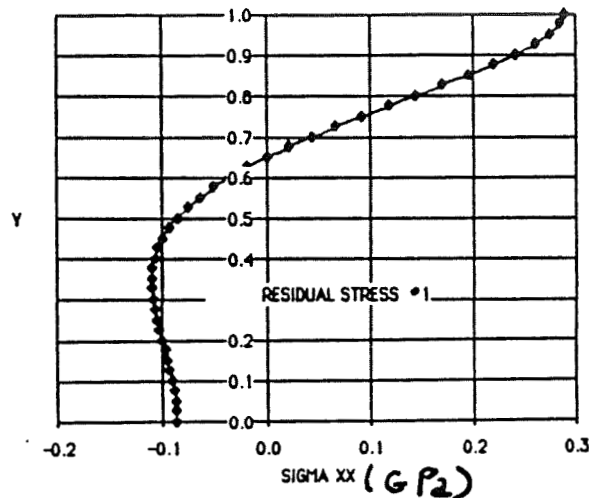
FIGURE 1.

COORDINATE FRAME & STRESS COMPONENTS
SIGN CONVENTION



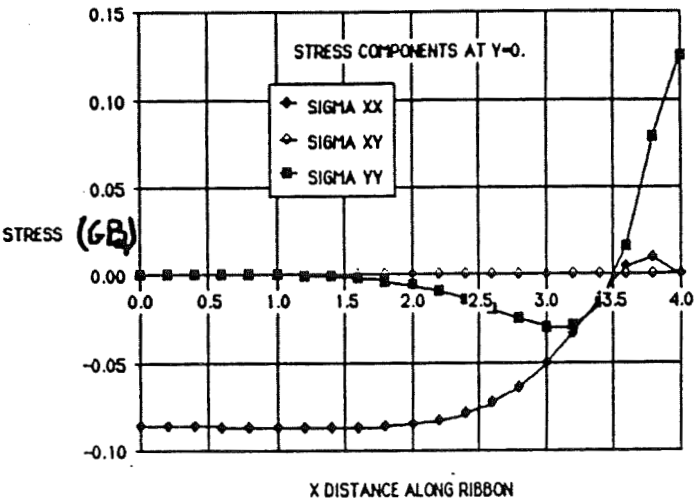
Residual Stress Distribution in Semi-Infinite Ribbon

Note $y=0$, is ribbon center line
Note σ_{xx} is plotted; other stress components are zero.

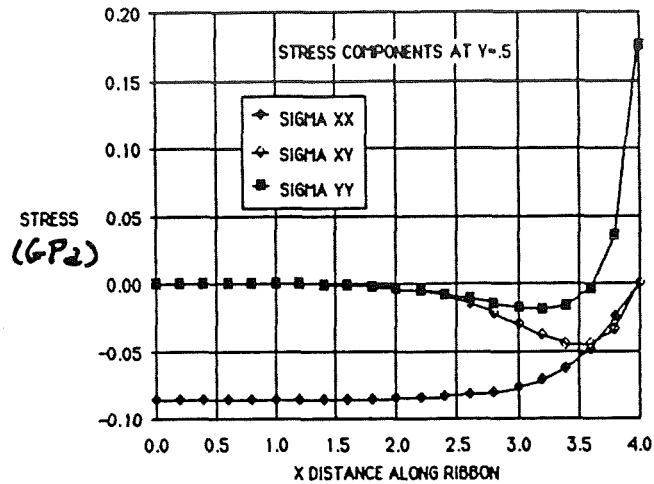


Stress Component Variation with "x" at $y = 0.0$

Note: Half length of ribbon $L = 4 \times$ (the half width)
Note: For x negative:
 σ_{xx} is symmetrical
 σ_{yy} is symmetrical
 σ_{xy} is a-symmetrical



Stress Component Variation with "x" at $y = 0.5$



Stress Redistribution in Finite Size Blanks: Summary

- METHOD FOR CALCULATING SHEAR FLOW DEVELOPED
 - CAN BE OBTAINED FOR ANY SIZE BLANK.
 - CAN BE RELATED TO GROWN-IN THERMOELASTIC STRESS IN SEMI-INFINITE SHEET.
- SIGNIFICANT STRESS REDISTRIBUTION AT BLANK END PRODUCES LARGE TENSILE NON-ZERO σ_{YY} COMPONENT.

Stress Relaxation Measurements in Silicon ($800^{\circ}\text{C} - 1200^{\circ}\text{C}$)

- PREVIOUS CREEP MEASUREMENTS OBTAIN

$$\frac{\partial \epsilon}{\partial T}, \sigma \text{ CONSTANT}$$

$$\text{CONSTITUTIVE LAW: } \dot{\epsilon} \sim F(T) \sigma^N$$

- RELAXATION MEASUREMENTS WILL OBTAIN

$$\frac{\partial \sigma}{\partial T}, \epsilon \text{ CONSTANT}$$

HIGH-PURITY SILICON CRYSTAL GROWTH INVESTIGATIONS

SOLAR ENERGY RESEARCH INSTITUTE

T. F. Ciszek

Investigators

T. F. Ciszek, Principal Investigator
T. Schuyler, Research Technician
J. L. Hurd, Associate Scientist (through 7/85)
M. Fearheiley, Postdoctoral Scientist (from 8/85)
C. Evans, Master Technician (from 3/86)
R. Elder, Summer Student (1985)

Goals

- * OPTIMIZE DOPANTS & MINORITY-CARRIER LIFETIME IN FZ MATERIAL
- * IMPROVE THE CONTROL OF LIFETIME DEGRADATION MECHANISMS (Impurities, Thermal History, Point Defects, etc.)
- * CHARACTERIZE LIFETIME-RELATED CRYSTALLOGRAPHIC DEFECTS

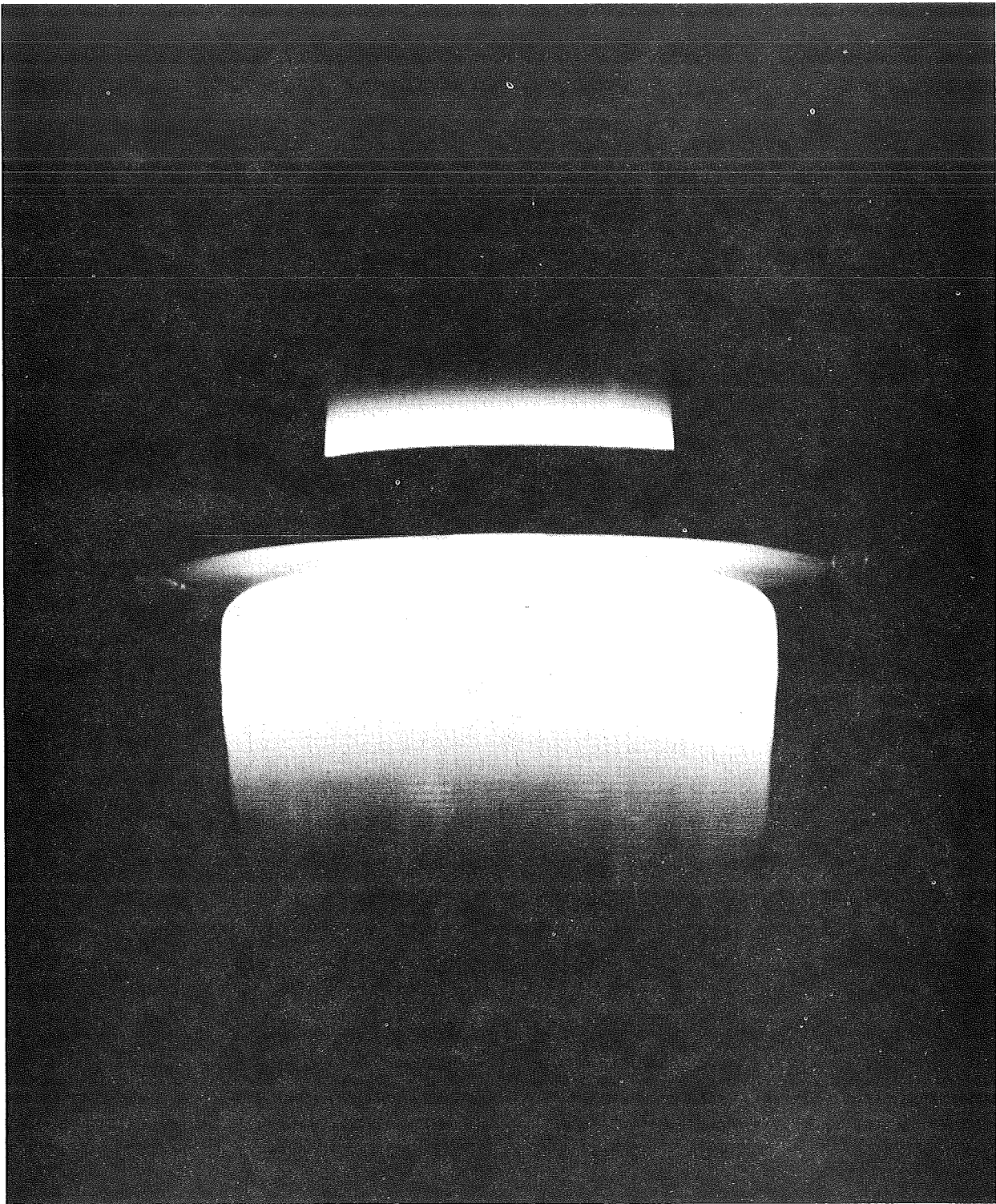
This work was supported by the U.S. Department of Energy under contracts DOE/JPL-WO8762-84-1 & DE-AC02-83CH10093: Sept. 1, 1984 - Mar. 31, 1986.

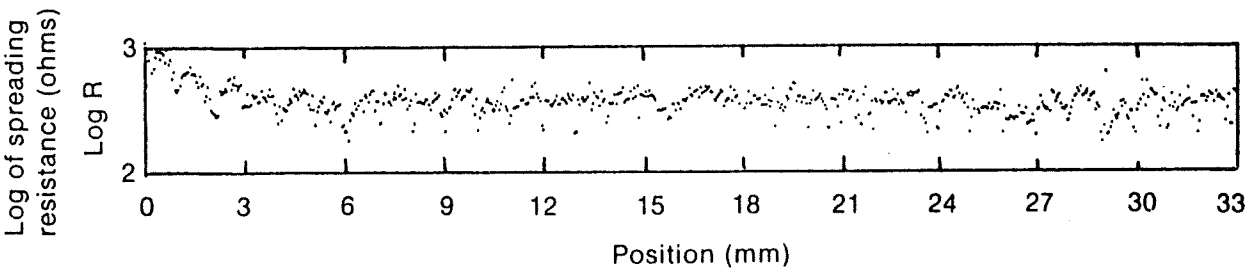
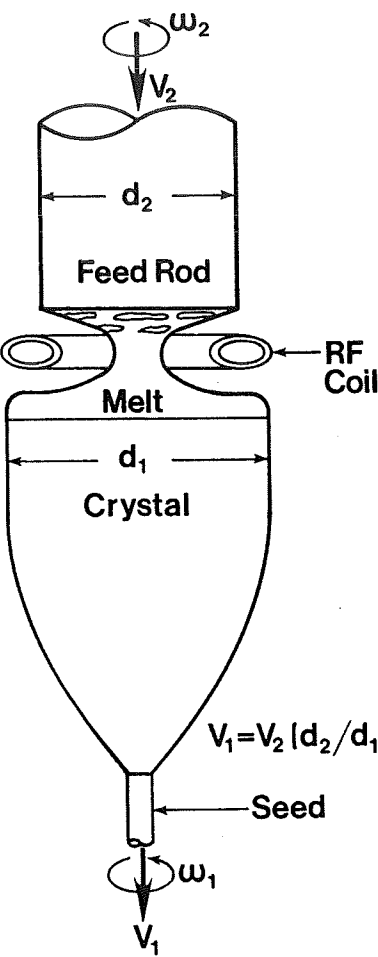
Topics

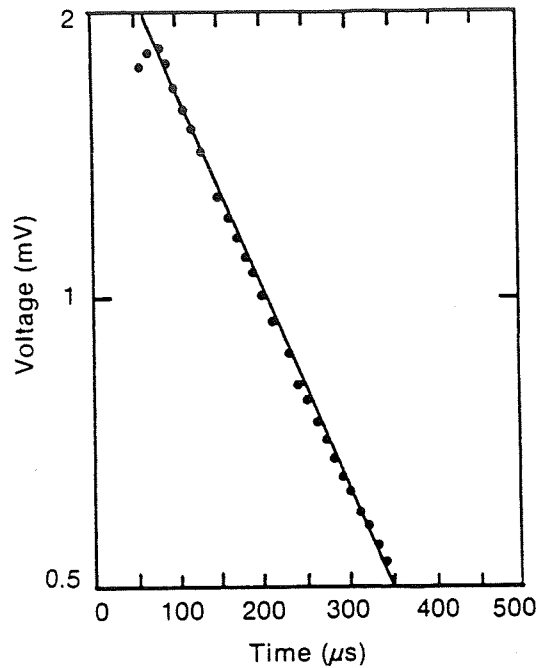
- * EVAPORATION AND SEGREGATION CONTRIBUTIONS TO IMPURITY PROFILES OF FZ CRYSTALS
- * HIGH-PURITY SILICON FLOAT ZONING (FZ)
- * MINORITY-CARRIER LIFETIME MEASUREMENT OF HEAVILY DOPED SILICON CRYSTALS
- * EFFECT OF SOME CRYSTAL GROWTH PARAMETERS ON MINORITY-CARRIER LIFETIME
 - feed rod cleaning procedures
 - crystal growth cooling rate
 - p-type dopant species and concentration
- * DEFECT INVESTIGATIONS BY X-RAY TOPOGRAPHY
 - dislocation-free FZ silicon
 - silicon ribbons grown by various methods

Comparison of Cz and FZ Growth Methods

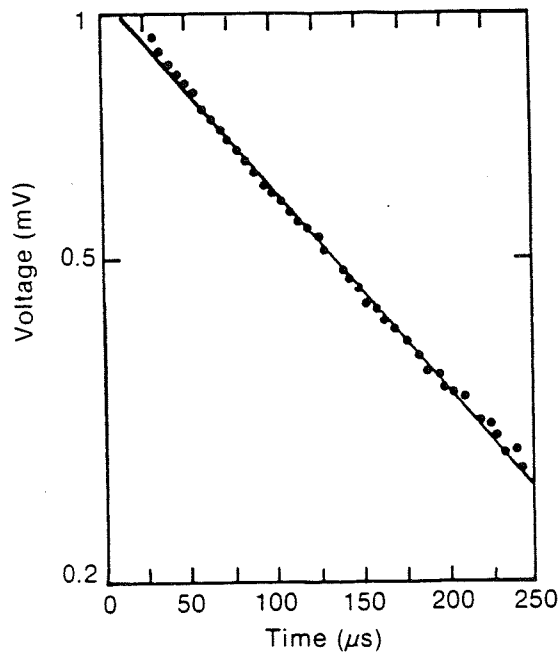
Method	CZ	FZ
Production diameter (mm)	150	125
Growth Speed (mm/min)	1 to 2	2 to 4
Crucible?	yes	no
Dislocation-Free?	yes	yes
Oxygen content (atom/cc)	$>1 \times 10^{18}$	$<1 \times 10^{16}$
Carbon content (atom/cc)	$>1 \times 10^{17}$	$<1 \times 10^{16}$
Metallic impurity content	high	low
Consumable material cost	high	low
Bulk lifetime (microsec.)	50	1000
Relative cell efficiencies	1	1 to 1.2
Heat-up/Cool-down time	large	small
Axial resistivity uniformity	poor	good
Typical # of pulls/crystal	one	two
poly feed form	any	crack-free rods
Mechanical strengthening	10^{18} O	10^{16} N
Degree of sophistication	less	more





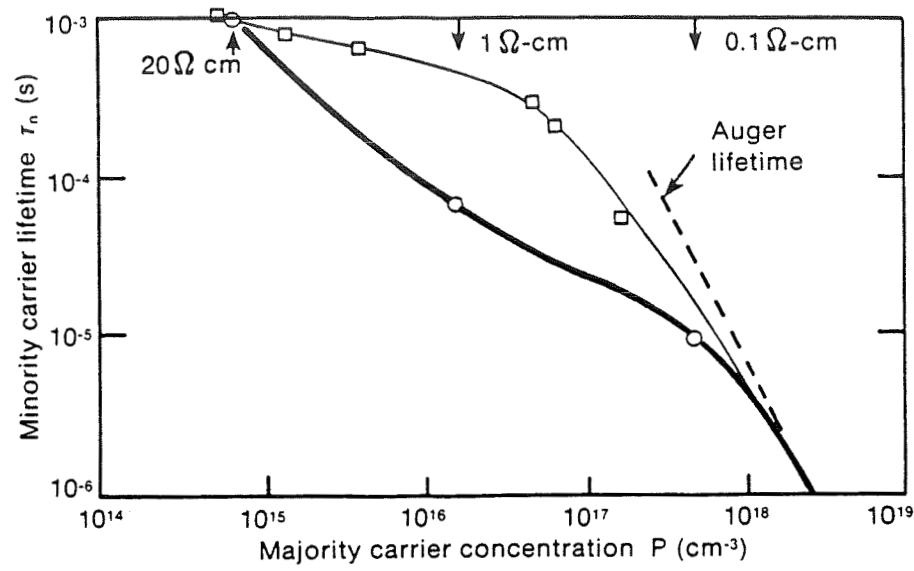


Crystal: 5032001
No. of passes: 4 (3 in vac.)
Orientation: [100], DF
Resistivity: 0.46 ohm-cm
Traces averaged: 20
Temperature: 27° C
Filament lifetime: 205 μs
Bulk lifetime: 303 μs
(@ $V_s/V = 0.002$)

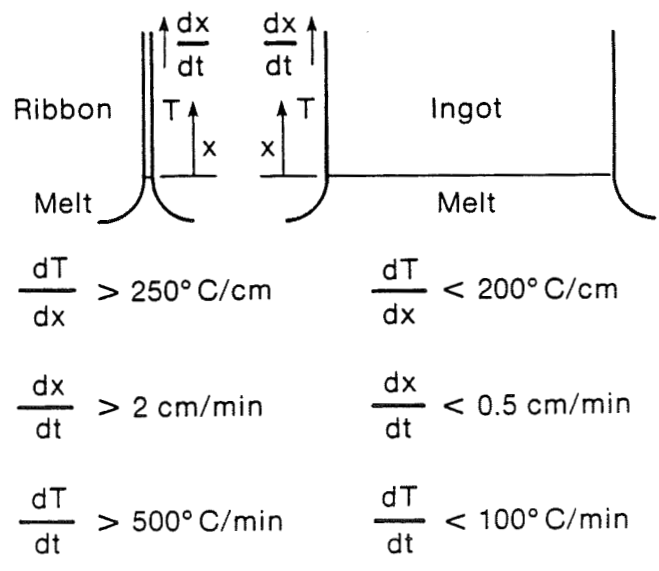


Crystal: 5041101
No. of passes: 4 (3 in vac.)
Orientation: [100], DF
Resistivity: 0.36 ohm-cm
Traces averaged: 100
Temperature: 26° C
Filament lifetime: 181 μs
Bulk lifetime: 231 μs

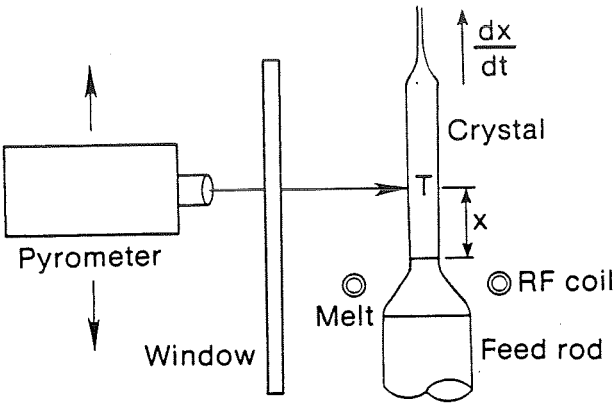
ADVANCED SILICON SHEET



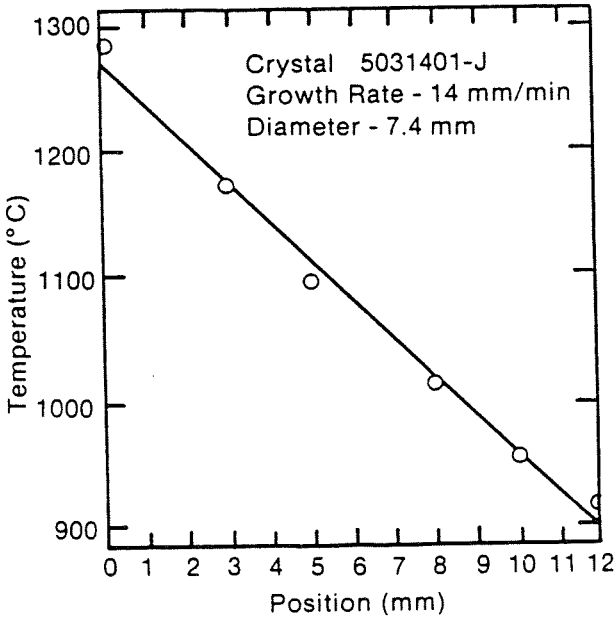
CLEANING PROCEDURE	RESISTIVITY (ohm-cm)	LIFETIME (microsec.)
Cold degreasing	760	790
NaOH etch	2220	600
3:1:2 mixed acid etch	2540	990
"RCA - clean"	4510	1040

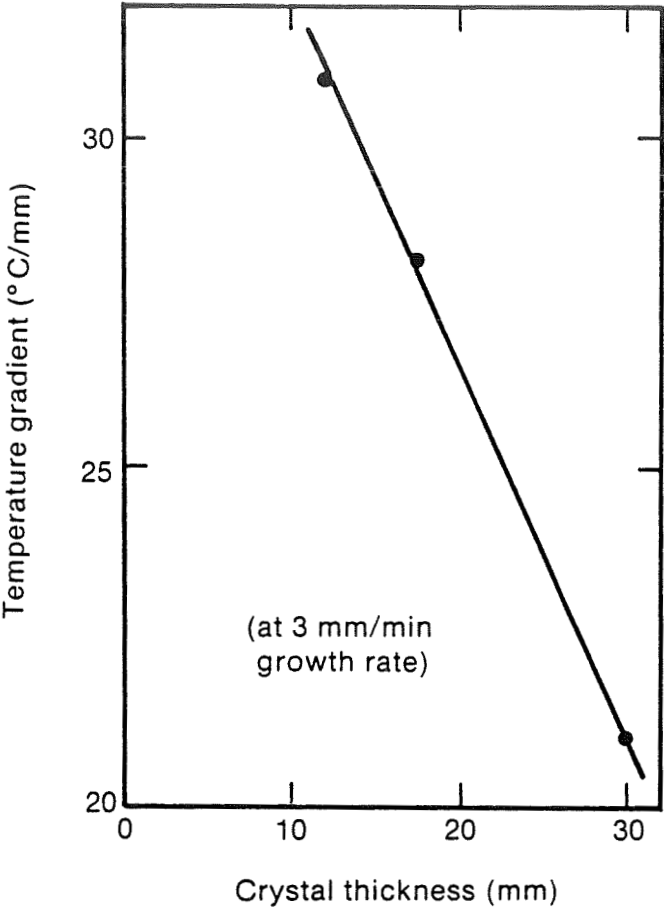


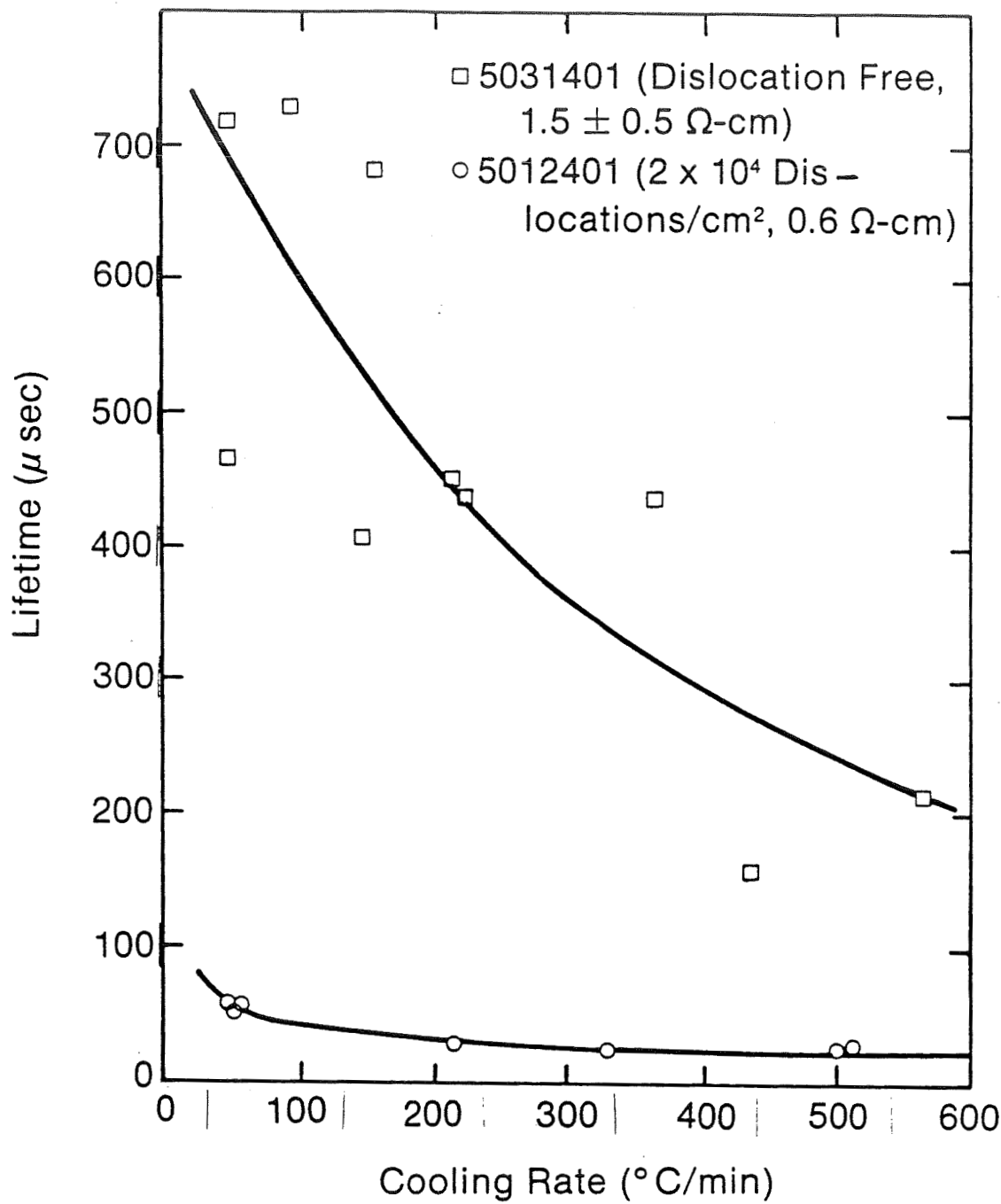
ADVANCED SILICON SHEET

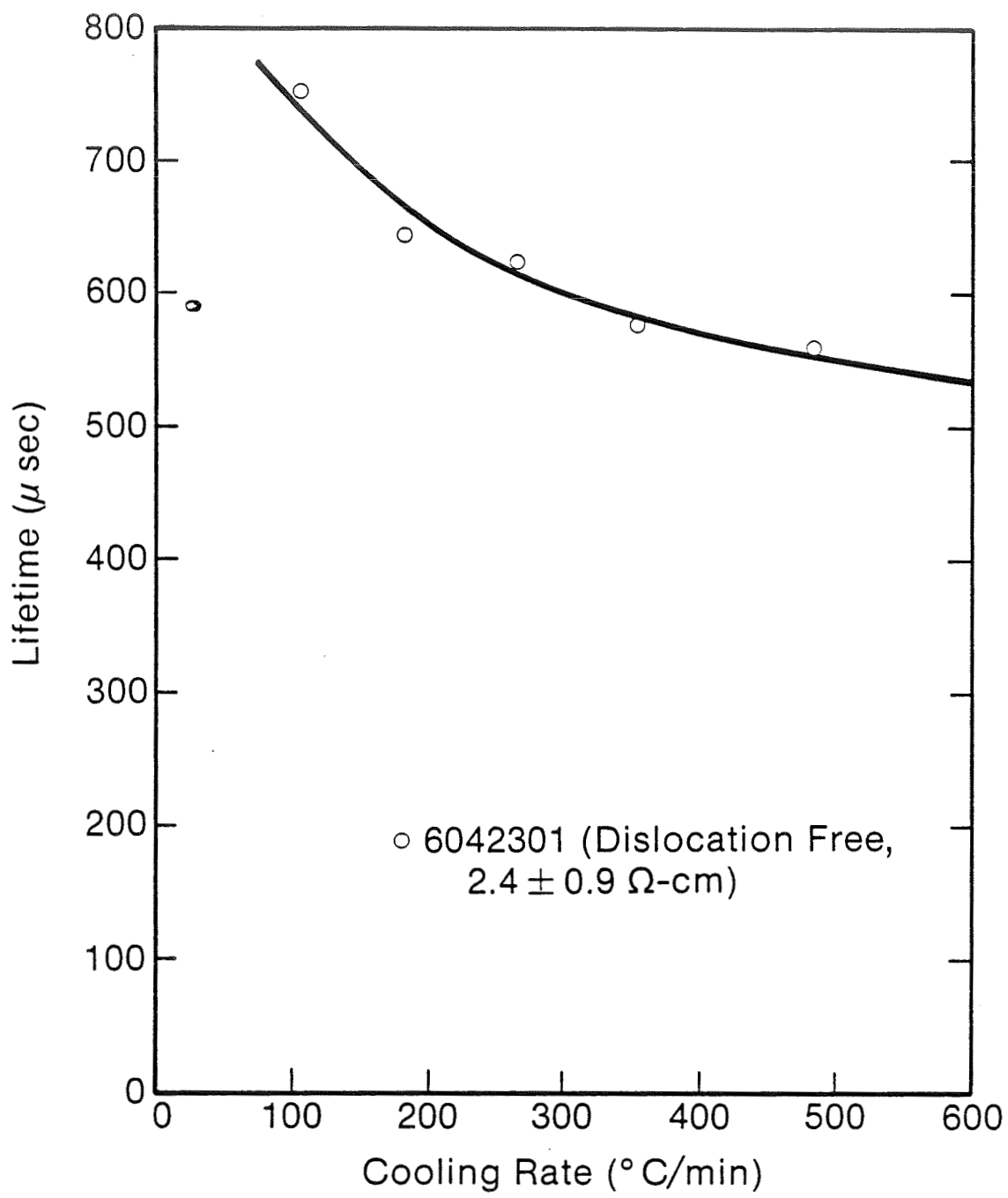


$$\frac{dT}{dt} = \frac{dx}{dt} \frac{dT}{dx}$$

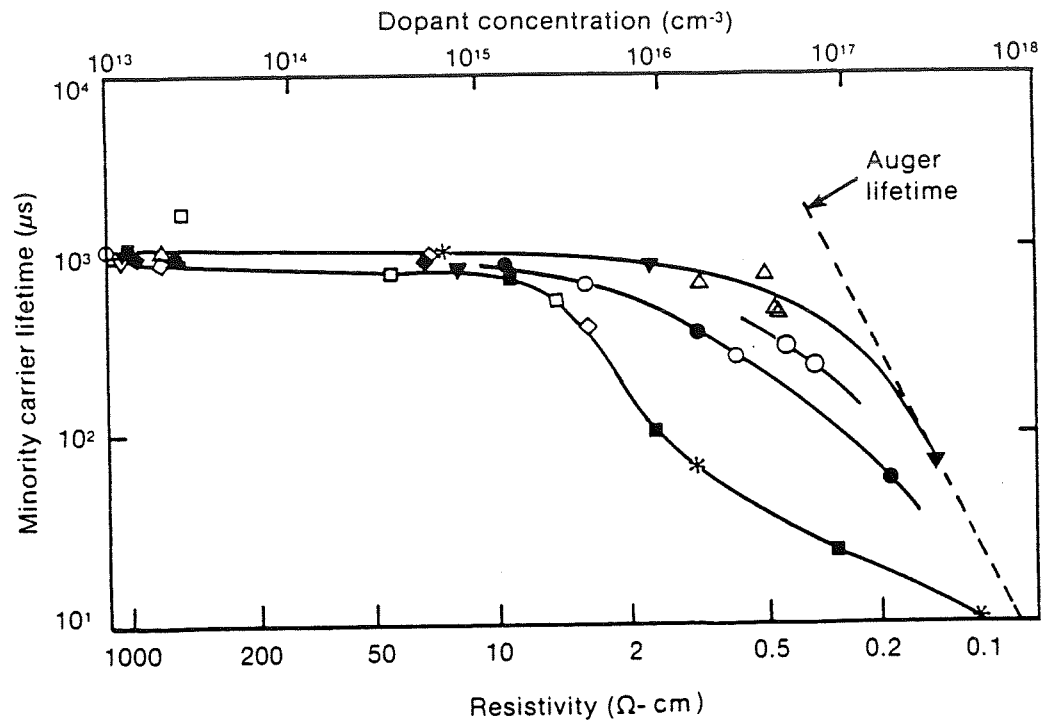






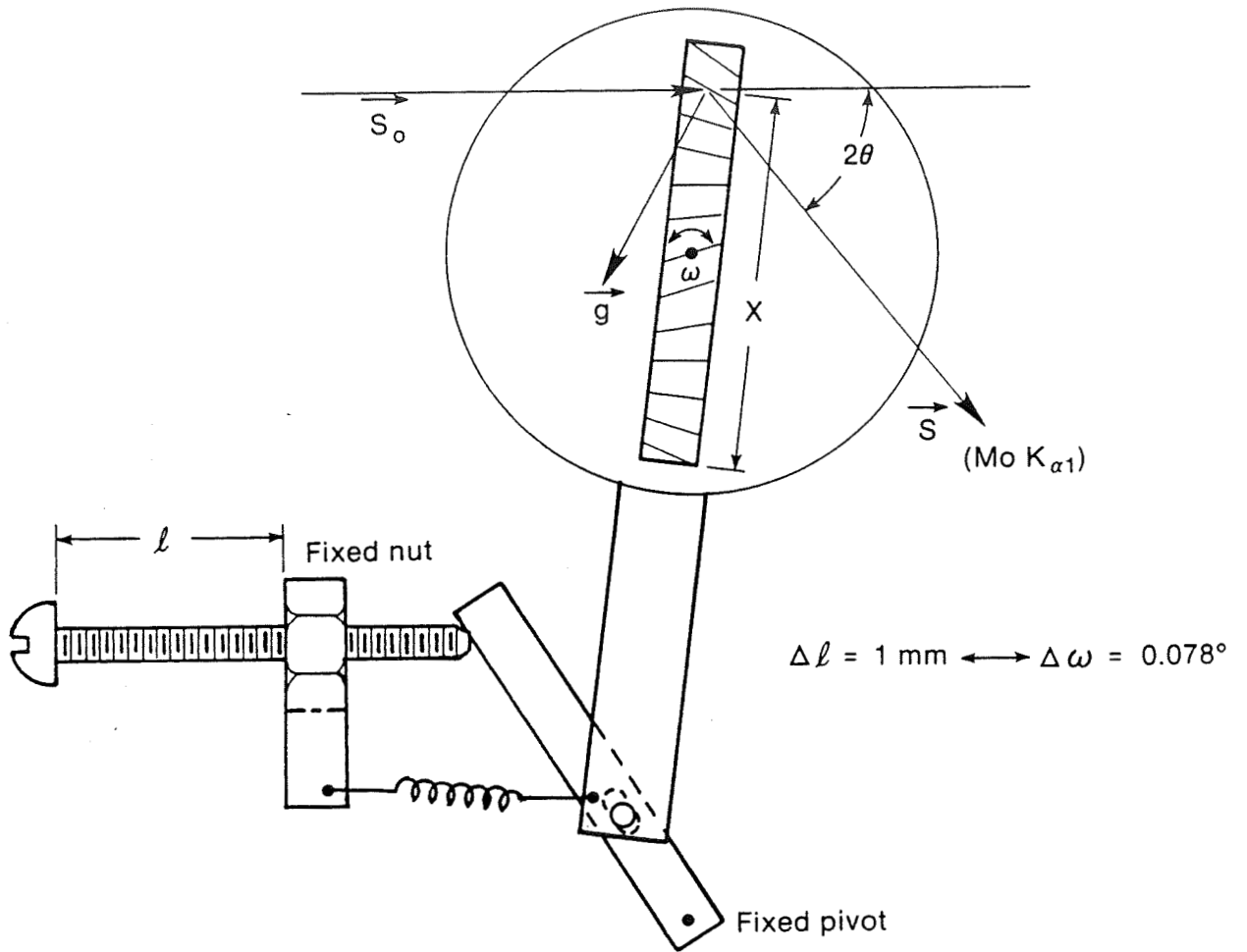


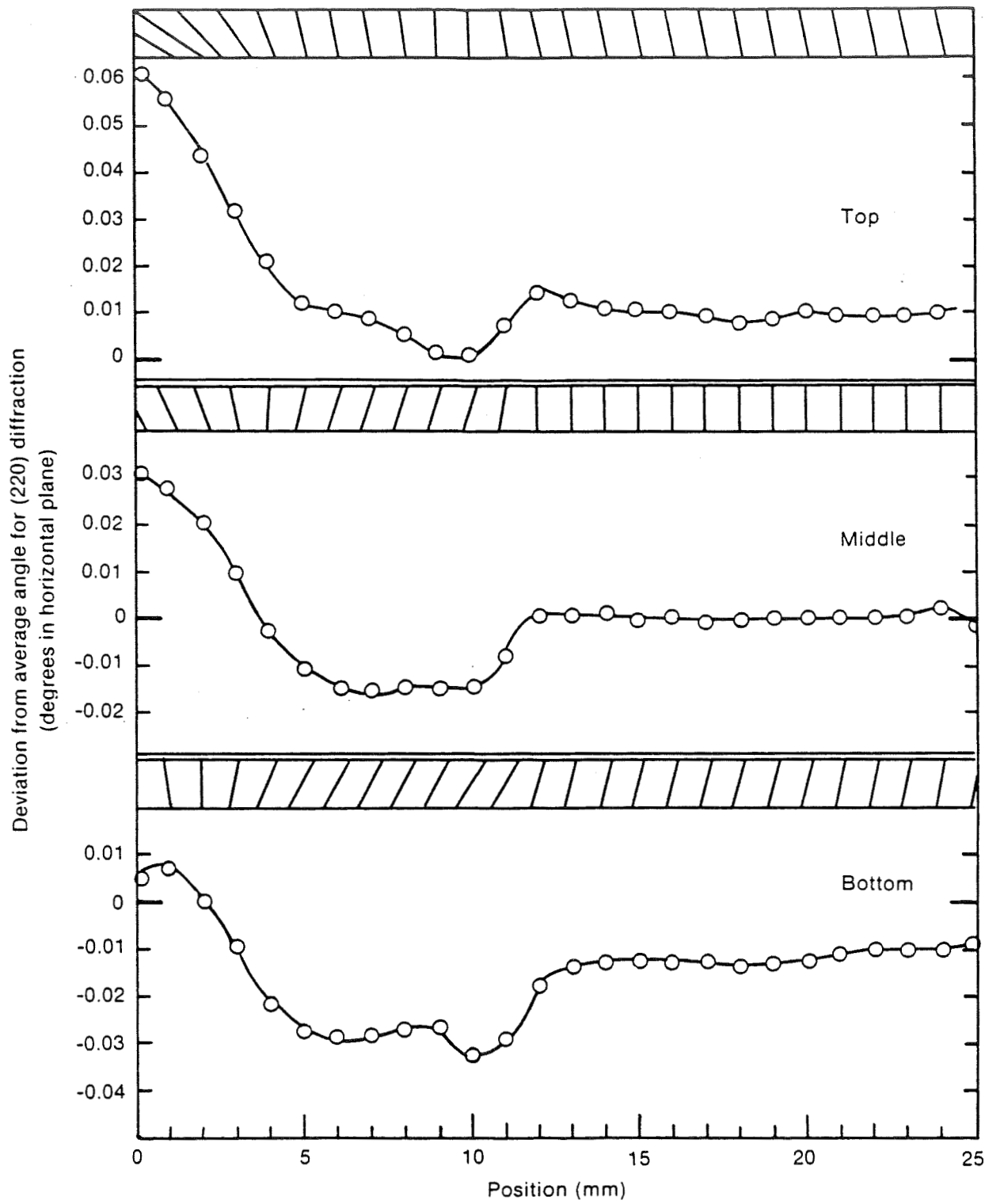
ADVANCED SILICON SHEET



- Al, 20 mm dia, poly Si vendor A
- Al, 20 mm dia, poly Si vendor B
- ▼ B, 20 mm dia, poly Si vendor A
- △ B, 20 mm dia, poly Si vendor B
- Ga, 20 mm dia, poly Si vendor A
- Ga, 20 mm dia, poly Si vendor B
- Ga, 34 mm dia, poly Si vendor B
- ◆ In, 20 mm dia, poly Si vendor A
- ◇ In, 20 mm dia, poly Si vendor B
- * Experts group best values

RESISTIVITY (ohm-cm)	LIFETIME (microsec.)
1	700
0.5	490
0.2	120
0.1	40





Summary and Conclusions

- * EVAPORATION CONTRIBUTES SUBSTANTIALLY TO IMPURITY REDUCTION WHEN FZ OR COLD-CRUCIBLE GROWTH IS CONDUCTED IN A VACUUM.
- * BORON AND GALLIUM MAY BE MORE FAVORABLE DOPANTS THAN INDIUM OR ALUMINUM FOR OBTAINING HIGH MINORITY-CARRIER LIFETIMES.
- * MINORITY-CARRIER LIFETIMES GREATER THAN 100 microseconds ARE FEASIBLE AT A $2 \times 10^{17} \text{ cm}^{-3}$ DOPING LEVEL.
- * MINORITY-CARRIER LIFETIME DECREASES WITH INCREASING CRYSTAL COOLING RATE AND ALSO WITH THE PRESENCE OF DISLOCATIONS.
- * THE METHOD USED TO CLEAN SILICON FEED RODS AFFECTS LIFETIME.
- * MICRODEFECT DENSITIES IN DISLOCATION-FREE FZ CRYSTALS APPEAR TO BE LOWER WITH Ga DOPING THAN WITH B DOPING.
- * A VARIETY OF SI RIBBONS WERE EXAMINED BY X-RAY TOPOGRAPHY; A METHOD FOR QUANTIFYING LATTICE PLANE BENDING WAS DEVELOPED.

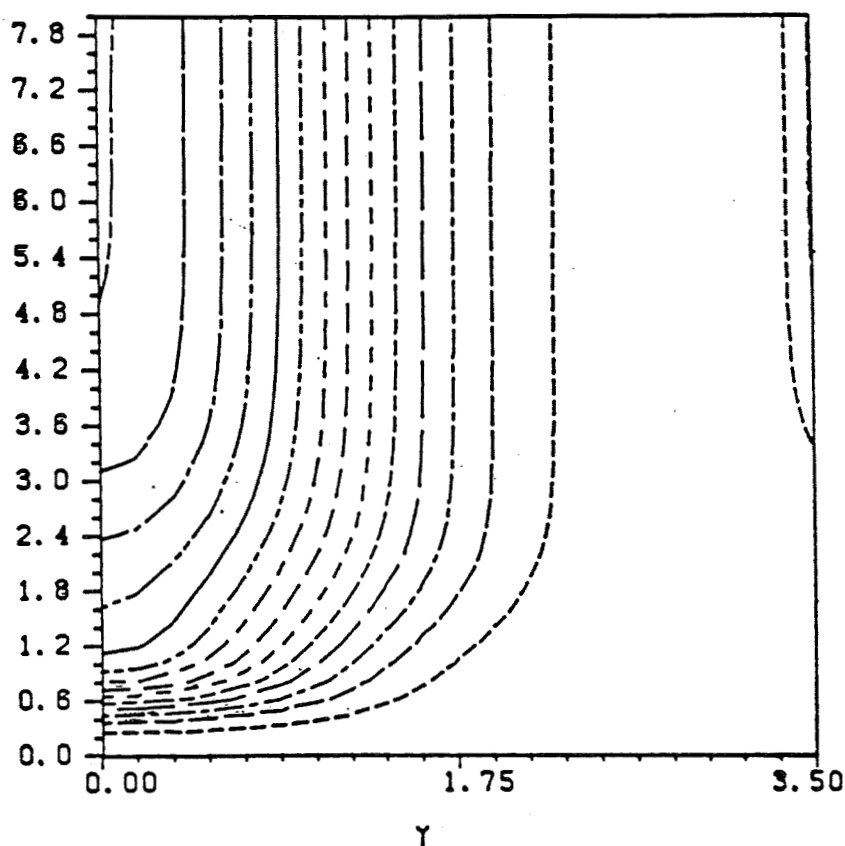
ANALYSIS OF SILICON STRESS/STRAIN
RELATIONSHIPS

UNIVERSITY OF KENTUCKY

O. Dillon

Dislocation Density Contour Plot

$$T = 1412 - 110.74X + 3.5X^2$$

UNIT OF X AND Y=CM, Z=1 PER CM²

LEGEND: Z

-----	0.5	-----	9.6
-----	18.	-----	27.
-----	36.	-----	46.
-----	55.	-----	64.
-----	73.	-----	82.
-----	91.	-----	100.
-----	109.	-----	118.
-----	127.		

Dislocation density contour plot for the parabolic thermal profile of Eq.(4-8), 8x7 cm ribbon and an initial dislocation density = 0.5 cm^{-2} .

Dislocation Density Along $Y = 0$ (Centerline)

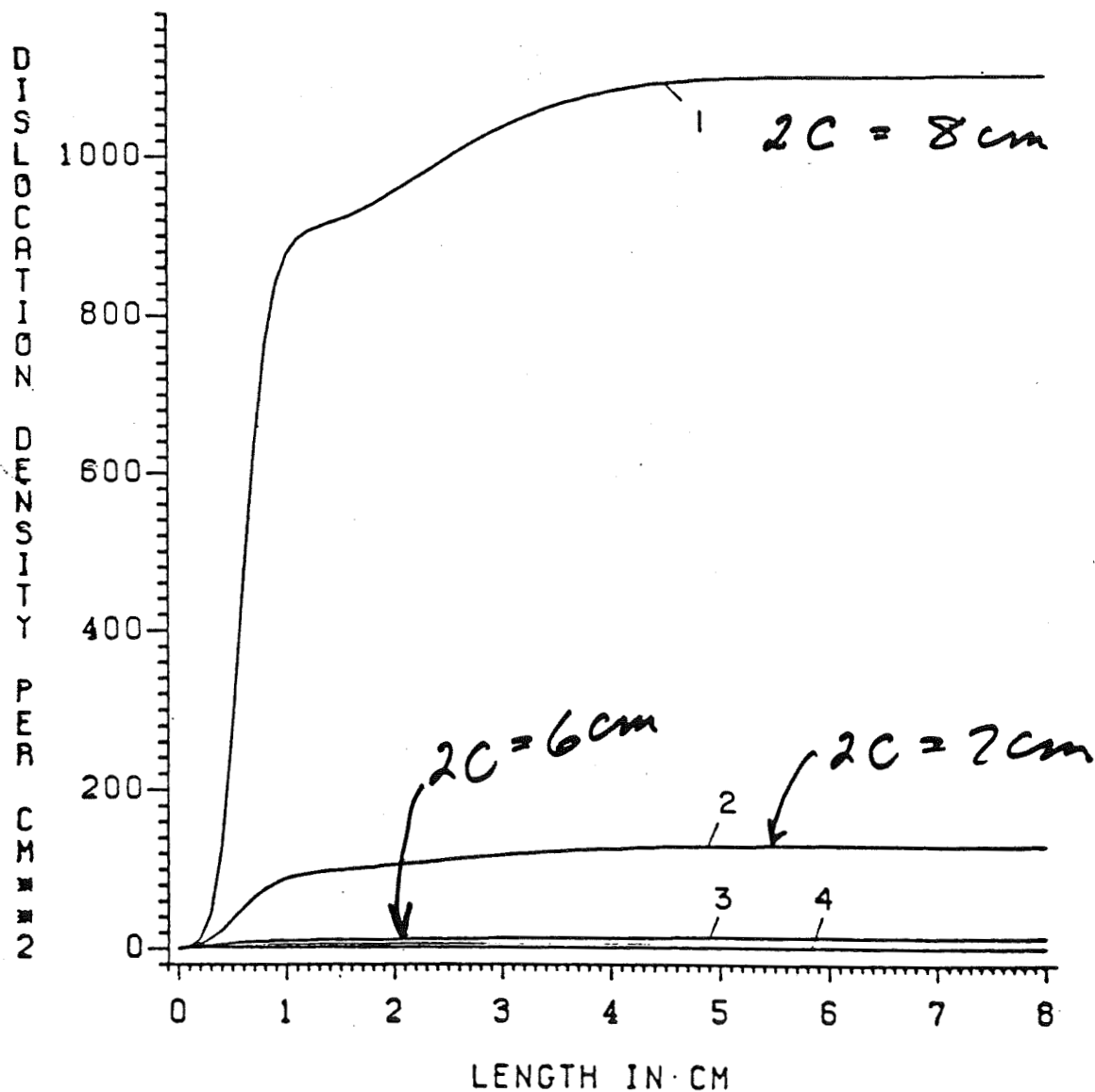
$$T = 1412 - 110.74X + 3.5X^2$$

LINE 1 FOR WIDTH=8 CM

LINE 2 FOR WIDTH=7 CM

LINE 3 FOR WIDTH=6 CM

LINE 4 FOR WIDTH=4 CM



Dislocation density along the centerline of the ribbon for the parabolic thermal profile of Eq. (4-8), initial dislocation density = 0.5 cm^{-2} , and width = 8, 7, 6, 4 cm.

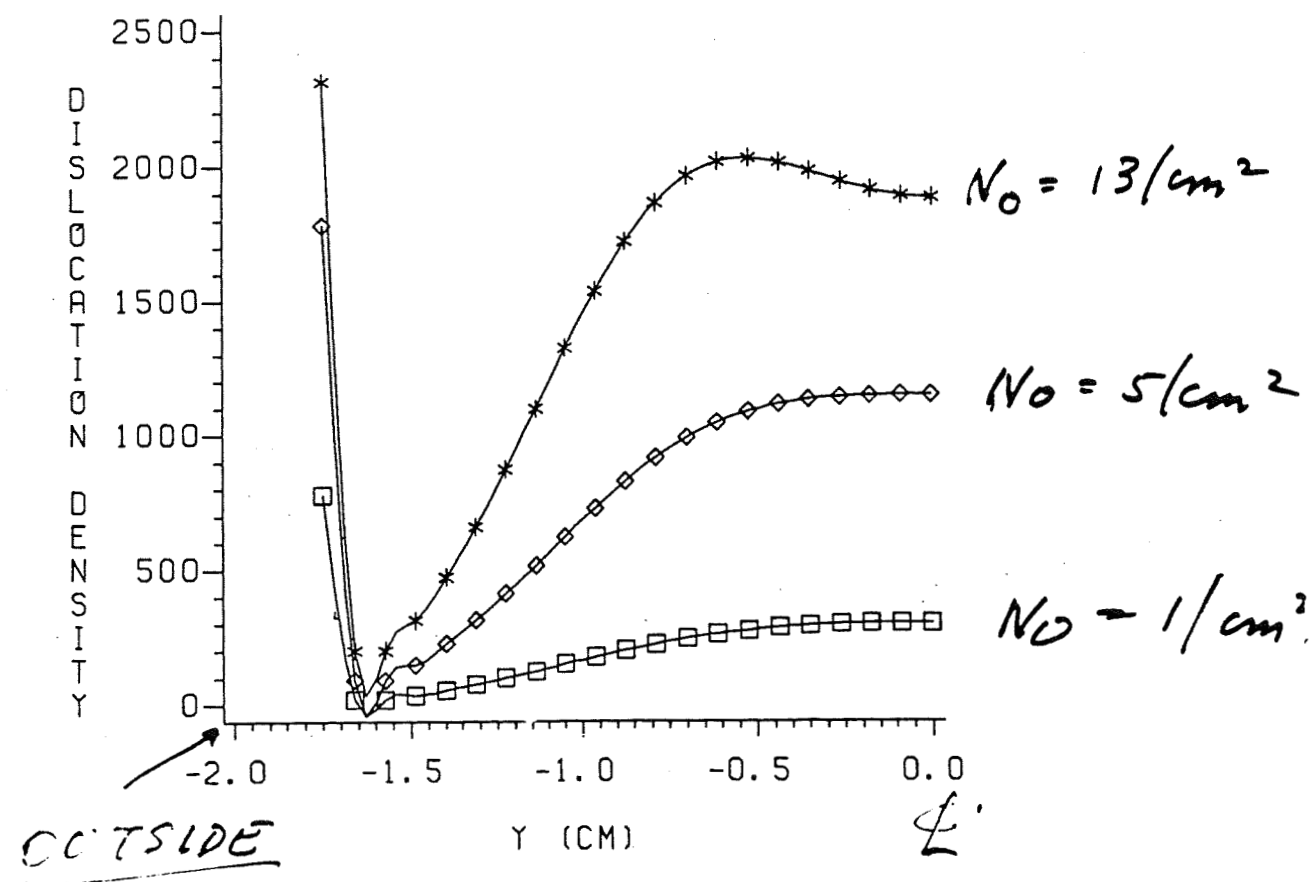
Final Dislocation Density Along the Ribbon
Width for Westinghouse Profile

LENGTH = 12 CM, WIDTH = 3.5 CM

STAR FOR $N_0 = 13 / \text{CM}^2$

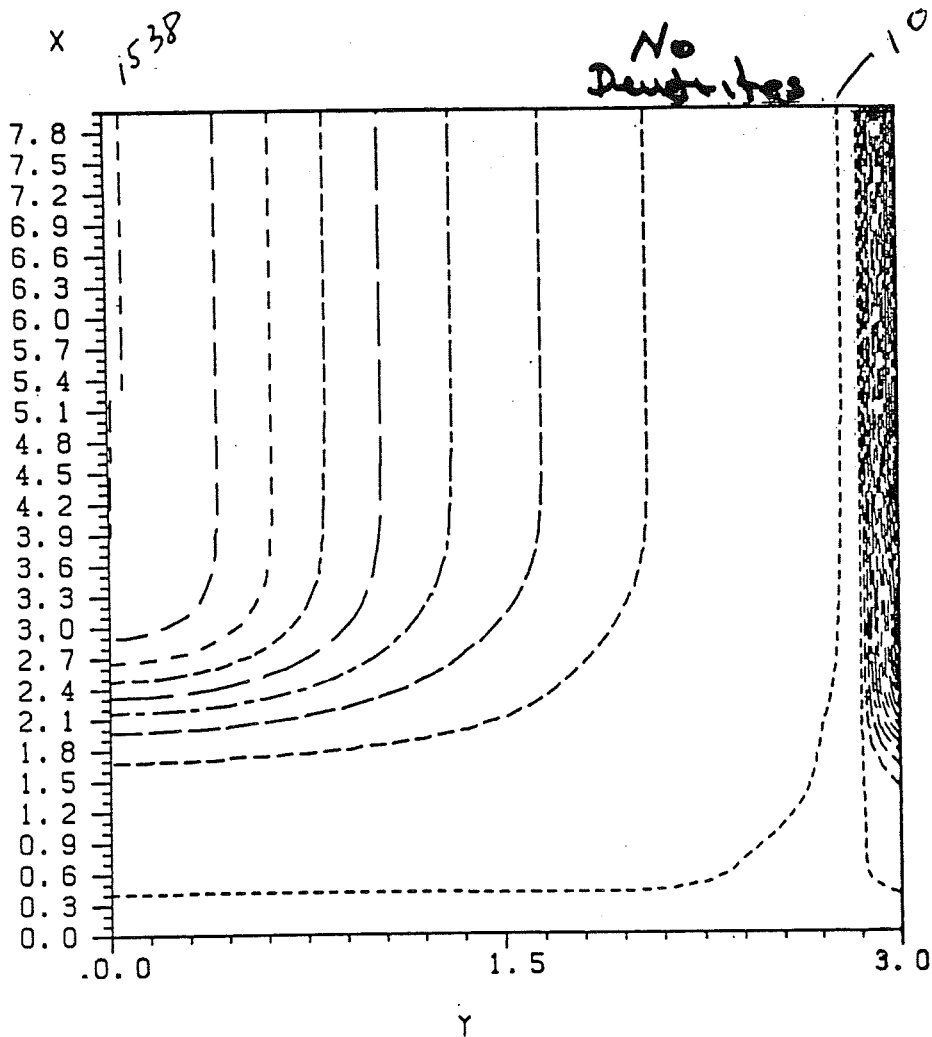
DIAMOND FOR $N_0 = 5 / \text{CM}^2$

SQUARE FOR $N_0 = 1 / \text{CM}^2$



Dislocation Density Contour Plot

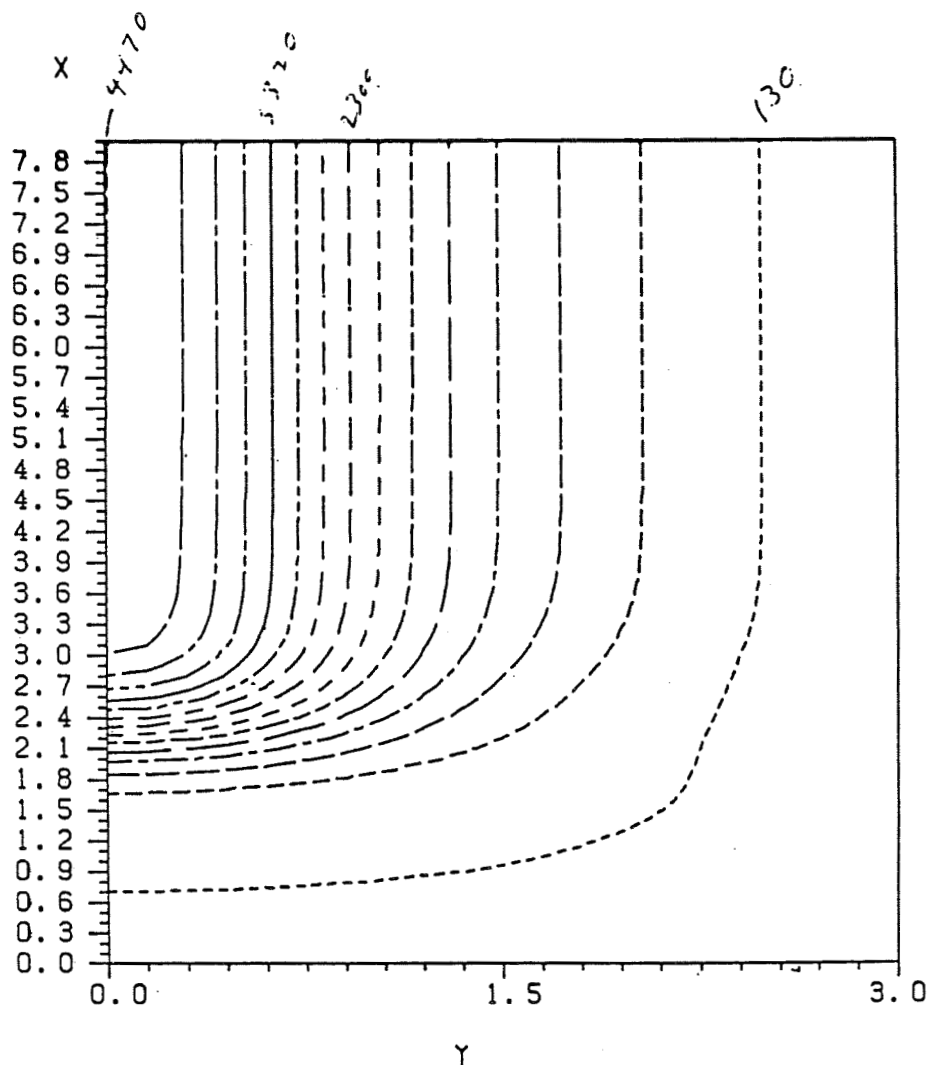
WESTINGHOUSE PROFILE, NO=0.25/CM**2, R/T=0
UNIT OF X AND Y=CM, Z=1 PER CM**2



LEGEND: Z	-----	10	-----	201
	-----	392	-----	583
	-----	774	-----	965
	-----	1156	-----	1347
	-----	1538	-----	1729
	-----	1920	-----	2111
	-----	2302	-----	2493
	-----	2684		

Dislocation Density Contour Plot

WESTINGHOUSE PROFILE, NO=0.375/CM**2
UNIT OF X AND Y=CM, Z=1 /CM**2, A/T=1.6667 M



*with
Densities*

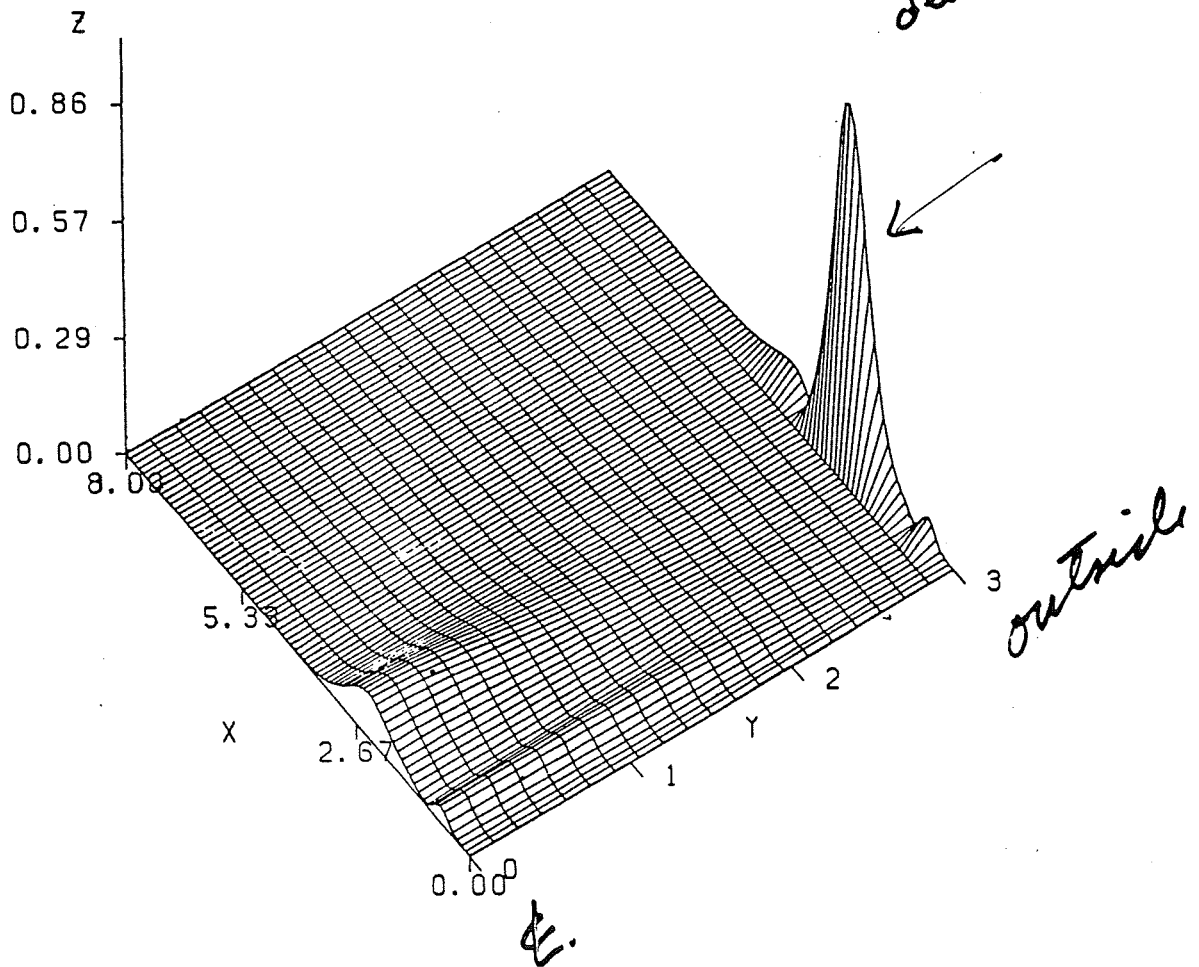
LEGEND: Z	----- 130	----- 440
	----- 750	----- 1060
	----- 1370	----- 1680
	----- 1990	----- 2300
	----- 2610	----- 2920
	----- 3230	----- 3540
	----- 3850	----- 4160
	----- 4470	

*Note
Low
Densities*

Effective Plastic Strain Rate

WESTINGHOUSE PROFILE, NO=0.25/CM \times 2
 WIDTH = 6 CM, LENGTH = 8 CM, A/T=0.
 UNIT OF X AND Y=CM, Z=10 \times -5 PER SEC

*PLASTIC STRAIN
RATE*

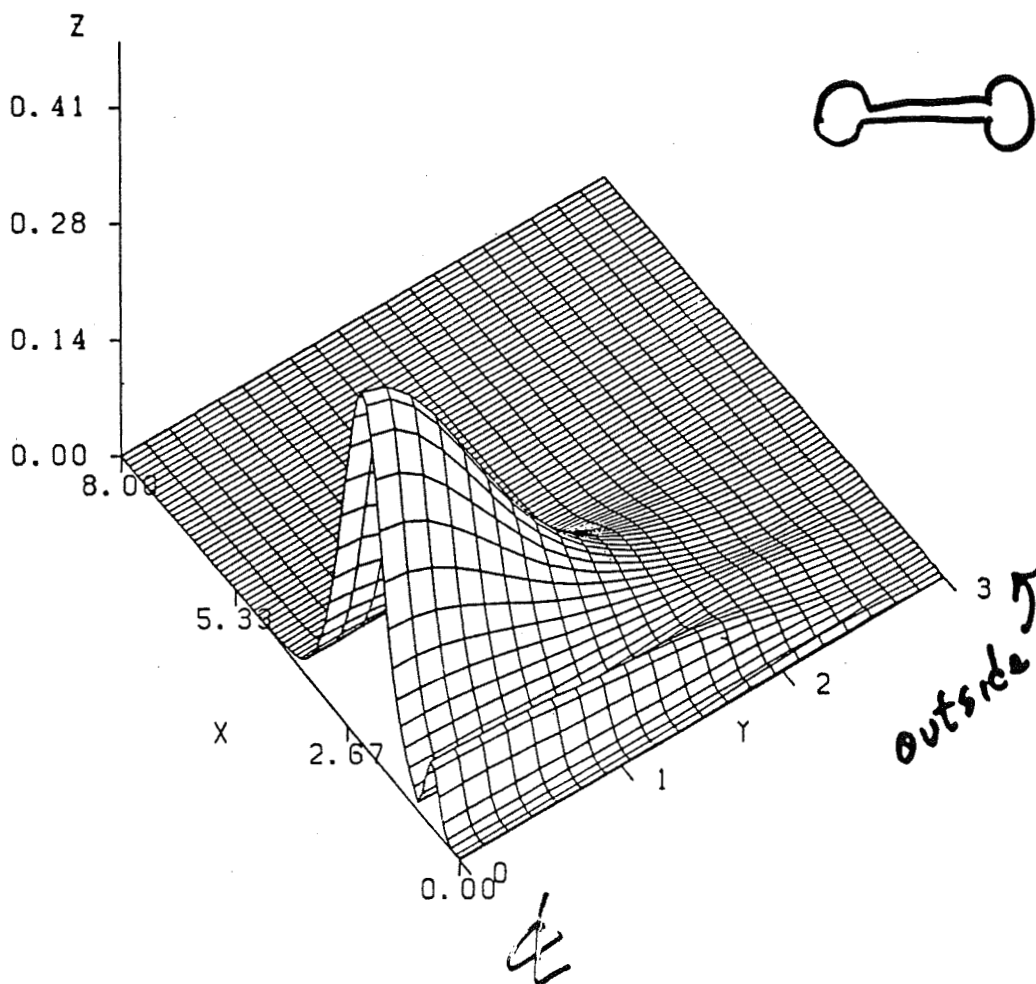


D

Effective Plastic Strain Rate

WESTINGHOUSE PROFILE, NO=0.375/CM**2
 WIDTH = 6 CM, LENGTH = 8 CM, A/T=1.6667 MM
 UNIT OF X AND Y=CM, Z=10**-5 PER SEC

PLASTIC STRAIN RATE



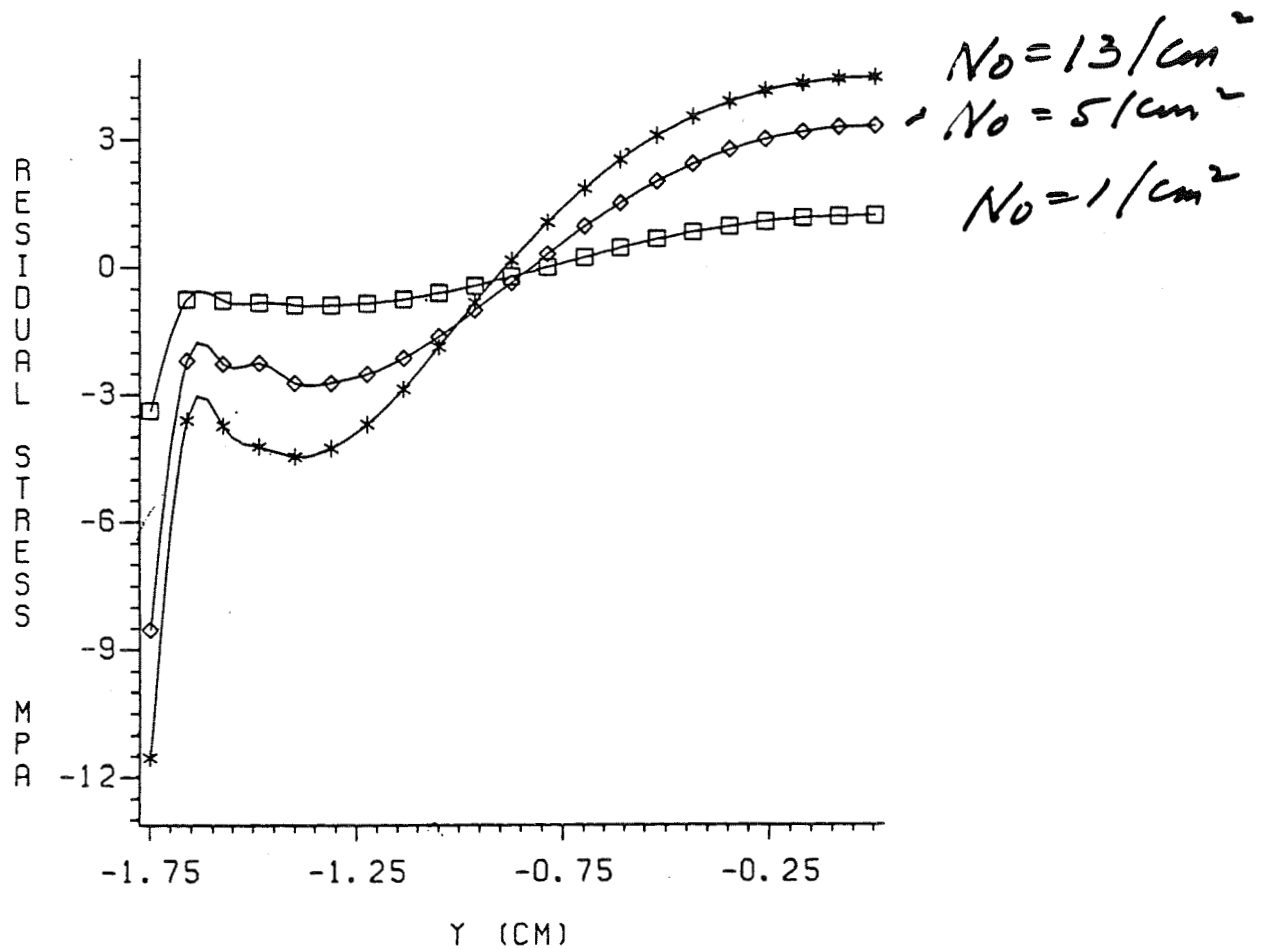
Residual Stress XX Along Ribbon
Width for Westinghouse Profile

LENGTH = 12 CM, WIDTH = 3.5 CM

STAR FOR NO = 13 /CM**2

DIAMOND FOR NO = 5 /CM**2

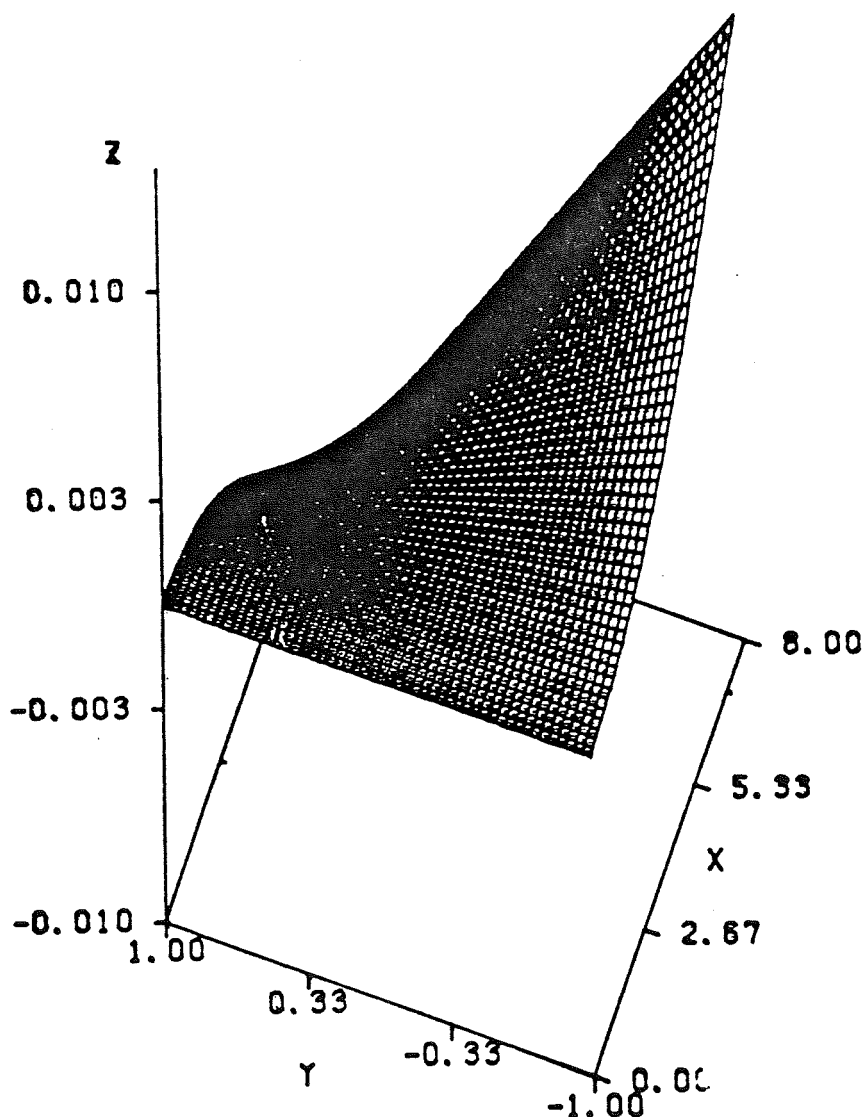
SQUARE FOR NO = 1 /CM**2



Deflection Shape

HALF-WIDTH (C)=1., LENGTH=8.0
DIAMETER OF DENDRITES IS 0.0 INCHES
CRITICAL THICKNESS = 0.00526 INCHES

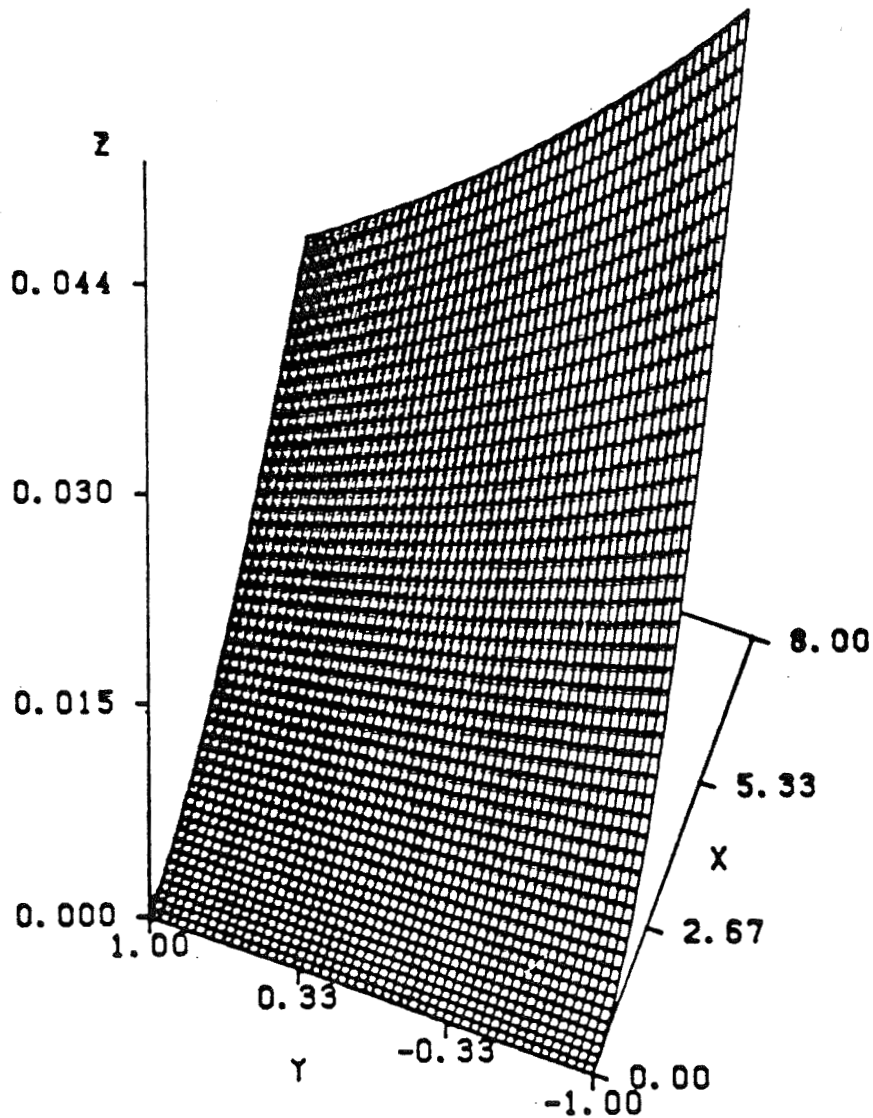
$$T(x) = \text{parabolic}$$



Deflection Shape

HALF-WIDTH (C)=1.0 LENGTH=8.0
 DIAMETER OF DENDRITES IS 0.2 INCHES
 CRITICAL THICKNESS = 0.057120 INCHES

$$T(x) = \text{parabolic}$$



Topics

1 Dislocation Motion

- A) Problem Formulation
- B) Calculation of Forces
- C) Tracking the motion of a single Dislocation

2 Dislocation Multiplication & Density

- A) Three methods of calculations - based on resolved shear stresses on each slip system
- B) Dislocation density by averaging the | shear stresses | in 0.5 cm. widths of ribbon. (starting at $x = 0.2$ cm.)

Possible Dislocations in the Silicon Crystal

burgers vector	tangent vector	slip plane type of dislocation
$\langle -1\ 0\ -1 \rangle$	$\langle -1\ 0\ -1 \rangle$	$(-1\ -1\ 1)$, left, screw
=	$\langle 0\ 1\ 1 \rangle$	= ,left, 60' (-120') ✓
=	$\langle 1\ -1\ 0 \rangle$	= ,left, 60' (+120')
=	$\langle 1\ -2\ -1 \rangle$	= ,left, edge
$\langle 0\ 1\ 1 \rangle$	$\langle 0\ 1\ 1 \rangle$	= ,left, screw
=	$\langle 1\ -1\ 0 \rangle$	= ,left, 60' (+120')
=	$\langle -1\ 0\ -1 \rangle$	= ,left, 60' (-120') ✓
=	$\langle -2\ 1\ -1 \rangle$	= ,left, edge
$\langle -1\ 1\ 0 \rangle$	$\langle -1\ 1\ 0 \rangle$	= ,left, screw
=	$\langle 0\ -1\ -1 \rangle$	= ,left, 60' (-120') ✓
=	$\langle 1\ 0\ 1 \rangle$	= ,left, 60' (+120') ✓
=	$\langle -1\ -1\ 2 \rangle$	= ,left, edge
$\langle 1\ 0\ -1 \rangle$	$\langle 1\ 0\ -1 \rangle$	$(-1\ 1\ -1)$, right, screw
=	$\langle -1\ -1\ 0 \rangle$	= ,right, 60' (-120') ✓
=	$\langle 0\ 1\ 1 \rangle$	= ,right, 60' (+120') ✓
=	$\langle -1\ -2\ -1 \rangle$	= ,right, edge
$\langle 0\ -1\ -1 \rangle$	$\langle 0\ -1\ -1 \rangle$	= ,right, screw
=	$\langle 1\ 1\ 0 \rangle$	= ,right, 60' (-120') ✓
=	$\langle -1\ 0\ 1 \rangle$	= ,right, 60' (+120')
=	$\langle -2\ -1\ 1 \rangle$	= ,right, edge
$\langle 1\ 1\ 0 \rangle$	$\langle 1\ 1\ 0 \rangle$	= ,right, screw
=	$\langle -1\ 0\ 1 \rangle$	= ,right, 60' (+120')
=	$\langle 0\ -1\ -1 \rangle$	= ,right, 60' (-120') ✓
=	$\langle -1\ 1\ -2 \rangle$	= ,right, edge
$\langle 0\ -1\ 1 \rangle$	$\langle 0\ -1\ 1 \rangle$	$(-1\ 1\ -1)$, transv., screw
=	$\langle 1\ 1\ 0 \rangle$	= ,transv., 60' (+120') ✓
=	$\langle -1\ 0\ -1 \rangle$	= ,transv., 60' (-120') ✓
=	$\langle 2\ 1\ 1 \rangle$	= ,transv., edge
$\langle 1\ 1\ 0 \rangle$	$\langle 1\ 1\ 0 \rangle$	= ,transv., screw
=	$\langle 0\ -1\ 1 \rangle$	= ,transv., 60' (+120')
=	$\langle -1\ 0\ -1 \rangle$	= ,transv., 60' (-120') ✓
=	$\langle 1\ -1\ 2 \rangle$	= ,transv., edge
$\langle 1\ 0\ 1 \rangle$	$\langle 1\ 0\ 1 \rangle$	= ,transv., screw
=	$\langle -1\ -1\ 0 \rangle$	= ,transv., 60' (-120') ✓
=	$\langle 0\ 1\ -1 \rangle$	= ,transv., 60' (+120')
=	$\langle -1\ -2\ 1 \rangle$	= ,transv., edge

- (1). Surface of the ribbon is $(1\ 1\ 1)$ plane.
- (2). Growth direction to the melt is $\langle 2\ -1\ -1 \rangle$.
- (3). For the motion of the dislocations, 60' dislocations that have -120 degree with the burger's vector will be chosen because these 60' dislocations may multiply themselves more than +120' type 60' dislocations as many investigators observed.

ORIGINAL PAGE IS
OF POOR QUALITY

Assumptions

- (1) The density of dislocation at the liquid solid interface is uniform
- ✱ (2) The pulling rate of the ribbon is 3cm/min.
- ✱ (3) Dislocations can move only in active slip systems that have their resolved shear stress higher than 95% of the most active slip system that has maximum Schmid Factor.
- (4) Average velocity of the dislocations in the presence of other dislocations is almost same as the velocity of isolated dislocation.
Equivalent to low dislocation density.
- ✱ (5) The velocity equation proposed by K.Sumino

$$V = V_0 \tau \exp(-E/kT)$$

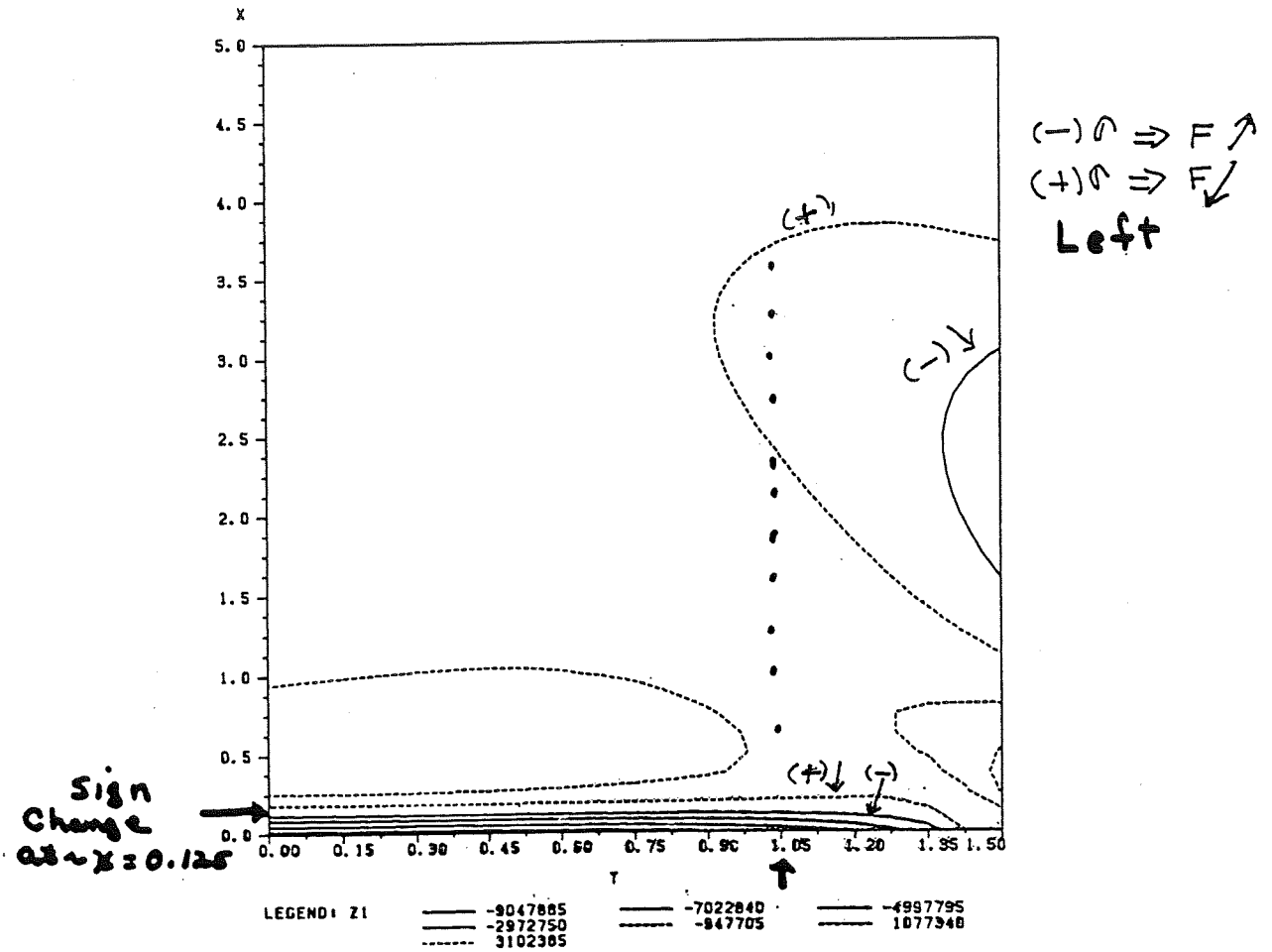
where E is 2.2 eV for 60' and 2.35 eV for screw,

V_0 is 0.035 for screw and 0.01 m³ / MN.sec for 60'.

is still valid at high temperature like around melting temperature.

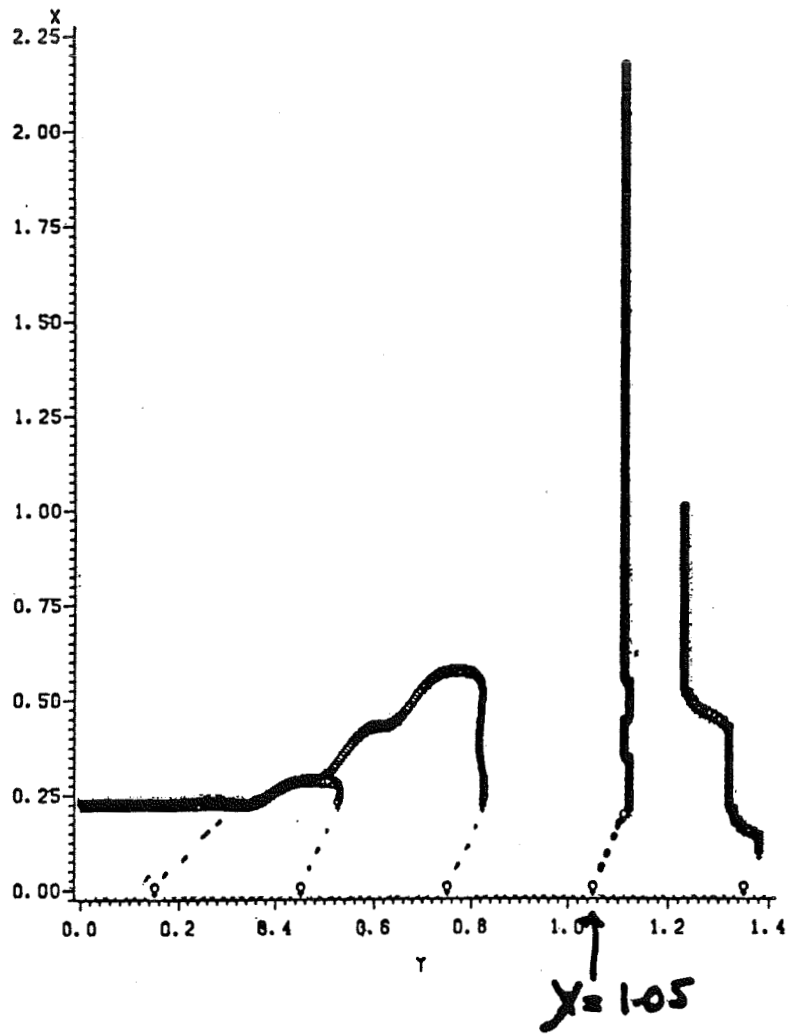
Resolved Shear Stress

ORIGINAL PAGE IS
OF POOR QUALITY



Motion of Dislocation

$B=A/2(-1 \ 1 \ 0), T=(1 \ 0 \ 1), M=(-1 \ -1 \ 1)$



UNIT OF AXES ARE CM

Motion of the Dislocations Emerging to the Surface

possible 60° dislocations emerging to the surface

burger's vector	tangent vector	plane	motion
$a/2(-1 \ 0 \ -1)$	$(0 \ 1 \ 1)$	$(-1 \ -1 \ 1)$	left strong
$a/2(-1 \ 1 \ 0)$	$(0 \ -1 \ -1)$	$(-1 \ -1 \ 1)$	*
$a/2(-1 \ 1 \ 0)$	$(1 \ 0 \ 1)$	$(-1 \ -1 \ 1)$	split
$a/2(0 \ 1 \ 1)$	$(-1 \ 0 \ -1)$	$(-1 \ -1 \ 1)$	right weak
$a/2(1 \ 0 \ -1)$	$(0 \ 1 \ 1)$	$(-1 \ 1 \ -1)$	right strong
$a/2(1 \ 0 \ -1)$	$(-1 \ -1 \ 0)$	$(-1 \ 1 \ -1)$	*
$a/2(1 \ 1 \ 0)$	$(0 \ -1 \ -1)$	$(-1 \ 1 \ -1)$	*
$a/2(0 \ -1 \ -1)$	$(1 \ 1 \ 0)$	$(-1 \ 1 \ -1)$	right weak
$a/2(0 \ -1 \ 1)$	$(-1 \ 0 \ -1)$	$(1 \ -1 \ -1)$	right strong
$a/2(0 \ -1 \ 1)$	$(-1 \ -1 \ 0)$	$(1 \ -1 \ -1)$	left strong
$a/2(1 \ 0 \ 1)$	$(-1 \ -1 \ 0)$	$(1 \ -1 \ -1)$	left weak
$a/2(1 \ 1 \ 0)$	$(-1 \ 0 \ -1)$	$(1 \ -1 \ -1)$	left weak

* ; These are forced into the liquid

Calculation of the Density of Dislocations

From the K. Sumino's equation of dislocation multiplication

$$\Rightarrow dN_m = K K_o N_{m1} (T_a - G b \sqrt{N_{m2}} / \beta)^{(m + \lambda)} \exp(-Q/kT) dt \quad \text{---(A)}$$

where $K, K_o, b, \beta, m, \lambda, k, Q$ are constants given by K. Sumino

N_m 's ; dislocation density

$N_{m1} \propto$ source density

N_{m2} is the density controlling the back stress

T_a ; applied stresses

T ; temperature

G ; shear modulus

t ; time

Three possible ways of application of the equation (A)

(1) N_{m1} and N_{m2} are total density of dislocations

(2) N_{m1} is the partial density of dislocations on each slip system and

N_{m2} is the total density of dislocations

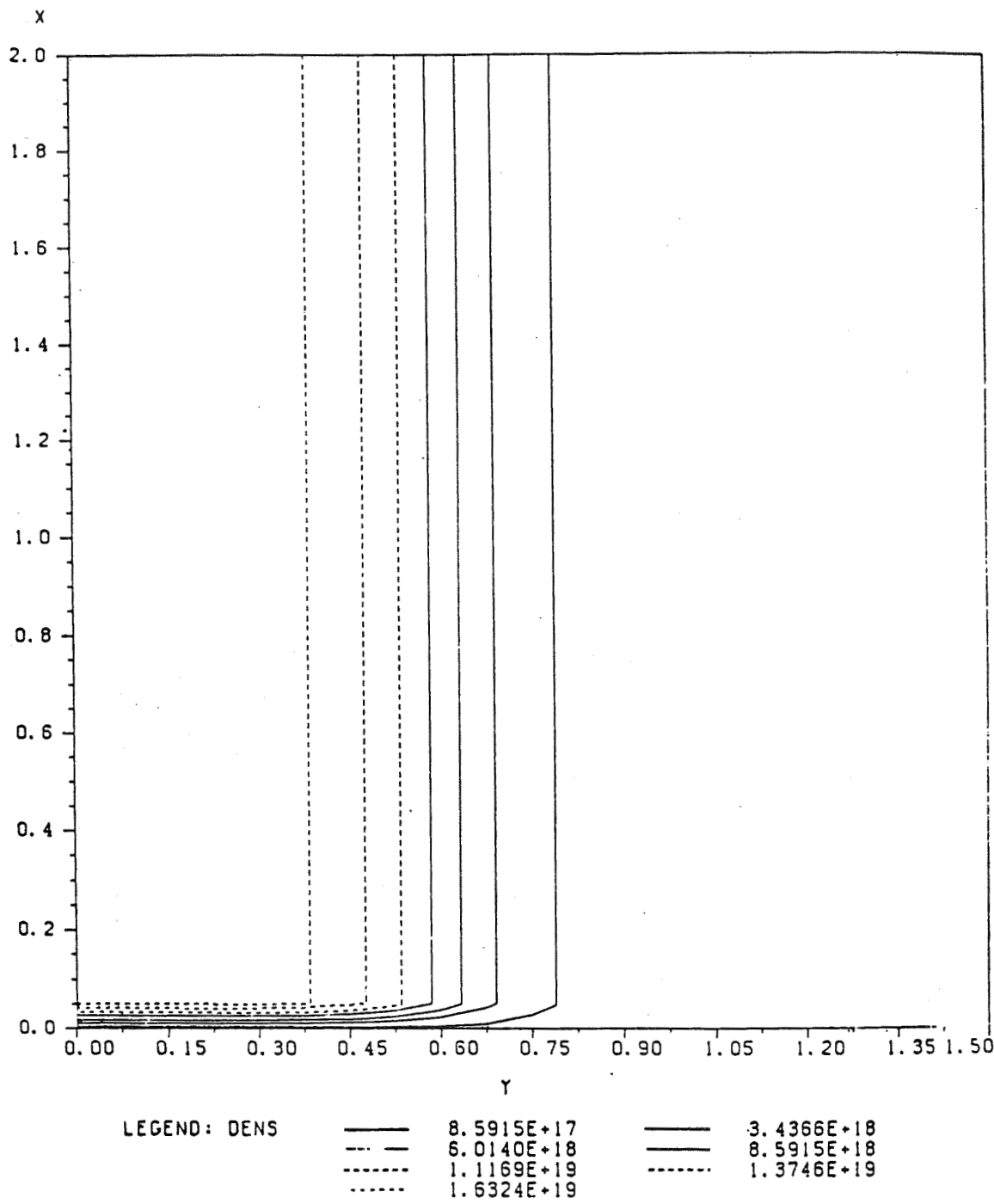
(3) Both N_m 's are partial densities of dislocations on each slip system

Method Calculating Dislocation Density

	Nm ₁	Nm ₂	
	-----	-----	
(1)	└->RSS _i	┌┌┌	total density = Nm ₁ = Nm ₂ dNm = dNm ₁ = dNm ₂
(2)	└->RSS _i	┌┌┌	total density = $\sum_i^9 (Nm_1)_i = Nm_2$ $dNm_2 = \sum_i^9 (dNm)_i$
(3)	└->RSS _i	┌┌┌	total density = $\sum_i^9 (Nm_1)_i = \sum_i^9 (Nm_2)_i$ (dNm ₁) _i = (dNm ₂) _i

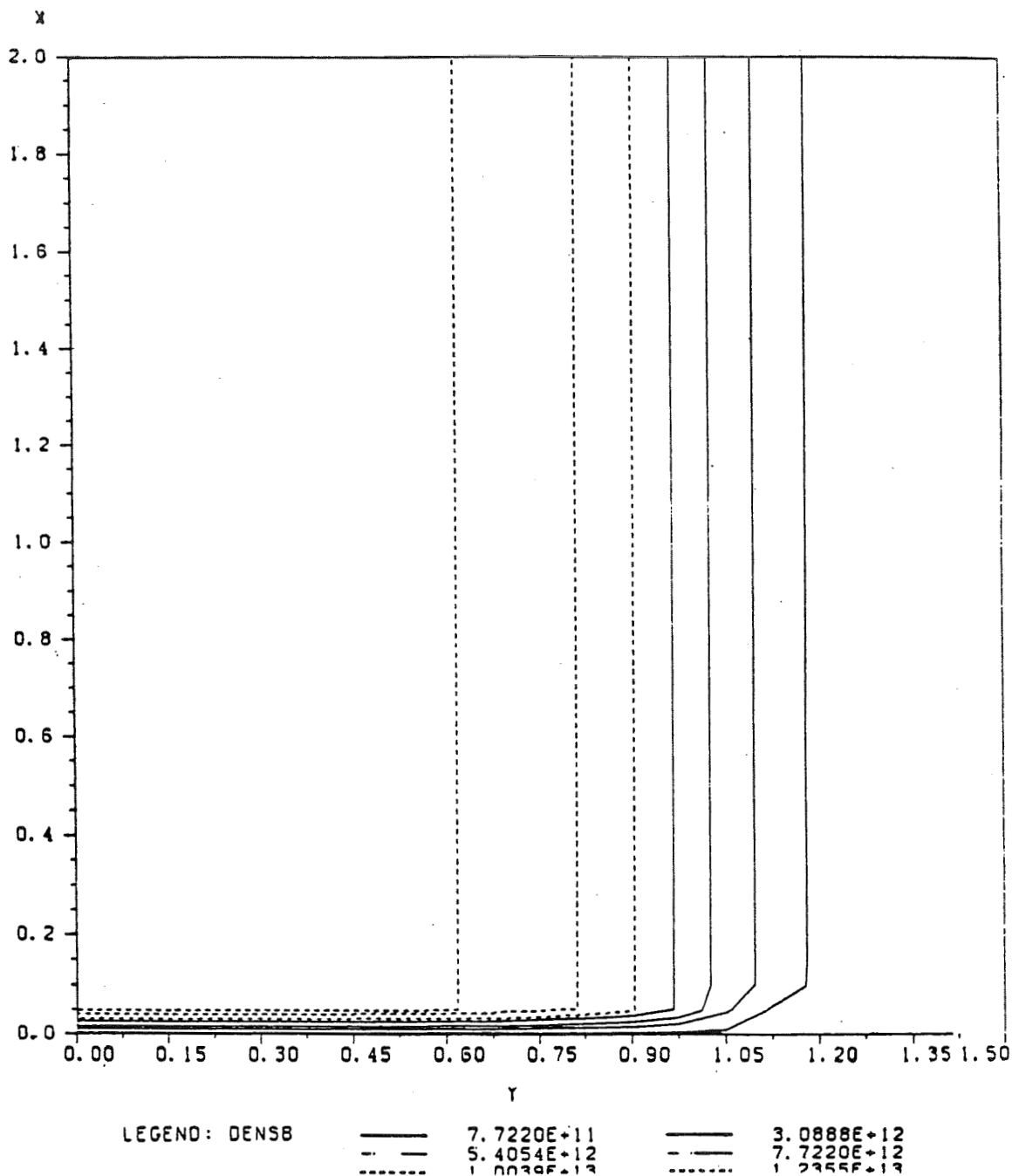
Total Density of Dislocation Using YI, YTOT and DGEAR

INITIAL TOTAL DENSITY IS 90/M**2 LAMDA IS 1.0

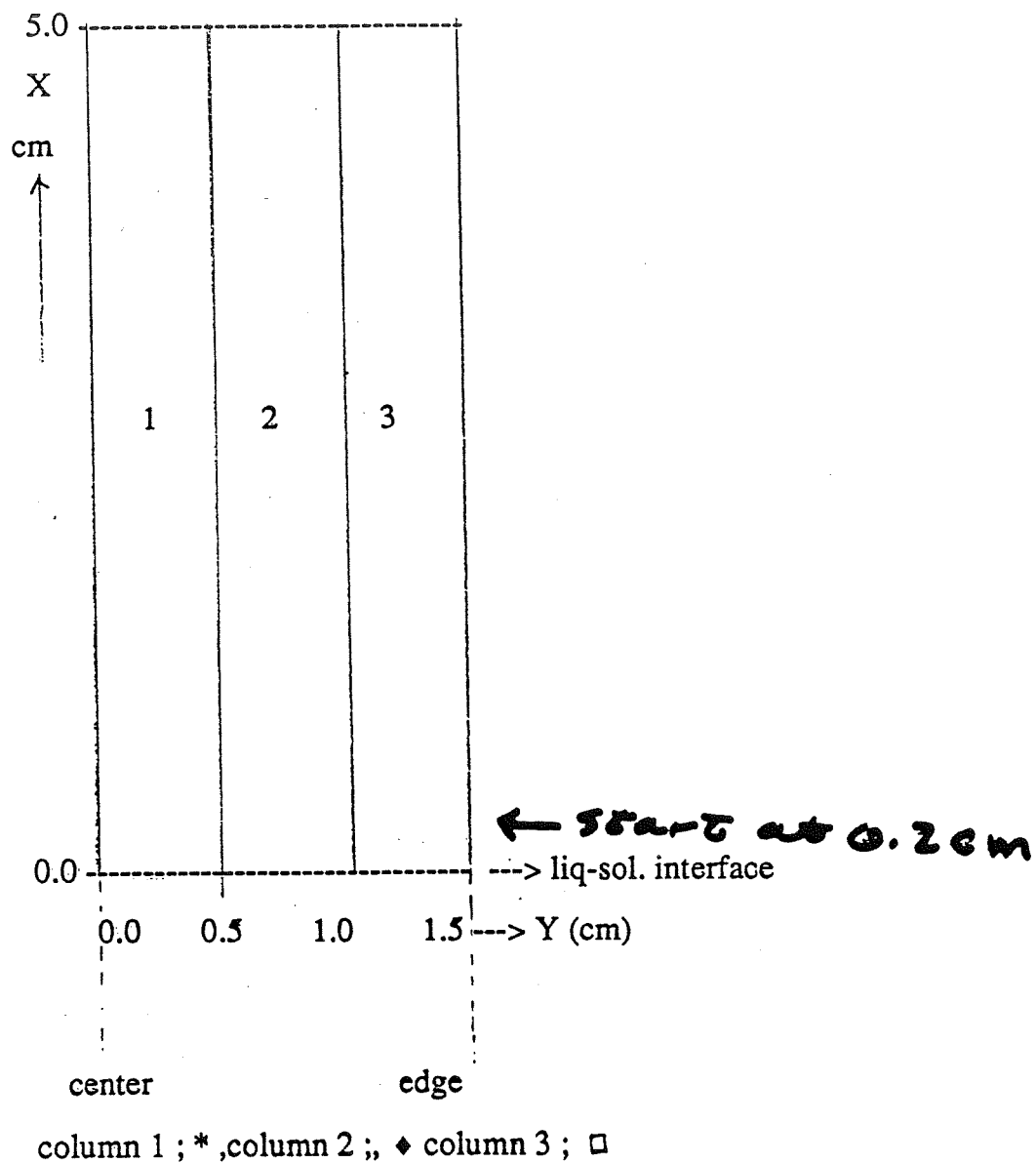


Total Density of Dislocation Using YI, YI and DGEAR

INITIAL TOTAL DENSITY IS $90/M^2$, LAMDA IS 1.0



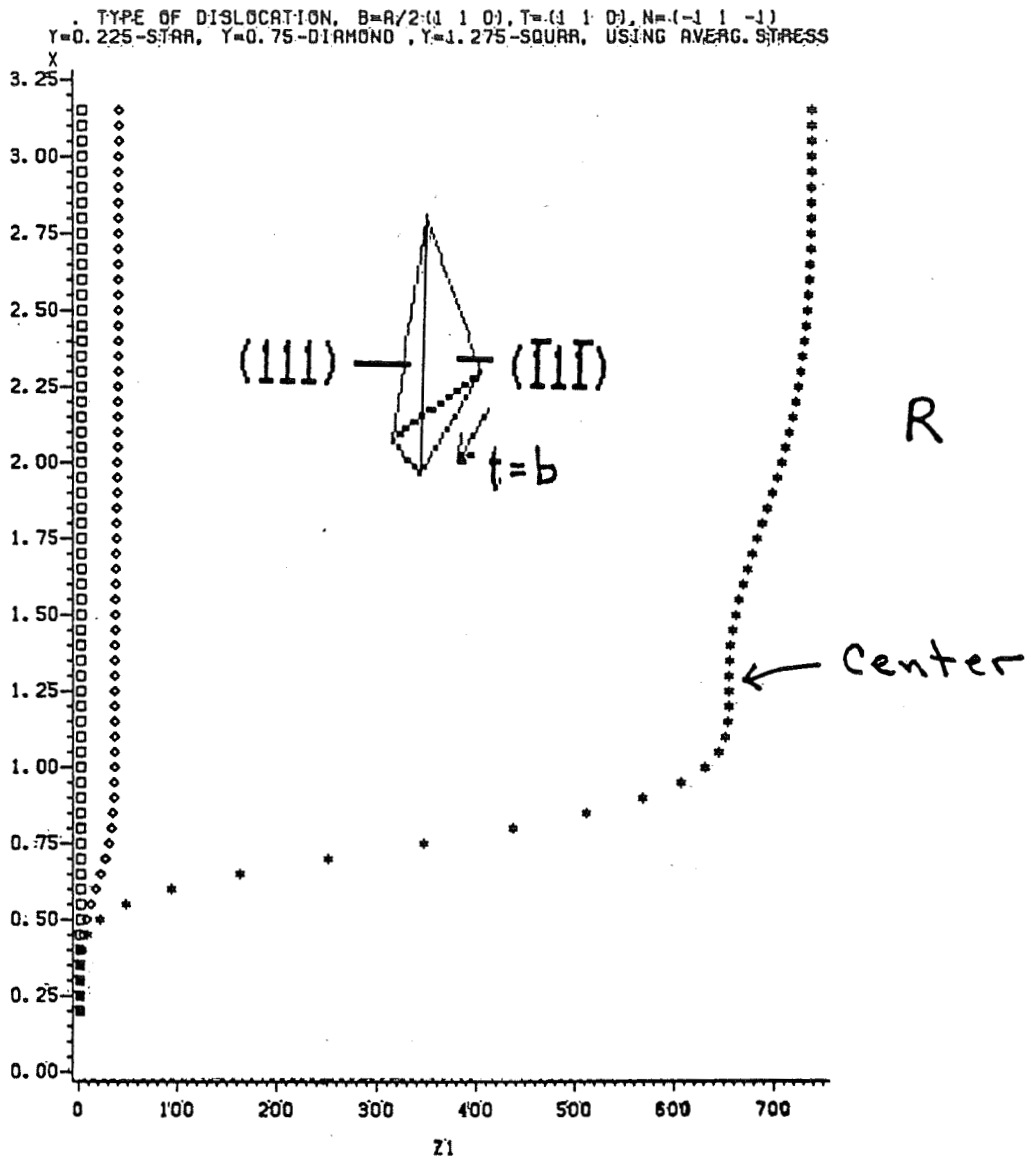
Averaging the $|\tau a|$ in Calculating Density



Nine Slip Systems

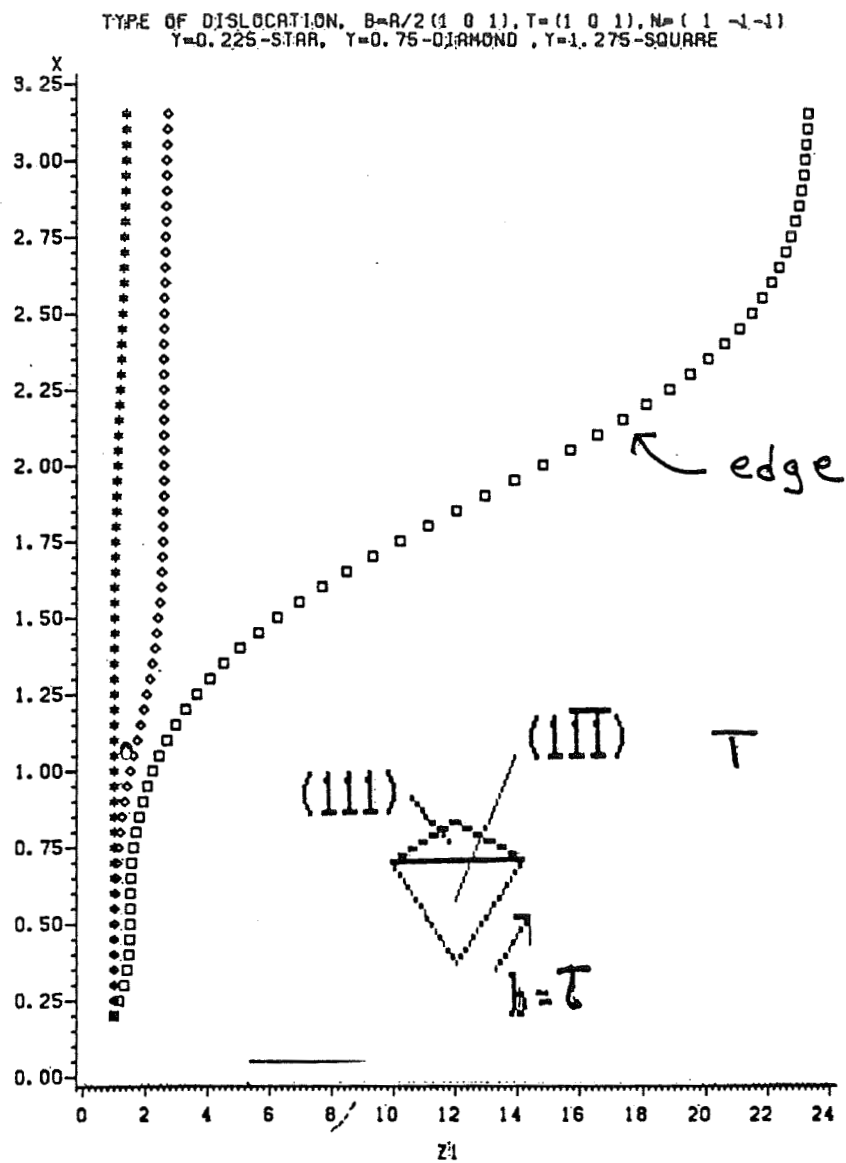
burger's vector	slip plane	type of plane
$a/2 (1\ 0\ 1)$	$(-1\ -1\ 1)$	left
$a/2 (0\ 1\ 1)$	$(-1\ -1\ 1)$	left
$a/2 (-1\ 1\ 0)$	$(-1\ -1\ 1)$	left
$a/2 (1\ 0\ -1)$	$(-1\ 1\ -1)$	right
$a/2 (1\ 1\ 0)$	$(-1\ 1\ -1)$	right
$a/2 (0\ 1\ 1)$	$(-1\ 1\ -1)$	right
$a/2 (0\ -1\ 1)$	$(1\ -1\ -1)$	transverse
$a/2 (1\ 0\ 1)$	$(1\ -1\ -1)$	transverse
$a/2 (1\ 1\ 0)$	$(1\ -1\ -1)$	transverse

Density of Dislocations When NO is 1 at $x = 0.2$ cm



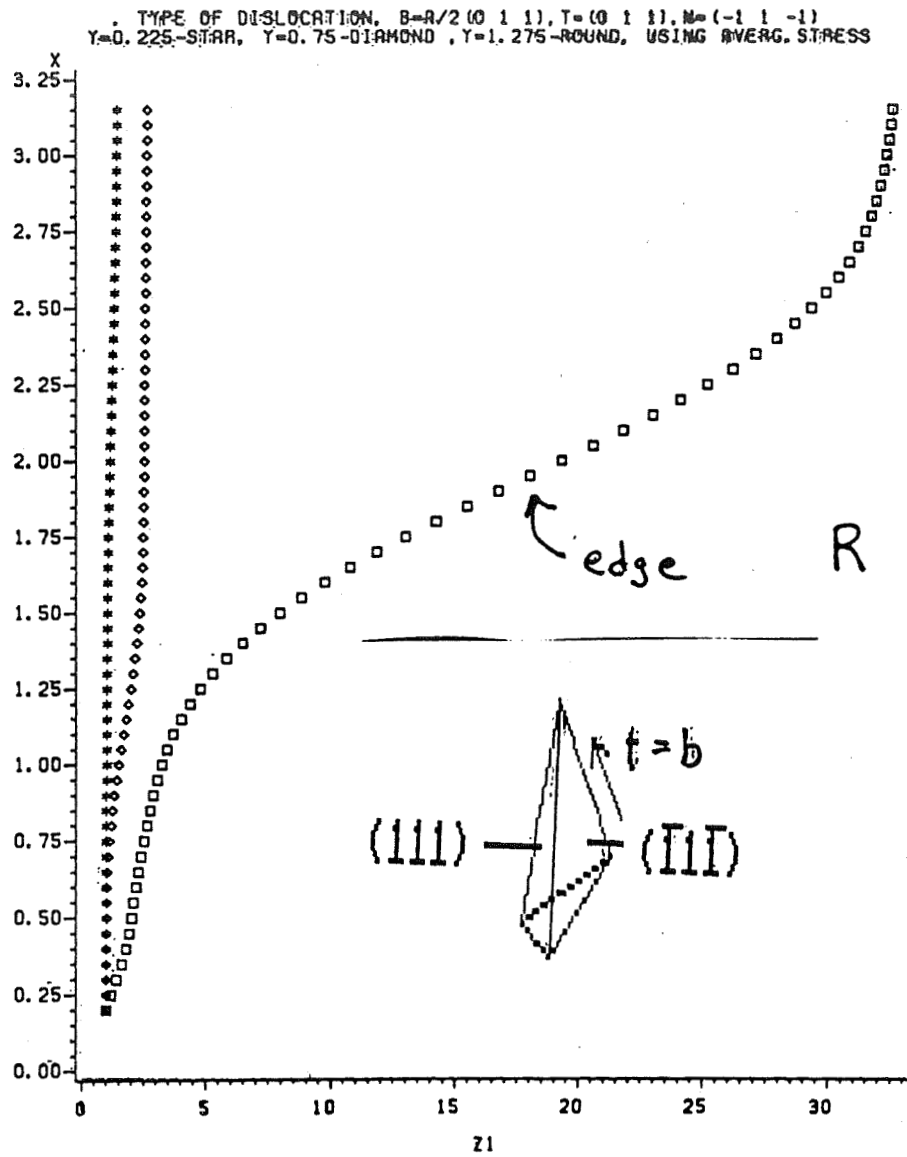
UNIT OF X IS CM, Z IS DENSITY IN $1/M^{**2}$

Density of Dislocations When NO is 1 at $x = 0.2 \text{ cm}$



UNIT OF X IS CM, Z IS DENSITY IN $1/M^2$

Density of Dislocations When NO is 1 at $x = 0.2$ cm

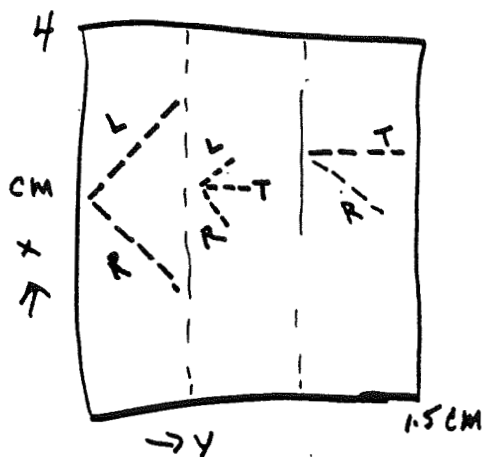


UNIT OF X IS CM, Z IS DENSITY IN $1/M^{**2}$

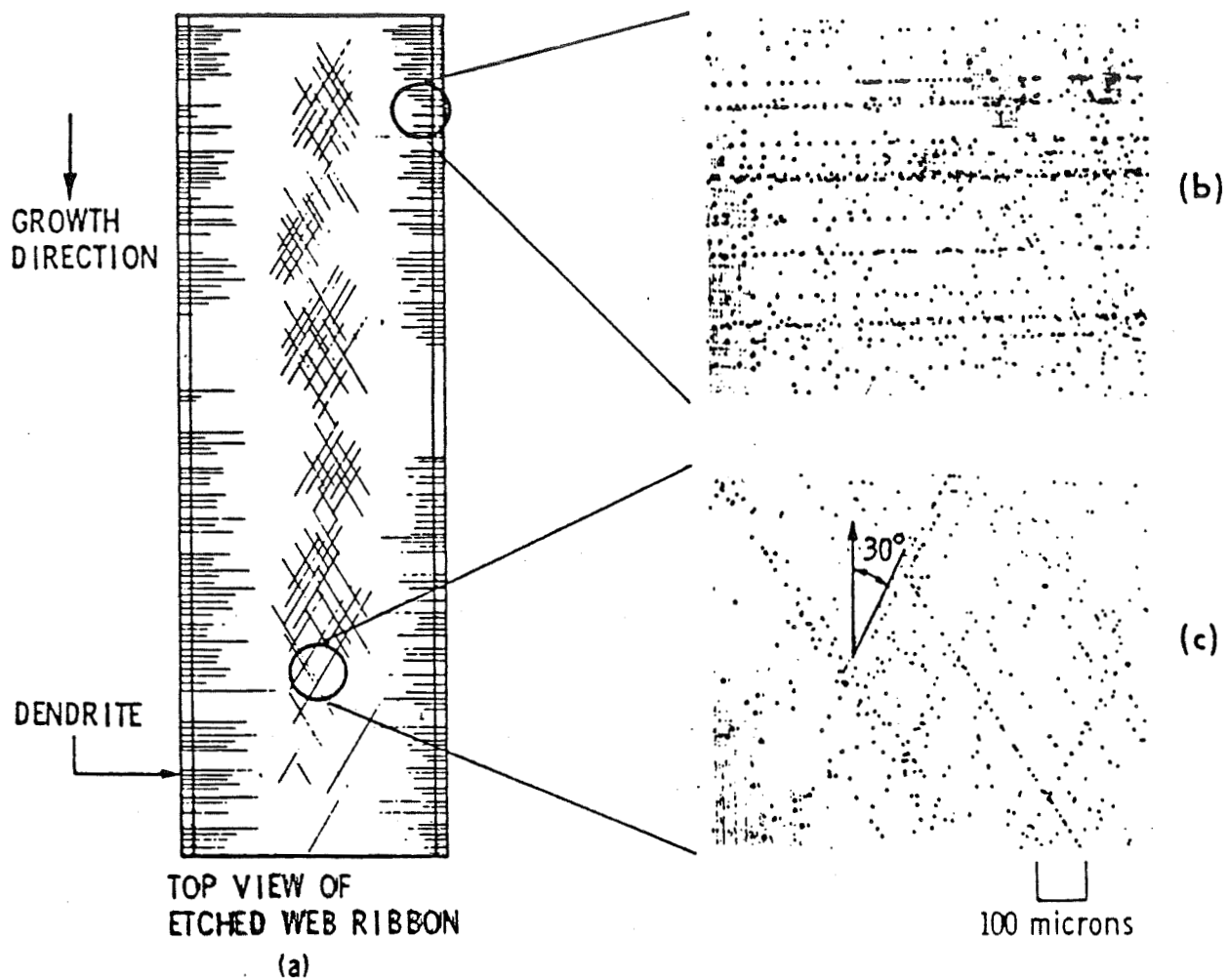
Dislocation Multiplication by Stress Averaging Over 0.5 cm

Dislocation Type			Multiplication Factor		
<u>b</u>	<u>N</u>	<u>Type</u>	<u>Center</u>	<u>Mid-Width</u>	<u>Edge</u>
[101]	[111]	L	750	50	1
[011]	[111]	L	2.5	3.5	5
[110]	[111]	L	23	1	2
[110]	[111]	R	750	50	1
[101]	[111]	R	12	1	50
[011]	[111]	R	1	2.5	35
[101]	[111]	T	1	3	24
[110]	[111]	T	2	3	10
[011]	[111]	T	1.5	66	37

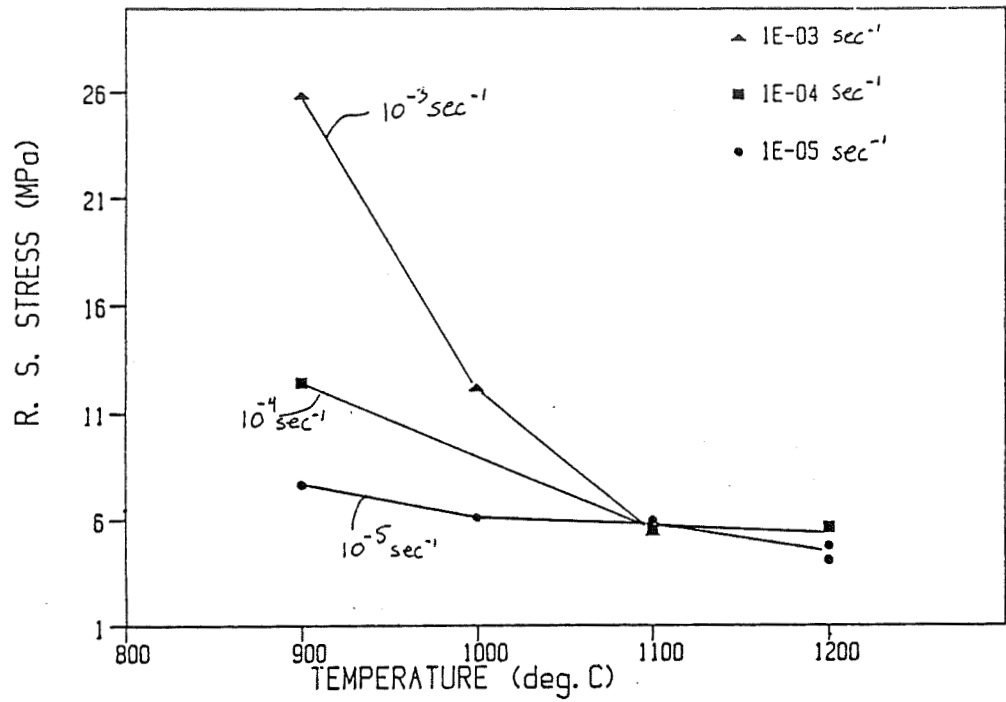
Calculations started at $x=0.2$ cm.



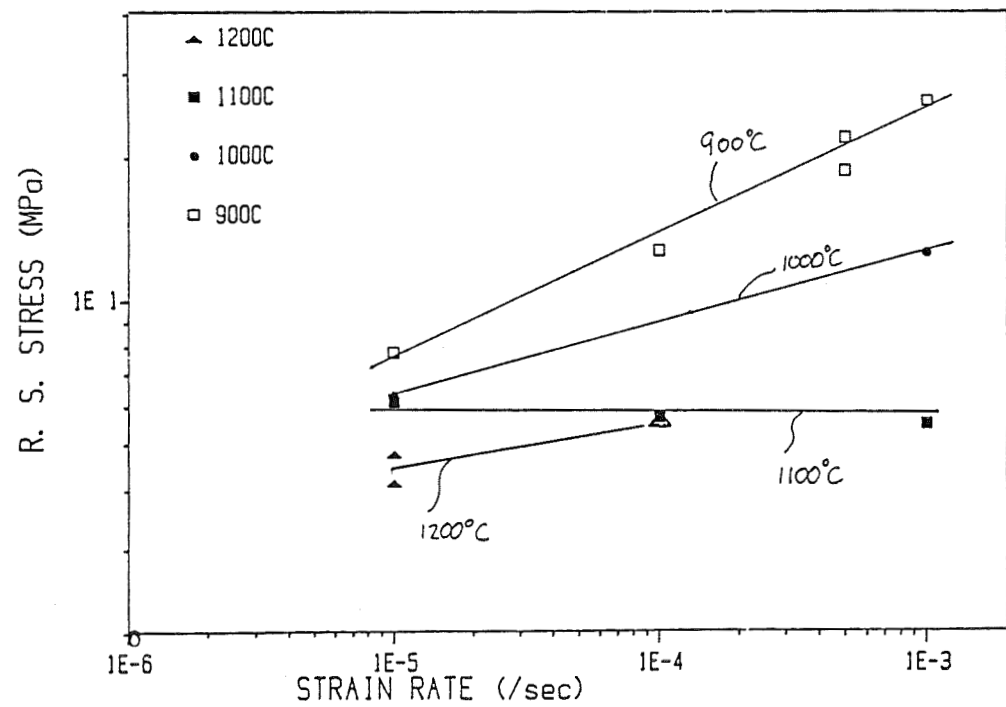
Dislocation Distribution in Web Dendrite Ribbon



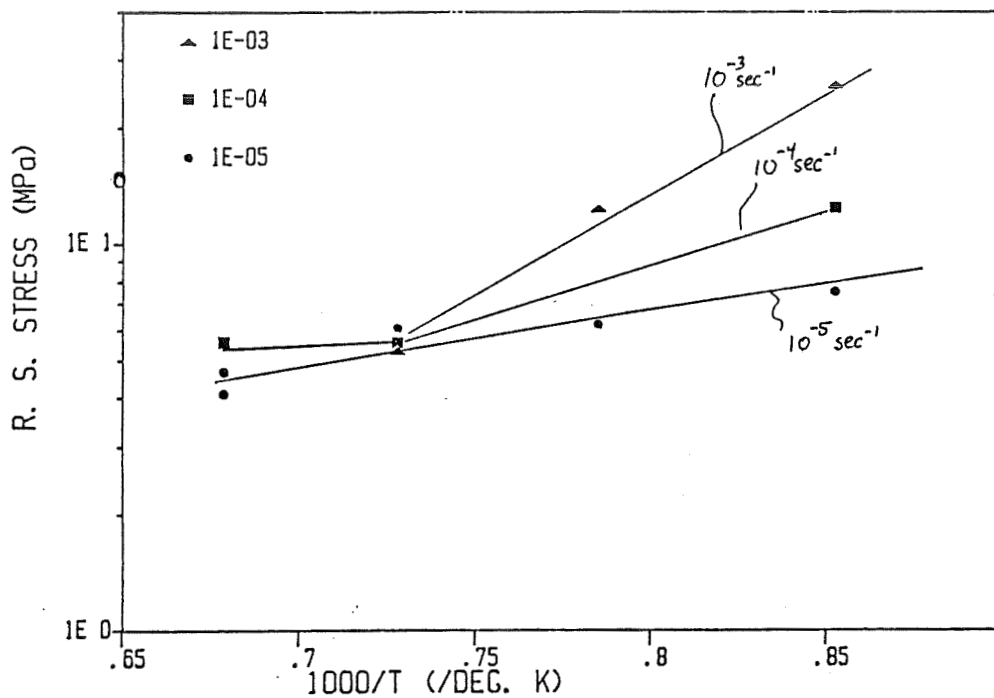
Cz Temperature Dependence



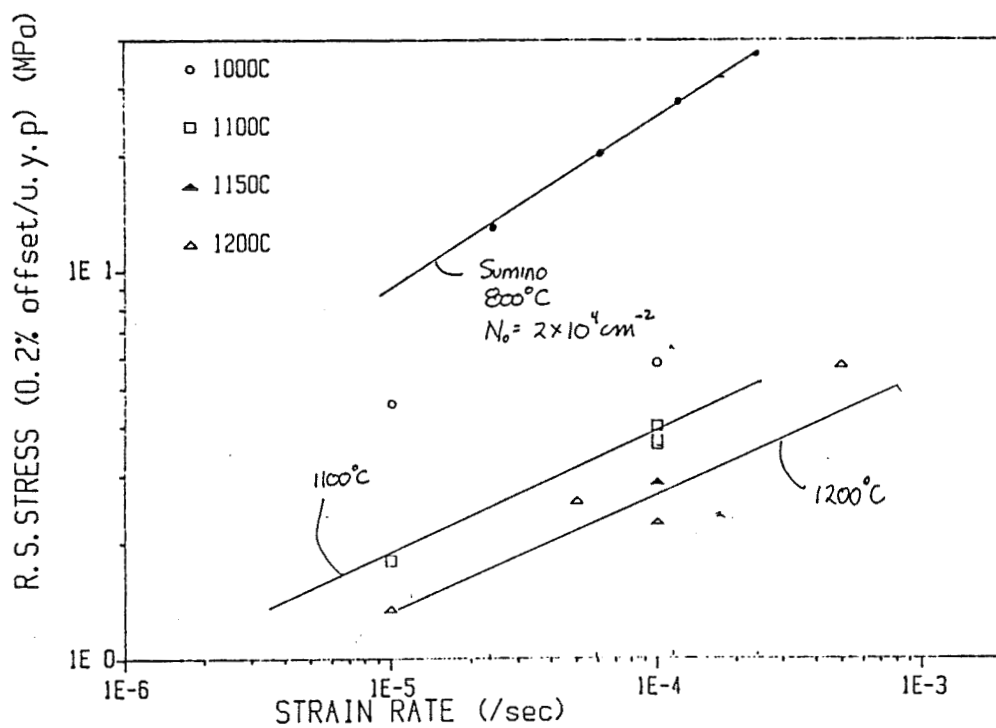
Cz Strain Rate Dependence



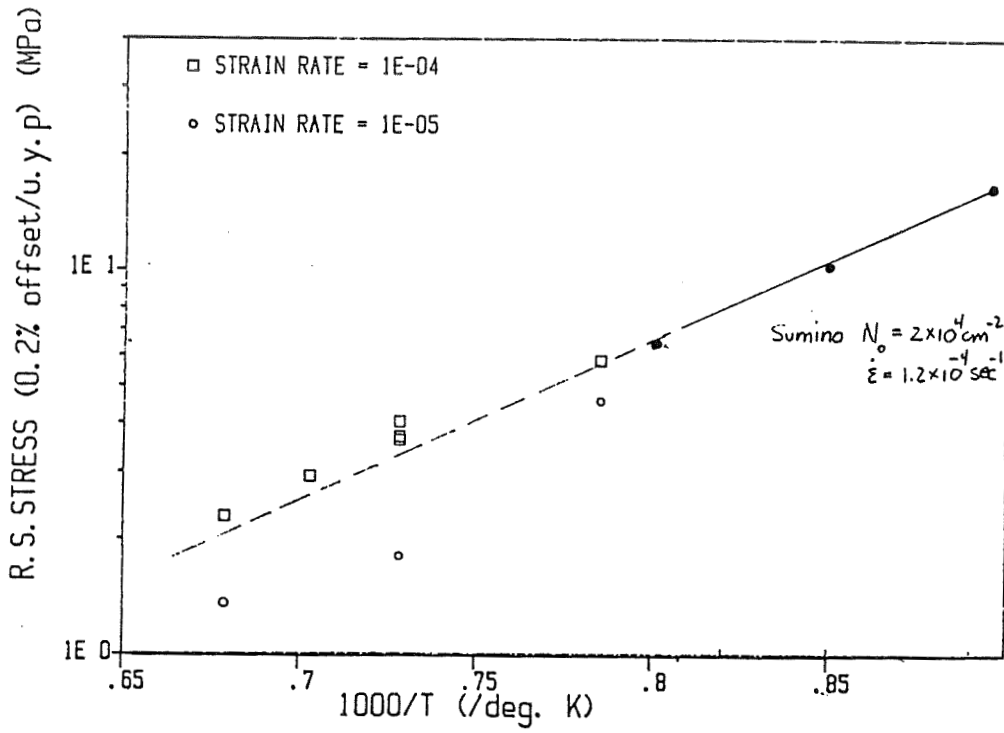
Cz Temperature Dependence



Web Ribbon: Strain Rate Dependence



Web Ribbon: Temperature Dependence



SILICON STRESS/STRAIN ACTIVITIES AT JPL

JET PROPULSION LABORATORY

C. P. Chen

Contents

- ° Highlight the important accomplishments of in-house efforts including:
 - ° Fracture Mechanics of Si
 - ° Stress/Strain Analysis
 - ° Thermal analysis
 - ° High Temperature Testing
- ° Recommend future work

Rationale: Fracture Mechanics of Silicon

- THE CRACKING CELL IS ONE OF THE MAJOR SOURCES OF SOLAR PANEL REJECTION AND FAILURE THAT CONTROL THE COST.
- F.M. DATA OF Si ARE CRITICALLY IMPORTANT FOR THE DESIGN OF RELIABLE SOLAR CELLS. NO DATA WAS AVAILABLE.

Objectives I: Fracture Mechanics

- DEVELOP FRACTURE MECHANICS (F.M.) METHODOLOGY
- GENERATE F.M. DATA
- CHARACTERIZE CRACK PROPAGATION IN Si

Key Accomplishments of Fracture Mechanics of Silicon

- ° Developed a "Standard test method for silicon solar cell strength" by a four-point twisting method. This method has been implemented in many PV manufacturers.
- ° Developed test methodology and generated FM data of Si. Results of this pioneering effort have enhanced production yields; improved cell reliability and durability and established mechanical design criteria which has reduced cell cost.
- ° FM technique has been utilized to modelling the silicon ingot wafering and to predict the limits and to improve the wafering conditions.
- ° FM technology has been recently extended to other semiconductors (e.g. GaAs).
- ° Published more than 30 papers in the area of FM of Si. Established a technology base at JPL on the fracture mechanics of Si.

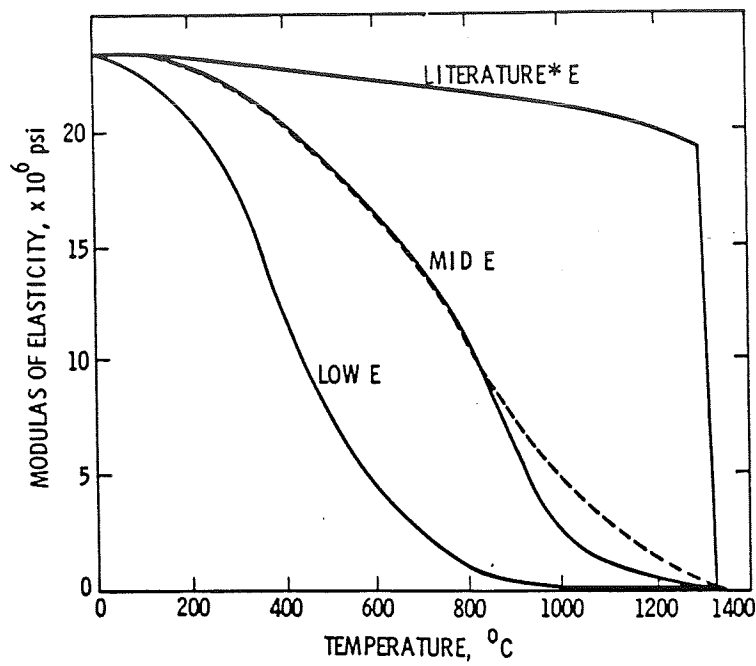
Future Work — I: Fracture Mechanics of Silicon

1. The effect of plastic zone propagation on the crack extension silicon at several temperatures.
2. Creep deformation of Si sheet at high temperature.
3. Fracture mechanics properties of other semiconductor materials (e.g., GaAs, Cd Te, InP).

Objective II: Nonlinear Stresses Analysis of Silicon Web

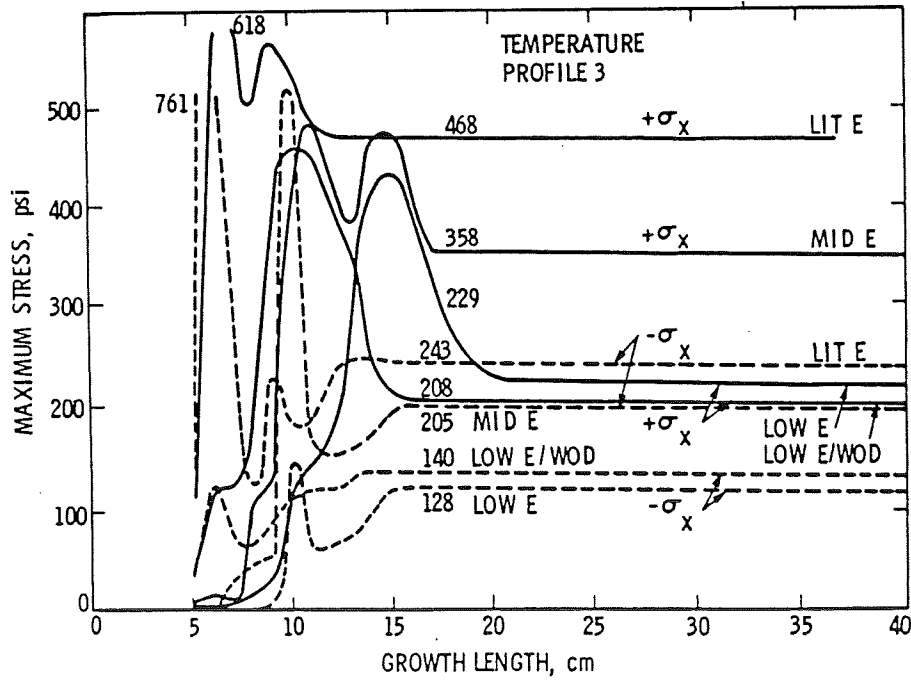
TO DETERMINE AN OPTIMAL TEMPERATURE PROFILE
IN A WEB SUCH THAT THE DETRIMENTAL STRESSES
ARE MINIMAL.

Modulus of Elasticity



*TEMPERATURE DEPENDANCE OF ELASTIC CONSTANTS OF SILICON, BY Yu A. BARENKOV AND S. P. NIKANOROV SOV. PHYS. SOLID STATE, VOL 16, No. 5, NOV 1974

Maximum Stresses



Steady State Maximum Stresses Versus Temperature Profile

(LOW E CASE)

TEMP PROFILE \ MAX STRESS	σ_x psi		σ_y	
	TENSION	COMPRESSION	TENSION	COMPRESSION
4	251	82	332	400
1	295	165	487	575
2	435	154	512	618
3	229	128	522	604

(LITERATURE E)

TEMP PROFILE \ MAX STRESS	σ_x		σ_y	
	TENSION	COMPRESSION	TENSION	COMPRESSION
3	468	243	911	1027
4	1747	775	2913	2114

Conclusion

- DETRIMENTAL STRESS ARE HIGHLY DEPENDENT UPON MATERIAL PROPERTIES
- STEADY STATE MAXIMUM σ_x (IN WIDTH WISE) IS ALWAYS LESS THAN TRANSIT STATE MAXIMUM AND MAXIMUM σ_y (IN LENGTH WISE) IS GRADUALLY INCREASED TO STEADY STATE MAXIMUM WITH GROWTH
- THE OPTIMAL TEMPERATURE PROFILE IS DEPENDENT UPON MATERIAL PROPERTIES (E, σ_y , α etc.)

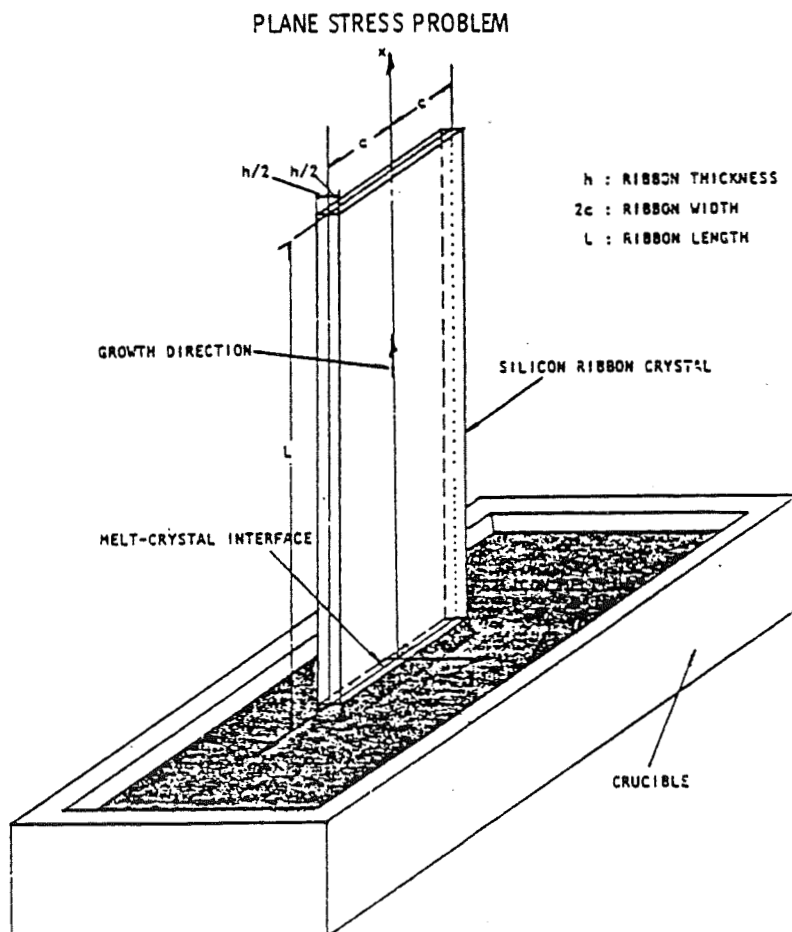
Future Work Planned — II

- 1) MORE MATERIAL PROPERTIES IN $20^{\circ}\text{C} \sim 800^{\circ}\text{C}$
- 2) LOCAL BUCKLING BEHAVIOR, STRESS STIFFNESS AND ITS EFFECTS IN BUCKLING MODES.
- 3) EFFECT OF WEB SIZE, PULL-UP SPEED

Objective III: Thermal Analysis

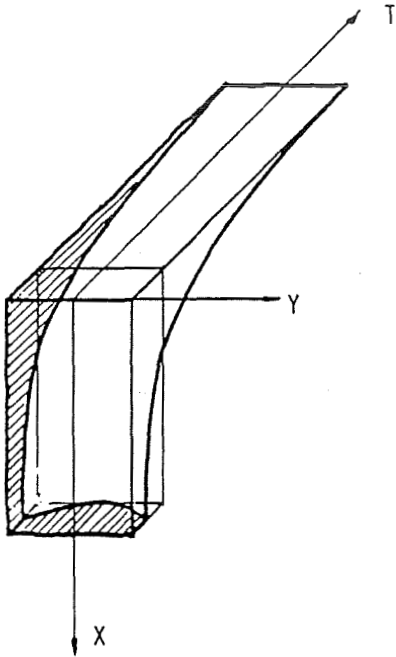
Analytical simulation of thermal stresses distribution in WEB during growth process.

Geometry of Ribbon and the Reference Coordinate System

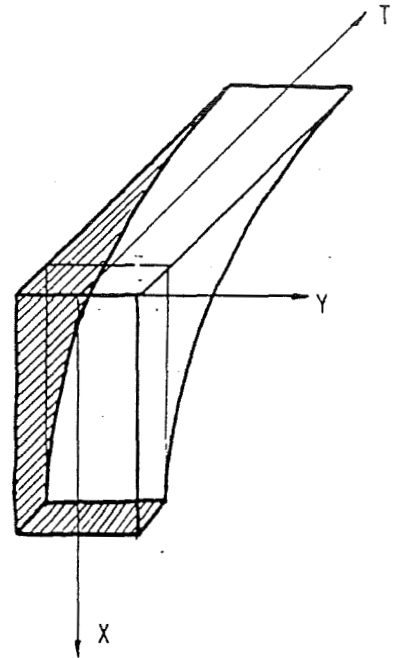


ADVANCED SILICON SHEET

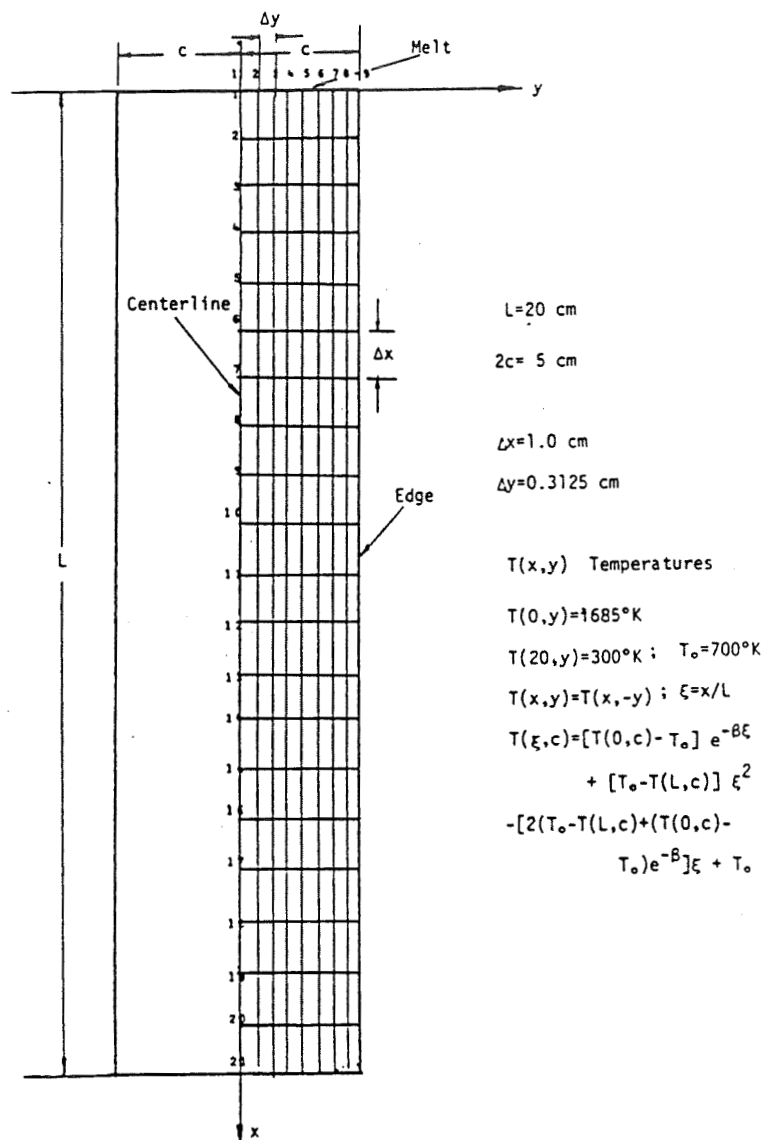
Frowning Temperature Distribution
No Thermal Stresses Develop



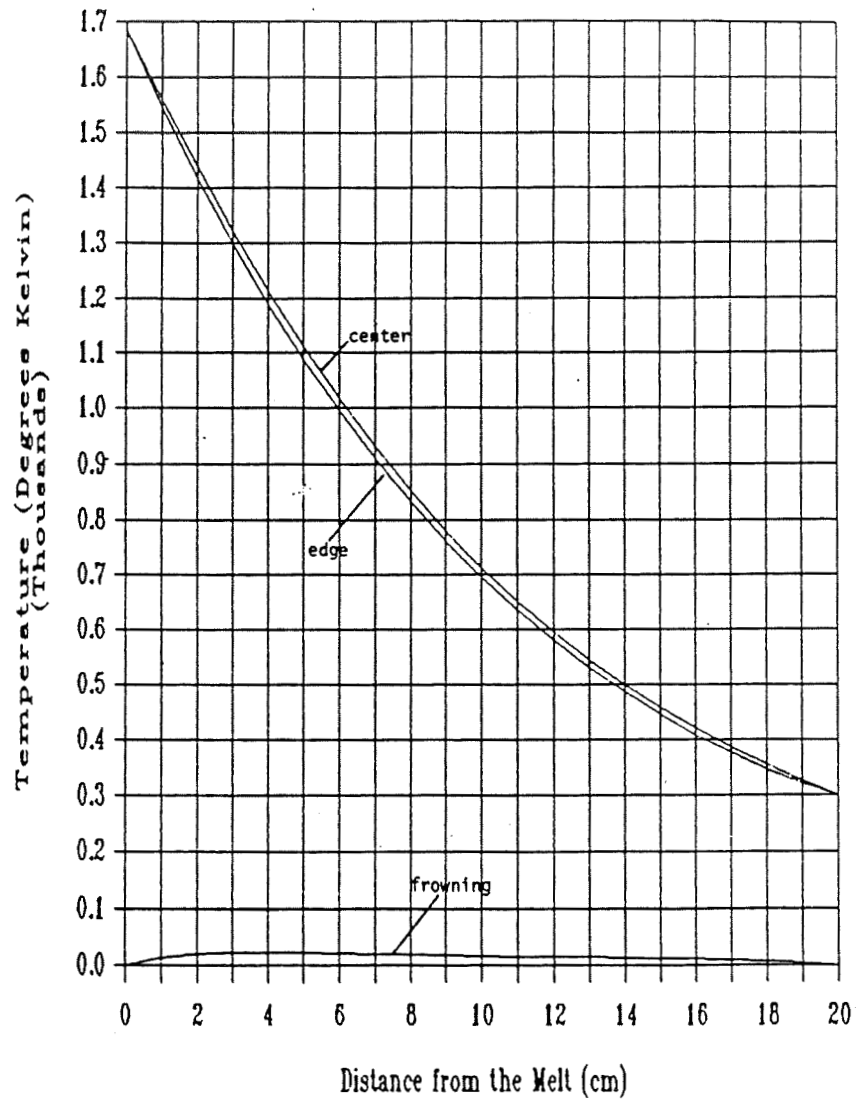
Uniform Temperature Distribution
Thermal Stresses Develop



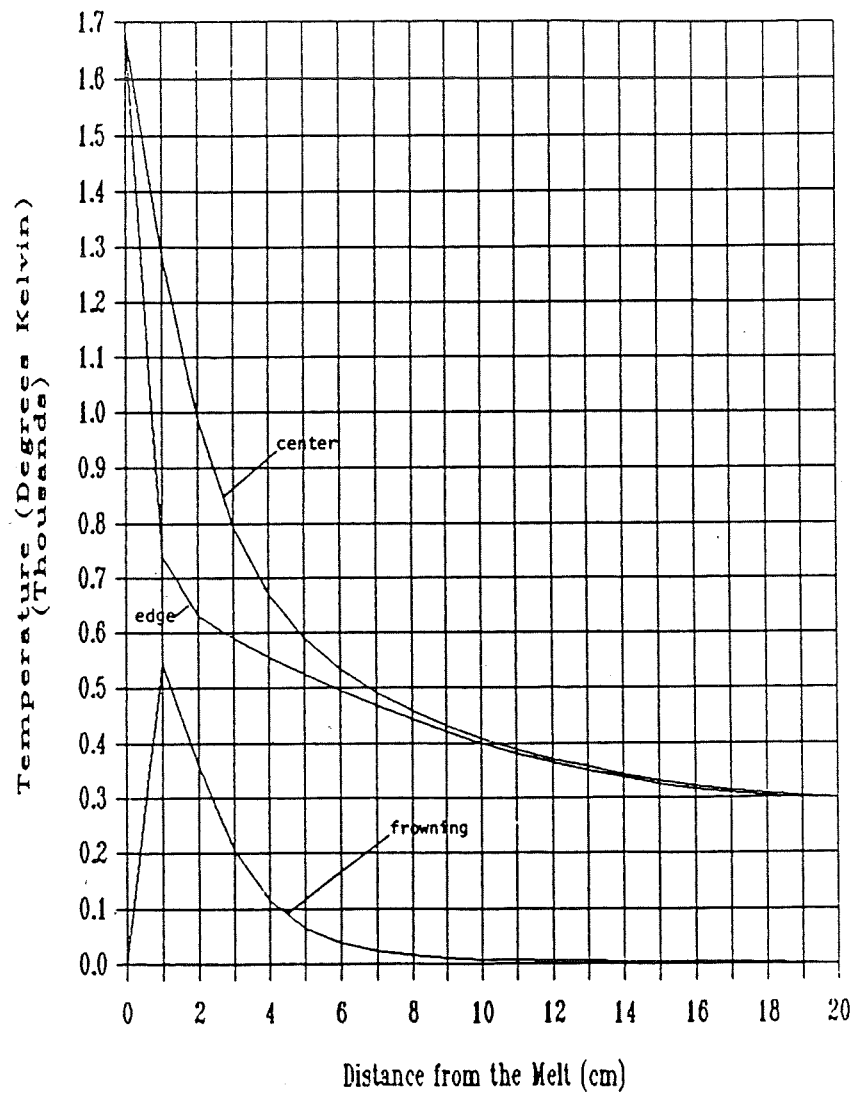
Keysketch for Determining Temperature Distribution Satisfying $\Delta^2 T = 0$



Center, Edge, and Frowning Temperatures for Beta = 2



Center, Edge, and Frowning Temperatures for Beta = 50



Conclusions

- o TEMPERATURE PROFILES MAY BE SLIGHTLY FROWNED TO ELIMINATE THE THERMAL STRESSES
- o IN THE NUMERICAL COMPUTATION OF THERMAL STRESSES NUMERICAL CONVERGENCE ANALYSIS IS VERY IMPORTANT
- o A SIMULATOR IS BEING DEVELOPED FOR THE ELASTO-THERMO-VISCO-PLASTIC BEHAVIOR OF THE SILICON RIBBON FOR ANY THERMAL LOADING. ELASTIC PORTION OF THE SIMULATOR IS COMPLETE, INCLUDING THE BUCKLING TENDENCY ANALYSIS
- o THERMO - VISCO - PLASTIC PART OF THE SIMULATOR IS BEING DEVELOPED.
- o IN ORDER TO MINIMIZE THE EXECUTION COST OF THE SIMULATOR, PARTITIONING OF THE MATRICES IS NECESSARY WHICH WILL BE IMPLEMENTED LATER.

Silicon High-Temperature Test Program: Objectives

- PERFORM UNIAXIAL, TENSILE, STRESS-STRAIN AND STRESS RELAXATION TESTS ON SILICON SHEET MATERIALS AT TEMPERATURES ABOVE 1000°C IN ORDER TO MEASURE THE LOW STRAIN (LESS THAN 1%) RESPONSE OF THESE MATERIALS.
- QUANTIFY THE EFFECT OF LOW STRAIN AND STRESS ON THE GENERATION OF RIBBON STRUCTURAL DEFECTS, PRIMARILY DISLOCATIONS.
- PROVIDE NEW HIGH TEMPERATURE MATERIAL PROPERTY DATA, SUCH AS CREEP CHARACTERISTICS, SO THAT SILICON STRESS-STRAIN MODELING COULD BE IMPROVED.

Silicon High-Temperature Test Program: Status

- BASED ON COMMENTS BY DR. SUMINO AND SCATTERED TEST DATA FROM DOZENS OF TESTS CONDUCTED IN 1985 THE TEST COUPON DESIGN/ PROCESSING WAS MODIFIED IN EARLY 1986.
- NO NEW TEST DATA YET.
- SOME CALIBRATION TESTS, SUCH AS MEASUREMENT OF EXTENSOMETER FRICTIONAL LOAD CONTRIBUTION AND LOW TEMPERATURE SPRING CONSTANT OF THE LOAD TRAIN HAVE BEEN COMPLETED.
- MEASUREMENT OF +1000°C LOAD TRAIN STIFFNESS HAS BEEN DIFFICULT.
- NEW TEST COUPONS OF ZERO DISLOCATION {211} ORIENTED CZ AND WEB RIBBON HAVE BEEN PRODUCED BY ULTRASONIC MACHINING AND SUBSEQUENT CHEMICAL EDGE-ONLY ETCHING.
- VACUUM CAPABILITY HAS BEEN ADDED TO THE TEST FURNACE.

Silicon High-Temperature Test Program: Future

- COMPLETE ELEVATED TEMPERATURE LOAD TRAIN STIFFNESS MEASUREMENTS.
- CONDUCT STRESS RELAXATION TESTS (CONSTANT TOTAL STRAIN) AT 1000°C AND 1200°C. INITIAL STRESS LEVELS WILL BE IN THE RANGE 3-20 MPA DEPENDING ON TEST TEMPERATURE. TOTAL STRAIN $\leq 1\%$. MEASURE TIME CONSTANT OF LOAD DECAY AND DEVELOP CONSTITUTIVE CREEP EXPRESSION BASED ON EXPERIMENTAL BEHAVIOR.
- USE X-RAY TOPOGRAPHY AND ETCH PIT STUDY TO CHARACTERIZED EXTENT OF LOW STRAIN STRUCTURE FORMATION.

CREEP OF WEB RIBBONS

CORNELL UNIVERSITY

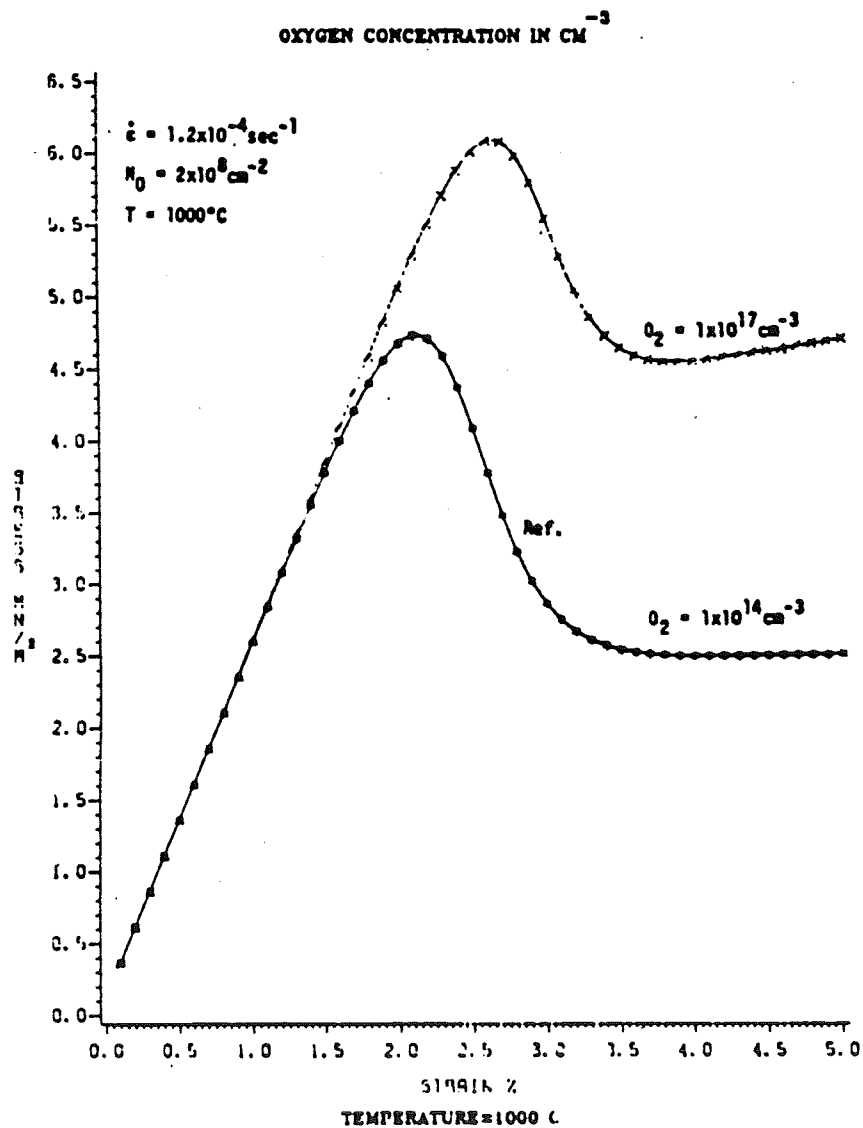
S. Hyland and D. G. Ast

1. Oxygen Content

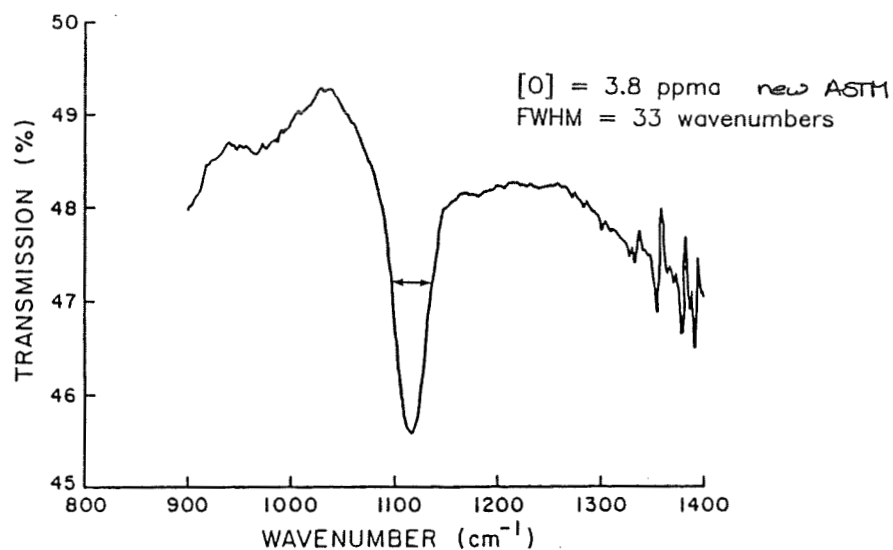
2. Creep Law

3. Microscopic Mechanisms

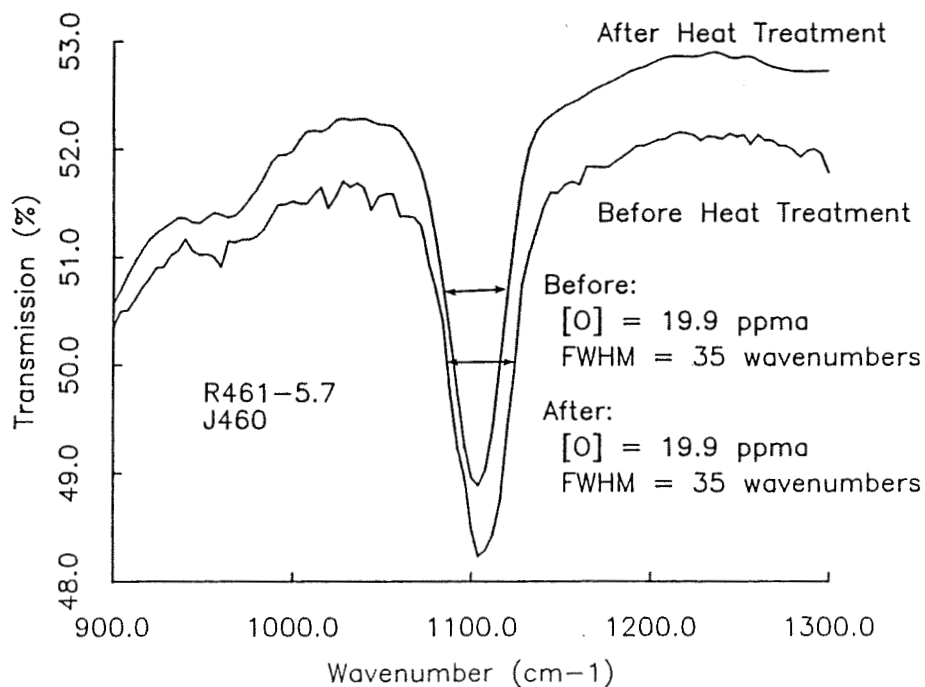
Silicon Sheet Growth and Characterization



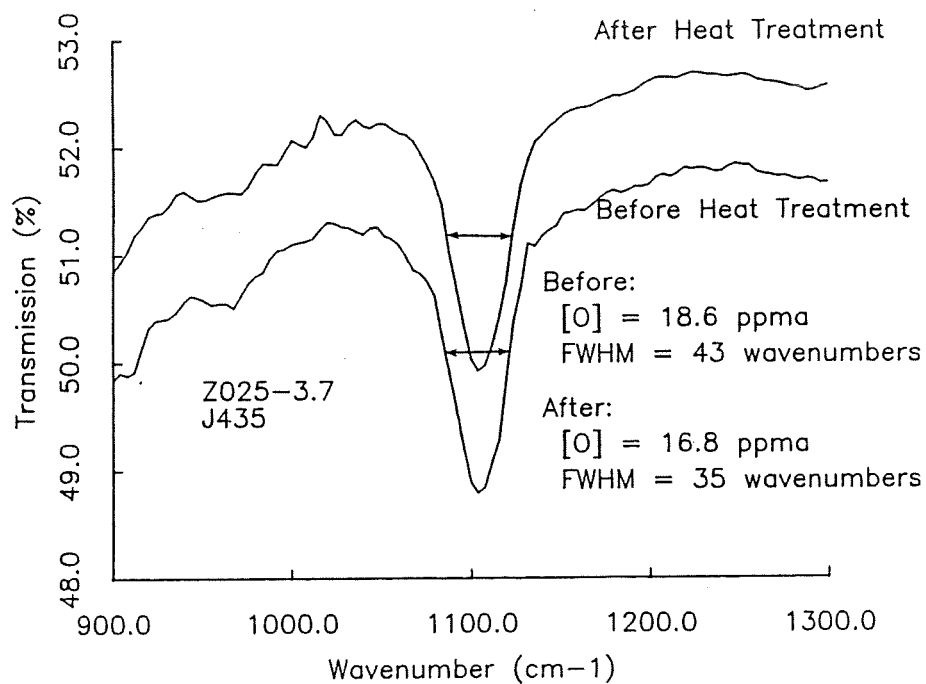
IR Transmission Versus Wavenumber for Cz Silicon



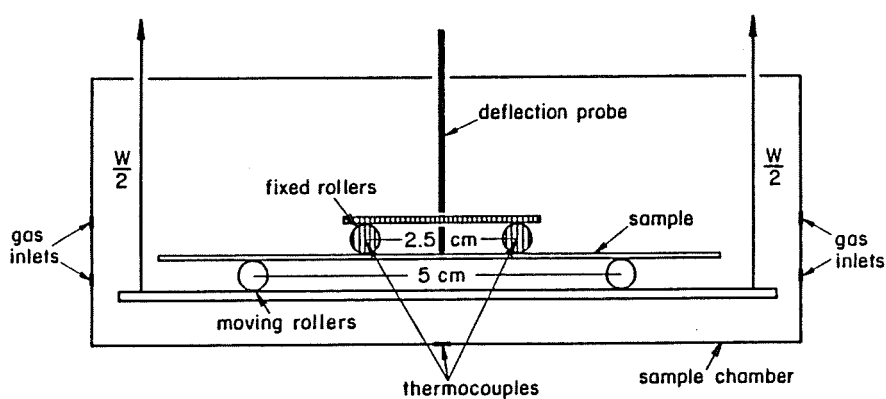
IR Transmission Versus Wavenumber for Low Stress Web Before and After 850°C, 24-Hour Heat Treatment



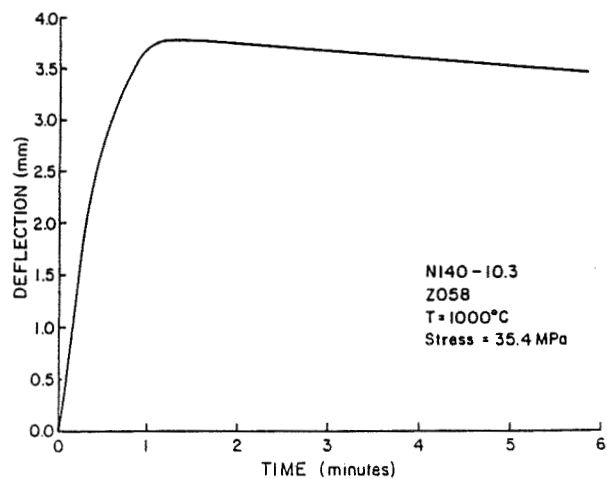
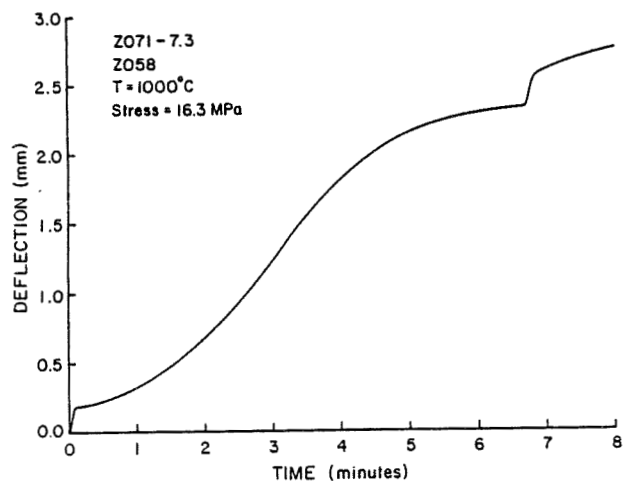
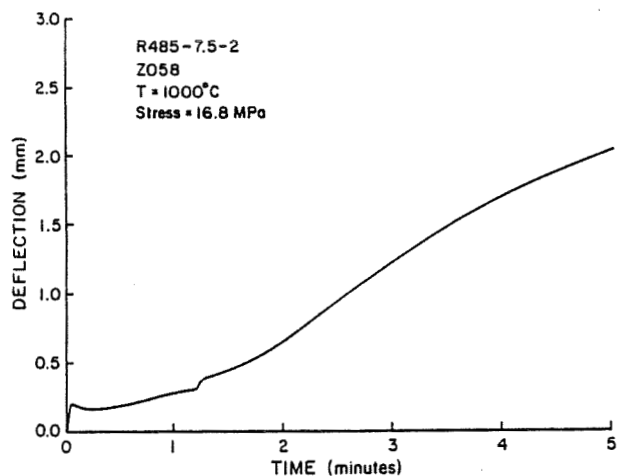
IR Transmission Versus Wavenumber for High Stress Web Before and After 850°C, 24-Hour Heat Treatment



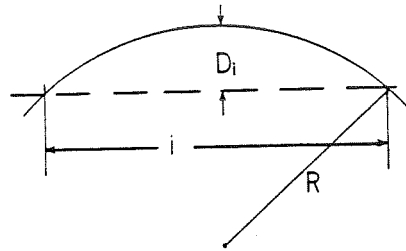
Four-Point Bending Rig at MSEC



Deflection Versus Time for Web Silicon Four-Point Bending



Preliminary Analysis of Four-Point Bending



h = sample thickness

B = sample width

ε_s = surface strain

σ_s = surface stress

$$R = h/(2\varepsilon_s)$$

$$D_i = R - R\cos[\arcsin\{i/(2R)\}] = i^2/(2R)$$

$$\text{for } D_i \ll R$$

combining:

$$\dot{\varepsilon}(z) = \frac{8\dot{D}_i}{i^2} z$$

Assuming a Power Law Creep

$$\dot{\varepsilon} = \dot{\varepsilon}_0 \sigma^n$$

$$\text{therefore, } \sigma(z) = [(\dot{\varepsilon}_0 i^2)/(\dot{D}_i)]^{1/n}$$

The stress can be determined from the slope of the deflection vs. time curve.

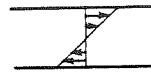
The moment is obtained from the stress:

$$\begin{aligned} M &= 2B \int_0^{h/2} \sigma(z) z dz \\ &= 2B [(\dot{\varepsilon}_0 i^2)/(\dot{D}_i)]^{1/n} \\ &\quad [n/(2n+1)] [h/2]^{(2n+1)/n} \end{aligned}$$

Preliminary Analysis of Four-Point Bending (Cont'd)

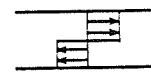
Under elastic loading:

$$\sigma_s = 6[M/(h^2B)]$$



Under plastic loading:

$$\sigma_s = 4[M/(h^2B)]$$



Kalejs uses an intermediate factor of 5.
We will use the plastic factor of 4.

experimentally,

$$\dot{\epsilon}_i = \frac{1}{7000} \sigma^3 \quad \begin{array}{l} i = 25 \text{ mm} \\ h = 0.153 \text{ mm} \end{array}$$

leading to: $\dot{\epsilon}_o = 8.8 \times 10^{-8} \text{ sec}^{-1}$

Creep Law:

$$\dot{\epsilon} = 8.8 \times 10^{-8} \sigma^3$$

 σ in MPa, $T = 1000^\circ\text{C}$

Data from Web Bending Tests

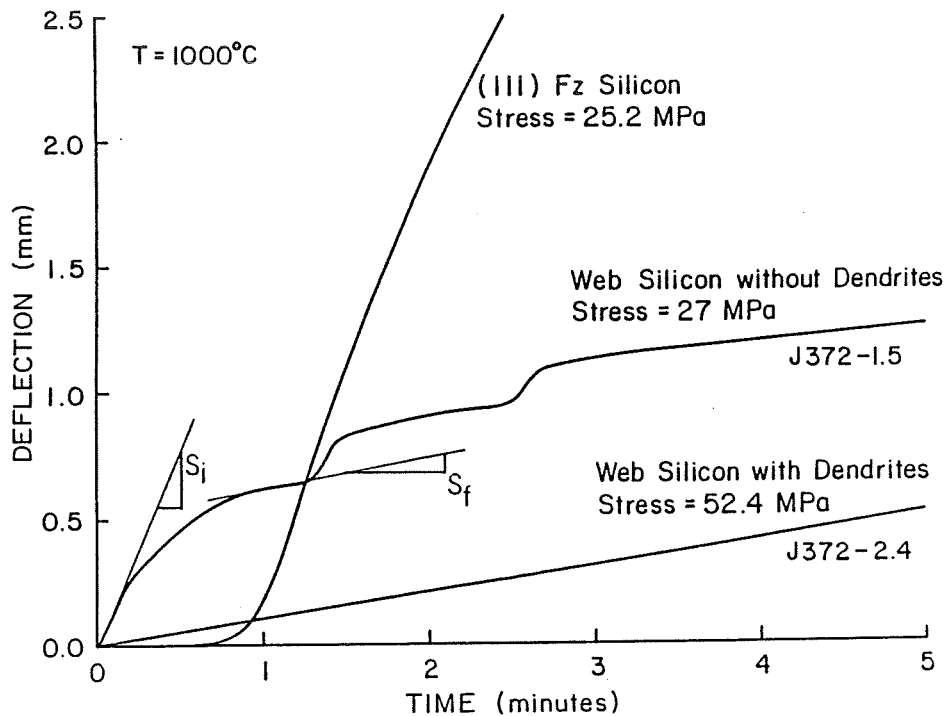
APPLIED STRESS (MPa)	EXPERIMENTAL S_I (MM/MIN)	POWER LAW FIT (MM/MIN) N=3
27	2	2.8
16.3	0.5	0.62
35.4	6	6.3
16.8	0.5	0.68
16.8	0.5	0.68
13*	0.1	0.3

* WEB WITH DENDRITES ON ASSUMING LOAD IS CARRIED BY SQUARE DENDRITES ONLY.

$$\text{POWER LAW FIT: } S_I = \frac{\sigma^3}{7000}$$

FROM FIT TO DATA

Deflection Versus Time for Web Silicon Four-Point Bending

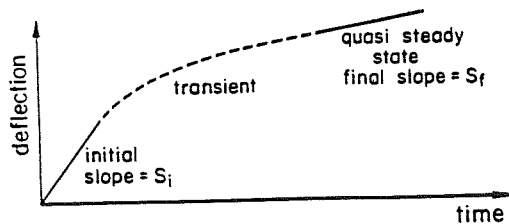


Predicted Deflection Versus Time Curve

$$S_f = S_i (1.5)^{-N}$$

APPROXIMATELY = 0.3 TO 0.36 S_i FOR $N = 2.5 - 3$

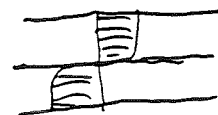
ASSUME THAT THE MATERIAL DOES NOT CHANGE DURING THE TEST.



Initial stress distribution:



Final stress distribution:



Analysis of Strain Transition

$$\text{Elastic: } D_i^e = [i^2/4Eh] \sigma_s$$

$$\text{Plastic: } D_i^p \cong \frac{1}{7000} \sigma_s^3 t \quad (\text{experimentally})$$

When does the elastic load distribution change to a plastic load distribution?

$$D_i^p = N D_i^e$$

assume $N = 5$:

$$\begin{aligned} \text{a) } \sigma_s &= 27 \text{ MPa} & h &= 0.153 \text{ mm} \\ i &= 25 \text{ mm} & E(111) &= 1.9 \times 10^5 \text{ MPa} \end{aligned}$$

$$t_{\text{transition}} = 15.5 \text{ sec}$$

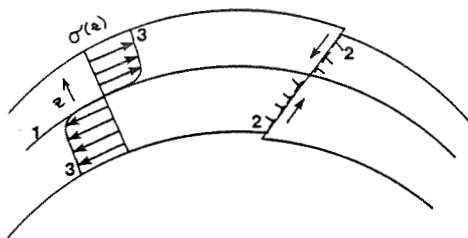
$$\text{b) } \sigma_s = 16 \text{ MPa}$$

$$t_{\text{transition}} = 44 \text{ sec}$$

This order of magnitude seen for transition from S_i to S_f .

Load redistribution is responsible for the transition.

Analysis of Strain Bursts

ORIGINAL PAGE IS
OF POOR QUALITY

There is no stress on a dislocation at the neutral axis(1).

A dislocation at the neutral axis will experience a stress due to the long range stress fields of following dislocations(2).

If the following dislocations are located in a part of the sample where they are under an applied stress(3), they may generate enough stress on the leading dislocation to push it through the neutral axis.

Therefore, if the length of a dislocation pile-up is some fraction of the thickness of the sample, such as in the case of Web silicon ribbons, there may be enough stress on dislocations at the neutral axis to cause them to move through, resulting in "strain bursts".

References

ORIGINAL PAGE IS
OF POOR QUALITY

1. Change of misorientation with deformation due to trapped reaction products (Ge): J.J.Bachmann, M.O.Gay and R.Touremine, Scripta Met. 16 (1982) 535.
2. Influence of coherent twins on mechanical behavior (Ni): L.C.Lim, Scripta Met. 18 (1984) 1139; L.C.Lim and R.Raj, Acta Met. 32 (1984) 727ff and 1183ff.
3. General discussion on interaction between grain boundary dislocations and lattice dislocations and their role in mechanical properties: L.C.Lim and R.Raj, Journal de Physique Colloque C4 (1985) 581.
4. Reactions between lattice dislocations and twins studied by TEM (Si): R.Gleichmann, M.D.Vaudin and D.G.Ast, Phil. Mag. A 51 (1985) 449.

Summary

4-Point Bending

Data consistent with

- transient due to load redistribution
- creep law, at 1000 deg C: $\dot{\epsilon} = 9 \times 10^{-8} \sigma^3$ (σ in MPa)

Observed creep slower for Web than for Cz

Oxygen Measurements

High Oxygen content of 20 ppma

Width of IR absorption peak greater for Web

Low stress ribbons—no change with annealing

High stress ribbons—width of peak decreases with annealing

Appearance of shoulder on IR peak is not predictable

SURFACE PROPERTY MODIFICATION OF SEMICONDUCTORS BY FLUID ABSORPTION

UNIVERSITY OF ILLINOIS AT CHICAGO

S. Danyluk

Objectives

- . Lubricated Cutting (wafering)
 - laboratory simulation
 - mechanism
 - model
- . Residual Stresses in Sheet
 - Develop Interferometry Technique
 - Apply to EFG and WEB

Lubricated Cutting in Simulated Laboratory Experiments

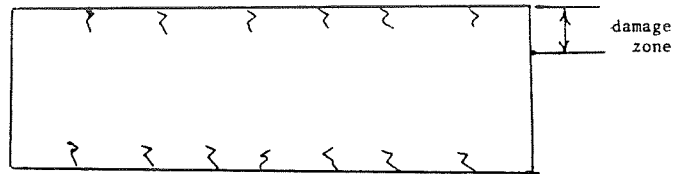
	Surface Morphology
	Hardness
Load, Temperature, Fluids	Wear rate
	Depth of Damage

Mechanism

Model

Silicon Wafer

cracks (propagate on
cleavage planes)



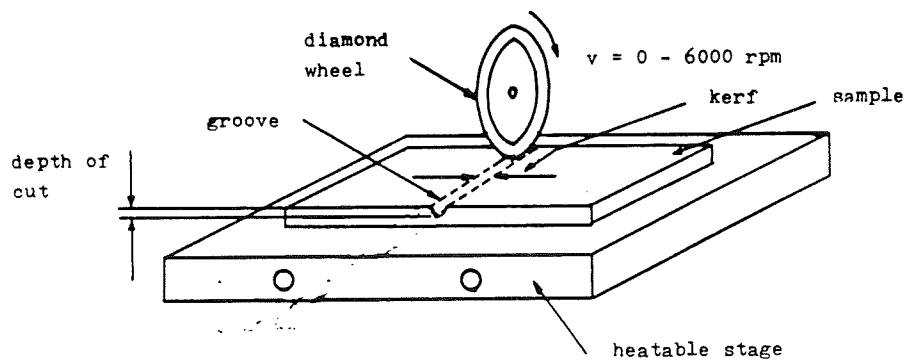
plasticity(?)
 . due to high compressive stresses
 . at crack tips

. Simulate Damage

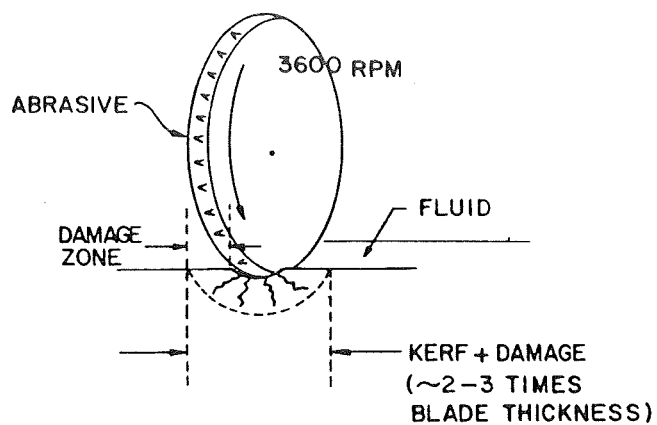
dicing (OD sawing)
 indentation (Vickers[®] dia)

. Identify critical parameters

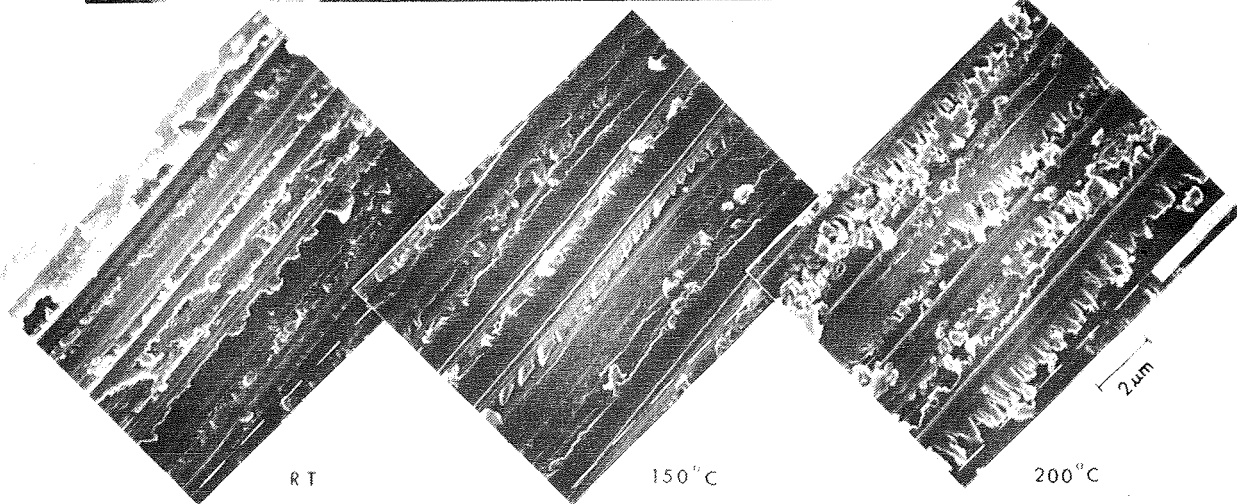
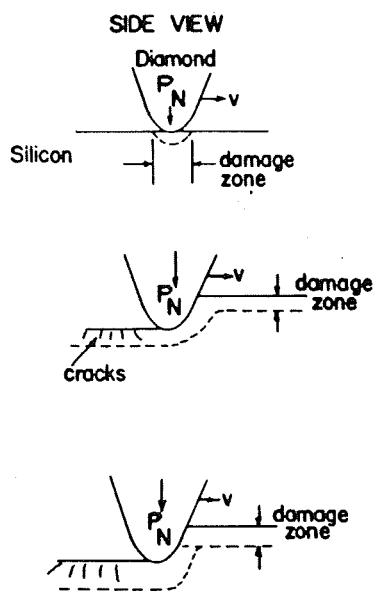
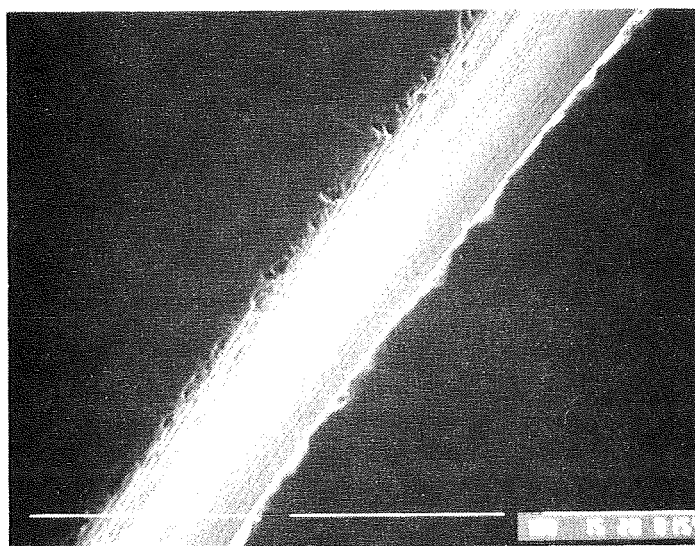
Load
 fluid
 temperature



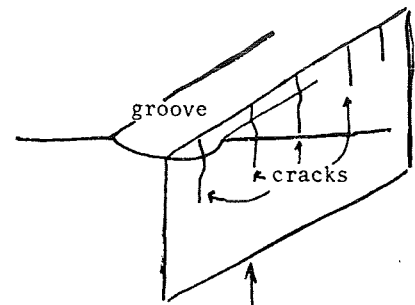
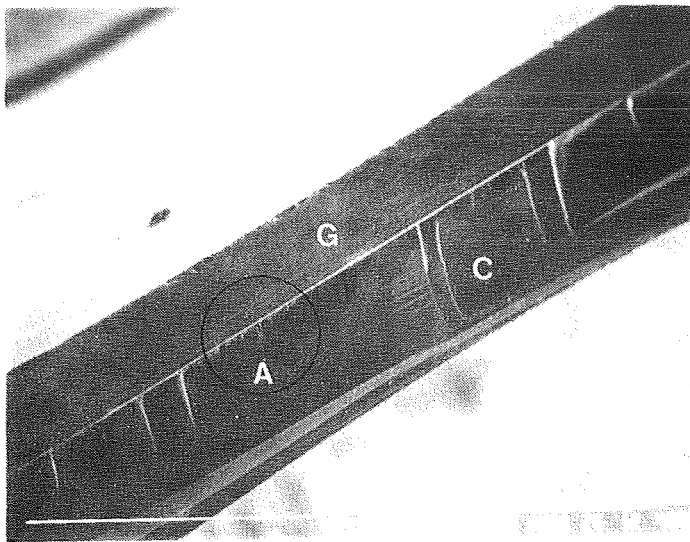
OD Sawing (Dicing)



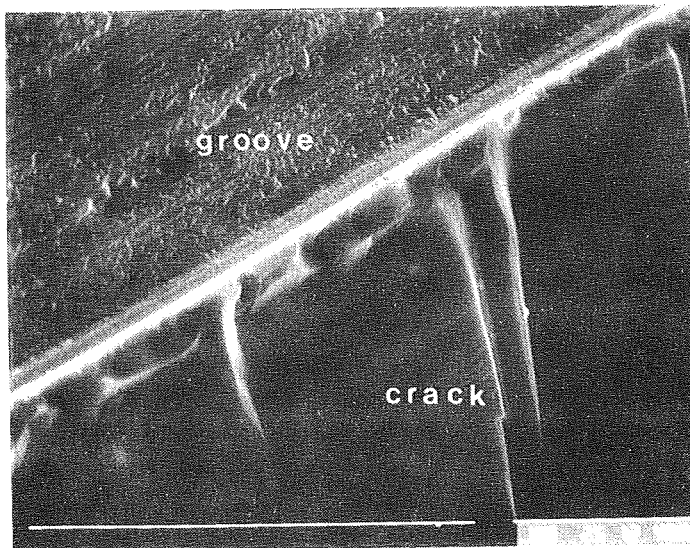
ORIGINAL PAGE IS
OF POOR QUALITY



Examples of Cracks at the Bottom of Grooves

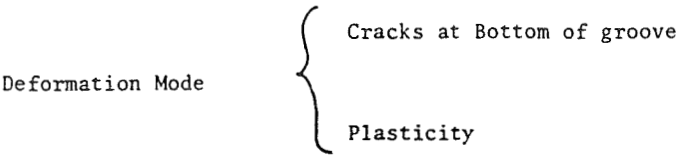


micrograph

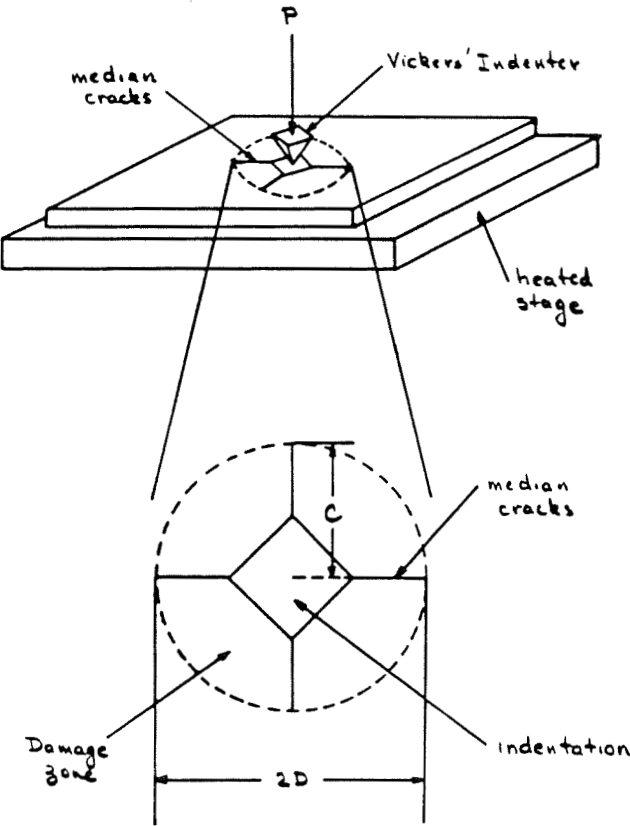


ORIGINAL PAGE IS
OF POOR QUALITY

Summary of High-Speed, Elevated Cutting



Fluids, Temperature--- influence surface morphology



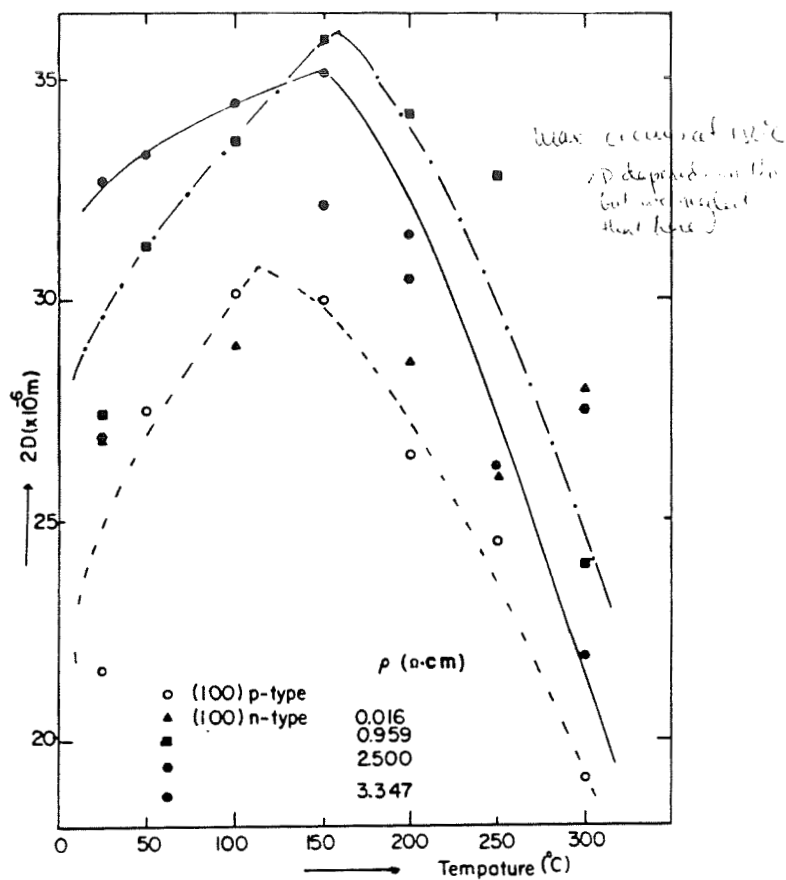
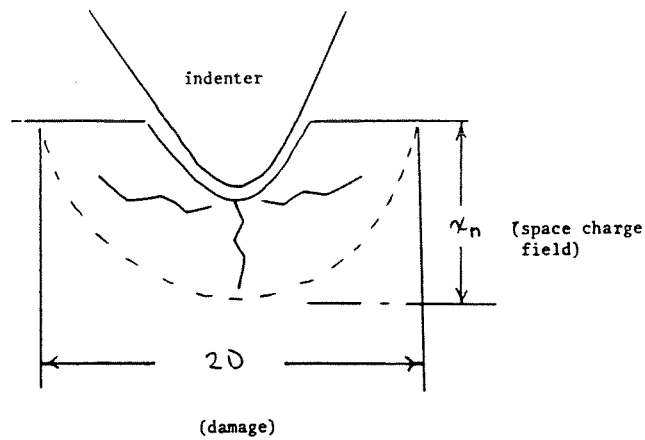


Figure 36. Damage size(2D) vs. indentation temperature for p-type and n-type Cz silicon. The indentation load was 0.49N. The n-type silicon had resistivities of 0.016, 0.959, 2.5, and 3.347 Ωcm .

Indentation Model



$$2D \propto X_n \quad \text{at low } P, \text{ space charge fields influence damage}$$

$$X_n = \frac{N_s}{N_D} \left[\frac{e^{\frac{(\mu_e - E_{ss})}{kT}}}{1 + e^{\frac{(\mu_e - E_{ss})}{kT}}} - 1 \right]$$

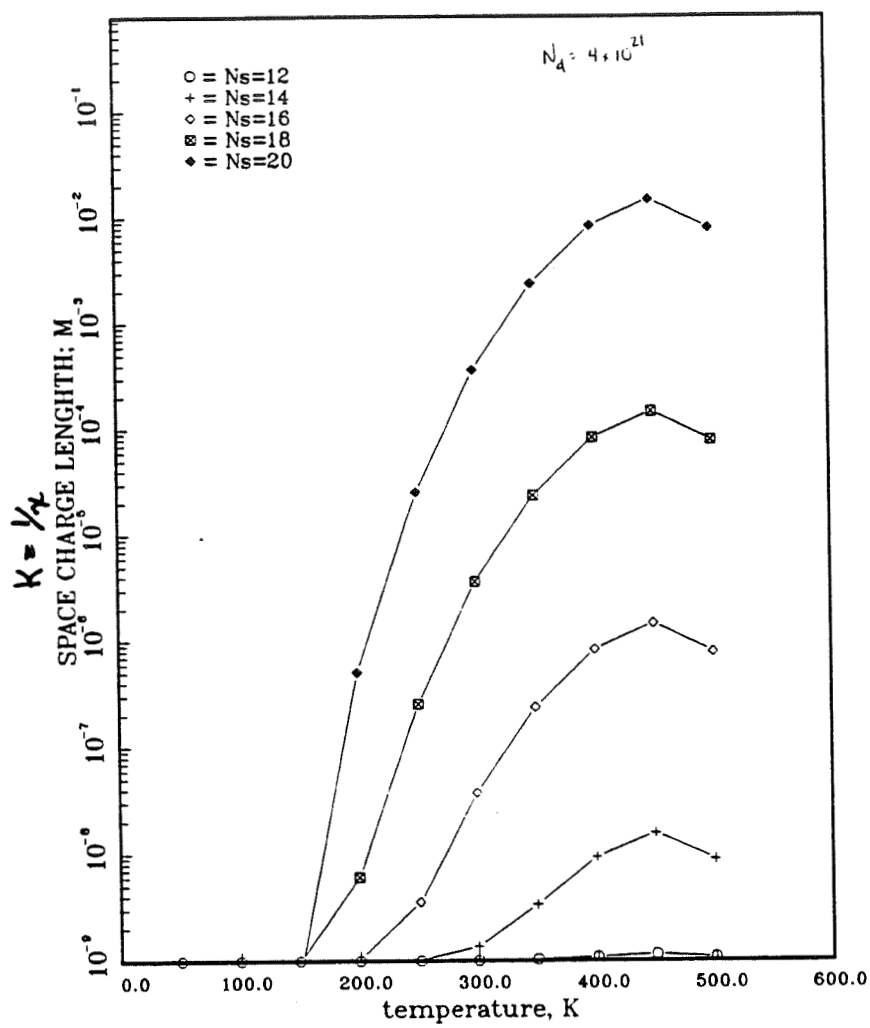
* N_s - finite number of surface states

* N_s , E_{ss} not known but extracted from expt.

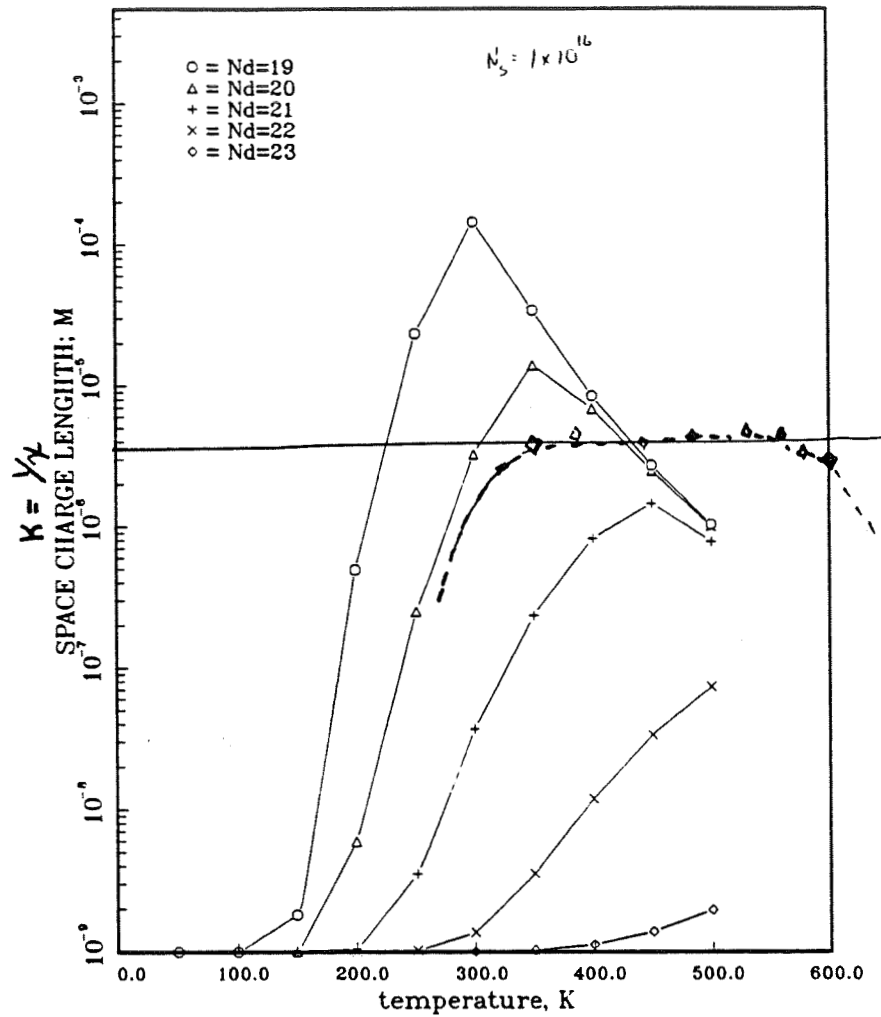
* μ_e , electrochemical potential

$$2D = f(N_D, N_s, E_{ss}, T)$$

Space Charge Length as a Function of Temperature



Space Charge Length as a Function of Temperature



Summary of Indentation Model

2D and x_n exhibit maximum at 150C

$$N_s = 10^{16} - 10^{18} / m^2$$

$$E_s = 0.79 \text{ eV}$$

Doping level influences 2D

Predict T, N_D variation with 2D


Summary of Silicon Results

. Wear rate

. Ethanol - highest

. air - lowest

. Damage

.load  plasticity, p 100gf
cracks, p 200gf

.temp

cracks, damage decreases
at T 250°C

. bulk doping

. fluid

Conclusions

Mechanisms of Wear

- . Wear rate and damage includes: cracks and plasticity
- . Laboratory simulation tests provide guidance in modifying industrial practices.
- . Wear rate may be optimized and damage may be minimized
 - Load (below 0.98N (100fg)
 - Fluid (alcohol-based vs. water-based fluids)
 - Temp (200-300°C)
- . Model allows parameters to be identified and range to be extrapolated.
- . Unresolved problems: Impact, fatigue

Residual Stresses

- . Interferometry is a promising NDT technique for sheet geometries
- . Edges - compressive
Center - tensile
- . EFG - $v_{\text{growth}} = 2 \text{ cm/min}$ - $\sigma_{\text{RS}} = \pm 10 \text{ MPa}$
WEB - $v_{\text{growth}} = \text{cm/min}$ - $\sigma_{\text{RS}} = \pm 1 \text{ MPa}$
- . Unresolved problems: anisotropy of E, ν
dendrite geometry

CZOCHELSKI CRYSTAL GROWTH: MODELING STUDY

CHEMICAL REACTION ENGINEERING LABORATORY
DEPARTMENT OF CHEMICAL ENGINEERING
WASHINGTON UNIVERSITY
ST. LOUIS, MO

M. P. Dudukovic, P. A. Ramachandran, R. K. Srivastava,
and D. Dorsey

Summary of Accomplishments: Modeling the Cz Growth of Silicon

Modeling Approach

During the past eighteen months the CREL group at Washington University has established itself as a leader in mathematical modeling of CZ growth of silicon. The unique approach of this modeling group was to relate in a quantitative manner, using models based on first principles, crystal quality to operating conditions and geometric variables. Superior quality Si crystals need to be of uniform diameter, of high, axially and radially uniform, resistivity and defect free. The resistivity profiles can readily be related to imbedded dopant and impurity concentrations, while the dislocations are a strong function of the interface shape and residual stresses in the crystal. In turn the dopant distributions, interface shape and diameter are governed by the heat balance at the interface. Thus, it can be concluded that crystal quality can directly be related, in a quantitative way, to the hydrodynamics, mass and heat transfer in the melt and to heat transfer in and from the crystal. These phenomena are dependent on: geometric variables which are fixed for a given puller (e.g., crucible and enclosure shape, heater shape, etc.), process variables which are governed by the selected operating schedule (e.g., melt depth, height of exposed crucible wall, etc.), manipulated variables which could be used for control (e.g., heater power,

crystal and crucible rotation speed, crystal pulling rate, heater position, gas flow rate, etc.). The variables to be controlled are crystal diameter and interface shape since they directly affect dopant distribution and residual stresses.

The systematic modular approach to this complex problem developed at CREL is shown schematically in Figure 1. The sketch of the puller is showing Figure 2. The finite element method is used for all calculations. The heat balance at the interface, which is the key element that governs crystal quality can be stated as:

$$(\text{Heat of Solidification}) \times (\text{Rate of Solidification}) =$$

$$(\text{Heat Loss into Crystal from the Interface}) - (\text{Heat Transfer from Melt to the Interface})$$

$$\rho V_G \Delta H \cos \alpha = (-k_c \frac{\partial T}{\partial n}) - (-k_m \frac{\partial T}{\partial n}) \quad (1)$$

$$I = II - III$$

Here term II is given by the heat transfer model for the crystal while term III is determined by the hydrodynamic and heat transfer model for the melt. Clearly, terms II and III dictate the interface shape through angle α and achievable pulling rate V_G at the fixed diameter. Equation (1) allows the general problem to be approached in a modular, sequential fashion. The rigorous model for the heat transfer in the crystal can be solved first and coupled with an approximate model for the melt. Melt models can be gradually improved and incorporated into the overall model as shown in Figure 1.

The above approach has been used successfully by the CREL group in modeling CZ of silicon and it should be directly extrapolable to modeling of GaAs.

Major Accomplishments

1. A rigorous model based on first principles was established to predict the heat transfer in the crystal and the interface shape [Ramachandran and Dudukovic, J. Crystal Growth 71 (1985): 399-408]. The model is the first to have considered properly both direct and reflected radiation in the crystal enclosure. The model established two dimensionless parameters: a dimensionless flux at the interface and a Biot number as the key factors in determining the interface shape. This is confirmed by experimental data. The effect of including reflected radiation on axial temperature profiles is shown in Figure 3. The effect is even more dramatic for interface shape.
2. A coupled problem for the puller was solved based on an approximate conductor dominated heat transfer in the melt [Srivastava, Ramachandran and Dudukovic, J. Crystal Growth 73 (1985); 487-504]. Both, the Laplace-Young equation for the melt meniscus shape and Gebhart's enclosure theory for radiation were used. This paper provides a detailed account for the effect of all variables on interface shape. It is shown that reflected radiation is important especially in the vicinity of the interface.
3. Radiation view factors for short crystals during necking and shoulder growth are reported for the first time [Srivastava, Ramachandran and Dudukovic, J. Crystal Growth (1986) in print]. These are essential in simulating properly the critical initial stages of growth.
4. The detailed model developed and described under item 2 was simplified. Useful simple relations were developed for growth rate and interface shape as shown in Figure 4. The various parameters A , B , b , C_1 , C_2 , C_3 can be correlated with operating conditions. The simple models can then be run on line. [Srivastava, Ramachandran and Dudukovic, J. Electrochem.

Soc. Solid State Sci. Techn. 133 (1985): 1007-1015]. The success of the simple models in matching the predictions of the detail models for growth rate versus radius and for interface shape versus radius are shown in Figure 5 and 6, respectively.

5. A novel concept of improving the controllability of the diameter and achieving decoupled diameter and interface shape control is introduced and numerically demonstrated [Srivastava, Ramachandran and Dudukovic, J. Crystal Growth (1986) in print]. The concept relies on regulating the convecting cooling component of the crystal by using gas jets.

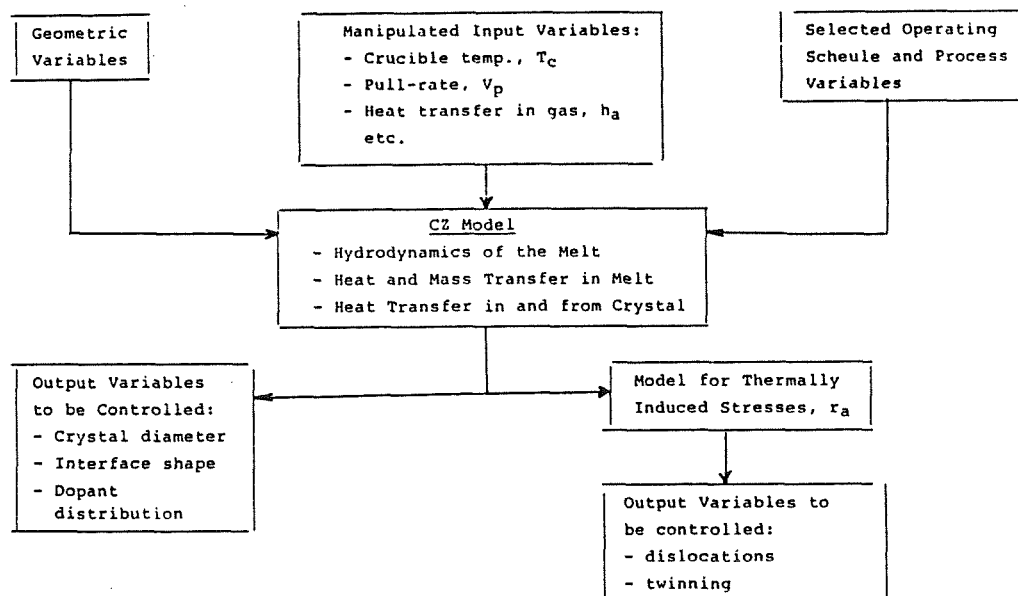
Variations of gas flow rate or gas pressure can also be used. Predicted increases in productivity with increased jet cooling are illustrated in Figure 7.

6. A preliminary steady state model for simulation of the hydrodynamics of the melt has been established [Dorsey, Ramachandran and Dudukovic, AIChE One Day Symp., St. Louis, April, 1985].

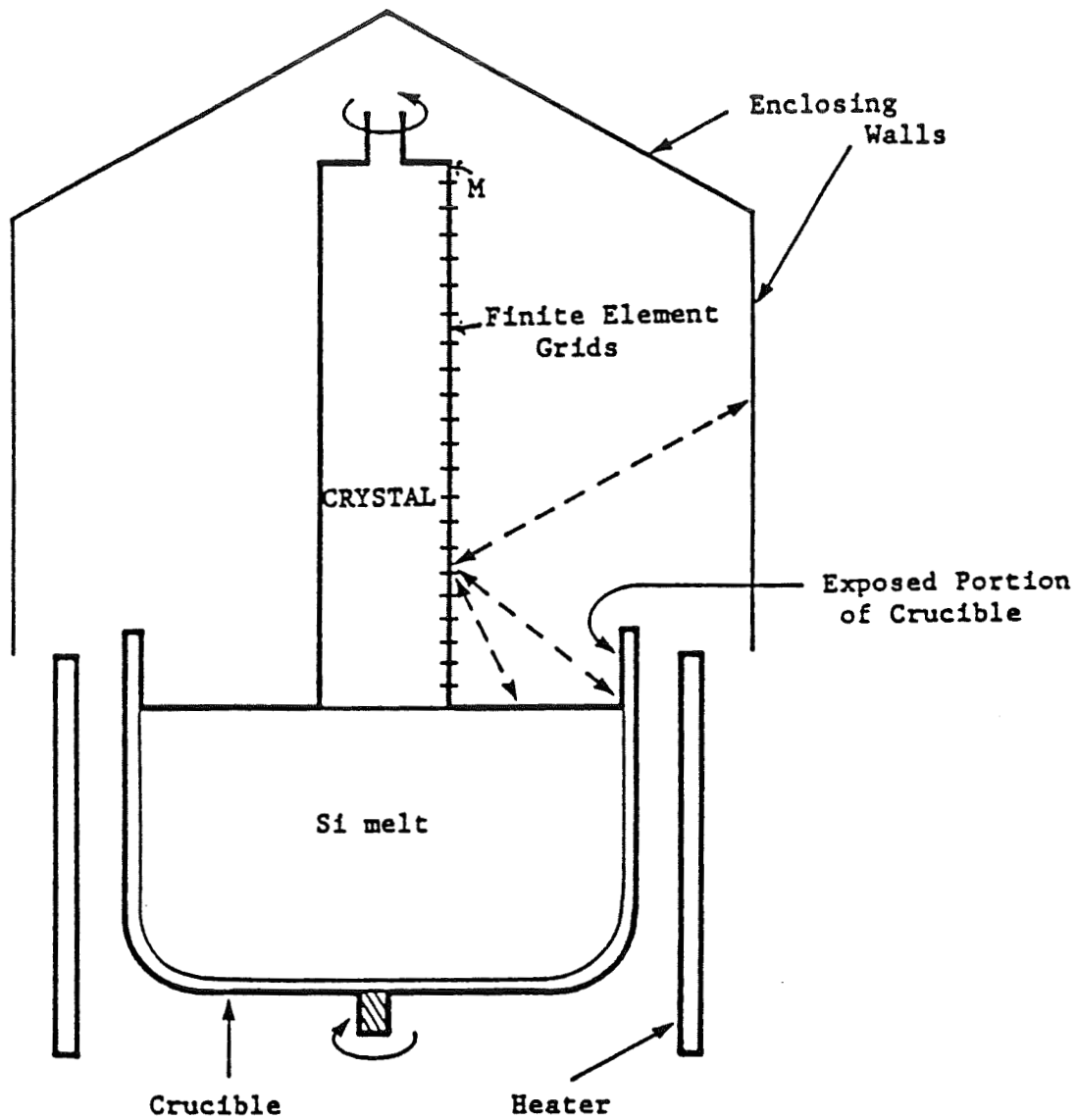
List of Publications Resulting from the Cz Modeling Work at CREL at Washington University

1. Ramachandran, P. A. and M. P. Duduković, "Simulation of Temperature Distribution in Crystals Grown by Czochralski Method", J. Crystal Growth 71 (1985): 399-408.
2. Srivastava, R. K., P. A. Ramachandran and M. P. Duduković, "Interface Shape in Czochralski Grown Crystals: Effect of Conduction and Radiation", J. Crystal Growth 73 (1985): 487-504.
3. Srivastava, R. K., P. A. Ramachandran and M. P. Duduković, "Radiation View Factors in Czochralski Crystal Growth Apparatus for Short Crystals", J. Crystal Growth (1986). In print.
4. Srivastava, R. K., P. A. Ramachandran and M. P. Duduković, "Czochralski Growth of Crystals: Simple Models for Growth Rate and Interface Shape", J. Electrochem. Soc.: Solid-State and Technology 133 (1985): 1009-1015.
5. Srivastava, R. K., P. A. Ramachandran and M. P. Duduković, "Simulation of Jet Cooling Effects on Czochralski Crystal Growth", J. Crystal Growth (1986). Accepted for publication.
6. Dorsey, D., P. A. Ramachandran and M. P. Duduković, "Numerical Simulation of the Hydrodynamics and Heat Transfer in Czochralski-Melts: Preliminary Results", AIChE One Day Symp., St. Louis, April 17, 1985.

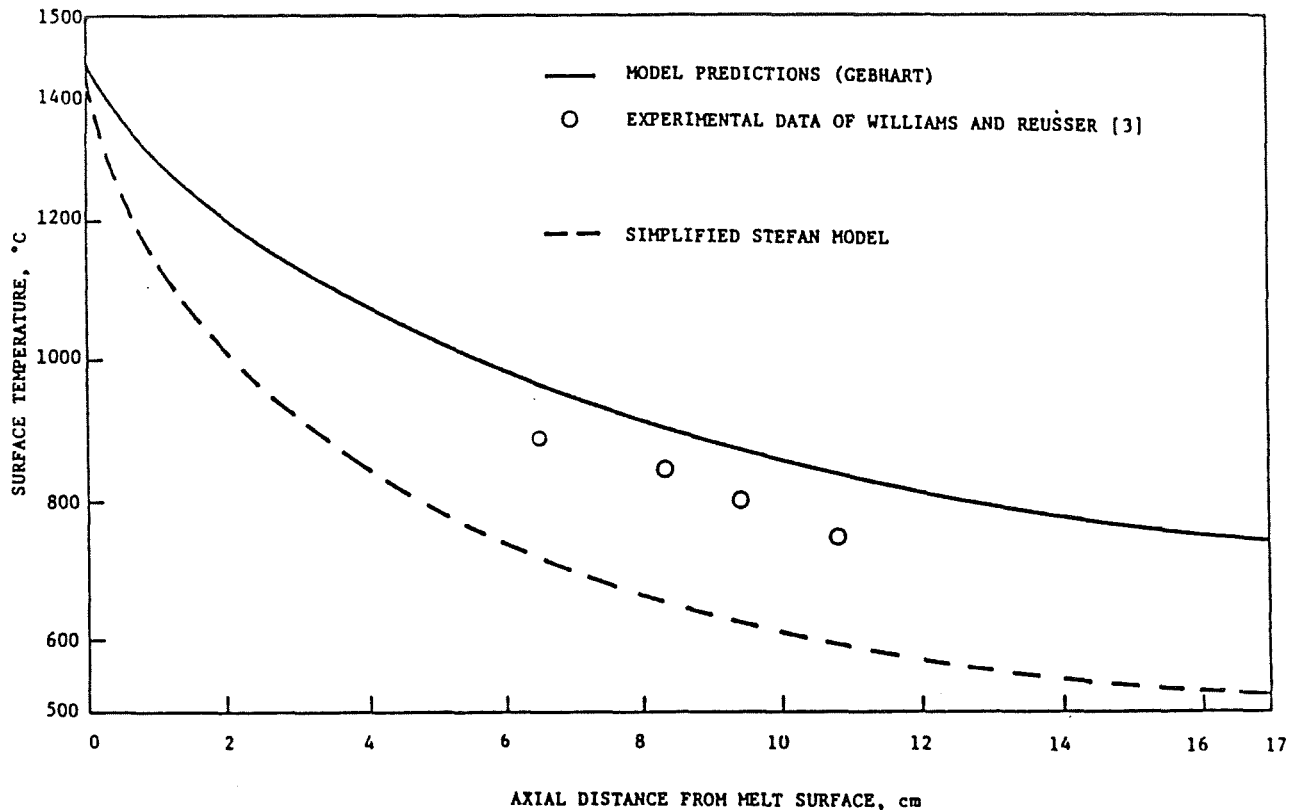
Overall Schematic of Cz Modeling



Schematic of Cz Single Crystal Puller
(---Indicates Radiation Interaction Between Various Surfaces)



Predicted Crystal Surface Temperatures Based on Gebhart and Stefan Models and Experimental Results of Williams and Reuser
[from Ramachandran and Dudukovic,
J. Crystal Growth (1985): 399-408]



Simple Models for Growth Rate and Interface Shape

Developed from the predictions of the detailed heat transfer model

1. Growth rate

At const. T_c $V_G = \frac{A}{R} - B$; A and B are constants, A depends on extent of jet cooling

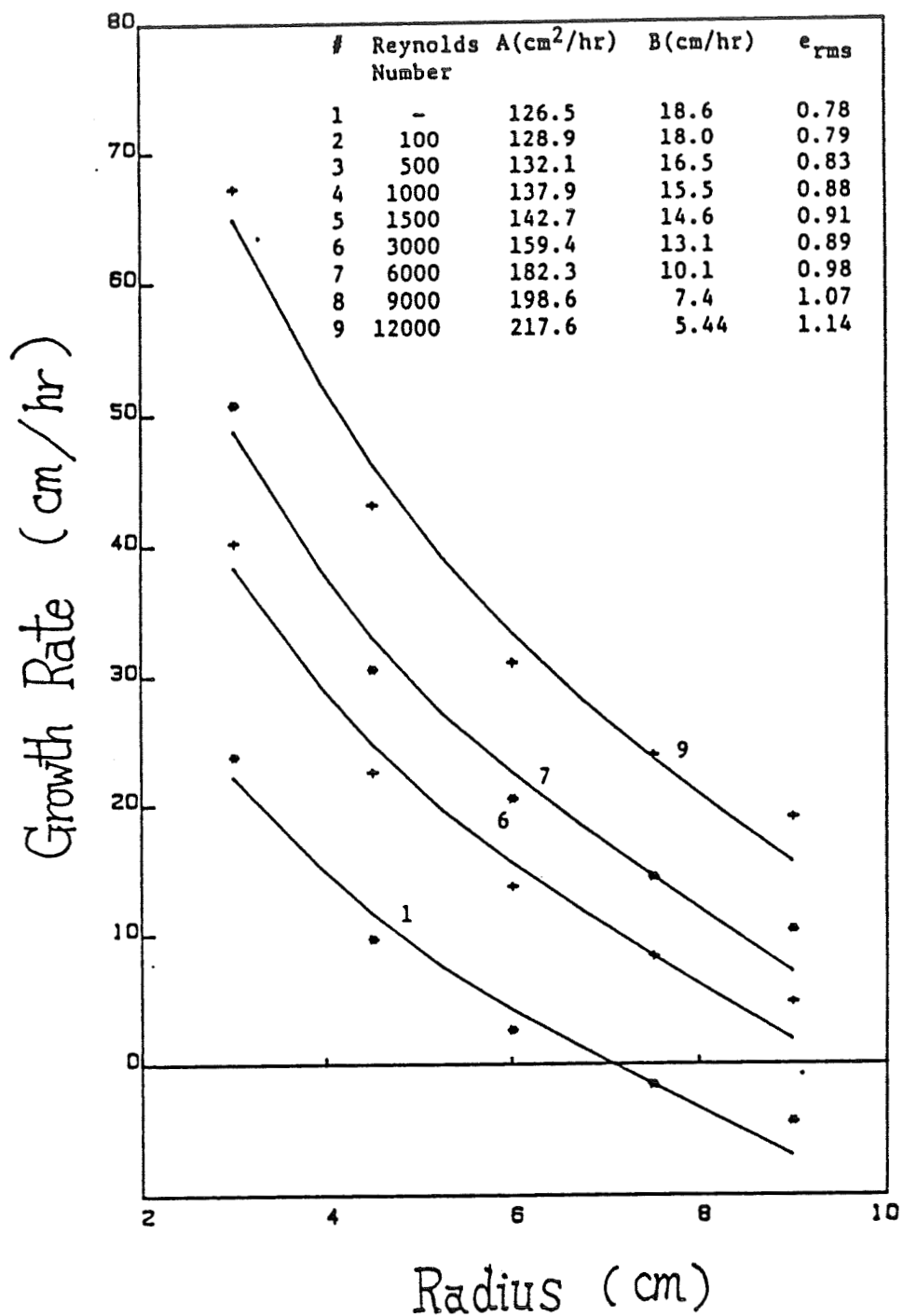
At const. R $V_G = V_{max} - b\Delta T$; $\Delta T = T_c - T_m$

2. Interface shape

At const. T_c $\Delta R = C_1 R - C_2 R^2$

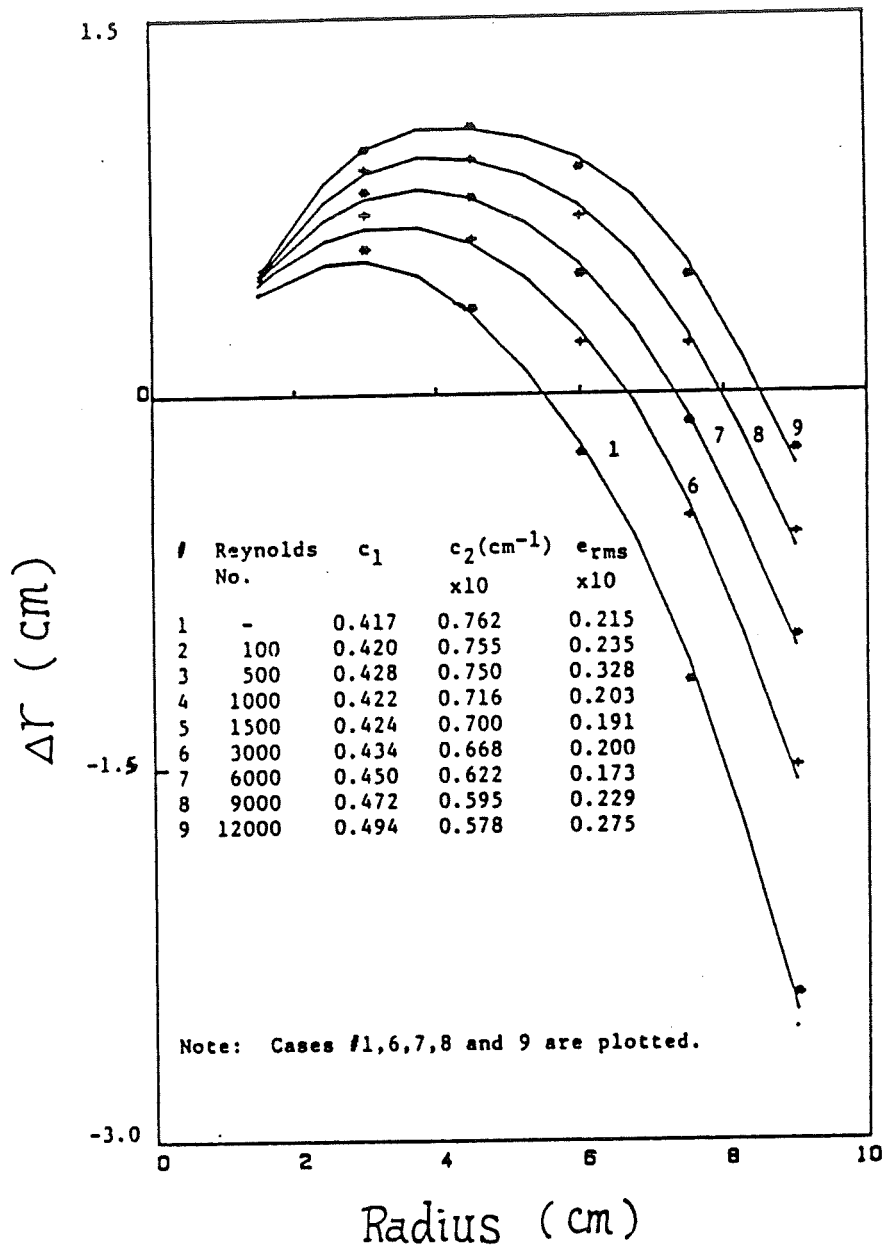
At const. R $\Delta R = \Delta R_0 - C_3 \Delta T$

Comparison of Pulling Rate Versus Crystal Radius (V Versus R)



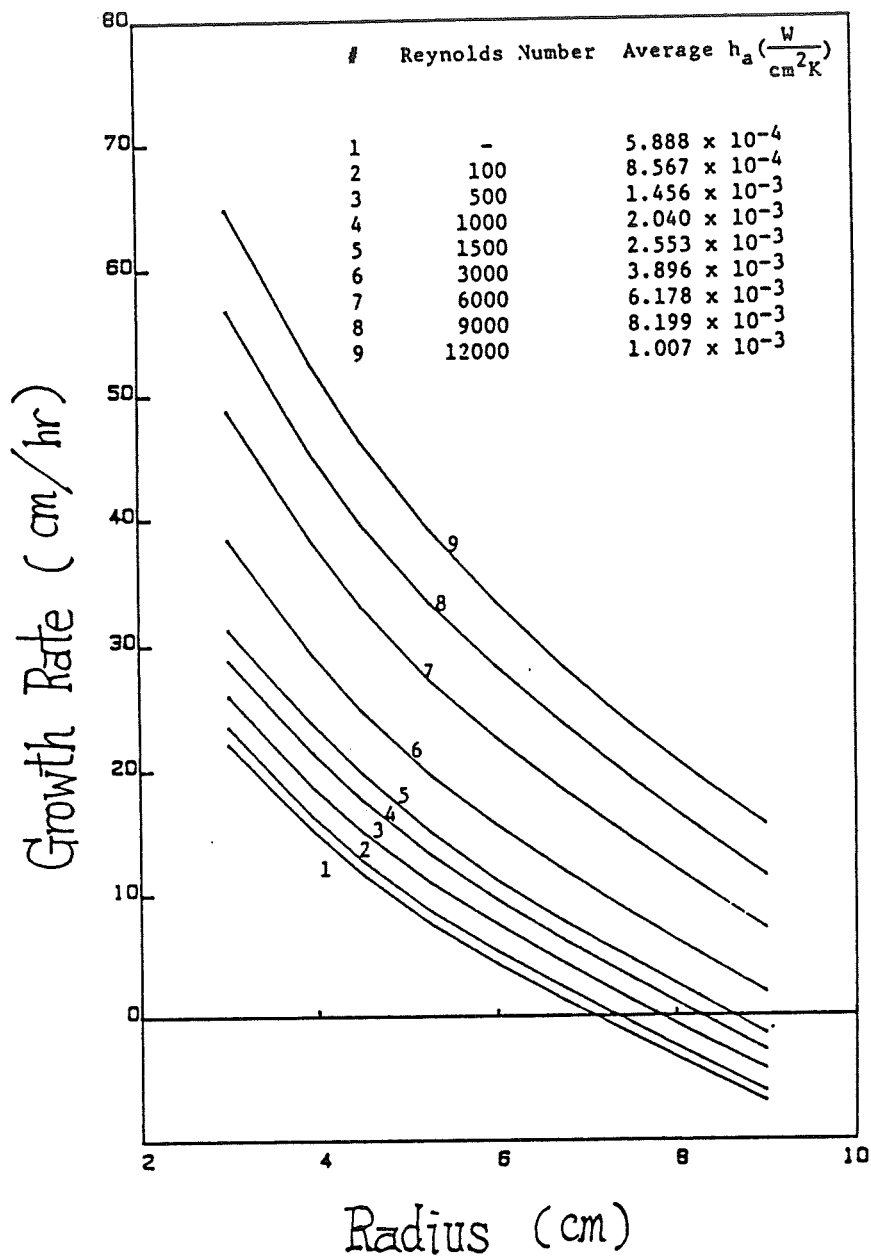
———— Detailed Simulation
 *** or +++ Approximate Equation

Variation of Interface Shape with Crystal Radius and Jet-Cooling



———— Detailed Model
 *** or ++ Approximate Equation

Variation of Growth Rate with Crystal Radius
at Different Levels of Jet-Cooling



HIGH-EFFICIENCY SOLAR CELLS

Paul Alexander, Chairman

Six presentations were made at this session on progress in high-efficiency solar cell research.

The presentation by the University of California, Los Angeles (UCLA), was on optimization methods for solar cell numerical models. A description was given on optimizing algorithms of solar cell models to simultaneously vary design variables such as impurity concentrations, front junction depth, back junction depth, and cell thickness to maximize predicted cell efficiency. The optimization methodology was demonstrated on Solar-Cell Analysis Program in One Dimension (SCAP1D), which is a computer program written by Purdue University, that relates a specific solar cell efficiency to a given set of input conditions such as cell thickness, impurity concentration, junction depth, etc. The UCLA optimization method, by iterating a set of input conditions from SCAP1D, provided a maximum solar cell efficiency related to ranges of input conditions that were derived from the SCAP1D inputs. UCLA presented curves of computer runs that demonstrated their optimization techniques.

The University of Pennsylvania described their work in identifying, developing, and analyzing techniques for measuring bulk recombination rates, and surface recombination velocities and rates in all regions of high-efficiency silicon solar cells. Professor M. Wolfe described their recent work of improving the accuracy of their previously developed DC measurement system by adding blocked interference filters. The system has been further automated by writing software that completely samples the unknown solar cell regions with data of numerous recombination velocity and lifetime pairs. The results can be displayed in three dimensions and the best fit can be found numerically using the simplex minimization algorithm. They also described a theoretical methodology to analyze and compare existing dynamic measurement techniques.

Stanford University presented their work on carrier transport and recombination parameters in heavily doped silicon. They presented data of minority carrier diffusivity in both p- and n-type heavily doped silicon covering a broad range of doping concentrations from 10^{15} to 10^{20} atoms per cm^3 . One of the highlights of their results showed that minority carrier diffusivities are higher by a factor of 2 in silicon compared to majority carrier diffusivities.

Professor R. Swanson, of Stanford University, described the construction of a 22.2% efficient single-crystal silicon solar cell fabricated at Stanford. The cell dimensions were 3×5 mm and $100 \mu\text{m}$ thick with a base lifetime of $500 \mu\text{s}$. The cell featured light trapping between a texturized top surface and a reflective bottom surface, small point contact diffusions, alternating between n-type and p-type in a polka-dot pattern on the bottom surface, and a surface passivation on all surfaces between contact regions. A V_{oc} of 0.681 V, a J_{sc} of $41.5 \text{ mA}/\text{cm}^2$, and a fill factor of 0.786 was reported for the 22.2% efficient cell.

HIGH-EFFICIENCY SOLAR CELLS

The University of Washington presented their work on investigating the passivation of silicon surfaces using SiN_x . They used high-frequency capacitance voltage (CV) measurements to determine the interface state density at midgap (D_{ss}). They indicated that the SiN_x/Si interface exhibits values of D_{ss} larger for n-type substrates than for p-type substrates and that, further, after heat treatment, this difference becomes even more pronounced. Also, it was found that the interface state density for $\text{SiN}_x/\text{p-type silicon}$ is essentially independent of dopant concentration, and the D_{ss} for $\text{SiN}_x/\text{n-type silicon}$ interface increases from 10^{12} to 10^{13} states $\text{cm}^{-2} \text{eV}^{-1}$ as the phosphorus concentration increases from 10^{16} to 10^{18} cm^{-3} . These results suggest that SiN_x can passivate a P^+/n cell more effectively than an n^+/p cell. The University of Washington also indicated that they are working on special structures that will allow measurement of both surface recombination velocity and interface state density.

Westinghouse described their work on achieving higher efficiency cells by directing efforts toward identifying carrier loss mechanisms, designing new cell structures, and developing new processing techniques. Their work, using techniques such as deep-level transient spectroscopy (DLTS), laser-beam-induced current (LBIC), and transmission electron microscopy (TEM), indicated that dislocations in web material rather than twin planes were primarily responsible for limiting diffusion lengths in web. They described their work in hydrogen implantation which indicated that they can improve lifetimes and cell efficiencies from 19 to 120 μm , and 8 to 10.3% (no AR), respectively, by implanting hydrogen at 1500 eV and a beam current density of 2.0 mA/cm^2 . Some of their processing improvements included use of a double-layer AR coating (ZnS and MgF_2) and an addition of an aluminum back surface reflector. Cells of more than 16% efficiency have been achieved.

OPTIMIZATION METHODS AND SILICON SOLAR CELL NUMERICAL MODELS

UNIVERSITY OF CALIFORNIA, LOS ANGELES

K. Girardini

Project Goal

The goal of this project is the development of an optimization algorithm for use with numerical silicon solar cell models. By coupling an optimization algorithm with a solar cell model it is possible to simultaneously vary design variables such as impurity concentrations, front junction depth, back junction depth, and cell thickness to maximize the predicted cell efficiency. An optimization algorithm has been developed and interfaced with the Solar Cell Analysis Program in 1 Dimension (SCAP1D). SCAP1D uses finite difference methods to solve the differential equations which, along with several relations from the physics of semiconductors, describe mathematically the operation of a solar cell. A major obstacle is that the numerical methods used in SCAP1D require a significant amount of computer time, and during an optimization the model is called iteratively until the design variables converge to the values associated with the maximum efficiency. This problem has been alleviated by designing an optimization code specifically for use with numerically intensive simulations, to reduce the number of times the efficiency has to be calculated to achieve convergence to the optimal solution. Adapting SCAP1D so that it could be called iteratively by the optimization code provided another means of reducing the cpu time required to complete an optimization. Instead of calculating the entire I-V curve, as is usually done in SCAP1D, only the efficiency is calculated (maximum power voltage and current) and the solution from previous calculations are used to initiate the next solution. Optimizations have been run for a variety of substrate qualities and levels of front and back surface passivation. This was done to determine how these variables affect the optimized efficiency and the values of the optimized design variables. The sensitivity of efficiency to each of the design variables was investigated by changing one variable and reoptimizing the others. Work is progressing to include variables associated with the design of an anti-reflection coating in the optimization.

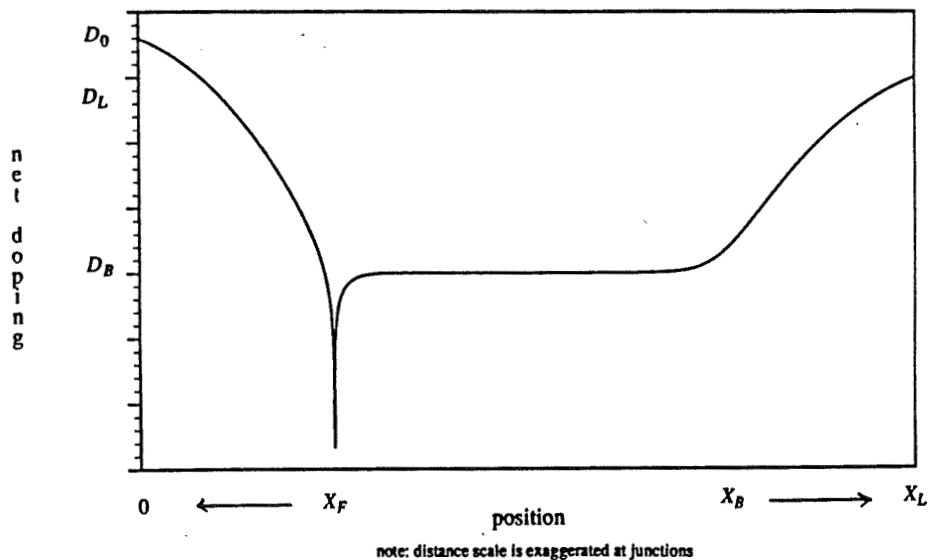
Problem Statement

How can all the inputs to a numerical model
of a silicon solar cell be simultaneously
varied to obtain the "optimal" design.

Outline

- I Define the Optimization Problem.
 - a) Objective, variables, and constraints
- II Solving the Optimization Problem
 - a) Outline of optimization algorithm
 - b) Calculating efficiency using SCAP1D
 - c) Adapting SCAP1D for an iterative environment
- III Results of Optimization
- IV Future Work

Doping Concentration Versus Position Use of *Cerf* Model for Doping



Optimization Model

$$\text{MAX Efficiency}(D_0, X_F, D_B, X_B, D_L, X_L)$$

$$14 \leq D_0 \leq 20.6$$

$$14 \leq D_B \leq 20.6$$

$$14 \leq D_L \leq 20.6$$

$$0.1 \leq X_F \leq 10.0$$

$$0.2 \leq X_B \leq 50.0$$

$$10.0 \leq X_L \leq 300.0$$

$$0.0 \leq D_L - D_B$$

$$0.1 \leq X_L - X_F - X_B$$

$$D_0 = \log[\text{Front surface doping concentration}] \quad \text{P atoms/cm}^3$$

$$D_B = \log[\text{Bulk doping concentration}] \quad \text{B atoms/cm}^3$$

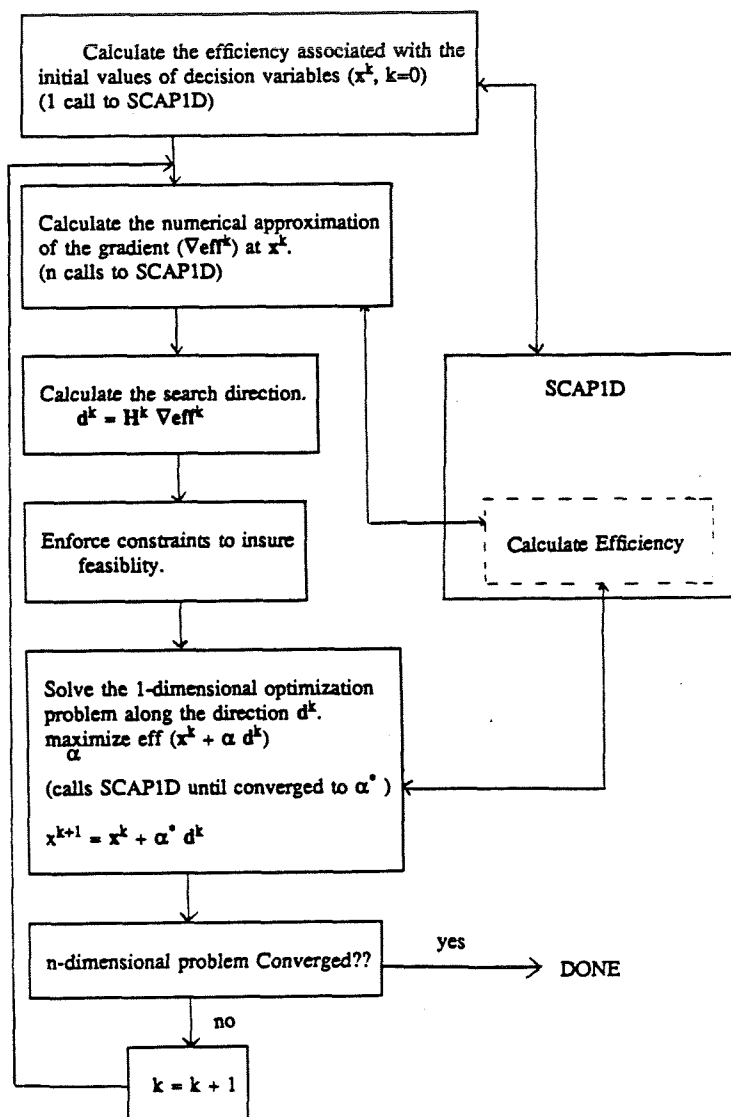
$$D_L = \log[\text{Back surface doping concentration}] \quad \text{B atoms/cm}^3$$

$$X_F = \text{Front junction depth} \quad \mu\text{m}$$

$$X_B = \text{Back junction depth} \quad \mu\text{m}$$

$$X_L = \text{Cell thickness} \quad \mu\text{m}$$

Optimization Model Flow Chart



SCAP1D (Solar Cell Analysis Program in 1 Dimension)

$$\text{Poisson's equation} \quad \nabla^2 V = \frac{q}{\epsilon} (n - p + N_D - N_A)$$

$$\text{Electron Continuity Equation} \quad \nabla J_n = q (R - G)$$

$$\text{Hole Continuity Equation} \quad \nabla J_p = -q (R - G)$$

Hole and Electron Carrier Transport Equations

$$J_n = -q \mu_n n \left[\nabla \left(V + \gamma \frac{\Delta_g}{q} \right) \right] + q D_n \nabla n$$

$$J_p = -q \mu_p p \left[\nabla \left(V - (1-\gamma) \frac{\Delta_g}{q} \right) \right] - q D_p \nabla p$$

where:

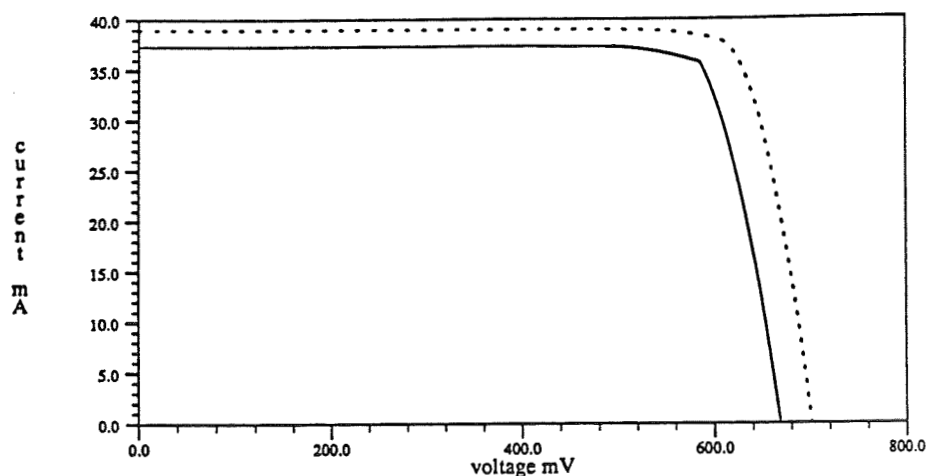
$$\text{effective gap reduction} = \Delta_g = \left[\Delta E_g + \Theta_n + \Theta_p \right]$$

$$\text{effective asymmetry factor} = \gamma = \frac{\Delta \chi + \Theta_n}{\Delta_g}$$

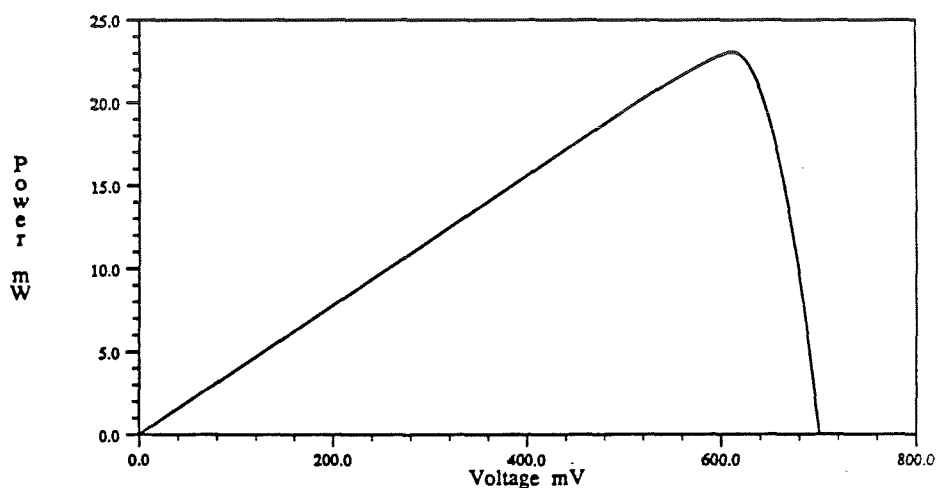
Several assumptions are required for the validity of these equations.

- (1) Complete ionization of the dopants.
- (2) The heavily doped regions are quasi-neutral and in low injection.
- (3) The parameters Δ_g and γ are functions of the carrier concentrations.
- (4) Δ_g and γ do not change when the device is not in equilibrium.

I-V Curves



Power Versus Voltage



Base Input Parameters

Constant Input Parameters

Illumination	100mW/cm ³ (AM 1.5)
Temperature	28 degrees C
Doping Profile	erfc
Shadowing (including reflection)	7%
Auger Recombination	considered
Band Gap Narrowing	Slootboom Degraff model

Inputs Varied Parametrically

Front surface recombination velocity (S_f)
 Back surface recombination velocity (S_b)
 Minority carrier lifetime (used same formulas as in last progress report)
 τ_{n0} is electron minority carrier lifetime.
 τ_{p0} is hole minority carrier lifetime (always taken as one half τ_{n0})
 For .2 ohm-cm substrate the input $\tau_{n0} = 2$ ms, 1 ms, .4 ms gives bulk minority carrier lifetimes of 54, 30, and 13 micro seconds respectively.
 R_b (back surface reflection, 1.0 or 0.0)

Inputs Varied Parametrically or Optimized

Front junction depth (X_f)
 Back junction depth (X_b)
 Cell thickness (X_L)
 Front surface doping concentration (D_0)
 Bulk doping concentration (D_B)
 Back surface doping concentration (D_L)

Optimal Solution for Case 2

Parameters Held Constant During Optimization

Front surface recombination velocity (S_f)	1,000.0	cm/s
Back surface recombination velocity (S_b)	1,000.0	cm/s
Electron minority carrier lifetime ¹ (τ_{n0})	1.00	ms
Hole minority carrier lifetime ¹ (τ_{p0})	0.50	ms

Optimal Values of Decision Variables

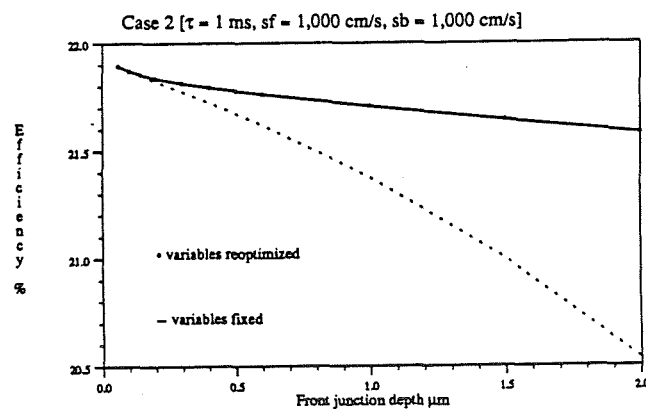
Front junction depth (X_F)	0.10	μm (lower bound)
Back junction depth (X_B)	0.20	μm (lower bound)
Cell thickness (X_L)	280.1	μm
Front surface doping concentration (D_0)	2.153×10^{19}	P atoms/ cm^3
Bulk doping concentration (D_B)	1.989×10^{16}	B atoms/ cm^3
Back surface doping concentration (D_L)	3.214×10^{19}	B atoms/ cm^3

Cell Performance Parameters

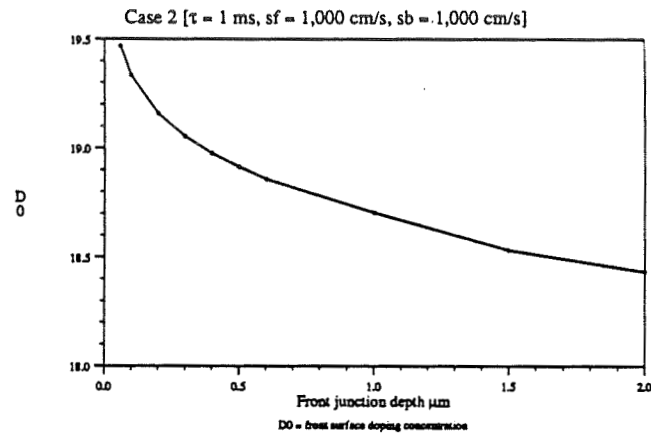
Efficiency	21.871	%
Open circuit voltage (V_{oc})	668.2	mV
Short circuit current density (J_{sc})	39.063	mA/cm^2
Maximum power voltage (V_{mp})	584.86	mV
Fill factor	0.8379	
Collection efficiency	99.23	%
Bulk resistivity	0.74	ohm-cm
Sheet resistance layer 1	988.0	ohm/ \square
layer 2	25.37	ohm/ \square

¹ Values in lightly doped silicon.

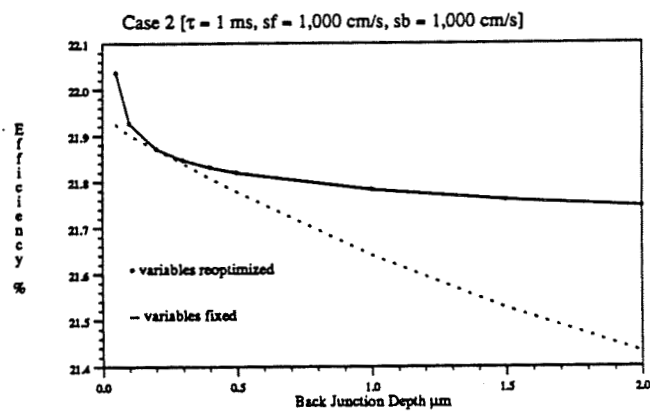
Efficiency Versus Front Junction Depth



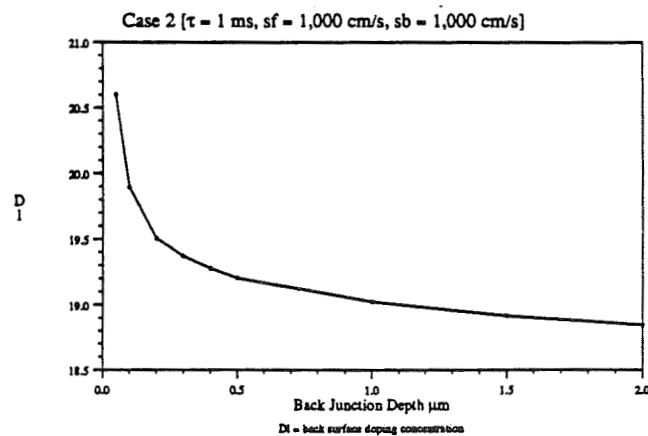
Optimal Front Surface Doping for Fixed Front Junction Depth



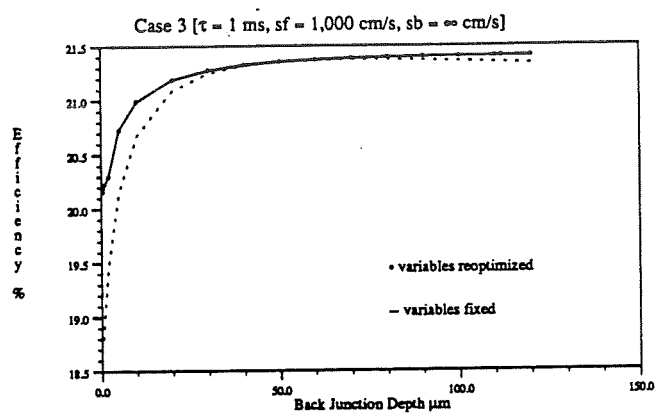
Efficiency Versus Back Junction Depth



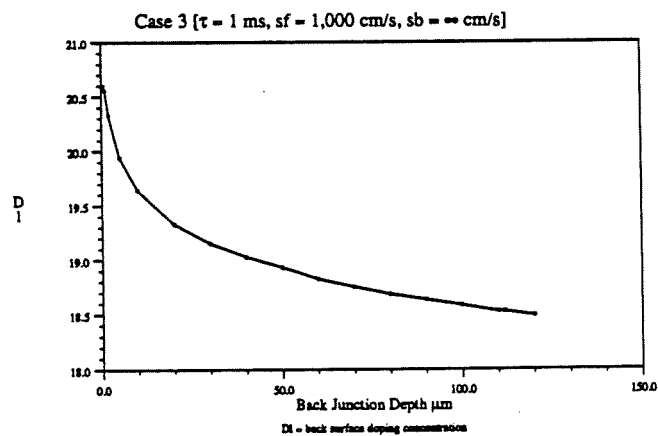
Optimal Back Surface Doping for Fixed Back Junction Depth



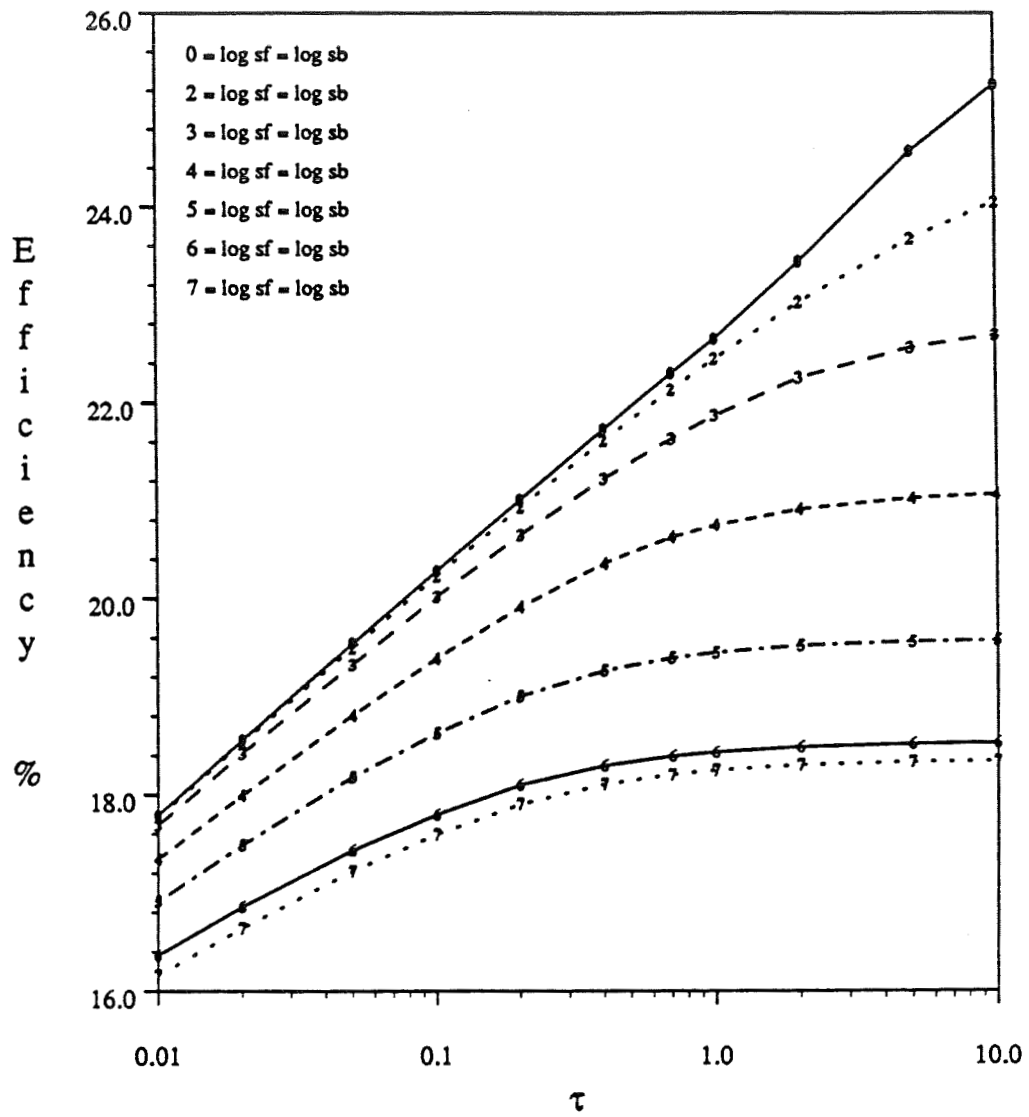
Efficiency Versus Back Junction Depth



Optimal Back Surface Doping for Fixed Back Junction Depth



Efficiency Versus τ at Different Levels of Surface Passivation

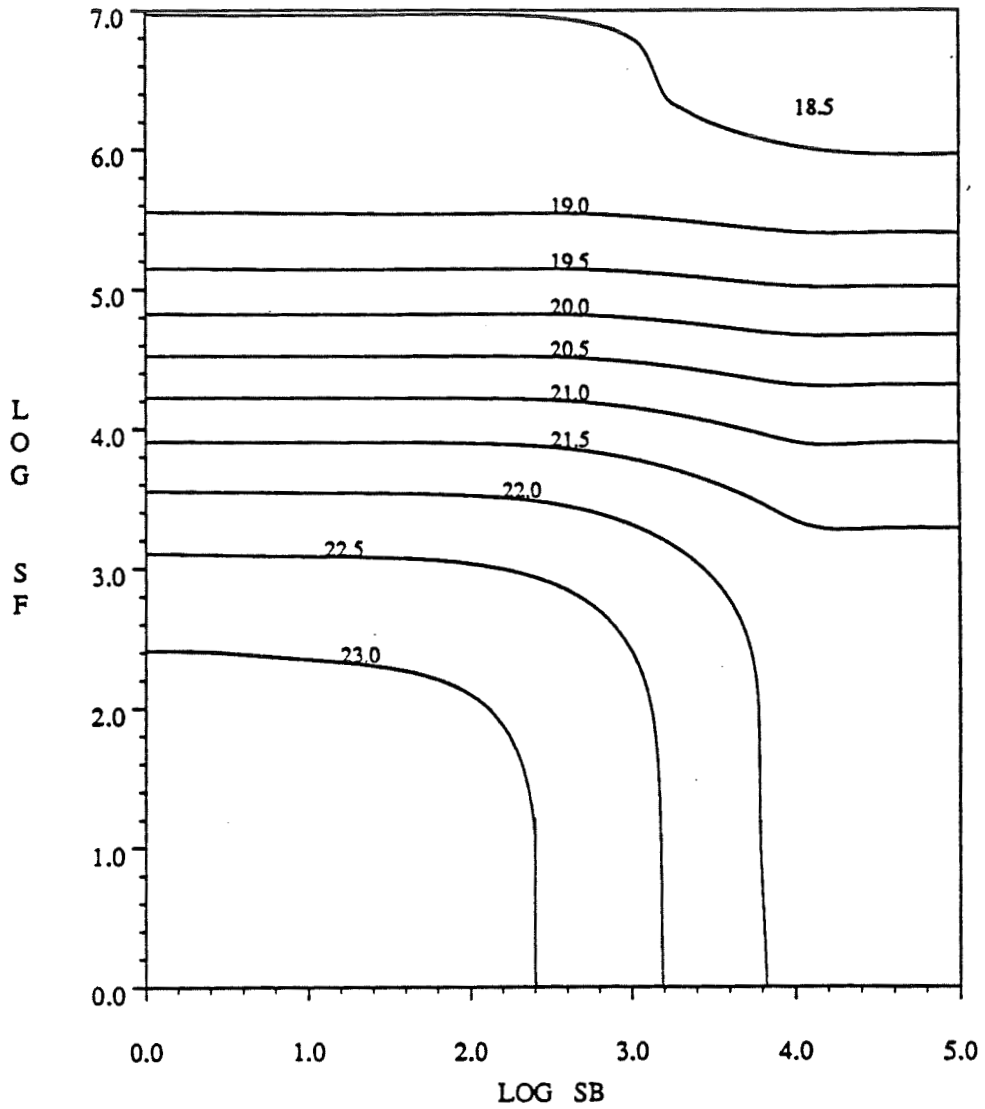


τ = Intrinsic electron minority carrier lifetime

sf [sb] = front [back] surface recombination velocity

Optimal Efficiency Contours Versus SB and SF

$\tau_{\text{aun}} = 2.0 \text{ ms}$, cell thickness < 300

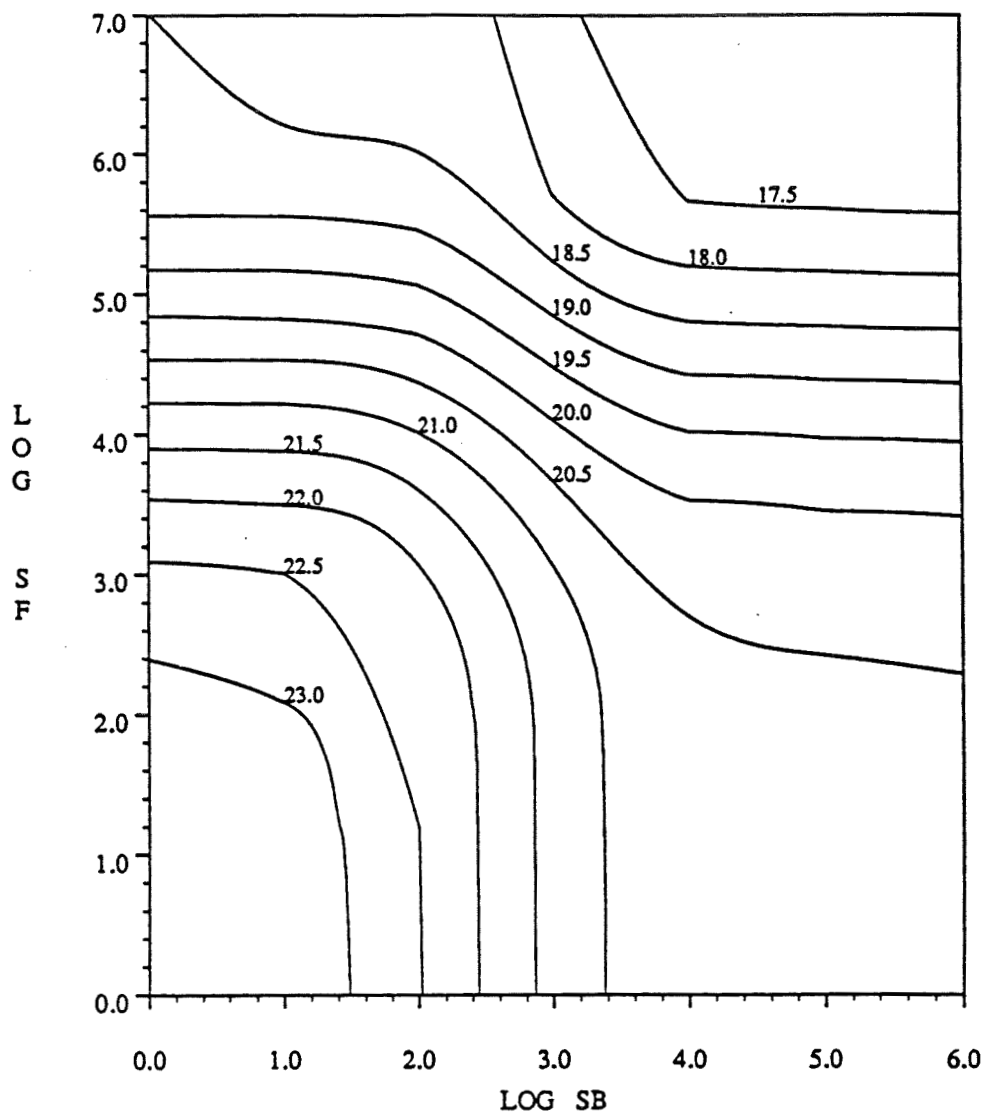


SB = effective back surface recombination velocity (cm/s)

SF = effective front surface recombination velocity (cm/s)

Optimal Efficiency Contours Versus SB and SF (Cont'd)

$\tau_{\text{aun}} = 2.0 \text{ ms}$, no BSF, cell thickness < 300



SB = effective back surface recombination velocity (cm/s)

SF = effective front surface recombination velocity (cm/s)

Summary

- (1) Significant computational savings can be realized by adapting a solar cell model for use with an optimization algorithm.
- (2) Comparisons should only be made between different values of a design variable after the other variables are optimized.
- (3) An optimization algorithm provides a systematic method for comparing different levels of technology and/or fabrication processes.
- (4) A model coupled with an optimization algorithm provides a very powerful tool for analyzing the system modeled.

Future Work

- (1) Analyze results of optimization runs.
- (2) Investigate other models for the doping concentrations.
- (3) Include a term for lateral resistance in the objective function.
- (4) Include the design of the anti-reflection coating in SCAP1D and possibly in the optimization.

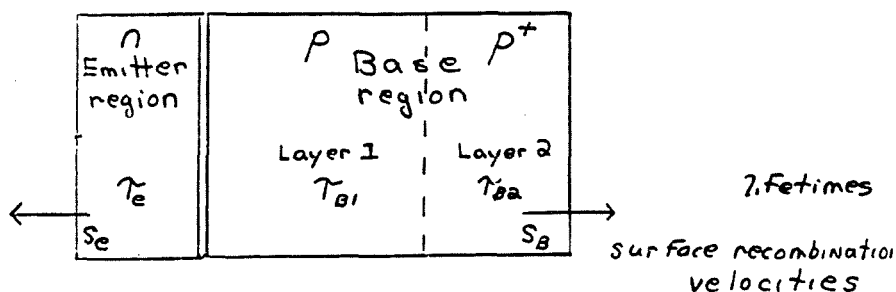
NOVEL MEASUREMENT TECHNIQUES (DEVELOPMENT AND ANALYSIS OF SILICON SOLAR CELLS NEAR 20% EFFICIENCY)

UNIVERSITY OF PENNSYLVANIA

M. Wolf and M. Newhouse

Typical High-Efficiency Device

Traditional lifetime measurement techniques have been directed at extracting a single bulk lifetime from rather simple structures in which nonuniformities, drift fields and surface recombination velocities were ignored.



Real devices have multiple unknown recombination and transport parameters

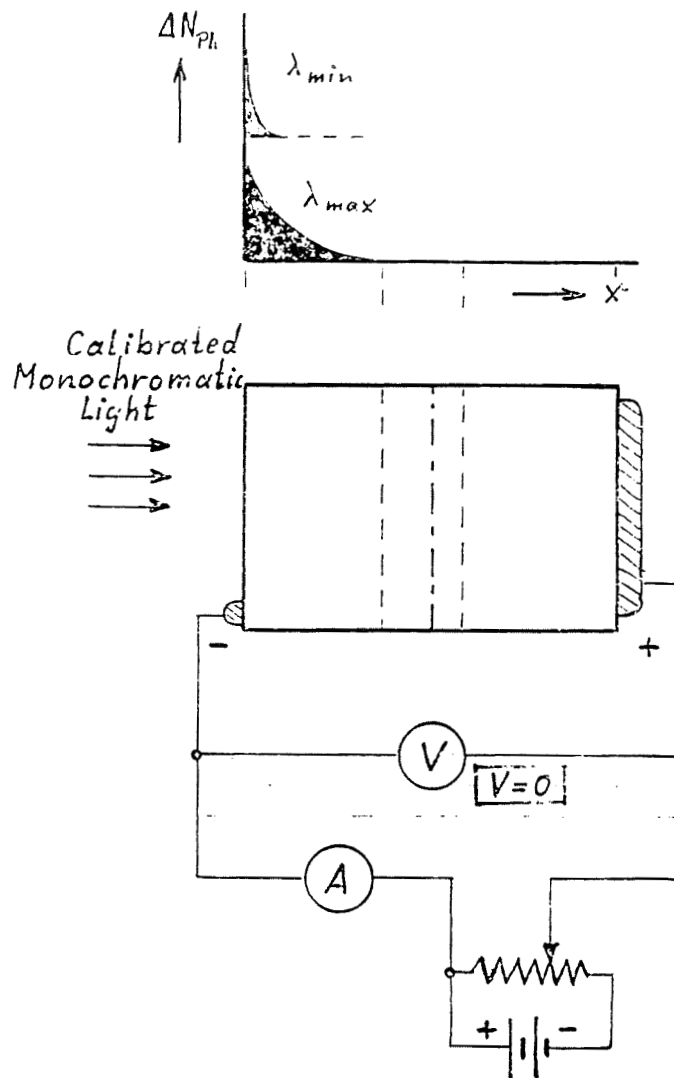
PRECEDING PAGE BLANK NOT FILMED

PRECEDING PAGE BLANK NOT FILMED

Objectives

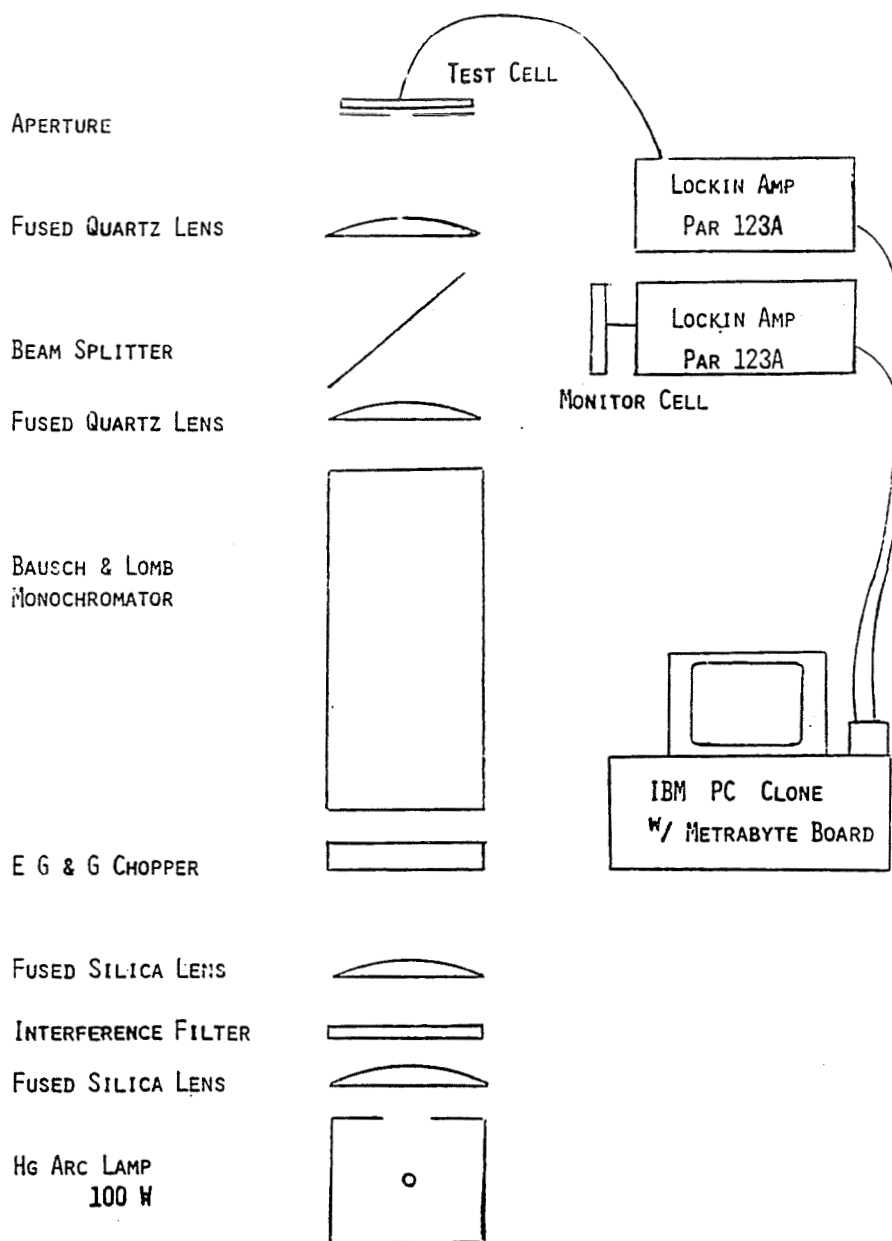
1. REFINE, AUTOMATE, AND APPLY ASLBIC METHOD.
2. DEVELOP GENERIC METHOD FOR EVALUATING AVAILABLE METHODS
FOR S AND τ DETERMINATION
IN COMPLEX DEVICE STRUCTURES (SOLAR CELLS):
 - A. ESTABLISH GENERAL THEORY.
 - B. APPLY TO DETERMINING RELATIVE ADVANTAGES,
LIMITATIONS OF CANDIDATE METHODS.
 - C. DERIVE METHODS FOR REDUCING MEASURED DATA
FROM THESE METHODS TO MEANINGFUL S, τ VALUES
IN RELEVANT PARTS OF COMPLEX DEVICES.
 - D. IF POSSIBLE, APPLY INSIGHTS GAINED
TO DEVELOPMENT OF MORE SUITABLE METHODS.
3. ESTABLISH TO WHAT EXTENT S AND AN "EFFECTIVE τ "
CAN BE DETERMINED IN THE COMMONLY USED "EMITTER"
($x_j \approx 0.2 \mu\text{m}$; $N_{D,S} \approx 10^{19} - 10^{20} \text{ cm}^{-3}$).
(EXAMPLE: FSA - COMMITTEE SOLAR CELL DESIGN)

Absolute Spectral Light Beam Induced Current (ASLBIC)

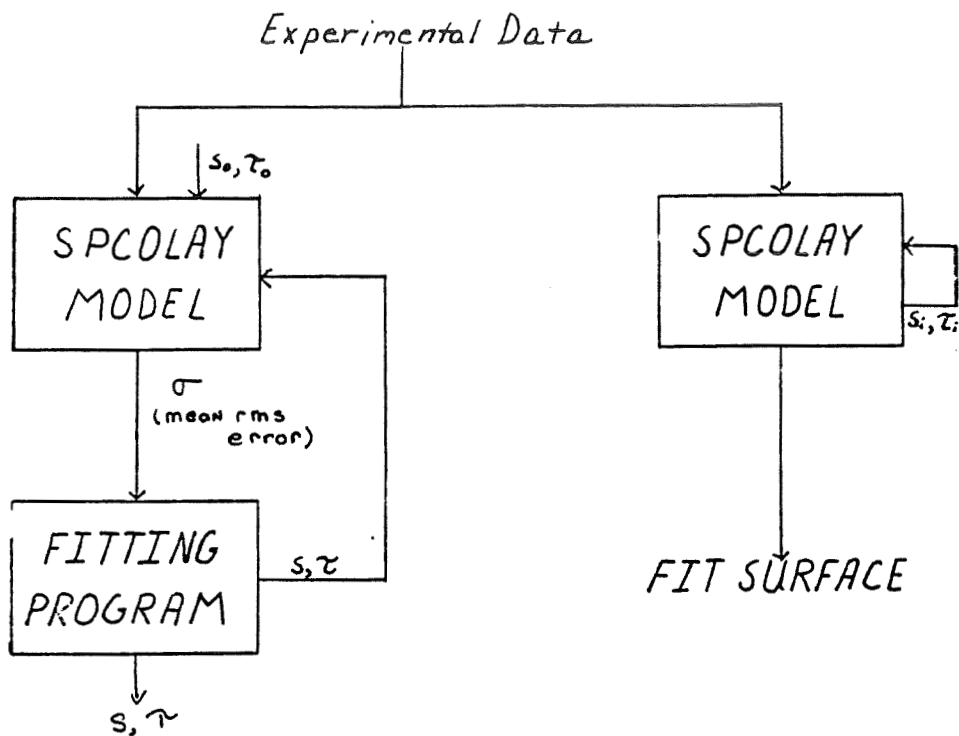


HIGH-EFFICIENCY SOLAR CELLS

ASLBIC Facility



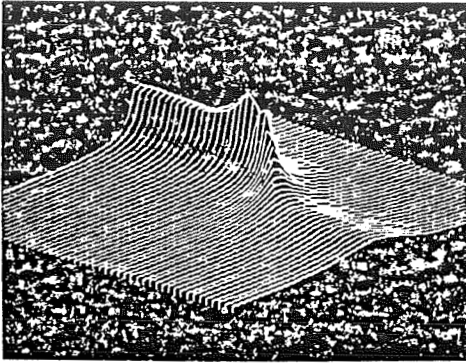
ASLBIC Fitting



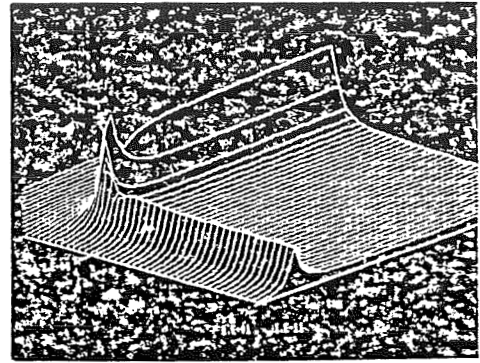
Two Fitting Methods

1. Steepest Descent
go down steepest hill
2. Simplex
NEW METHODS
NOT intuitive
works best

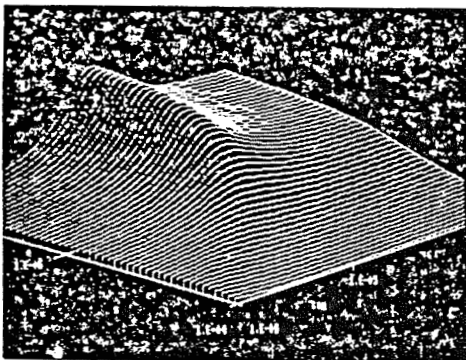
HIGH-EFFICIENCY SOLAR CELLS



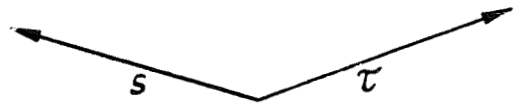
$3\mu\text{m}$ uniform (theor'l.)



Spire 4400 20B
 $0.3\mu\text{m}$ SIMS data \rightarrow 3 layers
 (same τ)



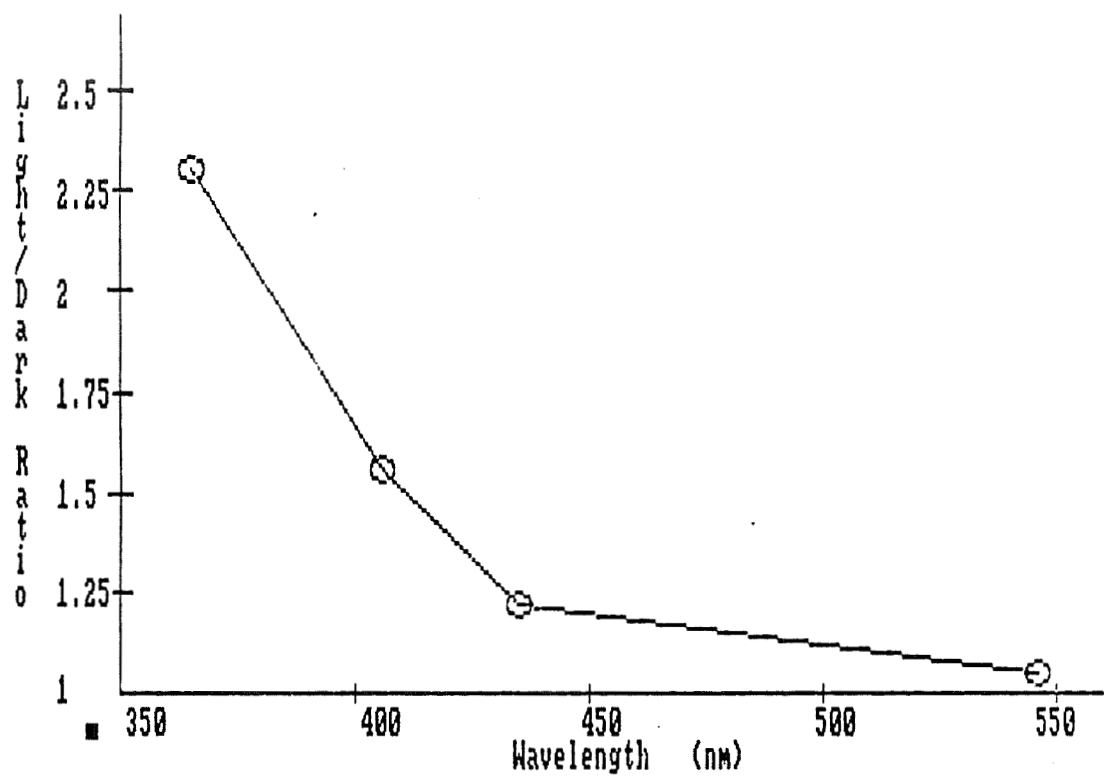
A-3-1-216/100-2-3, $100\mu\text{m}$ unif'm.



ORIGINAL PAGE IS
 OF POOR QUALITY



Effect of Bias Light Versus Wavelength for a-3-1-216/2-1-2



Measurement Types

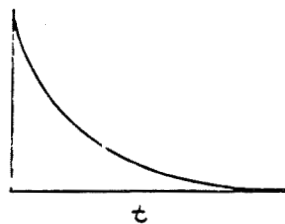
- Steady State

vs. wavelength
vs. distance
vs. voltage

- Relaxation Constant Measurements

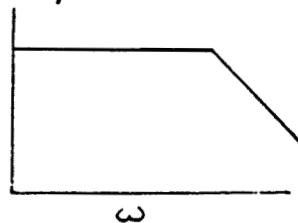
- Decay measurements

vs. time



- Modulation measurements

vs. frequency



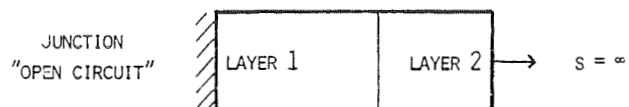
$$D \frac{\partial^2 n}{\partial x^2} - \frac{n}{\tau} = \begin{cases} G_n(x) & \text{steady state} \\ \frac{\partial n}{\partial t} & \text{free decay} \\ \frac{\partial n}{\partial t} - G_n(x, t) & \text{forced oscillation} \end{cases}$$

$$\begin{cases} [G_n(x) = N_{ph} \alpha e^{-\alpha x}] & n(x) = A e^{\frac{x}{L}} + B e^{-\frac{x}{L}} + C e^{-\alpha x} \\ [\underline{\underline{\frac{\partial n}{\partial t}}}] & n(x, t) = \sum_{i=1}^{\infty} A_i e^{-(\frac{1}{\tau} + \lambda_i) t} \phi_i(x) \\ [G_n(x, t) = G(x) e^{j\omega t}] & n(x, \omega) = \sum_{i=1}^{\infty} \frac{B_i^2 \phi_i(x)}{\frac{1}{\tau} + \lambda_i + j\omega} \int_0^d \phi_i(y) G_n(y) dy \end{cases}$$

The Meaning of the Constants in Decay Modes

- A. $\beta_i = \frac{1}{\tau} + \lambda_i$ ARE THE RELAXATION CONSTANTS OF THE SYSTEM.
THEY ARE OBSERVABLE.
-
- B. $1/\tau$ CHARACTERIZES THE EFFECTIVE MINORITY CARRIER RECOMBINATION RATE
IN THE VOLUME OF THE LAYER AT WHICH THE OBSERVATION IS MADE.
(IF THIS RATE IS UNIFORM IN THE VOLUME, THEN τ IS THE M.C. LIFETIME.)
-
- C. λ_i ARE THE EIGENVALUES WHICH DETERMINE THE DIFFUSIVE DECAY
OF THE M.C. IN THE LAYER UNDER OBSERVATION.
THEY ARE DETERMINED BY:
1. ANY "SINKS" OUTSIDE OF THE LAYER CONSIDERED
(SUCH AS: SURFACE WITH RECOMBINATION:
BOUNDARY TO JUNCTION IN NOT-FLAT-BAND CONDITION:
BULK RECOMBINATION),
 2. THE TRANSPORT PROPERTIES OF THE LAYER AND INTERVENING LAYERS.
-
- D. WHICH, AND HOW MANY, OF THE INFINITELY MANY λ_i ARE OF SIGNIFICANCE,
IS DETERMINED BY THE INITIAL EXCESS MINORITY CARRIER DISTRIBUTION
AND THE PROPERTIES OF THE LAYER.

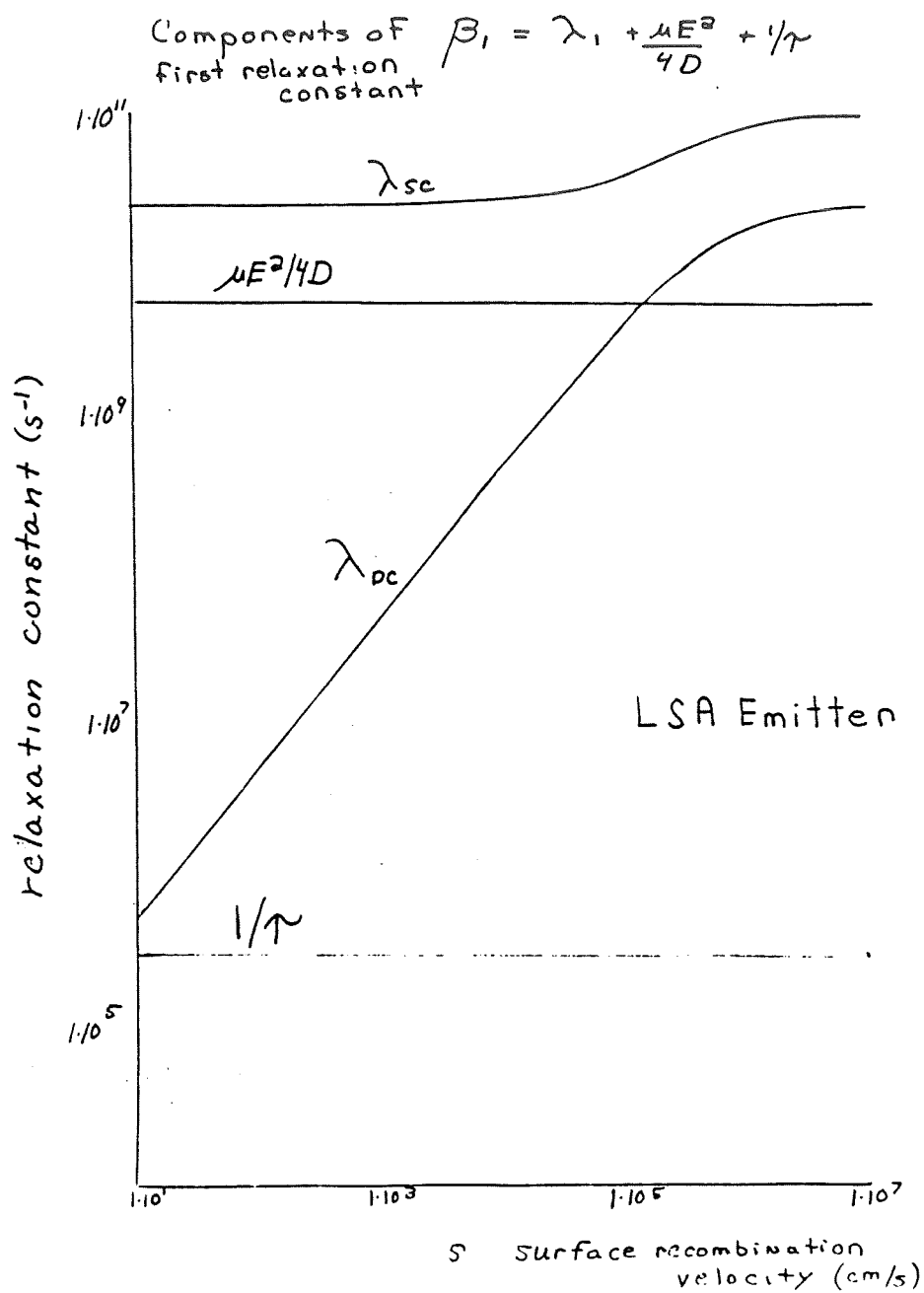
HIGH-EFFICIENCY SOLAR CELLS



VARIATION CASE	BASELINE CASE: UNIFORM (ONLY 1 LAYER)		DOPING		D		τ		LSA		LSA, BUT LOW τ IN LAYER 2	
	1	2	1	2	1	2	1	2	1	2	1	2
LAYER												
THICKNESS (μm)	60	40	→									
DOPING (cm^{-3})	5E16	5E16	5E16	2E18	5E16	5E16	→		5E16	2E18	→	
D (cm^2/s)	15.5	15.5	→		15.5	5.95			15.5	5.95	→	
τ (μs)	33	33	→				33	2	33	2	33	0.27
β_1	2.4		21.6		4.8		2.2		25.8		11.2	

ORIGINAL PAGE IS
OF POOR QUALITY

HIGH-EFFICIENCY SOLAR CELLS



MEASUREMENT OF MINORITY CARRIER LIFETIME, MOBILITY AND DIFFUSION LENGTH IN HEAVILY DOPED SILICON

STANFORD UNIVERSITY

S. E. Swirhun and R. M. Swanson

Outline

Introduction

Measurement of Minority Carrier Lifetimes in p^+ and n^+ Si

- photoluminescence decay technique
- data reduction
- fits of lifetime vs. doping data (p^+ and n^+)

Measurement of Diffusion Length and Mobility in p^+ and n^+ Si

- lateral transistor test structure
- typical diffusion length data
- diffusion length vs. doping in p^+ Si
- electron (minority carrier) mobility vs. doping
- hole (minority carrier) mobility vs. doping

PRECEDING PAGE BLANK NOT FILMED

Minority Carrier Lifetime in n^+ and p^+ Silicon
Recombination Paths

- Shockley-Read-Hall Recombination

$$\tau_p = (N_t v \sigma)^{-1}$$

– lifetime independent of doping, dependent on N_t

- Auger Recombination: Trap Assisted

$$\tau_p = (T_n n N_t)^{-1}$$

– lifetime dependent on doping, N_t

- Auger Recombination: Band to Band

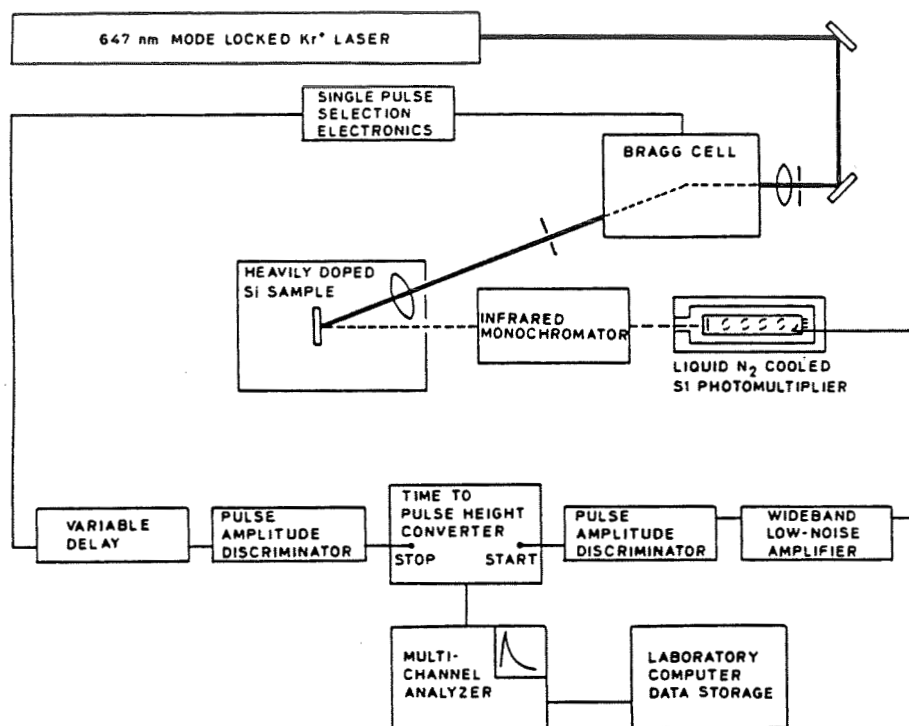
$$\tau_p = (C_n n^2)^{-1}$$

– lifetime dependent on doping only

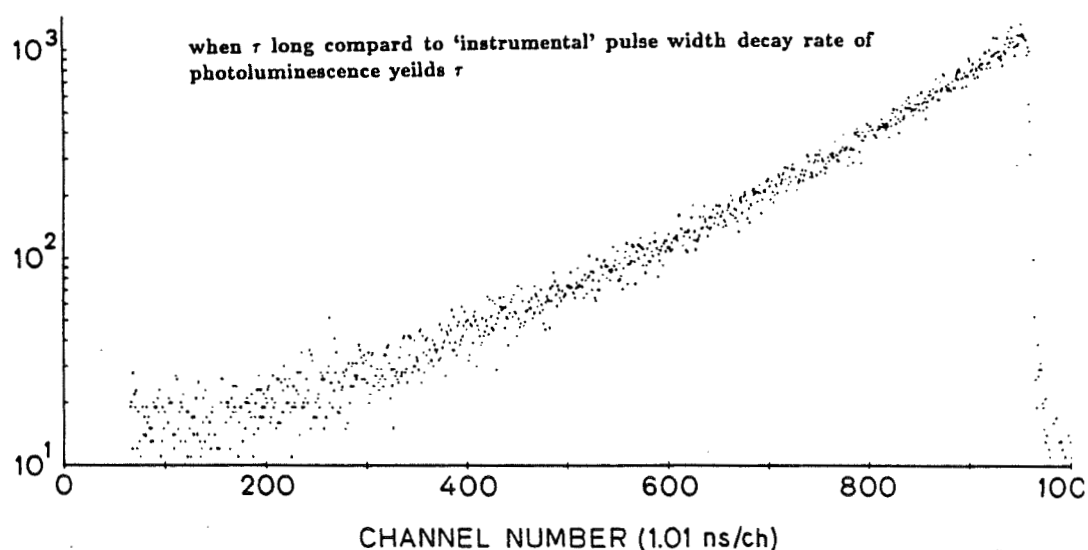
Photoluminescence Lifetime Decay

- short (200 ps) laser pulse generates minority carriers
- monitor decay of luminescence radiation

Photoluminescence Decay Lifetime Measurement Apparatus



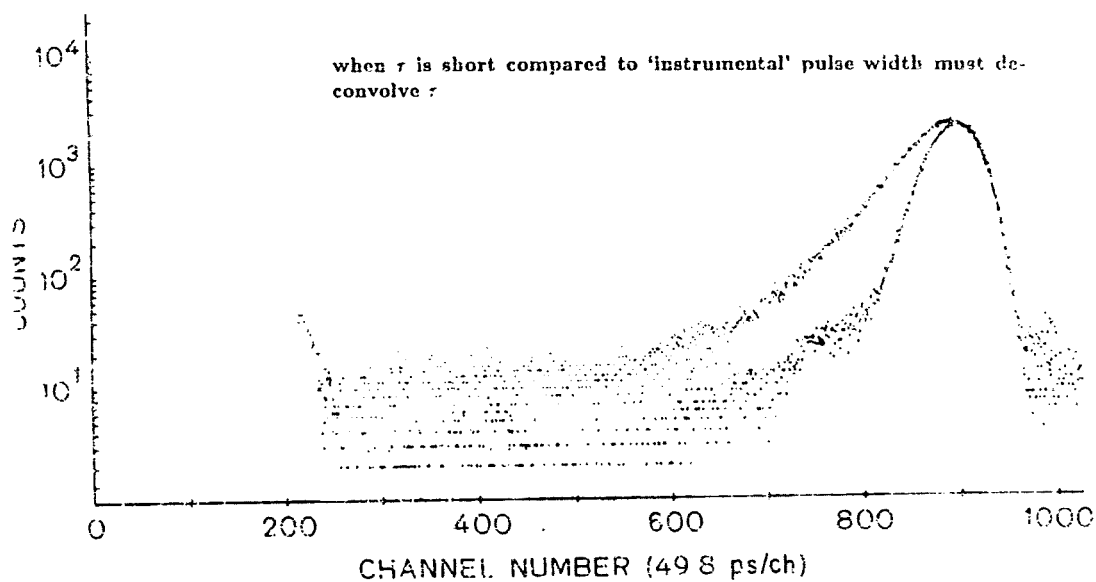
Photoluminescence Decay
 Si:Sb $4.2 \cdot 10^{18}$
 $\tau = 160 \text{ ns} \pm 10\%$



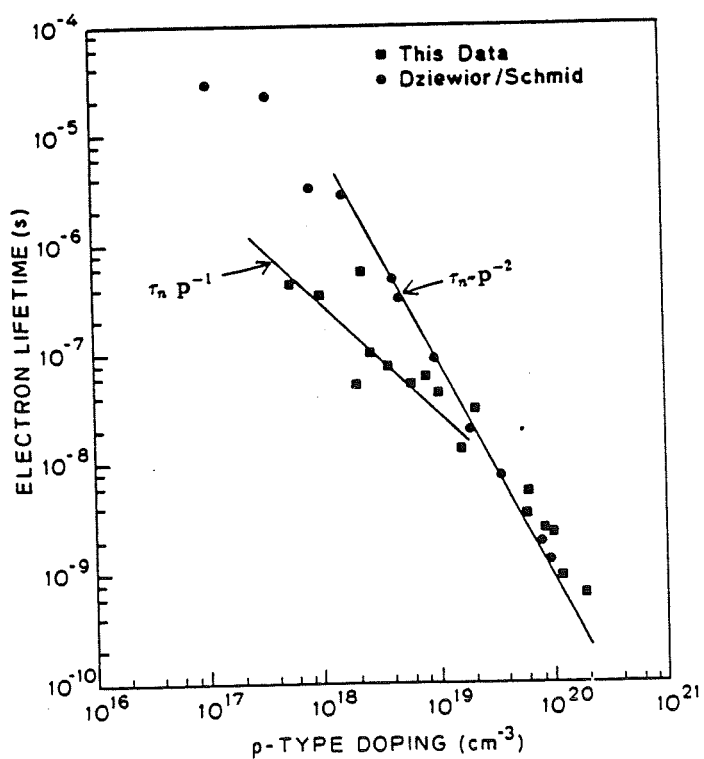
Photoluminescence Decay

Si:Ph $9.2 \cdot 10^{19}$

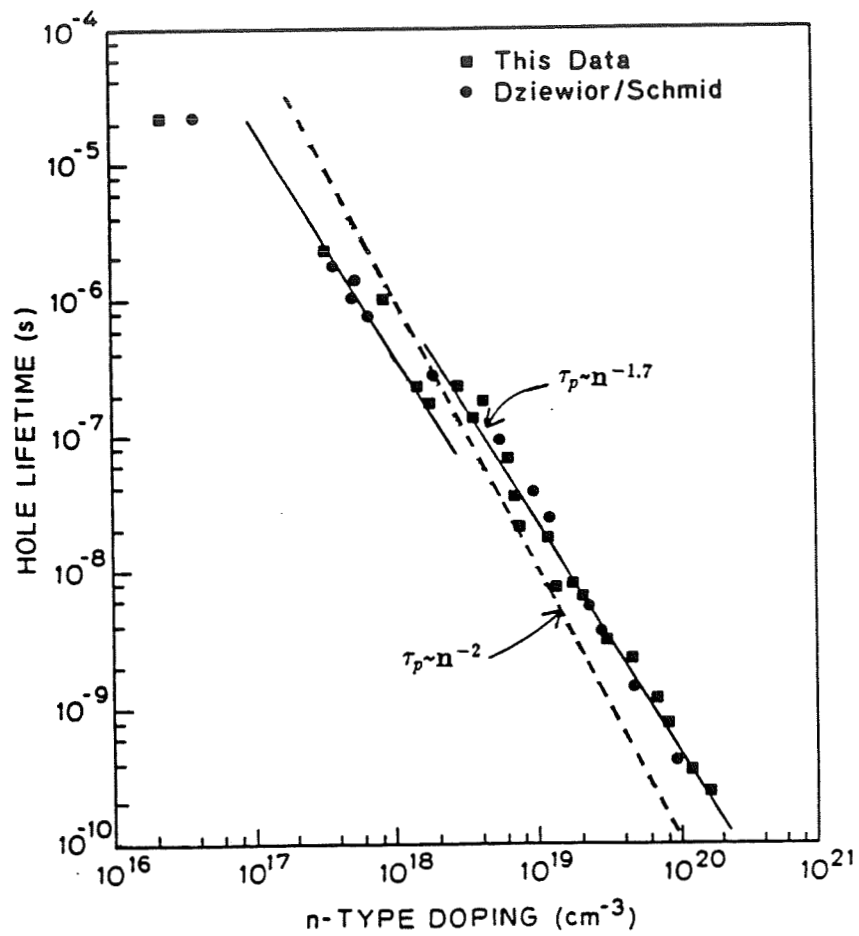
$$\tau = 880 \text{ ps} \pm 20\%$$



Electron Lifetime in p-Type Silicon



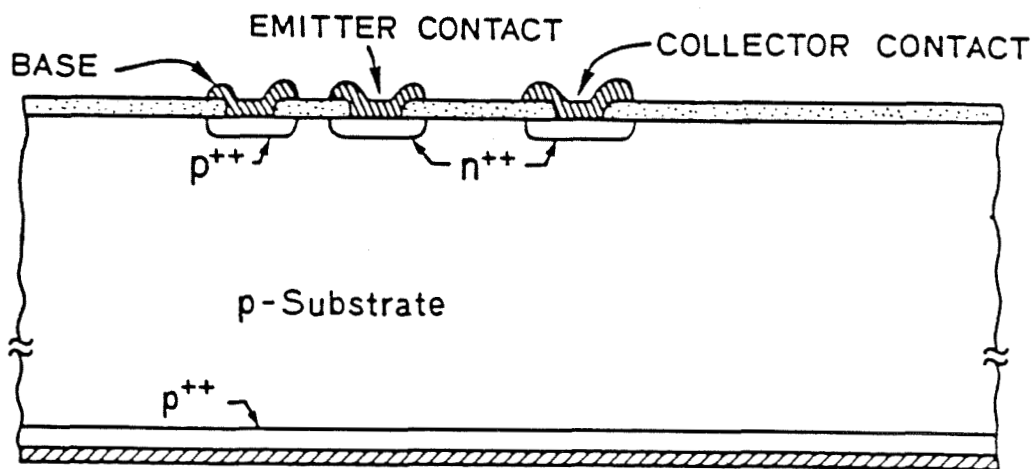
Hole Lifetime in n-Type Silicon



Measurement of Diffusion Length and Mobility

- Diffusion Length (electrons in p^+ Si) $L_n = \sqrt{D_n \tau_n}$
- Mobility (electrons in p^+ Si) $\mu_n = q/kT D_n$

Lateral Transistor to Measure L_n

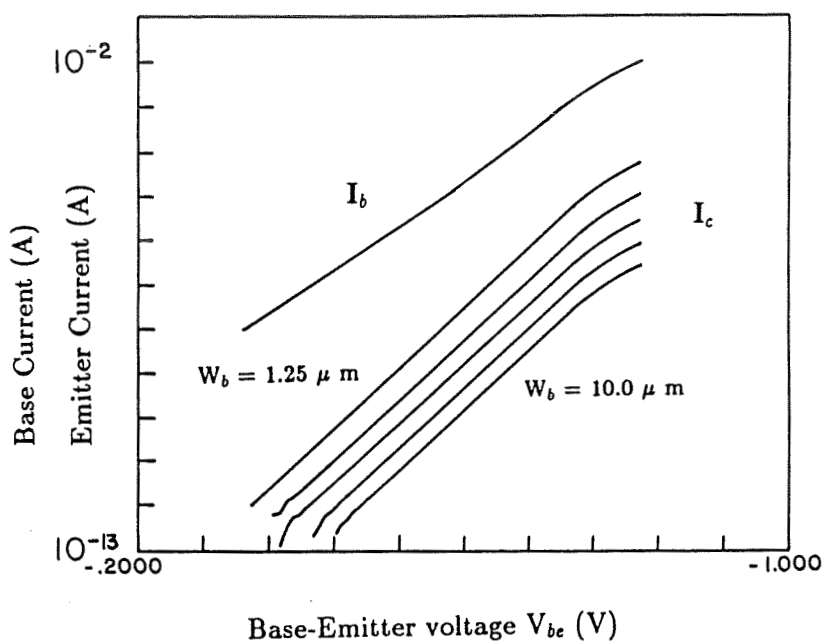


$$I_c = I_{c0}(e^{(qV_{be}/kT)} - 1)$$

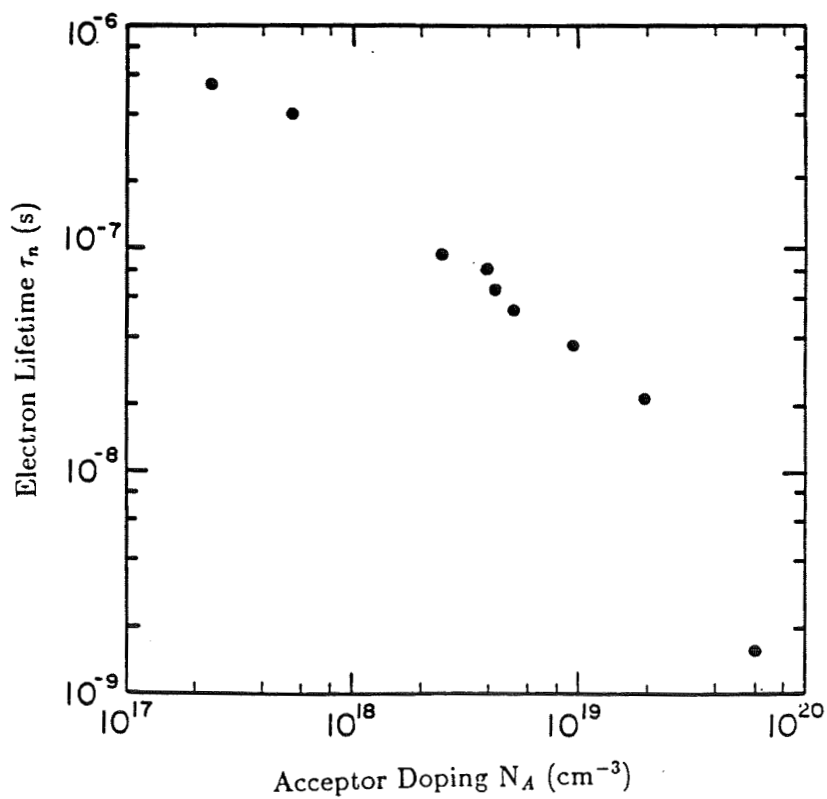
$$I_{c0} = \frac{qAn_0D_n}{L_n}e^{-(W_b/L_n)} \quad \text{when } W_b \gg L_n$$

use similar structures with varying W_b to obtain L_n

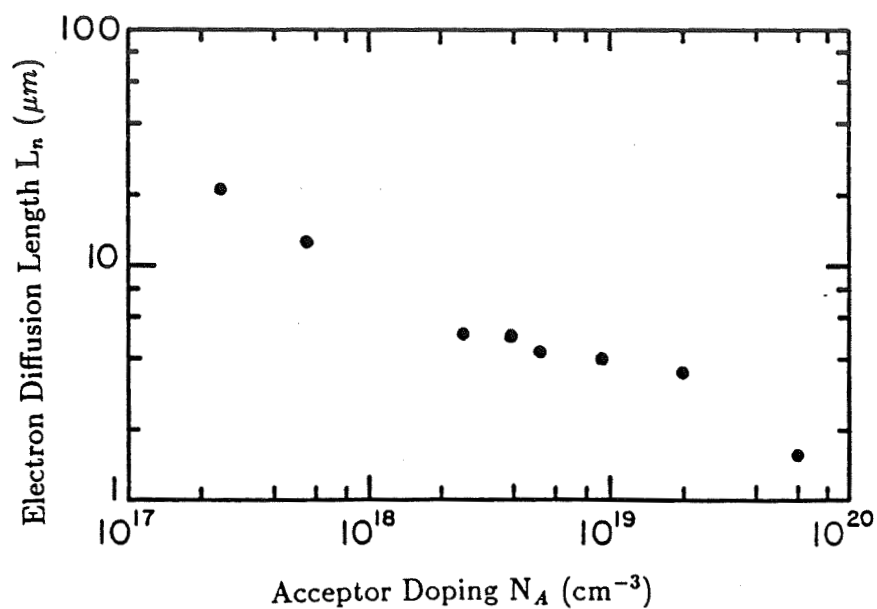
Gummel Plot of Lateral Bipolar Transistors



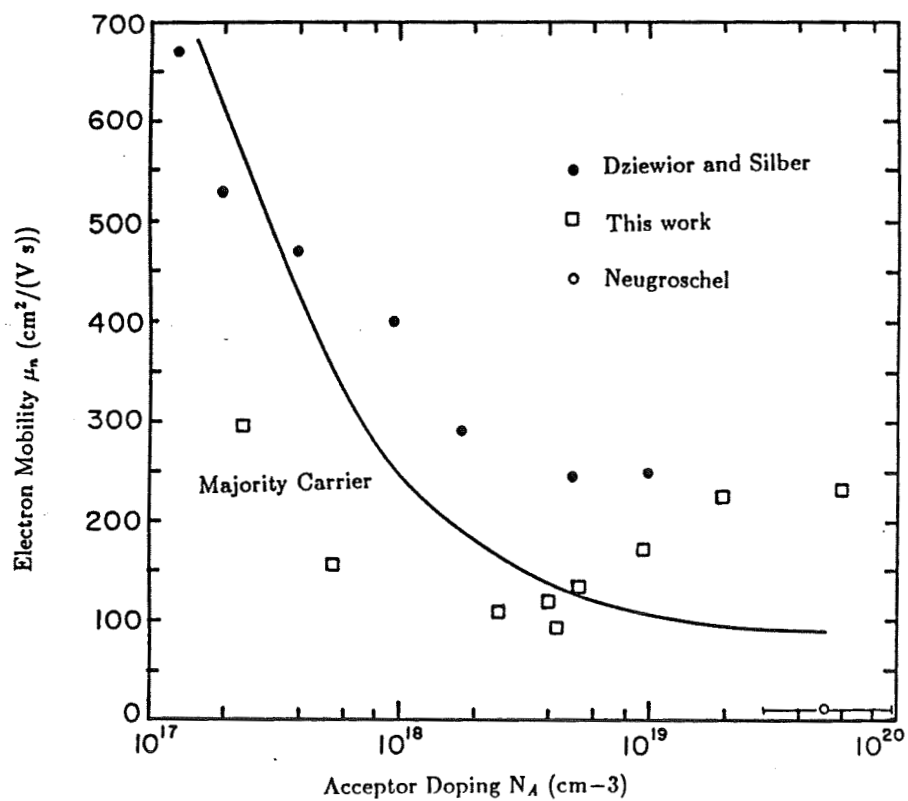
Electron Lifetimes of L_n Samples



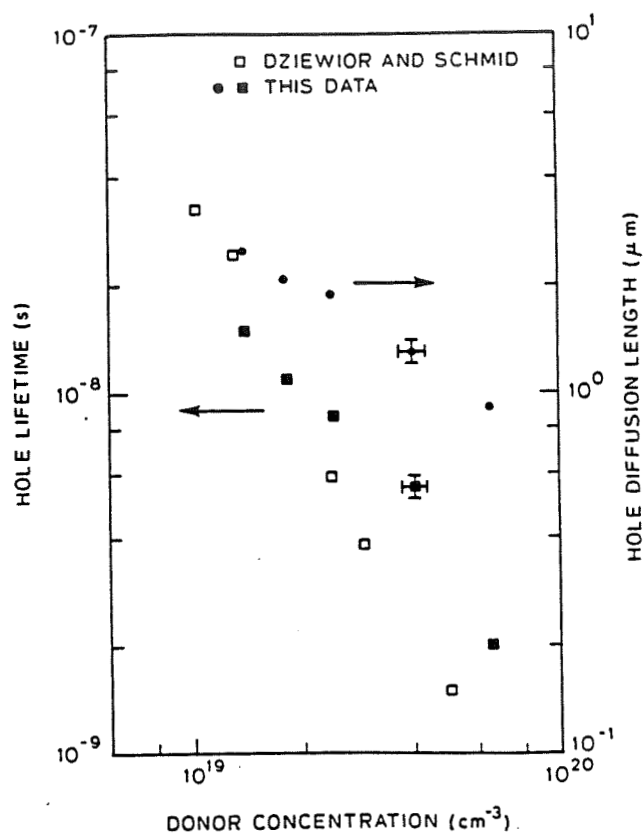
Extracted Electron Diffusion Lengths



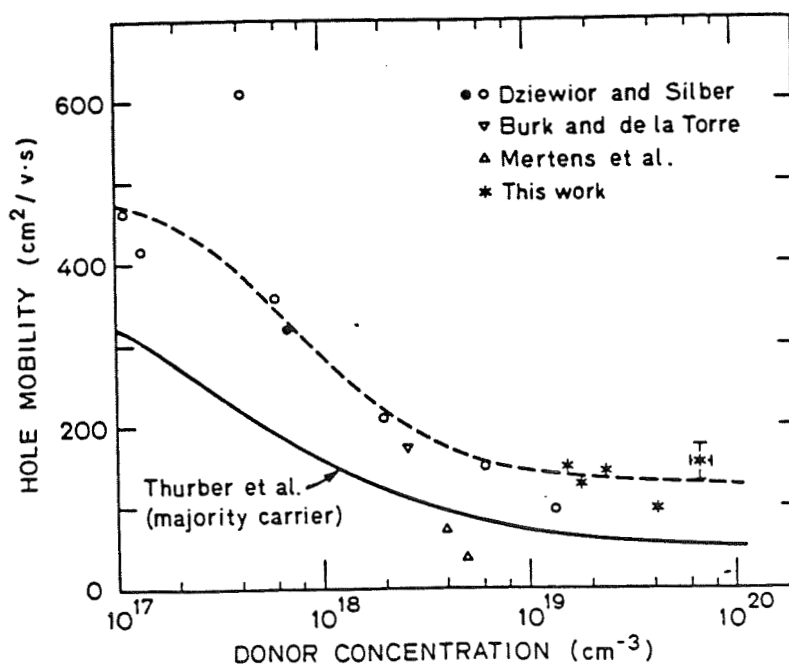
Electron Mobility at 300°K



L_p and τ_p in Heavily Doped Epitaxial Silicon



Hole Mobility in P epi Silicon



Conclusions

Lifetime in heavily doped Si

- first comprehensive measurements of τ_n , τ_p in *processed* heavily doped Si
- τ measurements extended into 10^{20} cm^{-3} doping range
- photoluminescence decay technique suitable and accurate
- τ_n in p^+ Si
 - ‘standard’ τ_n dependence with N_A^{-2} accurate in very limited range
 - lifetime modeled best by sum of inverse plus inverse square dependence on N_A
- τ_p in n^+ Si
 - previously observed τ_p dependence verified
 - use of N_D^{-2} dependence inadequate for wide doping range
 - data suggests better fit lifetime dependence of approximately $N_D^{-1.7}$

Diffusion Length and Mobility Measurement

- lateral transistor test structure used to measure L_n , L_p
- measurement of lifetimes allows extraction of μ_n , μ_p
- extraction of μ_n , μ_p in 10^{19} range shows that minority carrier mobilities exceed majority carrier mobilities

POINT CONTACT SILICON SOLAR CELLS

STANFORD UNIVERSITY

R. M. Swanson

The point contact cell has recently demonstrated 22 percent conversion efficiency at one sun and 27.5 percent at 100 suns. This cell derives its high efficiency from a synergistic combination of:

- Light trapping between a texturized top surface and a reflective bottom,
- Thin, high resistivity, high lifetime base,
- Small point contact diffusions, alternating between n-type and p-type in a polka-dot pattern on the bottom, and
- Surface passivation on all surfaces between contact regions.

The following figures are described below:

Figure 1: Light trapping is caused by the diffuse nature of scattering from a texturized surface. If a photon is not absorbed upon reaching the back surface it is reflected of the back surface reflector. If it is still not absorbed by time it reaches the top there is a very high probability (about 88 percent) that it will be beyond the angle for total internal reflection and hence will be reflected back into the cell.

Figure 2: For high efficiency it is necessary to reduce recombination as much as possible. This is to provide for:

- Collecting as large a fraction of the photo-generated carriers as possible,
- Generating as large a voltage (which goes exponentially in the p-n product) as possible, and
- Producing as much conductivity modulation in the base, and hence reducing base voltage drop, as much as possible. The point contact cell reduces recombination by passivating the surfaces with SiO_2 , using high lifetime float-zone silicon, and reducing the metal-semiconductor contact fraction through the point contact scheme.

¹This work supported in part by the Electric Power Research Institute and the Department of Energy through Sandia National Laboratories.

Figure 3: A three dimensional model has been developed to explore the potential of the cell and optimize the design. Important findings are:

- The contact spacing must be rather small to prevent excessive losses through base spreading resistance at the contact diffusions,
- The cell must be thin, in the 60 to 100 μm range,
- The base lifetime must be over 500 μsec ,
- The surface recombination velocity must be less than 10 cm/sec, and
- The cell is capable of efficiencies of around 29 percent at 27 °C if the above conditions are met.

Figure 4: This figure shows the structure of the test cells currently being made.

Figure 5: This table illustrates the importance of texturizing for improving the short circuit current. Salient one sun parameters are shown.

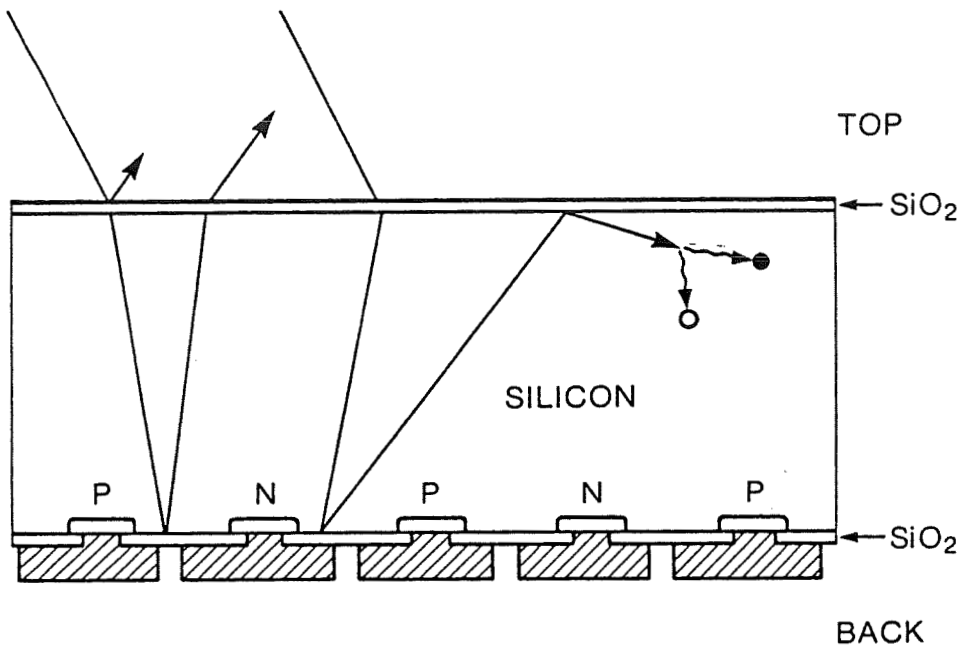
Figure 6: The spectral responsivity of a texturized and untexturized cell is shown. At shorter wavelengths the texturizing has reduced the reflectivity, resulting in improved response. Near the bandgap, however, the response has been dramatically increased due to light trapping.

Figure 7: The internal quantum efficiency is essentially unity until near the bandgap, where competing absorption mechanisms, such as absorption in the back surface mirror, become comparable to photo-absorption.

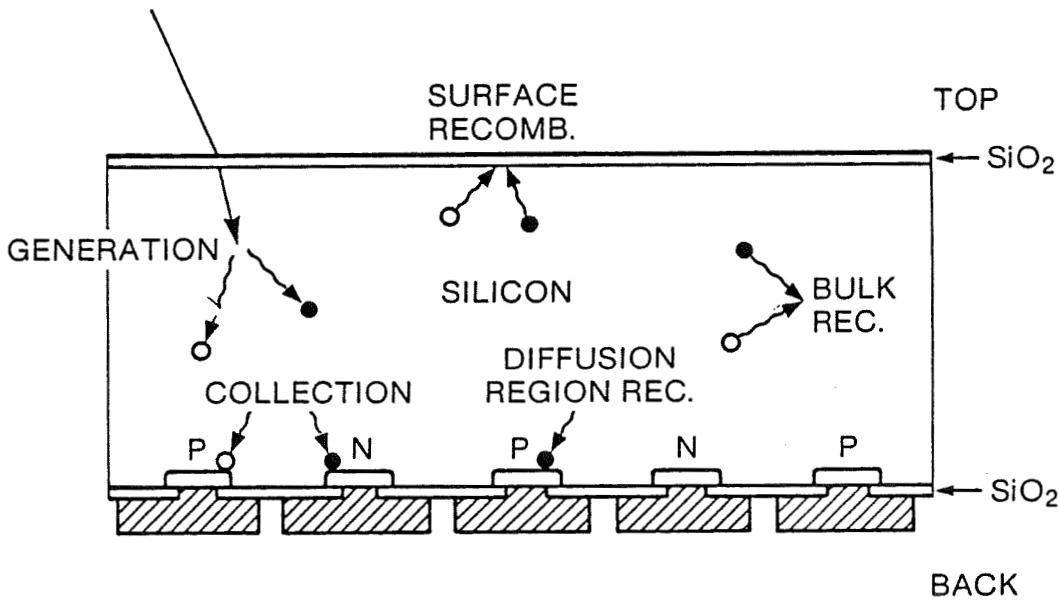
Figure 8: This slide shows the measured open circuit voltage and fill factor of a 113 μm texturized cell.

Figure 9: The measured efficiency of the cell from the previous slide is presented. The one sun efficiency is 22 %, increasing to 27.5 % at 100 suns. The major portion of the drop off above 100 suns is due to metal series resistance; however, a significant portion results from a decrease in internal quantum efficiency at high intensity due to Auger recombination in the dense electron-hole plasma generated by the light. A thinner cell will reduce this effect.

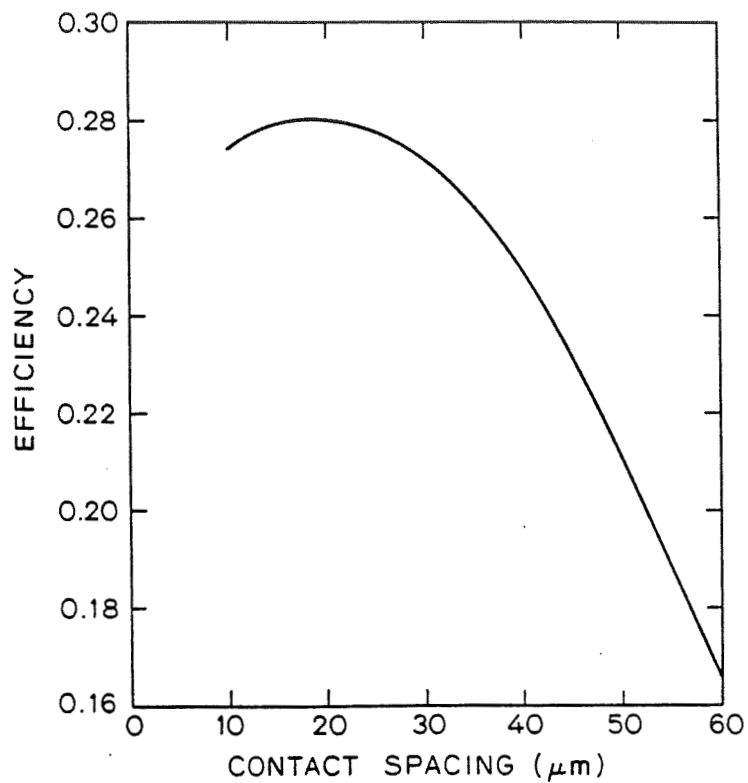
Light Trapping



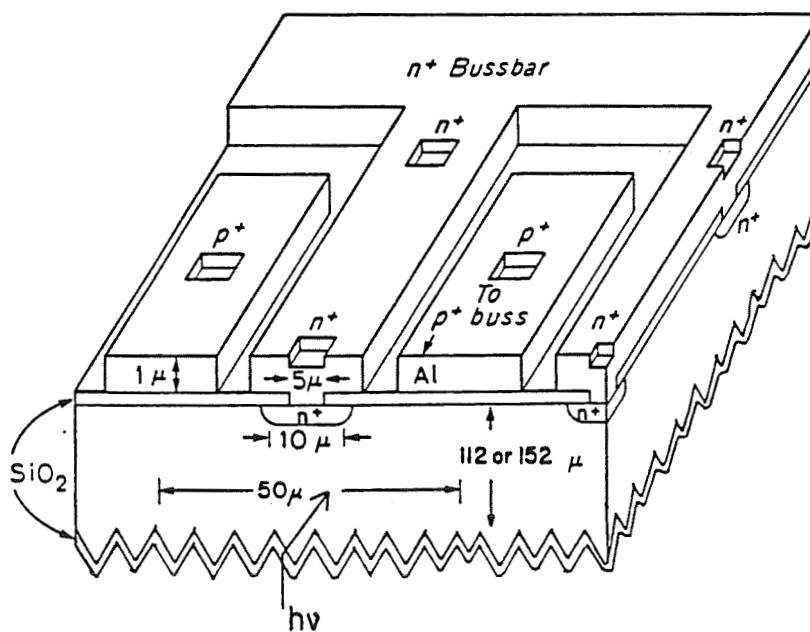
Collection and Recombination



Efficiency Versus Contact Spacing Derived from Three-Dimensional Model



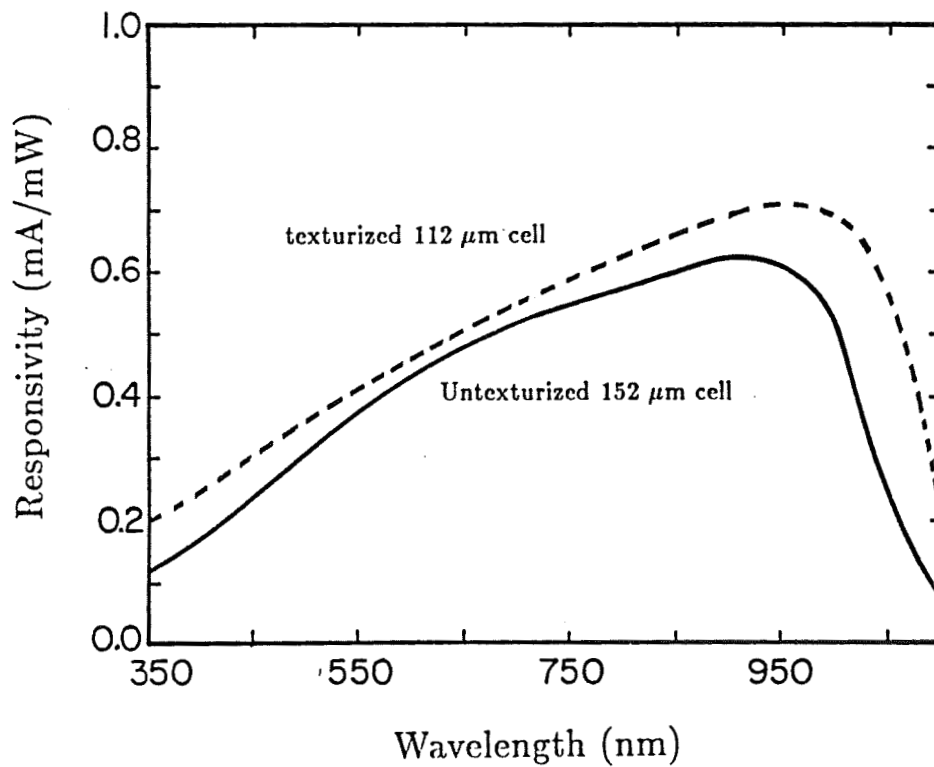
Structure of Test Cells Currently Being Made



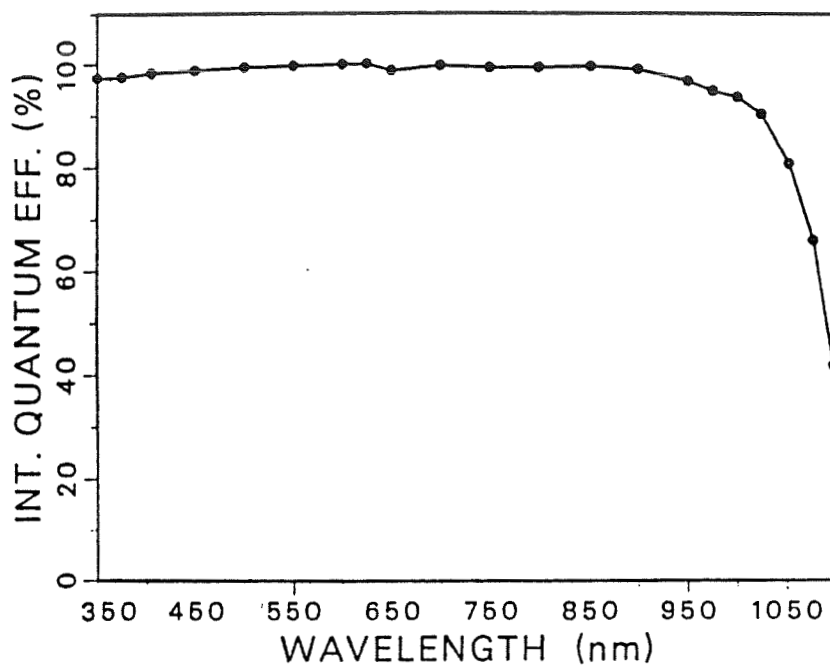
Importance of Texturizing for Improving the Short Circuit Current

One Sun Results AM1.5 100 mW/cm ²								
Cell	Thickness	Texturized	Efficiency	V _{oc}	J _{sc}	V _{mp}	Fill Factor	Temp
11-3B	112 μ m	Yes	22.2%	.681 V	41.5 mA/cm ²	.582 V	.786	24 °C
11-1A	152	No	18.5%	.678	35.0	.570	.778	26

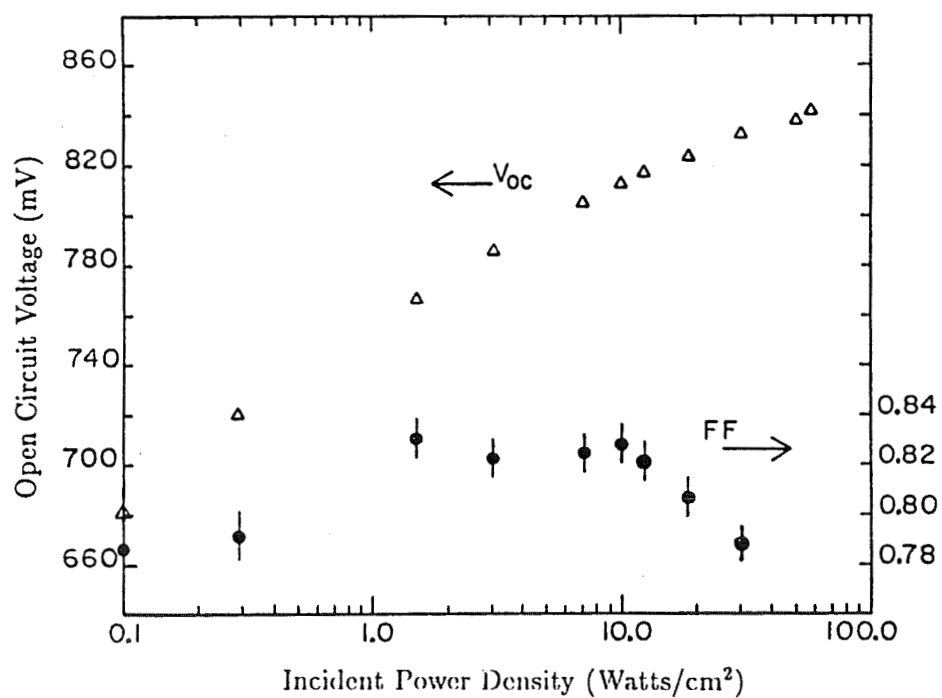
Spectral Responsivity of a Texturized and Untexturized Cell



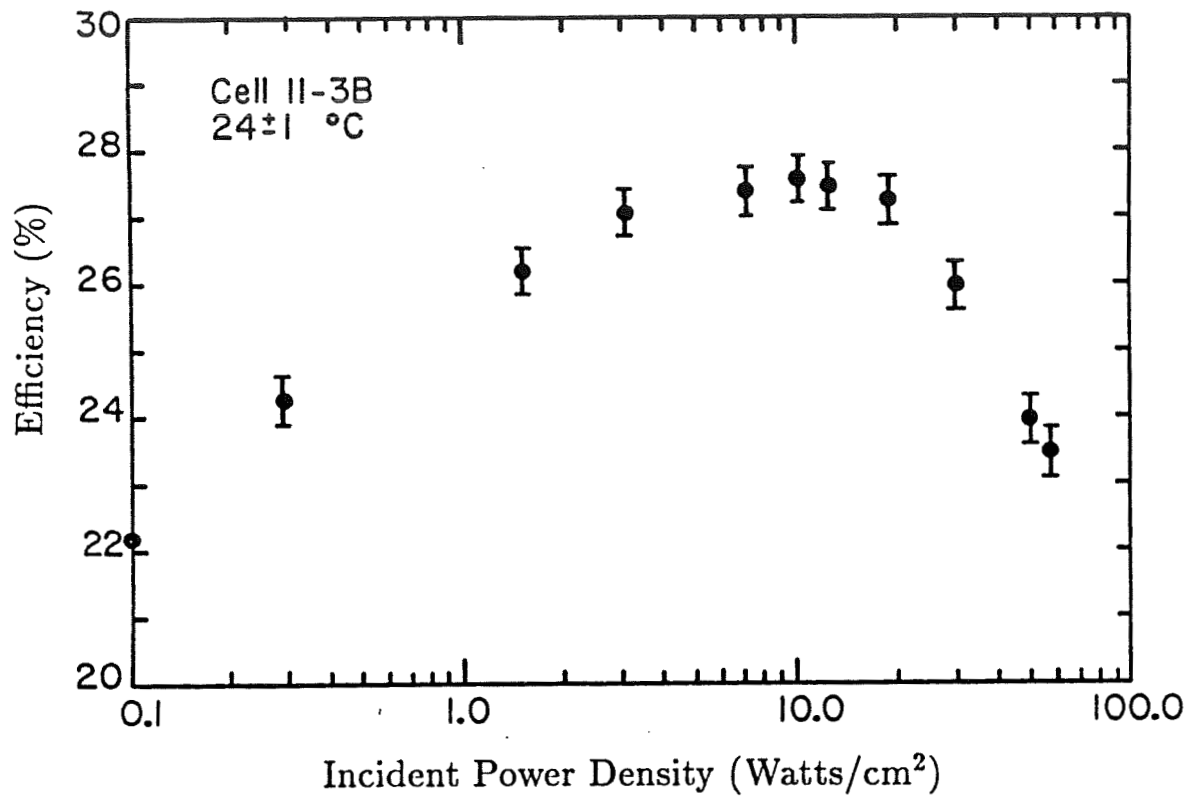
Internal Quantum Efficiency Versus Wavelength
(Stanford Point Contact Cell FT 11-3B)



Measured Open Circuit Voltage and Fill Factor
of a 113 μm Texturized Cell



Measured Efficiency of the Cell (from Figure 8)



SiN_x PASSIVATION OF SILICON SURFACES

UNIVERSITY OF WASHINGTON

L. C. Olsen

Objectives and Approach

OBJECTIVES

- RELATE SURFACE DENSITY TO SUBSTRATE DOPANT CONCENTRATION
- SURFACE CHARACTERIZATION OF HIGH EFFICIENCY n^+/p and p^+/n SILICON CELLS
- IDENTIFY DOMINANT CURRENT LOSS MECHANISMS IN HIGH EFFICIENCY CELLS

APPROACH

- MEASURE DENSITY OF STATES ON HOMOGENEOUSLY DOPED SUBSTRATES WITH HIGH FREQUENCY C-V AND $\text{Al/SiN}_x/\text{Si}$ STRUCTURES
- INVESTIGATE DENSITY OF STATES AND PHOTORESPONSE OF HIGH EFFICIENCY N^+/P and P^+/N CELLS.
- CONDUCT I-V-T STUDIES TO IDENTIFY CURRENT LOSS MECHANISMS IN HIGH EFFICIENCY CELLS

Presentation Outline

1. SURFACE PASSIVATION

- SiN_x DEPOSITION
- HOMOGENEOUSLY DOPED SUBSTRATES
- PHOTORESPONSE OF N^+/P AND P^+/N CELLS

2. SOLAR CELL STUDIES

- MINP CELL WITH TEXTURED SURFACE

3. CURRENT LOSS MECHANISMS

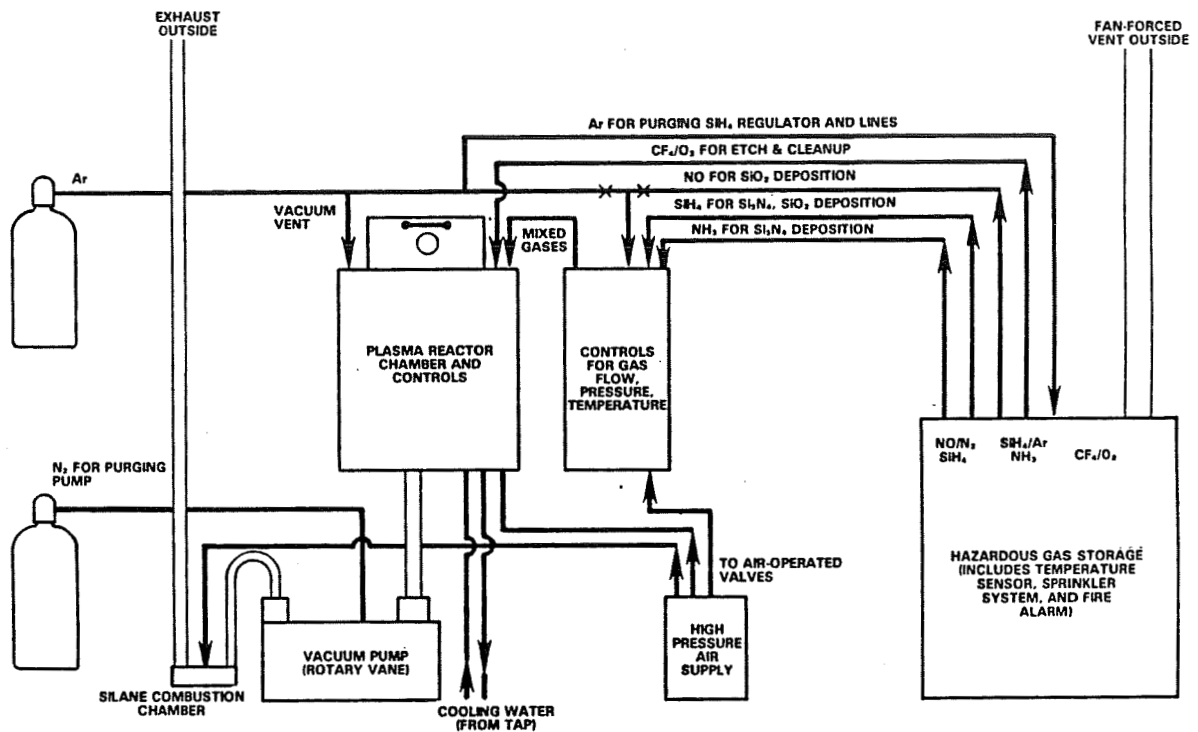
- LIGHT INDUCED CURRENT LOSS MECHANISM
- Mg MIS CONTACTS
- NEUTRON ACTIVATION

4. FUTURE WORK

- PASSIVATION OF P^+/N CELLS
- FINAL REPORT CONCERNING SiN_x PASSIVATION OF SILICON

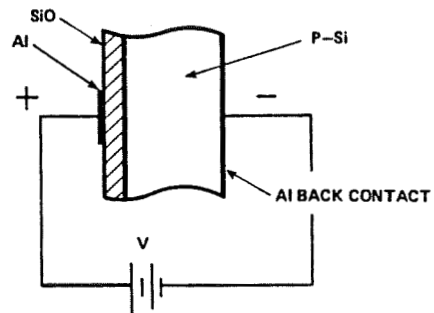
PRECEDING PAGE BLANK NOT FILMED

Schematic of PECVD System

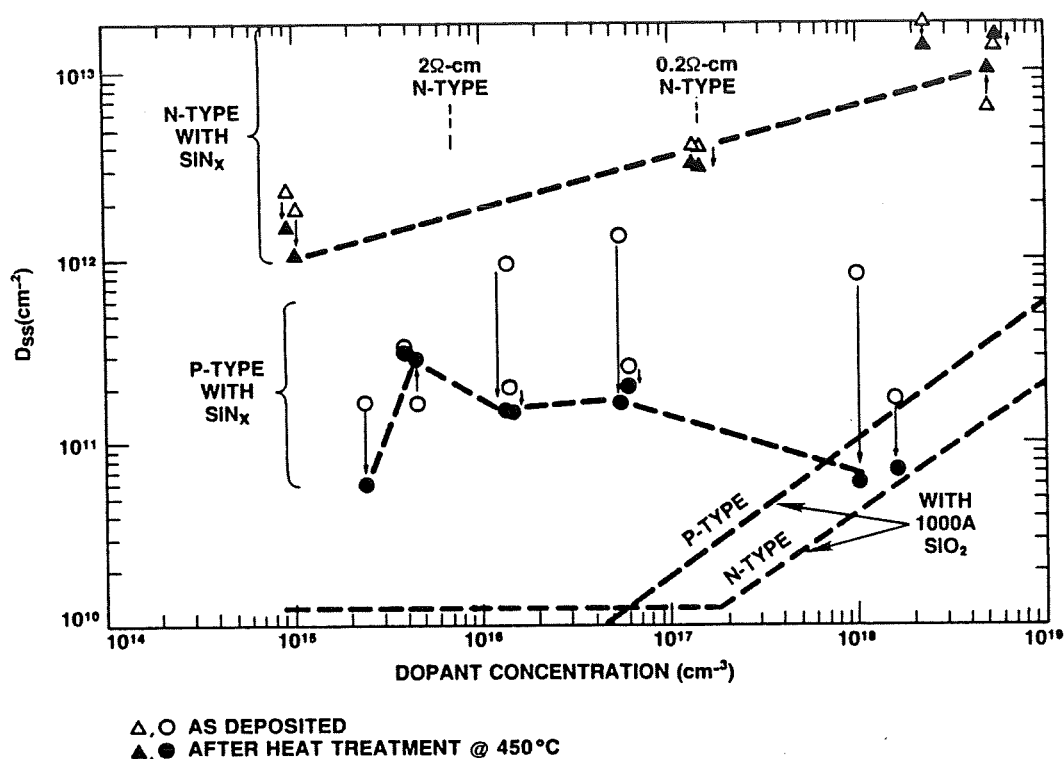


Fabrication of Al/SiN_x/Si MIS Structures

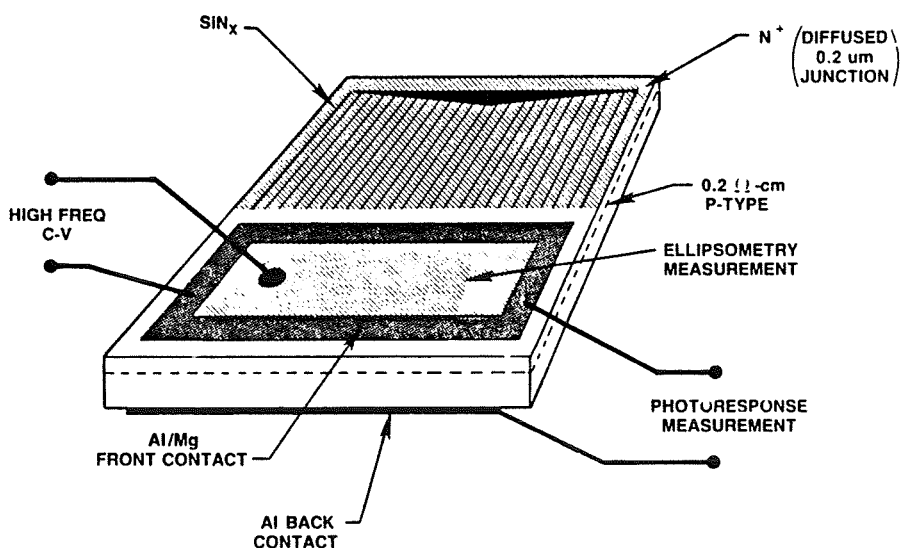
- CLEAN SILICON SUBSTRATES WITH RCA PROCESS
- SUBJECT SUBSTRATE TO NITRIDING STEP (LOW RF POWER WITH NH₃ @ 70 SCCM)
- DEPOSIT ≈ 100 Å SiN_x WITH SUBSTRATE AT 270°C AND RF POWER @ 212 W/cm²
- DEPOSIT ≈ 600 Å SiN_x WITH POWER @ 1225 W/cm²
- DEPOSIT ALUMINUM



Midgap Interface State Density Versus Dopant Concentration

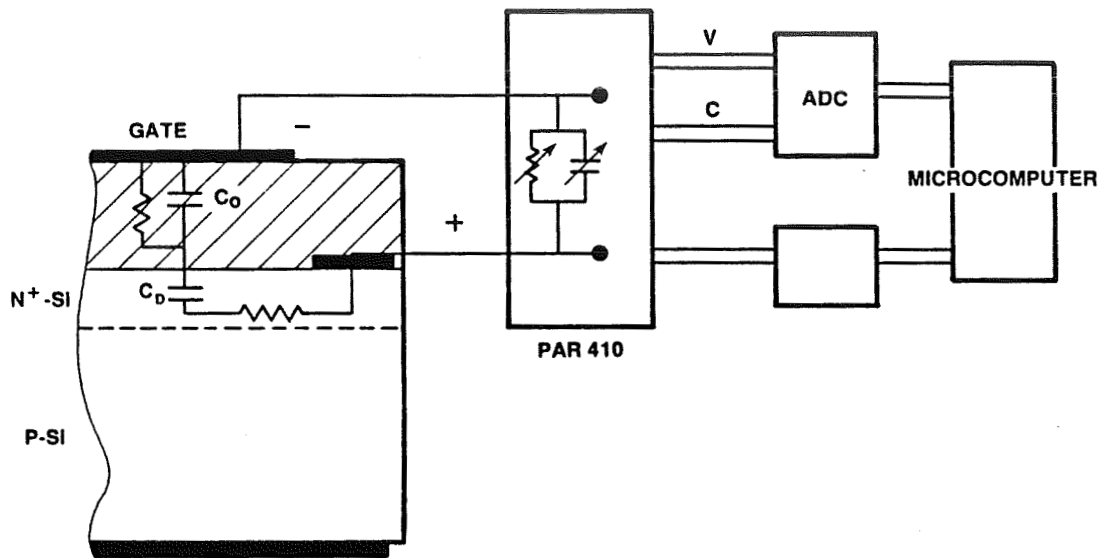


Device Structure for Surface Recombination Study

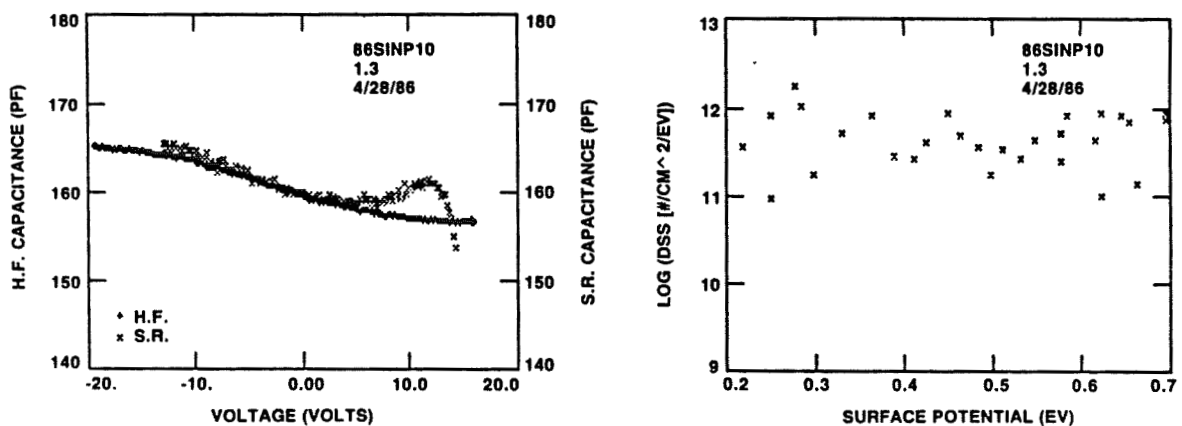


HIGH-EFFICIENCY SOLAR CELLS

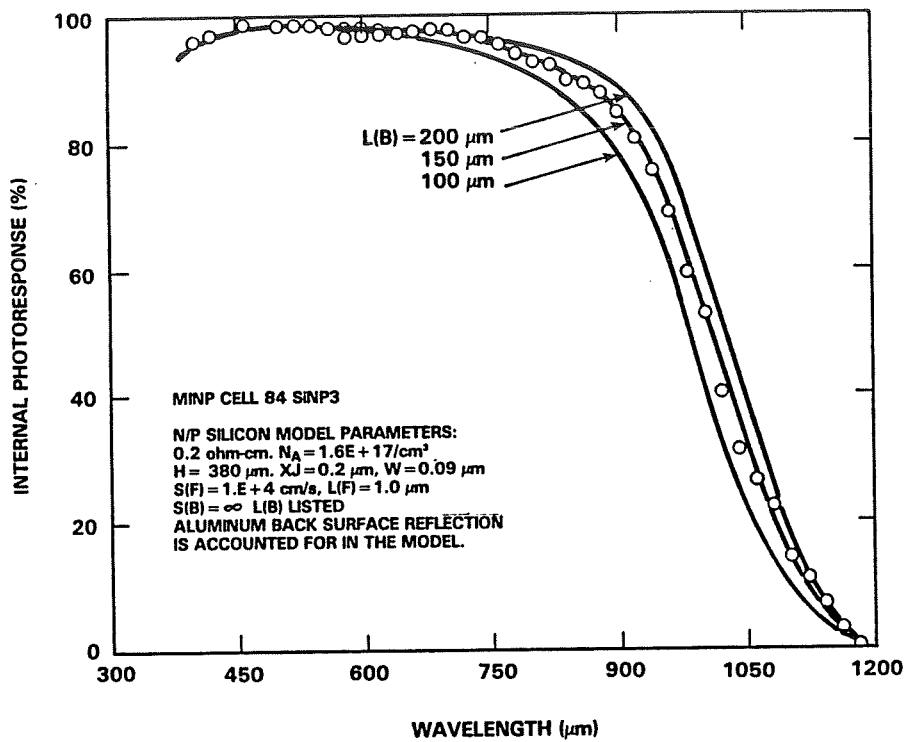
C-V Measurement of Interface Density at N^+ Surface of N^+/P Cell



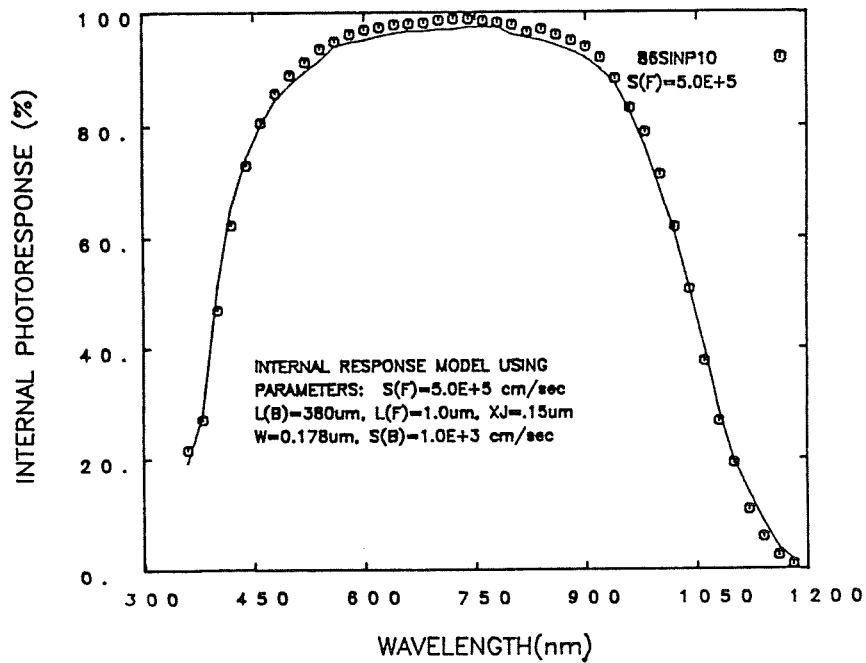
Density of States of Surface of P^+/N Cell



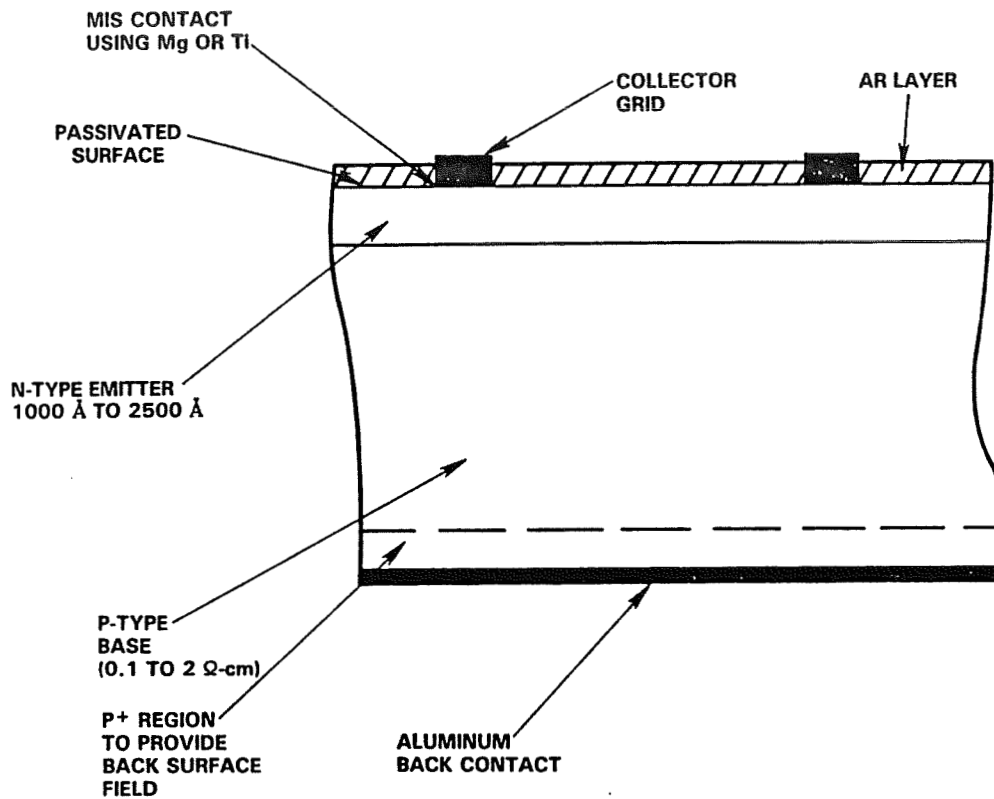
Internal Photoresponse for 0.2 ohm-cm MINP Cell



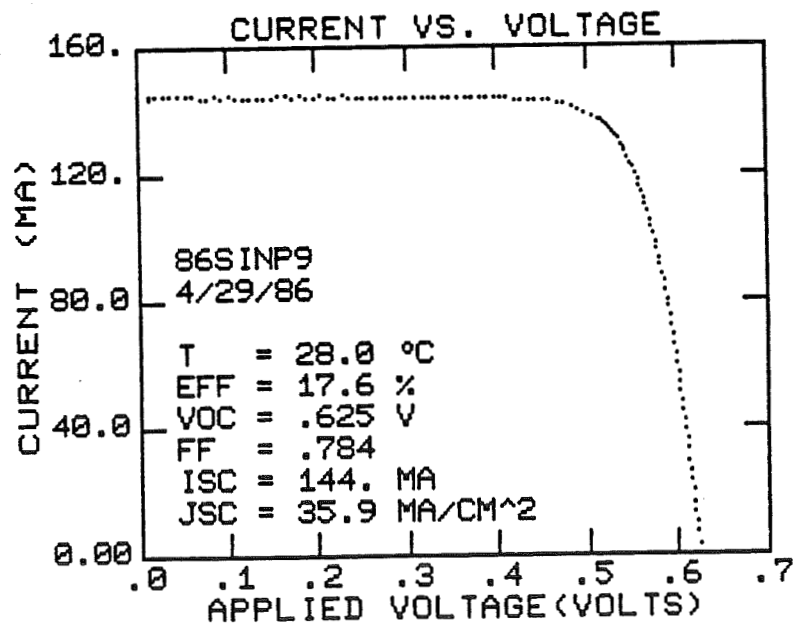
Internal Photoresponse for 0.2 ohm-cm P^+/N Cell



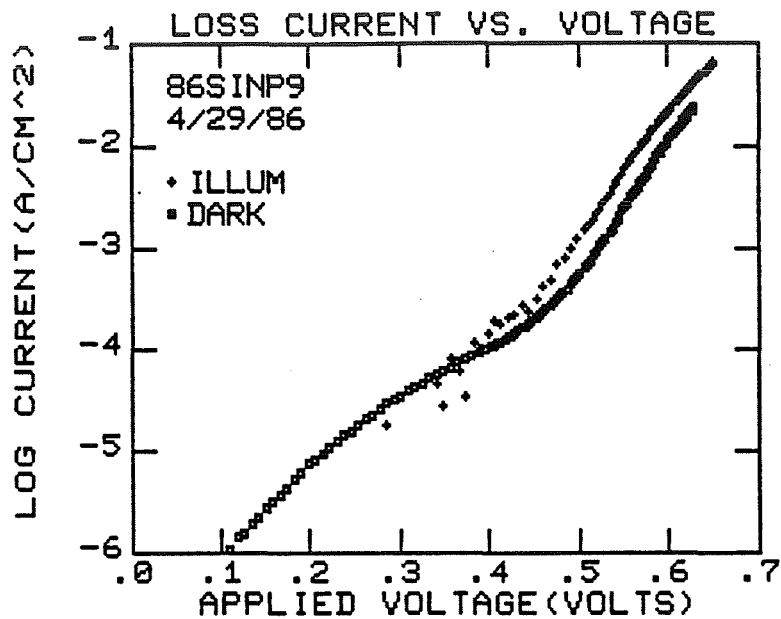
MINP Cell Concept



AM1 Characteristics of Textured MINP Cell



Loss Current Versus Voltage for Illuminated and Dark Characteristics of Textured MINP Cell



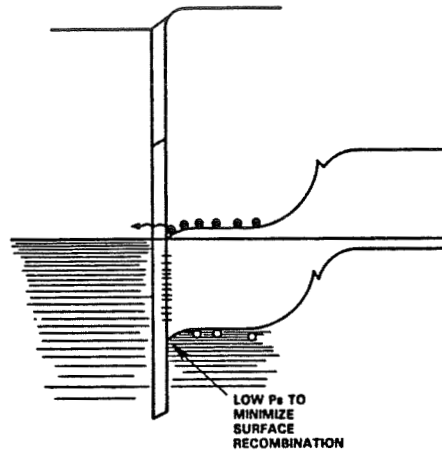
Neutron Activation Measurement of Impurity Concentration

SAMPLE	Au (ppma)	Co (ppma)	Sc (ppma)	Hg (ppma)	Fe (ppma)	COMMENT
AS RECEIVED	< 3E-6	< 2E-3	-	< 3E-4	< 2.5	AS RECEIVED FROM WACKER
AFTER DIFFUSION	< 1.6E-5	3.8 E-3	-	< 3E-4	< 2.0	AFTER P-DIFFUSION BY ASEC
84 SINP4	1.2 E-4	11 E-3	4.4 E-3	< 3E-4	< 2.5	DARK: $J_0 = 1.0 \text{ E-13 A/cm}^2$ $n = 1.00$ ILLUM: $J_0 = 2\text{E-11 A/cm}^2$ $N = 1.16$
85 SINP20	5.7 E-5	8.1 E-3	-	30 E-4	< 2.5	$L \approx 35 \mu\text{m}$ CONTAMINATE $\text{D}_2\text{H}_2\text{O}$
85SINP40	9.0 E-5	7.5 E-3	-	< 3E-4	< 2.5	$L \approx 220 \mu\text{m}$ GOOD TRANSLATION

Mg MIS Contact Study

METAL COVERAGE	HIGH VOLTAGE MECHANISM	
	J_0 (A/cm ²)	n
62%	1.5×10^{-12}	1.03
3.6%	1.2×10^{-12}	1.01
1.5%	1.8×10^{-12}	1.03

BASE RESISTIVITY = 0.2 Ohm-cm
JUNCTION DEPTH = 0.2 μ m



DEVELOPMENT OF HIGH-EFFICIENCY SOLAR CELLS ON SILICON WEB

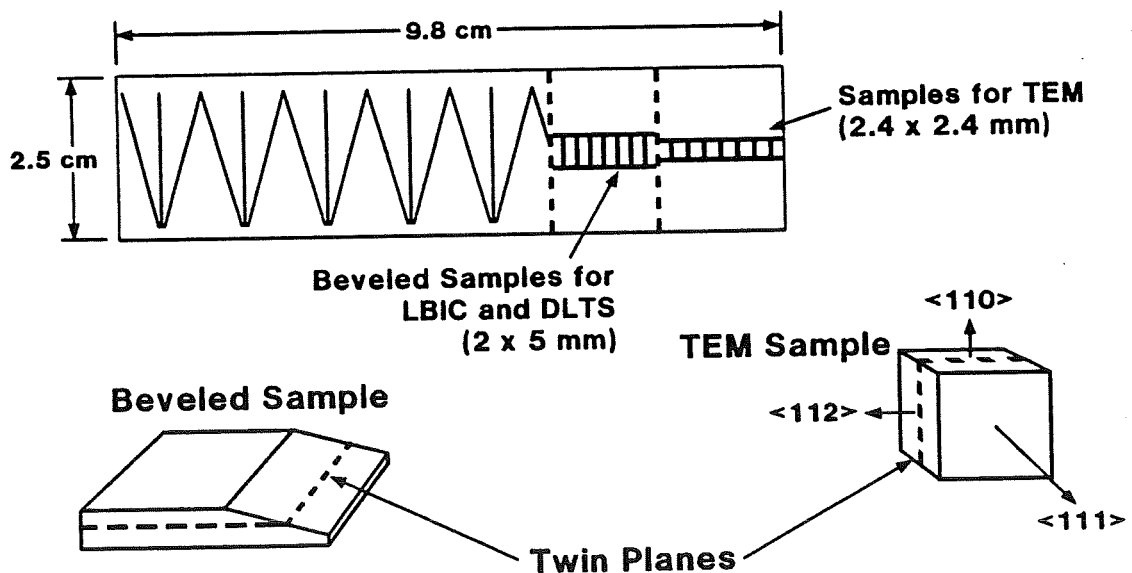
WESTINGHOUSE RESEARCH AND DEVELOPMENT CENTER

D. L. Meier

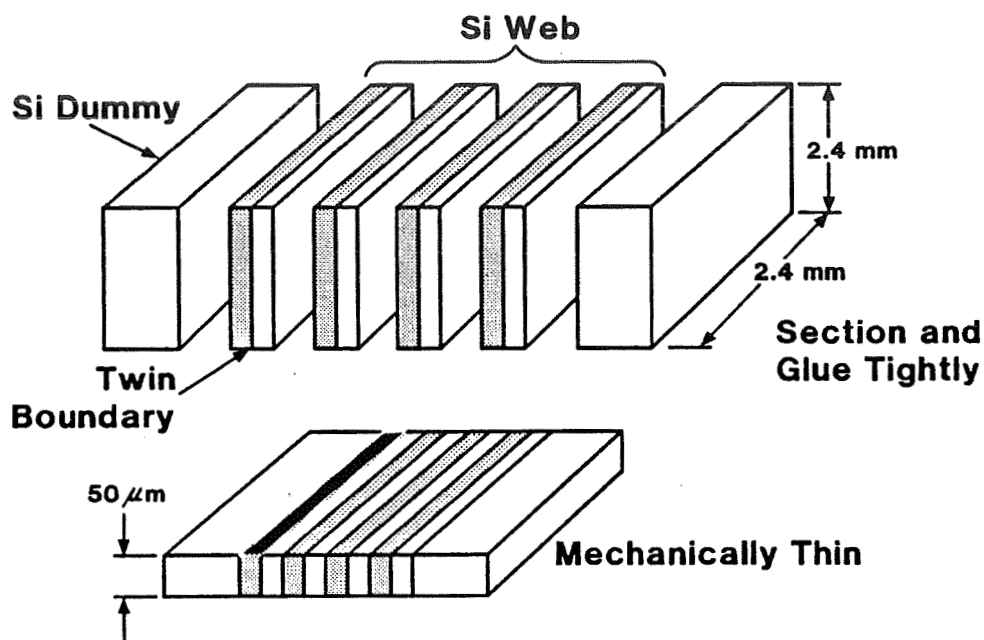
Topics

- **Determination of defect in web silicon which limits minority carrier diffusion length**
- **Passivation of defects by low energy, high dose hydrogen ion implantation**
- **Fabrication of web and float zone cells**

Location of TEM, LBIC, and DLTS Samples in Web Cell

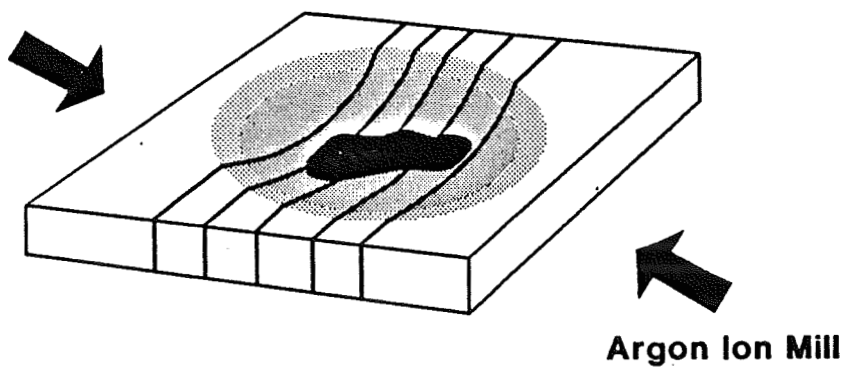


Cross-Sectional TEM Sample Preparation



Cross-Sectional TEM Sample

**FORMATION OF
THIN FOIL AT EDGE OF HOLE**



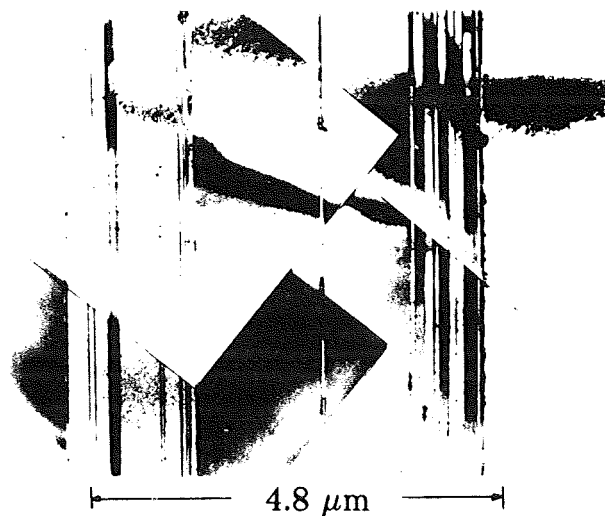
Electrical Parameters of Cells Examined by Cross-Sectional TEM

<u>Cell</u>	<u>L_n (SPV) (μm)</u>	<u>J_{sc} (mA/cm^2)</u>	<u>V_{oc} (V)</u>	<u>FF</u>	<u>η (%)</u>
17C	12	23.4	0.514	0.79	9.5
38A	156	31.0	0.584	0.79	14.9
40C	19	24.3	0.525	0.78	10.0
69A	135	31.2	0.580	0.78	14.3

Notes:

1. Cells have p-base (boron-doped) of nominal 4 ohm-cm resistivity.
2. Cell size is (2.0 x 9.8) cm or (2.5 x 9.8) cm.
3. Cells tested at $100 \text{ mW}/\text{cm}^2$, AM1 spectrum at room temperature.

Cell 40C: Low-Efficiency Twin Plane Region

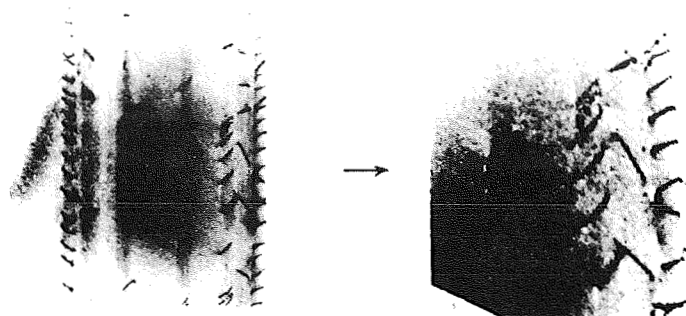


Twin Plane Vertical

Twin Plane Region:
Numerous Alternating Twins

Cell 40C: Low Efficiency

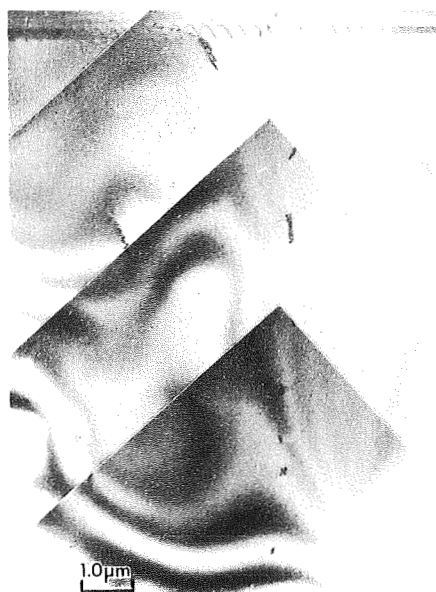
ORIGINAL PAGE IS
OF POOR QUALITY



← 4.8 μm →

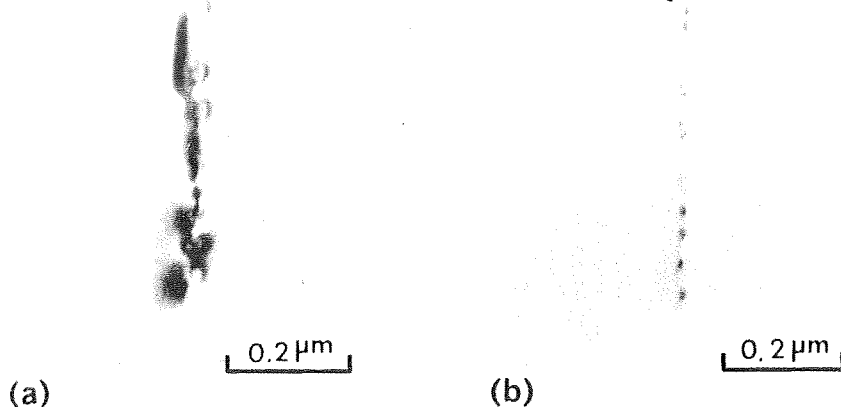
Twin Plane Tilted; Twins Out of Contrast

Numerous Dislocations Adjacent
to Twin Boundaries



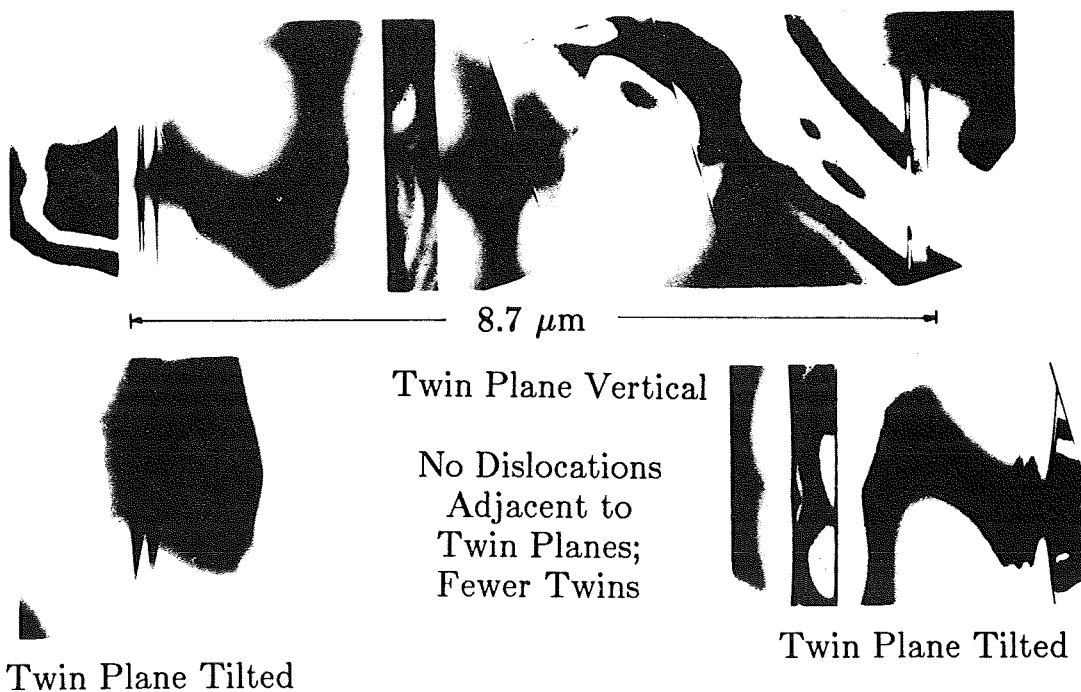
TEM micrograph showing dislocations in the bulk of low-efficiency cell 40C (10.0%). Note large density of dislocations in the heavily twinned region near the top of the micrograph.

ORIGINAL PAGE IS
OF POOR QUALITY



TEM micrograph showing possibility of impurity decoration at dislocations in low-efficiency cell 40C (10.0%): (a) two-beam dynamical condition showing strain fields, and (b) weak quasi-kinematical condition with strain fields minimized.

Cell 69A: High Efficiency

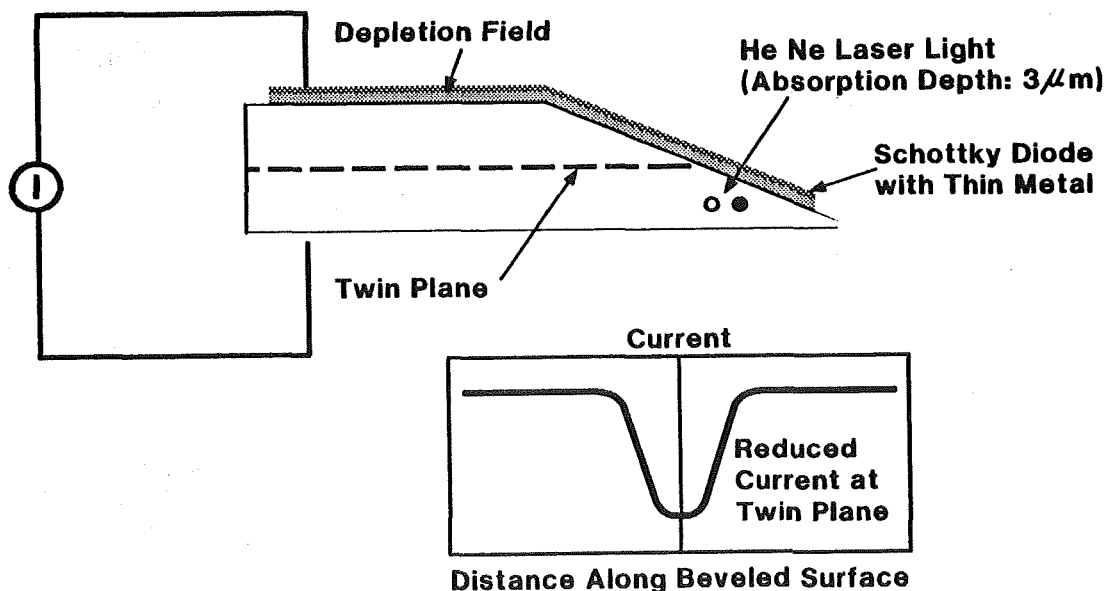


Summary of TEM Observations with Electrical Parameters

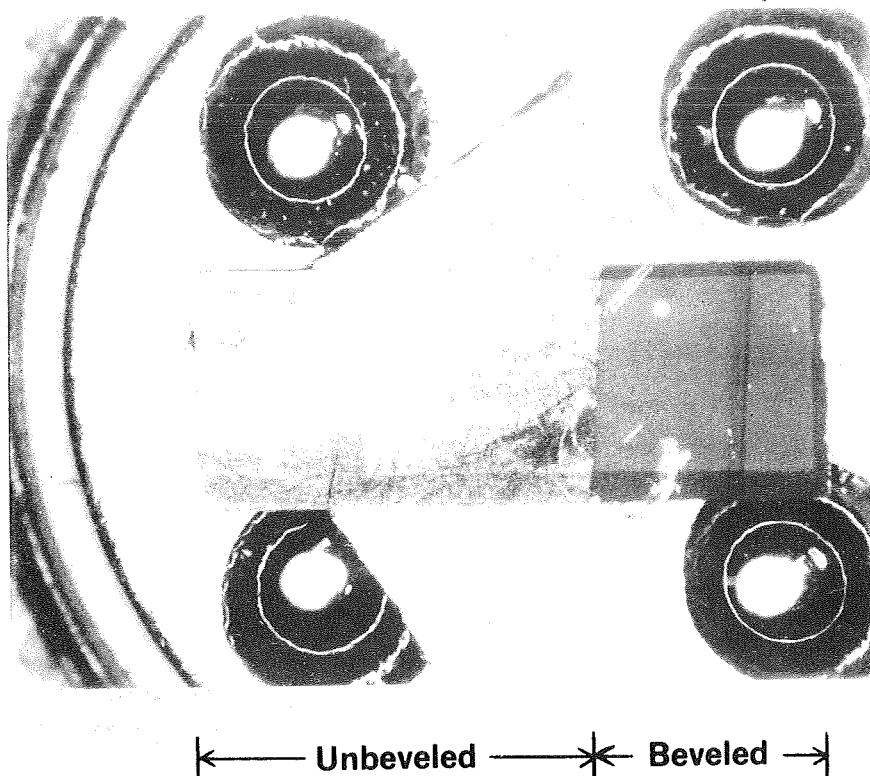
Cell	L_n (SPV) (μm)	η (%)	Number of Twin Boundaries	Width of Heavily Twinned Region (μm)	Dislocation Density (cm^{-2})	
					Twinned Region	Bulk
17C	12	9.5	27	5.7	2×10^8	$\approx 10^6$
38A	156	14.9	5	3.6	None Observed	One Observed
40C	19	10.0	41	4.8	3×10^8	$\approx 10^6$
69A	135	14.3	13	8.7	None Observed	None Observed

Note: Detection limit for dislocation density by TEM is $10^4 - 10^5 \text{ cm}^{-2}$.

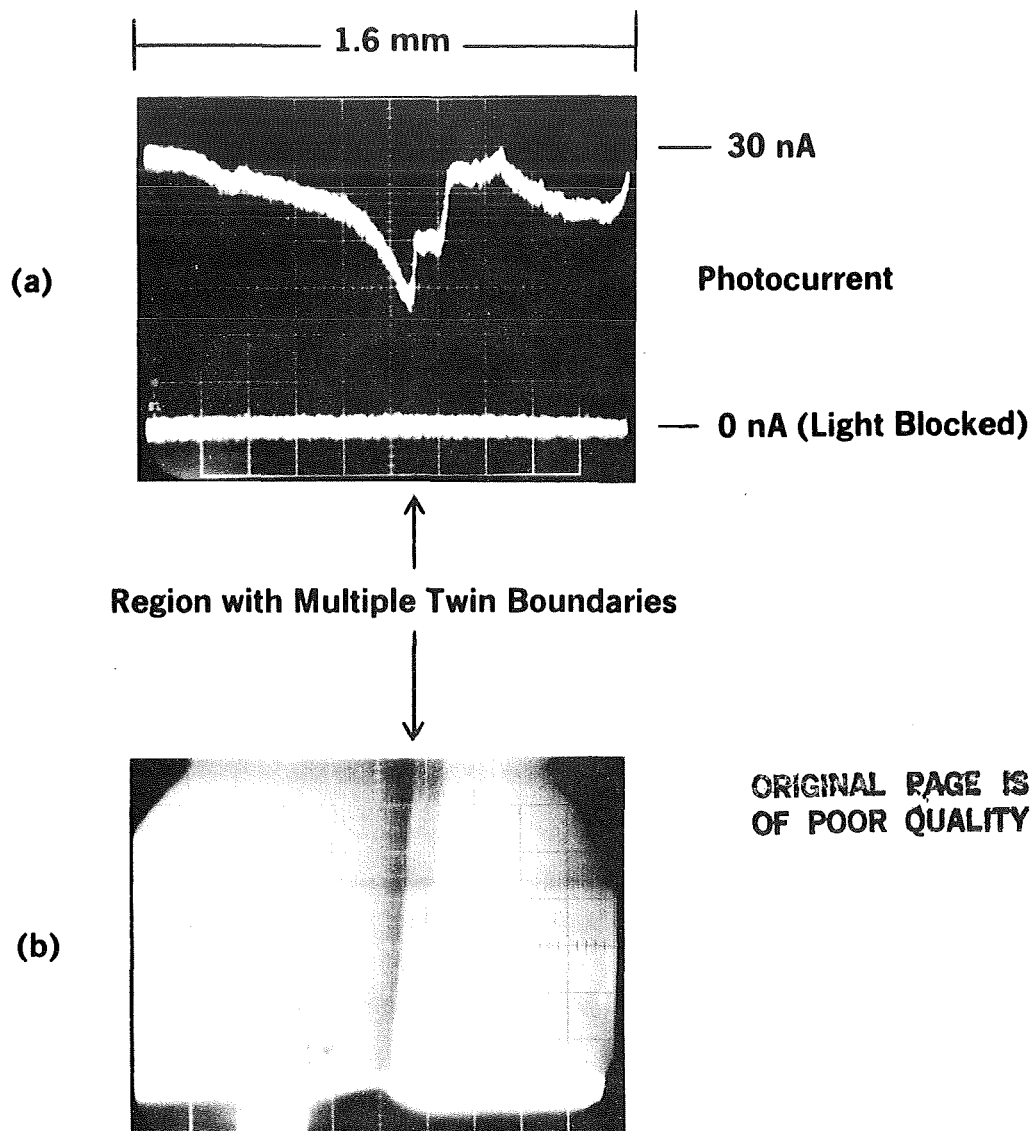
Sensing the Electrical Activity of the Twin Plane with Laser-Induced Current



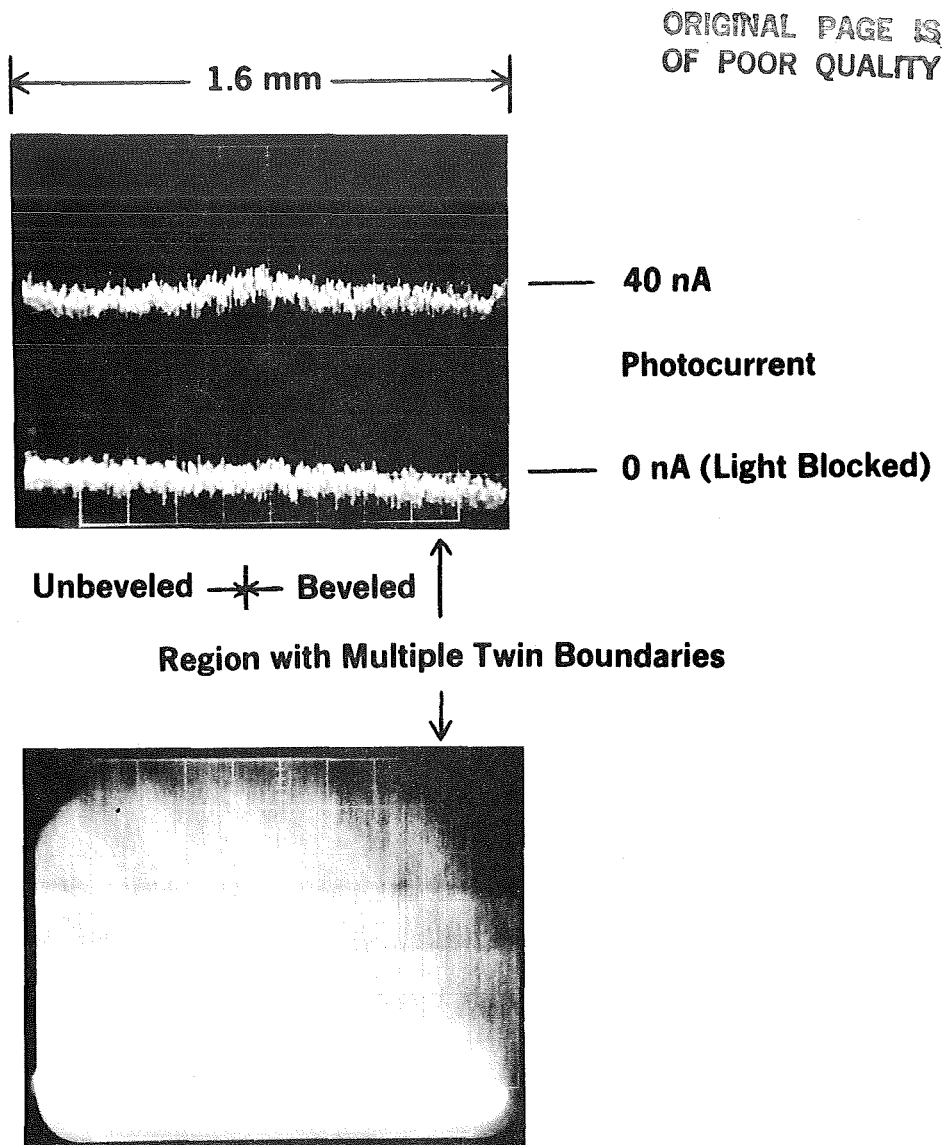
Multiple Twin Boundaries



Photograph of a (2 × 5) mm beveled sample prepared from cell 17C (9.5%) and mounted on a TO-5 header. Shown are the area of the sample covered with semitransparent metal to form the Schottky diode and the lines formed where the twin boundaries emerge from the beveled surface. (Sample #1, Run TP-10)



LBIC scans of beveled sample prepared from cell 17C (9.5%):
 (a) line scan showing 50% decrease in photocurrent in the vicinity of the twinned region as the laser beam is scanned down the beveled surface across the twin boundaries; (b) area scan showing uniform dark bands associated with excessive recombination within and near the twinned region. (Sample #1, Run TP-10)

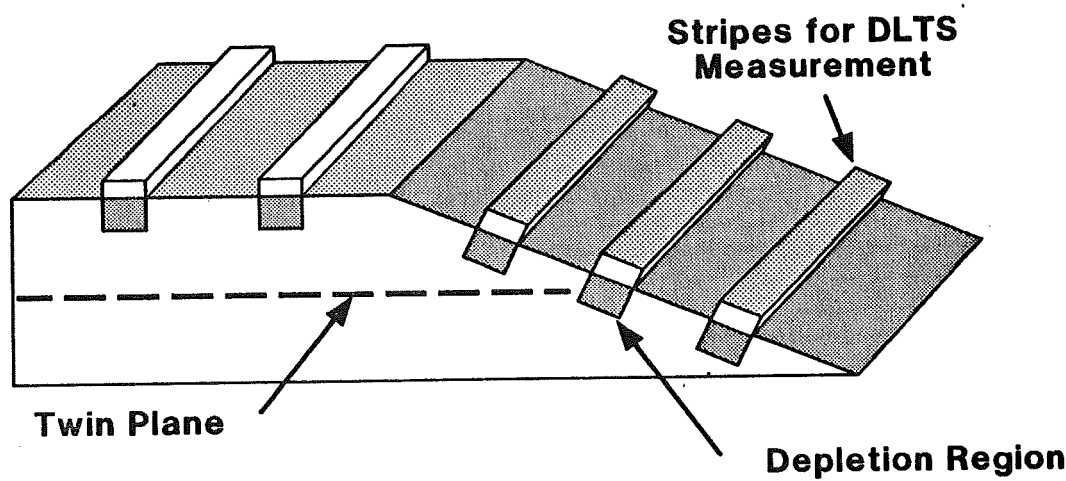


LBIC scans of beveled sample prepared from cell 38A (14.9%):
 (a) line scan showing no decrease in photocurrent in the vicinity of the twinned region; (b) area scan showing no features associated with the twinned region. (Sample #10, Run TP-10)

Comparison of Minority Carrier Diffusion Length with Twin Plane Depth

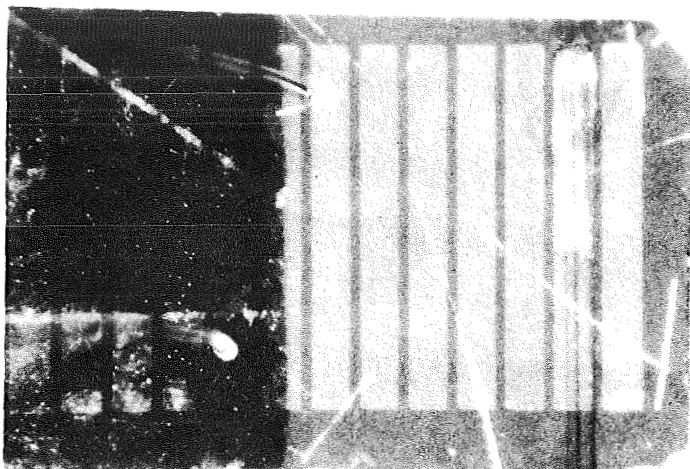
<u>Cell</u>	<u>η (%)</u>	<u>L_n (SPV) (μm)</u>	<u>Twin Plane Depth (μm)</u>	<u>Cell Thickness (μm)</u>
17C	9.5	12	60	158
38A	14.9	156	55	110
40C	10.0	19	65	148
69A	14.3	135	70	155

Impurity Depth Profile by DLTS



ORIGINAL PAGE IS
OF POOR QUALITY

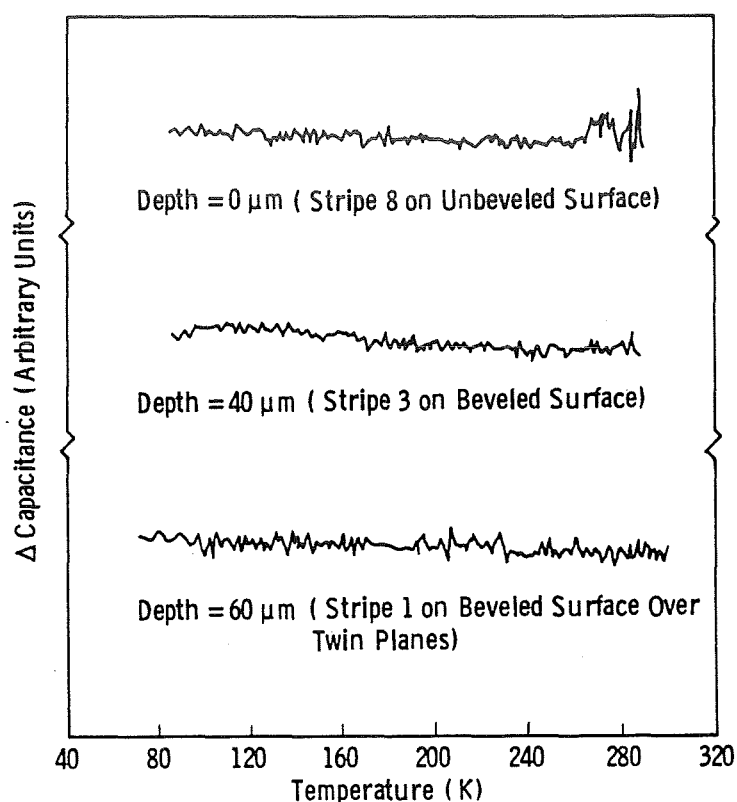
← 2.9 mm →



← Unbeveled → * → Beveled →

Multiple Twin Boundaries

Photograph of a beveled sample prepared from cell 17C (9.5%) showing Schottky diodes in the form of stripes for DLTS measurements. Note that the second stripe from the right is located directly over the lines which indicate twin boundaries emerging from the beveled surface. (Sample #3, Run TP-10)



DLTS scans for stripes on a beveled sample prepared from cell 17C (9.5%) showing that the concentration of electrically-active point defects is below the DLTS detection limit of $3 \times 10^{11} \text{ cm}^{-3}$. (Sample #5, Run TP-10)

Conclusions

1. **Low Efficiency (9.5%) Web Cells Have Many Boundaries (≥ 27) and a High Dislocation Density**
 - $2 \times 10^8 \text{ cm}^{-2}$ in Heavily Twinned Region
 - $\approx 10^6 \text{ cm}^{-2}$ in Bulk
2. **High Efficiency (14.9%) Web Cells Have Fewer Twin Boundaries (≤ 13) and Low Dislocation Density ($< 10^4 - 10^5 \text{ cm}^{-2}$)**
3. **A Significant Fraction of the Dislocations are Decorated with Precipitates**
4. **Twin Boundaries Without Dislocations are Transparent to Minority Carriers But Those with Dislocations are Electrically Active**
5. **In Low Efficiency Cells the Diffusion Length is Controlled by Dislocations Alone or Dislocations with Precipitates, Not by Dissolved Impurities**

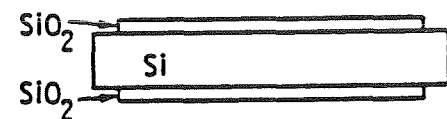
Effect of Hydrogen Ion Implantation on Web Cells

<u>Web Cell ID</u>	<u>H⁺ Implant</u>	<u>J_{sc} (mA/cm²)</u>	<u>V_{oc} (V)</u>	<u>FF</u>	<u>η (%)</u>	<u>SPV L (μm)ⁿ</u>
48-1	No	32.0	0.510	0.729	11.9	19
48H-1	Yes	36.4	0.574	0.770	16.1	120
52-1	No	36.8	0.586	0.773	16.7	130
52H-1	Yes	36.7	0.589	0.757	16.4	> 200

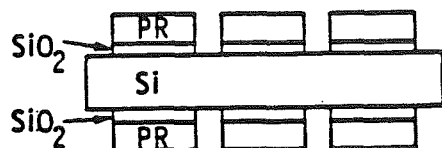
Notes:

1. Implant Conditions: 1500 eV, 2 mA/cm², 2 minutes with no stage cooling.
2. Hydrogen was implanted into the emitter side of the cells after boron and phosphorus diffusions.
3. Cell Size: 1 x 1 cm.
4. Test Conditions: AM1 (tungsten/halogen lamp), 100 mW/cm², room temperature (Run Cell-4).
5. Starting web material was boron-doped to 4 ohm-cm.
6. Anti-reflective coating: 600 Å ZnS and 1000 Å MgF₂

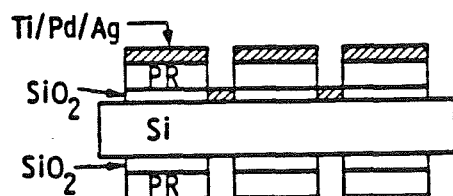
Process Sequence for Metal Contact to Silicon Along Grid Line Openings in Oxide



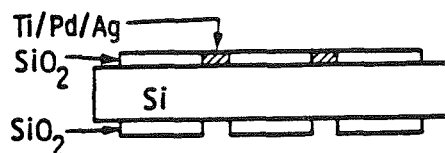
1. Oxide-Passivation Layers on Diffused Silicon



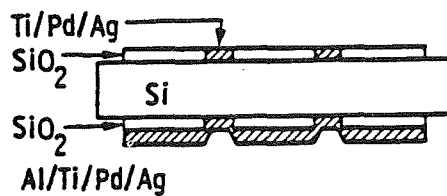
2. Grid Line Contact Windows Etched in Oxide Front and Back.



3. Front Metal Evaporation (Ti/Pd/Ag)

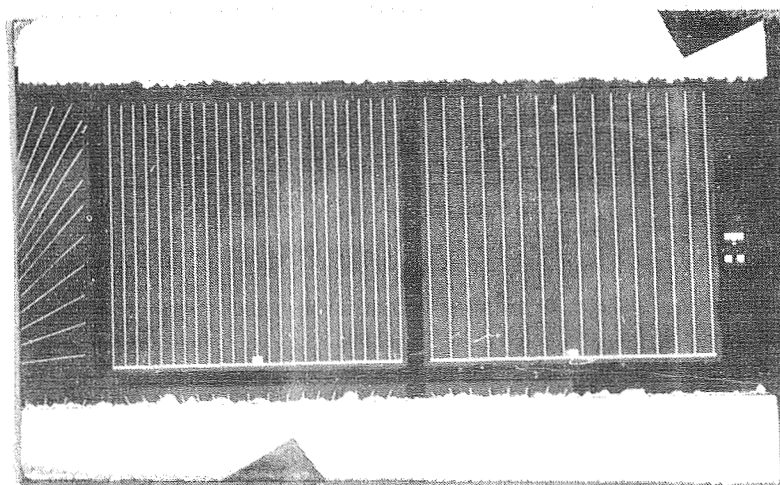
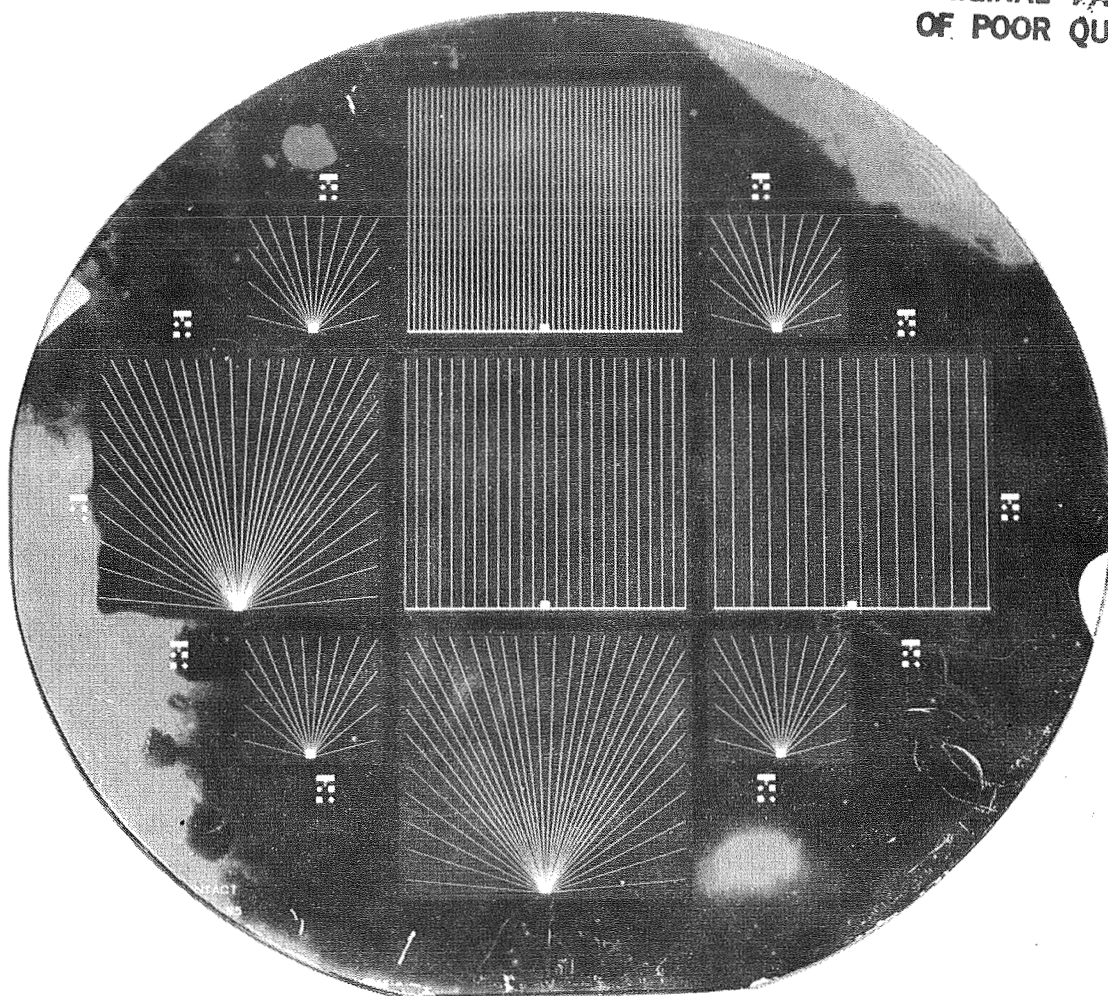


4. Metal Rejection; Front Grid Lines Contact Silicon



5. Back Metal Evaporation (Al/Ti/Pd/Ag) ; Back Grid Lines Contact Silicon

ORIGINAL PAGE IS
OF POOR QUALITY

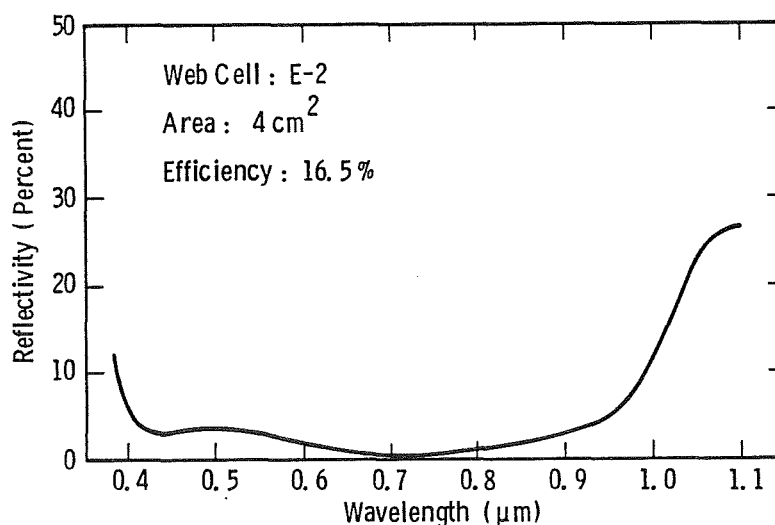


Cells Produced by the High-Efficiency Process (Run Cell-3)

Cell ID	Substrate	J_{sc} (mA/cm ²)	V_{oc} (V)	FF	η (%)	QE L (μ m) ⁿ	τ_{ocd} (μ s)	Thickness (μ m)
A-2	web	37.1	0.571	0.765	16.2	149	31	124
C-2	web	36.0	0.584	0.769	16.2	62	22	127
E-2	web	37.5	0.576	0.762	16.5	116	79	140
3FZH-7	float zone	35.9	0.626	0.812	18.3	210	36	394

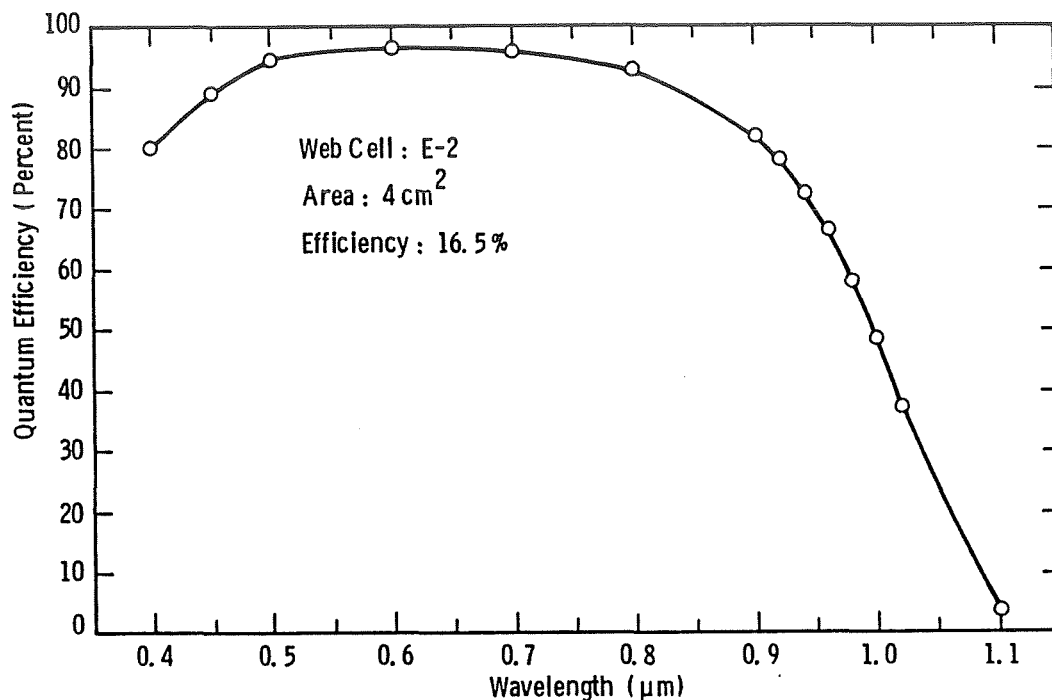
Notes:

1. Cell Size: 2 x 2 cm
2. Test Conditions: AM1 (tungsten/halogen lamp), 100 mW/cm² room temperature.
3. Web substrates were boron-doped to 4 ohm-cm (nominal); float zone substrates were boron-doped to 0.2 ohm-cm (Wacker 100)
4. Surface Passivation: 100 Å SiO₂ (front and back).
5. Anti-reflective coating: 430 Å ZnS and 1000 Å MgF₂ (evaporated)
6. Back surface reflector: 1000 Å Aluminum.
7. Forward current for τ_{ocd} measurement: 150 mA ($\sim I_{sc}$)



Reflectivity versus wavelength for Web Cell E-2 from Run Cell-3. Cell has double layer anti-reflective coating (430 Å ZnS and 1000 Å MgF₂) evaporated onto a passivated (100 Å SiO₂) silicon surface

HIGH-EFFICIENCY SOLAR CELLS



Quantum efficiency versus wavelength for web cell E-2 from Run Cell-3. Cell has surface passivation (100 Å SiO₂), double layer anti-reflective coating (430 Å ZnS and 1000 Å MgF₂) and aluminum back surface reflector. Web substrate is boron-doped to 4 ohm-cm and efficiency is 16.5%. Note high short wavelength response

Future Work for Web Cells

- Decrease resistivity from 4 ohm-cm to 0.2 ohm-cm
- Incorporate H⁺ implantation to improve diffusion length to 100 microns or more
- Retain oxide passivation, double layer AR coating, aluminum back surface reflector and standard cell thickness (120 microns)
- Anticipate efficiency > 17%

Summary

- Primary defect in silicon web cells which limits diffusion length is a dislocation decorated with impurity precipitates
- Precipitate may be SiO_x
- Twin boundaries in web cells are electrically benign
- Diffusion length and cell efficiency can be improved significantly in web cells by H^+ implantation at 1500 eV, 2 mA/cm² for 2 minutes
- Cells (4 cm²) have been fabricated from web substrates boron-doped to 4 ohm-cm having:

$$\eta = 16.5\%$$

$$\tau_{\text{ocd}} = 79 \mu\text{s}$$

PROCESSING

Brian D. Gallagher, Chairman

E. Kolawa, of the California Institute of Technology (Caltech), discussed the investigation of amorphous W-Zr and W-N alloys as diffusion barriers in silicon metallization schemes. Data were presented showing that amorphous W-Zr crystallizes at 900°C, which is 200°C higher than amorphous W-Ni films, and that both films react with metallic overlayers at temperatures far below the crystallization temperature. Also, W-N alloys (crystalline temperature of 600°C) have been successfully incorporated as a diffusion barrier in contact structures with both Al and Ag overlayers. The thermal stability of the electrical characteristics of shallow n⁺p junctions is significantly improved by incorporating W-N layers in the contact system. One important fact demonstrated during this investigation was the critical influence of the deposition parameters during formation of these barriers.

J. Parker, of Electrink, described the processing techniques and problems encountered in formulating metallo-organic decomposition (MOD) films used in contacting structures for thin solar cells. The use of thermogravimetric analysis (TGA) and differential scanning calorimetry (DSC) techniques performed at JPL in understanding the decomposition reactions lead to improvements in process procedures. The characteristics of the available MOD films were described in detail.

R. Vest described the status of the ink-jet printing program at Purdue University. The drop-on-demand printing system has been modified to use MOD inks. Also, an IBM AT computer has been integrated into the ink-jet printer system to provide operational functions and contact pattern configuration. The integration of the ink-jet printing system, problems encountered, and solutions derived were described in detail. The status of ink-jet printing using a MOD ink was discussed. The ink contained silver neodecanoate and bismuth 2-ethylhexanoate dissolved in toluene; the MOD ink decomposition products being 99 wt % Ag, and 1 wt % Bi.

D. Meier, of Westinghouse Electric, described the status of the investigation of laser-assisted solar cell metallization processing. This process was the laser pyrolysis of spun-on metallo-organic silver films by an argon ion laser beam. The MOD film is spun-on an evaporated Ti/Pd film to produce good adhesion. In a maskless process, the argon ion laser "writes" the contact pattern. The film is then built up to obtain the required conductivity using conventional silver plating processes. The Ti/Pd film in the field is chemically etched using the plated silver film as a mask. The width of the contact pattern is determined by the power of the laser. Widths as thin as 20 μ m were obtained using 0.66 W of laser power.

Cells fabricated with 50 μ m line widths of 4 ohm-cm FZ silicon-produced efficiencies of 16.6% (no passivation) which were equivalent to the best cells using conventional metallization/lithography and no passivation. Funding problems caused the premature cessation of this study before a process could be developed that would eliminate the need for the evaporative Ti/Pd film base.

PROCESSING

R. B. Campbell, of Westinghouse Advanced System Division, described the investigation of simultaneous diffusion of liquid precursors containing phosphorous and boron into dendritic web silicon to form solar cell structures. A novel, simultaneous junction formation technique was developed. The web material was subjected to a high-temperature, short-time pulse from tungsten-halogen flash lamps. Times of 5 to 15 s and temperatures of 1000 to 1150°C were investigated. It was determined that to produce high quality cells, an annealing cycle (nominal 800°C for 30 min) should follow the diffusion process to anneal quenched-in defects. Two ohm-cm n-base cells were fabricated with efficiencies greater than 15%. A cost analysis indicated that the simultaneous diffusion process costs can be as low as 65% of the costs of the sequential diffusion process.

G. A. Rozgonyi, of the Materials Engineering Department of North Carolina State University, discussed their investigation in rapid thermal processing (RTP) of Cz silicon substrates and the attendant effects on defects, denuded zones, and minority carrier lifetime. Preferential chemical etching and x-ray topography was used to delineate defects which were subsequently correlated with minority carrier lifetime; determined by a pulsed MOD test device. The x-ray delineation of grown-in defects was enhanced by a lithium decoration procedure.

Results, thus far, show excellent correlation between process-induced defects. Wafers with optimum RTP and implant processes suitable for solar cell evaluation will be available this summer.

S. J. Fonash, of Pennsylvania State University, investigated the use of low-energy hydrogen implants in the fabrication of high-efficiency crystalline silicon solar cells. The work established that low-energy hydrogen implants result in hydrogen-caused effects in all three regions of a solar cell: emitter, space charge region, and base. In web, Cz, and FZ material, low-energy hydrogen implants reduced surface recombination velocity. In all three, the implants passivated the space charge region recombination centers. In web cells, the implants passivated the base region. This was not the case, however, in the base region of Cz or FZ cells. In the case of web, it is proposed that the hydrogen is able to diffuse into the base region where it can passivate structural damage present in the web in the base. During the course of the investigation, it was established that hydrogen implants can alter the diffusion properties of ion-implanted boron in silicon, but not ion-implanted arsenic.

B. D. Gallagher, of JPL, discussed investigations involving the low-pressure chemical vapor deposition (LPCVD) of polycrystalline silicon. The physical system was described, as was the controlling process parameters and requirements for producing films for use as an integral portion of the solar cell contact system.

The film depositions were done in a conventional hot wall LPCVD reactor equipped with an Alcatel double-stage rotary pump. Both undoped and PH₃-doped polysilicon deposition processes were developed and characterized. Excellent cell structures were obtained using a [PH₃]/[SiH₄] concentration ratio of 250 to 1. The best results were obtained using a film thickness of 1 KÅ, resulting in cell characteristics of: V_{oc} 650.6, I_{sc} 130.0, FF 0.811, and an efficiency of 17.2%. The fill factor of 0.811 attests to the fact that a good ohmic contact was obtained.

AMORPHOUS DIFFUSION BARRIERS

CALIFORNIA INSTITUTE OF TECHNOLOGY

E. Kolawa, F. C. T. So, and M-A. Nicolet

Amorphous W-Zr Barrier

MOTIVATION

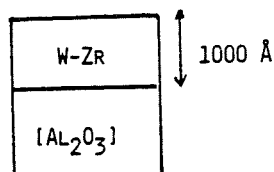
(PREVIOUS STUDIES: NI-W, NI-MO, CU-TA)

- SUBSTITUTE NI WITH ZR TO AVOID INTERFACIAL PENETRATION OF NI INTO SI SUBSTRATE AT LOW TEMPERATURES ($\sim 400^{\circ}\text{C}$)

NOTE:

- I) NI REACTS WITH SI AT $\sim 200^{\circ}\text{C}$
- II) NI IS THE MOVING SPECIES IN NI+SI REACTION
- III) ZR REACTS WITH SI AT $\sim 700^{\circ}\text{C}$
- IV) SI IS MOVING SPECIES IN ZR+SI REACTION

Crystallization

ANNEALED $500-900^{\circ}\text{C}$ (30')

X-RAY

 $T_c \sim 900^{\circ}\text{C}$

Experimental

RF SPUTTER DEPOSIT W-ZR FILMS FROM A W TARGET
COVERED WITH ZR STRIPES IN 10MTORR AR
(BASE PRESURRE < 1E-6 TORR)

2 COMPOSITIONS: $W_{70}Zr_{30}$

$W_{40}Zr_{60}$

DEPOSITION RATE: $\sim 400 \text{ \AA} / \text{MIN}$

AL DEPOSITION WITHOUT BREAKING VACUUM $\sim 120 \text{ \AA} / \text{MIN}$

ANNEALING IN VACUUM: PRESSURE < 5E-7 TORR

ANALYSIS:

RBS (ATOMIC DEPTH PROFILES)

SEM, EDAX (SURFACE MORPHOLOGIES)

X-RAY (PHASE IDENTIFICATION)

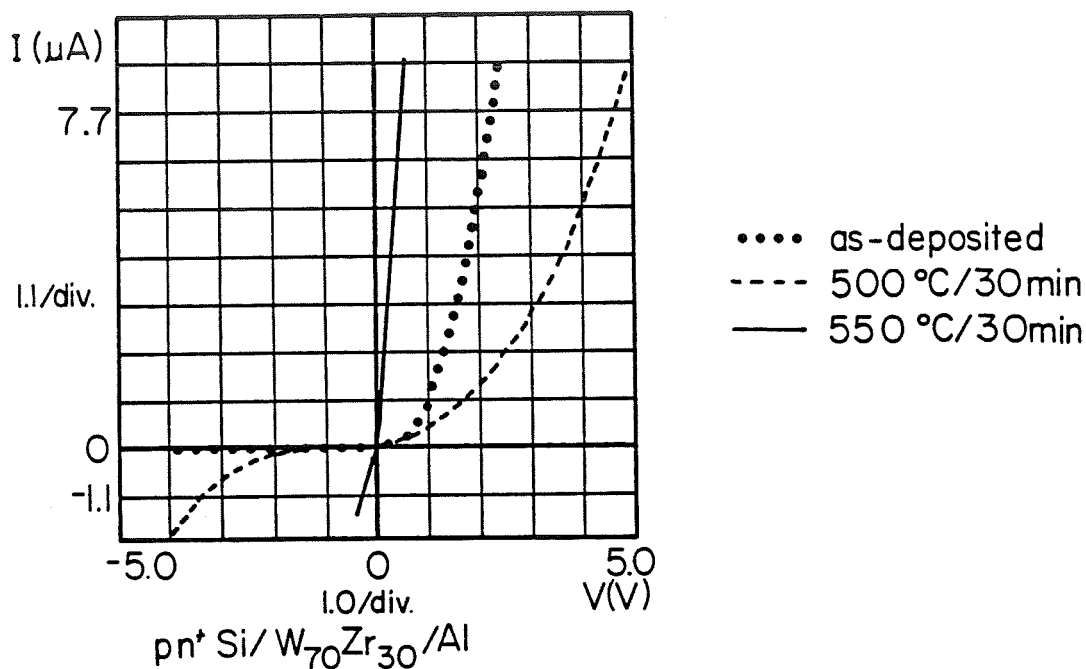
N⁺P Shallow Junctions

JUNCTION DEPTH : 0.35 μM

JUNCTION AREA : 500 x 500 μM^2

CONTACT AREA : 300 x 300 μM^2

AS SURFACE CONCENTRATION : $3E20 \text{ cm}^{-3}$

I-V Characteristic of n^+p Solar Cell with W-Zr Diffusion Barrier

Behavior of W-Zr Diffusion Barrier

1) INTERDIFFUSION IN [Si] / W-Zr / Al SETS IN

AT ~ 500°C DESPITE T_c IS AS HIGH AS 900°C

(Al+W 500°C

Al+Zr 400°C)

2) REACTION BETWEEN Al AND Zr-W IS LATERALLY

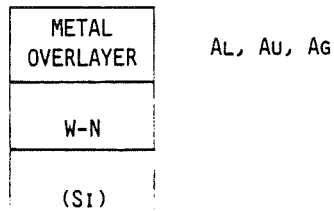
NONUNIFORM ---PITS FORMATION

** W-Zr CANNOT BE USED AS SACRIFICIAL BARRIER

** W-Zr EFFECTIVE BELOW 500°C

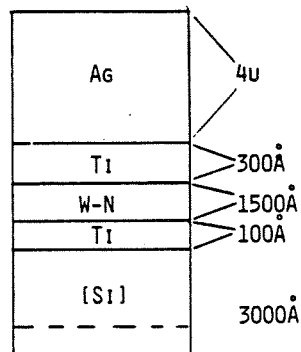
W-N Barriers

PREVIOUS WORK:

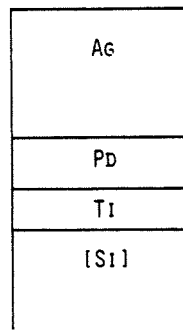


- W-N INHIBITS INTERDIFFUSION BETWEEN METAL OVERLAYER AND Si UP TO:
 - 550°C - 30 MIN. FOR AL
 - 800°C - 30 MIN. FOR AU
 - 700°C - 30 MIN. FOR AG

Experimental: Solar Cell with W-N Diffusion Barrier

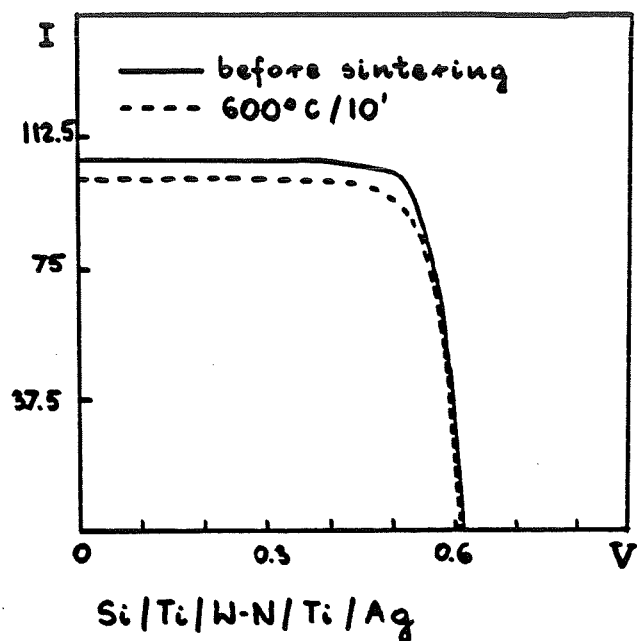


Experimental: Solar Cell with Ti-Pd-Ag Metallization

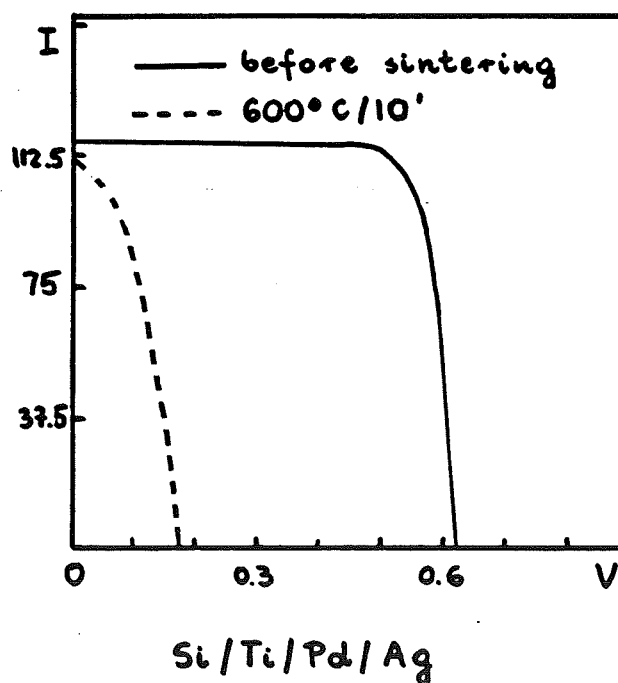


- ANNEALED IN FORMING GAS AT 400°C, 600°C FOR 10 MIN.
- I-V MEASURED UNDER AMO ILLUMINATION AT R.T.

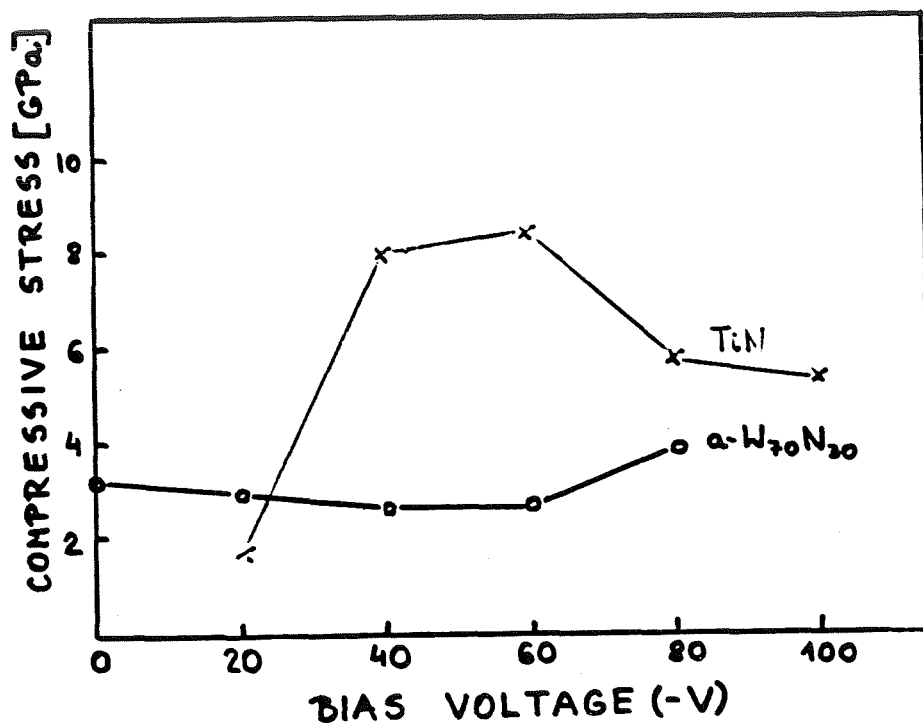
I-V Characteristic of n^+p Solar Cell with W-N Diffusion Barrier Under AMO Illumination at Room Temperature



I-V Characteristic of n^+p Solar Cell with Ti-Pd-Ag Metallization



Comparison Between Intrinsic Stress Properties of Magnetron-Sputtered TiN and α -W-N Films



Conclusions

- 1) W-Zr, Ni-W, Ni-Mo
 - FAILURE MECHANISM - REACTION WITH METAL OVERLAYER BELOW T_c
 - NEED TO FIND WAYS TO SUPPRESS THIS REACTION (E.G. NiNW)

- 2) WN

- EFFECTIVE BARRIER BETWEEN	$\left. \begin{array}{c} \text{AL} \\ \text{AG} \\ \text{AU} \end{array} \right\}$	AND Si UP TO	$\left\{ \begin{array}{l} 550^\circ\text{C}/30' \\ 700^\circ\text{C}/30' \\ 800^\circ\text{C}/30' \end{array} \right.$
-----------------------------	--	--------------	--

 - STABLE Si/Ti/WN/Ag CONTACT TO SOLAR CELLS UP TO 600°C/10'
 - LOWER STRESS W-N FILMS CAN BE PRODUCED BY APPLYING NEGATIVE SUBSTRATE BIAS VOLTAGE

METALLO-ORGANIC DECOMPOSITION (MOD)
FILM DEVELOPMENT

ELECTRINK, INC.

J. Parker

MOD Film Materials (Materials Made)

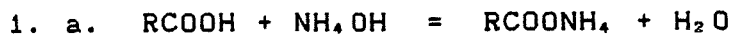
<u>I</u>	<u>Organometallic Compound</u>	<u>Purpose</u>
A	Silver neo decanoate	contact and circuit conductors
B	Bismuth 2-ethylhexanoate	adhesion enhancer for use in mixed organometallic solutions
C	Platinum 2-ethylhexanoate	to improve solder leach resistance in mixed systems
D	Nickel neo decanoate 2-ethylhexanoate	reduced cost solder leach resistance agent, barrier film possibility
E	Gold 2-ethylhexanoate	contact and circuit conductors
F	Aluminum neo decanoate	back surface field alloy ceramic layer
G	Mixed organometallics	various, eg. see above

MOD Film Materials (Compound Information)

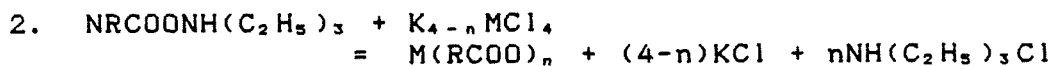
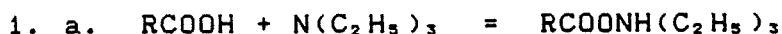
Product Compound	% Metal in compound	Decomp Temp. °C	Reagent compound	Metal Density gm/cc	metal Valence
Ag(C ₉ H ₁₉ COO)	38.7	230	AgNO ₃	10.5	<u>1</u>
Bi(C ₇ H ₁₅ COO) ₃	32.7	250	Bi(NO ₃) ₃	9.8	<u>3</u> , 5
Pt(C ₇ H ₁₅ COO) ₂	40.5	210	K ₂ PtCl ₄	21.4	<u>2</u> , 4
Ni(C ₉ H ₁₉ COO) ₂	14.6	310	Ni(NO ₃) ₂	8.9	<u>2</u> , 3
Ni(C ₇ H ₁₅ COO) ₂	17.0	300	"	"	" "
Au(C ₉ H ₁₉ COO) ₃	27.7	-	KAuCl ₄	19.3	1, <u>3</u>
Au(C ₇ H ₁₅ COO) ₃	31.4	-	"	"	" "
Al(C ₇ H ₁₅ COO) ₃	5.9	-	Al(NO ₃) ₃	2.7	<u>3</u>

MOD Film Materials (Chemical Reactions)

A Strong Acid Salts



B Weak Acid Salts



RCOOH is either neodecanoic acid, C₉H₁₉COOH or
2-ethylhexanoic acid, C₇H₁₅COOH.

M is a metal which has a valence n.

Mixed Organometallics

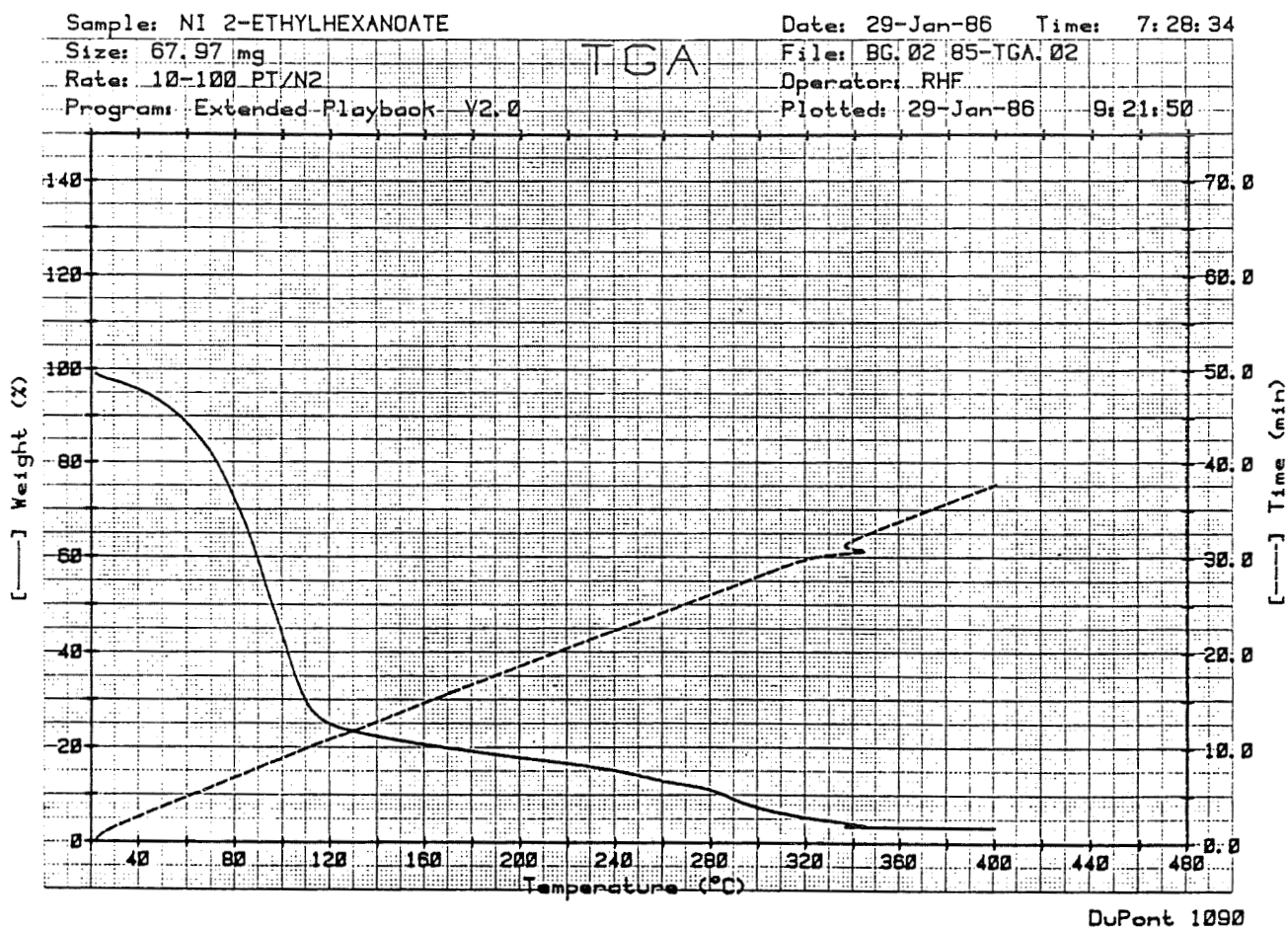
The adhesion of silver Metallo-Organic Decomposition (MOD) films is substantially improved by a small addition of bismuth which after oxidation during firing may serve as a bonding frit. Solder leaching of the metal film is reduced by the addition of a small amount of platinum. Both the bismuth and the platinum are added to the silver neodecanoate in xylene as the 2-ethylhexanoate. This mixed solution is designated AGS 13.30 and has the composition given in the table below.

Solution Composition

Compound	% Compound in Solution	% Metal in Compound	% Metal in Solution	% on Metal Solids
Silver Neo Decanoate	30.00	38.7	11.61	95
Bismuth 2-ethylhexanoate	0.37	32.7	.12	1
Platinum 2-ethylhexanoate	1.21	40.5	.49	4
Xylene	65.42	-	-	-
	100.00			100

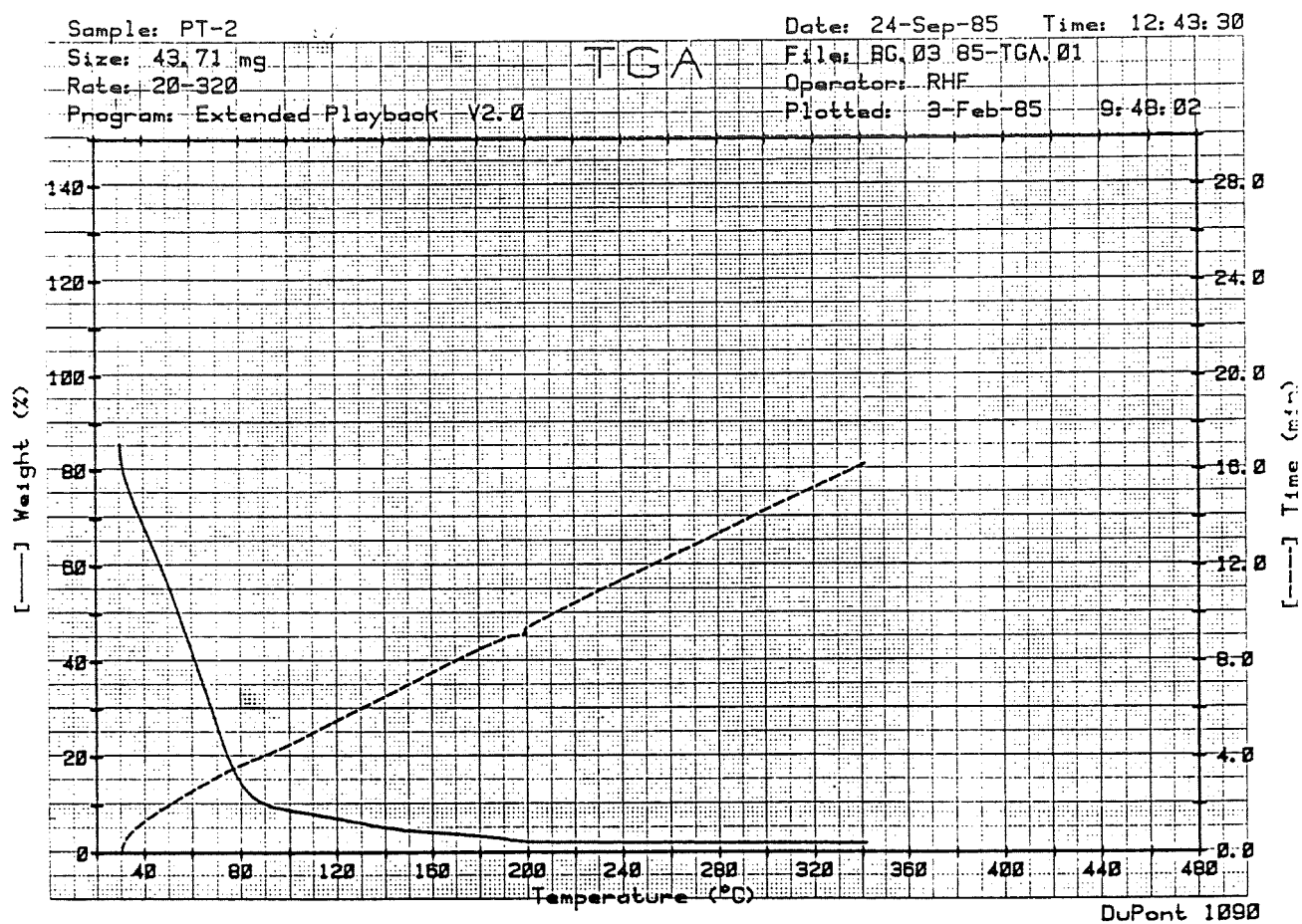
PROCESSING

Thermogravimetric Analysis: Ni 2-Ethylhexanoate

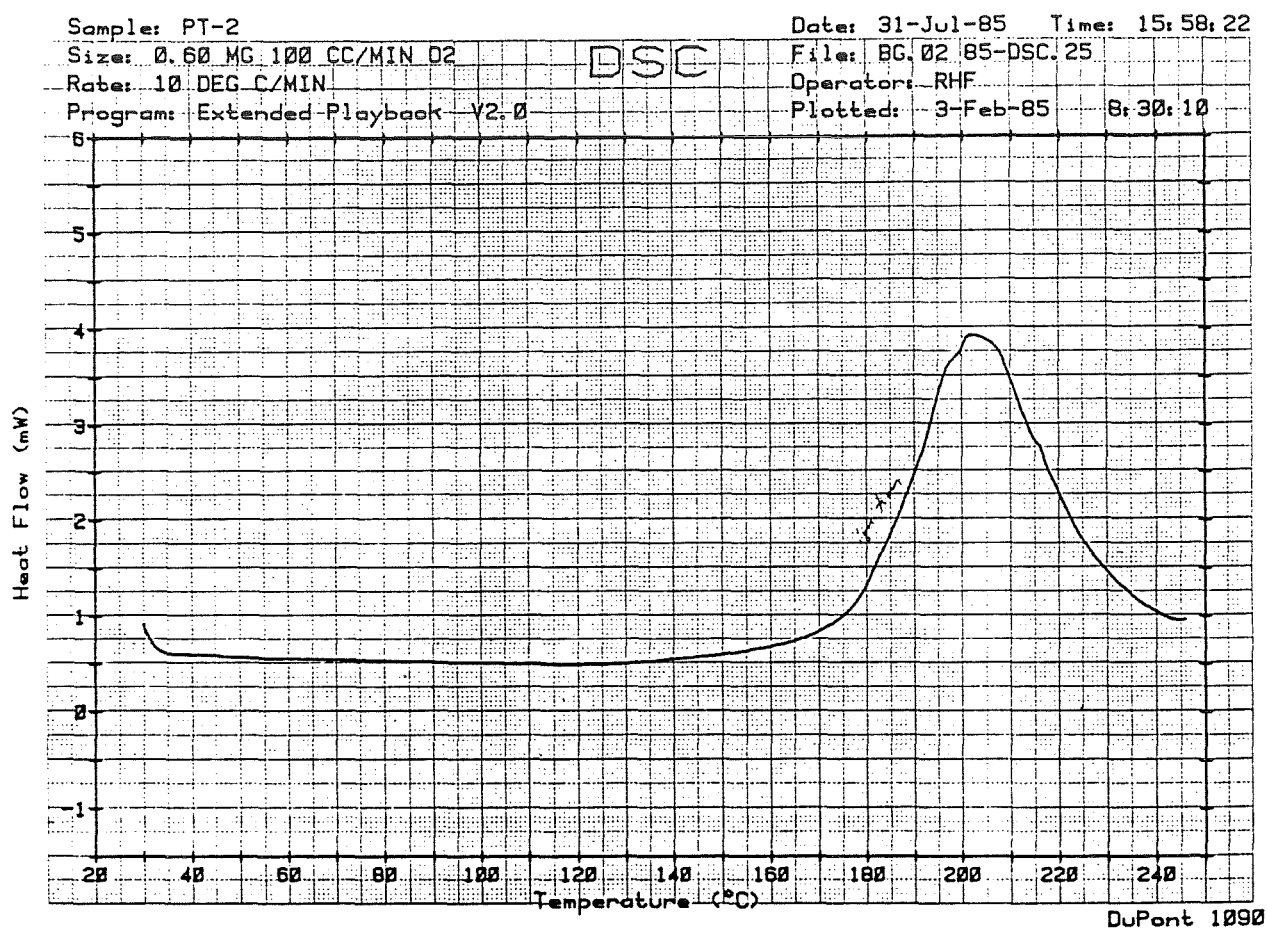


ORIGINAL PAGE IS
OF POOR QUALITY

Thermogravimetric Analysis: Pt 2-Ethylhexanoate



Differential Scanning Calorimetry: Pt 2-Ethylhexanoate



ORIGINAL PAGE IS
OF POOR QUALITY

PROCESSING

ORIGINAL PAGE IS
OF POOR QUALITY

Differential Scanning Calorimetry: Pt 2-Ethylhexanoate

Sample: PT-2

Size: 2.10 MG 100 CC/MIN N2

Rate: 10 DEG C/MIN

Program: Extended Playback V2.0

Date: 5-Aug-85 Time: 16:49:50

File: BG.03 85-DSC.24

Operator: RHF

Plotted: 3-Feb-85 8:15:48

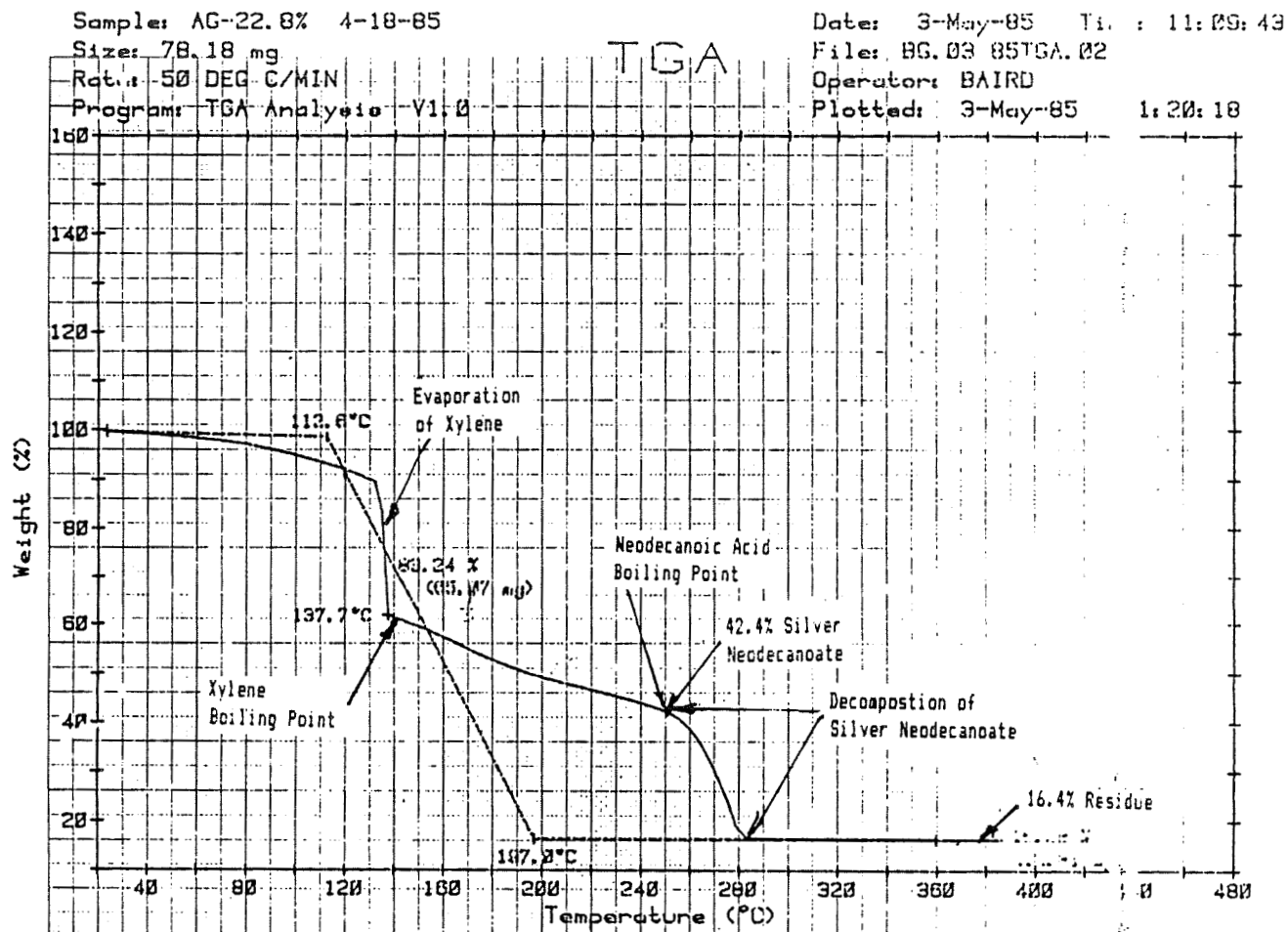
DSC



DuPont 1090

PROCESSING

Thermogravimetric Analysis of 42.4% Silver Neodecanoate in Xylene (50°C/min)



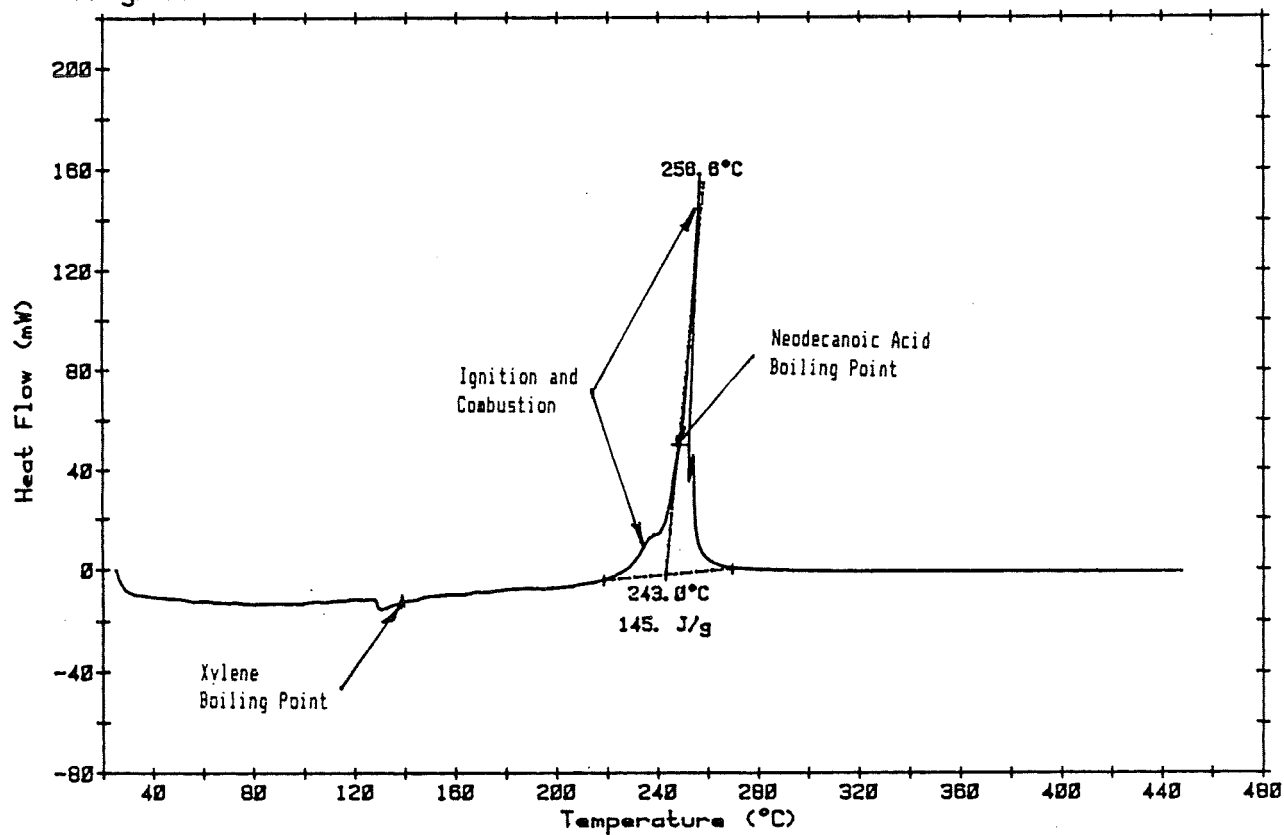
ORIGINAL PAGE IS
OF POOR QUALITY

Differential Scanning Calorimetry of 23% Silver Neodecanoate in Xylene (10°C/min)

Sample: SILVER INK Ag₂₃ in Xylene
Size: 36.6 MG
Rate: 10 DEG C/MIN IN AIR
Program: Interactive DSC V2.0

DSC

Date: 1-Dec-83 Time: 11:21:09
File: BG.02 83-DSCDAT-31
Operator: BRONSON
Plotted: 7-Dec-83 10:57:50

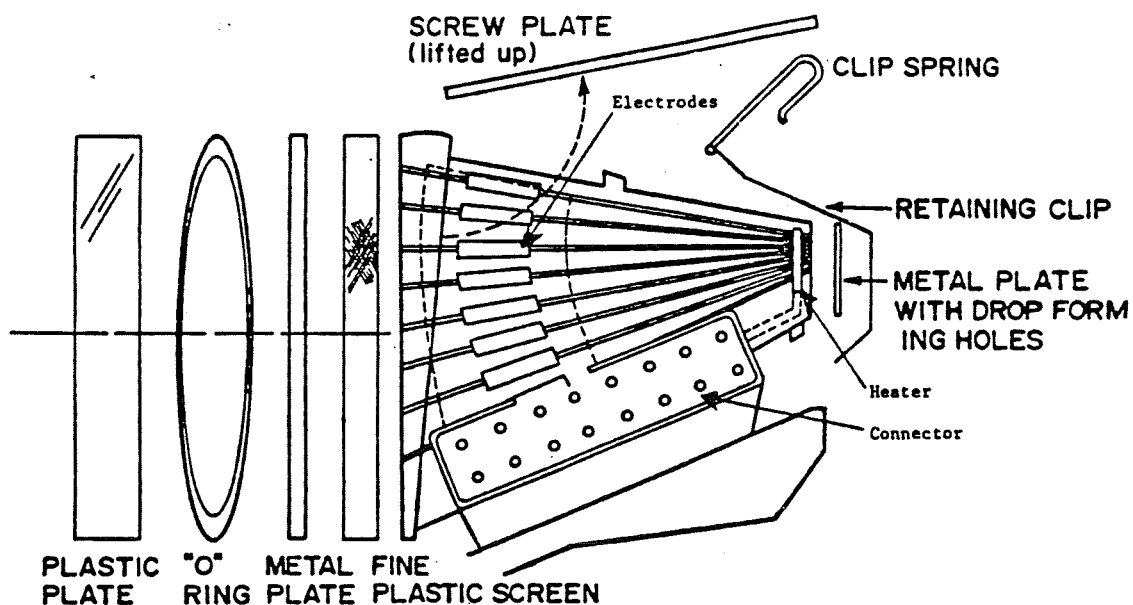


INK-JET PRINTING OF SILVER METALLIZATION
FOR PHOTOVOLTAICS

PURDUE UNIVERSITY

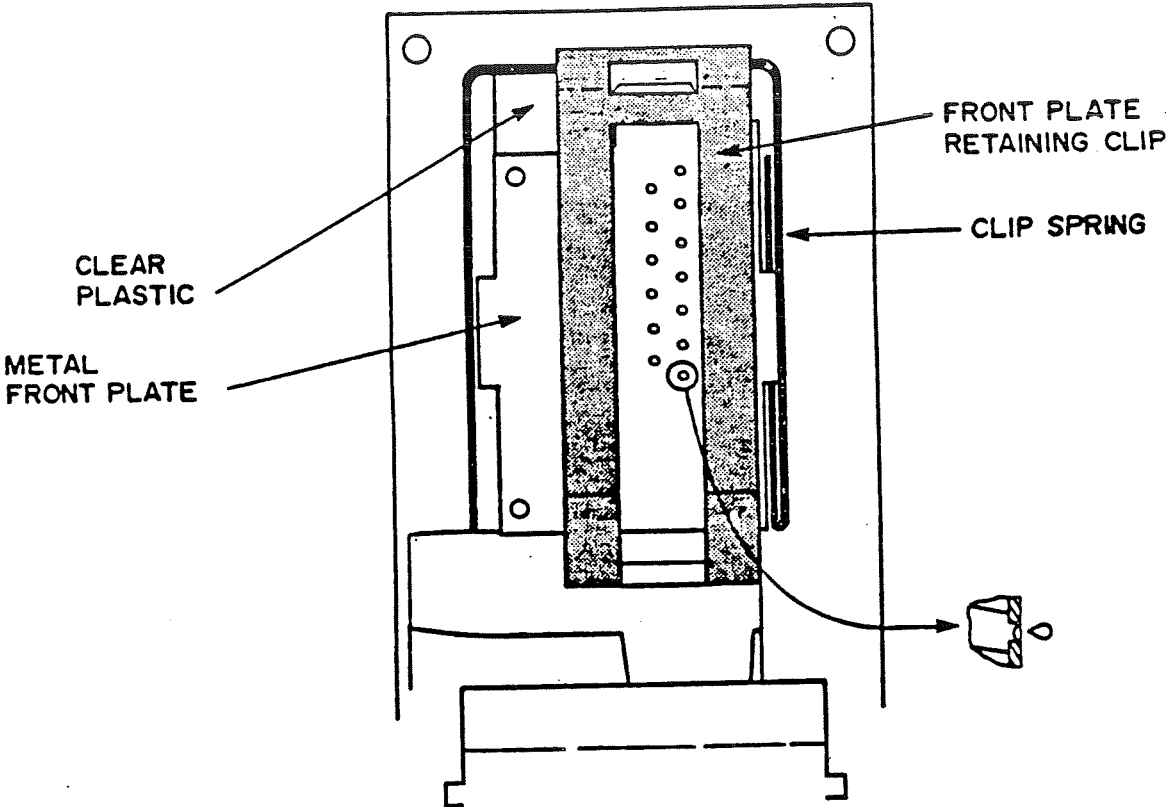
R. W. Vest

Nozzle Assembly (side view)

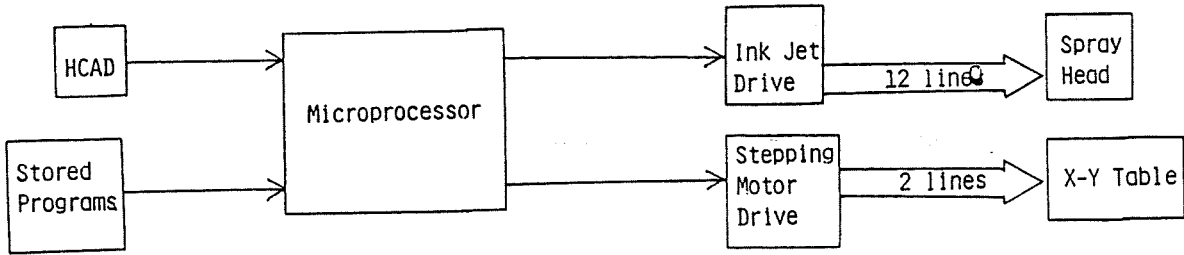


PRECEDING PAGE BLANK NOT FILMED

Nozzle Assembly (front view)



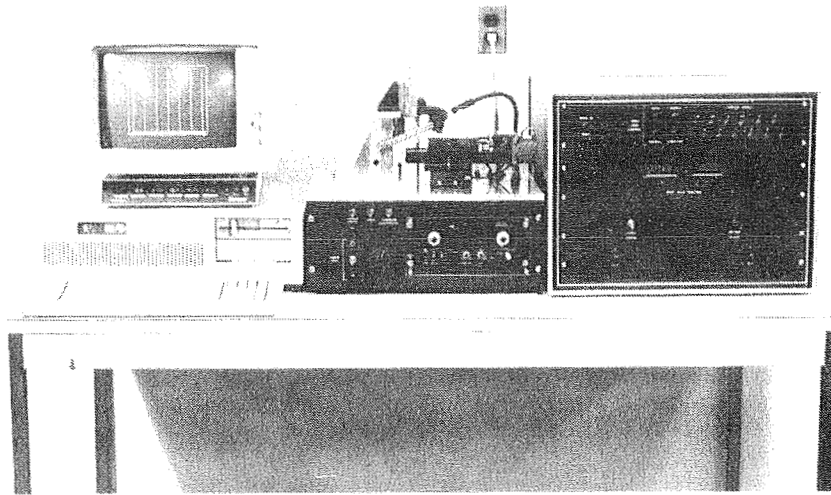
Flow Diagram of Ink-Jet Printer System



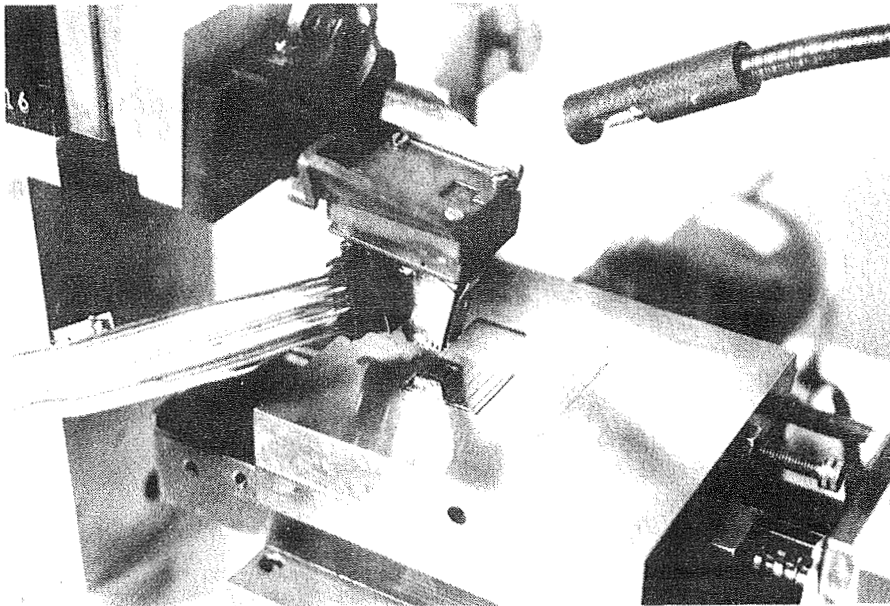
PROCESSING

Computer Controlled Ink-Jet Printer

ORIGINAL PAGE IS
OF POOR QUALITY



Print Head and Substrate Mount



PROCESSING

Ink Requirements

1. No Particulates
2. Low Viscosity
3. High Surface Tension
4. High Inorganic Content
5. Non Clogging
6. Stable

Ink Chemistry

1. Silver Compound
Ag neodecanoate
2. Adhesion Agent
Bi 2-ethylhexanoate
3. Solvent
toluene or xylene
4. Stabilizer
neodecanoic acid

Ink-Jet Printing Studies

Ink Parameters

1. viscosity
2. surface tension
3. metal content
4. solvent vapor pressure

Printer Parameters

1. pulse voltage
2. pulse frequency
3. ink pressure
4. nozzle diameter
5. nozzle-substrate separation

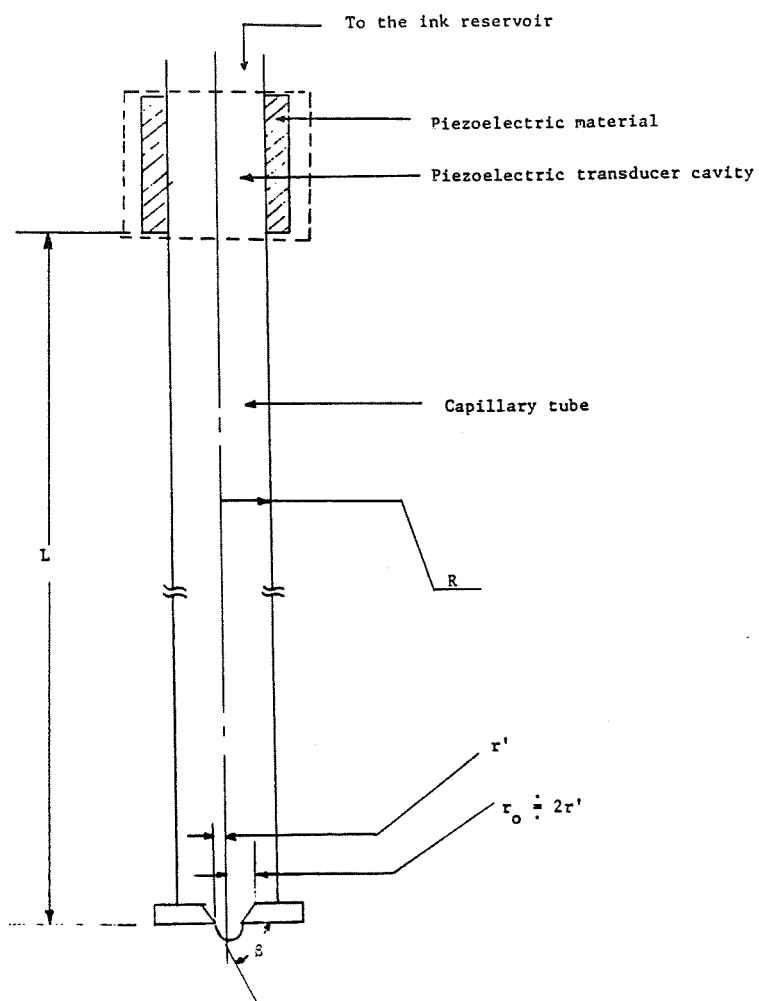
Substrate Parameters

1. velocity
2. temperature

Firing Parameters

1. heating rate
2. maximum temperature
3. time at maximum temperature

Diagram of the Ink-Jet Model



Ink-Jet Theory

$$Q_r = fT \frac{\pi R^2 r_0^2 K}{8\mu L} \left[1 - \frac{1}{2} \left[\frac{r_0}{R} \right]^2 \right] \left[C V^n - \frac{2\sigma \cos \beta}{r'} \right]$$

Ink Parameters

σ = surface tension

β = contact angle

μ = viscosity

Mechanical Parameters

r' = nozzle radius

$r_0 = 2r'$

Electrical Parameters

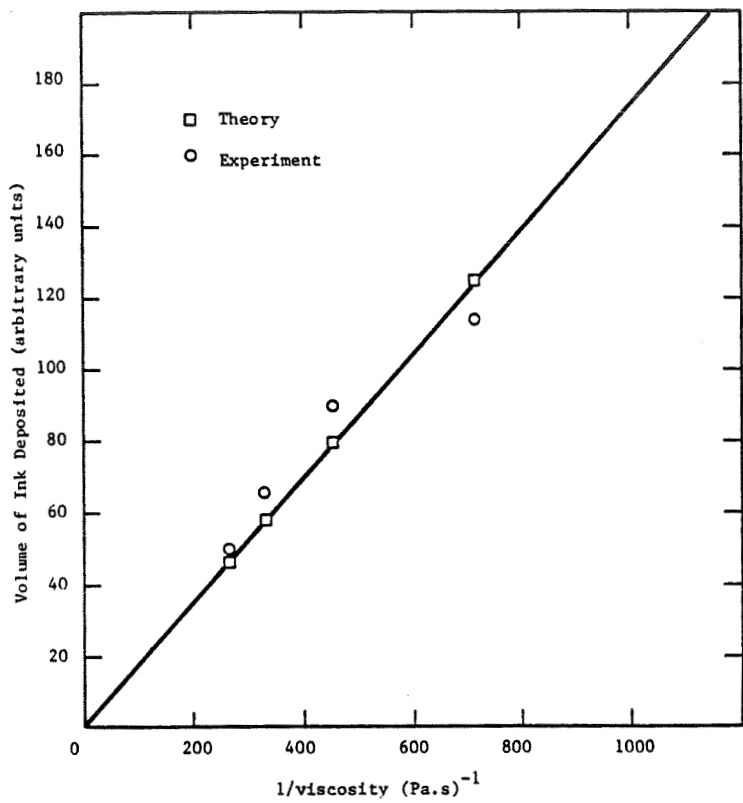
V = pulse voltage

T = pulse duration

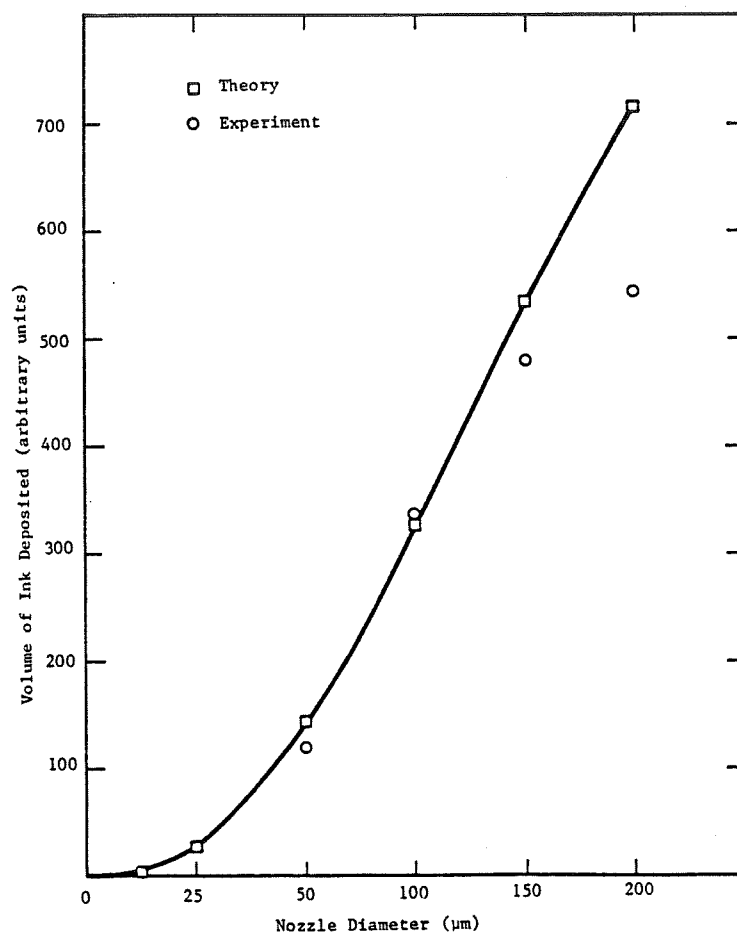
f = pulse frequency

R , K , L , C and n are constant for a given printer.

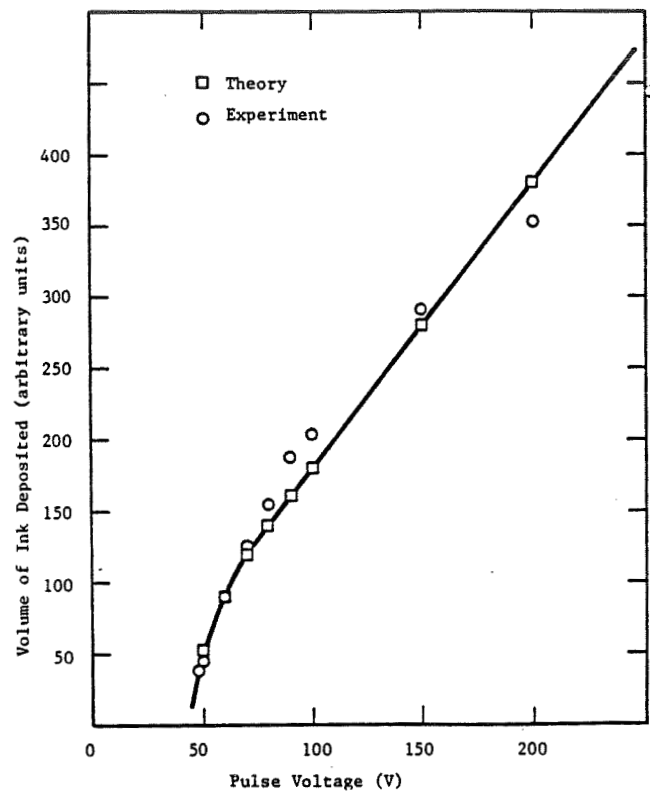
Relationship of Ink-Flow Rate and Ink Viscosity



Relationship of Ink-Flow Rate and Nozzle Diameter

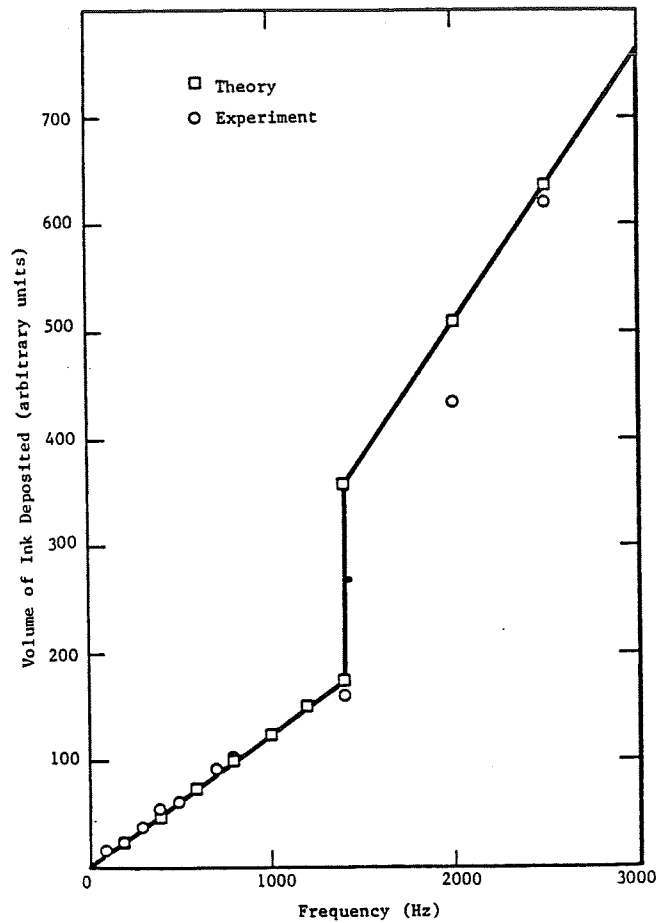


Relationship of Ink-Flow Rate and Pulse Voltage Applied to the Piezoelectric Transducer



PROCESSING

Relationship of Ink-Flow Rate and Frequency of Pulses to the Piezoelectric Driver



Thermal Processing

Belt Furnace

$T_{\max} = 280^{\circ}$ to 400°C

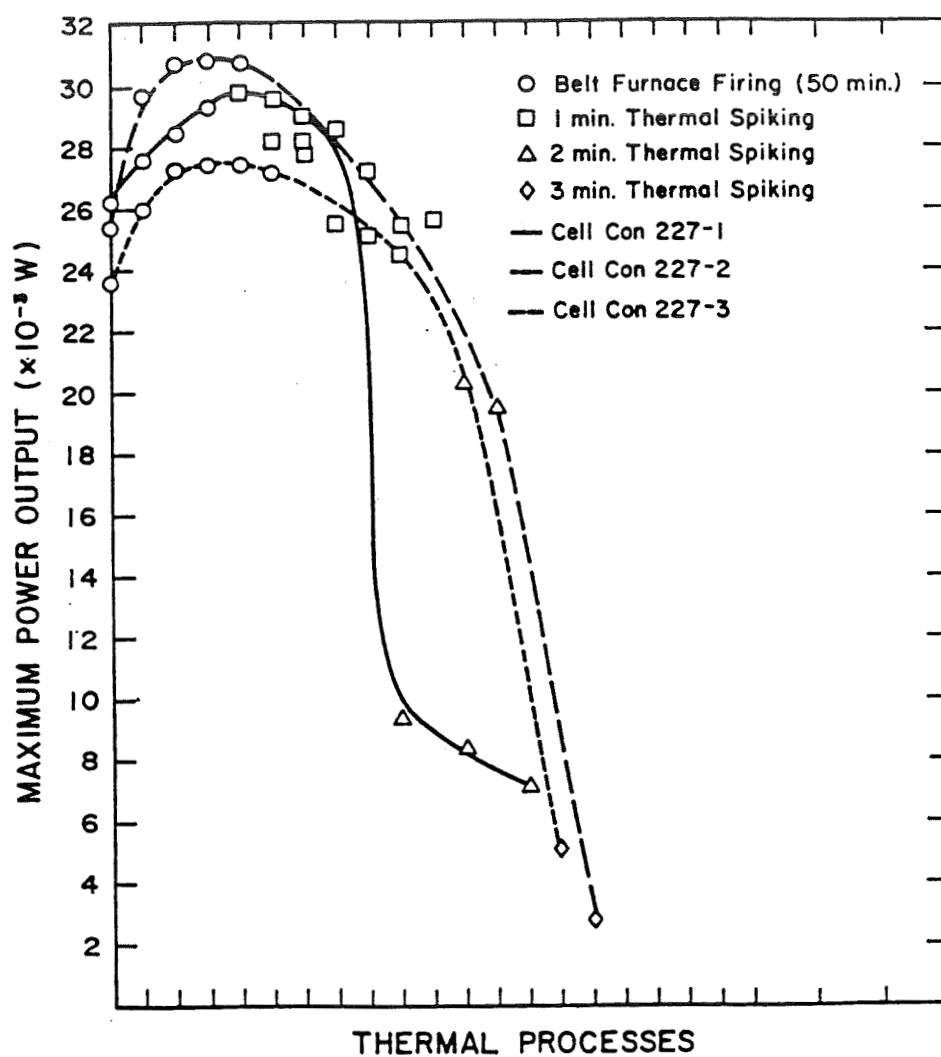
cycle time = 40 - 70 minutes

Thermal Spike

750° to 850°C

45 to 180 seconds

Thermal Effects on Performance of Thin-Film (Control) Solar Cells



Fired Film Properties

Composition

99% Ag - 1% Bi_2O_3

Adhesion

excellent (Scotch tape)

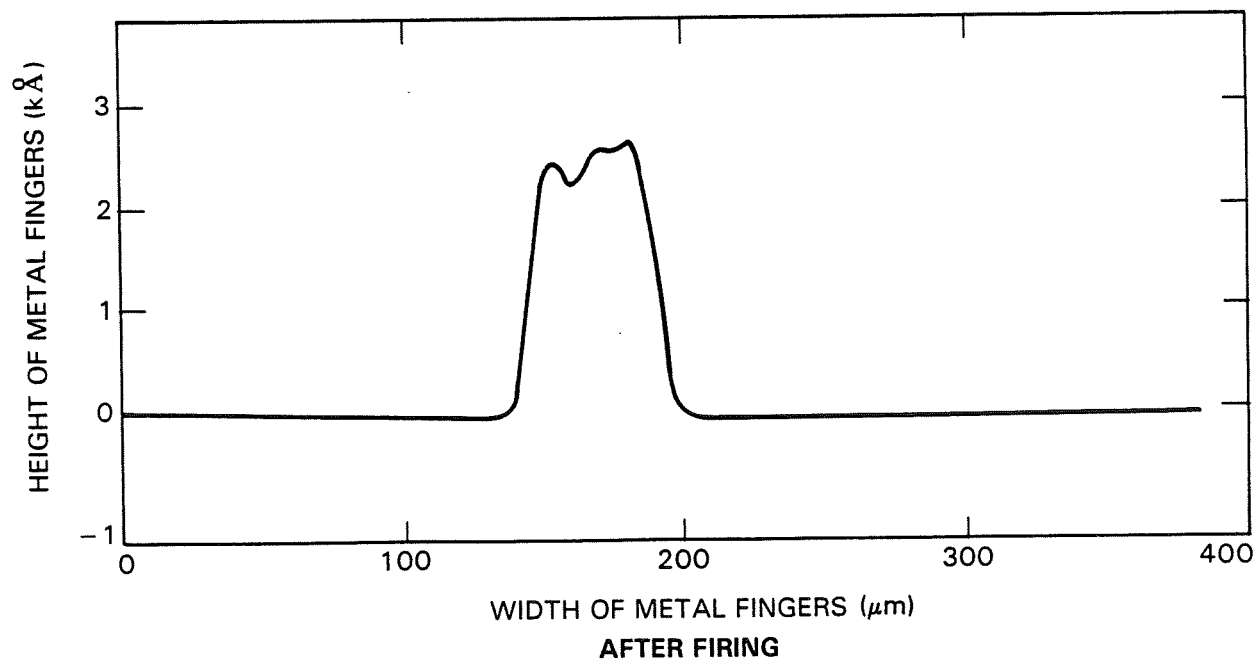
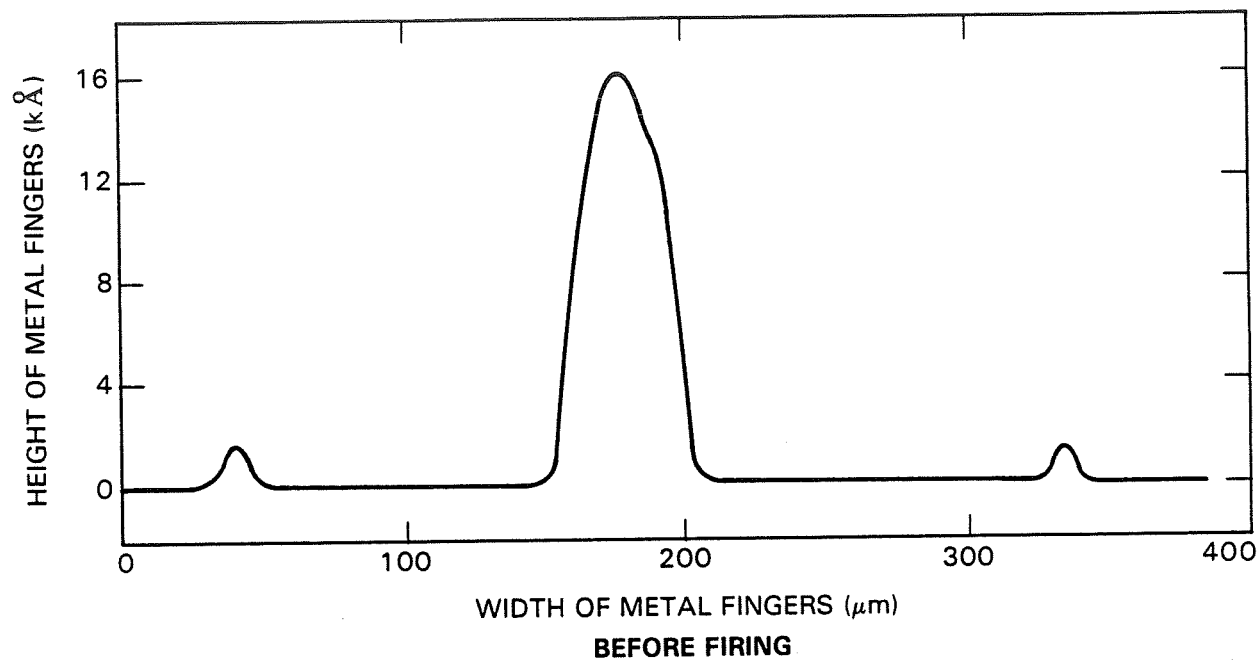
Solderability

excellent (100% acceptance)

Solder Leach Resistance

excellent (30 second dip)

Height Versus Width of Metal Fingers



PROCESSING

Measured Finger-to-Finger Resistances (R_{ff}) and Series Resistance (R_{SE}) Calculated from I-V Curves for Solar Cells with Different Processing

No. of Layers of Ag	Thermal Treatment Sequence (a)										JPL Control Cells	
	(1) B+60S		(2) B+60S+B		(3) B+60S+B ²		(4) B+60S+B ² +15S		(5) B+60S+B ² +15S ²			
	R _{ff}	R _{SE}	R _{ff}	R _{SE}	R _{ff}	R _{SE}	R _{ff}	R _{SE}	R _{ff}	R _{SE}	R _{ff}	R _{SE}
5	9.38 ±1.22	10.05 ±1.79	8.26 ±0.13	-	8.13 ±0.42	9.48 ±1.33	8.76 ±0.59	10.92 ±0.67	8.57 ±0.40	10.59 ±1.57		
10			5.52 ±0.35	-	5.13 ±0.39	7.98 ±0.89	3.48 ±0.18	7.16 ±0.48	3.41 ±0.18	6.73 ±0.43		
20							2.44 ±0.12	4.35 ±1.77	1.65 ±0.05	5.40 ±0.71		
											5.22 ±1.32	1.49 ±0.09 0.63 ^(b) ±0.12

(a) thermal treatments

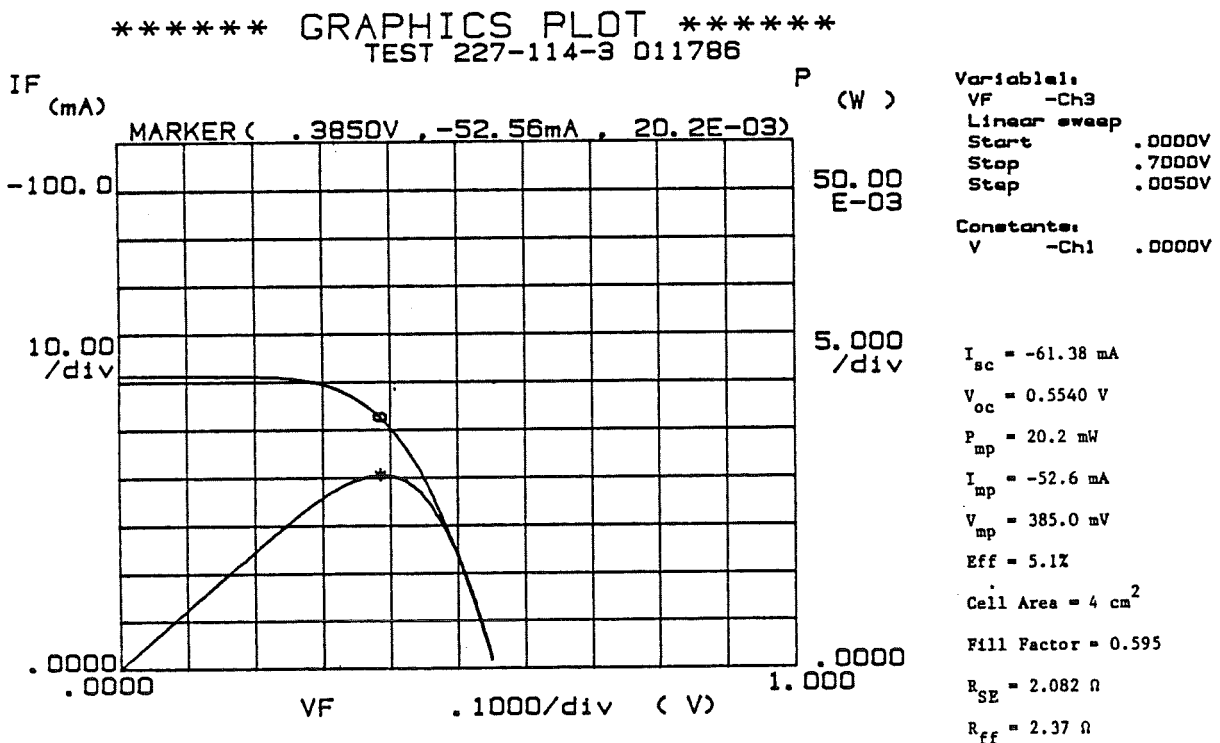
B = belt furnace with 70 minute cycle and 300°C maximum temperature

60S = sixty seconds at 800°C

15S = fifteen seconds at 800°C

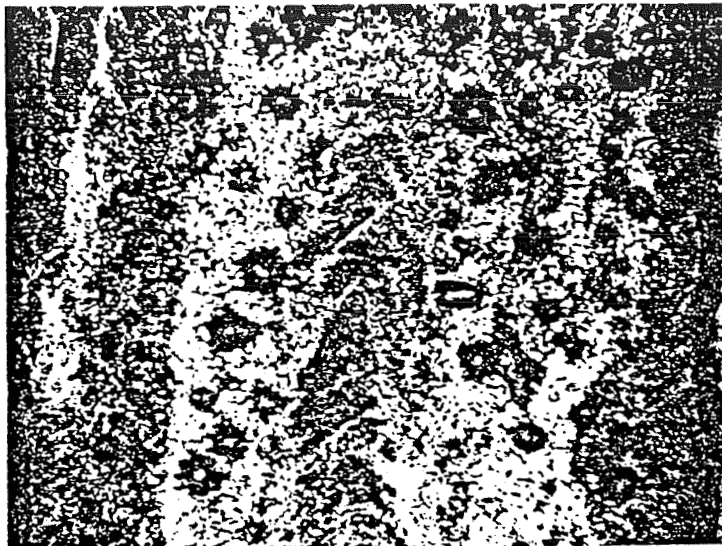
(b) calculated from the I-V curves supplied by JPL

Current-Voltage Curve for 20-Layer Cell 114-3 After Thermal Treatment Step 4

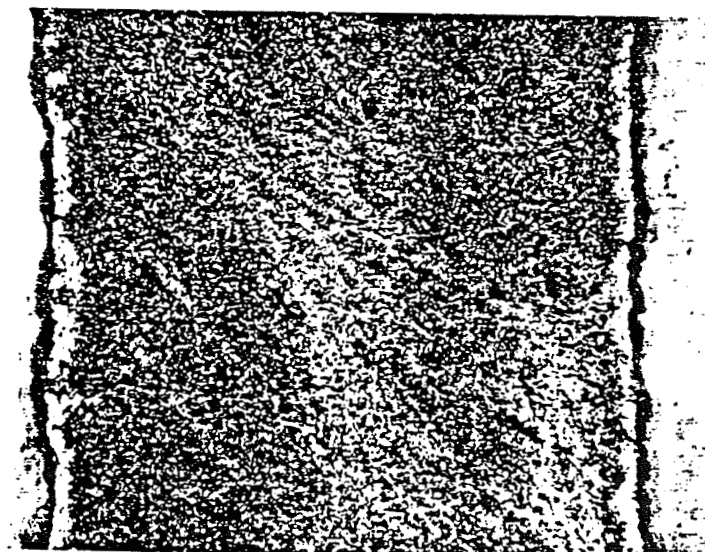


Current-Voltage Curve for 20 Layer Cell 114-3 After Thermal Treatment Step 4.

Effect of Quality of the Metal Film on Solar Cell Quality



(a) Cell 227-15 Poor Metal Film and Poor Solar Cell



(b) Cell 227-14 Good Metal Film and Good Solar Cell

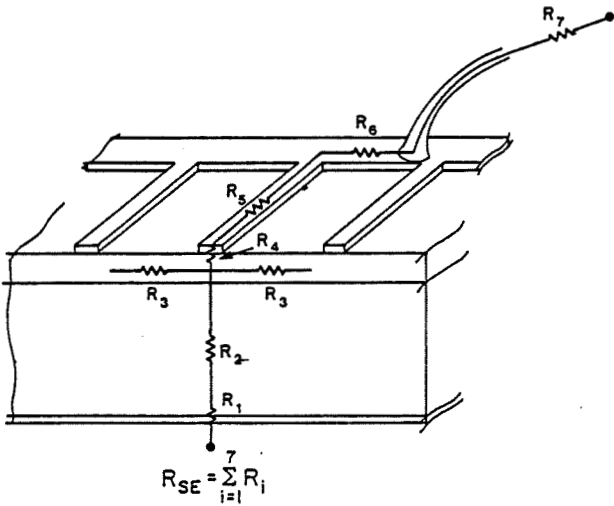
ORIGINAL PAGE IS
OF POOR QUALITY

Comparison of Series Resistance (R_{SE}) and Fill Factor (FF) for Solar Cells Metallized with MOD Silver With and Without a Ti/Pd Underlayer

No. of Layers of Ag	Thermal Treatment Sequence (a)								JPL Control Cells			
	B + 60S				B + 60S + B				Purdue Data		JPL Data	
	No Ti/Pd		With Ti/Pd		No Ti/Pd		With Ti/Pd		R_{SE}	FF	R_{SE}	FF
	R_{SE}	FF	R_{SE}	FF	R_{SE}	FF	R_{SE}	FF				
5	39.78 ±10.09	0.22 ±0.02	2.48 ±0.79	0.51 ±0.07	32.67 ±15.15	0.24 ±0.02	1.78 ±0.25	0.57 ±0.04				
10					20.04 ±3.12	0.24 ±0.01	1.75 ±0.41	0.58 ±0.03				
									1.70 ±0.36	0.56 ±0.04	0.69 ±0.04	0.65 ±0.03

(a) thermal treatments
B = belt furnace with 70 minute cycle and 300°C maximum temperature
60S = sixty seconds at 800°C

Seven Factors that Contribute to the Measured Series Resistance of a Solar Cell



- R_1 = Back Contact
- R_2 = Bulk
- R_3 = Diffused Layer
- R_4 = Front Contact
- R_5 = Grid Lines
- R_6 = Bus Lines
- R_7 = Measuring Circuit

Summary

1. A computer controlled ink jet printing system was developed.
2. A theoretical model which adequately describes the ink jet printer was developed.
3. A MOD silver ink was developed for use with the printer.
4. Grid patterns with suitably low sheet resistance can be produced.
5. Line definition to 50 μm can be achieved.
6. Good adhesion and solder leach resistance was demonstrated.
7. The contact resistance must be reduced in order to produce high efficiency cells.

LASER-ASSISTED SOLAR CELL METALLIZATION PROCESSING

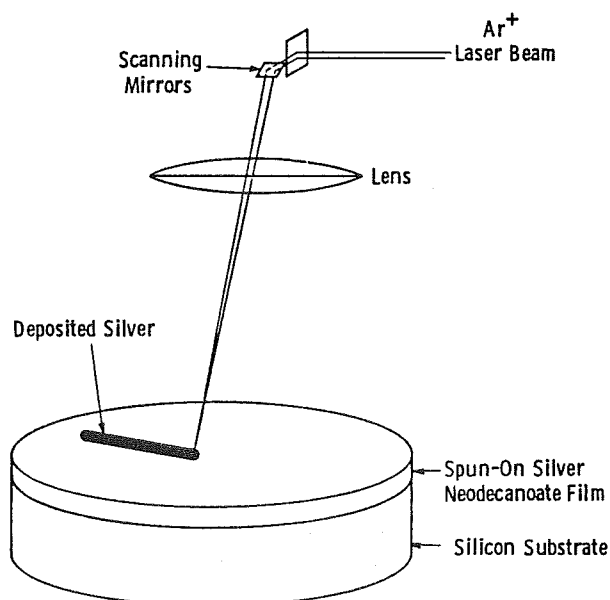
WESTINGHOUSE ELECTRIC CORPORATION
RESEARCH AND DEVELOPMENT CENTER

D. L. Meier

Topics

- **Basic Concept**
- **Linewidth**
- **Cells Fabricated Without Masks**
- **Alternative Metals for Improved Adherence**

Laser Pyrolysis of Spun-On Metallo-Organic Film



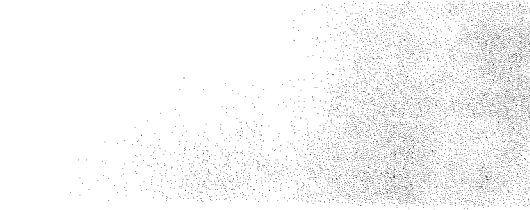
Sample Base Temperature 75°C

Focussed Laser Spot Decomposes Spun-On Film

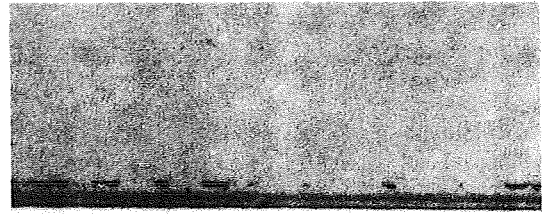
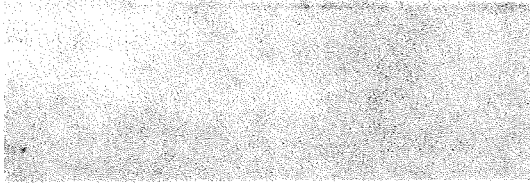
Silver Metallization Patterns are Formed by Direct-Writing

PROCESSING

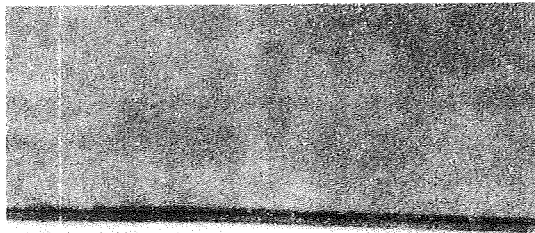
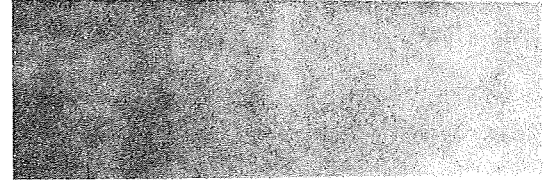
Effect of Laser Power on Laser-Metallized Linewidth After Rinsing the Silver Neodecanoate Film



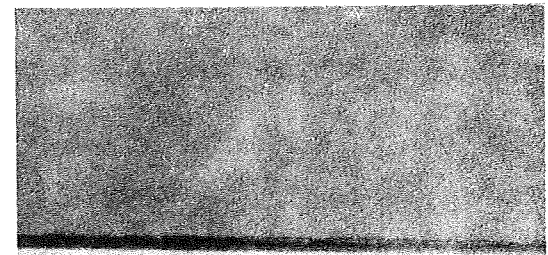
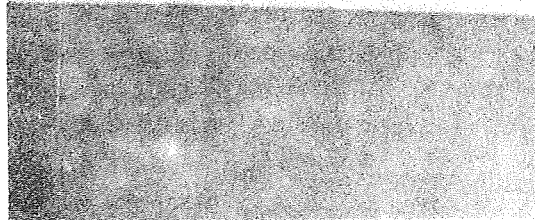
Maximum Power: 8.5 watts
Width: 60 μm



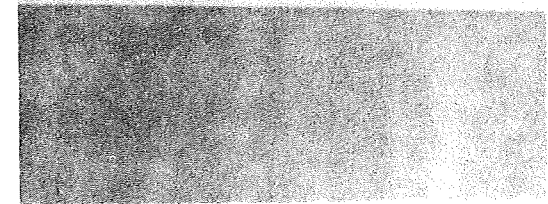
Maximum Power: 6.9 watts
Width: 60 μm



Maximum Power: 4.9 watts
Width: 55 μm

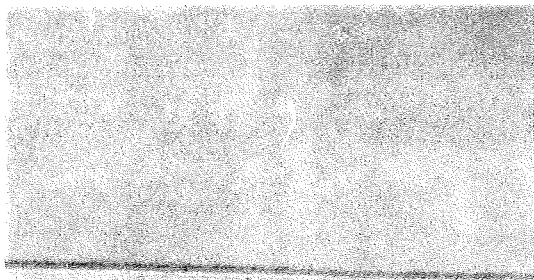


Maximum Power: 4.1 watts
Width: 50 μm

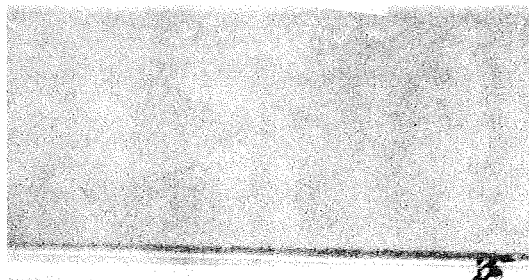


**ORIGINAL PAGE IS
OF POOR QUALITY**

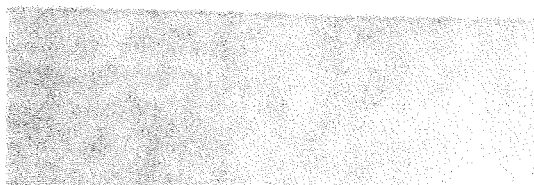
Effect of Laser Power on Laser-Metallized Linewidth After
Rinsing the Silver Neodecanoate Film (Cont'd)



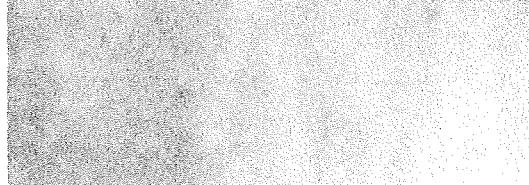
Maximum Power: 2.6 watts
Width: 40 μ m



Maximum Power: 1.8 watts
Width: 40 μ m



Maximum Power: 1.2 watts
Width: 30 μ m



Maximum Power: 0.7 watt
Width: 20 μ m

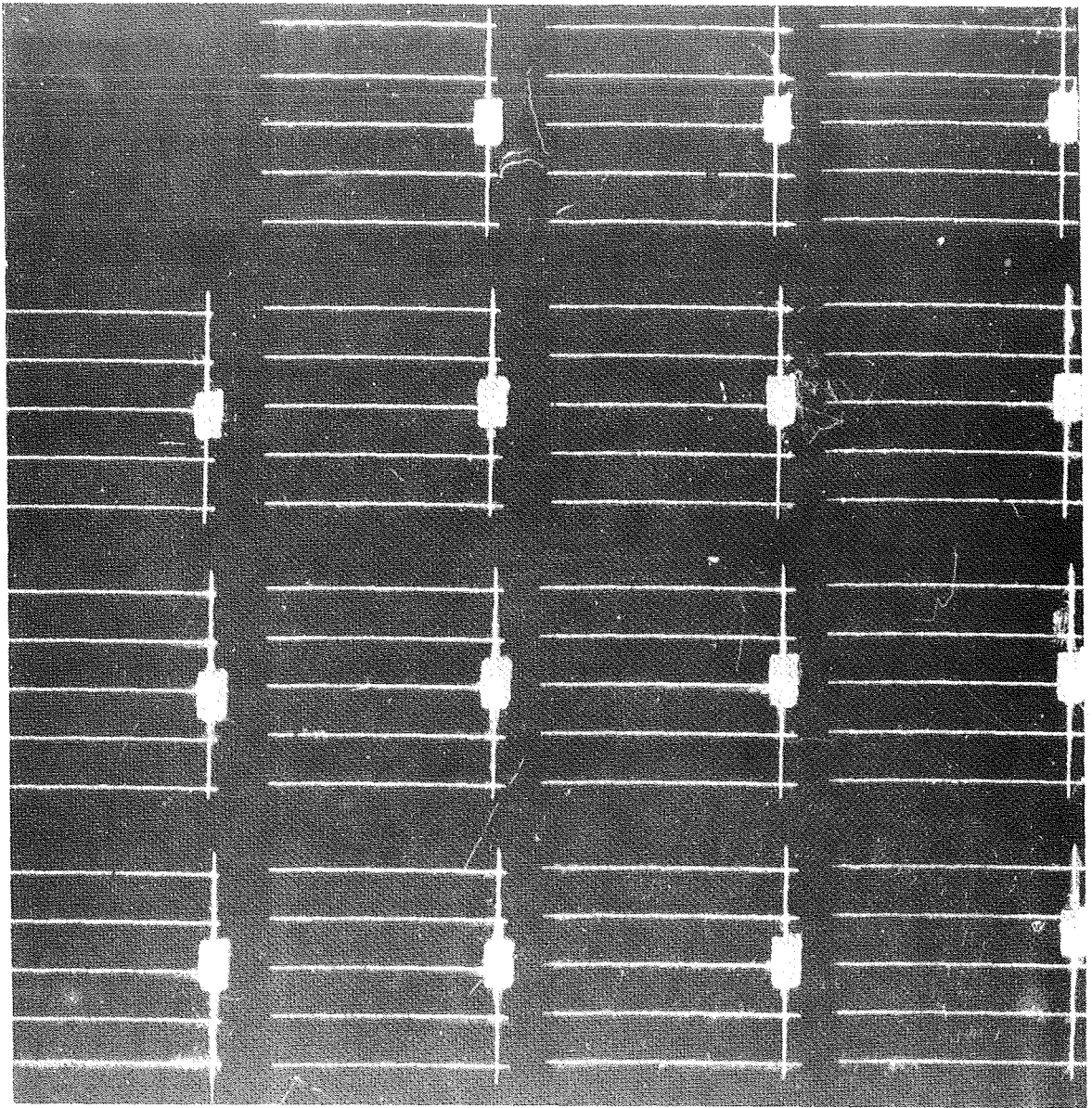
Linewidths as a Function of Laser Power With 50 mm Lens
Before and After Film Rinse

Laser Power (W)	Before <u>Film Rinse</u>	After <u>Film Rinse</u>
8.50	85 μm	60 μm
7.50	75	65
6.90	75	60
6.36	75	60
5.70	70	60
4.92	70	55
4.14	65	50
3.30	60	50
2.55	55	40
1.80	50	40
1.20	45	30
0.66	25	20

Sequence of Laser-Assisted Maskless Metallization Process

- Evaporate 1500 Å Ti (adherence) and 500 Å Pd (cap) over entire Si wafer
- Spin solution of silver neodecanoate in xylene on wafer
- Write Ag lines (50 μm) with Ar^+ laser (8 W) at 20 cm/sec scan speed
- Dissolve undecomposed silver neodecanoate film in acetone
- Electroplate 8 μm Ag on laser-deposited Ag lines
- Etch Ti and Pd leaving only grid lines

Laser-Metallized Cells



ORIGINAL PAGE IS
OF POOR QUALITY

PROCESSING

Effect of Laser Power on the Performance of Cells Fabricated by Laser-Assisted Metallization Process

<u>Cell ID</u>	<u>Laser Power Watt</u>	<u>J_{sc} (mA/cm²)</u>	<u>V_{oc} (mV)</u>	<u>FF</u>	<u>η (%)</u>
1	8.5	33.5	577	.787	15.2
2	7.0	34.3	582	.792	15.9
3	6.0	34.6	579	.788	15.8
4	4.0	35.1	582	.781	16.0
5	3.0	34.9	582	.785	16.0
6	2.0	34.5	584	.786	15.9
7	1.0	34.1	573	.761	15.2

PROCESSING

Laser-Metallized Solar Cells on 4 ohm-cm Float-Zone Silicon After AR Coating

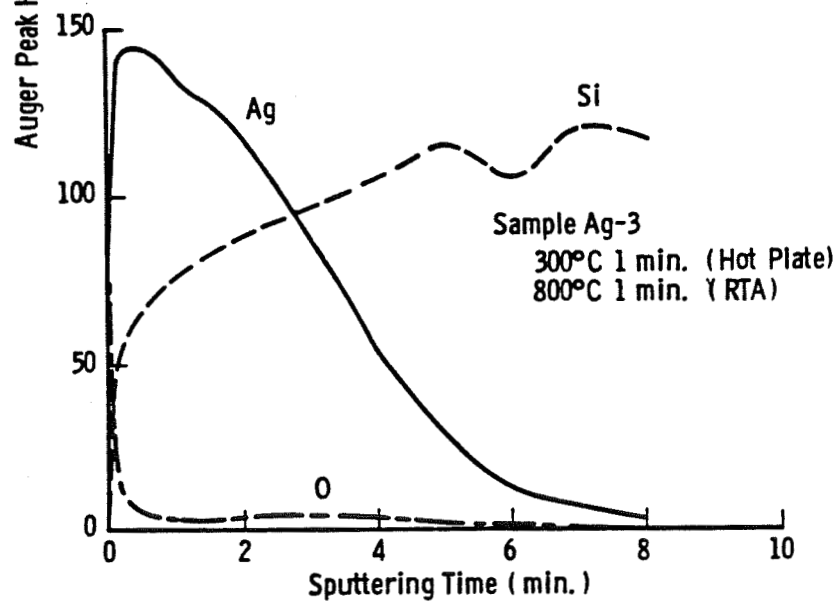
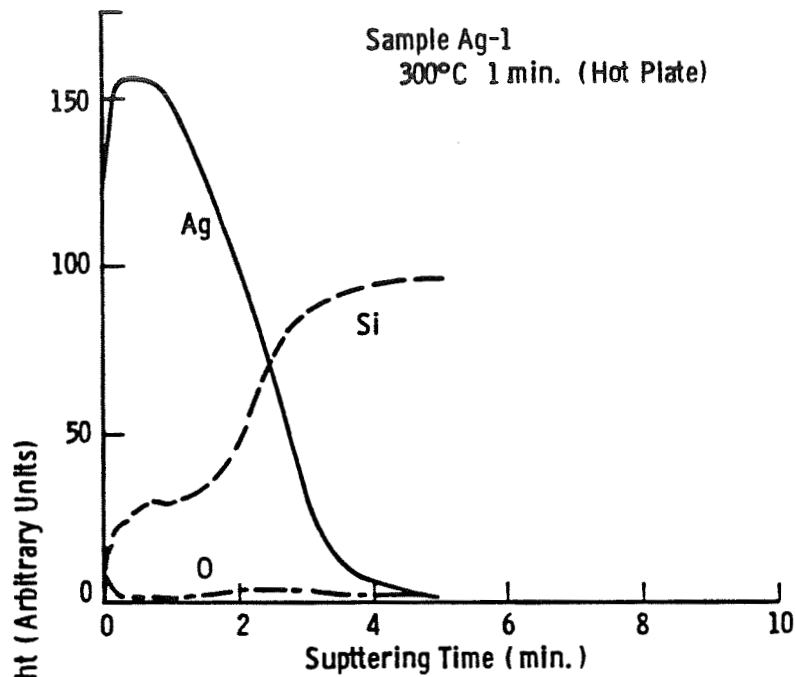
<u>Cell ID</u>	<u>J_{sc} (mA/cm²)</u>	<u>V_{oc} (mV)</u>	<u>FF</u>	<u>η (%)</u>
2	35.0	606	.754	16.0
3	34.9	603	.768	16.2
4	35.5	603	.750	16.0
5	34.8	601	.781	16.3
6	35.0	601	.779	16.4
7	35.4	603	.780	16.6
10	34.5	598	.778	16.1
11	33.8	604	.785	16.1
14	34.3	603	.789	16.3
15	34.3	604	.782	16.2
Q1+	35.1	609	.790	16.9

+Conventional Metallization/Lithography and no
passivation

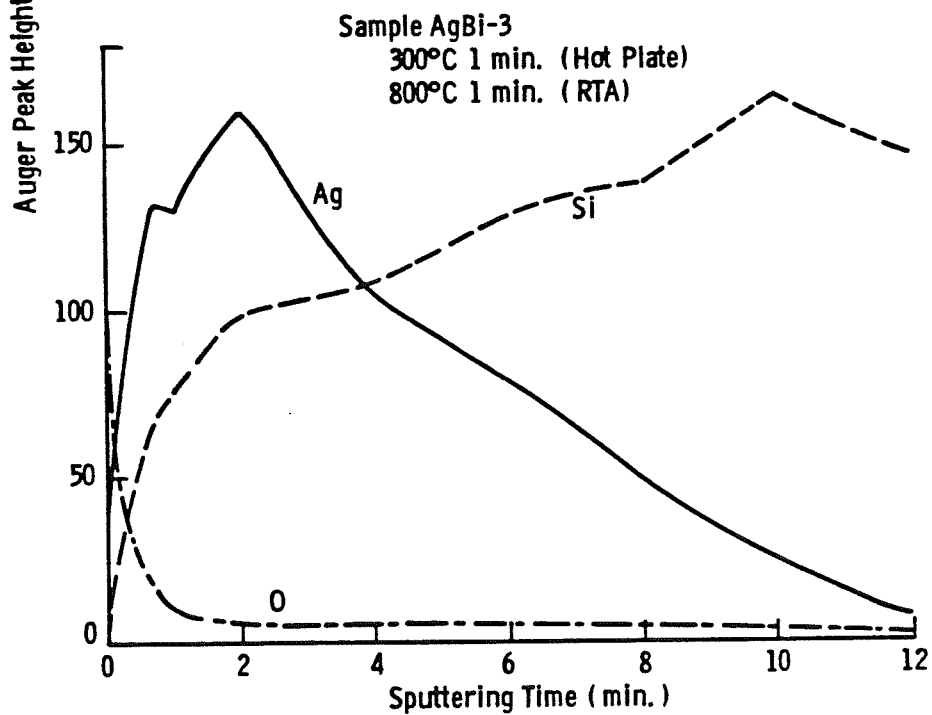
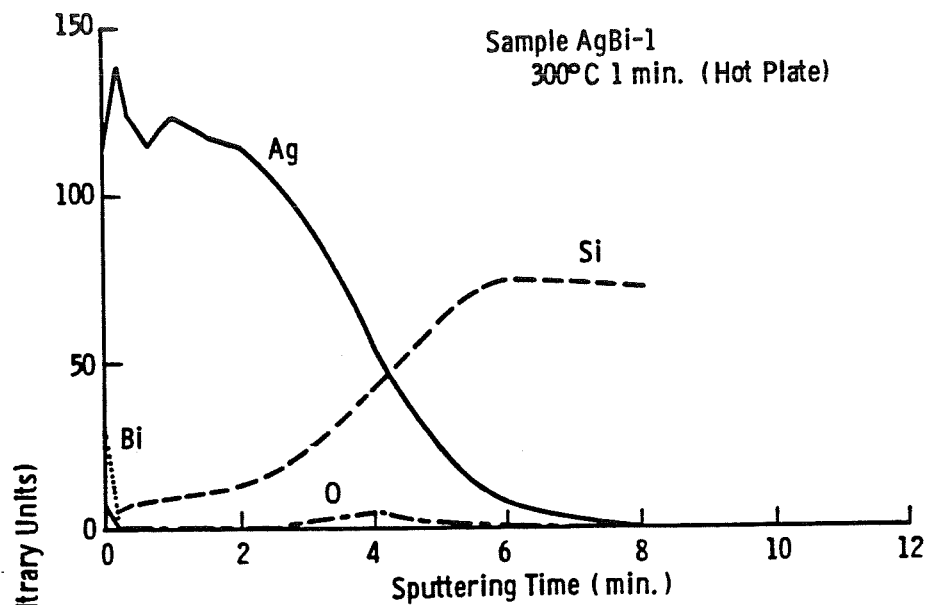
A Comparison of Lighted and Dark I-V Data of 16.6% Laser-Metallized Cell and 18.4% Cell Fabricated by Conventional Metallization and Photolithography

<u>Parameter</u>	<u>16.6% Laser-Metallized Cell</u>	<u>18.4% Oxide-Passivated Conventionally Metallized Cell</u>
J_{sc}	35.4 mA/cm ²	36.7 mA/cm ²
V_{oc}	604 mV	621 mV
FF	0.780	0.804
η	16.6%	18.4%
R_s	0.69 Ω -cm ²	0.56 Ω -cm ²
R_{sh}	103 k Ω -cm ²	150 k Ω -cm ²
J_o	1.4×10^{-12} A/cm ²	0.5×10^{-12} A/cm ²

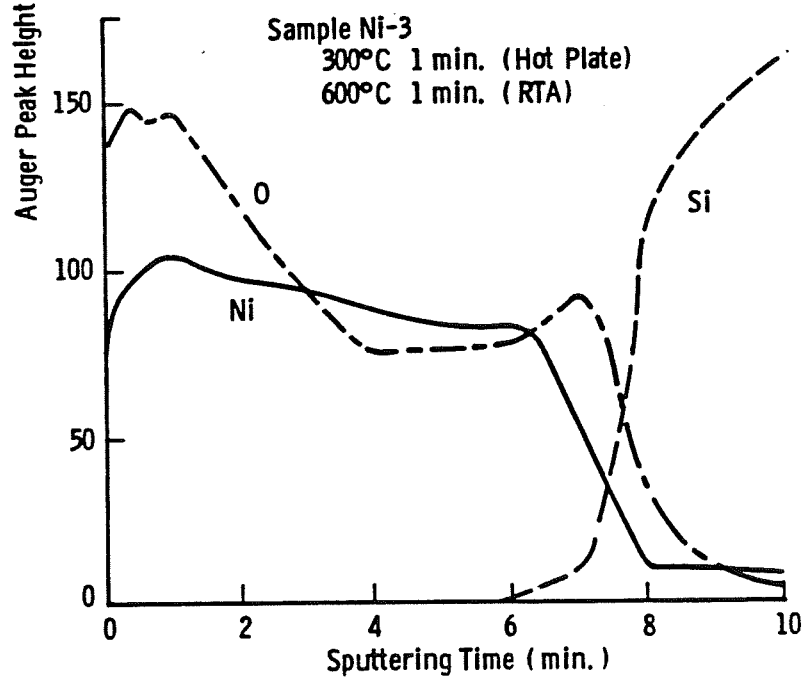
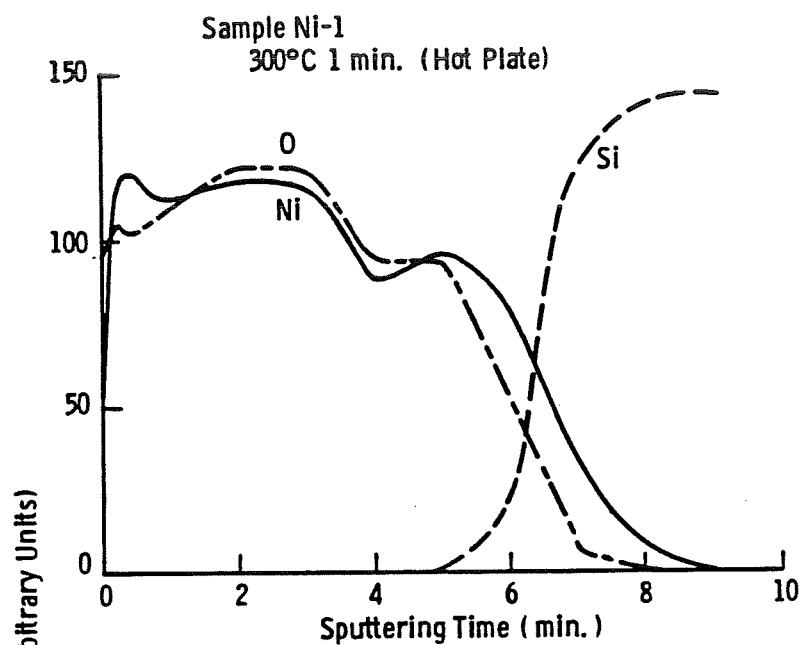
Relationship of Auger Peak Height Versus Sputtering Time



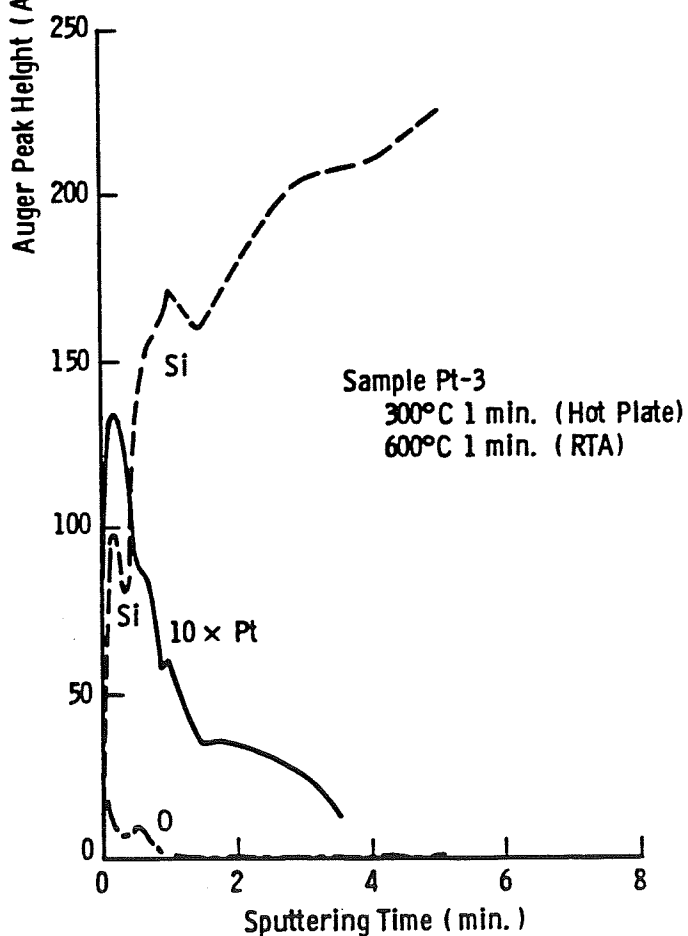
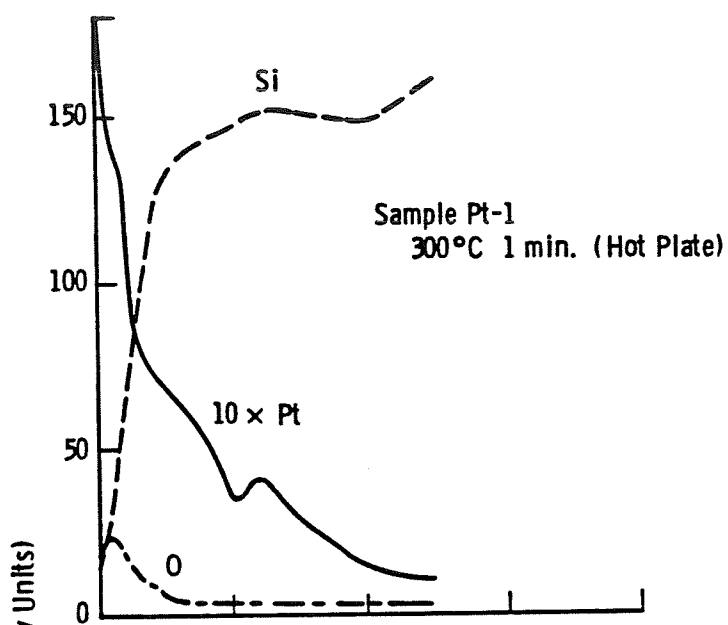
Relationship of Auger Peak Height Versus Sputtering Time (Cont'd)



Relationship of Auger Peak Height Versus Sputtering Time (Cont'd)



Relationship of Auger Peak Height Versus Sputtering Time (Cont'd)



Summary

- **Linewidths of 20 μm demonstrated**
- **Cells with efficiency up to 16.6% fabricated with a hybrid laser/evaporation maskless process**
- **Adherence of Ag to Si poor**
- **Alternative materials (Ag/Bi, Ni, Pt) also poorly adherent (preliminary result)**

PROCESS RESEARCH OF NON-CZOCHELSKI SILICON MATERIAL

WESTINGHOUSE ELECTRIC CORPORATION
ADVANCED ENERGY SYSTEMS DIVISION

R. B. Campbell

Contract Objectives

- INVESTIGATE SIMULTANEOUS DIFFUSION OF LIQUID PRECURSORS INTO DENDRITIC WEB SILICON TO FORM SOLAR CELL STRUCTURES
- INVESTIGATE PROCESS CONTROL PARAMETERS
- PERFORM COST ANALYSIS OF THE SIMULTANEOUS JUNCTION FORMATION PROCESS

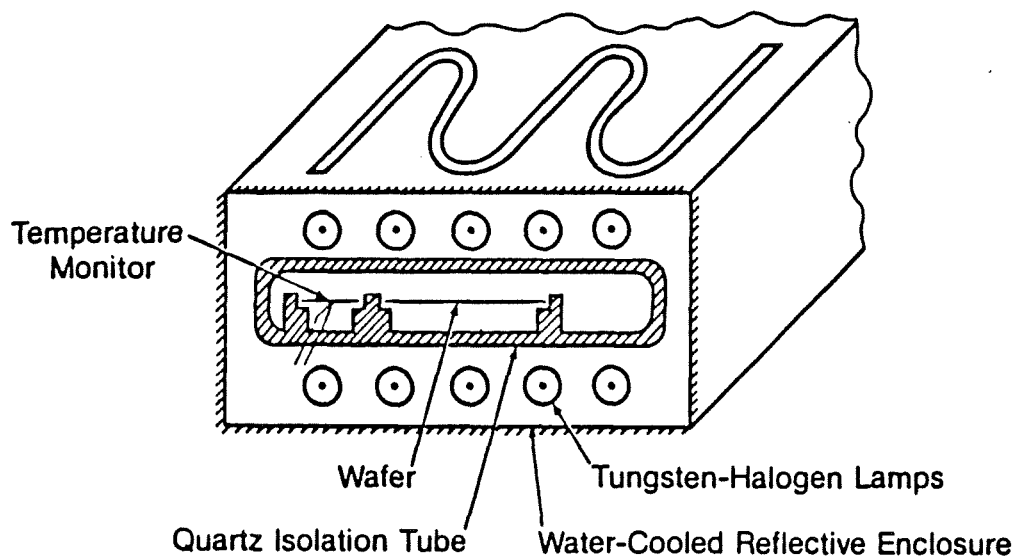
Potential Benefits of Simultaneous Diffusion

- REDUCE NUMBER OF PROCESSING STEPS
- LESS COSTLY PROCESSING (CAPITAL EQUIPMENT, MATERIALS)
- MORE RAPID PROCESSING
- MORE UNIFORM CELL PARAMETERS

Simultaneous Junction Formation by Flash Diffusion

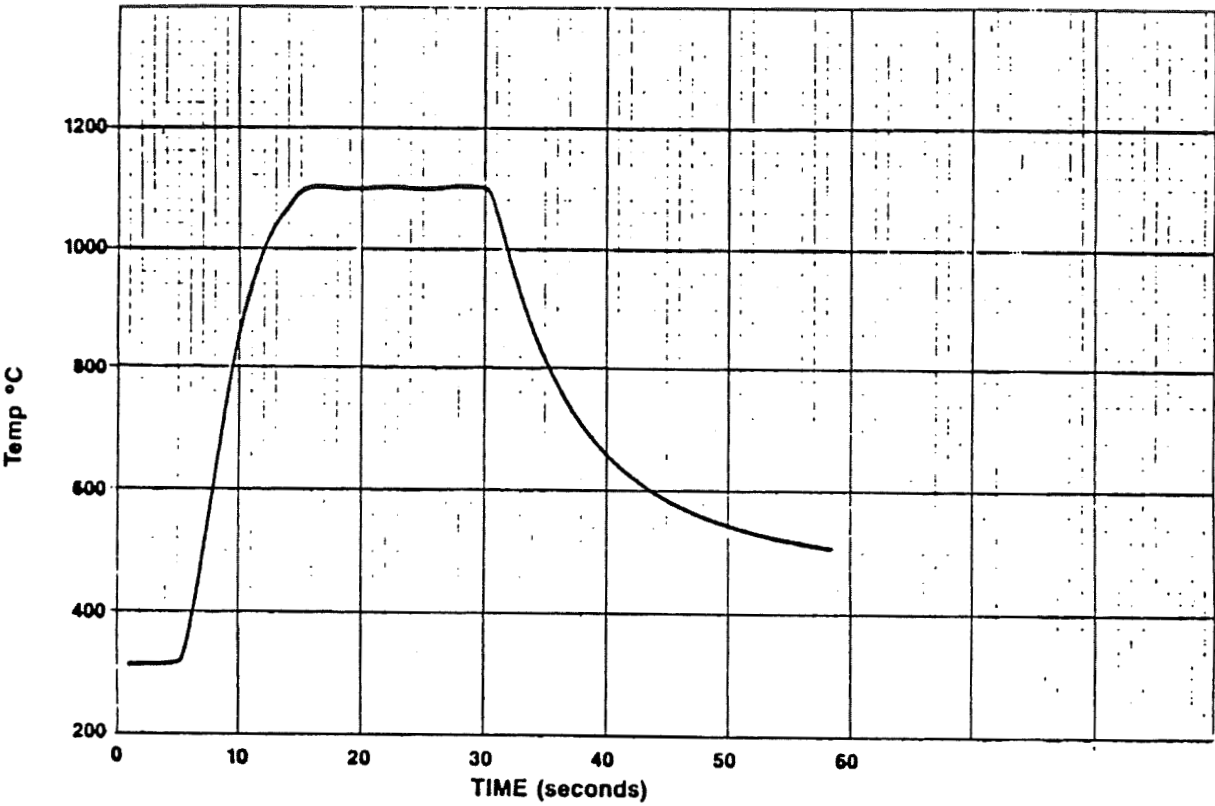
- NOVEL TECHNIQUE DEVELOPED TO ACHIEVE SIMULTANEOUS DIFFUSION WITHOUT CROSS-DOPING
- WEB STRIPS COATED WITH LIQUID PRECURSORS (B AND P DOPED) AND HEATED WITH A TUNGSTEN - HALOGEN LIGHT SOURCE.
- NOMINAL TIMES - 10-20 SEC
NOMINAL TEMPERATURE - 1050°C - 1150°C
- N^+PP^+ AND P^+NN^+ CELLS FABRICATED
- NO CROSS CONTAMINATION NOTED

HeatpulseTM Annealing Chamber

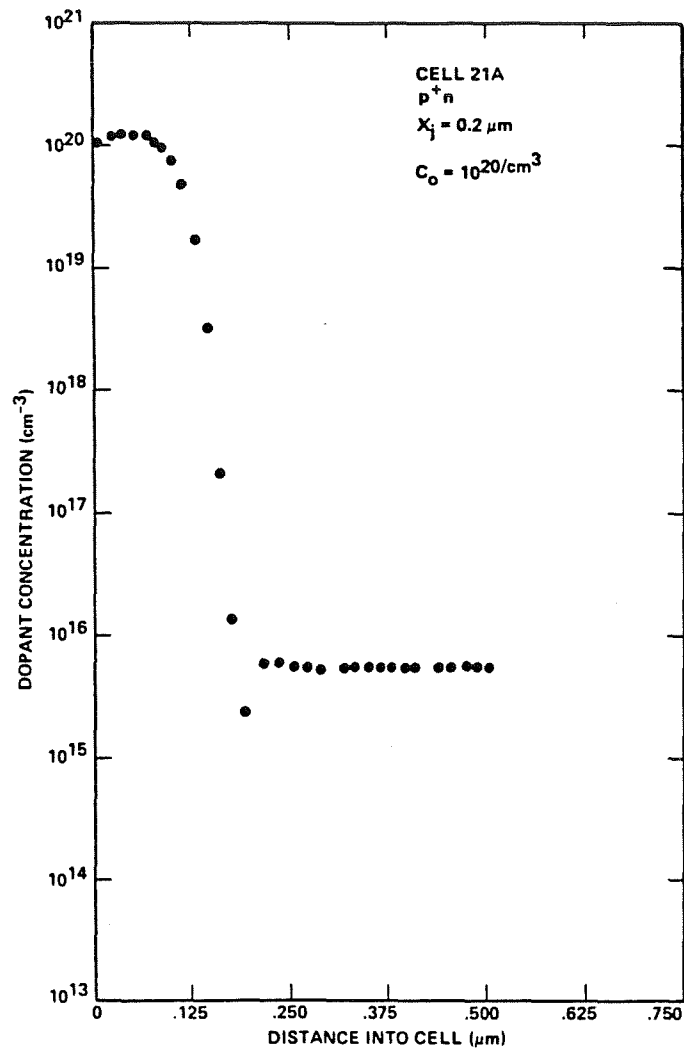


HeatpulseTM Temperature-Time Profile

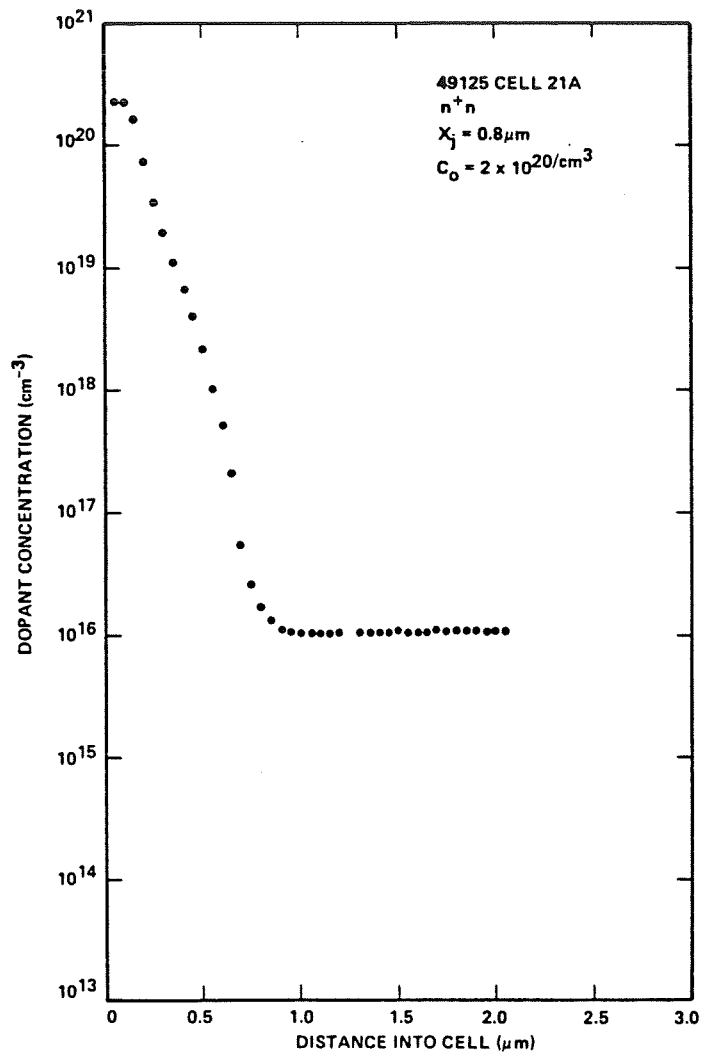
Sample No. WESTINGHOUSE - DENDRITIC WEB



Flash Diffusion: N-Type WEB Front Junction
(Dopant Concentration Versus Distance into Cell)



Flash Diffusion: N-Type WEB Back Junction
(Dopant Concentration Versus Distance into Cell)



Simultaneous Junction Formation by Flash Diffusion

OVERALL RESULTS

- SUITABLE JUNCTION DEPTHS ACHIEVED FOR N-TYPE DENDRITIC WEB
 P^+N - 0.15 μM TO 0.25 μM
 N^+N - 0.25 μM TO 0.80 μM
- FOR P-TYPE MATERIAL FRONT N^+P JUNCTION DEEPER THAN OPTIMUM TO ACHIEVE REQUIRED P^+P BSF
- ANNEALING OF DIFFUSED MATERIAL REQUIRED TO ACHIEVE HIGHEST EFFICIENCY - 750-800°C FOR 10 - 30 MIN
- EFFICIENCIES GREATER THAN 15.2% OBTAINED ON N-BASE CELLS - 24.5 cm^2 AREA
- P BASE CELLS GAVE MAXIMUM EFFICIENCY OF 12.5%

Flash Diffusion Verification

- 48 WEB STRIPS EACH OF:
0.4 ΩCM P TYPE GROWTH RUN
6 ΩCM P TYPE R499

0.2 ΩCM N TYPE GROWTH RUN
2 ΩCM N TYPE 5332
STRIPS 3 CM X 13 CM
- RUN R499 - 130 μM NOMINAL THICKNESS
RUN 5332 - 100 μM NOMINAL THICKNESS
- COAT WITH LIQUID PRECURSORS (B & P DOPED)
- DIFFUSE AT 1100°C/10 SEC IN ARGON
- LESS THAN 1% OF STRIPS BROKEN DURING DIFFUSION
- ANNEAL AT TEMPERATURES 900°C TO 750°C AND TIMES 10 MIN. TO 60 MIN. (6 CONDITIONS)
- FINISH BASELINE PROCESS

PROCESSING

Flash Diffusion Verification: Samples Diffused 1100°C/10 s Back Surface Reflector (No Passivation)

ANNEALING (TEMP. °C)	ANNEALING TIME (MIN)	CELL EFFICIENCY (%)			
		N BASE CELLS		P BASE CELLS	
		0.2 - 0.3 ΩCM	2 ΩCM	0.4 - 0.6 ΩCM	6-8 ΩCM
900	30	13.8	14.2	11.4	12.2
900	10	12.8	--	10.4	11.1
800	60	13.5	14.6	10.8	11.4
800	30	14.4	14.6	11.4	11.5
800	10	14.3	14.8	11.0	11.5
750	60	14.0	15.1	12.1	11.5

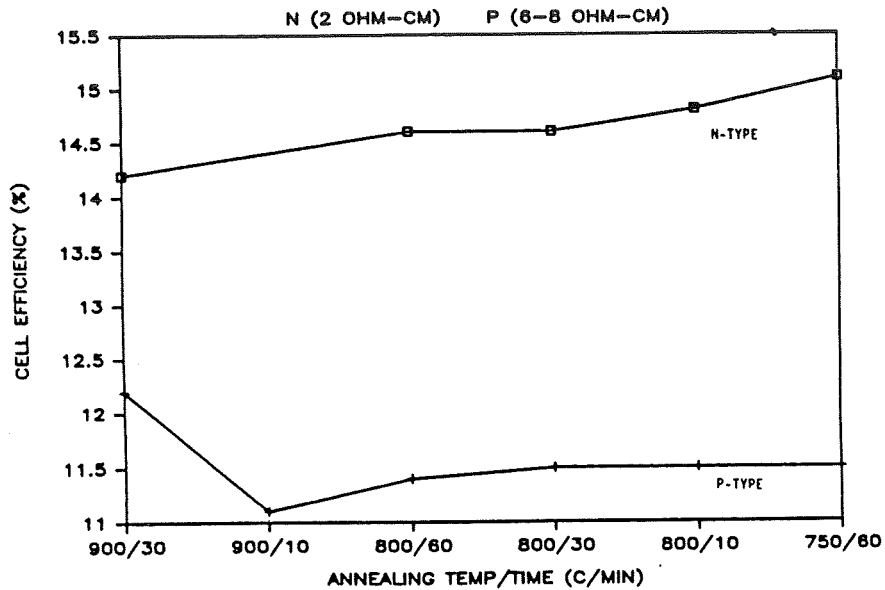
Diffusion Length in Flash-Diffused Cells

ANNEAL TEMP. (°C)	ANNEAL TIME (MIN)	DIFFUSION LENGTH (μM) BY SPV			
		P TYPE CELLS		N TYPE CELLS	
		0.2 ΩCM	6-8 ΩCM	0.2 ΩCM	2 ΩCM
900	30	--	50	---	160
900	10	--	25	125	185
800	60	--	92	---	145
800	30	--	75	---	168
800	10	--	75	---	130
750	60	65	--	---	165

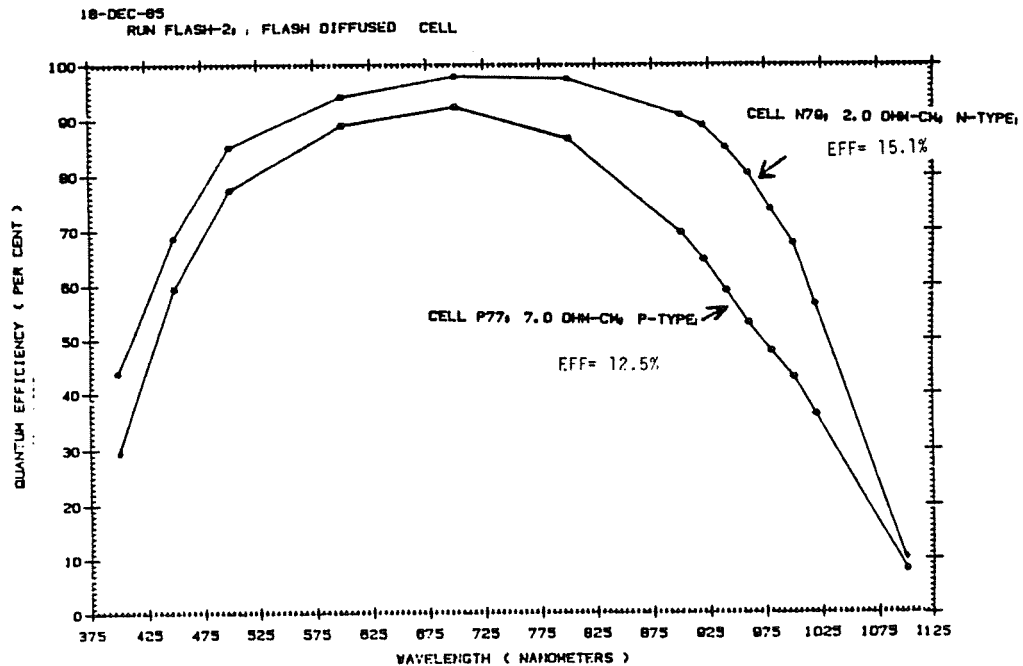
Representative Data from Selected Flash-Diffused Cells

Cell ID	Base Conductivity	Resistivity (Ω-cm)	Anneal Cycle (°C/min)	Eff. (%)	J ₀₁ (A/cm ²)	J ₀₂ (A/cm ²)	Ln (μm)
7N	N	0.32	900/30	13.4	4.1E-12	2.8E-4	---
10N	N	0.32	900/10	13.1	1.1E-12	1.8E-5	125
47N	N	2.0	900/30	14.2	1.2E-12	2.5E-5	170
58N	N	2.0	800/60	14.9	1.1E-12	2.8E-6	135
65N	N	2.0	800/30	14.7	1.2E-12	1.2E-6	168
79N	N	2.0	750/60	15.2	8.9E-13	7.1E-6	160
48P	P	9.0	900/30	12.5	3.3E-12	4.2E-8	50
57P	P	8.0	800/60	11.8	2.2E-12	9.8E-9	92
71P	P	8.0	800/30	12.2	3.7E-12	2.7E-8	70
77P	P	7.0	800/10	12.2	5.1E-12	6.0E-8	72

Flash Diffusion Results (Cell Efficiency Versus Annealing Temperature/Time)



Quantum Efficiency Plot



PROCESSING

Simultaneous Junction Formation by Flash Diffusion: Cost Analysis

- COMPARE SIMULTANEOUS JUNCTION FORMATION (FLASH DIFFUSION) WITH SEQUENTIAL DIFFUSION
- TWO PRODUCTION LEVELS CONSIDERED
 - 1 MW/YR - SEMI-AUTOMATED
 - 25 MW/YR - FULLY AUTOMATED
- COSTS CALCULATED IN 1985 \$ FOR DIFFUSION PROCESS STEP
- FORMAT A'S PREPARED

Cost Analysis

ALL COSTS - 1985 \$/WATT

PROCESS STEP COST (DIFFUSION)		
PRODUCTION LEVEL (MW/YR)	SIMULTANEOUS - FLASH DIFFUSION	SEQUENTIAL DIFFUSION
1	0.57	0.92
25	0.072	0.134

Simultaneous Junction Formation by Flash Diffusion: Conclusions

CONCLUSIONS:

- SIMULTANEOUS JUNCTION FORMATION BY FLASH DIFFUSION VERIFIED
- NO CROSS-CONTAMINATION NOTED
- ANNEALING REQUIRED AFTER DIFFUSION TO ACHIEVE HIGHEST CELL EFFICIENCY
- TECHNIQUE IS COMPATIBLE WITH WESTINGHOUSE BASELINE PROCESS SEQUENCE
- N-BASE CELLS WITH EFFICIENCIES OF 15.2% FABRICATED USING FLASH DIFFUSION (AREA = 24.5 CM²)
- COST ANALYSIS SHOWS SAVING OF 60 - 85% IN DIFFUSION PROCESS STEP

RAPID THERMAL PROCESSING OF CZOCHRALSKI SILICON SUBSTRATES: DEFECTS, DENUDED ZONES, AND MINORITY CARRIER LIFETIME

NORTH CAROLINA STATE UNIVERSITY

G. S. Rozgonyi, D. K. Yang, Y. H. Cao, and Z. Radzimski

Rapid Thermal Processing of Czochralski Silicon: Objectives

To evaluate rapid thermal processing as a viable procedure for:

1. Czochralski substrate modification using high temperature defect-dissolution treatments,
2. Rapid junction activation following ion implantation

Diagnostic Tools

1. MOS Capacitor -- minority carrier lifetime
2. X-Ray Topography -- defect delineation
3. Nomarski Optical Microscopy & Preferential Chemical Etching -- defect delineation
4. Fourier Transform Infrared Microscopy -- oxygen precipitation kinetics

Metal Oxide Semiconductor Capacitor - C

1. Capacitance-voltage (C-V) measurements
2. Capacitance-time (C-t) measurements
3. C-V, C-t measurements at different temperatures T
4. Minority carrier generation and recombination lifetime (τ_g and τ_r)

PRECEDING PAGE BLANK NOT FILMED

Change of Inversion Layer Charge Density with Time

$$\frac{dn_s}{dt} = \underbrace{\left(\frac{n_i (W - W_F)}{\tau_g} + n_i s \right)}_A + \underbrace{\left(\frac{n_i^2 D_n}{N_A L_n} \right)}_B$$

Room temperature $A \gg B$ (Zerbst, 1966)

Elevated temperature $A \ll B$ (Schroder, 1984)

n_s - inversion layer charge density

W_F - final space charge region width

W - space charge width

n_i - intrinsic carrier density

D_n - diffusion constant

L_n - diffusion length

N_A - substrate doping concentration

τ_g - generation lifetime

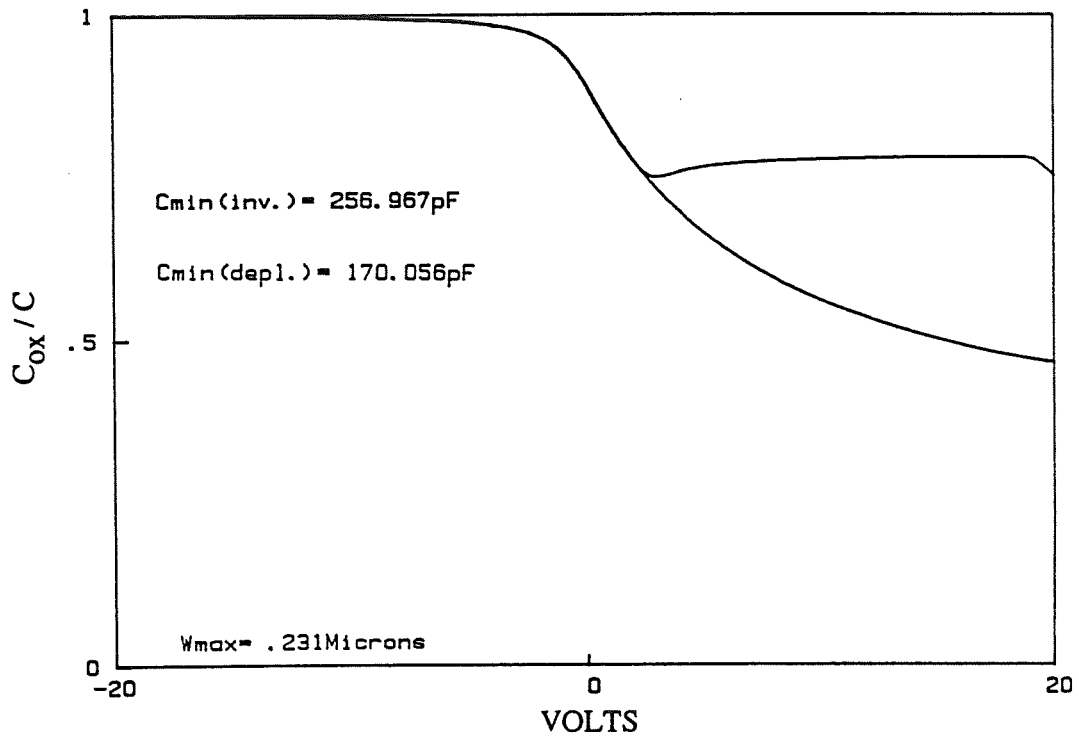
s - surface recombination velocity

τ_r - recombination lifetime ($\tau_r = L_n^2/D_n$)

PROCESSING

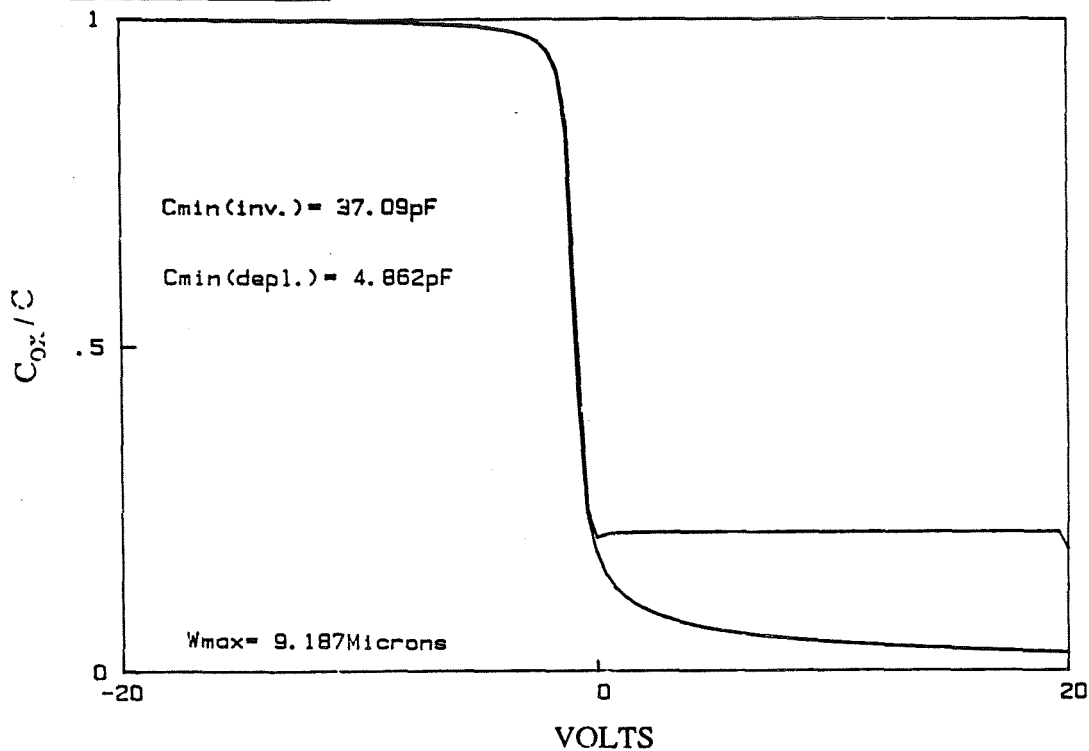
Capacitance Versus Voltage (Sample Y2)

Cox= 340.278pF	Cfb= 327.203pF	
Cmin/Cmax= .755	Cfb/Cox= .962	Qss= 2.272E+11ions/cm ²
Area= 7.58528E-03cm ²	Vfb(0)=-1.738Volts	Sample number = Y2
<u>Nsub= 1.96658E+17cm⁻³</u>	Vt= 4.374Volts	

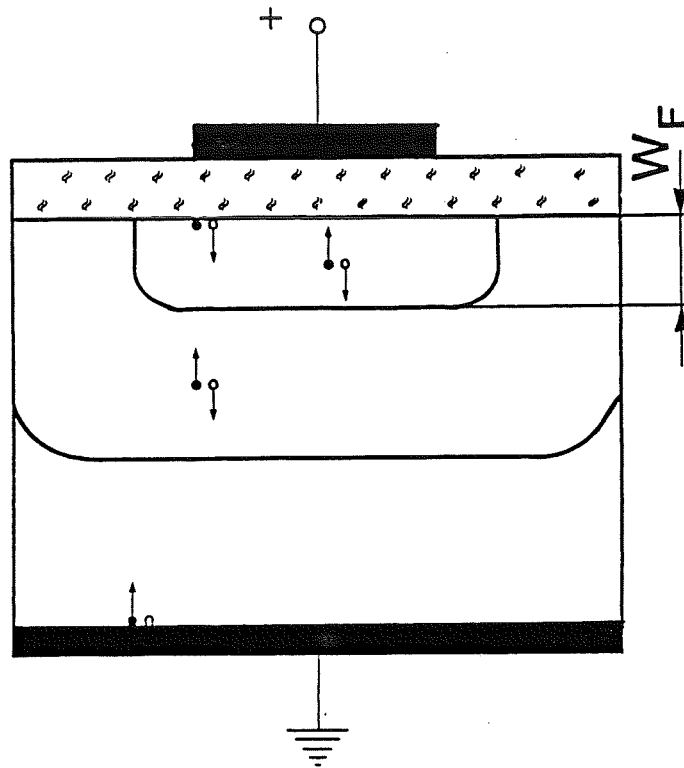


Capacitance Versus Voltage (Sample Z27)

Cox= 198.3pF Cfb= 119.474pF Qss= 3.66E+10ions/cm²
Cmin/Cmax= .187 Cfb/Cox= .602 Sample number = Z27
Area= .0044204cm² Vfb(0)= -.912Volts
Neub= 7.213E+14cm⁻³ Vt= -.091Volts



Zerbst Analysis (Room Temperature)

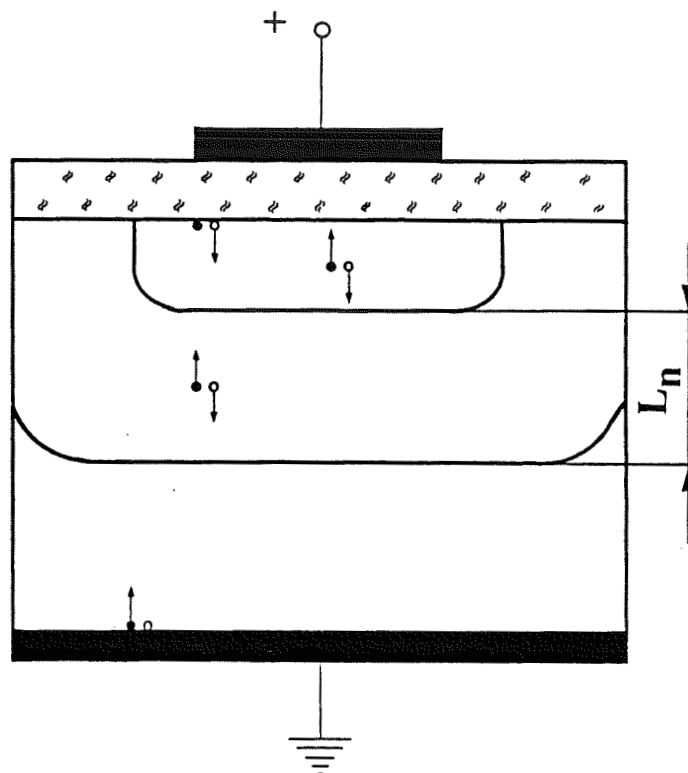


$$\frac{-d(C_{ox}/C)}{dt} \quad \text{vs} \quad \frac{C_F}{C-1}$$

$\tau_g \propto \text{slope}$

$s \propto \text{intercept}$

Schroder Analysis (Elevated Temperature)

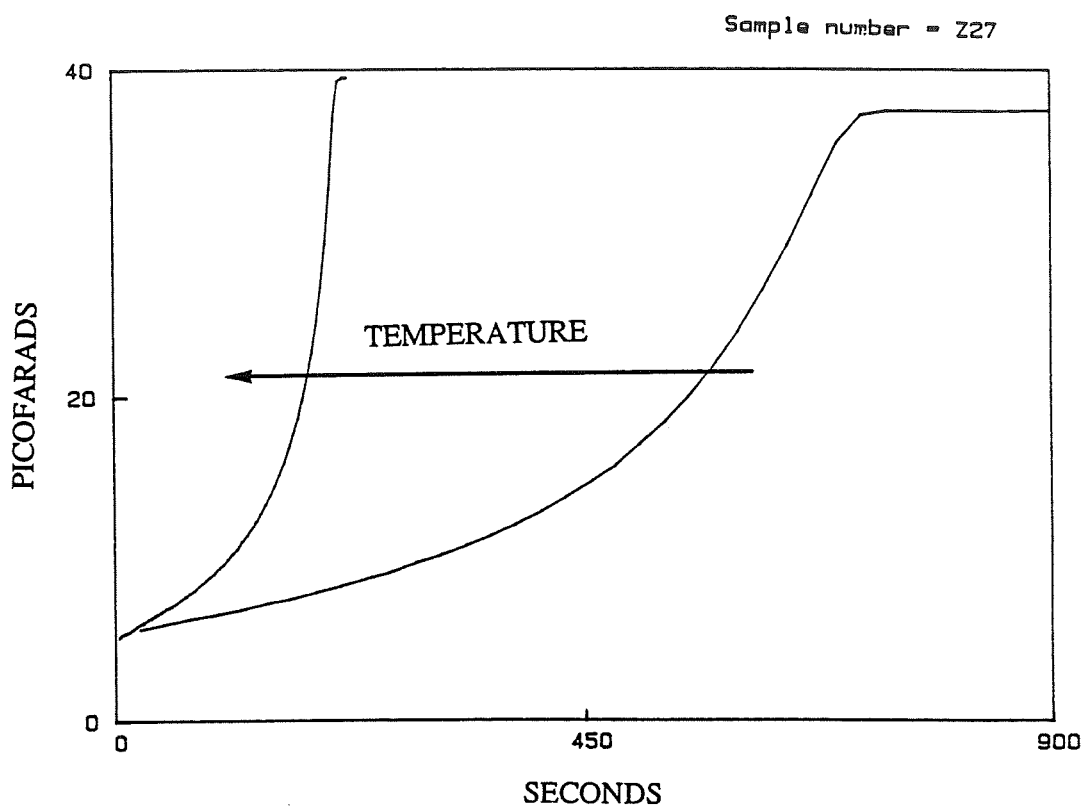


$1 - (C_F / C)^2$ vs time

$$\tau_r \propto L_n^2$$

$$L_n \propto \text{slope}$$

Capacitance Versus Time (Sample Z27)



X-Ray Topography

1. X - Ray Source: Marconi-Elliot GX-21
(15kW, Rotating anode)

2. Cameras: - Lang Transmission
- Double Crystal

3. Sample treatment conditions:

- i. Virgin
- ii. Lo-Hi + RTP combination
- iii. Li decoration

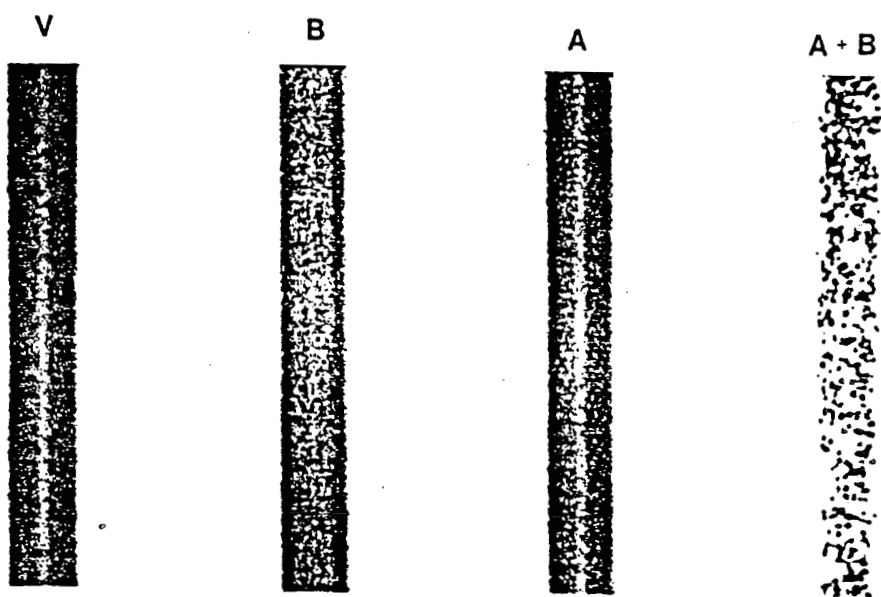
Surface Recombination Velocity/X-Ray Topography

MoK α 220 X30

V: Virgin

A: 700°C / 16 h dry O₂ + 0.0425HCL

B: 1100°C / 10min dry O₂ + 60minwet O₂ + 10mindry O₂



Nomarski Optical Microscopy and Preferential Chemical Etching

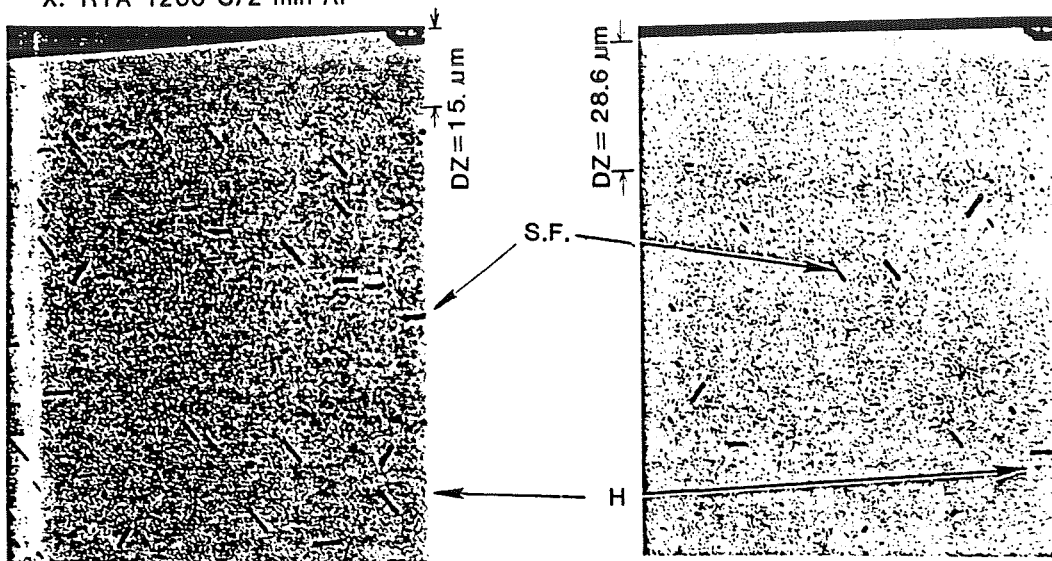
Etchant: Secco

Observation: 1. Depth of denuded zone (DZ)
2. Density and size of oxygen precipitates, stacking faults and dislocation.

P: $700^{\circ}\text{C}/16\text{h dry O}_2+2\% \text{ HCl}+1100^{\circ}\text{C}/(10\text{min dry}+65\text{min wet}+10\text{min})\text{O}_2+2\% \text{ HCl}$
 $+1100^{\circ}\text{C}/15\text{min dry O}_2+2\% \text{ HCl}$

V: Virgin

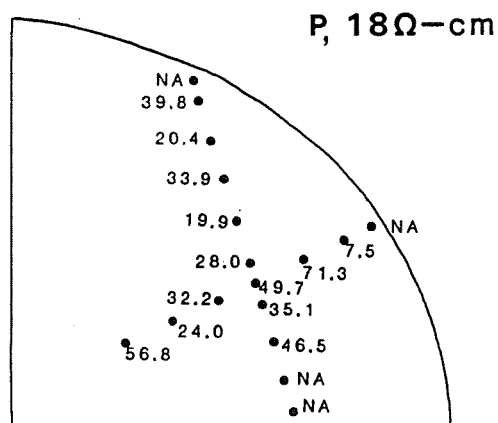
X: RTA $1200^{\circ}\text{C}/2 \text{ min Ar}$



V + P

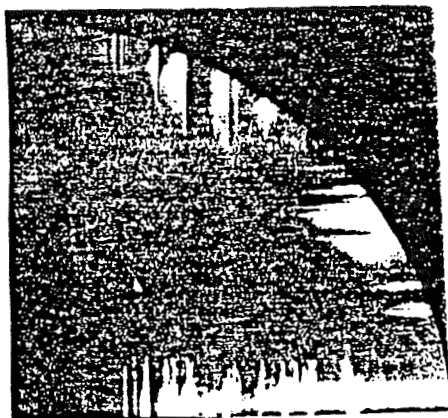
X + P

Minority Carrier Lifetime (Units in μs)



Heat Treatment

RTP(1200°C/2min) in Ar
+1100°C/(10min dry+65min wet+10min dry)O₂



Heat Treatment of Samples

- A : 700°C/16h dry O₂ + 2% HCl
- B : 1100°C/(10 min dry+65 min wet+10 min dry)O₂ + 2% HCl
- C : 1100°C/15 min dry O₂
- V : Virgin
- X : RTP 1200°C/2 min in Ar
- Y : 1200°C/30 min in Ar
- Z : 1250°C/30 min in dry O₂ + 2% HCl
- w : 1250°C/30 min in Ar

Arrays of Heat Treatments

	C	A+C	B+C	A+B+C
V	V+C	V+A+C	V+B+C	V+A+B+C
X	X+C	X+A+C	X+B+C	X+A+B+C
Y	Y+C	Y+A+C	Y+B+C	Y+A+B+C
Z	Z+C	Z+A+C	Z+B+C	Z+A+B+C
W	W+C	W+A+C	W+B+C	W+A+B+C

Heat Treatment of Samples

- A : 700°C/16h dry O₂ + 2% HCl
B : 1100°C/(10 min dry+65 min wet+10 min dry)O₂ + 2% HCl
C : 1100°C/15 min dry O₂ + 2% HCl

V : Virgin	}	C
X : RTP 1200°C/2 min in Ar		A + C
Y : 1200°C/30 min in Ar		B + C
Z : 1250°C/30 min in dry O ₂ + 2% HCl		A + B + C
W : 1250°C/30 min in Ar		

Minority Carrier Lifetime (τ_g , μs)

	V+C	X+C	X+A+B+C
Group Z1	111.0	15.6	83.8
Group Z2	57.5	85.7	159.0
	V+C	Z+C	Z+A+B+C

USE OF LOW-ENERGY HYDROGEN ION IMPLANTS IN HIGH-EFFICIENCY CRYSTALLINE-SILICON SOLAR CELLS

PENNSYLVANIA STATE UNIVERSITY

S. J. Fonash, R. Singh, and H. C. Mu

Basic Effects of Low-Energy H^+ Implants

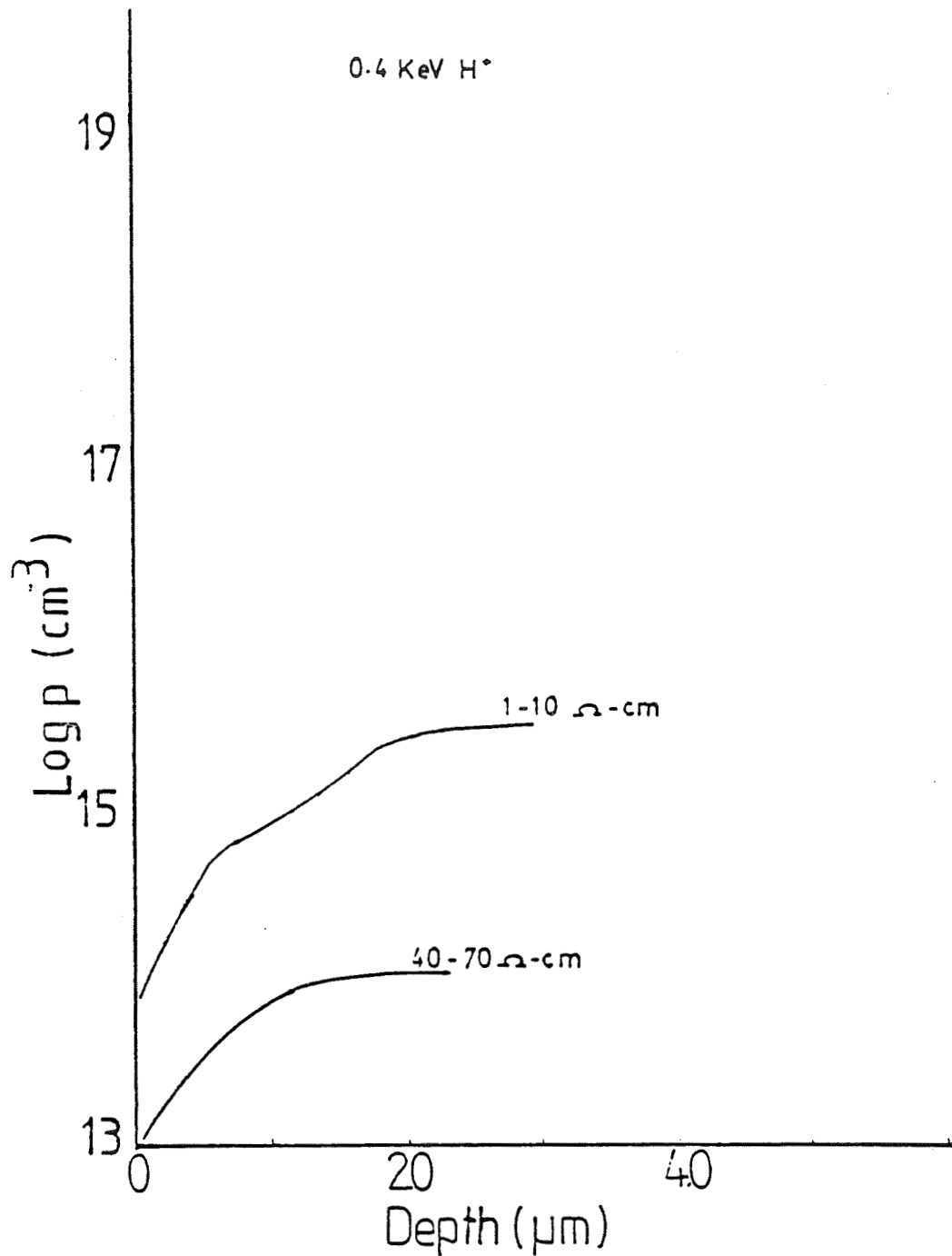
- A. BORON NEUTRALIZATION
- B. EFFECT ON ELECTRICALLY ACTIVE METALLIC IMPURITIES
- C. PASSIVATION OF DANGLING BONDS
- D. DEEP PERMEATION
- E. HYDROGEN CAUSED DAMAGE - SYNERGISTIC EFFECTS

Effects of Low Energy H^+ Implants on Solar Cell Behavior

- A. EFFECT ON BASE
- B. EFFECT ON SPACE CHARGE LAYER
- C. EFFECT ON EMITTER

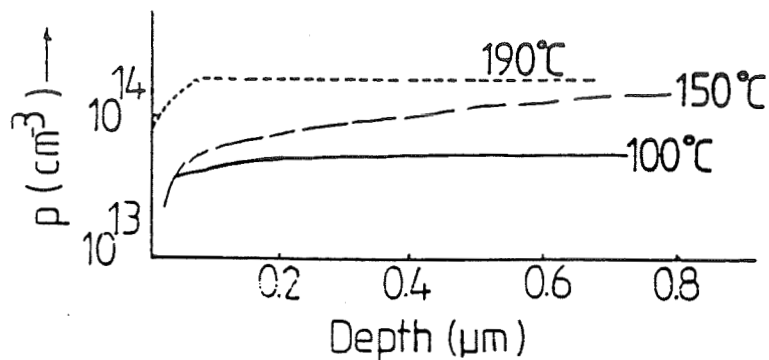
PRECEDING PAGE BLANK NOT FILMED

Hole Concentration Profiles (Moderately Doped p-type Si)



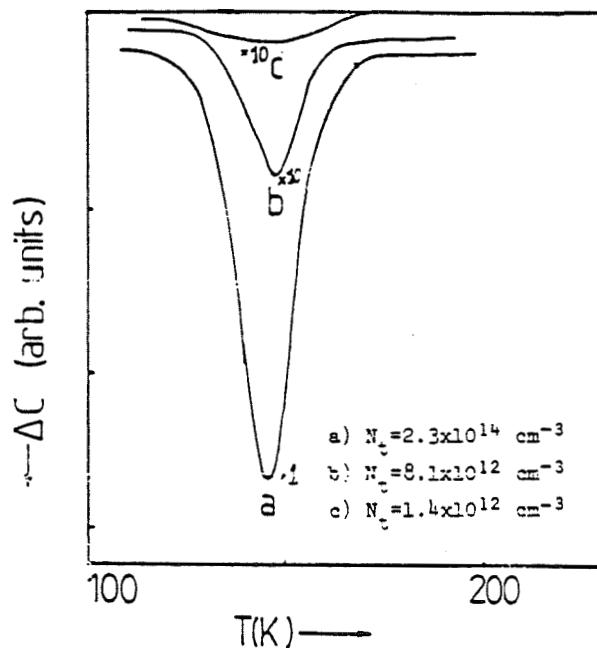
Spreading resistance plots showing the hole concentration in moderately doped (10^{15}cm^{-3} and $2 \times 10^{14}\text{cm}^{-3}$) p-type Si samples after exposing them to 0.4KeV H^+ ions for 1 minute. The incident fluence of H ions was 10^{18}cm^{-2} .

Hole Concentration Profiles (B-doped p-type Si)



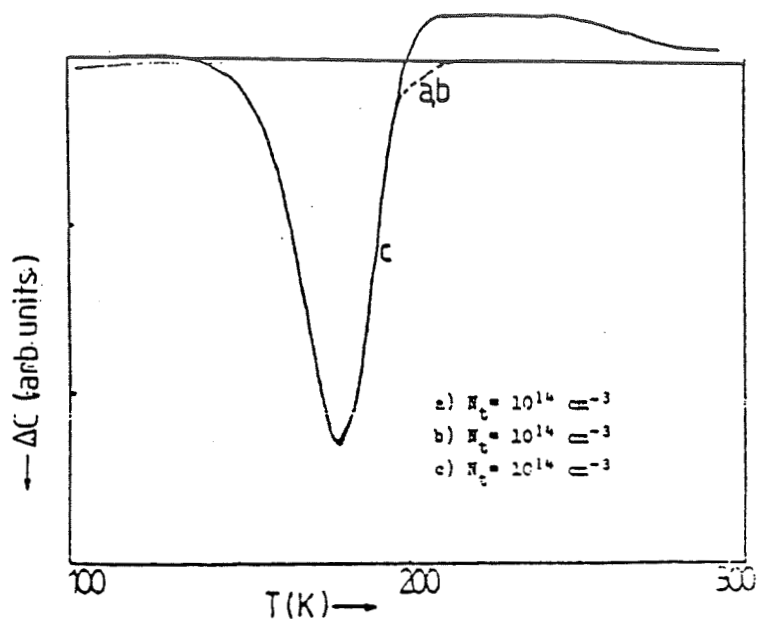
Hole concentration in H-ion-bombarded p-Si doped with $2 \times 10^{14} \text{ cm}^{-3}$ boron atoms after annealing for 1 hr at the temperature shown. Note that a 190 °C heat treatment anneals out all the compensating defects at the surface.

Deep Level Transient Spectra (Cr-doped p-type Si)



Curves showing the DLTS spectra obtained from Schottky-diodes made on Cr doped p-Si, as a function of processing; a) no treatment. b) 300 °C 1hour anneal in an inert ambient. c) 0.4KeV H^+ implant for 5 minutes. Note that although the concentration of the Cr levels decreases after both heat treatment and after H^+ bombardment, the reduction is much more pronounced in the latter case.

Deep Level Transient Spectra (Ti-doped p-type Si)

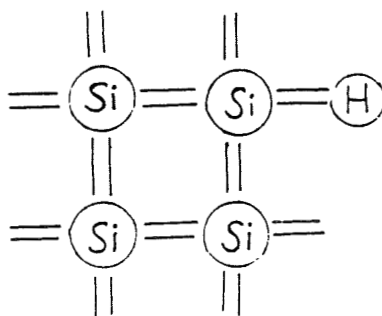


Curves showing the DLTS spectra obtained from Schottky-diodes made on Ti doped p-Si, as a function of processing; a) no treatment. b) 300 °C 1 hour anneal in an inert ambient. c) 0.4 KeV H^+ implant for 5 minutes. Note that the concentration of the Ti levels is insensitive to these processes.

Data from DLTS Spectra Establish that H^+ Low-Energy Implants:

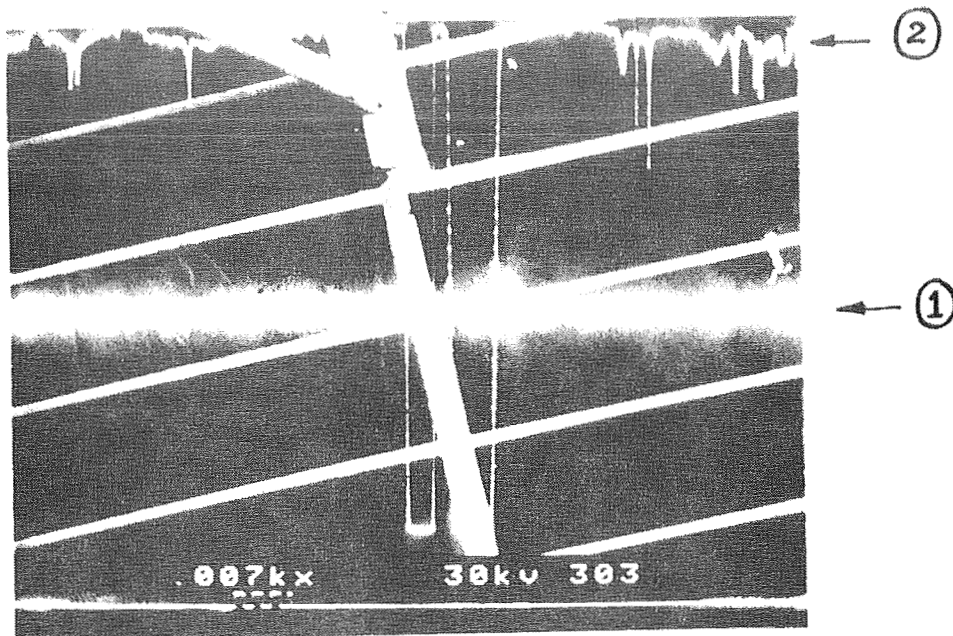
- A. DEFINITELY DO NOT AFFECT ALL METALLIC DEEP LEVELS.
- B. ONLY AFFECT THE LEVELS OF FAST DIFFUSERS.
- C. PASSIVATION OF FAST DIFFUSERS? ENHANCED DIFFUSION OF FAST DIFFUSERS (DUE TO RADIATION) AND GETTERING?

Passivation of Dangling Bonds

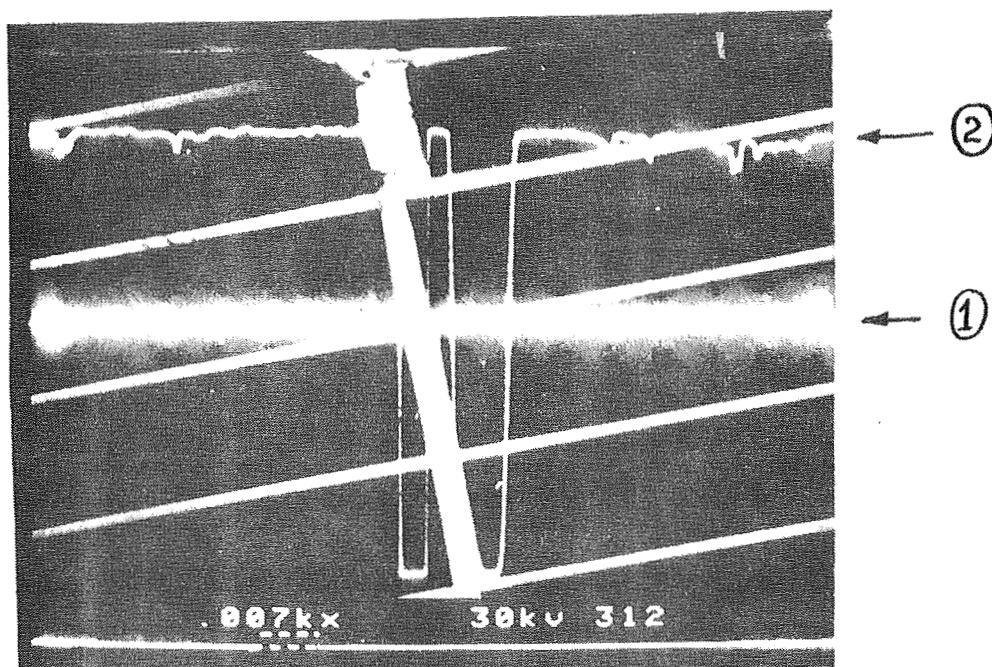


Electron Beam Induced Current Scans

ORIGINAL PAGE IS
OF POOR QUALITY

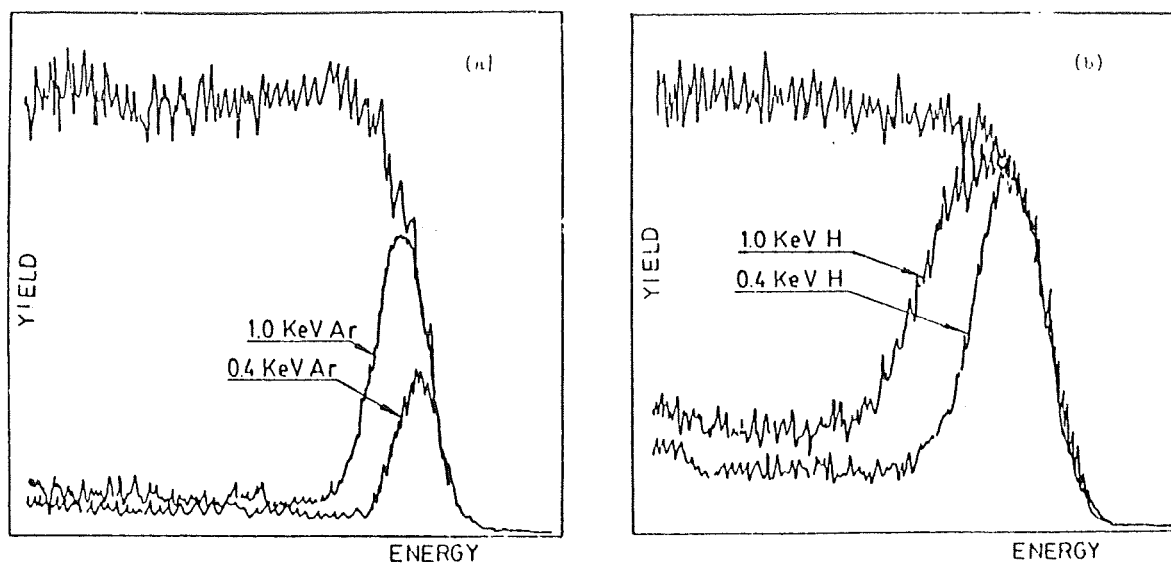


EBIC Scans taken on the front surface before any H^+ treatment.



Scans taken on the front surface after implanting the device with H^+ on the back of the wafer.

Rutherford Backscattering Spectra



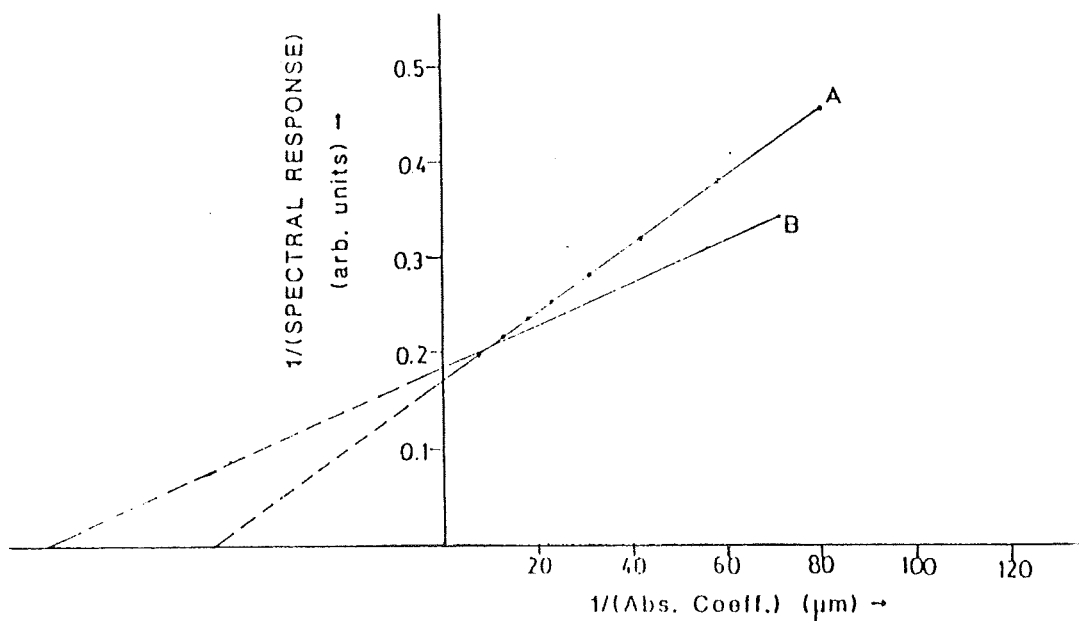
Rutherford backscattering data in the channeling and random mode from Si samples subjected to low-energy ion-beams. Note that as the energy of the incident ions is increased, more damage is introduced at the Si surface. Further, note that H ions introduce more lattice damage than Ar ions.

Spectral Response

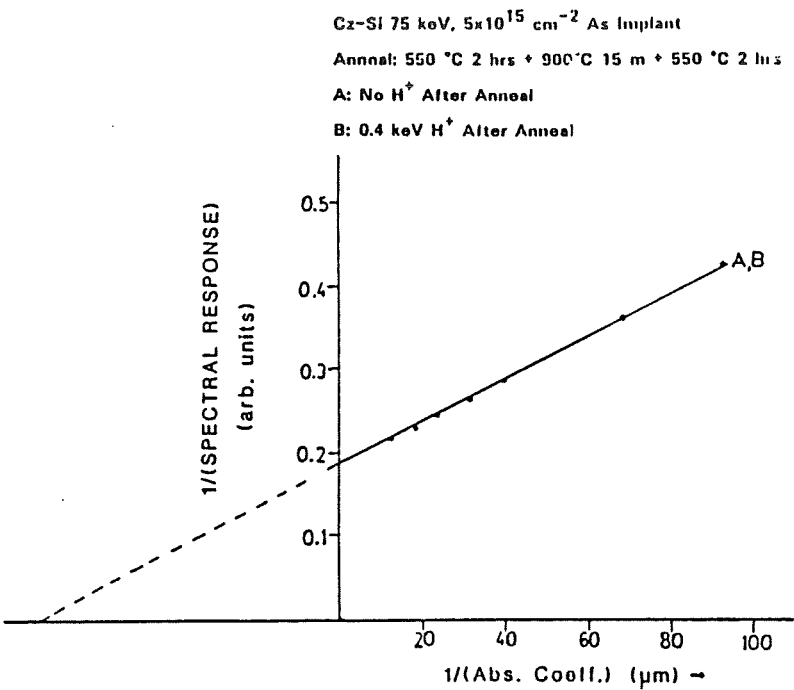
Dendritic Web Solar Cell 15-3

A: no H^+

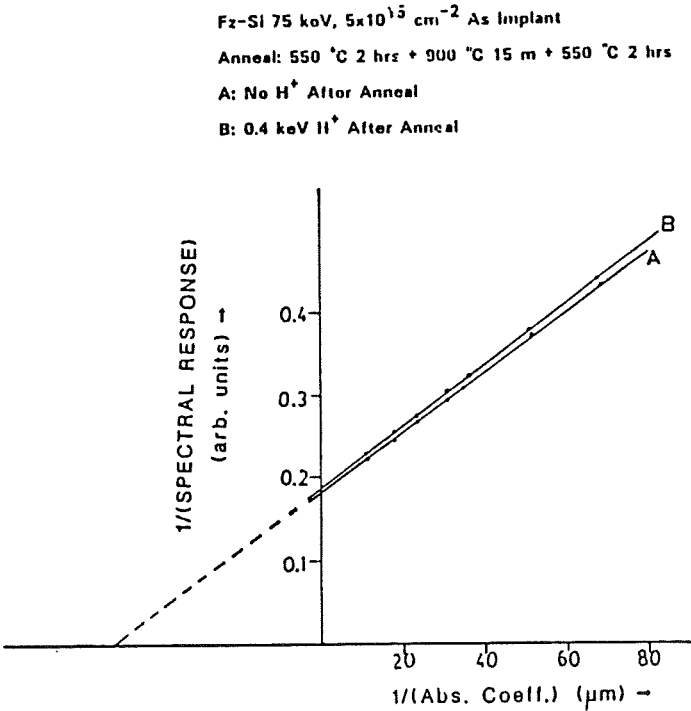
B: 0.4 keV H^+



Spectral Response



Spectral Response



Effect of H on Space Charge Region of Solar Cells

Device	L_n Before H^+	L_n After H^+	I_0 before H^+ (A/cm ²)	I_0 after H^+ (A/cm ²)	I_0 base (A/cm ²) Theoretical
S7 Cz-Si	75	75	3.096×10^{-9}	6.47×10^{-11}	1.1×10^{-11}
S25 (Fz-Si)	51	51	1.667×10^{-9}	1.57×10^{-10}	10^{-12}

Total Saturation Current and Saturation Current Component
Due to Emitter Transport for Different Devices

Processing	J_0 (pA/cm ²)	J_{0e} (pA/cm ²)
4412-5C as is	3.78	1.71
4412-5C no oxide	7.13	5.06
4412-5C no oxide after H^+	3.90	1.83

$$J_{0b} = 2.07 \times 10^{-10-2} \text{ A.cm}^2$$

Surface Recombination Velocity Values for Different Devices

Model	S_p with oxide	S_p no oxide	S_p no oxide with H^+
-------	---------------------	-------------------	------------------------------

$$\text{Roulston} \quad 1.53 \times 10^4 \quad 5.66 \times 10^4 \quad 1.65 \times 10^4$$

$$J_{0e} \text{ (with oxide)} = 3.786 \times 10^{-12} \text{ A.cm}^2.$$

$$J_{0e} \text{ (without oxide)} = 7.13 \times 10^{-12} \text{ A/cm}^2.$$

$$J_{0e} \text{ (no oxide + 0.4 keV } H^+) = 3.90 \times 10^{-12} \text{ A/cm}^2.$$

Conclusions

A. HYDROGEN IMPLANTS ARE VERY USEFUL BECAUSE

1. CAN PASSIVATE DANGLING SI BONDS AT BULK AND SURFACE DEFECTS.
2. CAN PERMEATE DEEPLY DOWN DISLOCATIONS AND GRAIN BOUNDARIES.
3. CAN GETTER (OR PASSIVATE) FAST DIFFUSING METALLIC IMPURITIES (BUT NOT SLOW DIFFUSING IMPURITIES - AT LEAST IF DOPED FROM THE MELT).

B. HYDROGEN IMPLANTS CAN IMPROVE CELLS THROUGH IMPROVEMENT OF

1. BASE
2. SPACE CHARGE LAYER
3. EMITTER (AND EMITTER SURFACE)

C. CAUTIONS

1. HYDROGEN IMPLANTS THEMSELVES CAUSE DAMAGE.
2. HYDROGEN CAUSES BORON NEUTRALIZATION (WHICH ANNEALS OUT IF $T \geq 180^{\circ}\text{C}$ OR IS NOT PRESENT IF PROCESSING TEMPERATURE $\geq 150^{\circ}\text{C}$).

LOW-PRESSURE, CHEMICAL VAPOR DEPOSITION POLYSILICON

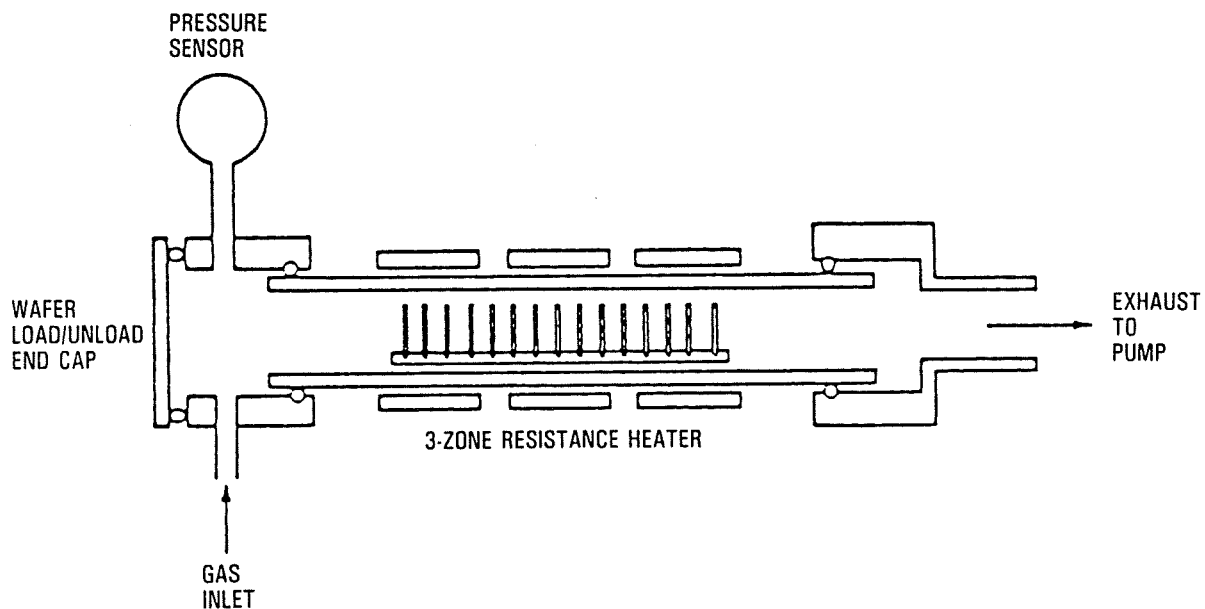
JET PROPULSION LABORATORY

B. D. Gallagher and G. C. Crotty

Polysilicon is Used for Contact Passivation to:

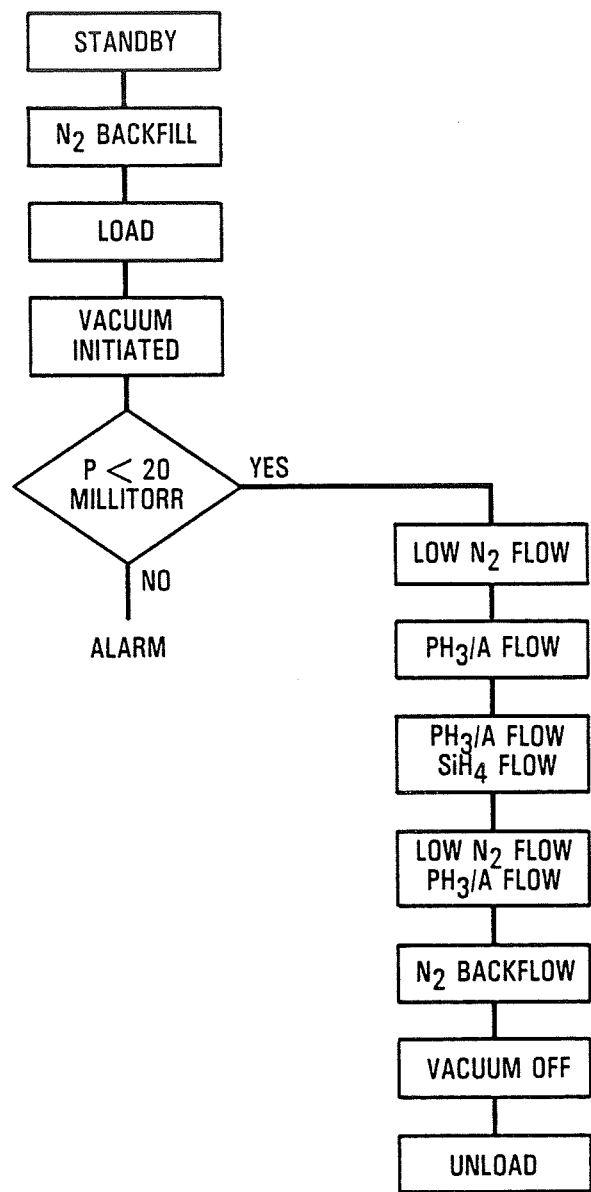
- Lower surface recombination velocity
- Increase Voc
- Increase cell efficiency

Reactor for LPCVD Polysilicon

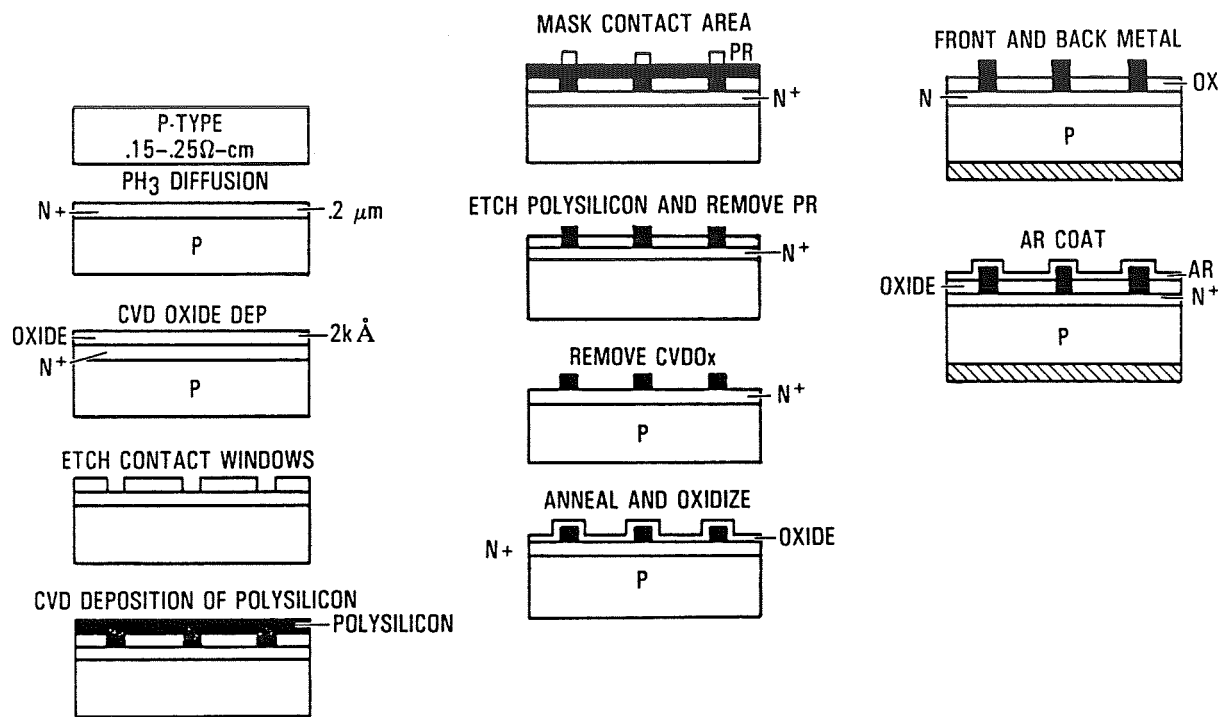


PRECEDING PAGE BLANK NOT FILMED

Algorithm for the LPCVD Polysilicon Process



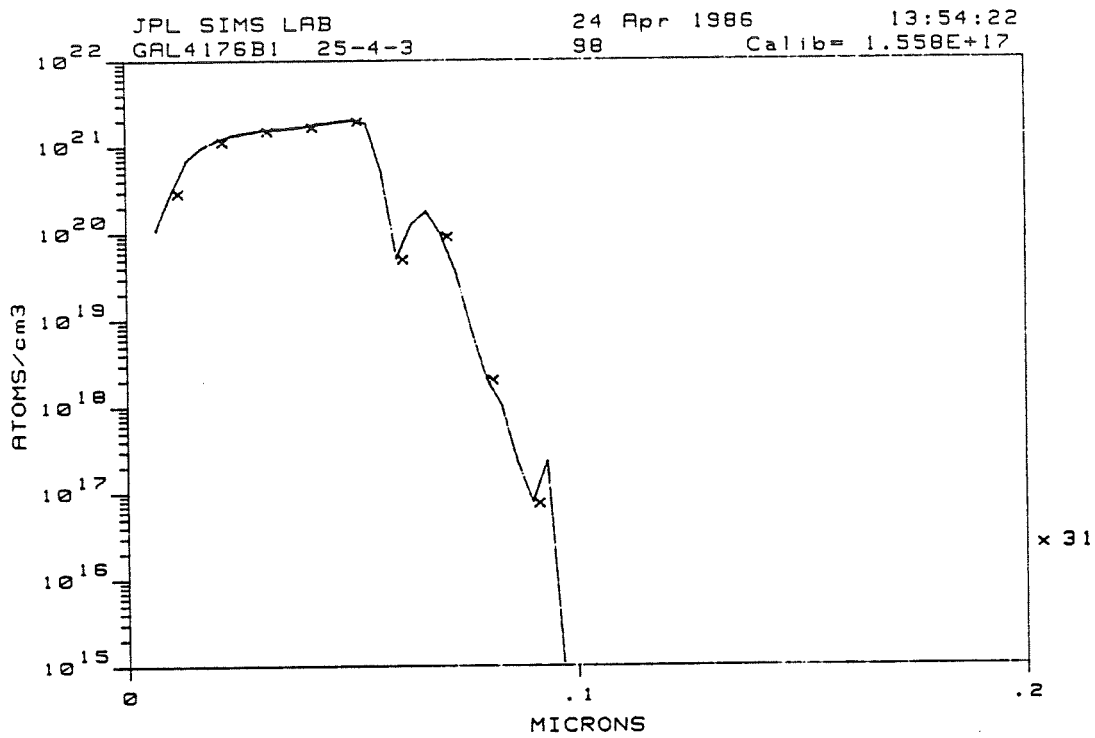
Flow Diagram for the LPCVD Polysilicon Process



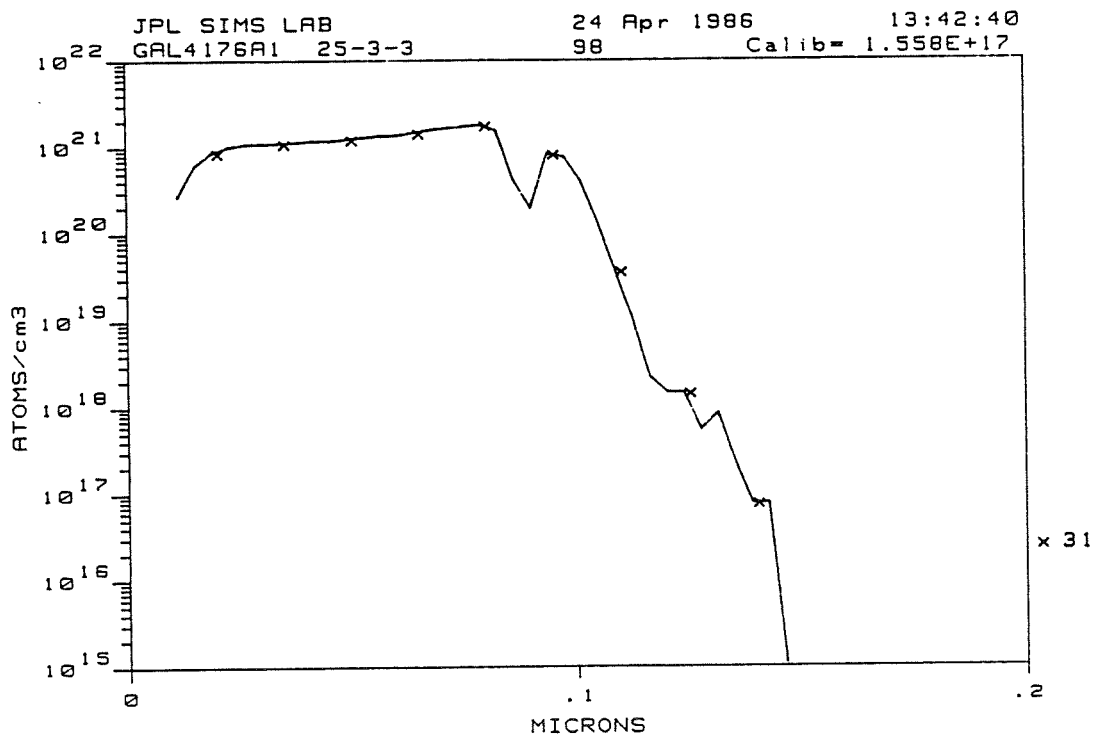
Sheet Resistance

[PH ₃]/[SiH ₄]	TIME (min)	AS DEPOSITED (ohms/square)	POST ANNEAL (ohms/square)
2.5 x 10 ⁻²	90	2320	178
	120	1616	138
	180	863	70

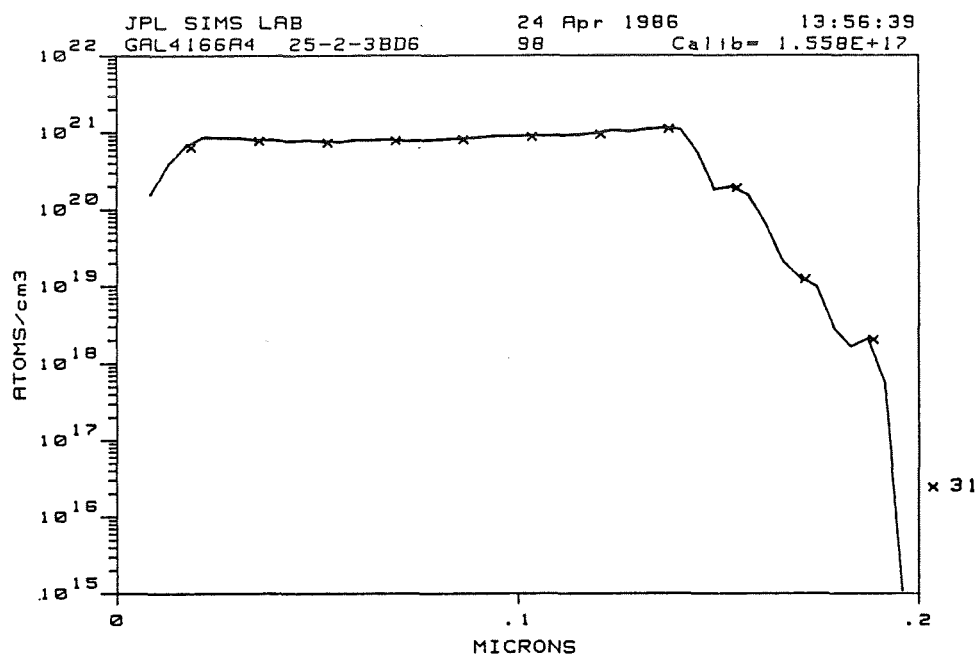
Secondary Ion Mass Spectroscopy Plot (25-4-3)



Secondary Ion Mass Spectroscopy Plot (25-3-3)



Secondary Ion Mass Spectroscopy Plot (25-2-3BD6)



Preliminary Electrical Results
 (In-Situ Polysilicon Doped with $[PH_3]/[SiH_4]$ Ratio of 2.5×10^{-2})

	Voc	Isc	FF	η	t	ρ_s
151-1	639.5	128.5	813	16.72	1.5 μA	70
151-2	638.5	127.5	812	16.52	30-40 μA	VL
151-3	645.3	125.0	811	16.36	400 μA	VL
151-4	637.2	132.8	807	17.08	1.5 μA	VL
151-5	650.6	130.0	811	17.15	1 μA	138
151-6	648.0	128.6	811	16.81	200 μA	VL
151-7	643.9	129.5	799	16.65	Control	

Conclusions

- LPCVD System Operational
- Preliminary Electrical Results Encouraging

Module and Reliability Technology

MODULE TECHNOLOGY

Melvin I. Smokler, Chairman

R. Mueller, of JPL, described the measurement system requirements to obtain accurate electrical performance measurements of amorphous silicon cells and modules, and reviewed progress in modifying the JPL system toward that objective.

R. Ross, Jr., of JPL, discussed the JPL program of developing qualification tests necessary for amorphous silicon modules, including appropriate accelerated environmental tests that reveal degradation due to illumination. Data were given showing the results of temperature-controlled field tests and the results of accelerated tests in an environmental chamber.

J. Lathrop, of Clemson University, reported progress and initial data on accelerated stress tests on small amorphous silicon test samples from several manufacturers. The test samples included both single and tandem junction devices.

D. Otth, of JPL, presented the results of a current set of accelerated long-term endurance tests on crystalline silicon modules of various constructions. Cell materials include single crystal, semicrystal, EFG ribbon, and dendritic web ribbon. The latest data set is for the equivalent of 20-year life and showed satisfactory performance.

P. Willis, of Springborn Laboratory, reviewed work on identifying and developing low-cost module encapsulation materials. Test results were displayed for a variety of materials. The improved prospects for modeling encapsulation systems for life prediction were reported.

M. Smokler, of JPL, presented the results of a program of qualification testing of commercial crystalline silicon modules from nine manufacturers in five countries. The outcome demonstrated the effective role of the Block V Qualification Tests in the development of reliable modules.

M. Spitzer, of Spire Corp., reported success in meeting the long-sought goal of manufacturing a crystalline silicon module with efficiency of 15% or better. Encapsulated cell efficiencies as high as 17.6% were obtained.

B. Jackson, of JPL, reviewed the role and some results of the project analysis and integration function in the FSA Project. Activities included supporting the decision-making process, preparation of plans for Project direction, setting goals for Project activities, measuring progress within the Project, and the development and maintenance of analytical models.

PRECEDING PAGE BLANK NOT FILMED

ACCURACY AND LONG-TERM STABILITY OF AMORPHOUS-SILICON MEASUREMENTS

JET PROPULSION LABORATORY

R. Mueller

Presentation Overview

- MEASUREMENT SYSTEM REQUIREMENTS
- CAPABILITIES OF FSA BLOCK V JPL LAPSS SYSTEM
- CONCERNS RELATING TO α -SILICON MEASUREMENTS
- LAPSS SYSTEM IMPROVEMENTS ADDRESSING THE CONCERNS
- OBSERVATIONS OF EXISTING LAPSS SYSTEM
- CONCLUSIONS AND RECOMMENDATIONS

Measurement System Requirements

- DATA ACQUISITION
 - HIGH RESOLUTION AND LINEARITY OF MEASUREMENTS
 - VOLTAGE AND CURRENT MEASUREMENTS TRACEABLE TO NBS
 - LONG-TERM REPEATABILITY OF MEASUREMENTS
 - DEVICE MEASUREMENTS INDEPENDENT OF LEAD RESISTANCE
 - MINIMAL APPLICATION OF BIAS VOLTAGE TO DEVICE
 - SIMULTANEOUS MEASUREMENT OF REF. CELL AND DEVICE
 - ACQUIRE TRUE DEVICE I-V CURVE SHAPE
 - DATA CORRECTION TO DESIRED TEMPERATURE AND INTENSITY

PRECEDING PAGE BLANK NOT FILMED

Measurement System Requirements (Cont'd)

- LIGHT SOURCE
 - HIGH STABILITY OF INTENSITY LEVEL
 - LONG-TERM STABILITY OF SPECTRAL IRRADIANCE DISTRIBUTION
 - CLOSE MATCH OF SPECTRAL IRRADIANCE DISTRIBUTION TO THE DESIRED ASTM E 892 AM1.5 GLOBAL SPECTRUM
 - LOW NON-UNIFORMITY OF IRRADIANCE AT TEST PLANE
 - MINIMAL HEATING OF DEVICE
- REFERENCE DEVICE
 - FAST RESPONSE TIME AND STABLE OUTPUT
 - SPECTRAL RESPONSE SIMILAR TO DEVICE
 - CALIBRATION DIRECTLY TRACEABLE TO SUNLIGHT MEASUREMENTS USING ACCEPTABLE ASTM METHOD

FSA Block V JPL LAPSS System Capabilities

- DATA ACQUISITION
 - EXCELLENT LINEARITY AND IMPROVED RESOLUTION
 - FULL SCALE ACCURACY OF $\pm 0.1\%$ TRACEABLE TO NBS
 - IMPROVED LONG-TERM REPEATABILITY, STD. DEV. $\leq 1.0\%$
 - 4-TERMINAL CONNECTIONS TO DEVICE
 - REF. CELL AND DEVICE OUTPUT MEASURED SIMULTANEOUSLY EVERY 20 μ SEC DURING LAMP FLASH
 - DEVICE I-V CURVE SHAPE VERIFIABLE USING FIXED LOAD DURING LAMP FLASH
 - DATA CORRECTED TO DESIRED TEMPERATURE AND INTENSITY USING PREDETERMINED DEVICE TEMPERATURE COEFFICIENTS
 - ADJUSTABLE REVERSE BIAS FOR TRUE I_{SC} MEASUREMENT

FSA Block V JPL LAPSS System Capabilities (Cont'd)

- LIGHT SOURCE
 - LAPSS INTENSITY STABLE TO $\pm 0.5\%$ WITHOUT CORRECTION
 - INSIGNIFICANT CHANGE IN LAPSS SPECTRAL IRRADIANCE DISTRIBUTION THROUGHOUT LAMP LIFETIME
 - NON-UNIFORMITY OF IRRADIANCE IS $\leq \pm 1\%$ OVER A 4 x 6 FT TEST PLANE AREA
 - SIGNIFICANTLY SUPERIOR TO A CLASS A SIMULATOR RATING AS DEFINED BY ASTM E 927
 - INSIGNIFICANT HEATING OF TEST DEVICES DUE TO SHORT PERIOD OF ILLUMINATION
 - OPTICALLY FILTERED LAPSS SPECTRAL IRRADIANCE CLOSE TO DESIRED ASTM E 891 AM1.5 DIRECT SPECTRUM
- REFERENCE CELL
 - FAST RESPONSE, STABLE CRYSTALLINE SILICON CELL
 - SPECTRAL RESPONSE SUFFICIENTLY SIMILAR TO ALL CRYSTALLINE SILICONE DEVICES
 - CALIBRATION PERFORMED IN DIRECT NORMAL SUNLIGHT USING PROPOSED ASTM METHOD

Concerns Relating to Amorphous-Silicon Measurements

- POSSIBLE DEVICE DAMAGE FROM EXCESSIVE BIAS APPLIED DURING LAPSS SYSTEM TESTING
- POSSIBLE TEMPORARY SOFTENING OF I-V CURVE KNEE DUE TO LENGTHY APPLICATION OF FORWARD BIAS
- STABILITY AND RESPONSE TIME OF REFERENCE CELL
- SPECTRAL RESPONSE OF REFERENCE CELL
- SPECTRAL IRRADIANCE DISTRIBUTION OF LAPSS

Improvements in the LAPSS System that Addresses the Concerns

- NEGATIVE BIAS LIMITED TO 0.7 VOLTS WITH A PROTECTIVE DIODE
- POSITIVE BIAS OF UP TO 15 VOLTS PRESENT DURING STAND-BY PERIOD ELIMINATED BY CHANGING PROCEDURE
- FAST RESPONSE, STABLE CRYSTALLINE SILICON DEVICE CONTINUED AS REFERENCE CELL
- REFERENCE CELL NOW HAS BUILT-IN IR FILTER TO PROVIDE CLOSE MATCH TO TYPICAL α -SILICON DEVICES
- SPECTRAL IRRADIANCE DISTRIBUTION OF LAPSS OPTICALLY FILTERED FOR CLOSE MATCH TO ASTM E 892 AM1.5 GLOBAL SPECTRUM

Observations of Existing LAPSS System

- PROVIDES RELIABLE AND REPEATABLE MEASUREMENTS OF α -SILICON DEVICE OUTPUT
- INTERNATIONAL COMPARISON OF α -SILICON REFERENCE CELL CALIBRATION SHOWS JPL AND 6 OTHERS WITHIN 2.0% STANDARD DEVIATION OF THE AVERAGE AND JPL MEASUREMENTS NEARLY THE SAME AS SEVERAL PARTICIPANTS
- OBTAINED LIMITED TEMPERATURE COEFFICIENT MEASUREMENTS ON SEVERAL α -SILICON MODULES USING THE LAPSS
- NEW I-R FILTERED REFERENCE CELL HAS LOW SPECTRAL MISMATCH TO A VARIETY OF α -SILICON DEVICES
- OCCASIONAL DIFFICULTY CONTACTING α -SILICON COUPONS WITH PROBES WHEN TESTING WITH LAPSS
- MOST α -SILICON I-V CURVES SHOW A 2 TO 5% SOFTENING OF KNEE AT P_{MAX}

International Comparison of Measurements
of Amorphous-Silicon Reference Cell

CELL NO.	MEASUREMENTS (RATIO FROM AVERAGE)						
1	1.022	1.018	1.005	0.992	1.005	0.983	0.975
2	1.039	1.018	1.009	0.996	0.970	0.983	0.983
3	1.027	1.019	1.011	0.994	0.994	0.977	0.977
AVERAGE	1.029	1.018	1.008	0.994	0.990	0.981	0.978

Temperature Coefficients of Amorphous-Silicon Modules
(17 to 32°C)

MODULE TYPE	I COEFF ($\mu\text{A}/\text{cm}^2/^{\circ}\text{C}$)	E COEFF ($\mu\text{V}/\text{CELL}/^{\circ}\text{C}$)	K COEFF ($\text{m}\Omega/\text{cm}^2/^{\circ}\text{C}$)	P COEFF ($\%/^{\circ}\text{C}$)
ARCO GENESIS 100	5.5	-2672	-186	-0.15
SOVONICS TANDEM	8.2	-5216	-637	0
SOLAREX	7.2	-4356	-183	-0.14

**Spectral Mismatch Parameters of Hypothetical Amorphous-Silicon Devices
Versus JPL Pseudo Amorphous-Silicon Reference Cell
(JPL Global Filtered LAPSS Versus Proposed New ASTM E 892 Spectrum)**

HYPOTHETICAL CELL	WAVELENGTHS FOR 50% RESPONSE		SPECTRAL MISMATCH
	UV	IR	
1	340 nm	TO 680 nm	0.9991
2	360 nm	TO 680 nm	0.9993
3	380 nm	TO 680 nm	0.9998
4	380 nm	TO 700 nm	0.9992
5	380 nm	TO 720 nm	0.9988

Conclusions and Recommendations

- THE VARIANCE AMONG PARTICIPANTS IN INTERNATIONAL CALIBRATION COMPARISON NEEDS TO BE INVESTIGATED
- PRIMARY GLOBAL CALIBRATION OF REFERENCE CELLS IS NEEDED
- SINGLE-POINT LOAD TEST ALWAYS REQUIRED FOR FINDING TRUE P_{MAX}
- MULTIPLE-FLASH WITH SEGMENTED I-V DATA MAY BE DESIRABLE
- MORE RELIABLE PROBE CONTACTING METHOD FOR α -SILICON COUPONS OR USE ONLY DIRECTLY BONDED/ SOLDERED CONNECTIONS
- THE PRESENT JPL LAPSS SYSTEM APPEARS TO BE THE MOST DESIRABLE SYSTEM FOR OBTAINING ACCURATE MEASUREMENTS ON α -SILICON MODULES OF ALL SIZES

LONG-TERM STABILITY OF AMORPHOUS-SILICON MODULES

JET PROPULSION LABORATORY

R. G. Ross, Jr.

Amorphous Silicon Module Test Program Objectives

Objective

- Assess reliability characteristics of amorphous silicon modules
- Assess attributes of various test methods
- Establish research priorities

Approach

- Establish strawman mechanism-specific reliability goals
- Test a number of first-generation amorphous silicon modules using a wide variety of tests
 - Block V qualification tests
 - Field aging (various electrical loading points)
 - Field aging (at elevated temperatures)
 - Dark oven aging (various electrical biases)
 - Photothermal oven aging

Life-Cycle Cost Impacts and Allowable Degradation Levels for Thin-Film Modules

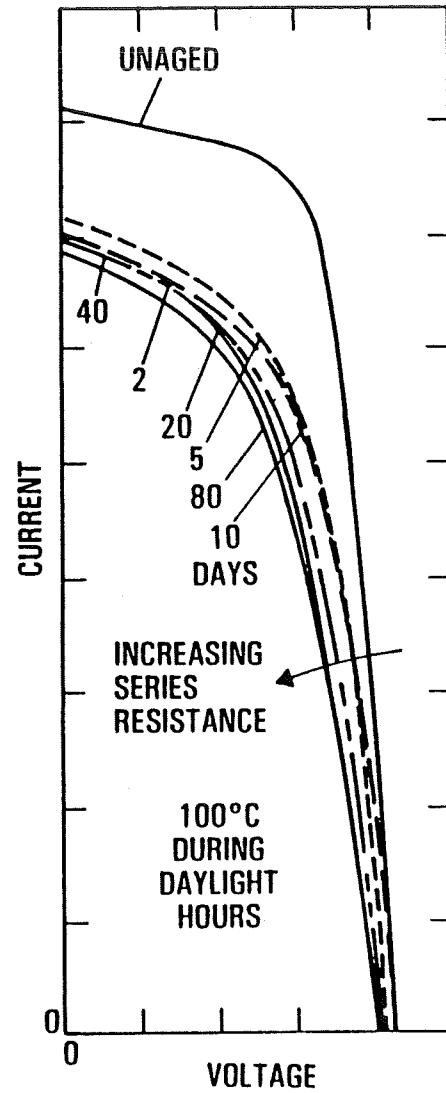
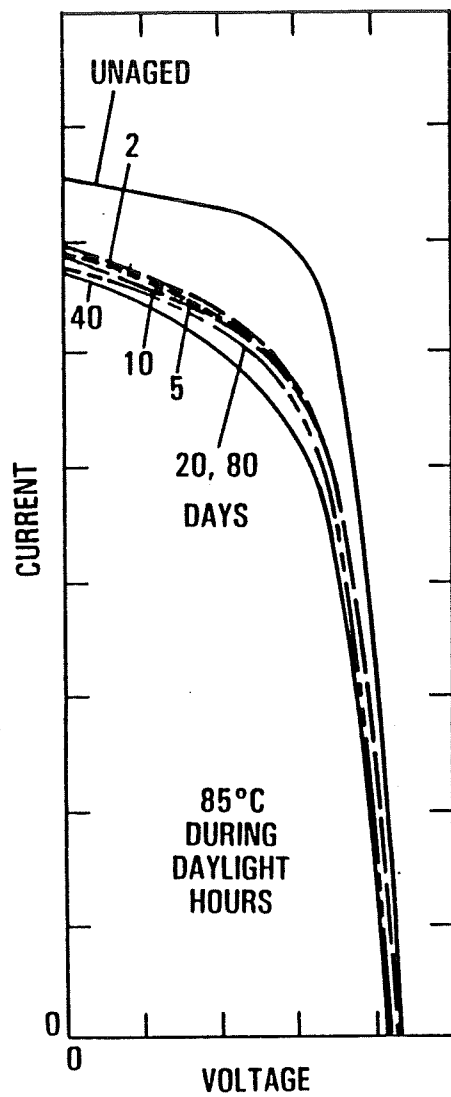
Type of Degradation	Failure Mechanism	Units of Degrad.	Level for 10% Energy Cost Increase*		Allocation for 30-Year-Life Module	Economic Penalty
			k = 0	k = 10		
Component failures	Open-circuit between cells	%/yr	0.08	0.13	0.02	Energy
	Short-circuit cells	%/yr	0.24	0.40	0.05	Energy
Power degradation	Light induced effects	%	10	10	5	Energy
	Cell gradual power loss	%/yr	0.67	1.15	0.20	Energy
	Module optical degradation	%/yr	0.67	1.15	0.02	Energy
	Front surface soiling	%	10	10	3	Energy
Module failures	Module glass breakage	%/yr	0.33	1.18	0.1	O&M
	Module open circuits	%/yr	0.33	1.18	0.1	O&M
	Module hot-spot failures	%/yr	0.33	1.18	0.1	O&M
	Bypass diode failures	%/yr	0.70	2.40	0.05	O&M
	Module shorts to ground	%/yr ²	0.022	0.122	0.01	O&M
	Module delamination	%/yr ²	0.022	0.122	0.01	O&M
Life-limiting wearout	Encapsulant failure due to loss of stabilizers	Years of life	27	20	35	End of life

*k = Discount rate

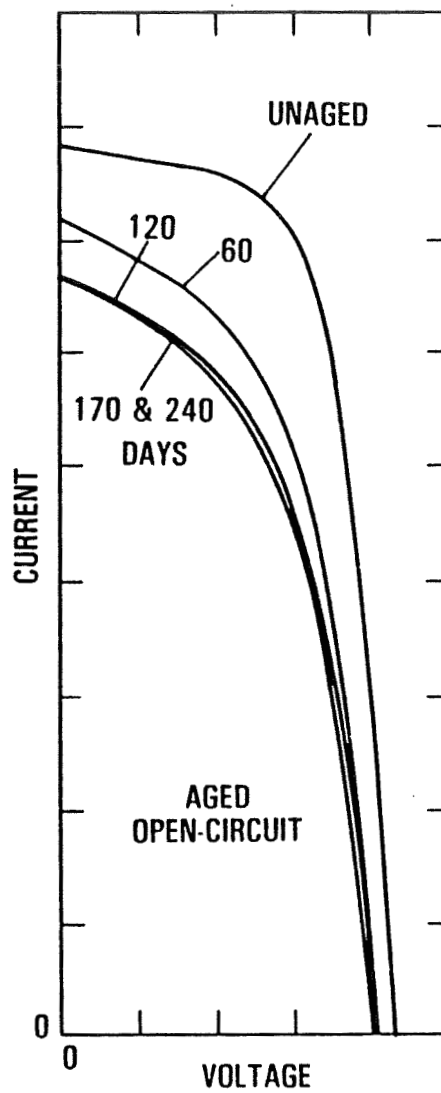
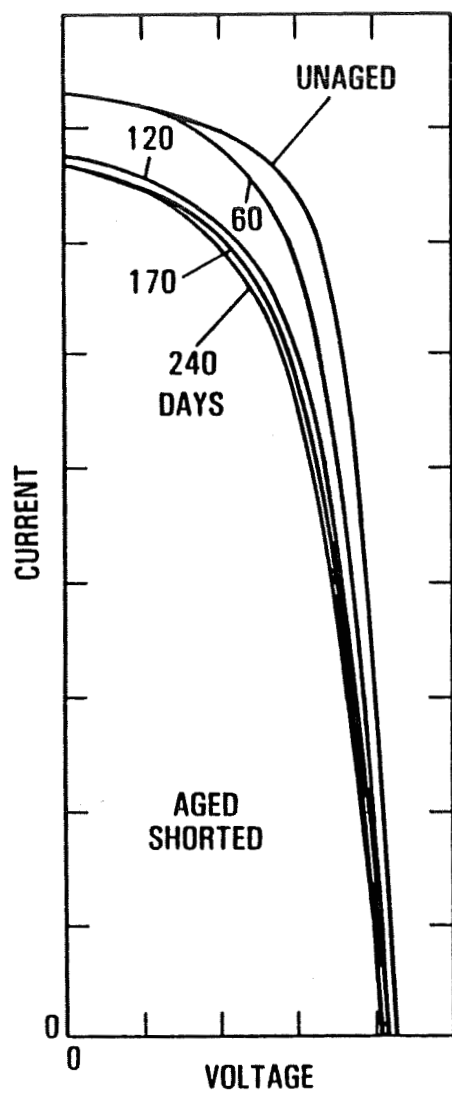
Block-V Qual Testing of Amorphous Silicon Modules

- Good performance in mechanical loading tests
 - Mechanical cycling at 50 psf
 - Hail impact with 1 in. ice balls
- Slight degradation (10%) in thermal cycle and humidity tests
 - Corrosion of monolithic interconnects
 - Some open-circuiting of monolithic interconnects
- Good performance in hot-spot test
- Mixed performance with encapsulant system
 - Frame softening
 - Some delamination of non-EVA systems

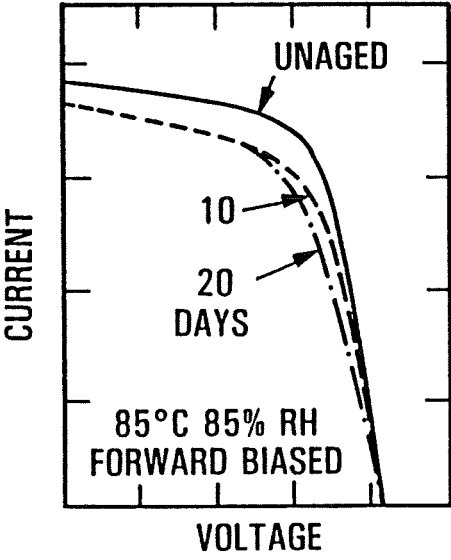
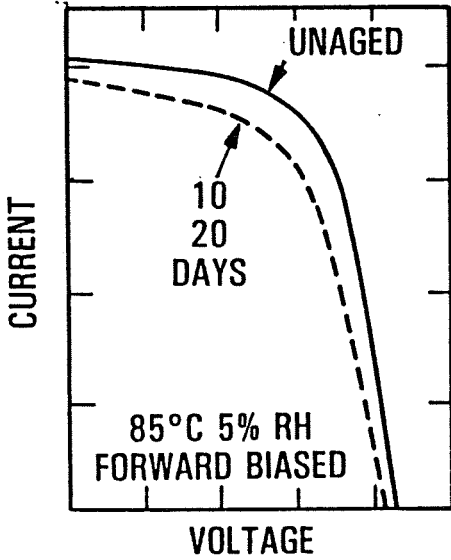
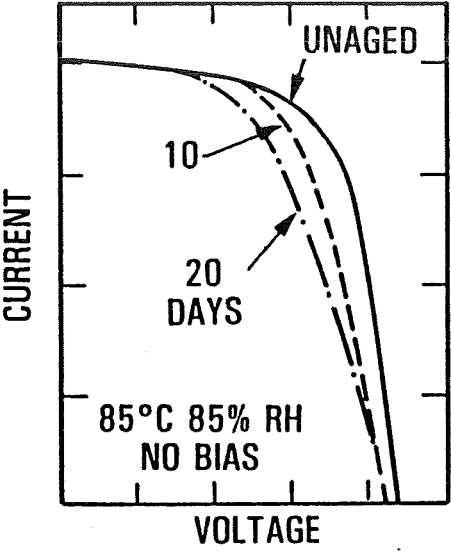
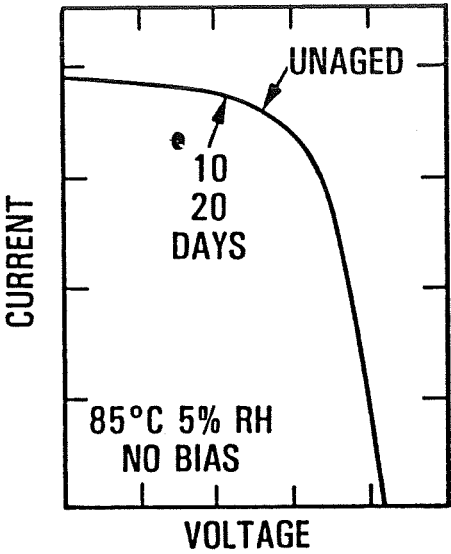
Amorphous-Silicon Module Field Performance
(Ambient-Temperature Aging)



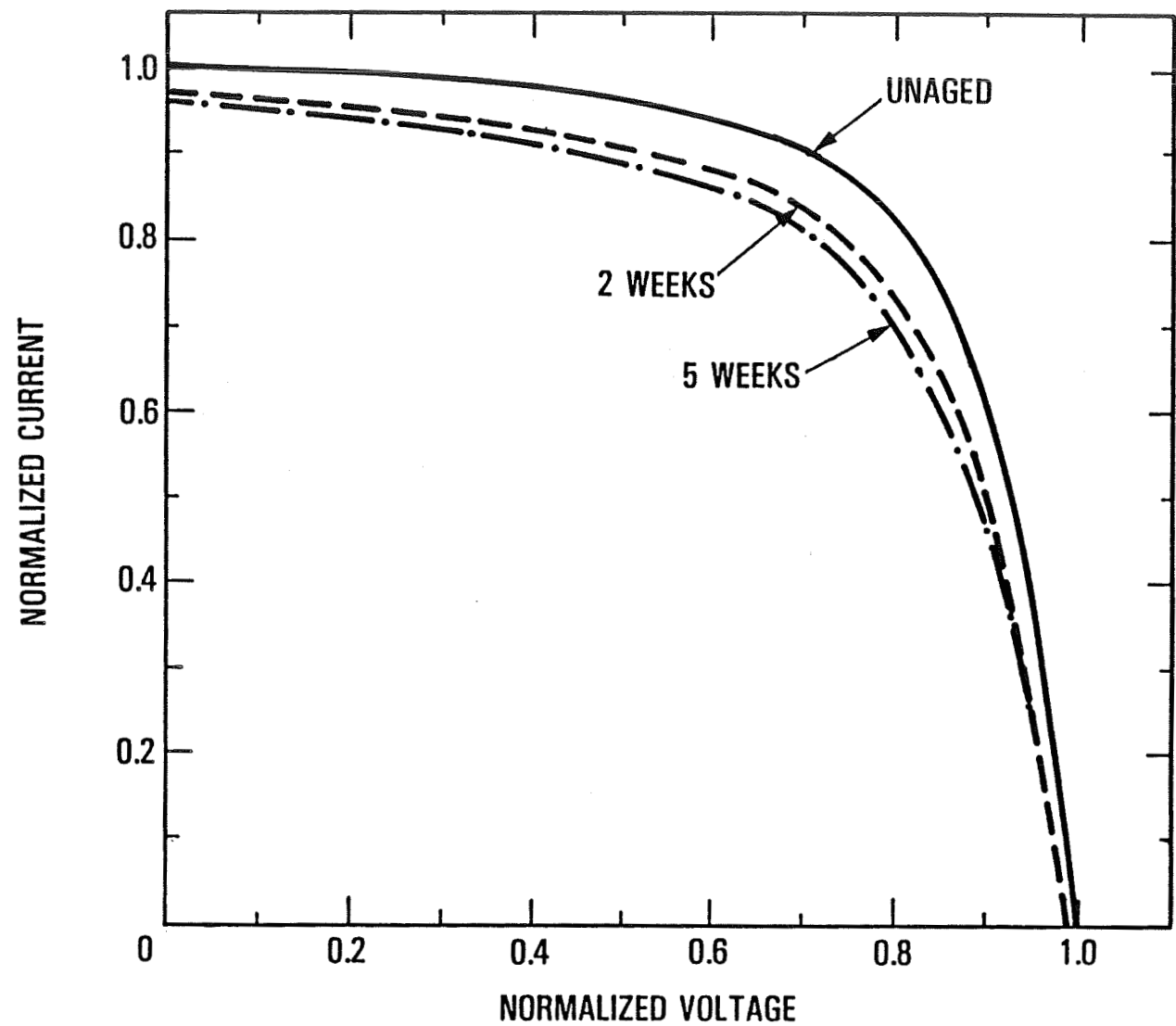
Amorphous-Silicon Field Performance
(Elevated-Temperature Aging)



Amorphous Silicon Module I-V Performance
(Dark Oven Aging)



Amorphous Silicon Cell Photothermal Aging Performance
(85°C, 5% RH, 1 Sun UV)



Summary

- Block V crystalline-silicon qualification test insufficient for amorphous silicon modules
 - Good indicator of mechanical and hot-spot endurance
 - Poor indicator of electrical stability of amorphous silicon
- Electrical stability of amorphous silicon modules is very complex
 - Light induced effects
 - Sensitive to electrical loading point (Voc, Isc, Pmp)
 - Complex temperature dependency
 - Corrosion induced effects
 - Strong (Arrhenius) temperature dependency
 - Strong humidity dependency
- Accelerated laboratory and field testing must address the complex parameter dependencies
- Tests appropriate for amorphous silicon procurement specifications do not exist at this time

Present Research Thrusts

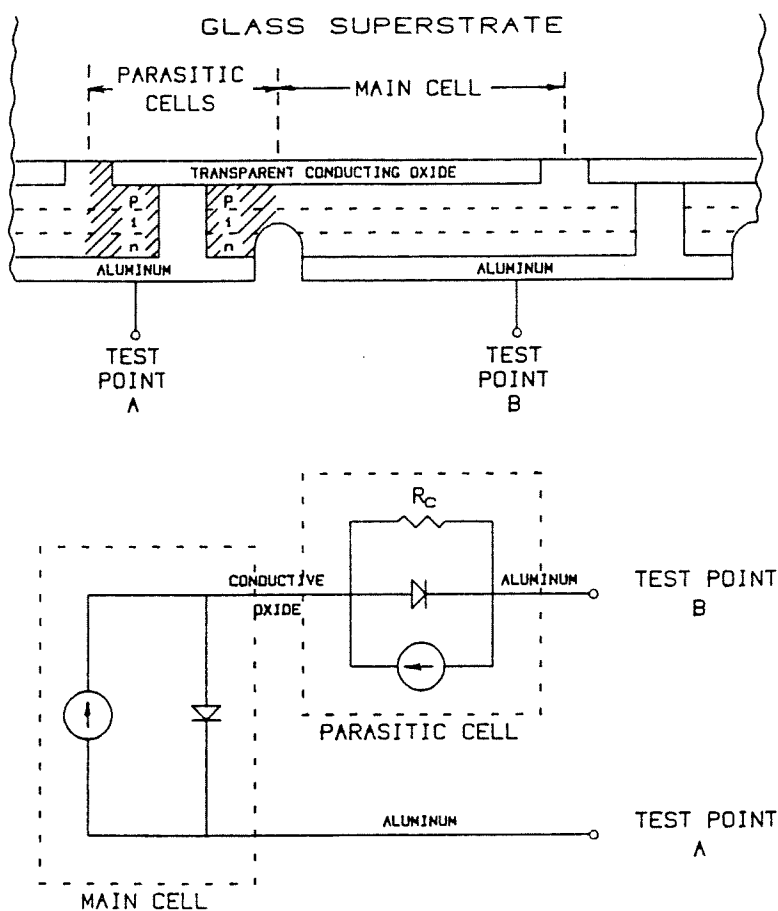
- Developing useful accelerated test for amorphous silicon electrical stability
- Developing solutions to corrosion-induced effects
- Continuing broad-spectrum testing to identify research priorities

SOLAR CELL RELIABILITY TESTING

SOLAR CELL DESTRUCTION LABORATORY
CLEMSON UNIVERSITY

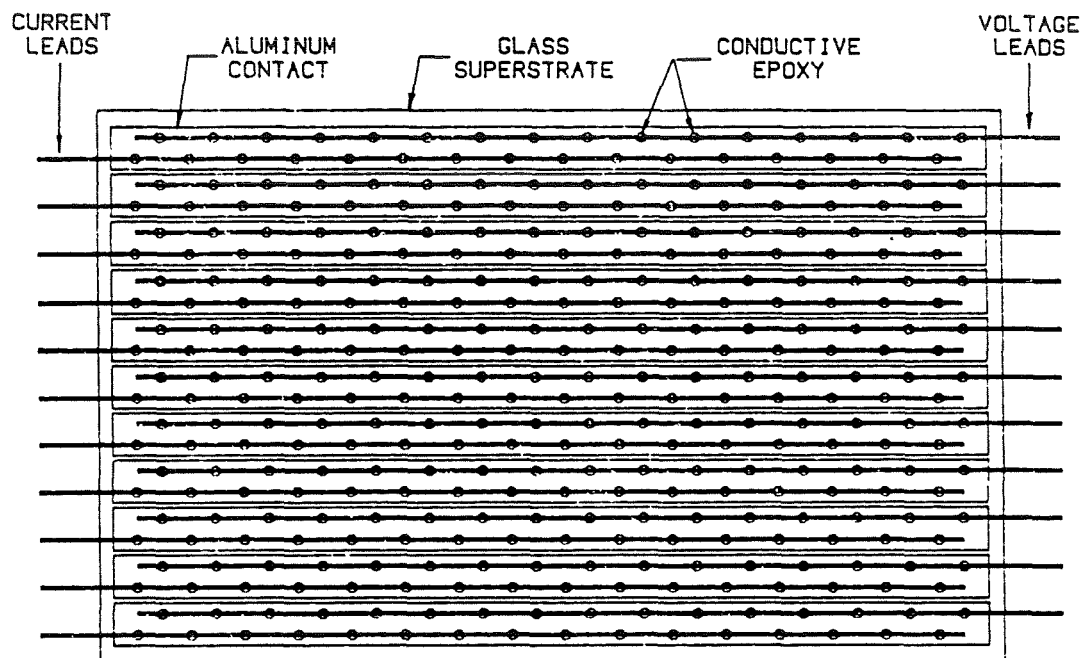
J. Lathrop

Equivalent Circuit of Series Connected Amorphous Silicon Cell

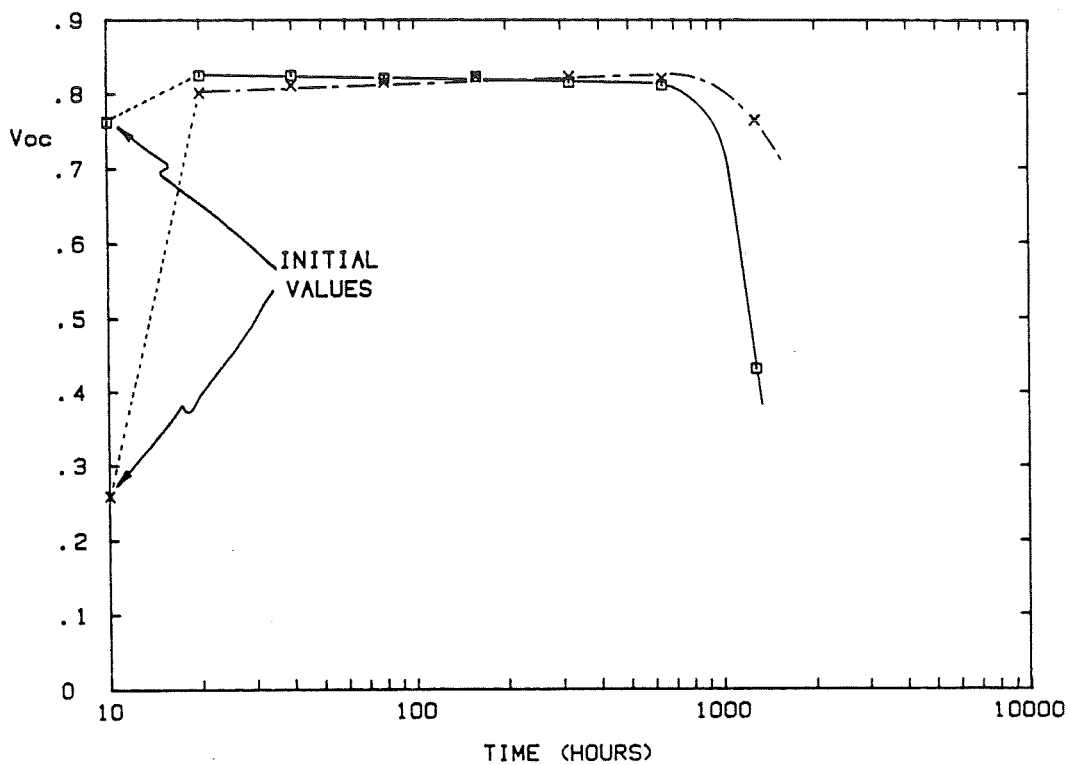


PRECEDING PAGE BLANK NOT FILMED

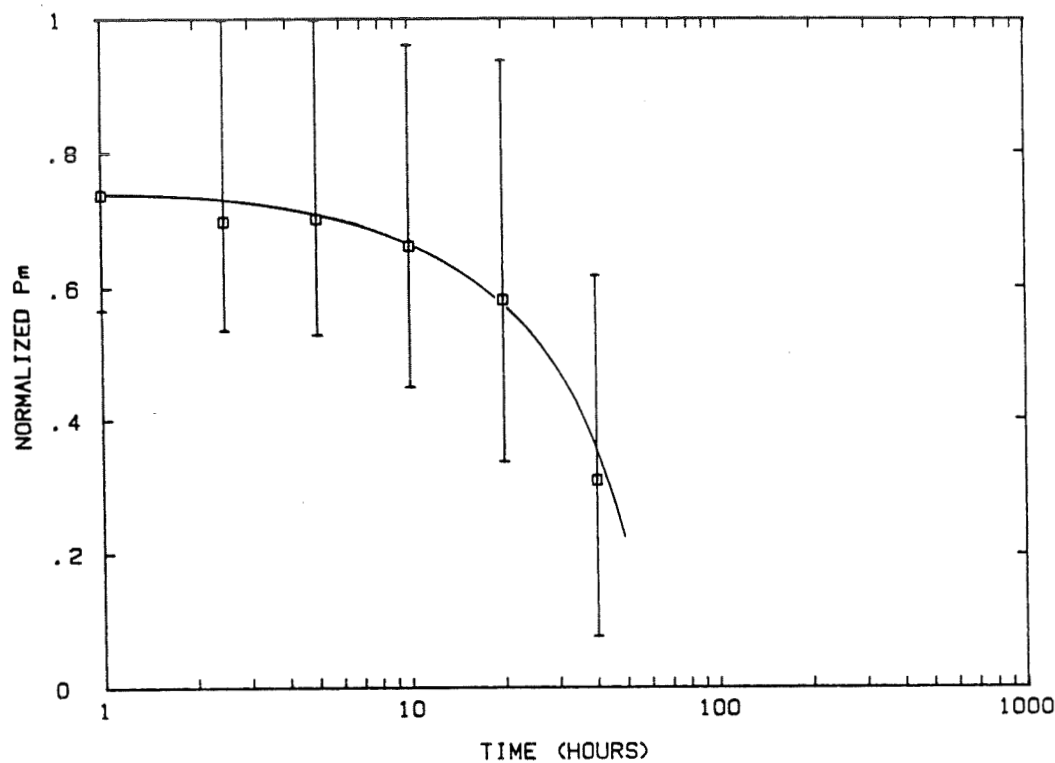
Bottom View of Unencapsulated Amorphous Silicon Module Showing
Attachment of Kelvin Probe Contacts for Individual Cell
Measurement



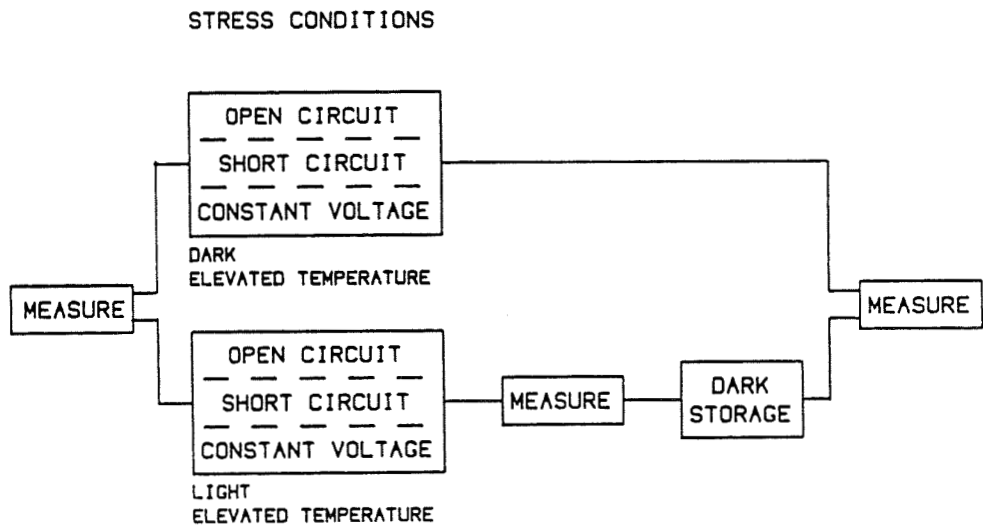
Cell Type "A" Non-Illuminated 140°C Stress Test



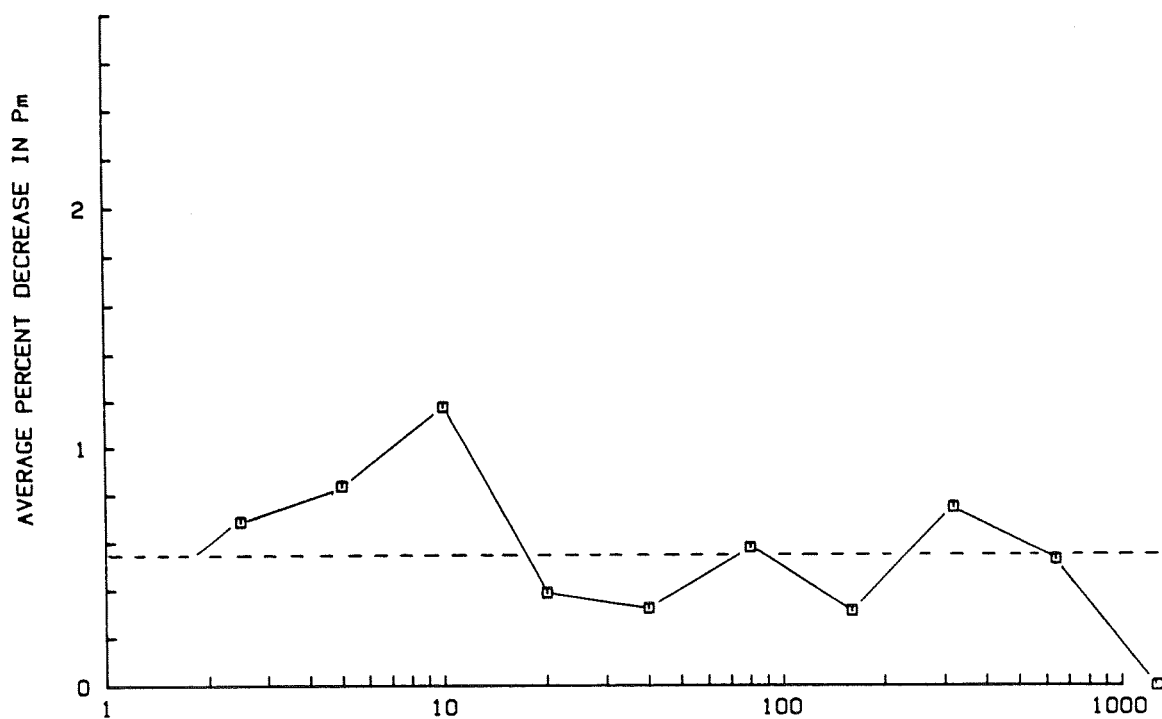
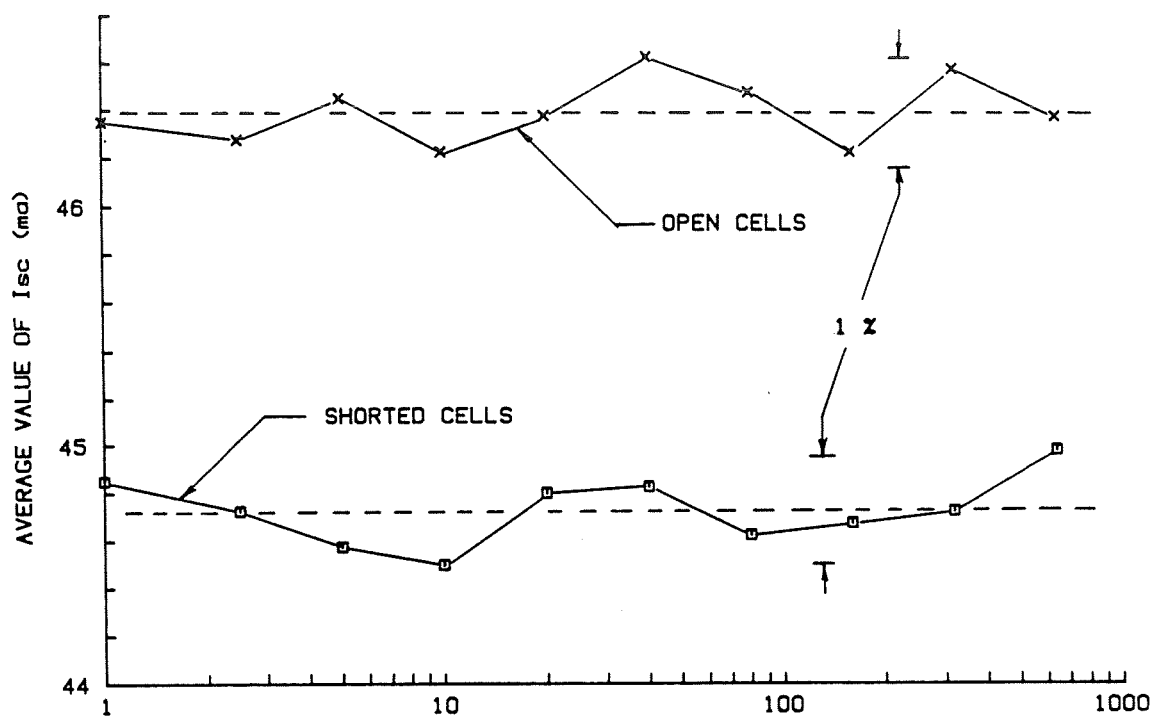
Cell Type "B" Non-Illuminated 140°C Stress Test



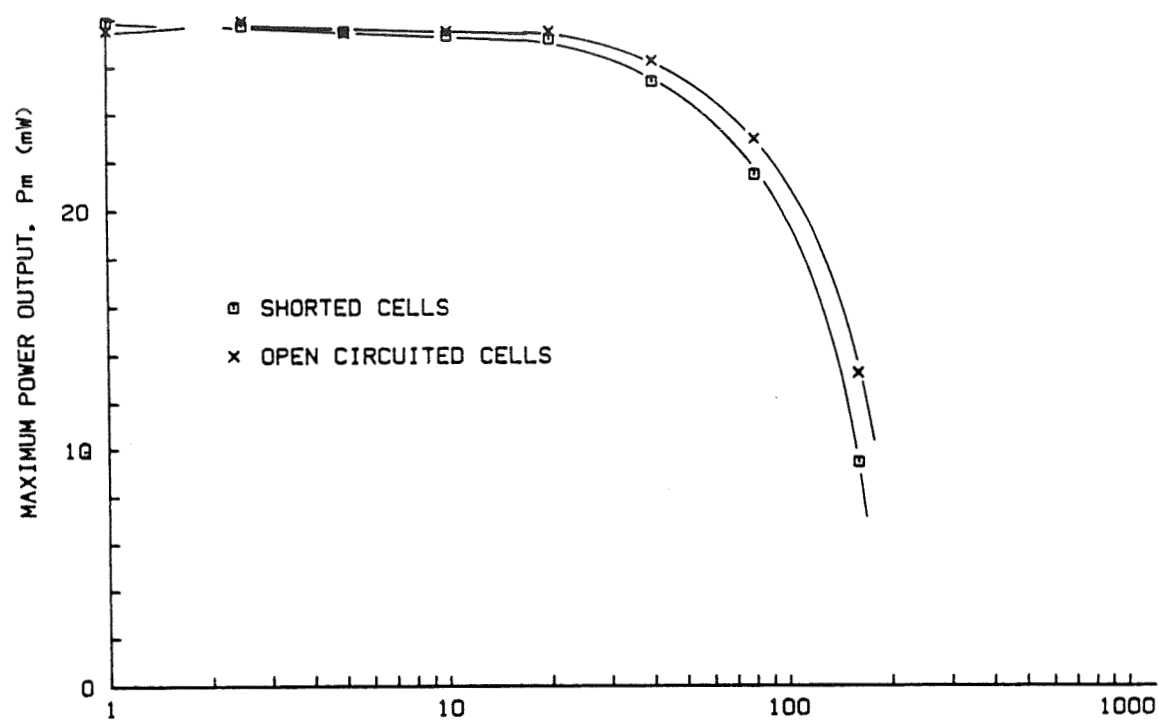
Amorphous Silicon Accelerated Stress Test Plan



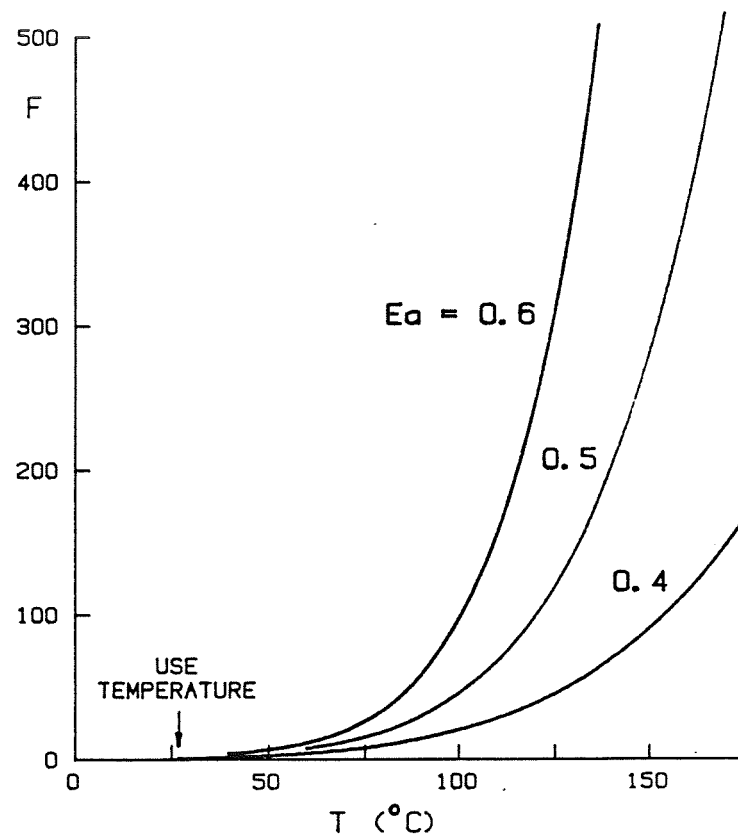
Cell Type "C" 16-Cell Non-Illuminated Control Module



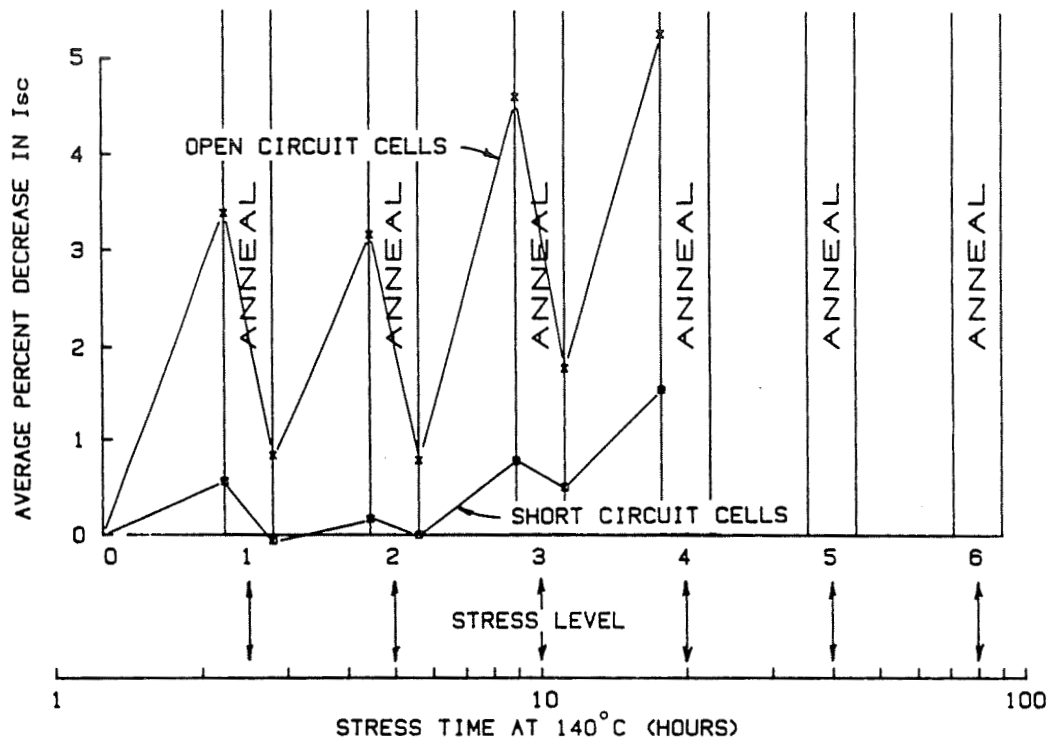
Cell Type "C" Non-Illuminated 140°C Stress Test



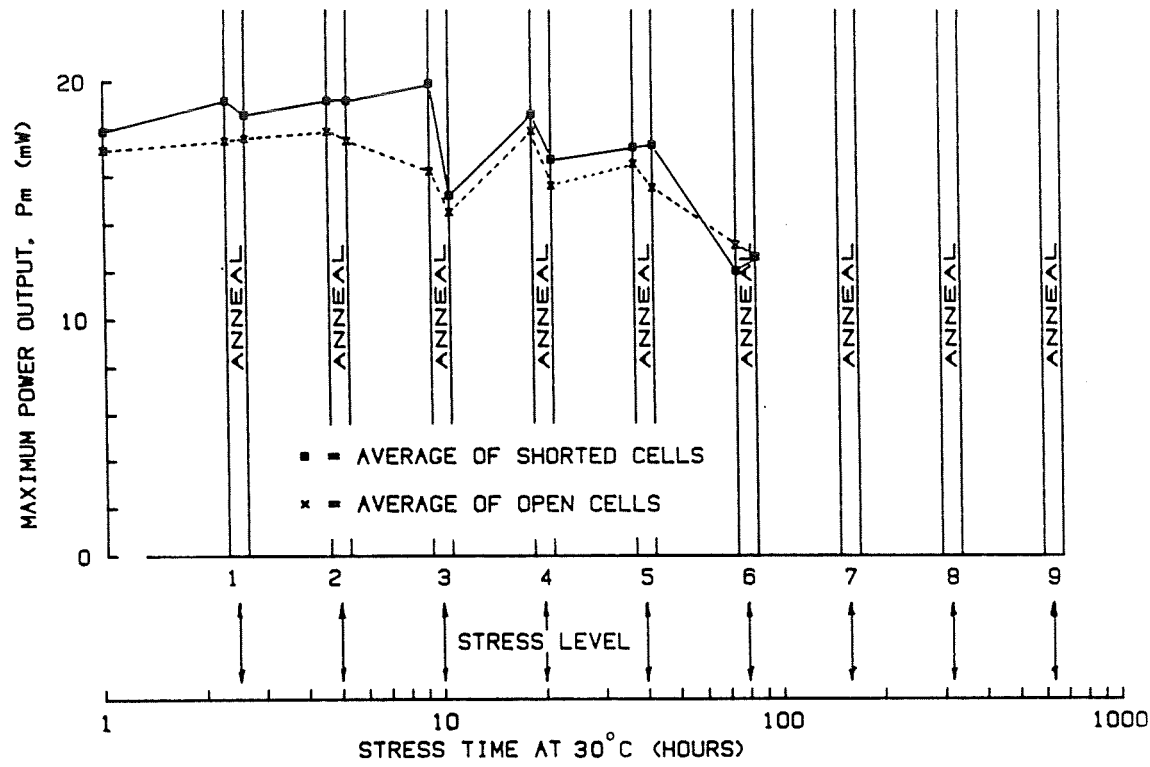
Acceleration Factor "F" as a Function of Stress Temperature



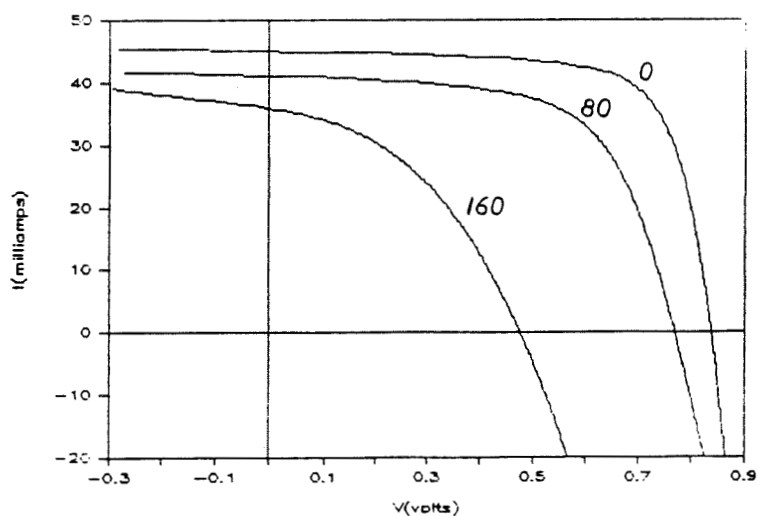
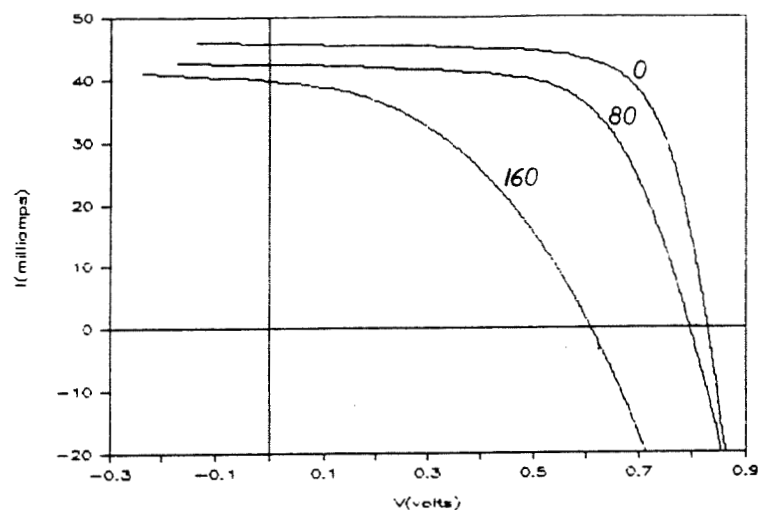
Cell Type "C" Illuminated Control Module



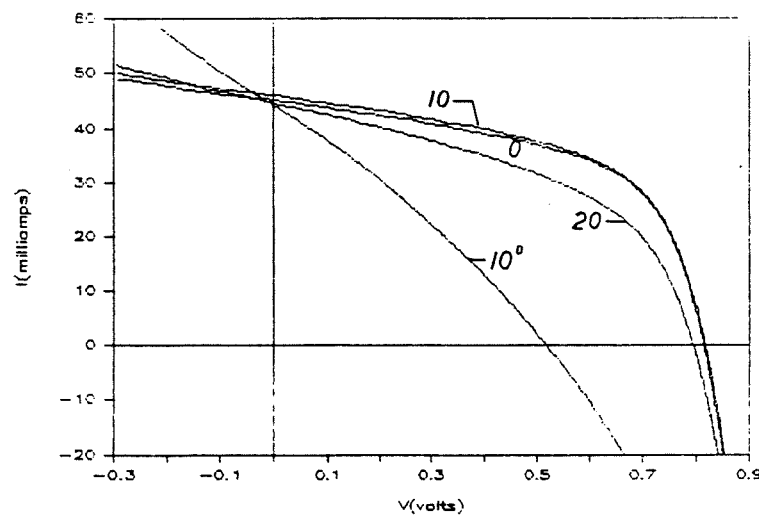
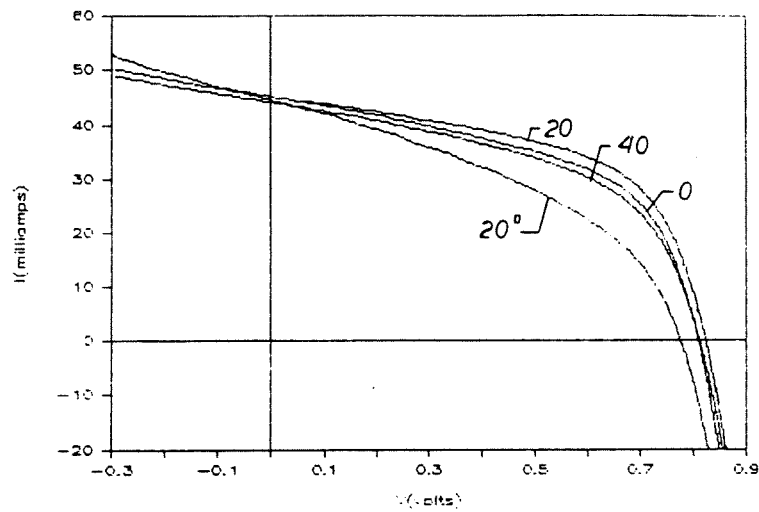
Cell Type "C" Illuminated Stress Test



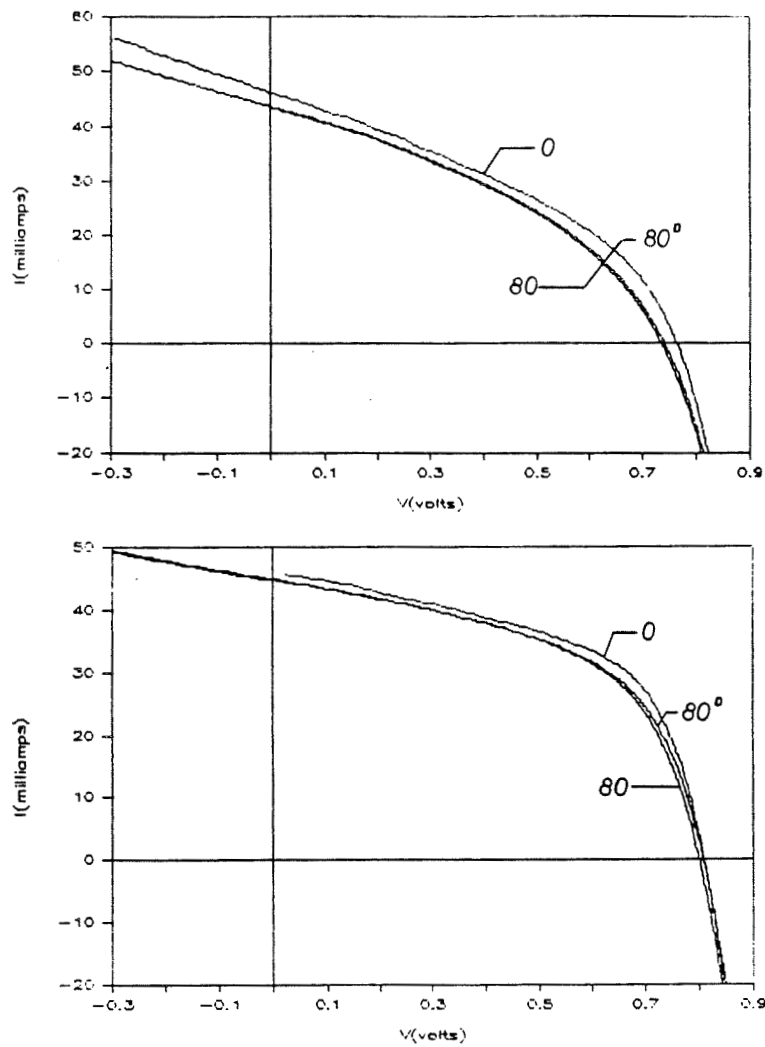
I-V Characteristics Initially and After 80 and 160 Hours for
Two Type "C" Cells Subjected to 140°C
(Non-Illuminated Stress Under Shorted Conditions)



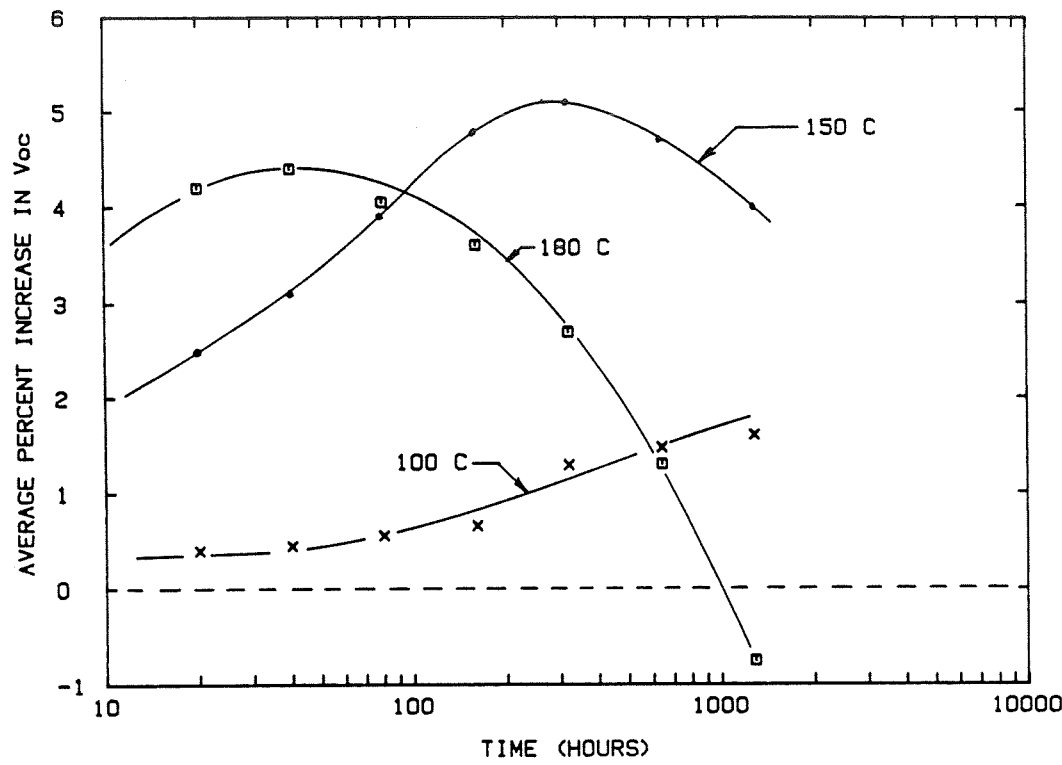
I-V Characteristics for Two Type "C" Cells as a Function of Hours at 140°C Under Illumination and While Shorted
 (□ Indicates Measurement Taken Following 2.5 Hours 100°C Anneal)



I-V Characteristics for Two Type "C" Cells as a Function of Hours at 140°C Under Illumination and While Open Circuited
(\square Indicates Measurement Taken Following 2.5 Hours 100°C Anneal)



Tandem Cells: Non-Illuminated Stress



Conclusions

- MEASUREMENT SYSTEM FOR ACCELERATED TESTING OF α -Si CELLS WITH 1% REPEATABILITY DEMONSTRATED
- WELL MADE MODULES SHOW INITIAL V_{oc} (P_m) IMPROVEMENT UNDER ELEVATED TEMPERATURE STRESS (CAN BE DRAMATIC FOR LOW V_{oc} CELLS)
- SINGLE JUNCTION CELLS SHOW IRREVERSIBLE DEGRADATION UNDER ELEVATED TEMPERATURE STRESS IN THE DARK

T	TIME	P_m LOSS
140 C	50 hours	10 %
140 C	150 hours	50 %
30 C	3 years	50 % ($E_a = 0.5$ eV)
- SINGLE JUNCTION CELLS SHOW THE SAME LONG TERM IRREVERSIBLE DEGRADATION WHEN STRESSED IN LIGHT AS IN THE DARK, BUT WITH REVERSIBLE LIGHT INDUCED CHANGES SUPERIMPOSED
- LIGHT INDUCED EFFECTS AT ELEVATED TEMPERATURES AFFECT CELL CHARACTERISTICS DIFFERENTLY THAN AT ROOM TEMPERATURE
- MACROSCOPIC PHYSICAL OBSERVATION APPEARS TO CONFIRM THAT IRREVERSIBLE DEGRADATION AT ELEVATED TEMPERATURES IS THE RESULT OF A SOLID STATE REACTION BETWEEN ALUMINUM AND α -Si FILMS
- TANDEM JUNCTION CELLS SHOW LITTLE DEGRADATION UNDER ELEVATED TEMPERATURE STRESS IN THE DARK

T	TIME	P_m LOSS
180 C	1000 hours	<1 %
30 C	>30 years	50 % ($E_a = 0.5$ eV)

LONG-TERM MODULE TESTING AT WYLE LABORATORIES

JET PROPULSION LABORATORY

D. H. Otth

Objectives

- Identify temperature/humidity-bias failure mechanisms in important photovoltaic designs
 - Modules in application experiments
 - R & D modules
 - Commercial modules
- Identify synergisms among the module elements
 - Cells, encapsulants, interconnects
 - Back covers, edge seals

Wyle Laboratories Module Test Set

- Application Experiment Modules
 - Arco Solar - SMUD, Phase 1
 - Solarex - SMUD, Phase 2
 - Mobile Solar - SMUD, Phase 2
 - Solarex - Georgetown
- R & D Modules
 - Westinghouse
- Commercial Modules
 - Tideland Signal
 - Solec

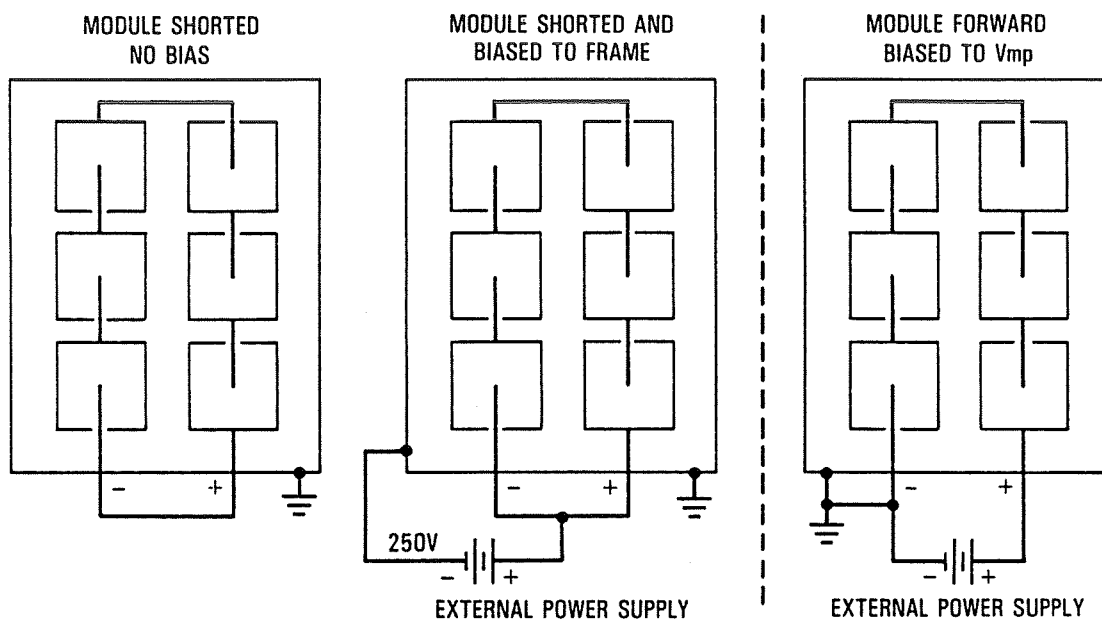
Module Materials

Design Details	Prior Tests	Current Test
Front cover	glass, Tedlar/none	glass
Encapsulants	silicone, PVB, EVA	EVA, APU, silicone
Cell types	CZ (p/n, n/p), semi-Xtl	semi-Xtl, CZ, EFG ribbon, D-web, a-Si
Cell metallization	Ni-Sn, Ti-Pd-Ag, print Ag, Pd-Ni-Sn	Ti-Pd-Cu, print Ag, Ti-Pd-Ag, Ni-Cu-Sn
Back cover	Tedlar, mylar, T-P-T T-Al-T	Tedlar, T-P-T, glass, P-Al-T, T-Al-T, white RTV
Frame	Al, stainless steel	Al, stainless steel
Edge seals	EPDM, RTV, acrylic tape, FRP, PS, butyl, silicone	EPDM, FRP, acrylic tape, mylar tape, none

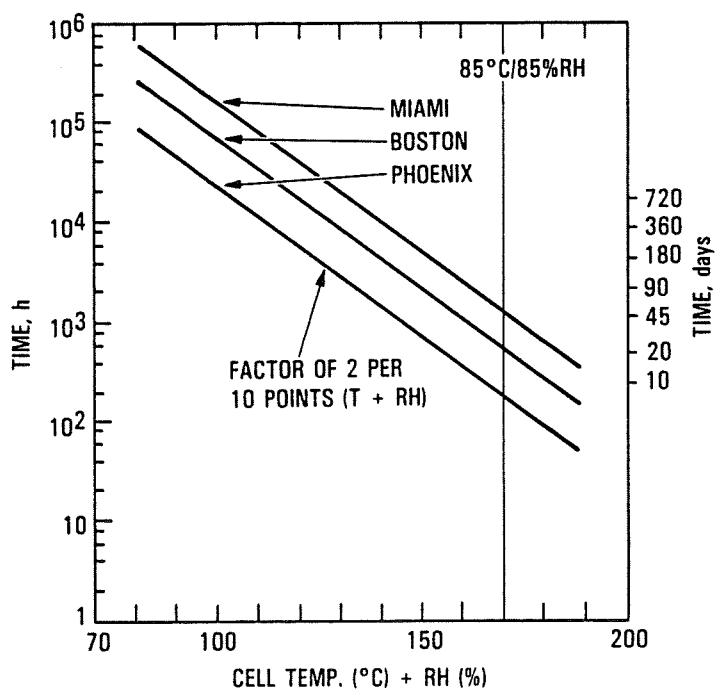
Long-Term Module Testing Schedule at Wyle Laboratories

TEST	1981	1982	1983	1984	1985	1986
T/H 85°C/85%RH					<div> LEGEND BLKS I, II, III BLKS III, IV BLK IV BLK V, COMM. INSPECTION POINTS </div>	
40°C/93%RH						
TEMP 85°C 100°C						
MID T/H 70°C/85%RH 85°C/70%RH						
T/H 85°C/85%RH 85°C/5%RH						

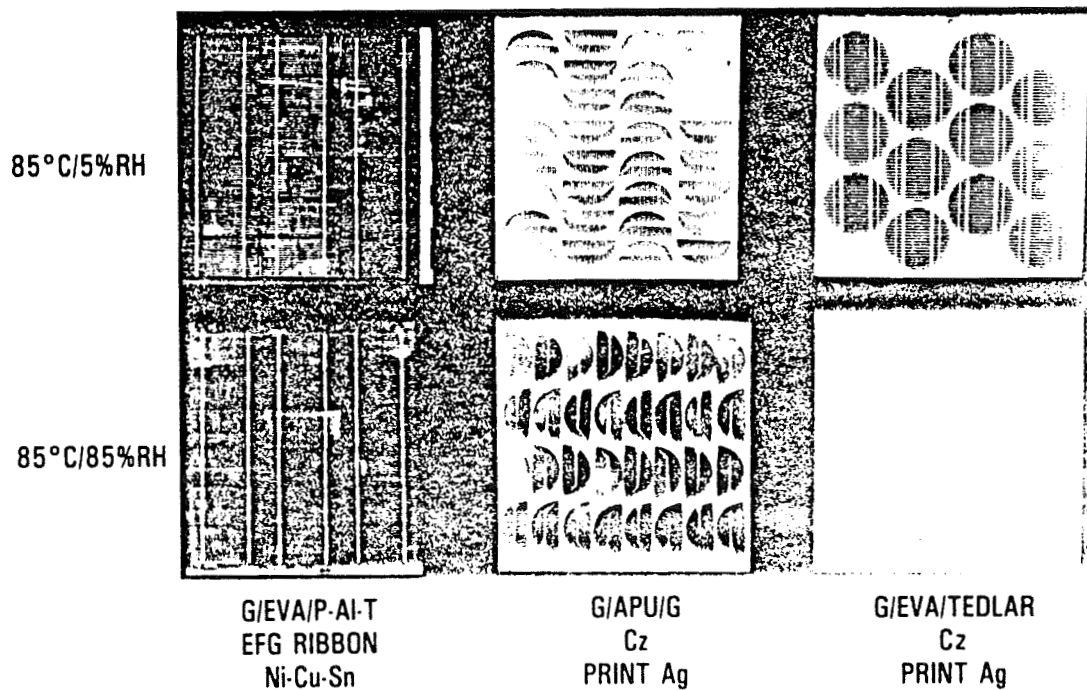
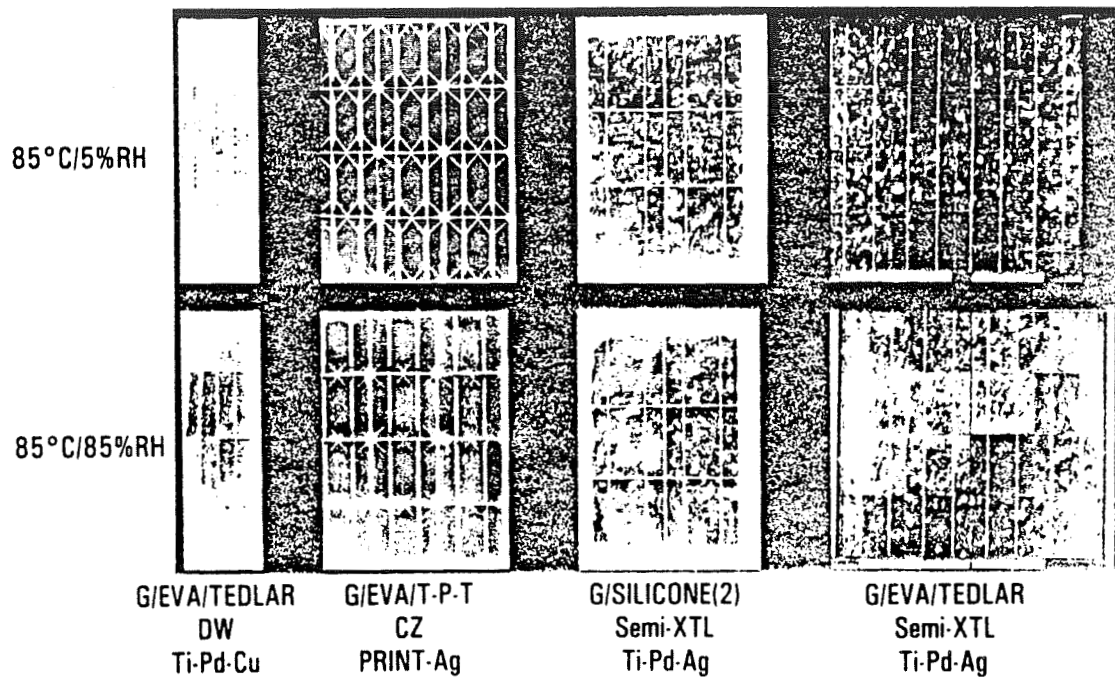
Wyle Laboratories Voltage-Bias Circuits



Combined Environment Tests (Temperature/Humidity Durations Equivalent to a 20-Year Field Exposure)

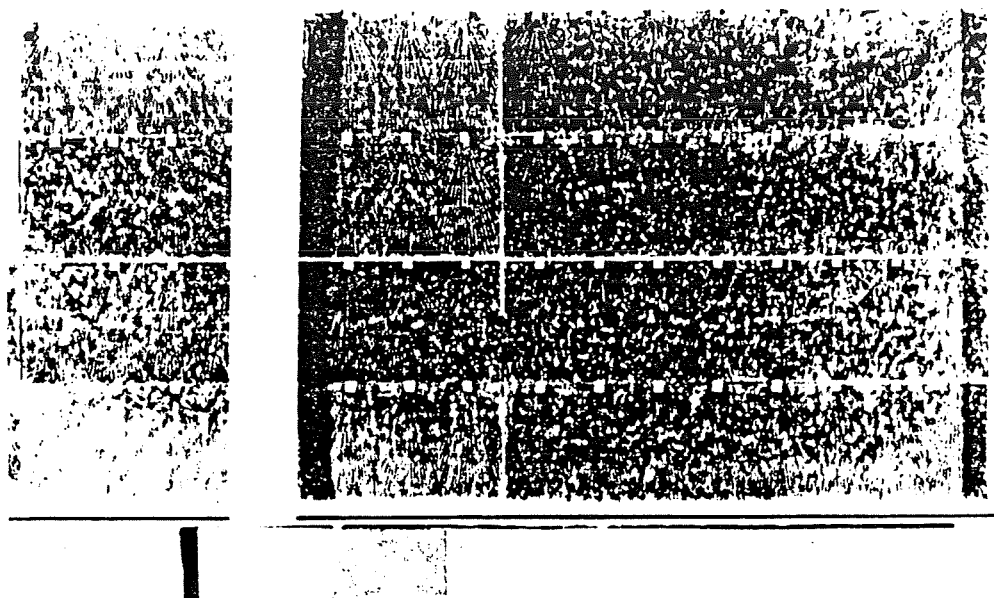


Combined Environment Results: Comparison After 40 Days of
Various Module Designs



ORIGINAL PAGE IS
OF POOR QUALITY

Electrochemical Degradation of Glass/EVA/Tedlar Module (at Day 40)



Performance Degradation After 40 Days at 85°C/85% RH
(Approximately Equivalent to 20 Years in the Field)

Encapsulant	Metallization	P/P ₀ Power Loss	
		Transmissivity	Series Resistance
Glass/EVA/Tedlar	Print-Ag	0.99	0.82
	Ti-Pd-Cu	0.96	1.00
	Ti-Pd-Ag	0.95	0.99
Glass/EVA/T-P-T	Print-Ag	0.96	0.91
Glass/EVA/Foil	Ni-Cu-Sn	0.99	0.99
Glass/APU/Glass	Print-Ag	0.97	0.99
Glass/Silicone	Ti-Pd-Ag	0.99	0.97
Strawman 20-year goal for total degradation in all environments		0.96	0.96

Conclusions

- A variety of present module types are consistent with 20-year life with respect to typical temperature/humidity site stress
- Degradation mechanisms identified include:
 - Discoloration of encapsulants
 - Electrochemical corrosion of cell metallization
 - Material diffusion from edge seals
 - Delamination (foil), and embrittlement of back covers
- Important to have voltage-bias in qualification tests
- Important to include both temperature/humidity and temperature-only test for identifying degradation mechanisms

MODULE ENCAPSULATION TECHNOLOGY

SPRINGBORN LABORATORIES

P. Willis

Phase I

IDENTIFY AND DEVELOP LOW COST
MODULE ENCAPSULATION MATERIALS

- POTTANTS
- COVER FILMS
- SUBSTRATES
- ADHESIVES/PRIMERS
- ANTI-SOILING TREATMENTS

Phase II

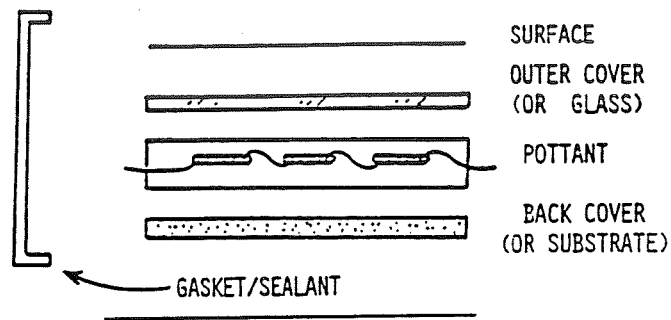
TASK 1: MATERIALS RELIABILITY

- AGING AND LIFE ASSESSMENT
- ADVANCED STABILIZERS
- ADHESIVE BOND DURABILITY
- HUMIDITY SENSITIVITY
- ELECTRICAL ISOLATION

TASK 2: PROCESS SENSITIVITY

- INTERRELATIONSHIPS OF
 - FORMULATION VARIABLES
 - PROCESS VARIABLES
- IDENTIFY FAILURE MODES
- INDUSTRIAL GUIDANCE

Module Components



CURRENT EMPHASIS ON MATERIALS AND MODULE PERFORMANCE CHARACTERISTICS

- DETERMINE CURRENT LEVEL OF PERFORMANCE
- ENHANCE PERFORMANCE (E.G. REFORMULATION)
- SERVICE LIFE PROGNOSIS

PERFORMANCE CRITERIA

- ENVIRONMENTAL DEGRADATION
- MAXIMUM SERVICE TEMPERATURE
- ADHESIVE BOND DURABILITY
- ELECTRICAL INSULATION DURABILITY
- HYDROLYTIC (WATER) STABILITY
- WHAT ARE DOMINANT TYPES OF FAILURE ?
- WHERE IS STABILIZATION NEEDED ?

Accelerated Aging Test Program

CONDITIONS USED INITIALLY

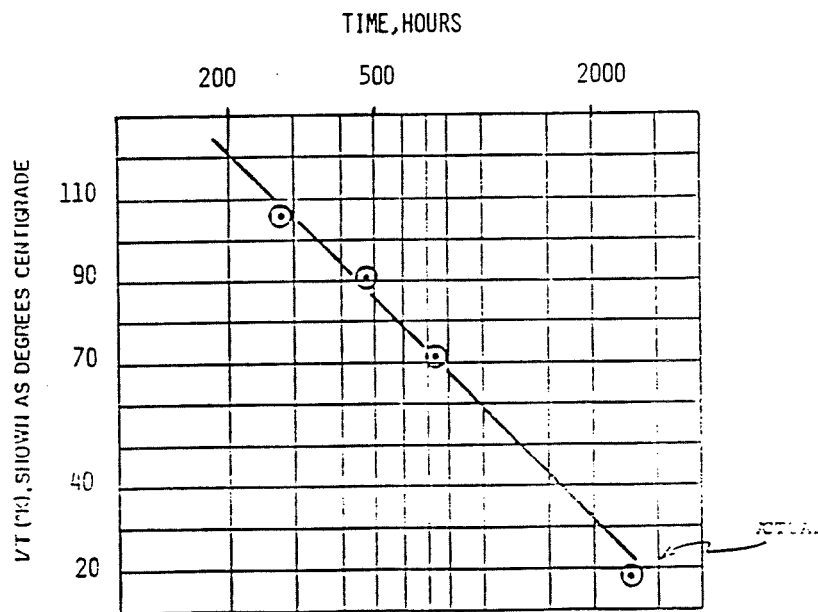
<u>METHOD</u>	<u>DEFICIENCIES</u>
• THERMAL (AIR OVEN)	• UNNATURAL LIGHT
• RS/4 50°C	• NO " WEATHER "
• RS/4 WET SPRAY	• NO PREDICTIVE METHODS
• RS/4 85°C	• <u>LONG</u> EXPOSURE TIMES

OUTDOOR PHOTOTHERMAL AGING REACTORS (OPTAR)

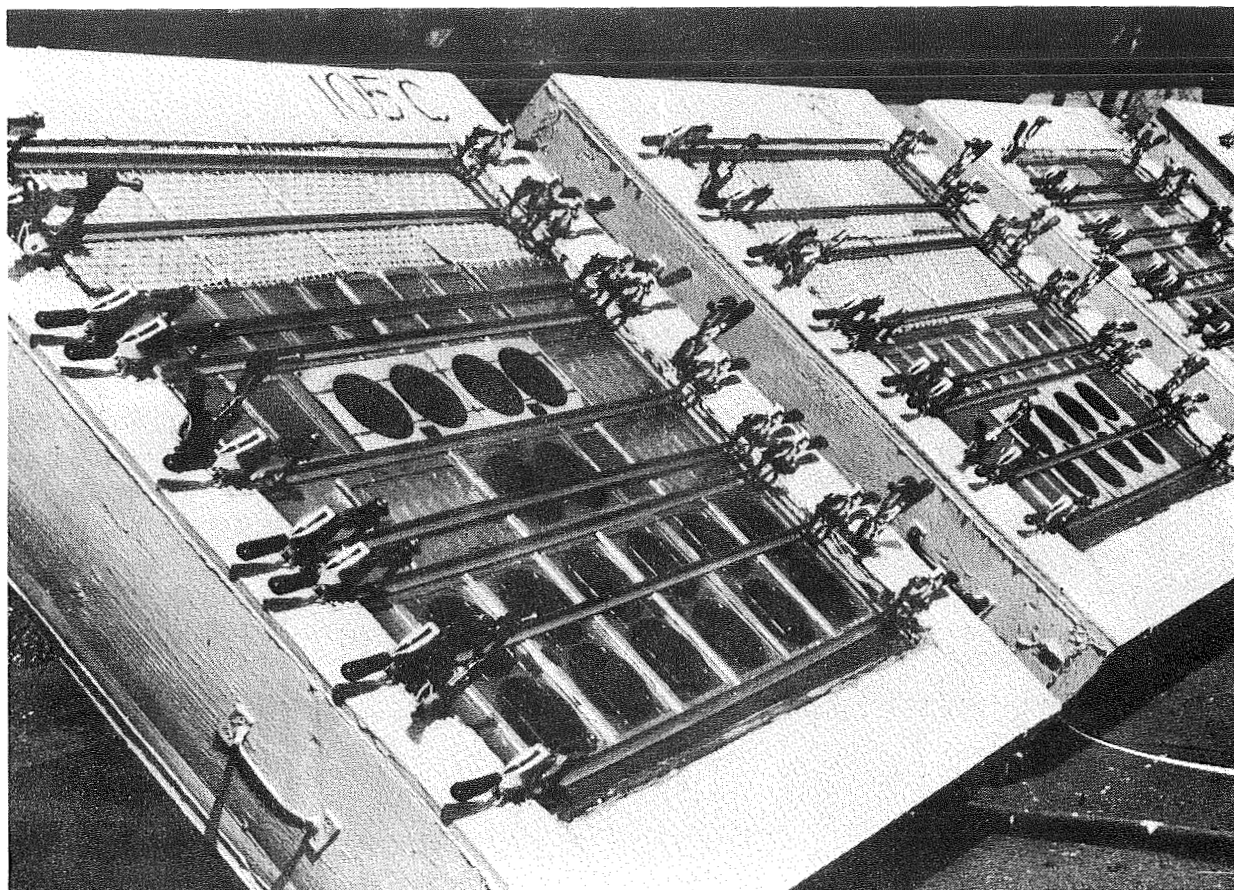
- USE NATURAL SUNLIGHT, AVOIDS SPECTRAL DISTRIBUTION PROBLEMS WITH ARTIFICIAL LIGHT SOURCES
- USE TEMPERATURE TO ACCELERATE THE PHOTO-THERMAL REACTION
- INCLUDES DARK CYCLE REACTIONS
- INCLUDES DEW / RAIN EXTRACTION
- INTENDED PRIMARILY FOR MODULE EXPOSURE
- EXTRAPOLATE EFFECTS TO LOWER TEMPERATURES

Accelerated Aging

- USEFUL FOR EVALUATING CANDIDATE FORMULATIONS - COMPARISON
- WHOLE MODULES UNDER EXPOSURE
- DETERMINE UPPER LEVEL SERVICE TEMPERATURES
- MODELLING:
 - TIME TO ONSET OF DEGRADATION (INDUCTION PERIOD, t_i)
EXAMPLE: POLYPROPYLENE
 - ARRHENIUS: $\log t_i$ vs, $1/K^0$
 - PREDICT SERVICE LIFE BY EXTRAPOLATION TO LOWER TEMPERATURES



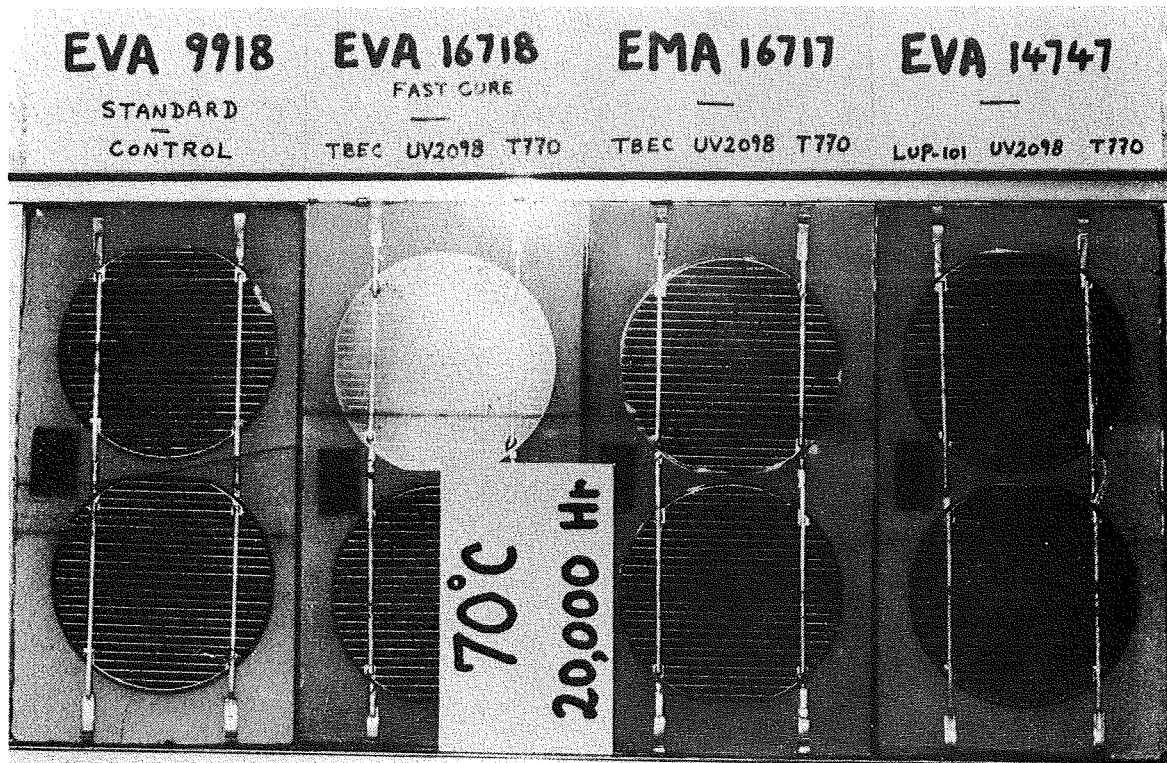
Outdoor Photothermal Aging Reactors (OPTAR), Enfield, Connecticut
(70, 90, and 105°C)



MODULE AND RELIABILITY TECHNOLOGY

OPTAR/70°C, 20,000 Hours

- SOME COPPER REACTION W/ EVA 9918
- NO OTHER EFFECTS NOTICEABLE



ORIGINAL PAGE IS
OF POOR QUALITY

OPTAR/90°C, 20,000 Hours

ORIGINAL PAGE IS
OF POOR QUALITY

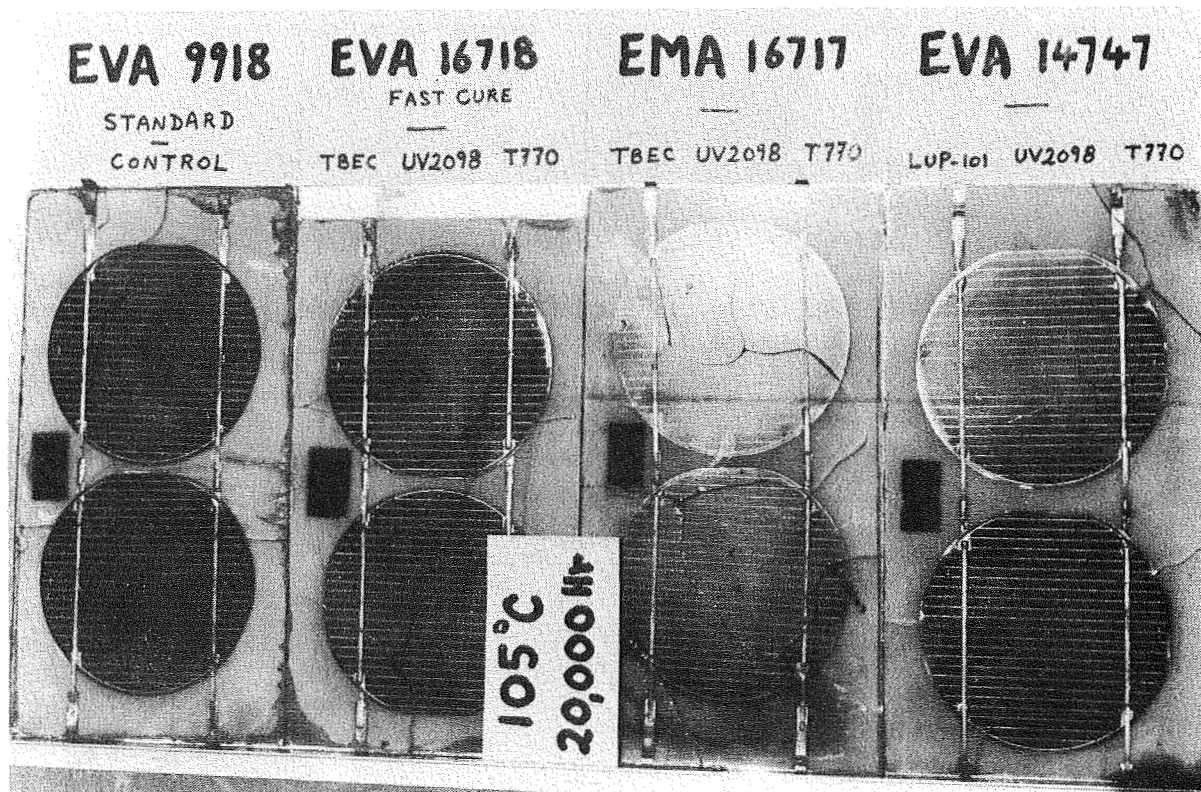
- COPPER REACTION IN LUPERSOL-101 RESINS
- OVERALL CONDITION: VERY GOOD



MODULE AND RELIABILITY TECHNOLOGY

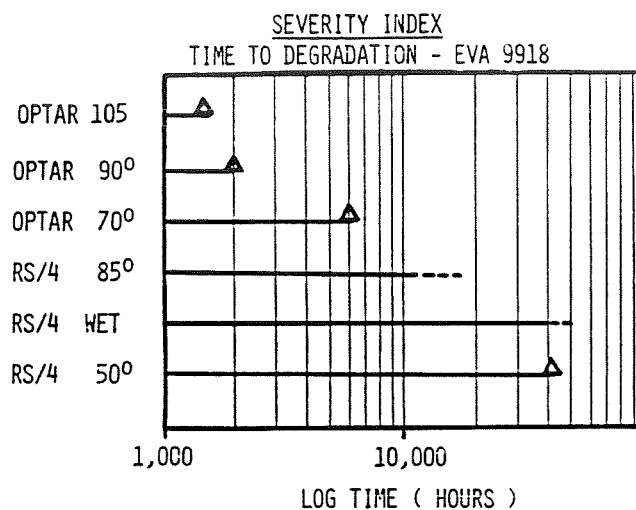
OPTAR/105°C, 20,000 Hours

- ALL SHOW SEVERE COPPER REACTION
- BEST PERFORMANCE: EVA-ADVANCED STABILIZER
TBEC, UV-2098, TINUVIN 770



ORIGINAL PAGE IS
OF POOR QUALITY

Accelerated Aging: Summary of Investigations



- OPTARS MOST EFFICIENT AGING TECHNIQUE
- MODULES HAVE VERY HIGH ENDURANCE
NO EFFECT: 20,000 HRS - 70°C / SUNLIGHT
- DEGRADED MODULES SHOW NO POWER LOSS
- EVA 9918 (STANDARD FORMULA) PERFORMS VERY WELL
- OPTIMIZED EVA FORMULATION:

LUPERSOL TBEC	CURING AGENT
CYASORB UV-2098	UV SCREENER
TINUVIN 770	STABILIZER
- RADIOMETER INSTALLED ON OPTAR DEVICES - POSSIBILITY
FOR MODELING BASED ON HEAT PLUS LIGHT ???

Adhesion Experiments

STATUS:

- PRIMER FORMULATIONS IDENTIFIED FOR ALMOST ALL INTERFACES IN MODULES
 - POLYMER / METAL
 - POLYMER / INORGANIC
 - POLYMER / ORGANIC
- DR. PLUEDDEMANN - DOW CORNING
- DR. JIM BOERIO - UNIVERSITY OF CINCINNATI
- SELF-PRIMING FORMULATIONS OF EVA (TO GLASS, CELLS) DEVELOPED: AVAILABLE - SPRINGBORN
- NEW PRIMER AVAILABLE - DOW CORNING WITH IMPROVED PROPERTIES - UNDER TEST

Adhesion Diagnostics

- NEW METHOD DEVELOPED
- EVA COMPOUNDED WITH HIGH LOADINGS OF SILANE TREATED GLASS BEADS - RESEMBLES GLASS REINFORCED POLYMER
- EQUILIBRIUM WATER ABSORPTION VALUES MAY PROVIDE NEW METHOD OF EVALUATING ADHESIVE BONDS - INDICATES " DAMAGE " TO BONDS AT THE INTERFACE IS REVERSIBLE UP TO A LIMIT
- DETERMINE DEGRADATION RATES (KINETICS)
- ASSESS SERVICE LIFE
- GENERAL CONCLUSION - BOND DURABILITY - EXCELLENT

Electrical Isolation

- POTTANTS AND COVER FILMS SERVE AS ELECTRICAL INSULATION
- NEED TO KNOW THICKNESS REQUIRED FOR VOLTAGE STANDOFF
- VARIATION WITH TEMPERATURE, ABSORBED WATER ?
- NEED TO KNOW VARIATION DIELECTRIC STRENGTH WITH AGING:
LIGHT, HEAT, HUMIDITY, FIELD STRESS

METHOD:

- HV-DC POWER SUPPLY, SYMMETRIC ELECTRODES
- SPECIFIED RATE OF RISE (500 V/SEC)
- PLOT AVERAGE BREAKDOWN VOLTAGE, V_A VS THICKNESS
- STRAIGHT LINE RELATIONSHIP: SLOPE EQUALS " INTRINSIC
DIELECTRIC STRENGTH " (DC)
- MEASUREMENTS TO DATE:
EVA 9918, $DV/DT = 3.48$ KV/MIL

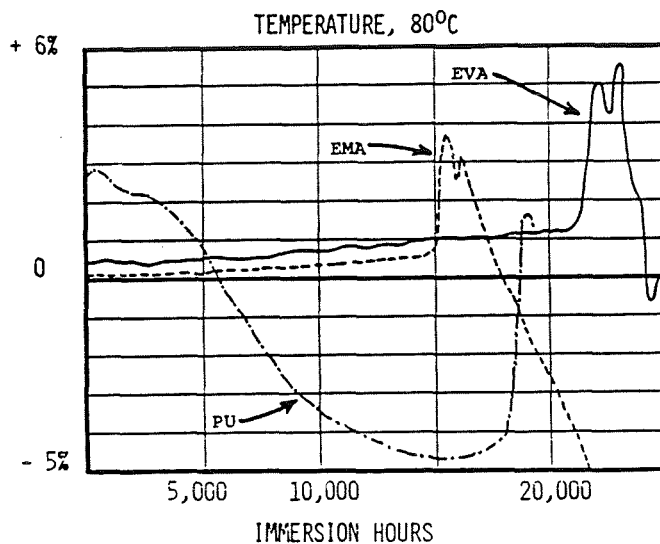
RESULTS TO DATE: EVA A9918

			Δ
RS/4 (50°C)	4,000 HR	3.24 KV/MIL	93%
RS/4 (85°C)	4,000 HR	1.98 KV/MIL	57%
RS/4 WET	4,000 HR	4.12 KV/MIL	118%
OPTAR 70°C	2,000 HR	2.85 KV/MIL	82%
OPTAR 90°C	2,000 HR	3.14 KV/MIL	90%
OPTAR 105°C	2,000 HR	- - UNTESTABLE - -	

- NEW SPECIMEN GEOMETRY NEEDED - NOW UNDER TEST
- SOME EVIDENCE FOR DECREASE IN DIELECTRIC STRENGTH WITH
ACCELERATED AGING
- INCREASE IN STRENGTH WITH WATER EXPOSURE

Hydrolytic Stability

- CANDIDATE POTENTIALS - WATER IMMERSION
AT 40°, 60°, 70°, 80° AND 90°
- MEASURE CHANGE IN WEIGHT VERSUS TIME



	TIME TO ONSET OF CHANGE, HOURS		
	70°	80°	90°
EVA	?	21,000	14,000
EMA	?	15,000	9,800
PU	----- CONTINUAL -----		

- EVA VERY HYDROLYTICALLY STABLE
- DATA WILL BE USED FOR KINETICS

Anti-Soiling Treatments

SURFACE CHEMISTRY:

- HARD
- SMOOTH
- HYDROPHOBIC
- OLEOPHOBIC
- ION FREE
- LOW SURFACE ENERGY

SURFACE INVESTIGATED:

- SUNADEX GLASS
- TEDLAR (100 BG 30 UT)
- ACRYLAR (ACRYLIC FLIM)

MOST EFFECTIVE TREATMENT:

- E-3820 PERFLUORODECANOIC ACID/
SILANE (DOW CORNING)
- STILL EFFECTIVE AT 56 MONTHS
OUTDOOR EXPOSURE
- RESULTS IN IMPROVED POWER OUTPUT
OF 1% TO 4% - DEPENDING ON SURFACE
- FLUOROALKYL SILANE CHEMISTRY
APPEARS TO BE MOST EFFECTIVE

NEW TREATMENTS:

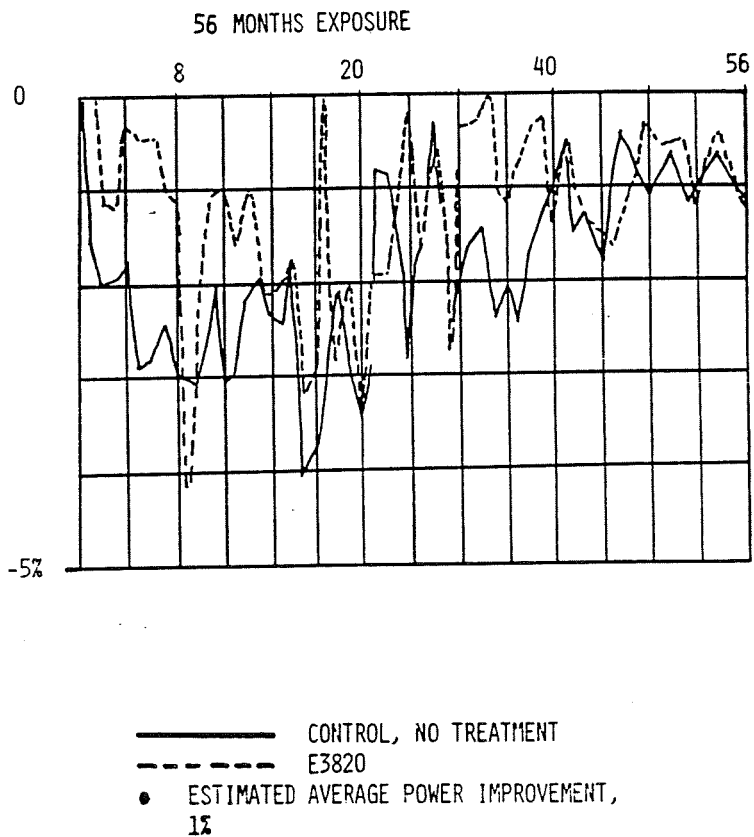
- TWO NEW CANDIDATES FROM DOW CORNING
STARTED

Soiling Experiments

FIFTY-SIX MONTHS EXPOSURE

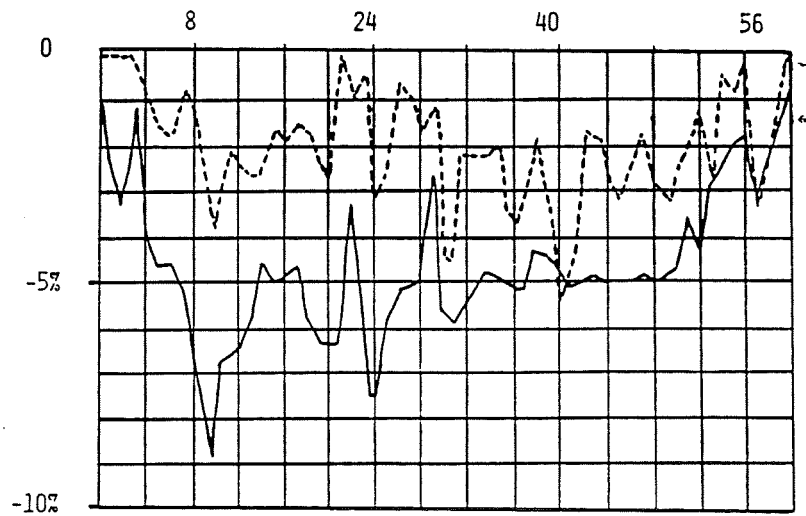
ENFIELD, CONNECTICUT

% LOSS IN I_{sc} WITH STANDARD CELL TREATED
SUNDEX GLASS



Soiling Experiments (Cont'd)

FIFTY-SIX MONTHS EXPOSURE
ENFIELD, CONNECTICUT
% LOSS IN I_{sc} WITH STANDARD CELL TREATED
TEDLAR 100B6300UT
(SUPPORT ON GLASS)
56 MONTHS EXPOSURE



— CONTROL, NO TREATMENT

- - - E3820

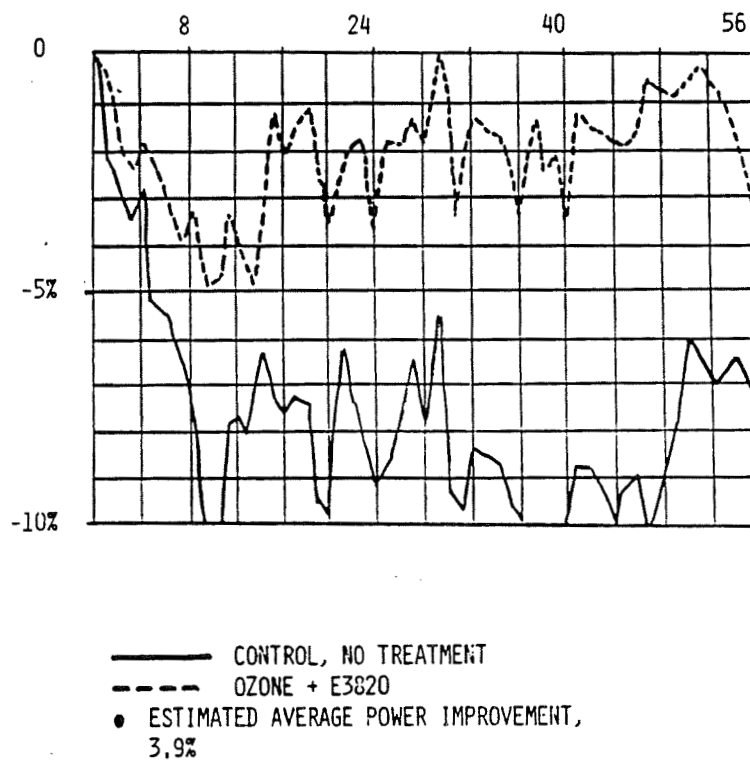
• ESTIMATED AVERAGE POWER IMPROVEMENT, 3.8%

Soiling Experiments (Cont'd)

FIFTY-SIX MONTHS EXPOSURE
ENFIELD, CONNECTICUT

% LOSS IN I_{sc} WITH STANDARD CELL TREATED ACRYLAR
(SUPPORTED ON GLASS)

56 MONTHS EXPOSURE



Process Sensitivity

GOALS:

- UNDERSTAND RELATIONSHIPS BETWEEN ALL MANUFACTURING VARIABLES
- DEFINE FAILURE / ACCEPTABILITY CRITERIA
- STATISTICAL ANALYSIS OF RESULTS
- DEFINE OPTIMUM CONDITIONS
- PREDICT MANUFACTURING YIELD
- PROVIDE DOCUMENTATION TO INDUSTRY

VARIABLES

FORMULATION:

- POTANT COMPOSITION
- CURING AGENTS
- PRIMERS
- STORAGE CONDITIONS

PROCESSING:

- VACUUM PRESSURE
- TEMPERATURE, ULTIMATE, °C
- TEMPERATURE, RATE OF RISE, °C / MIN.
- DWELL TIMES
- RATE OF COOLING

Testing and Performance Criteria

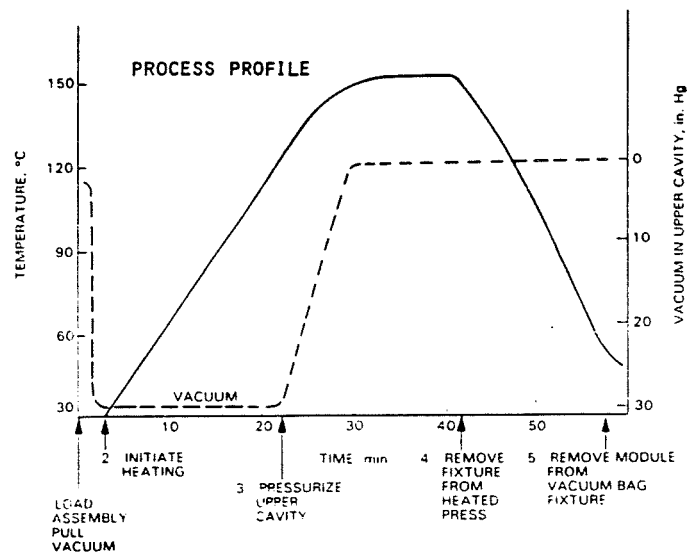
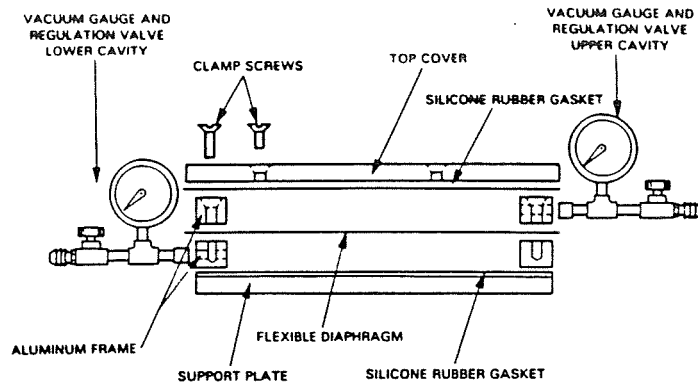
- METHOD:
- PREPARE TEST MODULES AND / OR OTHER TEST SPECIMENS WITH CHANGE IN SIGNIFICANT VARIABLE(S)
 - DEVELOPED STANDARD TEST SPECIMEN
 - DEVELOPED STANDARD TEST PROTOCOL
 - COLLECTED UNIFORM DATA SETS
 - QUANTITATE THE EFFECTS

<u>COMPONENT</u>	<u>CRITERION</u>	<u>TEST</u>
POTTANT	ADEQUATE CURE	PERCENT GEL THERMAL CREEP
	TRAPPED BUBBLES	VISUAL
	DISCOLORATION	VISUAL
CELLS	BREAKAGE	VISUAL, RESISTANCE
	INTERCONNECT	RESISTANCE
	REGISTRATION	VISUAL
COVER FILMS	TEARS / PUNCTURES	VISUAL
	WARPING / SHRINKAGE	VISUAL
GLASS (SUPERSTRATE)	FRACTURE	VISUAL
ADHESION	BOND STRENGTH	PEEL TEST
	ENDURANCE	WATER SOAK (50°C)

Process Equipment

ORIGINAL PAGE IS
OF POOR QUALITY

EXPERIMENTAL LAMINATOR



- MICROPROCESSOR CONTROLLED EXPERIMENTAL LAMINATOR CONSTRUCTED
- STUDIES STARTED ON PROCESSING PROFILES
 - RATE OF HEATING (HOW SLOW, HOW FAST ?)
 - VACUUM TIMING
 - RATE OF COOLING

Process Sensitivity: Observations and Recommendations

FORMULATION VARIABLES

- EVA FORMULATIONS RELATIVELY INSENSITIVE TO QUANTITY OF PEROXIDE BUT VERY SENSITIVE TO AIR EXPOSURE - EVAPORATION
- EVA WITH LUPERSOL - TBEC MUCH LESS SENSITIVE
- UNWRAP / CUT EVA JUST BEFORE MODULE MANUFACTURING - LIMIT AIR EXPOSURE
- SELF-PRIMING GRADE WORKS WELL

PROCESS VARIABLES

- UPPER AND LOWER LIMITS DETERMINED:
 - ULTIMATE TEMPERATURE
 - RATE OF RISE - TEMPERATURE
 - BACKPRESSURE TIMING
- DOMINANT FAILURE : ADHESION (POTTANT / GLASS)
 - BOUNDS THE NARROWEST PROCESSING " WINDOW "
- EVA WITH LUPERSOL-TBEC HAS WIDER WINDOW THAN EVA 9918
 - STORAGE : MORE STABLE TO EXPOSURE
 - PROCESSING : WIDER RANGE OF CONDITIONS
- INDUSTRIAL " TROUBLE SHOOTING GUIDE " PREPARED

Thin-Film Encapsulation

(AMORPHOUS PHOTOVOLTAICS)

TYPES:

- SUPERSTRATE - ON GLASS
- SUBSTRATE - ON STAINLESS STEEL

FAILURE MECHANISMS:

CORROSION , BREAKAGE (GLASS) , ABRASION,
ELECTRICAL SHORTING, OTHERS ? ? ?

Encapsulation Requirements (Anticipated)

<u>COMPONENT</u>	<u>PROPERTY</u>
OUTER COVER	<ul style="list-style-type: none">● INHERENTLY WEATHERABLE● ABRASION / CUT RESISTANT
BACK COVER	<ul style="list-style-type: none">● WHITE (EMISSIVE)● WEATHER RESISTANT
POTTANT	<ul style="list-style-type: none">● PROCESSABLE <100°C● CURABLE - CREEP RESISTANT● LOW WATER ABSORPTION● HIGH OPTICAL TRANSMISSION
DURABLE BONDING	<ul style="list-style-type: none">● ALL INTERFACES● LONG SERVICE LIFE● LOW COST

Manufacture/Process

- FAST
- AUTOMATABLE
- INEXPENSIVE

Thin-Film Encapsulation: Candidate Materials and Processes

BACK COVERS

- WHITE TEDLAR

OUTER COVERS

- FLUOROPOLYMERS BEST CHOICE
- FEP CURRENTLY FAVORED DUE TO HIGH TRANSPARENCY AND OUT-STANDING WEATHERABILITY

<u>FILM</u>	<u>REF. INDEX</u>	<u>% T</u>	<u>COST \$/FT²/MIL</u>
FEP	1.34	93.6	0.10

POTTANTS:

CONDUCTING INVESTIGATIONS

<u>MATERIAL CLASS</u>	<u>MANUFACTURER</u>	<u>\$/LB</u>
ETHYLENE/VINYL ACETATE	DU PONT, USI	.60 - .80
ETHYLENE/ACRYLIC	DOW, GULF	.80 - 1.00
IONOMER	DU PONT	1.08 - 1.60
ALIPHATIC URETHANE	UPJOHN	1.70 - 2.50
HOT MELT ADHESIVES (HYDROCARBON, POLYAMIDE POLYETHER, ACRYLIC)	MANY	.80 - 2.50

CURE METHOD:

- MOISTURE CURE (MODIFIED CHEMISTRY)
- PEROXIDE DECOMPOSITION (HEAT)
- UV CURE (PHOTOINITIATION)
- MOISTURE CURABLE SELF - PRIMING POTTANT UNDER DEVELOPMENT . SILANE / ACRYLIC CHEMISTRY

ENCAPSULATION METHOD:

- FILM LAMINATION: EXTRUDE THE POTTANT ON AN OUTER COVER FILM AS A CARRIER, USE COMBINATION FOR LAMINATION.

Conclusions

ACCELERATED AGING:

- " OPTAR " METHOD BEST AGING TECHNIQUE DISCOVERED SO ARE
- MODELING / LIFE PREDICTION ENCOURAGING
 - 70° & 90°C VERY GOOD CONDITION
 - COPPER REACTIONS NOT AS SEVERE AS ANTICIPATED - EXCEPT AT 105°C
 - LUPERSOL - TBEC CURED FORMULATIONS APPEAR MORE STABLE
 - BEST STABILIZERS : UV-2098 SCREENER, TINUVIN 770 (BOTH CYANAMIDE)
 - MODULE PERFORMANCE - EXCELLENT (OPTAR 90°C - 20,000 HR - NO CHANGE)

ADHESION:

- NEW TEST METHOD FOR PRIMER EVALUATION AND BOND DURABILITY
- CAN DEMONSTRATE BOND RECOVERY & LIMIT OF REVERSIBILITY
- SELF-PRIMING EVA WORKS WELL

ELECTRICAL ISOLATION:

- INTRINSIC DIELECTRIC TEST METHOD DEVELOPED
- SOME EVIDENCE OF DECREASE IN DIELECTRIC STRENGTH WITH ACCELERATED AGING

Conclusions (Cont'd)

HYDROLYTIC STABILITY:

- EVA APPEARS EXCELLENT

PROCESS SENSITIVITY:

- DOMINANT PROCESS FAILURE MODE : ADHESION
- EVA STORAGE ESSENTIAL
- LUPERSOL TBEC FORMULATIONS - WIDER PROCESS LATITUDE, BETTER STORAGE STABILITY

SOILING:

- TREATMENTS STILL EFFECTIVE AFTER 56 MONTHS

THIN-FILM PV:

- CANDIDATES BEING SELECTED / DEVELOPED

COMMERCIAL MODULE TEST PROGRAM

JET PROPULSION LABORATORY

M. I. Smokler

Purpose

- Investigate state of the art of module design and manufacture
- Identify problems requiring additional research

Approach

- Obtain commercial PV modules in current production
- Perform Block V Qualification Tests
- Perform failure analysis
- Obtain modules with defects corrected
- Repeat qualification tests

Module Manufacturers

AEG Telefunken	West Germany
Helios	Italy
Photowatt	France
Hoxan	Japan
Kyocera	Japan
Siemens	West Germany
Solavolt	USA
Solec	USA
Toyomenka	Japan

Efficiency Comparisons

Module Manufacturer	Power, Module (W)	Efficiency, Module (%)	Efficiency, Encapsulated Cell (%)	Efficiency, Module, at 0.9 Packing Factor (%)
Single-XTL Cells				
Helios	41.7	9.4	11.6	10.4
Hoxan	37.5	9.3	13.9	12.5
Siemens	130.8	8.7	11.6	10.4
Toyomenka	40.3	10.5	11.7	10.5
Semi-XTL Cells				
AEG Telefunken	38.7	7.9	9.8	8.8
Photowatt	36.1	7.5	10.0	9.0
Kyocera	42.8	9.8	12.0	10.8
Solavolt	38.6	8.4	10.6	9.5
Solec	40.3	10.5	11.7	10.5

The above data are based on JPL power measurements of one sample of the type module obtained for qualification testing and on nominal dimensions of module and cell areas.

Module Description

Manufacturer: Helios, Italy

Mechanical**Dimensions**

Module: 131 cm x 34.0 cm

Cell: 10.0 cm²

Packing factor: 0.81

Materials

Cells: Single XTL Silicon

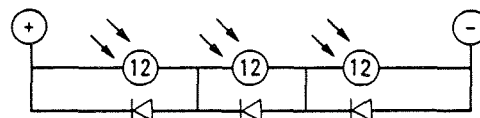
Superstrate: Tempered glass

Encapsulant: EVA

Back cover: Tedlar

Edge seal: Silicon rubber

Frame: Aluminum

Electrical**CIRCUIT****Sample Performance (Standard Conditions)**

Power, max: 41.7 W

Voltage: 15.8 V

Current: 2.64 A

V_{oc}: 20.2 V

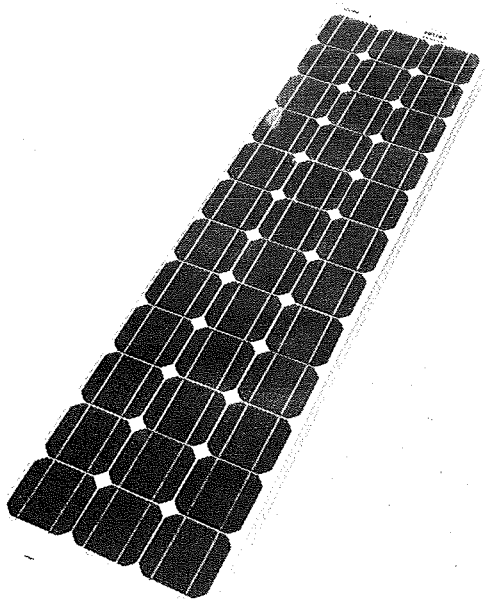
I_{sc}: 3.02 A

η, module: 9.4%

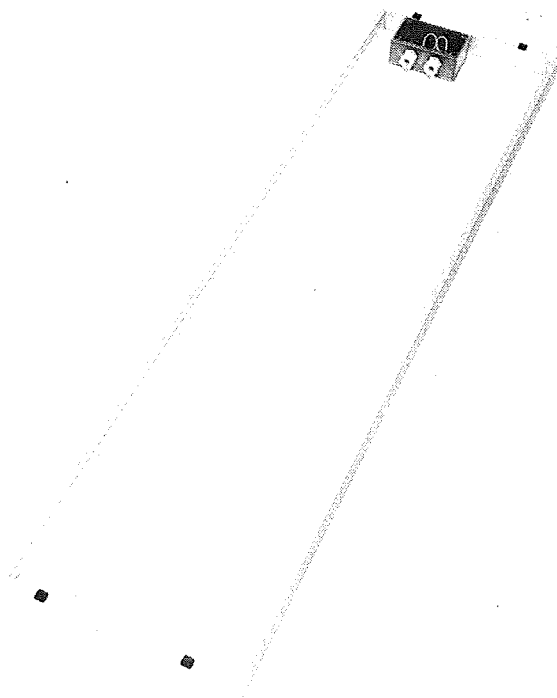
η, encapsulated cell: 11.6%

Photovoltaic Module (Top View)
Manufacturer: Helios, Italy

ORIGINAL PAGE IS
OF POOR QUALITY

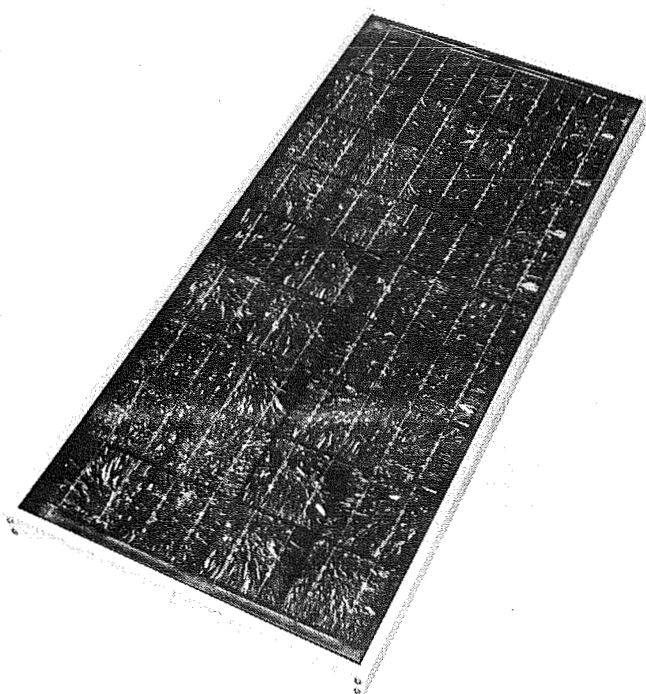


Photovoltaic Module (Bottom View)
Manufacturer: Helios, Italy

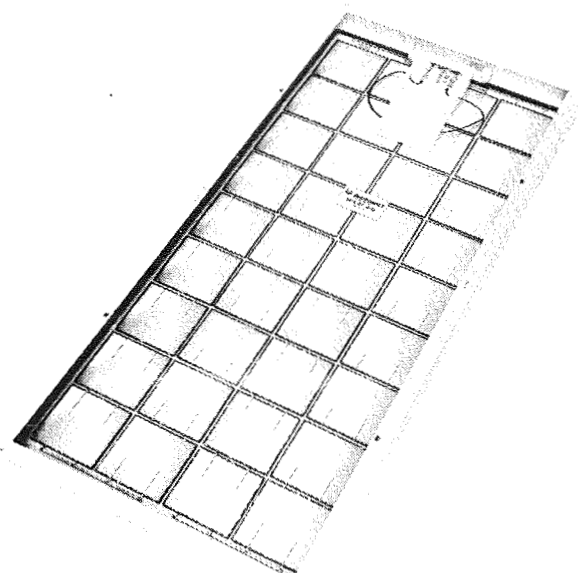


Photovoltaic Module (Top View)
Manufacturer: Photowatt, France

ORIGINAL PAGE IS
OF POOR QUALITY



Photovoltaic Module (Bottom View)
Manufacturer: Photowatt, France



C-7

Module Description Manufacturer: Photowatt, France

Mechanical

Dimensions

Module: 104.3 cm x 46.2 cm

Cell: 10.0 cm²

Packing factor: 0.75

Materials

Cells: Semi XTL Silicon

Superstrate: Tempered glass

Encapsulant: PVB

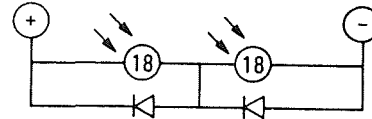
Back cover: Tempered glass

Edge seal: Silicon rubber

Frame: Aluminum

Electrical

CIRCUIT



(Standard Conditions)

Power, max: 36.1 W

Voltage: 16.3 V

Current: 2.22 A

V_{oc}: 20.1 V

I_{sc}: 2.46 A

η, module: 7.5%

η, encapsulated cell: 10.0%

Module Description Manufacturer: Siemens, West Germany

Mechanical

Dimensions

Module: 146.9 cm x 102 cm

Cell: 10.0 cm diameter

Packing factor: 0.75

Materials

Cells: Single XTL Silicon

Superstrate: Tempered glass

Encapsulant: PVB

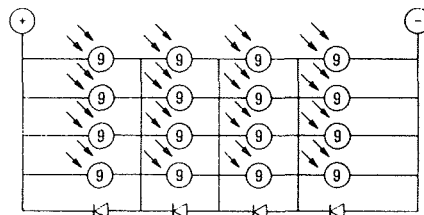
Back cover: Tedlar/Al/Tedlar

Edge seal: Foil tape/rubber

Frame: Aluminum

Electrical

CIRCUIT



Sample Performance (Standard Conditions)

Power, max: 130.8 W

Voltage: 16.5 V

Current: 7.91 A

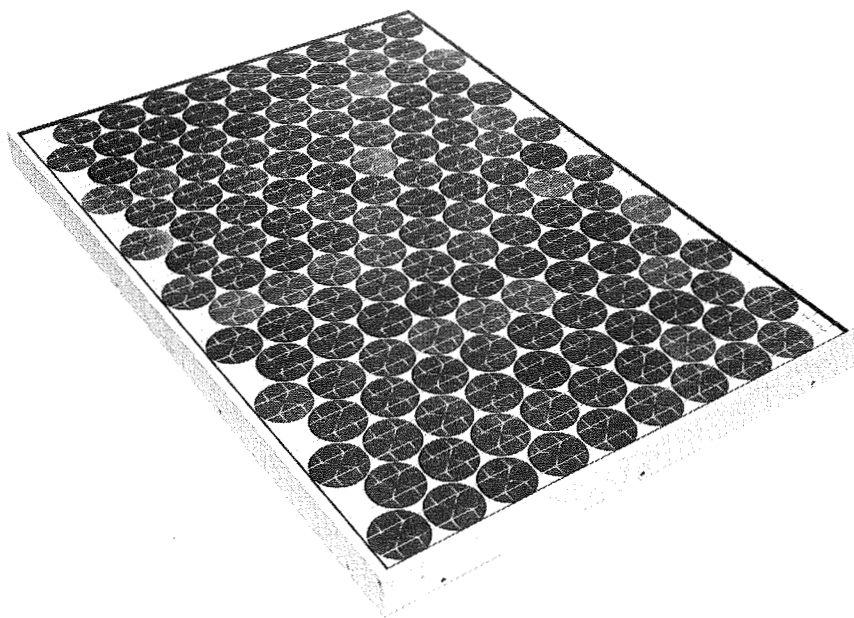
V_{oc}: 21.3 V

I_{sc}: 8.76 A

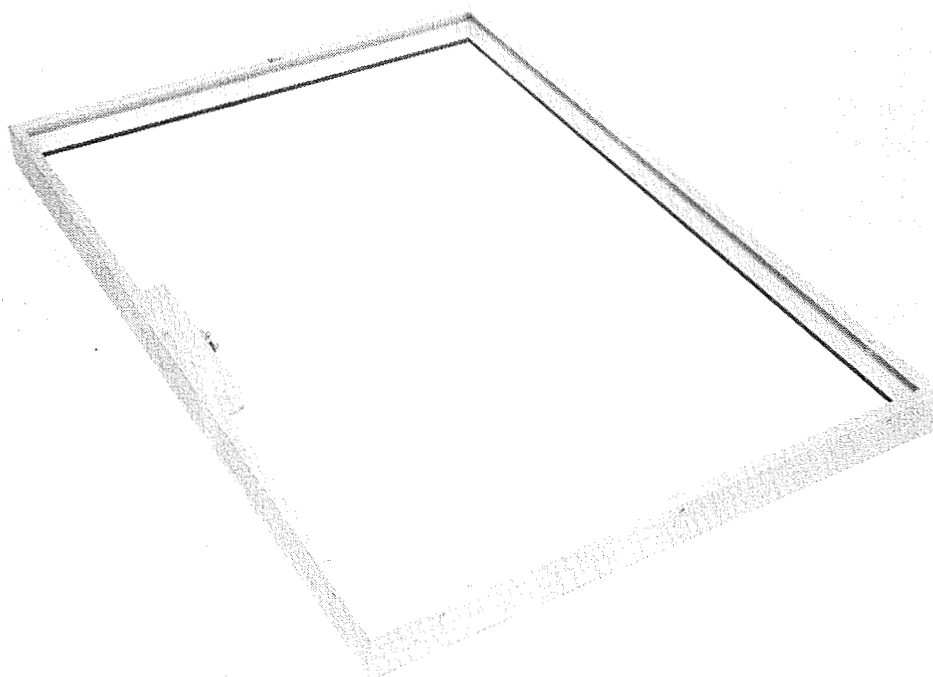
η, module: 8.7%

η, encapsulated cell: 11.6%

Photovoltaic Module (Top View)
Manufacturer: Siemens, West Germany



Photovoltaic Module (Bottom View)
Manufacturer: Siemens, West Germany



Qualification Test Record

Module Designs Tested	12
Number Passed	6
Number Failed	6

Failure Record

Test	Failed Designs	Failure Mode
T-50	1	Cracked interconnects. Power down
	1	Cracked cells. Power down
T-200	1	Encapsulant delamination
MI-10K	1	Cracked interconnects. Power down
Hot-Spot	2	Blistered Tedlar. Burn marks on Tedlar and encapsulant

Conclusions

- Most commercial modules use Block V technology
- Most commercial module designs do not pass the Block V Qualification Tests at the first attempt. (The Project phaseout plan precluded correction of defects and repetition of tests for the designs that failed)
- Semi-crystalline cell modules with one bypass diode per 36 series cells may pass the Hot-Spot test, but cell temperatures reach 150°C
- Although the precise cause of the cell cracks that caused power degradation was not determined, it seems clear that excess degradation would not have occurred if Block V (failure tolerant) cell/interconnect designs had been used
- It could not be determined whether the interconnect failures were caused by hitherto unexpected causes; failure analysis was terminated because of funding limitations
- The Block V Qualification Tests have again demonstrated their effective role in the development of reliable modules

HIGH-EFFICIENCY MODULE DESIGN

SPIRE CORPORATION

M. B. Spitzer

Principal Results

- DELIVERED 75.2 WATT MODULE WITH EFFICIENCY OF 15.2 %, AND ENCAPSULATED CELL EFFICIENCY OF 16.9%.
- OBTAINED ENCAPSULATED CELL EFFICIENCY OF 17.6% IN A 12-CELL MINI-MODULE.
- FABRICATED LARGE -AREA CELLS WITH EFFICIENCY OF OVER 18%.
- EVALUATED THE USE OF BSR CELLS TO REDUCE NOCT.
- HIGH EFFICIENCY WAS OBTAINED WITH CZ.

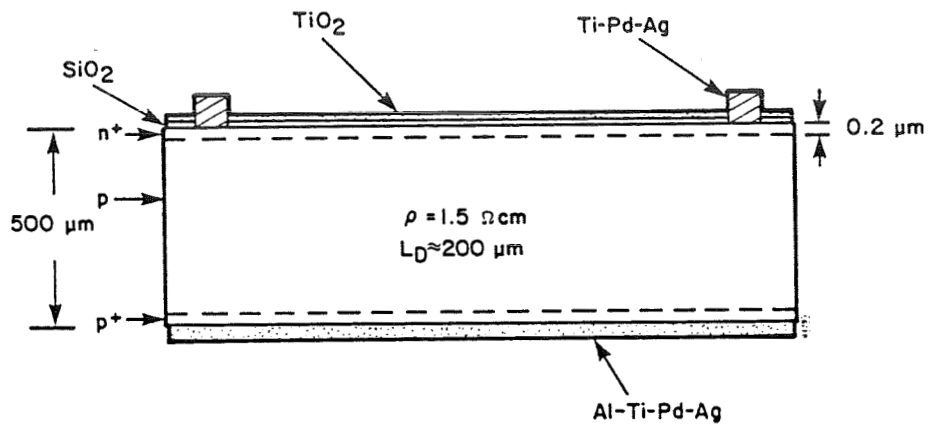
Objectives

- FABRICATION OF MODULES WITH EMPHASIS ON REDUCED OPERATING TEMPERATURE.
- FABRICATION OF HIGHLY EFFICIENT MODULES.
- EVALUATION OF POSSIBLE TRADE-OFF BETWEEN HIGH EFFICIENCY AND LOW NOCT.

PRECEDING PAGE BLANK NOT FILMED

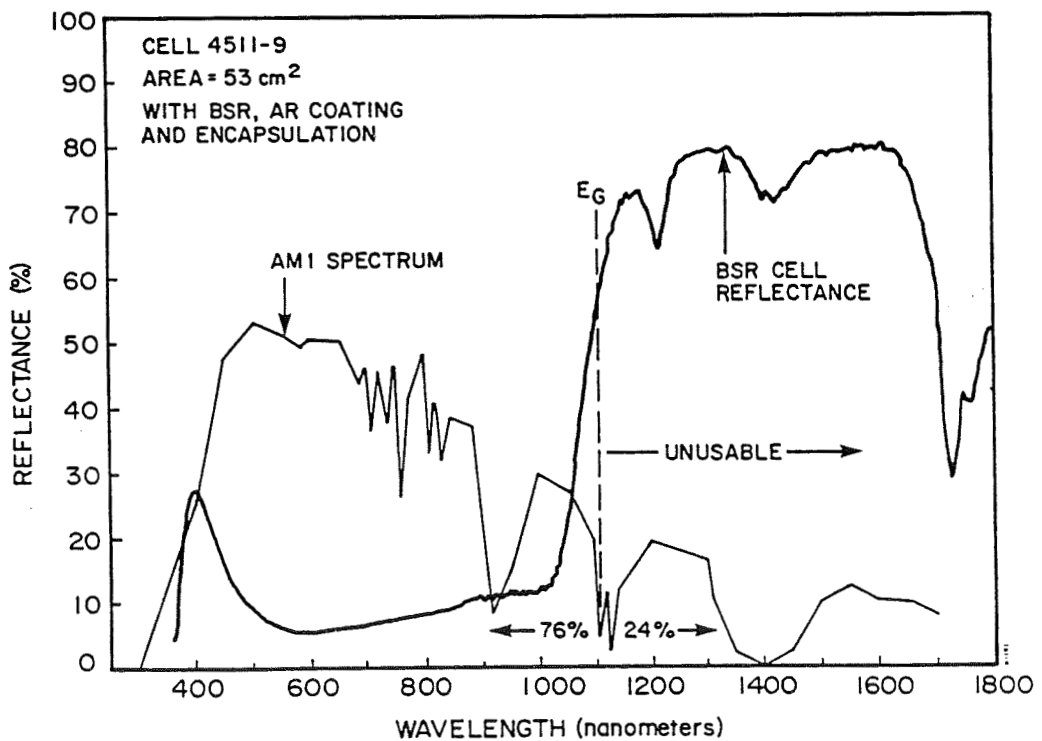
PRECEDING PAGE BLANK NOT FILMED

Cell Design

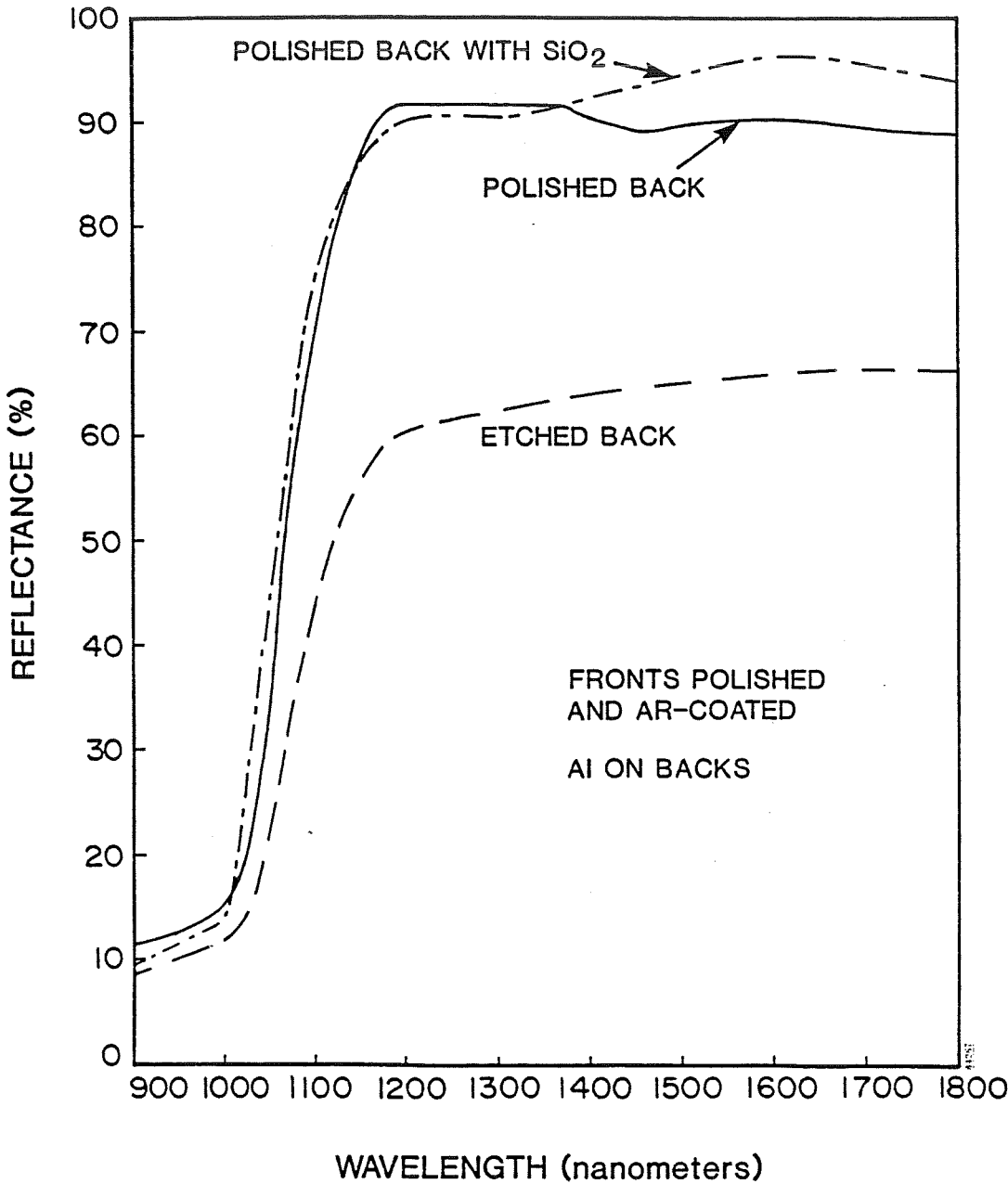


- AI USED FOR BSR
- SiO_2 USED TO PASSIVATE SURFACE
- NO EDGE PASSIVATION USED

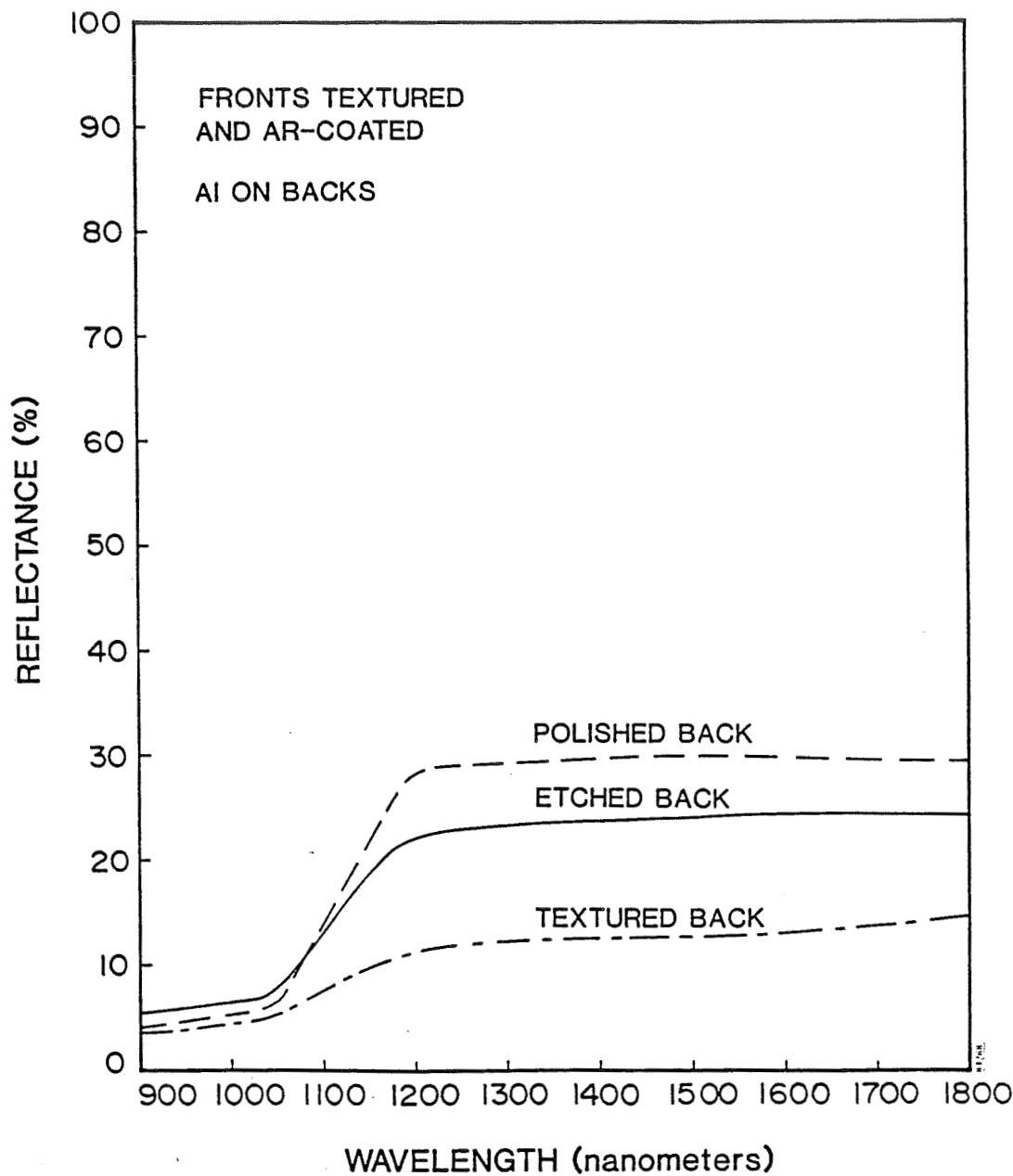
Reflectance Versus Wavelength (Cell 4511-9)



Reflectance Versus Wavelength
(Various Cell Backings With Fronts Polished and AR-Coated)



Reflectance Versus Wavelength
(Various Cell Backings With Fronts Textured and AR-Coated)



Mini-Module Fabrication and Performance Data

MINI-MODULE	CELL FRONT SURFACE	CELL BACK SURFACE	AVE.CELL EFFICIENCY ⁽¹⁾	ENCAP.CELL EFFICIENCY ⁽²⁾	MODULE EFFICIENCY ⁽²⁾	NOCT (°C)	MODULE EFF. AT NOCT ⁽³⁾
1	POLISHED	POLISHED	16.2 (0.2)	15.9	13.2	45	11.9
2	TEXTURED	ETCHED	17.9 (0.3)	16.8	14.0	50	12.2
3	TEXTURED	POLISHED	17.6 (0.2)	16.8	14.0	49	12.3
4	POLISHED	ETCHED	15.7 (0.2)	15.5	12.9	47	11.5

Notes: (1) Cell efficiency is the average of the 12 cells in the module. The standard deviation is shown in parenthesis. Spectrum was direct, AM1.5, 100mW/cm². T=25°C.

(2) Measured at JPL, global spectrum, AM1.5, 100mW/cm², T corrected to 25°C.

(3) Measured at JPL, global spectrum, AM1.5, 100mW/cm², T corrected to NOCT.

Characteristics of High-Efficiency Cell No. 10

Lot: 4751

Cell: 10

Area: 53.04 cm²

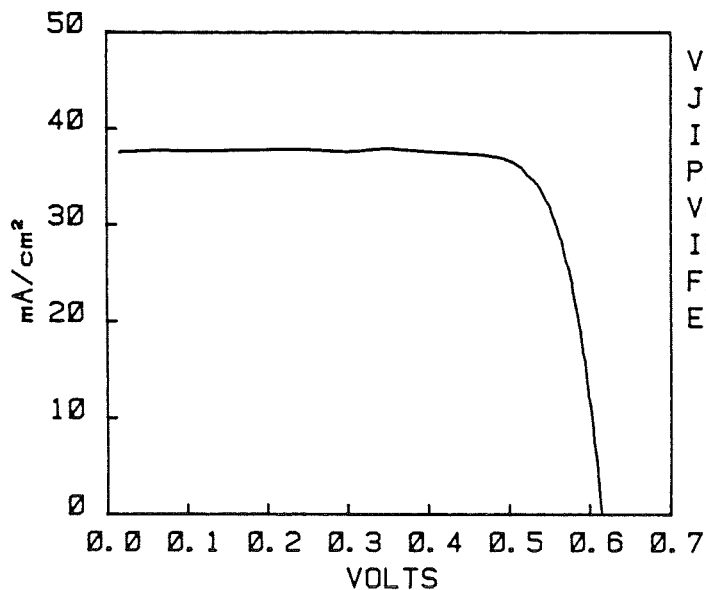
Material: Si

AM1.5, 28°C

Date: 12/19/85

Time: 13:45:07

AR Coating: TiO₂



$V_{oc} = 0.615 \text{ V}$
 $J_{sc} = 37.7 \text{ mA/cm}^2$
 $I_{sc} = 2.002 \text{ A}$
 $P_m = 0.9804 \text{ W}$
 $V_m = 0.509 \text{ V}$
 $I_m = 1.928 \text{ A}$
 $FF = 79.7 \%$
 $Eff = 18.5 \%$

MODULE AND RELIABILITY TECHNOLOGY

Performance Data for Ten Deliverable Cells

CELL	V _{oc} (mV)	J _{sc} (mA/cm ²)	FF (%)	EFF (%)
1	607	33.5	74.8	15.2
2	604	33.3	76.8	15.4
3	604	33.4	74.4	15.0
4	607	33.2	77.6	15.6
5	604	33.3	78.2	15.7
6	604	33.0	77.3	15.4
7	607	33.4	76.8	15.6
8	609	33.5	77.3	15.8
9	609	33.6	77.2	15.8
10	601	33.7	76.9	15.6

NOTES: INSOLATION WAS AM1.5, 100 mW/cm². T=28°C.
AREA=53 cm².

MODULE AND RELIABILITY TECHNOLOGY ORIGINAL PAGE IS
OF POOR QUALITY

Characteristics of High-Efficiency Module Cells

Lot: 4751

Originator: LMG

Date: 12/19/85

Comment: Module Cells

Resistivity: 1.50 Ω -cm

Material: Si

Spire Corporation
Illumination: AM1.5 (100 MW/cm²)

Temperature: 28 C

Thickness: 20 mils

Surface: Tex

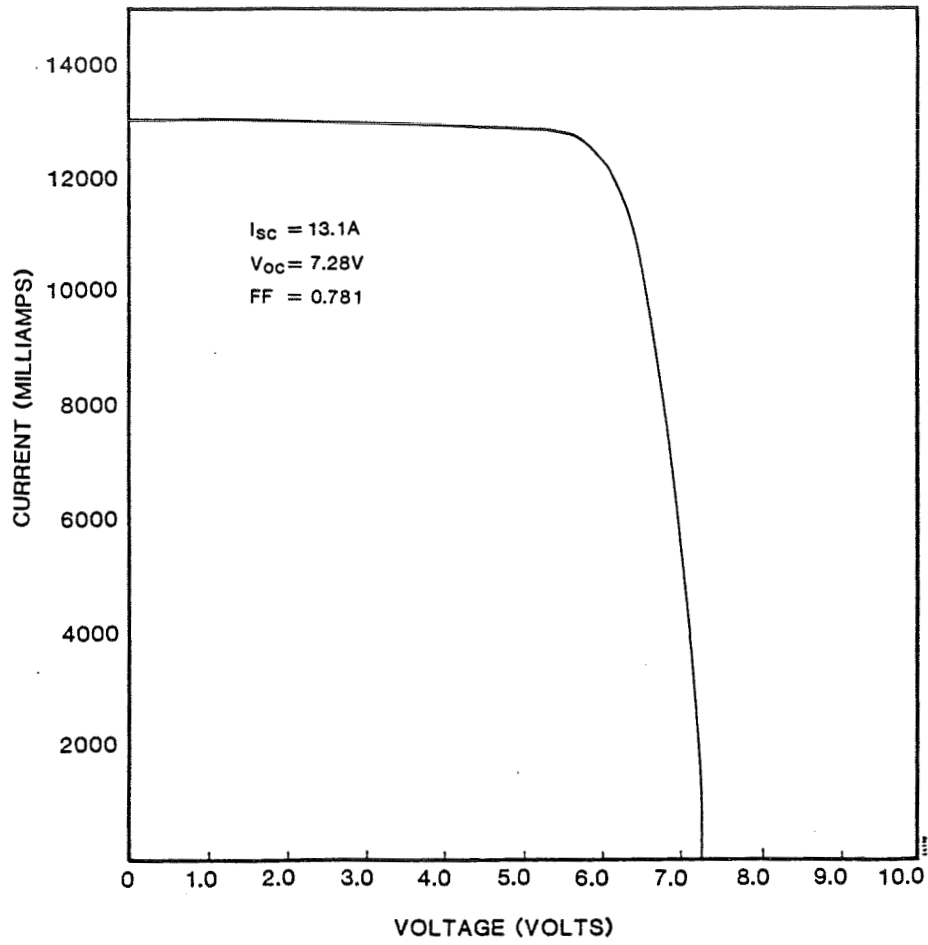
AR Coat: TiO₂

Cell	Area (cm ²)	Voc (V)	Isc (A)	Jsc mA/cm ²	Pm (W)	Vm (V)	Im (A)	FF (%)	Eff. (%)
1	53.04	0.616	2.007	37.8	0.9639	0.498	1.934	78.0	18.2
2	53.04	0.615	2.020	38.1	0.9685	0.510	1.898	78.0	18.3
3	53.04	0.614	2.001	37.7	0.9686	0.511	1.895	78.9	18.3
4	53.04	0.608	1.964	37.0	0.9417	0.518	1.816	78.8	17.8
5	53.04	0.613	1.989	37.5	0.9702	0.521	1.862	79.6	18.3
6	53.04	0.612	1.987	37.5	0.9553	0.504	1.895	78.6	18.0
7	53.04	0.613	1.988	37.5	0.9656	0.504	1.915	79.3	18.2
8	53.04	0.608	1.948	36.7	0.9477	0.510	1.857	80.0	17.9
9	53.04	0.612	1.979	37.3	0.9625	0.519	1.856	79.5	18.1
10	53.04	0.615	2.002	37.7	0.9804	0.509	1.928	79.7	18.5
11	53.04	0.614	1.999	37.7	0.9787	0.519	1.885	79.7	18.5
12	53.04	0.606	1.934	36.5	0.9036	0.494	1.831	77.0	17.0
13	53.04	0.613	1.992	37.5	0.9730	0.509	1.912	79.6	18.3
14	53.04	0.610	1.962	37.0	0.9411	0.508	1.851	78.6	17.7
15	53.04	0.612	1.963	37.0	0.9531	0.510	1.868	79.3	18.0
16	53.04	0.610	1.961	37.0	0.9575	0.521	1.836	80.0	18.1
17	53.04	0.610	1.962	37.0	0.9554	0.524	1.824	79.8	18.0
18	53.04	0.613	1.972	37.2	0.9710	0.509	1.906	80.3	18.3
19	53.04	0.611	1.974	37.2	0.9625	0.507	1.900	79.8	18.1
20	53.04	0.611	1.971	37.2	0.9475	0.507	1.870	78.7	17.9
21	53.04	0.614	1.988	37.5	0.9699	0.514	1.888	79.4	18.3
22	53.04	0.607	1.944	36.6	0.9356	0.518	1.806	79.3	17.6
23	53.04	0.612	1.981	37.3	0.9613	0.511	1.880	79.2	18.1
24	53.04	0.613	1.991	37.5	0.9593	0.506	1.895	78.6	18.1
25	53.04	0.614	1.997	37.7	0.9755	0.520	1.877	79.6	18.4
<hr/>									
mean		0.612	1.979	37.3	0.9588	0.511	1.875	79.2	18.1
std dev		0.002	0.021	0.4	0.0165	0.007	0.034	0.8	0.3

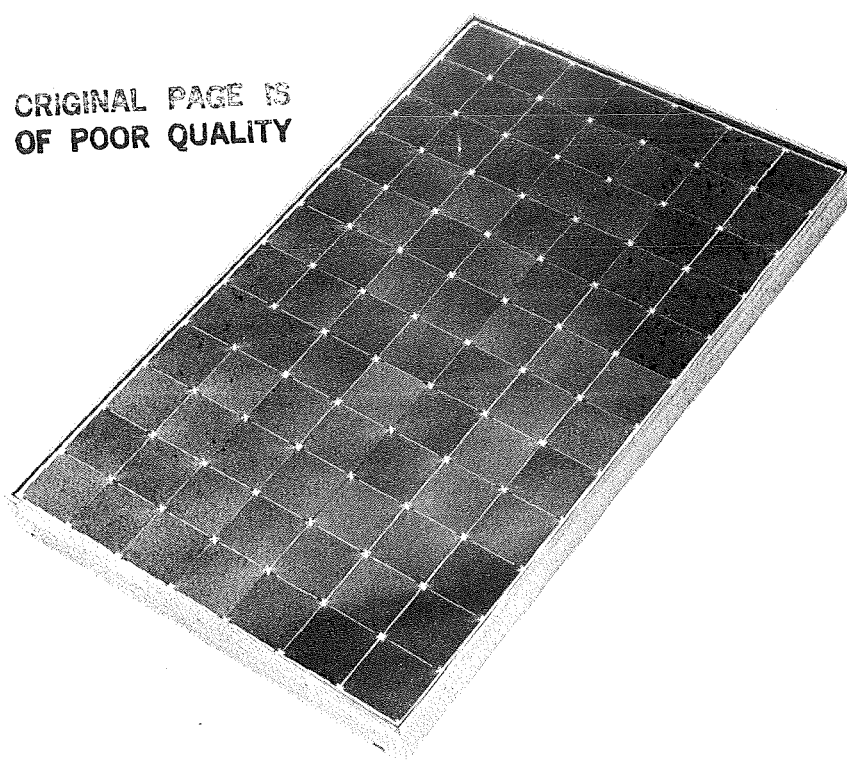
Delete: 12,

mean	0.612	1.981	37.3	0.9611	0.512	1.877	79.3	18.1
std dev	0.002	0.019	0.4	0.0121	0.007	0.034	0.6	0.2

I-V Curve for SPIRE High-Efficiency Solar Cell Module



SPIRE High-Efficiency Solar Cell Module



Mini-Module Performance

<u>MODULE</u>	<u>ENCAP. CELL EFFICIENCY (%)</u>	<u>V_{oc} (V)</u>	<u>I_{sc} (A)</u>	<u>MODULE EFF. (%)</u>
BEST FZ MINI-MODULE	17.6	7.33	1.92	14.7
BEST CZ MINI-MODULE	17.0	7.13	2.00	14.2

NOTES: INSOLATION WAS AM1.5, 100 mW/cm². T=25°C PACKING DENSITY IS 0.833. CELL AREA IS 53.04 cm². 12 CELLS PER MODULE.

Findings

- BSR's CAN REDUCE NOCT BY REFLECTION OF SUB-BANDGAP RADIATION.
- HIGH EFFICIENCY TECHNIQUES CAN BE UTILIZED IN LARGE-AREA CELLS.
- MODULES WITH EFFICIENCY GREATER THAN 15% CAN BE FABRICATED.
- THE ABOVE RESULTS CAN BE APPLIED TO CZ SILICON.

MEASURING RESEARCH PROGRESS IN PHOTOVOLTAICS

JET PROPULSION LABORATORY

B. Jackson and P. McGuire

Role of PA&I

SUPPORTING THE DECISION-MAKING PROCESS

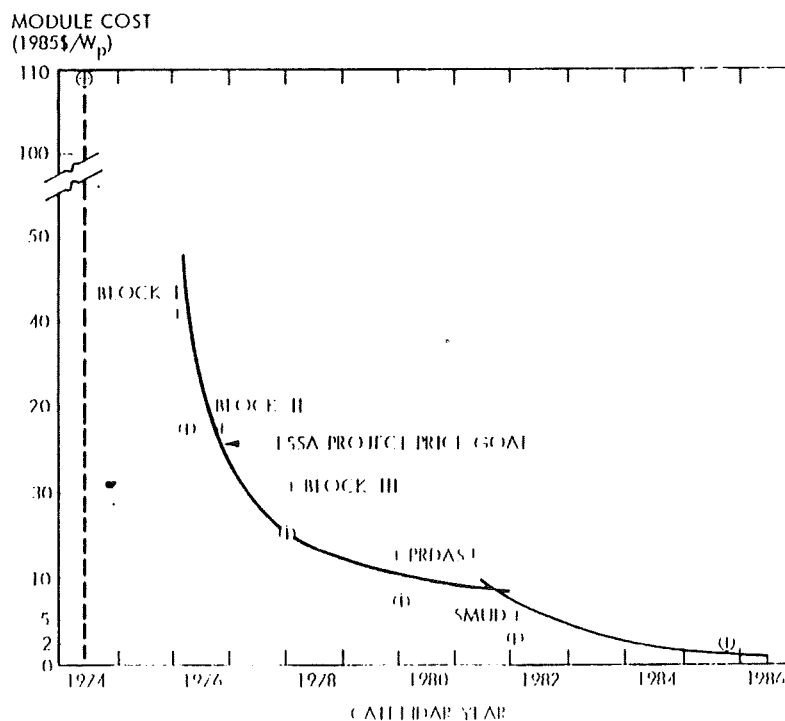
PREPARATION OF PLANS FOR PROJECT DIRECTION

SETTING GOALS FOR PROJECT ACTIVITIES

MEASURING PROGRESS WITHIN THE PROJECT

DEVELOPMENT AND MAINTENANCE OF ANALYTICAL MODELS

Module Cost Versus Time



Original Goals of FSA Project

MODULE PERFORMANCE:

50¢/Wp (1974 DOLLARS)

10% MODULE EFFICIENCY

20 YEAR LIFETIME

26¢/kWh (1985 DOLLARS)

Costs Involved in the Use of State-of-the-Art
Czochralski Silicon Technology

PROCESS	1985\$
SILICON MATERIAL	0.390
INGOT GROWTH	0.368
INGOT SAWING	0.304
CELL FABRICATION	0.208
MODULE ASSEMBLY	0.179
TOTAL COST (1985\$)	\$1.45/Wp
ENERGY COST (Using Baseline Parameters of the National PV Program)	\$0.275/kWh

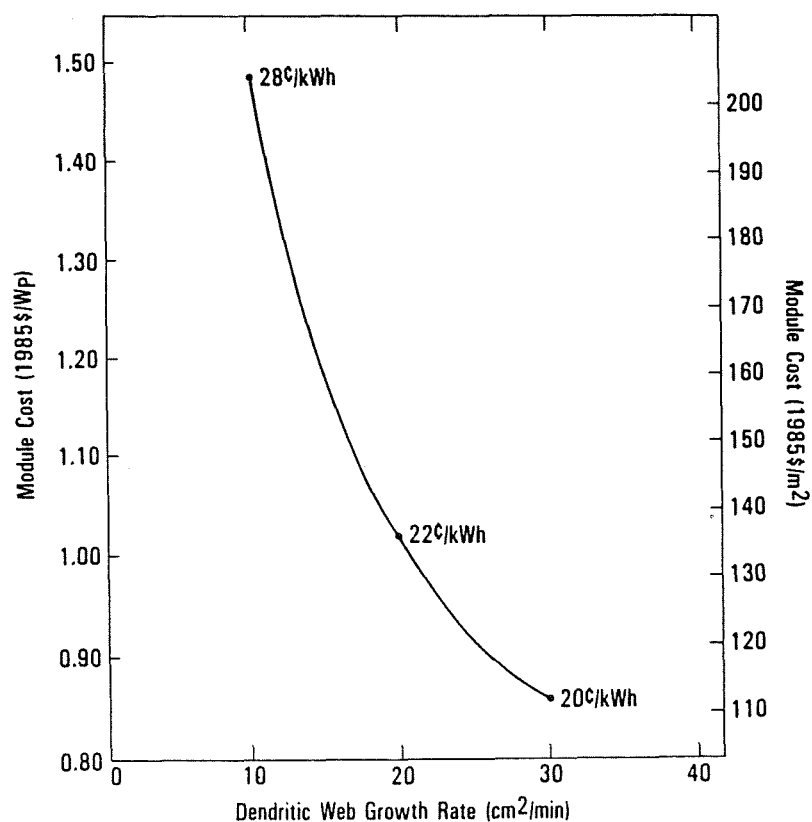
Assumptions Made in Arriving at Costs Involving Czochralski Silicon

FACTORY SIZE	25 MWp/yr
YEAR OF PRODUCTION	1988
SILICON COST, 1985\$/kg	\$43/kg
CRYSTALLIZATION RATE	1.5 kg/hr (Cz)
INGOT DIAMETER	5 in.
SAWING SLICE + KERF	19 mil
SAWING BLADE PLUNGE RATE	2.0 in./min
SAWING YIELD	95%
CELL SIZE	9.83 x 9.83 cm MODIFIED SQUARE
AREA PER CELL	94.6 cm ²
PACKING FACTOR	91.4%
MODULE SIZE	122 cm x 61 cm (4 ft x 2 ft)
MODULE POWER	101 Wp
ENCAPSULATED CELL EFFICIENCY	14.8%
MODULE EFFICIENCY, STC	13.5%

Costs Involved in the Use of Dendritic Web Technology (Projection)

PROCESS	1985\$
SILICON MATERIAL	0.153
WEB GROWTH	0.341
CELL FORMATION	0.119
METALLIZATION	0.162
MODULE ASSEMBLY	0.244
TOTAL COST (1985\$)	\$1.02/W_p
ENERGY COST (Using Baseline Parameters of the National PV Program)	\$0.220/kWh

Module Cost Versus Dendritic Web Growth Rate



National Research Program Goals

REVISED SINCE BEGINNING OF PROJECT

SLOWER INCREASES IN CONVENTIONAL ENERGY COST
HIGHER BALANCE OF SYSTEM COST

PRESENT PROGRAM GOALS

17.1¢/KWH (1985 DOLLARS) FOR LIFECYCLE ENERGY COST

SAMICS Methodology

ESTIMATES MODULE PRODUCTION COSTS

COSTS DEVELOPED FROM INDIVIDUAL PROCESS DESCRIPTIONS

BASED ON COMPANY DESIGNED SPECIFICALLY FOR MODULE PRODUCTION

METHODOLOGY ASSURES COMPARABILITY OF FINDINGS

Annual Cost for Each Process Step in the Production of Solar Cell Modules (in 1975 \$/W_p)

	VALUE ADDED	CAPITAL COSTS	DIRECT LABOR	MATERIALS & SUPPLIES	UTILITIES	INDIRECT EXPENSES	YIELD
SILICON PREP*	0.043			0.0434			
SHEET FAB	0.145	0.0630	0.0312	0.0140	0.0049	0.0320	0.800
P + BACK	0.002	0.0010	0.0004	0.0002	0.0000	0.0005	0.998
ETCH	0.010	0.0036	0.0018	0.0033	0.0000	0.0018	0.994
ION IMPLANT	0.012	0.0067	0.0018	0.0000	0.0003	0.0032	0.998
PULSE ANNEAL	0.006	0.0038	0.0004	0.0000	0.0003	0.0011	0.992
BACK METAL	0.036	0.0108	0.0013	0.0206	0.0005	0.0030	0.980
FRONT METAL	0.036	0.0111	0.0013	0.0202	0.0005	0.0030	0.980
AR COAT	0.009	0.0038	0.0018	0.0014	0.0002	0.0016	0.990
INTERCON	0.033	0.0104	0.0040	0.0135	0.0000	0.0054	0.995
ENCAPSULATE & ASSEMBLE	0.130	0.0368	0.0062	0.0750	0.0001	0.0120	0.999
TEST	0.001	0.0003	0.0002	0.0000	0.0000	0.0002	0.980
PACKAGE	0.001	0.0002	0.0001	0.0002	0.0000	0.0001	0.9999
TOTAL	0.464	0.1515	0.0505	0.1916	0.0068	0.0639	-

*BASED ON 10 \$/KG SILICON

SAMIS Personal Computer

SAMIS

COMPLETE COST STRUCTURE SIMULATION
PROVIDES DETAILED REPORTS

SAMPEG

QUICK PROCESS COST ESTIMATES
COSTS SUMMARIZED BY MAJOR CATEGORIES

IPEG

RAPID SENSITIVITY STUDIES
ANALYZE IMPACT OF CHANGES IN FINANCIAL PARAMETERS

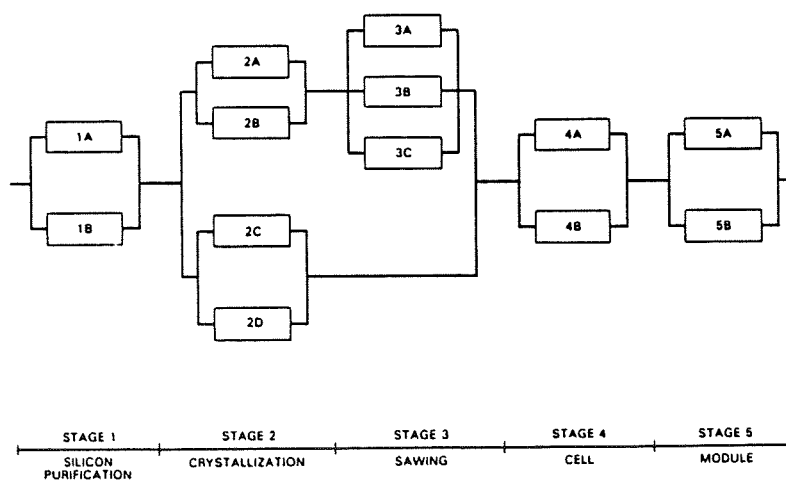
SIMRAND Methodology

EVALUATION OF COMPLEX R&D DECISIONS

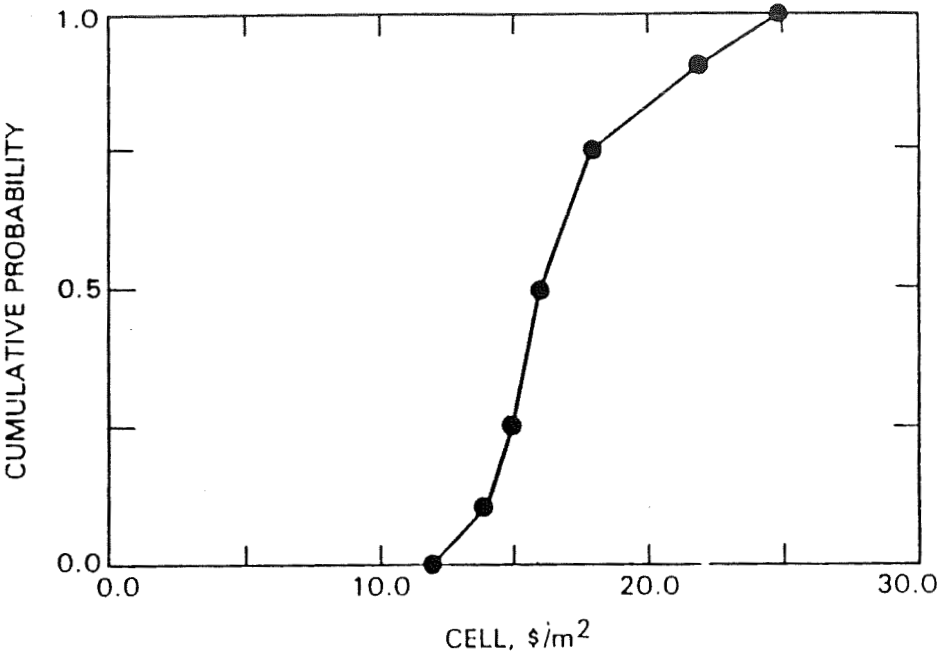
SIMULTANEOUS CONSIDERATION OF SEVERAL PATHS OF ACTION

ELEMENTS OF EACH PATH CAN BE DESCRIBED AS UNCERTAIN

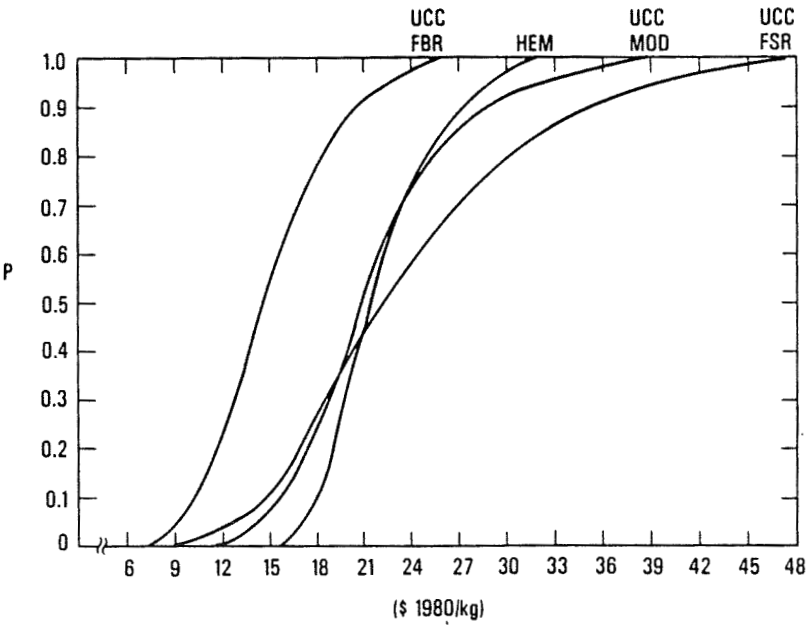
Task Network for Solar-Cell Module Production (SIMRAND)



Cumulative Probability Versus Solar Cell Cost



Comparison of Cumulative Probability Versus Cost for Various Ways to Produce Silicon



MODULE AND RELIABILITY TECHNOLOGY

LCP Methodology

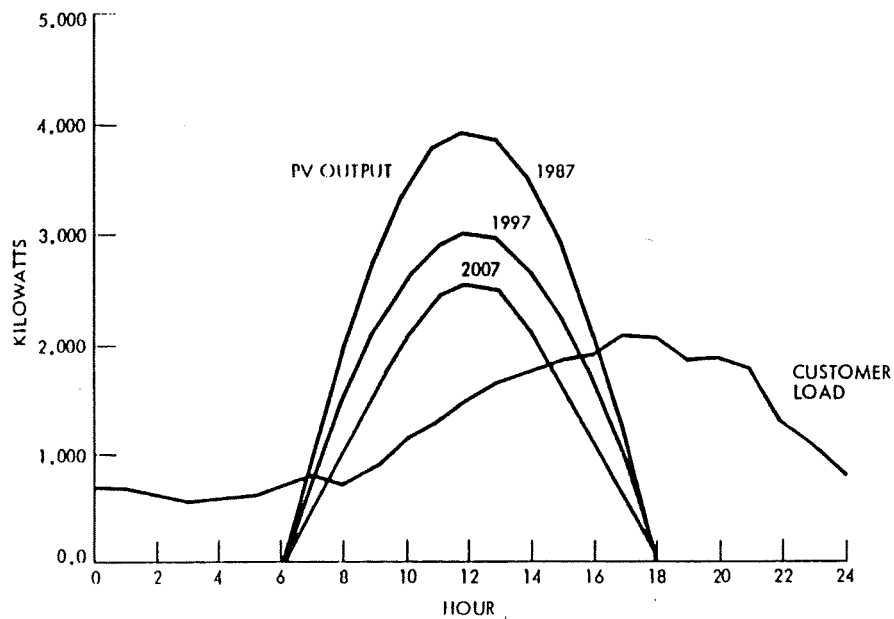
SIMULATES LIFETIME PERFORMANCE OF PV SYSTEM

ESTIMATES SYSTEM OUTPUT, REVENUES AND COSTS

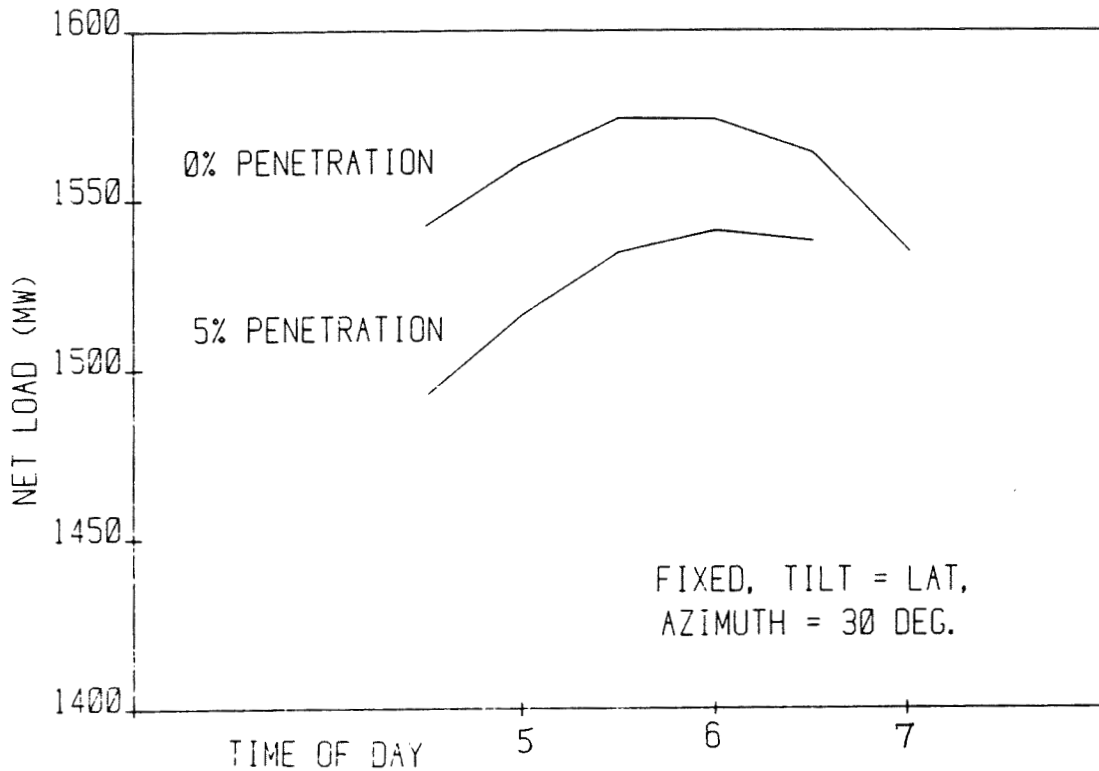
MODELS LOCATION SPECIFIC ENVIRONMENT

APPLICABLE TO UTILITY, RESIDENTIAL OR COMMERCIAL
INSTALLATIONS

LCP Simulation



SMUD Net Load Versus Time of Day
(0 and 5% Penetration on a July Peak Day)



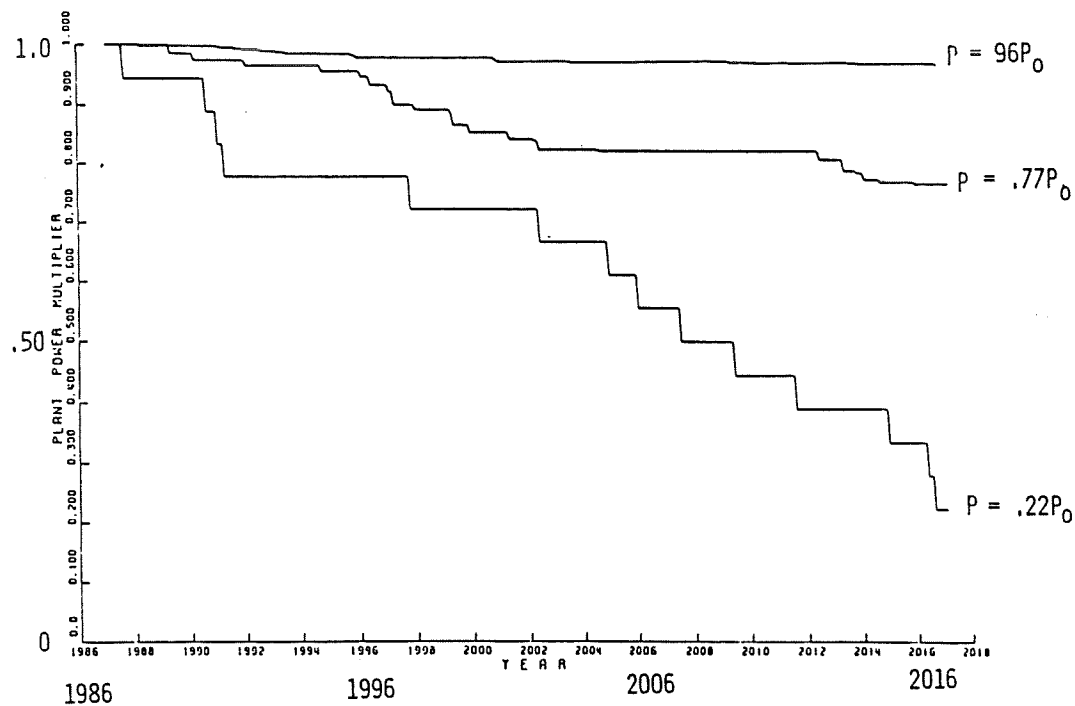
PVARRAY Methodology

USED TO OPTIMIZE ARRAY DESIGN

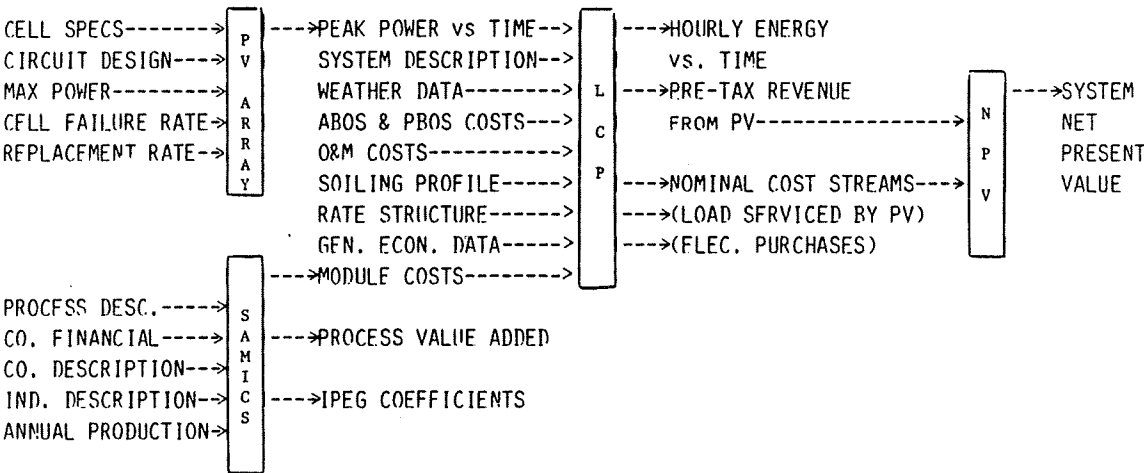
SELECT DIODE PLACEMENT

COMPARE ALTERNATE MODULE REPLACEMENT STRATEGIES

Fraction of Array Power Versus Time
(Cell Failure Rate = 1×10^{-4} /year)



Economic Evaluation Methodology for PV Array Design



SAMICS: SOLAR ARRAY MANUFACTURING INDUSTRY COSTING STANDARDS
LCP: LIFETIME COST AND PERFORMANCE MODEL

RELIABILITY PHYSICS

Edward Cuddihy, Chairman

This session consisted of eight presentations on reliability physics.

R. Liang, of JPL, reported that there have been observations of cracks forming in Tedlar back cover films on PV modules mounted outdoors in the natural environment. The cracks appear to approximate reasonable straight lines and, in general, are parallel to each other. It is implied that the directionality of these cracks may be in some way related to film orientation. Preliminary results from JPL studies investigating the causes of these cracks indicate that Tedlar does not become brittle on aging. It was speculated that perhaps compounding ingredients employed in EVA may migrate into the Tedlar film, thus causing a potential for chemical effects. This will be investigated.

On another topic, an experimental technique called "Flash Electron Spin Resonance (ESR)" was described which offers the promise of a quick method for identifying upper temperature limits for accelerated testing of module encapsulation materials.

The presentation by C. Gonzalez, of JPL, described a new, combined environmental aging chamber that was developed at JPL. The chamber has an ultraviolet (UV) light source that can be varied between 1 to 2 suns, temperature control from -40 to +175°C, and adjustable relative humidity. Results from two initial aging experiments (Tedlar and amorphous silicon solar cells) were presented.

J. Guillet reported that the University of Toronto is developing a computer program to simulate the photothermal degradation of materials exposed to terrestrial weathering environments. Input parameters would include the solar spectrum, the daily levels and variations of temperature and relative humidity, and materials such as EVA. A brief description of the program, its operating principles, and how it works was initially described. After that, the presentation focused on the recent work of simulating aging in a normal, terrestrial day-night cycle. This is significant, as almost all accelerated aging schemes maintain a constant light illumination without a dark cycle, and this may be a critical factor not included in acceleration aging schemes. For outdoor aging, the computer model is indicating that the night dark cycle has a dramatic influence on the chemistry of photothermal degradation, and hints that a dark cycle may be needed in accelerated aging schemes.

E. Plueddemann reported that Dow Corning is developing the primers employed in bonding together the various material interfaces in a PV module (such as EVA to glass, for example). The Dow Corning approach develops interfacial adhesion by generating actual chemical bonds between the various materials being bonded together. Dr. Plueddemann described the current status of this program, and the progress toward developing two general purpose primers for EVA, one for glass and metals, and another for plastic films.

J. Boerio reported that the University of Cincinnati is studying the aging behavior of chemically bonded interfaces between metals and pollutants, such as EVA, using the Dow Corning primer systems. As part of this study, it

RELIABILITY PHYSICS

has been observed that the primers seem to function as anticorrosion agents on metal surfaces. Dr. Boerio has been able to demonstrate that EVA, and the A-11861 EVA/glass primer will stop corrosion of the aluminum used on the back surfaces of crystalline silicon solar cells. However, this same treatment does not seem to work for the aluminum on the back surfaces of amorphous silicon solar cells. This is being investigated.

G. Mon reported that leakage currents are being experimentally measured by JPL in PV modules undergoing natural aging outdoors, and in PV modules undergoing accelerated aging in laboratory environmental chambers. The intent is to identify the significant contributors to module leakage currents, with a long-term goal to develop corrective technologies to reduce or stop module leakage currents. For outdoor aging in general, module leakage current is relatively insensitive to temperature fluctuations, but is very sensitive to moisture effects such as dew, precipitation, and fluctuations in relative humidity. Comparing EVA and polyvinyl butyral (PVB), module leakage currents are much higher in PVB as compared to EVA for all environmental conditions investigated. Leakage currents proceed in series along two paths, bulk conduction followed by interfacial (surfaces) conduction. It is being experimentally observed that leakage current is limited by bulk conduction in EVA modules, but that bulk conduction and interfacial conduction is about the same in PVB modules.

A theoretical modeling of leakage current in EVA and PVB modules is being developed and was described by A. Wen, of JPL. The modeling effort and the experimental effort, described by G. Mon, are two parts of a comprehensive study. The modeling effort derives mathematical relationships for the bulk and surface conductivities of EVA and PVB, the surface conductivities of glass and polymer films, and the interfacial conductivity between glass, polymer films, and the EVA and PVB pottants, all as functions of environmental parameters (temperature, RH, etc.). Some results from the modeling indicate that for glass/EVA, the glass surface controls the interfacial conductivity, although EVA bulk conductivity controls total leakage current. For PVB/glass, the interface conductivity controls leakage currents for RH less than 40 to 50%, but PVB bulk conductivity controls leakage current above 50% RH. This modeling work is continuing.

J. Orehtsky, of Wilkes College, reported that the interface between plastic film back covers and EVA or PVB in PV modules can influence water permeation, and electrical properties of the composite such as leakage current and dielectric constant. The interface can either be of two dissimilar materials in physical contact with no intermixing, or the interface can constitute a thin zone which is an interphase of the two materials having a gradient composition from one material to the other. The former condition is described as a "discrete interface," and Professor Orehtsky was able to develop a discrete interface model to predict water permeation, dielectric strength, and leakage currents for EVA, EMA, and PVB coupled to Tedlar and Mylar films. At this PIM, he compared experimental data with predicted data, and speculated that, in general, EVA and EMA form discrete interfaces, whereas PVB tends to form an interface with an interphase. This developing theory is intended to explain the deviations from expectations for some combinations of materials, on the basis that the properties of the gradient composition interphase controls the interface. His work continues to develop an interphase model for property prediction.

RELIABILITY PHYSICS

intended to explain the deviations from expectations for some combinations of materials, on the basis that the properties of the gradient composition interphase controls the interface. His work continues to develop an interphase model for property prediction.

MECHANISTIC STUDIES OF PHOTOTHERMAL AGING

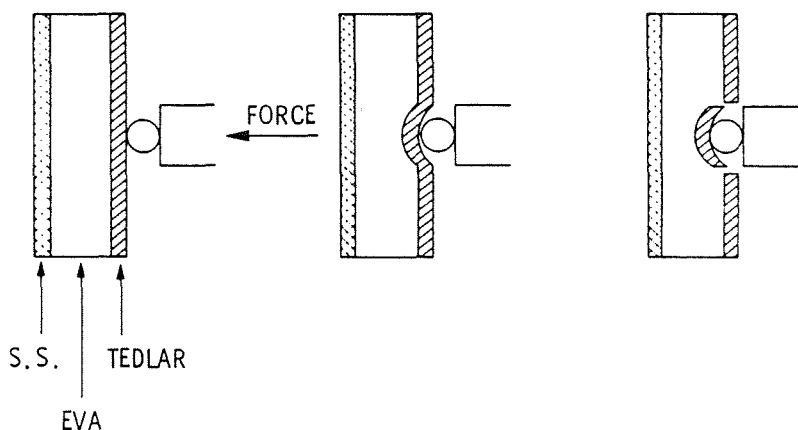
JET PROPULSION LABORATORY

R. H. Liang

Objective and Approaches

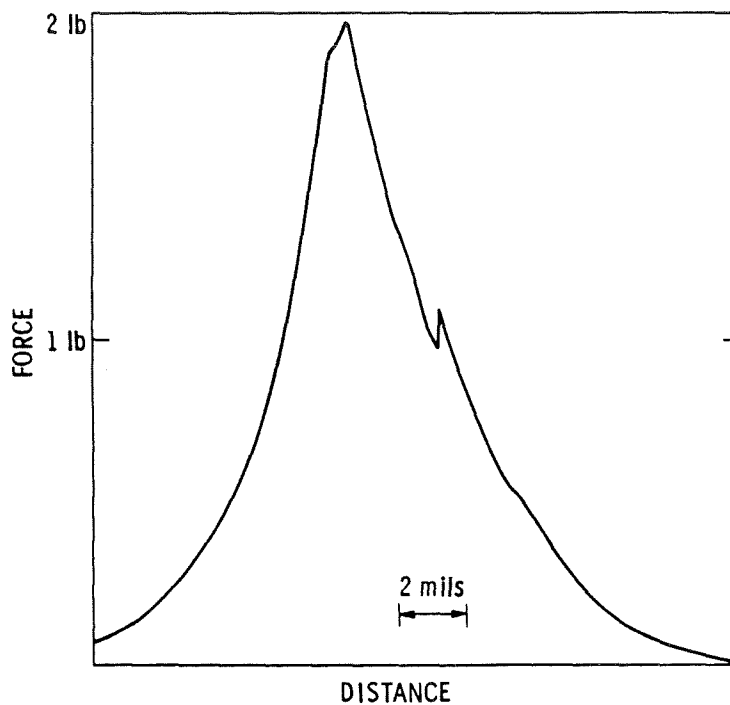
- OBJECTIVE
 - TO DEVELOP METHODOLOGY WHICH IS CAPABLE OF PREDICTING LONG-TERM BEHAVIOR OF POLYMERIC MATERIALS FOR OUTDOOR APPLICATIONS
- APPROACH
 - TO UNDERSTAND MECHANISMS OF DEGRADATION
 - TO DEVELOP VALID ACCELERATED TESTING FOR MATERIAL EVALUATION

Compression Testing of Tedlar/EVA/Stainless Steel Module



PRECEDING PAGE BLANK NOT FILMED

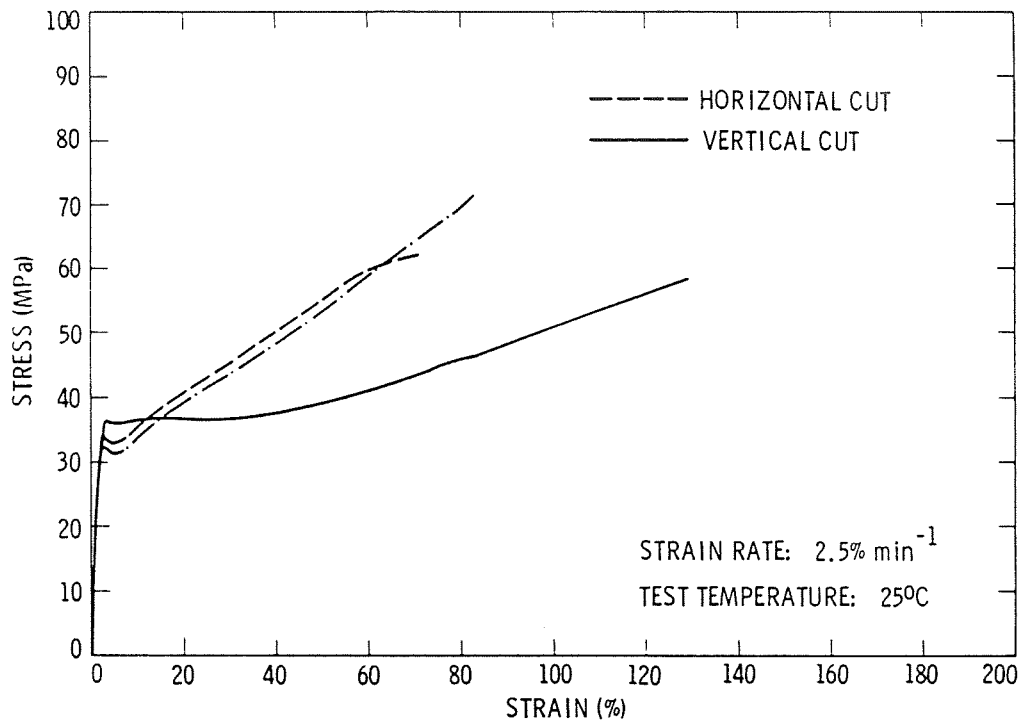
Compression Test of Outdoor Aged (500 Days) Tedlar/EVA/Stainless Steel Module



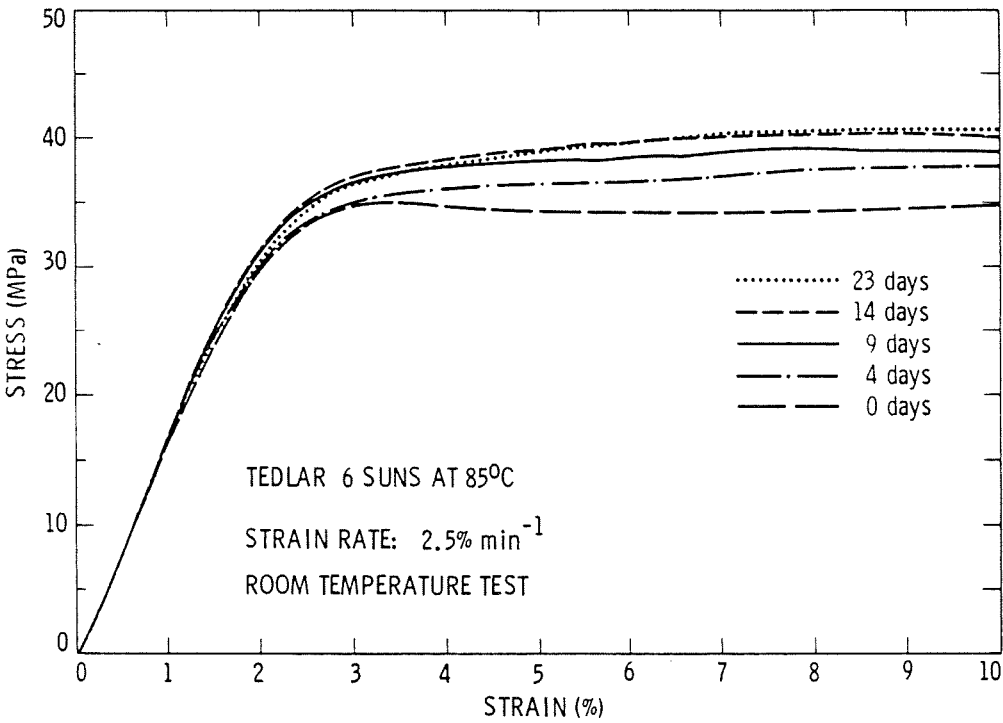
Compression Testing of Tedlar/EVA/Stainless Steel Module

SAMPLE	FORCE AT BREAK (lb)
CONTROL	31
OUTDOOR (500 days)	1.2
85°C, 8 SUNS (6.5 days)	1.0
98°C, 5.5 SUNS (6.5 days)	DID NOT BREAK

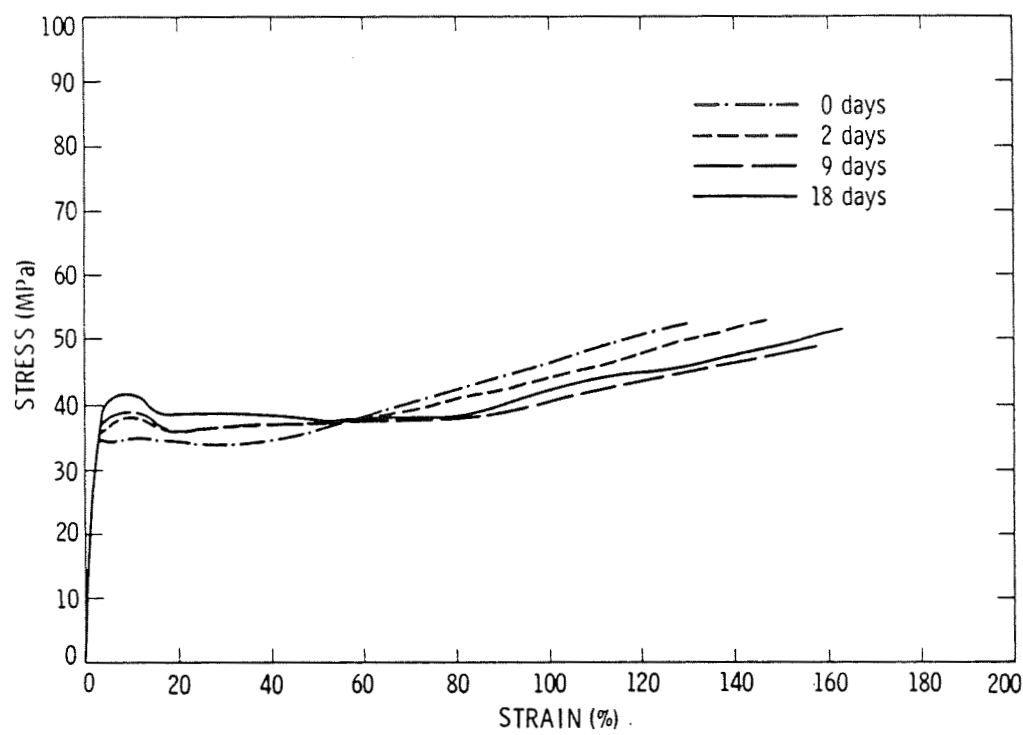
Tedlar Controls (As Received)



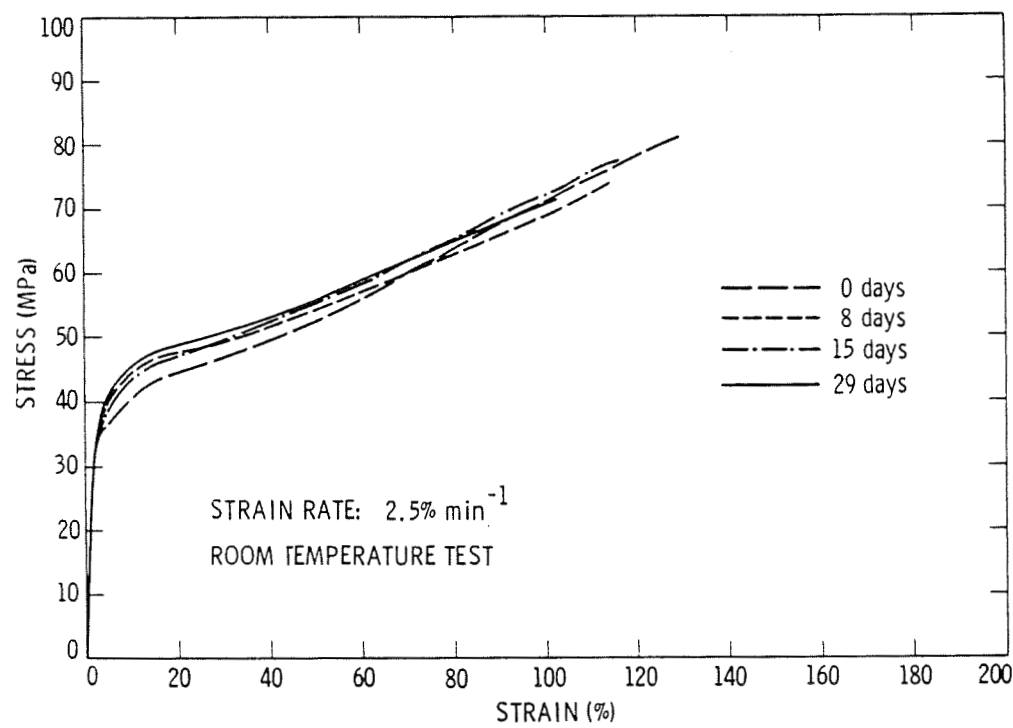
Stress-Strain as a Function of Exposure Time (Days)



Stress-Strain Curve of Tedlar Aged at 6 Suns and 85°C



Stress-Strain Curve of Laminated Tedlar Aged at 6 Suns and 85°C



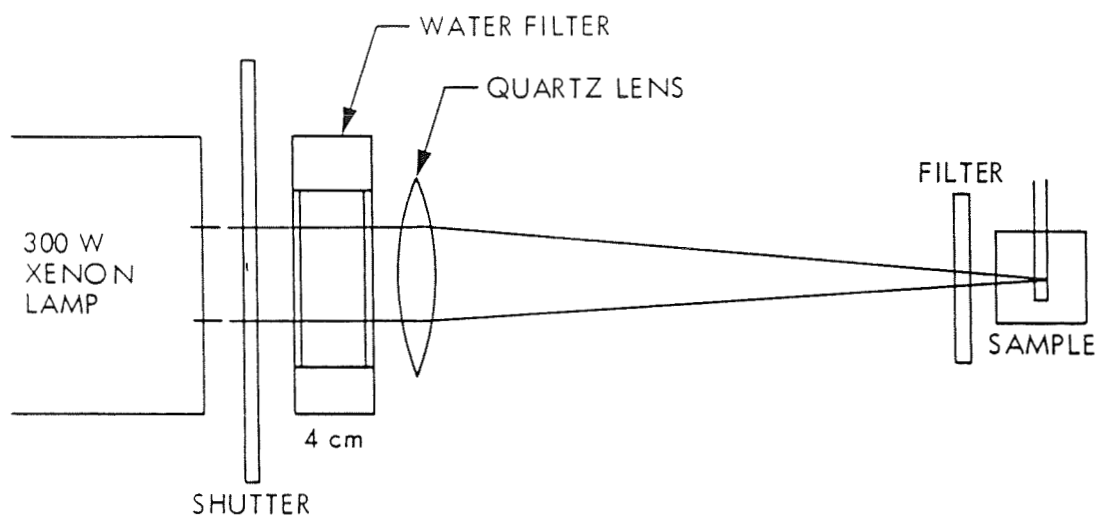
Conclusions for Tedlar Studies

- TEDLAR DAMAGE IS CHIEFLY UV DRIVEN
- QUAL TEST TEMPERATURE SHOULD BE $\leq 85^{\circ}\text{C}$
- DIAGNOSTIC TECHNIQUE HAS BEEN DEVELOPED
- SYNERGISTIC EFFECT OF TEDLAR AND EVA IS BEING EVALUATED

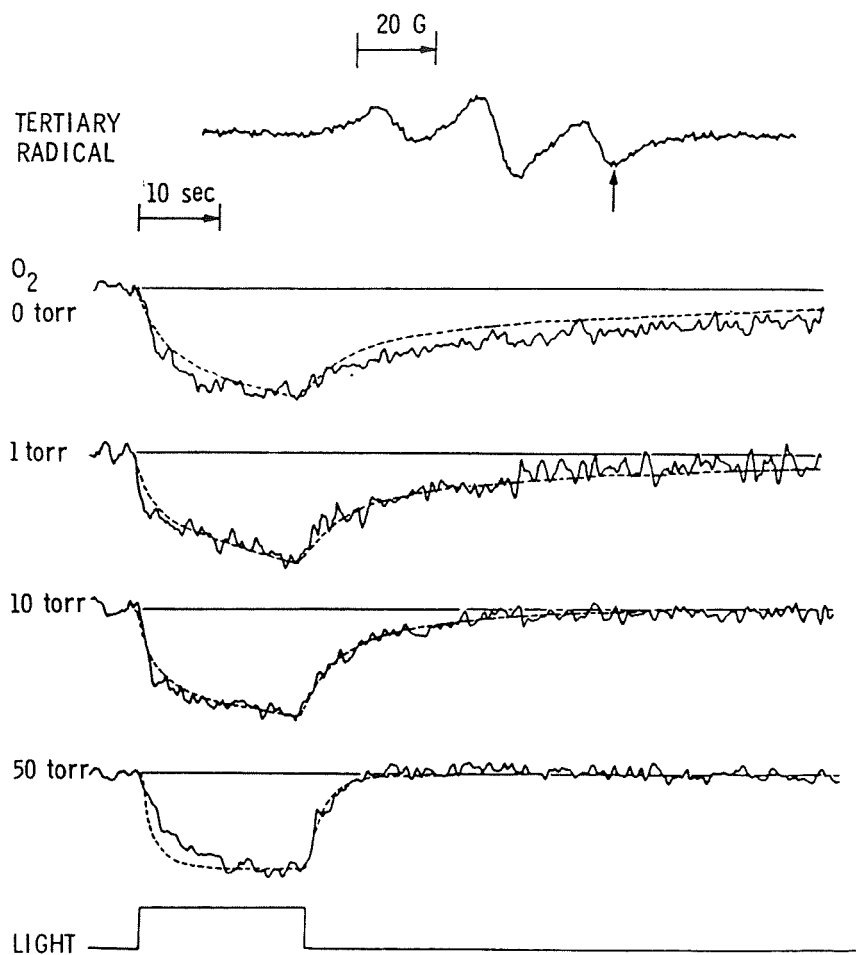
Mechanistic Studies of Photothermal Degradation

- OBJECTIVE
 - TO STUDY MECHANISTIC PATHWAYS OF PHOTOTHERMAL DEGRADATION
 - TO DETERMINE DEGRADATIVE REACTION RATES FOR MOLECULAR MODELING
- APPROACH
 - IDENTIFY FAILURE MODES
 - DETERMINE DEGRADATION MECHANISM
 - DEVELOP ACCELERATING CRITERIA
 - DEVELOP ACCELERATING METHODOLOGY
 - DEVELOP DIAGNOSTIC TECHNIQUES

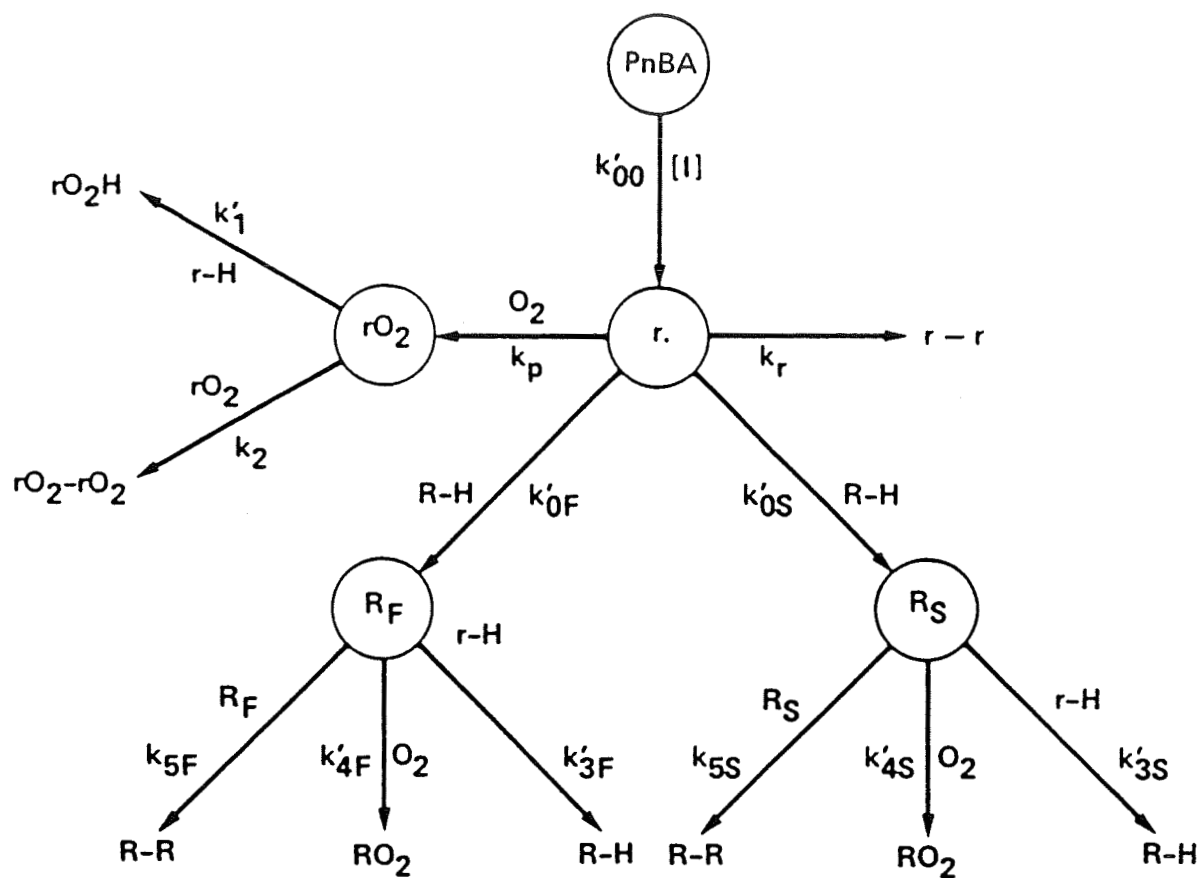
Flash Electron Spin Resonance Apparatus



Kinetic Studies of Photogenerated Tertiary Radical at Various Oxygen Pressures



Mechanism of Photooxidation of Poly-n-Butyl Acrylate



Kinetic Parameters of Poly-n-Butyl Acrylate Photooxidation

RADICAL	RATE CONSTANTS (25°C)
INTERMEDIATE	$k_p' = 700 \text{ l m}^{-1} \text{ s}^{-1}$ $k_r = 8 \times 10^5 \text{ l m}^{-1} \text{ s}^{-1}$
TERTIARY	$k_{OF} = 5 \times 10^{-1} \text{ s}^{-1}$ $k_{OS} = 1 \times 10^{-1} \text{ s}^{-1}$ $k_{3F}' = 1.3 \times 10^{-1} \text{ s}^{-1}$ $k_{3S}' = 8 \times 10^{-3} \text{ s}^{-1}$ $k_{4F}' = 700 \text{ l m}^{-1} \text{ s}^{-1}$ $k_{4S}' = 300 \text{ l m}^{-1} \text{ s}^{-1}$ $k_{5F} = 5 \times 10^4 \text{ l m}^{-1} \text{ s}^{-1}$ $k_{5S} = 3 \times 10^3 \text{ l m}^{-1} \text{ s}^{-1}$
PEROXY	$k_1' = 2 \times 10^{-2} \text{ s}^{-1}$ $k_2 = 5 \times 10^4 \text{ l m}^{-1} \text{ s}^{-1}$

UV-T-RH COMBINED ENVIRONMENTAL TESTING

JET PROPULSION LABORATORY

C. C. Gonzalez

Objectives

- To determine the combined effects of controlled amounts of UV radiation, heat and humidity upon the mechanical properties of module cover materials and the electrical properties of a-Si cells
- To develop the relationships required to relate experimental results obtained in accelerated and controlled-environment tests to field observations

Approach

- Use controlled environment for given period of time
 - Initial calibration of oven with lower-limit environments
 - 85 deg C, 10% RH, 1-2 suns UV
 - Use of increased levels for subsequent tests
- Monitor changes in selected key chemical and physical properties that are expected to control long-term performance
- Correlate controlled-environment test results with outdoor exposure

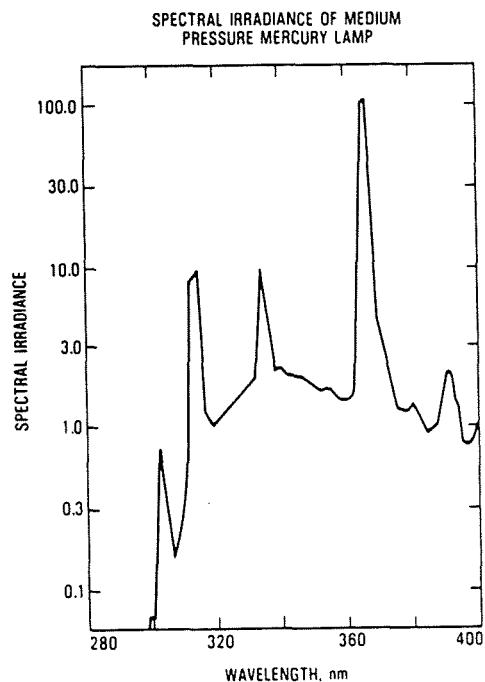
PRECEDING PAGE BLANK NOT FILMED

Description of Test Equipment

- Environmental chamber
 - Air-interchange, heat-and-refrigeration unit (-40 deg C to 175 deg C)
 - Varying humidity (10-100% (up to 90 deg C))
- UV lamp system
 - 2000 W UV (1-2 suns)
 - Water cooled
 - Dry-nitrogen purge

Ultraviolet Radiation Source

- Manufacturer: Canrad-Hanovia
- Type: Medium pressure mercury vapor lamp
- Lamp power consumption: 2100 W
- Lamp power output prior to filtering by cooling jacket: 1100 W



Environmental Parameter Measurements

- UV lamp
 - Integrated measurements
 - Actinometers
 - Radiometer
 - Spectral-radiometric measurements
 - Monochrometer
 - Lamp output vs time (qualitative)
- Oven temperature (continuous)
- Relative humidity (periodic)
- Selected sample temperatures

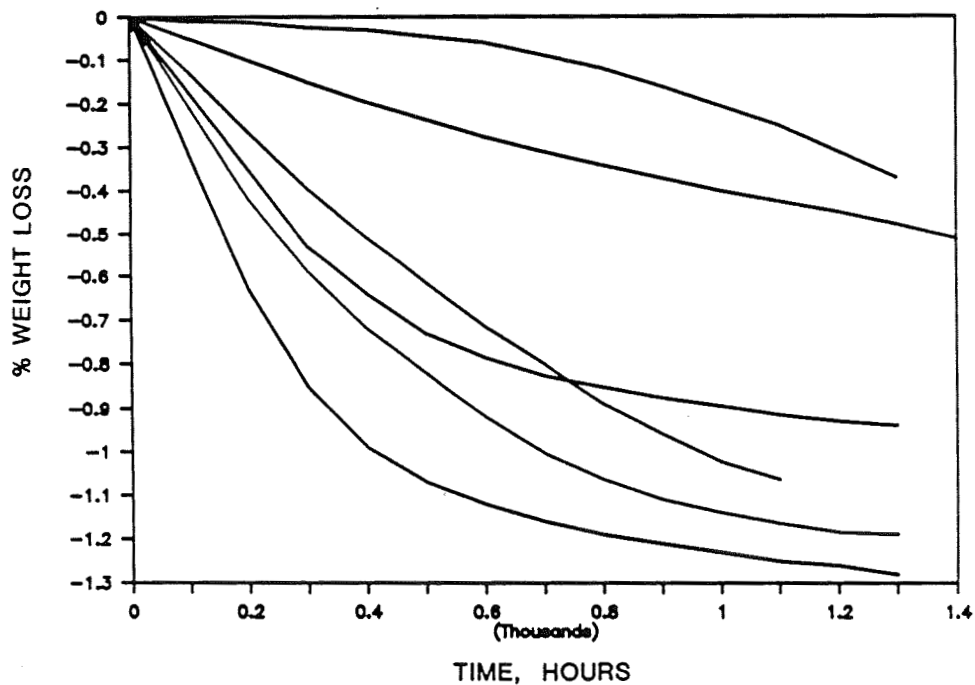
Sample Types

- Module encapsulant & cover materials
 - Material types
 - Tedlar
 - Varying amounts of additives
 - Clear and opaque
 - EVA
 - Size and configuration
 - 3/4" x 4" bare strips
 - 4" x 4" laminated tedlar-EVA-glass coupons
 - 4" x 4" submodules with tedlar front cover
- Amorphous-silicon 4" x 4" submodules

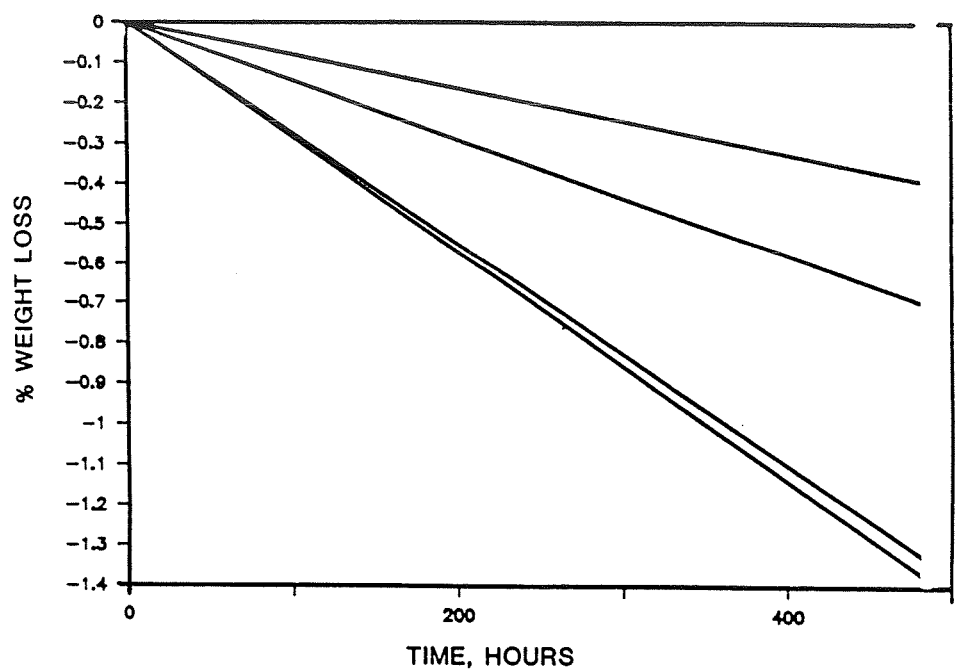
Material Parameters Measured
(Cover and Encapsulation Materials)

- Weight loss
 - Monitor loss of additives and volatiles
 - Correlate with shrinkage
- Changes in absorbance/transmission
 - Related to loss of absorbers and to chemical degradation (loss of transmission at 400nm related to yellowing)
- Tensile Modulus
 - May not establish rate and trend of photothermal degradation in early stages
- Visual inspection
 - Determine pliability of material by depressing laminated material

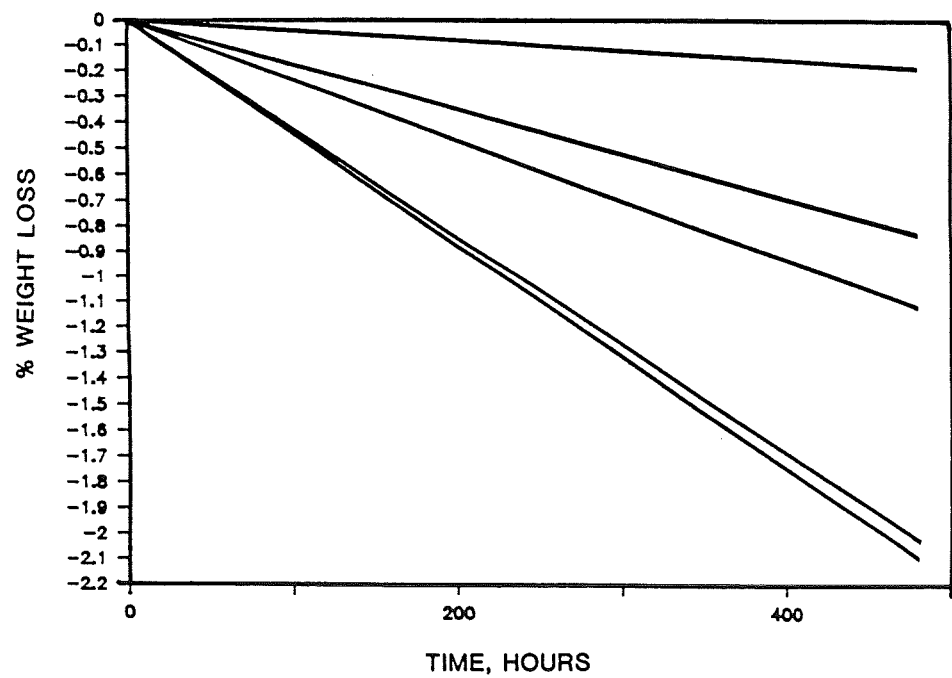
Tedlar: Percent Weight Loss Versus Time



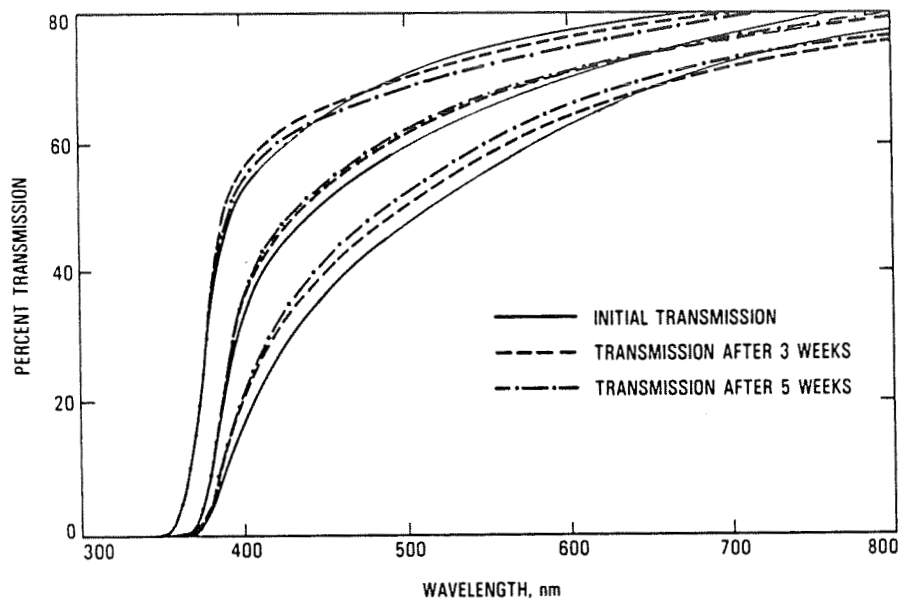
Tedlar (Dry Oven): Percent Weight Loss Versus Time



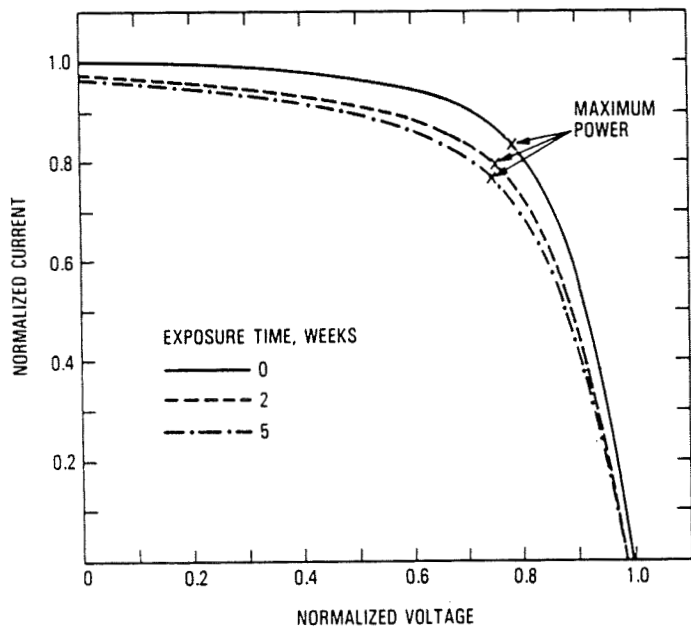
Tedlar (Vacuum Oven): Percent Weight Loss Versus Time



Module Front Cover Material: Percent Transmission Versus Exposure Time



Changes in I-V Curves of Amorphous Silicon Cells Versus Oven Exposure



Test Results Summary

- **Cover materials**
 - **Weight loss**
 - $\leq 1.35\%$ after 7-weeks exposure
 - **Changes in absorbance/transmission**
 - Results ranged from no change to about 15% gain after 5 weeks
 - **Mechanical properties**
 - Visual observations reveal no significant changes except for one case
- **Amorphous-silicon cells**
 - **IV-curve changes**
 - Average max-power loss of 10-15% after 3-5 weeks exposure

Future Work

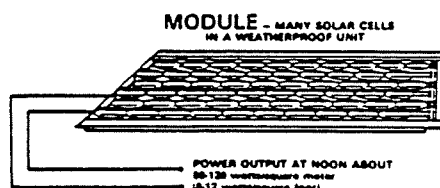
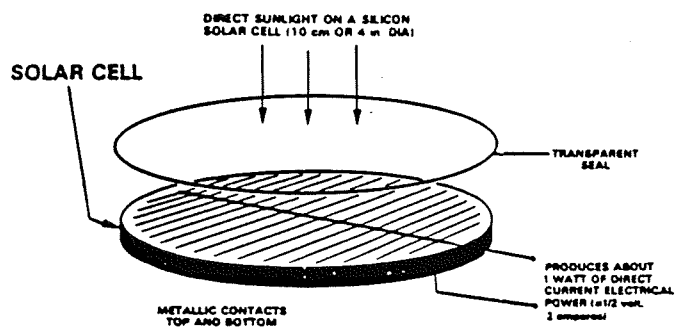
- **Refine existing test and sample measurement procedures**
(Develop new ones, if required)
- **Use high-humidity environment and increased temperature levels**
- **Vary UV levels by adding/removing screens and changing sample distance to lamp**
- **Perform parallel sample exposures in dry-heat and vacuum ovens**

COMPUTER MODELING OF PHOTODEGRADATION

UNIVERSITY OF TORONTO

J. Guillet

Construction and Operation of Solar Cells, Modules, and Arrays



ARRAY - MANY MODULES ELECTRICALLY AND PHYSICALLY CONNECTED TOGETHER

PRECEDING PAGE BLANK NOT FILMED

Chemical Weathering Factors

- SOLAR (UV) CYCLE
- TEMPERATURE CYCLES
- OXYGEN
- MOISTURE
- POLYMER COMPOSITION
 - STRUCTURE
 - FORMULATION
 - IMPURITIES
 - ADDITIVES

Chemical Weathering Effects

MOLECULAR WEIGHT CHANGES

Scission: Embrittlement
Permeability

Crosslinks: Shrinking
Wrinkles

PHOTOTHERMAL OXIDATION

Unsaturation: Discoloration
Transparency

Polar groups: Electrical properties
Wettability

RELIABILITY PHYSICS

Computer Simulation

INPUT

Mechanism (rates)

Conditions

Integration parameter

INTERFACE

Block of ordinary differential equations

SOLUTION

Numerical integration

STIFF · GEAR

OUTPUT

Concentration vs. time

10-20 years

Starting Conditions

SUBSTRATE *RH (cf. amorphous linear PE)*

INITIATORS *Ketone 10^{-3} M*
Hydroperoxide
Fortuitous

OXYGEN *Constant 10^{-3} M*

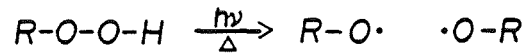
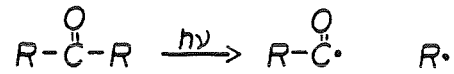
TEMPERATURE *Ambient*

RATES *Literature (cf. fluid)*

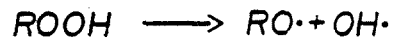
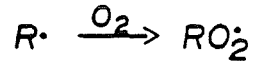
SOURCE *Daylight*

The Mechanism: A Model of 51 Elementary Reactions

INITIATION



PROPAGATION



TERMINATION

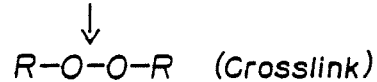
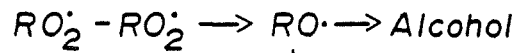


Table 1. Data Set: Photooxidation Reaction Scheme and Activation Parameters

	Reaction matrix	A	E kcal/mol
1.	Ketone \longrightarrow KET*	0.70×10^{-9}	0
2.	KET* \longrightarrow SMRO ₂ + SMRCO	0.59×10^9	4.8
3.	SMRCO \longrightarrow SMRO ₂ + CO	0.80×10^{17}	15
4.	KET* \longrightarrow Alkene + SMKetone	0.56×10^6	2.0
5.	SMKetone \longrightarrow SMKET*	0.70×10^{-9}	0
6.	SMKET* \longrightarrow SMRO ₂ + CH ₃ CO	0.32×10^{13}	6.5
7.	SMKET* \longrightarrow Alkene + Acetone	0.56×10^9	2.0
8.	ROOH \longrightarrow RO + OH	0.13×10^9	0
9.	RO ₂ + RH \longrightarrow ROOH + RO ₂	0.10×10^{10}	17.0
10.	SMRO ₂ + RH \longrightarrow SMROOH + RO ₂	0.10×10^{10}	17.0
11.	SMROOH \longrightarrow SMRO + OH	0.13×10^{-9}	0
12.	SMRO + RH \longrightarrow SMROH + RO ₂	0.16×10^{10}	6.2
13.	RO + RH \longrightarrow ROH + RO ₂	0.16×10^{10}	6.2
14.	RO \longrightarrow SMRO ₂ + Aldehyde	0.32×10^{16}	17.4
15.	KET* + ROOH \longrightarrow Ketone + RO + OH	0.25×10^{10}	11.6
16.	SMKET* + ROOH \longrightarrow SMKetone + RO + OH	0.25×10^{10}	11.6
17.	SMRCO + O ₂ \longrightarrow SMRCOOO	0.80×10^{14}	9.6
18.	SMRCO + RH \longrightarrow RO ₂ + Aldehyde	0.10×10^{10}	7.3
19.	SMRCOOO + RH \longrightarrow SMRCOOOH + RO ₂	0.10×10^{10}	17.0
20.	SMRCOOOH \longrightarrow SMRCOO + OH	0.13×10^{-9}	0
21.	SMRCOO \longrightarrow SMRO ₂ + CO ₂	0.10×10^{15}	6.6

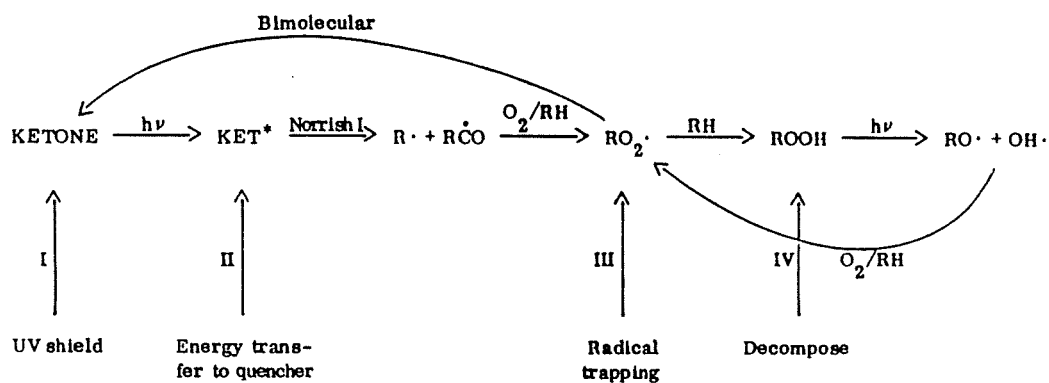
Table 1. (Cont'd)

22.	$\text{SMRCOO} + \text{RH} \longrightarrow$	Acid + RO_2	0.10×10^{10}	17.0
23.	$\text{OH} + \text{RH} \longrightarrow$	$\text{RO}_2 + \text{Water}$	0.10×10^{10}	0.5
24.	$\text{CH}_3\text{CO} + \text{RH} \longrightarrow$	$\text{RO}_2 + \text{CH}_3\text{CHO}$	0.10×10^{10}	7.3
25.	$\text{CH}_3\text{CO} + \text{O}_2 \longrightarrow$	CH_3COOO	0.89×10^{14}	9.6
26.	$\text{CH}_3\text{COOO} + \text{RH} \longrightarrow$	$\text{CH}_3\text{COOOH} + \text{RO}_2$	0.10×10^{10}	17.0
27.	$\text{CH}_3\text{COOOH} \longrightarrow$	$\text{CH}_3\text{COO} + \text{OH}$	0.13×10^{-9}	0
28.	$\text{CH}_3\text{COO} + \text{RH} \longrightarrow$	$\text{CH}_3\text{COOH} + \text{RO}_2$	0.10×10^{15}	6.6
29.	$\text{KET}^* \longrightarrow$	Ketone	0.10×10^9	0
30.	$\text{SMKET}^* \longrightarrow$	SMKetone	0.10×10^9	0
31.	$\text{KET}^* + \text{O}_2 \longrightarrow$	Ketone + SO_2	0.89×10^{14}	9.6
32.	$\text{SMKET}^* + \text{O}_2 \longrightarrow$	SMKetone + SO_2	0.89×10^{14}	9.6
33.	$\text{RO}_2 + \text{RO}_2 \longrightarrow$	$\text{ROH} + \text{Ketone} + \text{SO}_2$	0.25×10^{10}	11.6
34.	$\text{RO}_2 + \text{ROH} \longrightarrow$	$\text{ROOH} + \text{Ketone} + \text{HOO}$	0.10×10^{10}	15.3
35.	$\text{HOO} + \text{RH} \longrightarrow$	$\text{HOOH} + \text{RO}_2$	0.32×10^9	15.0
36.	$\text{HOO} + \text{RO}_2 \longrightarrow$	$\text{ROOH} + \text{SO}_2$	0.32×10^9	2.1
37.	$\text{RO}_2 + \text{Ketone} \longrightarrow$	$\text{ROOH} + \text{Peroxy CO}$	0.13×10^5	8.9
38.	$\text{Peroxy CO} + \text{RH} \longrightarrow$	$\text{PEROOH} + \text{RO}_2$	0.10×10^{10}	17.0
39.	$\text{PEROOH} \longrightarrow$	$\text{PERO} + \text{OH}$	0.13×10^{-9}	0
40.	$\text{PERO} + \text{RO}_2 \longrightarrow$	$\text{DKetone} + \text{ROOH}$	0.25×10^{10}	11.6
41.	$\text{RO}_2 + \text{ROOH} \longrightarrow$	$\text{ROOH} + \text{Ketone} + \text{OH}$	0.25×10^8	11.6
42.	$\text{RO}_2 + \text{SMROH} \longrightarrow$	$\text{ROOH} + \text{Aldehyde} + \text{HOO}$	0.10×10^{10}	15.3
43.	$\text{RO}_2 + \text{Aldehyde} \longrightarrow$	$\text{ROOH} + \text{SMRCO}$	0.25×10^{10}	11.6
44.	$\text{RO}_2 + \text{RO}_2 \longrightarrow$	$\text{ROOR} + \text{SO}_2$	0.38×10^{12}	16.0

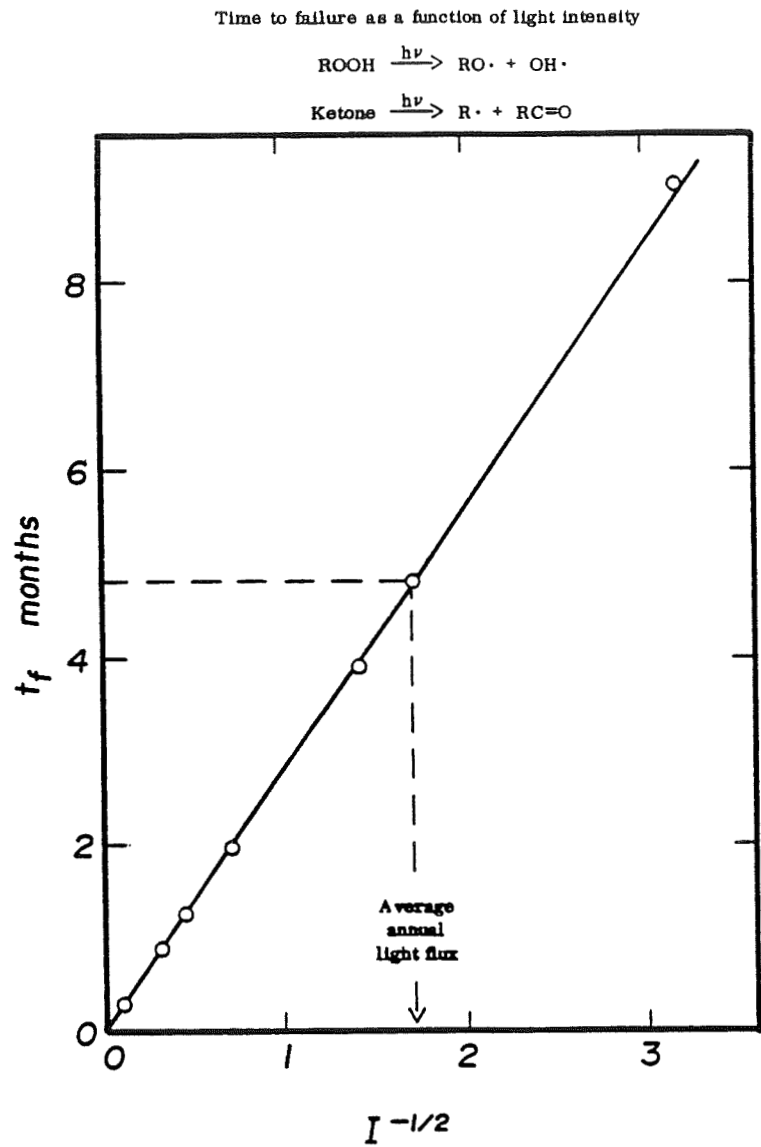
Table 1. (Cont'd)

45.	$\text{SO}_2 \longrightarrow \text{O}_2$	0.63×10^5	0
46.	$\text{SO}_2 + \text{Alkene} \longrightarrow \text{ROOH}$	0.20×10^{14}	10.0
47.	$\text{RO}_2 + \text{Alkene} \longrightarrow \text{Branch}$	0.16×10^9	11.6
48.	$\text{SMRO}_2 + \text{Alkene} \longrightarrow \text{ROOH}$	0.16×10^9	11.6
49.	$\text{RO}_2 + \text{QH} \longrightarrow \text{ROOH} + \text{Q}$	0.16×10^8	5.2
50.	$\text{KET}^* + \text{Q1} \longrightarrow \text{Ketone} + \text{Heat}$	0.80×10^{13}	9.5
51.	$\text{ROOH} + \text{QD} \longrightarrow \text{PRODS}$	0.80×10^{13}	9.5
52.	$\text{ROOH} \longrightarrow \text{RO}\cdot + \text{OH}\cdot$	0.63×10^{15}	35
53.	$\text{SMROOH} \longrightarrow \text{SMRO} + \text{OH}$	0.63×10^{15}	35
54.	$\text{SMRCOOH} \longrightarrow \text{SMRCOO} + \text{OH}$	0.63×10^{15}	35
55.	$\text{CH}_3\text{COOOH} \longrightarrow \text{CH}_3\text{COO} + \text{OH}$	0.63×10^{15}	35
56.	$\text{PEROOH} \longrightarrow \text{PERO} + \text{OH}$	0.53×10^{15}	35

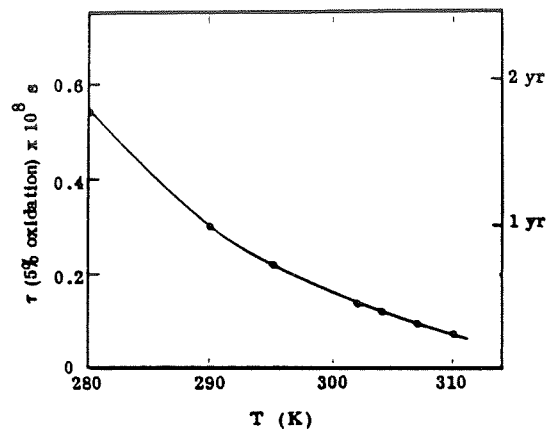
Stabilization Mechanisms



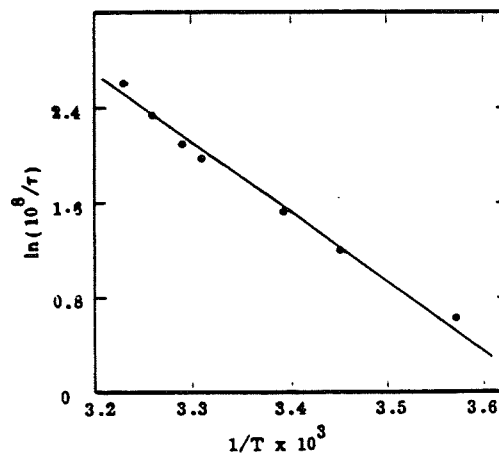
Photooxidation of Unstabilized Polyethylene



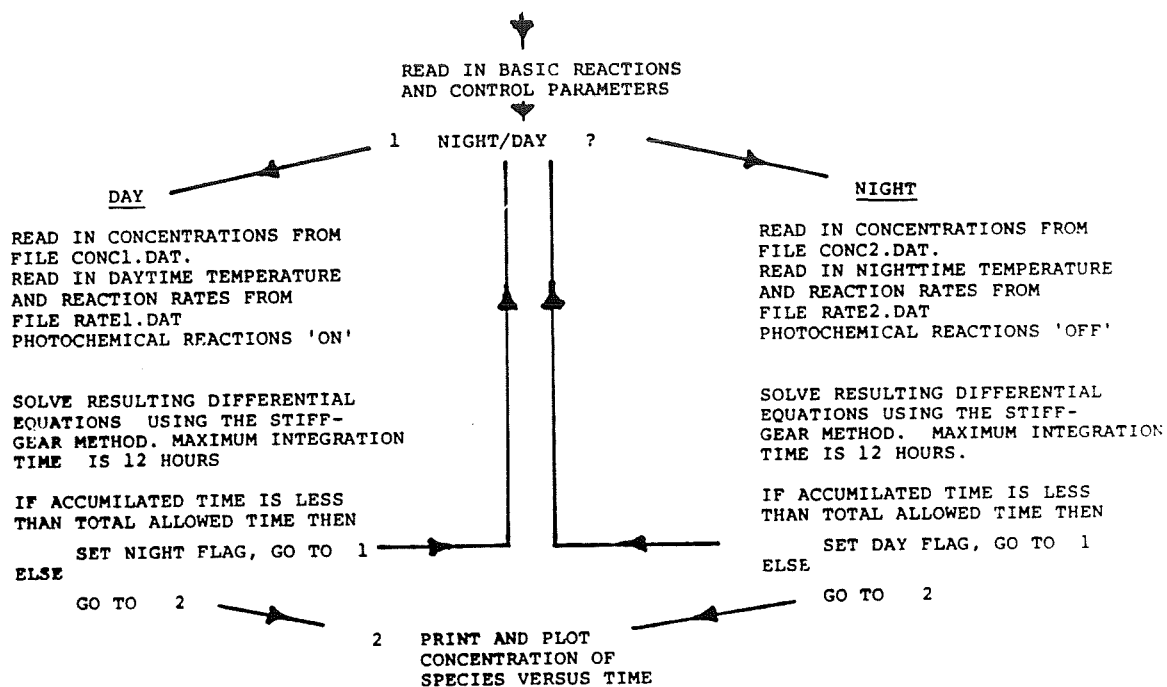
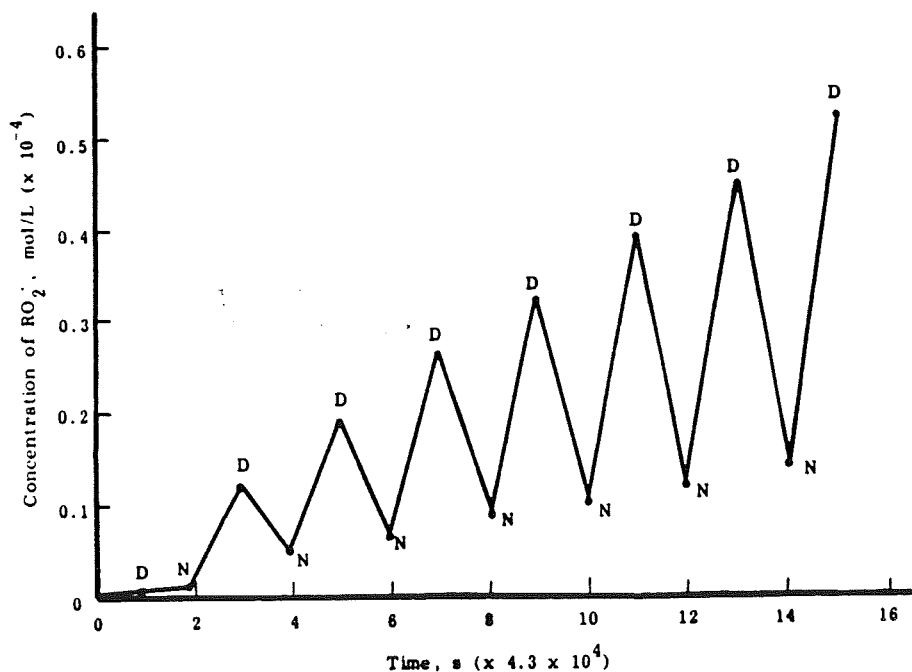
Time to Failure as a Function of Temperature



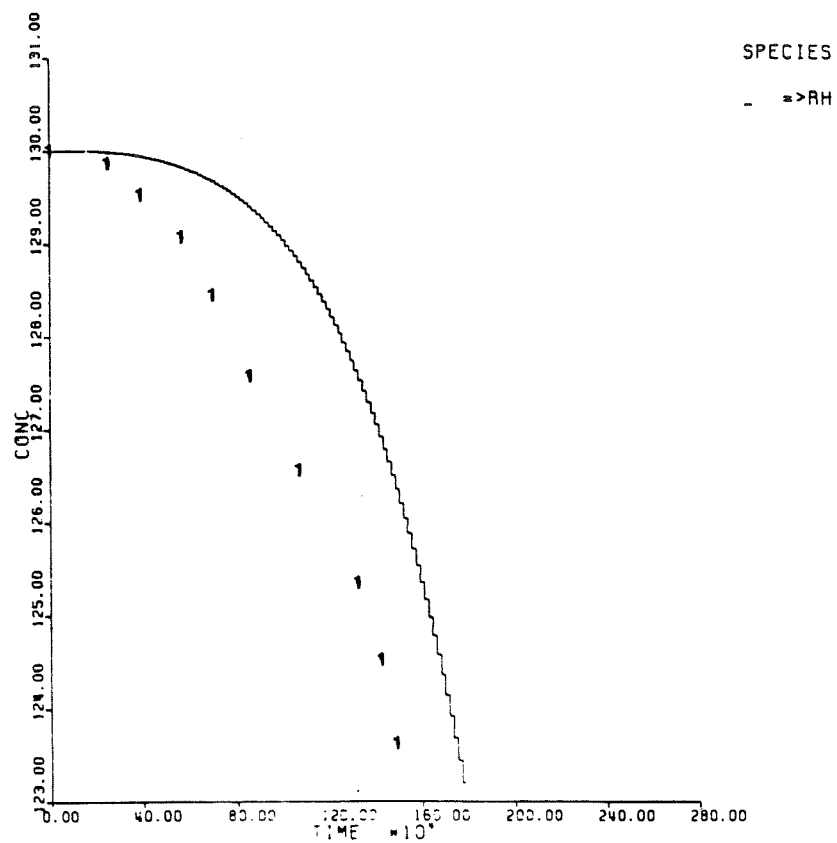
Arrhenius Plot of Rate of Oxidation (k Versus $1/T$)



Flow Diagram for Computer Modelling

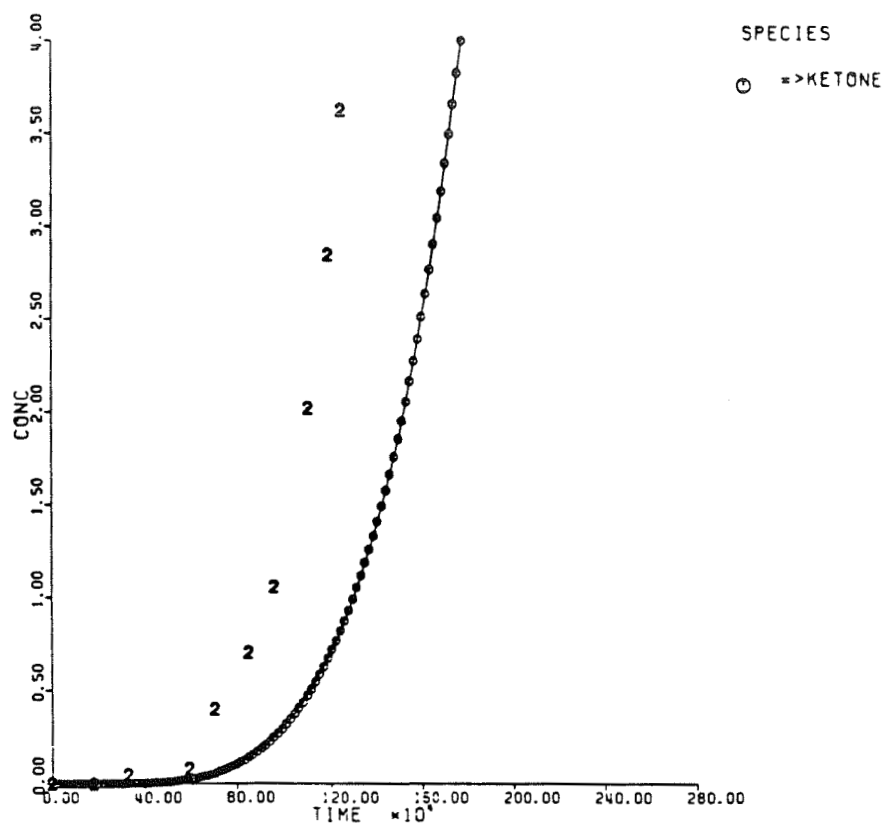
Concentration of RO_2^\bullet Versus Time

Concentration of RH Species Versus Time

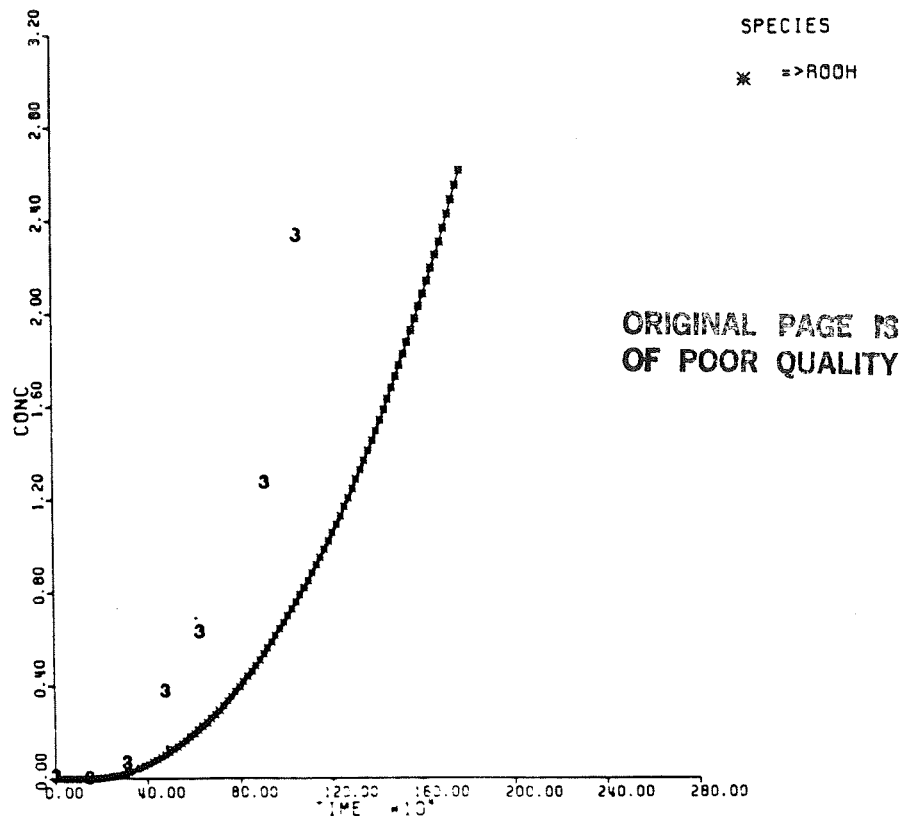


ORIGINAL PAGE IS
OF POOR QUALITY

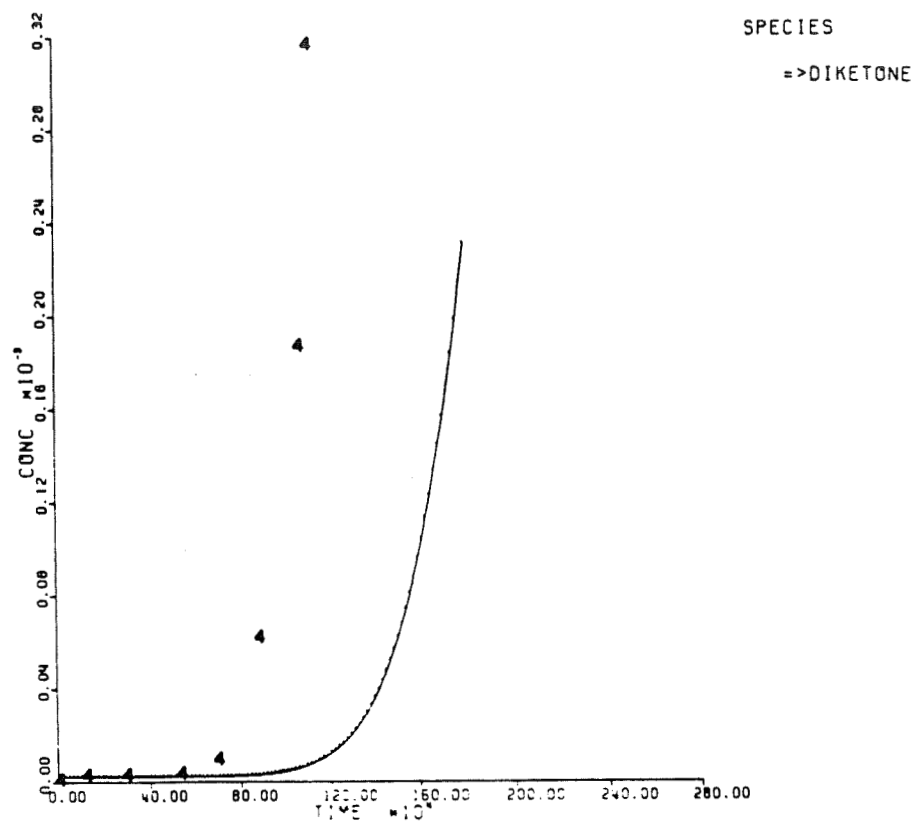
Concentration of Ketone Species Versus Time



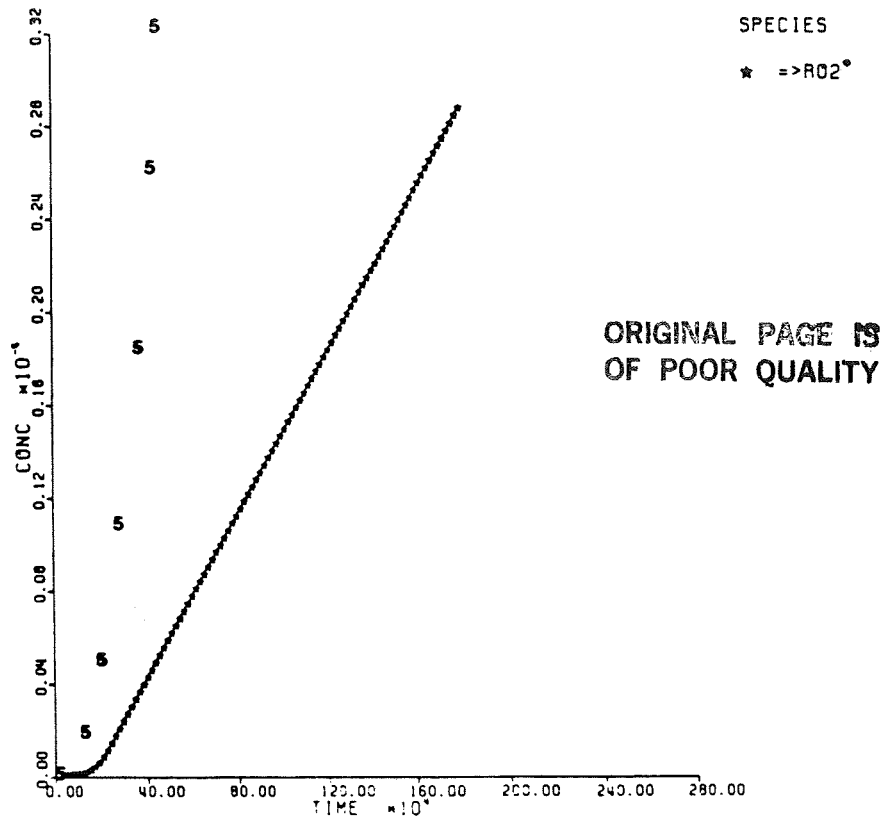
Concentration of ROOH Species Versus Time



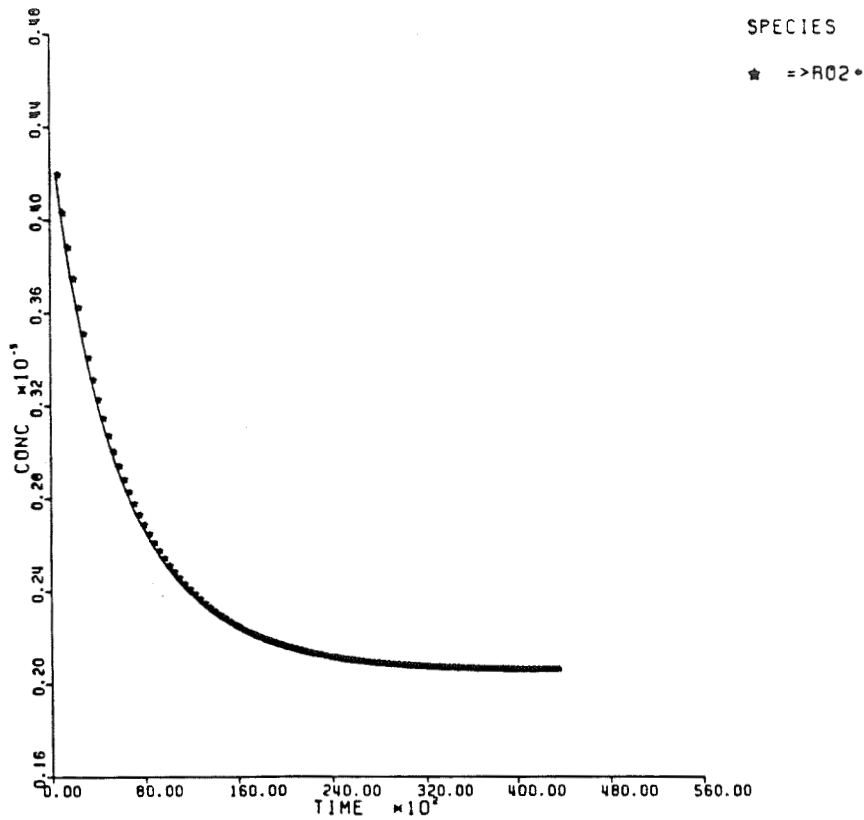
Concentration of Diketone Species Versus Time



Concentration of ROO• Species Versus Time



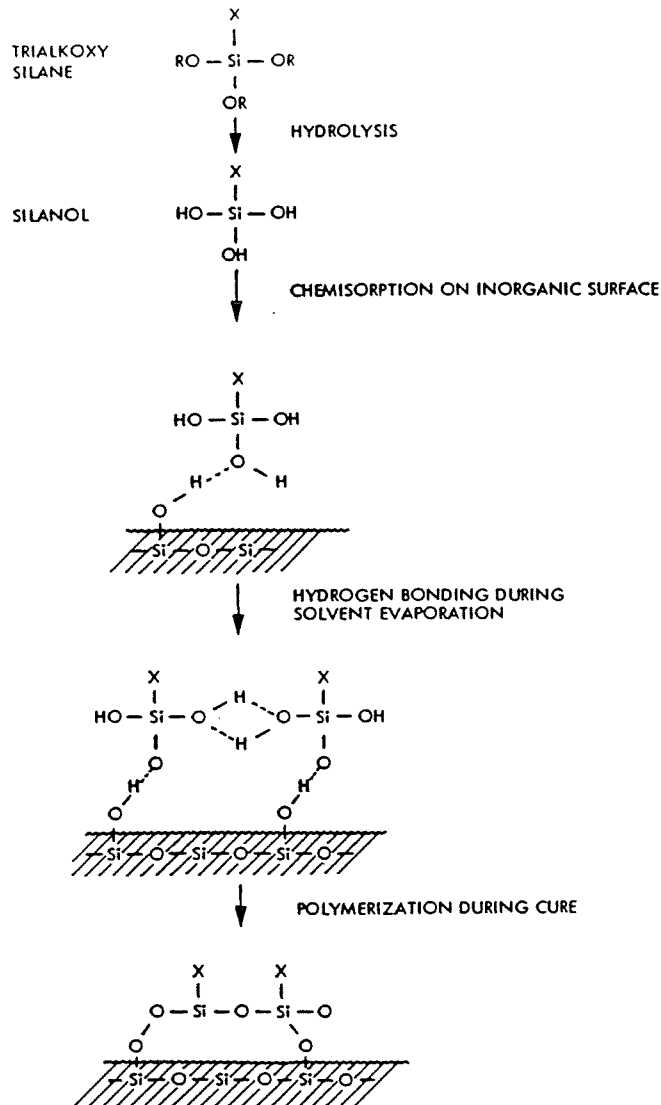
Concentration of ROO• Species Versus Time



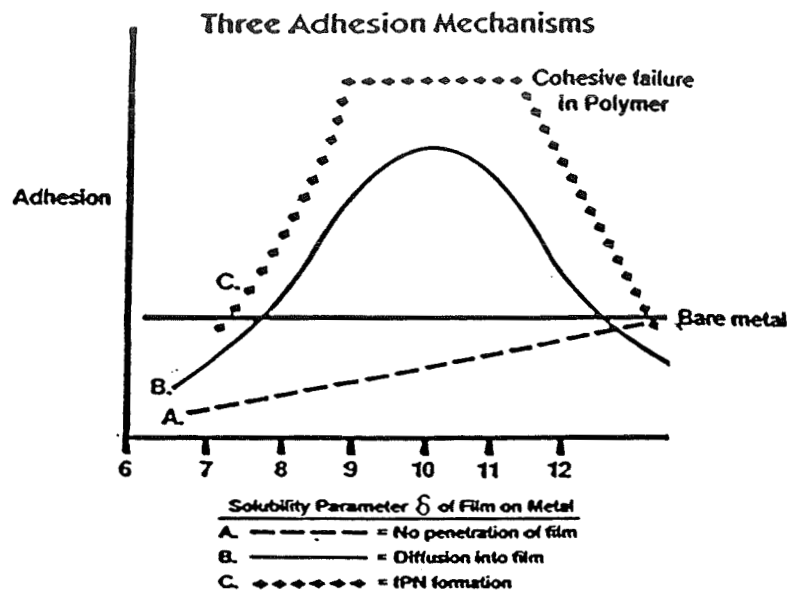
CHEMICAL BONDING TECHNOLOGY

DOW CORNING CORPORATION

E. Plueddemann

Formation of Polysiloxane on Glass Surface
(Bonding of Trialkoxysilanes to Glass and Metals)

Bonding with the Polymer



How Much Should Primer be Pre-Cured?
 (PVC Plastisol on Glass with Aminosilane Primer)
 Plastisol Fused 20 min at 150°C

Dry Primer 15 min. at Temperature (°C)	Peel Adhesion of PVC Film (N/cm)	
	Dry	1 day in 50° C water
100° C	(c)	1.08
125	(c)	1.27
150	(c)	15.8
150 (30 min.)	(c)	13.1
175	4.35	—
200	2.50	250
No primer	0.3	—

(c) = cohesive failure in film at about 25 N/cm

Bonding EVA Copolymers to Glass Through the Use of Commercial Silanes

Commercial designation	Functional group of primer (on Si, Cr, etc.)	Thermoplastic	X-linkable
		CXA 2202	A-9918
A-1100	Aminopropyl	-	+
Z-6020	Diamine	-	+
Z-6030	Methacrylate	++	++
Z-6032	Vinylbenzyl cationic	-	+
Z-6040	Epoxy	-	-
Z-6062	Mercaptan	+	-
Z-6076	Chloropropyl	+	-
Q9-6300	Vinyl	+	+
Q1-6106	Epoxy-melamine resin	++	-
" + Z-6030		++	++
Z-6020 + 2 Mal. Anhyd.		-	++
X1-6100	Mixed Ph/Z-6020 90/10	-	+
Z-6020 + IEHA	Methacrylate-urea	++	+++

+++ = best

++ = good

+ = fair

- = not recommended

Peroxides in Z-6030 Primer for EVA 9918 Peel Strength (Pounds/Inch)

Add 0.5% peroxide to Z-6030 + 1% BDMA	C.R. Steel		Stainless steel		Aluminum	
	Dry	2 hr. boil	Dry	2 hr. boil	Dry	2 hr. boil
None	6.6	9.5	c	c	c	3.3
t-Bu perbenzoate	11.0	c	c	3.3	c	1.8
Lupersol 101	13.2	c	c	c	6.2	-
Lupersol TBEC	c	c	c	c	c	c
Dicumyl peroxide	5.5	9.0	c	c	c	c
Luazo-85 (azo compd.)	c	9.0	c	c	c	c

101 = 2,5-Dimethyl-2,5-bis(t-butylperoxy)hexane

TBEC = t-Butyl-2-ethylhexyl monoperoxycarbonate

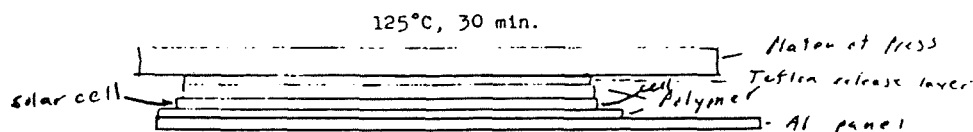
c = cohesive failure in film at over 15 lb/linear inch

Forced Drying of Primers for EVA on Steel

Primer on C.R. Steel	Drying T°C	Adhesion after 2 hour water boil(pli)
	15 min.	A-9918
Z-6030 + 1% BDMA	r.t.	11.0
	80	8.1
	120	4.4
" " + Lupersol 101	r.t.	c
	80	11.7
	120	4.4
1% Z-6030 in 1205	r.t.	15.4
	80	7.2
	120	2.4
" " + ZnCrO ₄	r.t.	c
	80	c
	120	5.5

c = cohesive failure in polymer at over 15 pli

Adhesion Testing of Formulated EVA and EMA (from Springborn Labs, Inc.) on Solar Cells



This configuration also gave me an opportunity to check the adhesion of polymers to aluminum. Observations :

Peel strength of cured polymers on solar cells and Al (Kg/in)

Polymer (Springborn)	Primer	Adhesion to Solar Cells		Aluminum
		grey side	black side	
9918-P	none	4.5	4.0	0.3
15295-P	none	1.6	2.2	1.4
9918	mod. 1205 ⁽¹⁾	c	c	c
15295	"	c	c	c

(1) mod. 1205 = D.C. 1205 primer with 1 percent added Z-6030

c = cohesive failure in polymer at over 5 Kg/in ≈ 20 N/cm

Recovery of Adhesion by Drying After Being Boiled in Water
(EVA Compounds Cured on C.R. Steel 15 min at 125°C)

Primer on Steel(or Ti)	Adhesion to steel - peel str. (Kg/in)		
	Dry	after 2 hr. boil	after 1 day in air
<u>EVA A-9918</u>			
Z-6030 + BDMA in iPA	c	3.7	5.2
D.C. 1205 + Z-6030	c	3.3	c
<u>EVA 15295</u>			
Z-6030 + BDMA	c	0.2	2.0
D.C. 1205 + Z-6030	c	2.2	8.0
<u>EVA 15295 On Titanium</u>			
D.C. 1205 + Z-6030	c	4.6	8.0

c = cohesive failure in polymer at over 8 Kg/in

Two Primers for X-Linkable EVA to All Surfaces

I. Glass, ceramic, and metalsAdd 1% Z-6030 to Dow Corning 1205 primer. A trace of added ZnCrO₄ improved water resistance of bond to certain metals.II. Plastic Surfaces, Kapton, Tedlar, Mellinex, Scotchpar, Araylar, Korad, etc.

Add 10% Z-6030 to Dow Corning Q1-6106, and dilute to 10% solids with i-PA.

or-

10 parts Z-6040

10 parts Z-6030

80 parts melamine resin (Monsanto Resimene 740)

dilute to 10% solids in i-PA (isopropanol)

Bonding Cross-Linkable EVA to Polymer Surfaces

Primer on Polymer	EVA A-9918							
	Kapton	Mellinex	Tedlar	Scotch-par	Acrylar	EH-723	Korad	Chemplex c-20
Unprimed	+ -	- -	+ +	- -	c c	- -	- -	+ -
Z-6030+1%BDMA	c +	+ -	c +	c -	c c	+ -	c c	c +
" + Lup. 101	c c		c c	c c	c c	+ -	+ -	+ -
Z-6030/40/Resimene	c c	c c	c c	c c	c c	c c	c c	c +
1% Z-6030 in 1205	c c	+ -	c c	c -	+ +	+ -	- -	c c
<u>EVA 15295</u>								
Unprimed	+ -	- -	+ +	- -	- -	- -	- -	+ -
Z-6030 + 1% BDMA	c +	c -	c +	c -		+		c c
Z-6030/40/Resimene	c c	c c	c c	c c	c c	+ -	c c	c c
1% Z-6030 in 1205	c c	+ -	c c	+ -		+		c c

Ratings 1st symbol = dry, 2nd = after 2 hours in boiling water

c = cohesive failure in polymer at over 15 pli

+ = peel strength 2 to 15 pli

- = peel strength less than 2 pli

Bonding Cross-Linkable EVA and EMA to Metal Surfaces

EMA 16717										
Primer on Surface	Glass	Alumin.	C.R. Steel	Stainless Steel	Tin on Steel	Zn galv Steel	Titanium	Brass	Solder on cu	
1% Z-6030 in 1205	c c	c c	c c	c c	c c	c c	c c	c c	c c	c c
2-6030/40/Resimene	c +	C +	c +	c -	c c	c +	c -	c +		
EVA 9918										
Unprimed	+ -	+ -	- -	- -	+ -	- -	- -	+ -	+ -	
1% Z-6030 in 1205	c c	c +	c -	c +	c +	c c	c -	c c		
" " + ZnCrO ₄	c c	c c	c +	c c	c c	c c	c +	c c	c c	
EVA 15295										
1% Z-6030 in 1205	c c	c +	c +	c c	c c	c c	c -	c +	c c	
" " + ZnCrO ₄	c c	c c	c +	c c	c c	c c	c c	c +	c c	

Ratings 1st symbol = dry, 2nd = after two hours in boiling water
 c = cohesive failure at over 15 pli (pounds per linear inch)
 + = peel strength 2' to 15 pli
 - + peel strength less than 2 pli

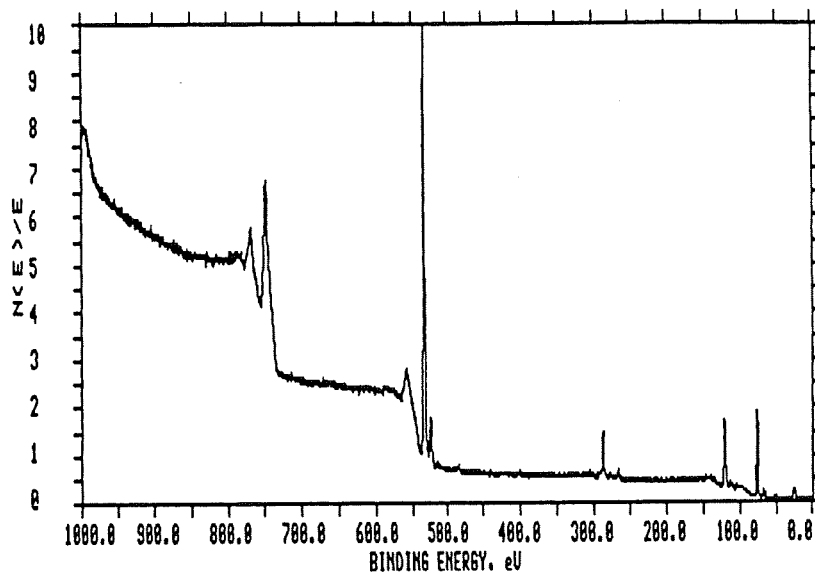
ORIGINAL PAGE IS
OF POOR QUALITY

ANTICORROSION STUDIES

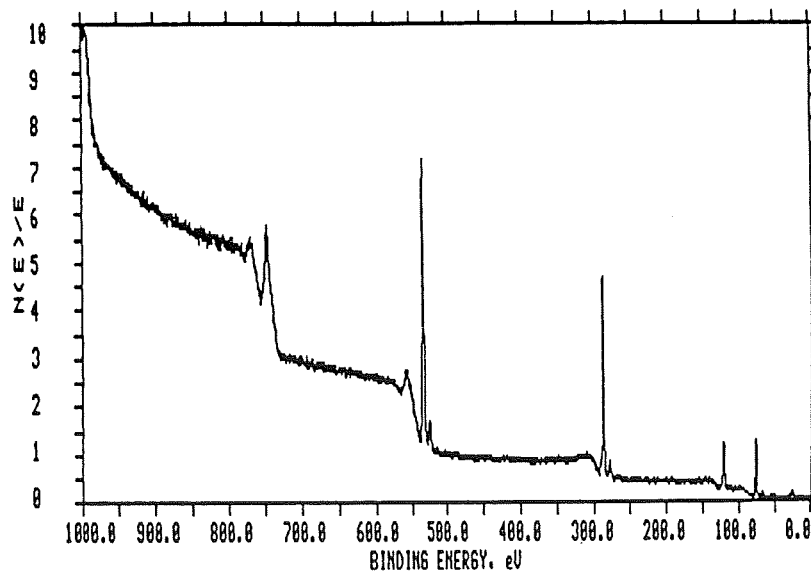
UNIVERSITY OF CINCINNATI

J. Boerio

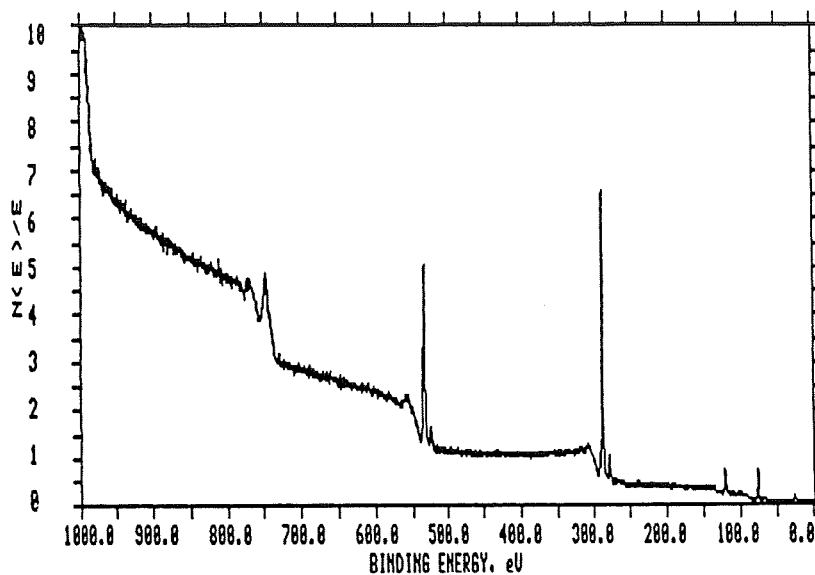
XPS Spectrum from Aluminized Back Side of As-Received Solar Cell
(Exit Angle of 45°)



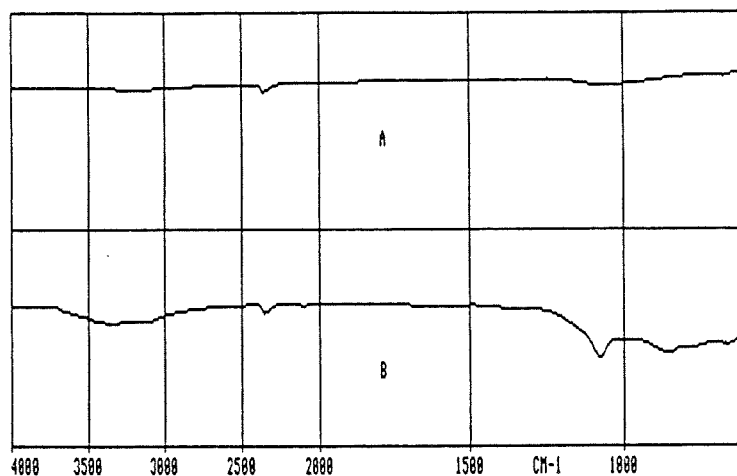
XPS Spectrum from Back Side of Solar Cell Coated with EVA
(Cell Boiled in Water 1 h Before Coating was Peeled Off)



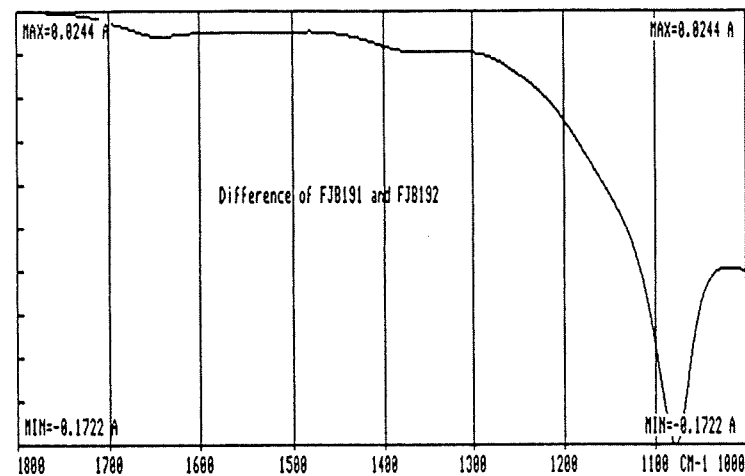
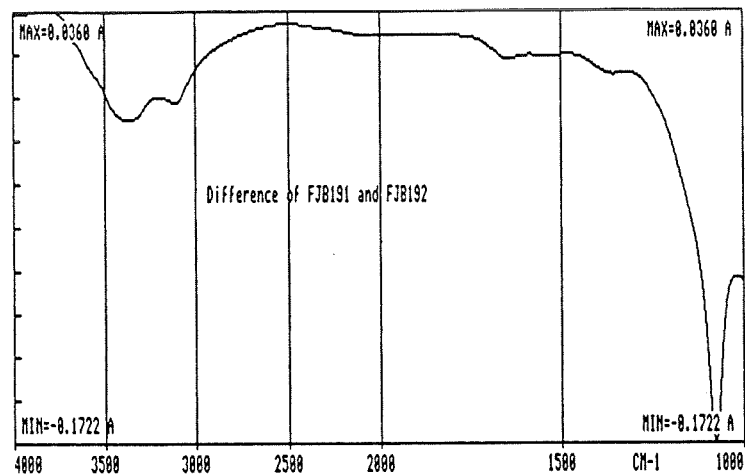
XPS Spectrum from Back Side of Solar Cell
Coated with EVA and A-11861
(Cell Boiled in Water 1 h Before EVA was Peeled Off)



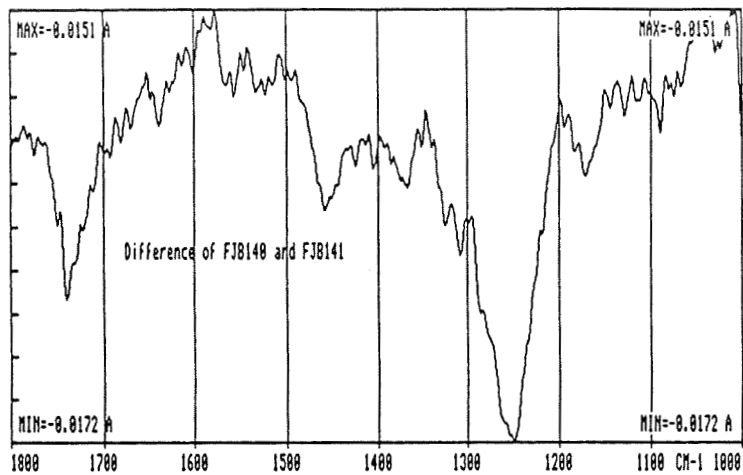
Effect of Immersion, of Thin Amorphous Silicon Cell in Boiling Water
for 10 min, on the Infrared Spectra from Aluminum Film on Back Side
(A, Before Immersion; B, After Immersion)



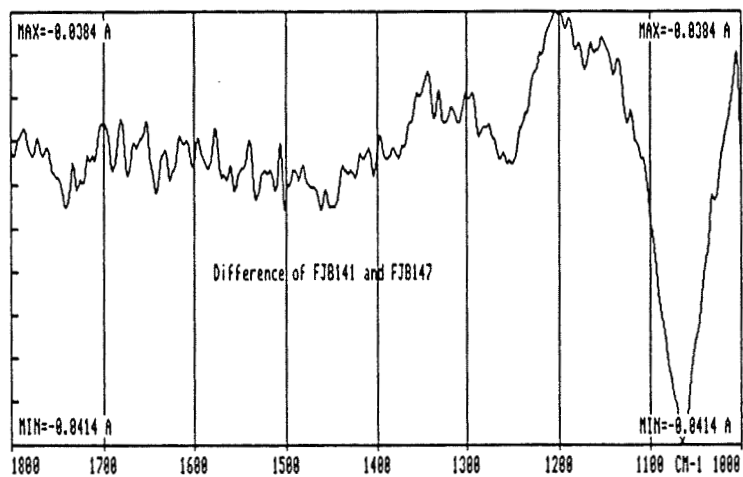
Difference of Infrared Spectra from Aluminum Film on Back Side of a Thin Amorphous Silicon Cell Before and After Immersion in Boiling Water for 10 min



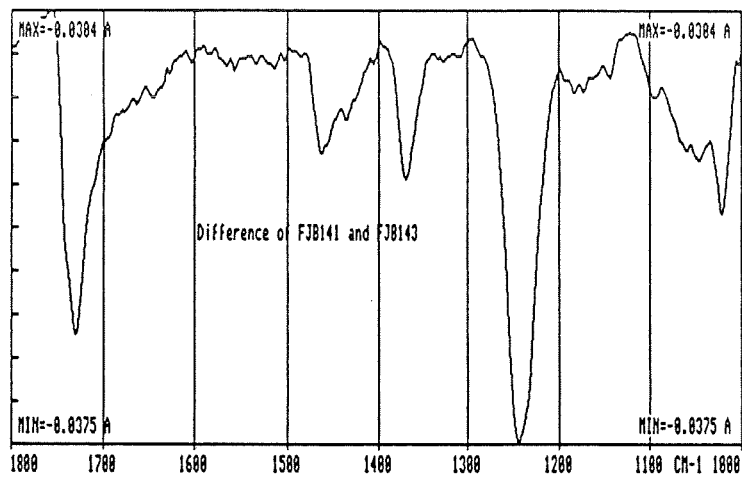
Infrared Spectrum of Silicon Cell Coated with EVA



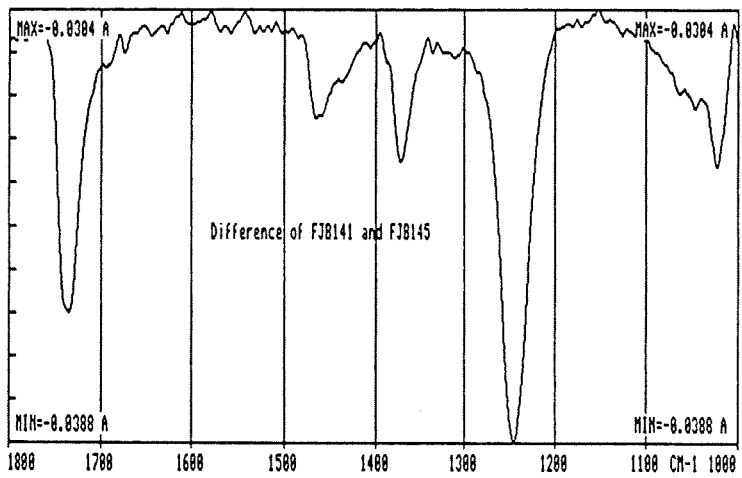
Infrared Spectrum: Silicon Cell Coated with EVA and then Boiled in Water for 30 min



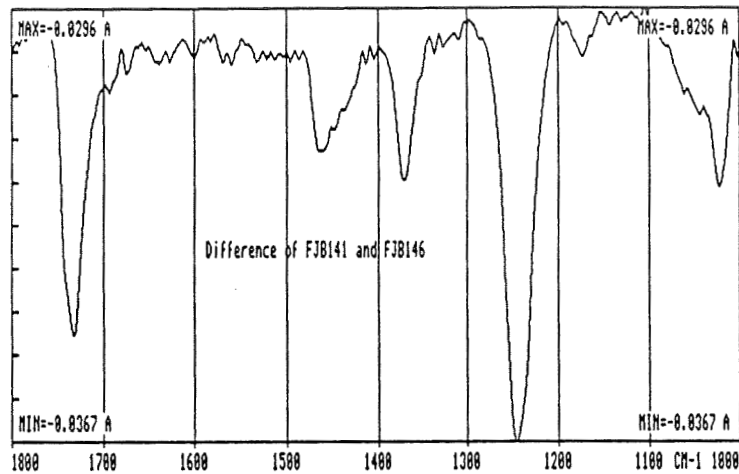
Infrared Spectrum: Silicon Cell Coated with Primer A-11861 and EVA



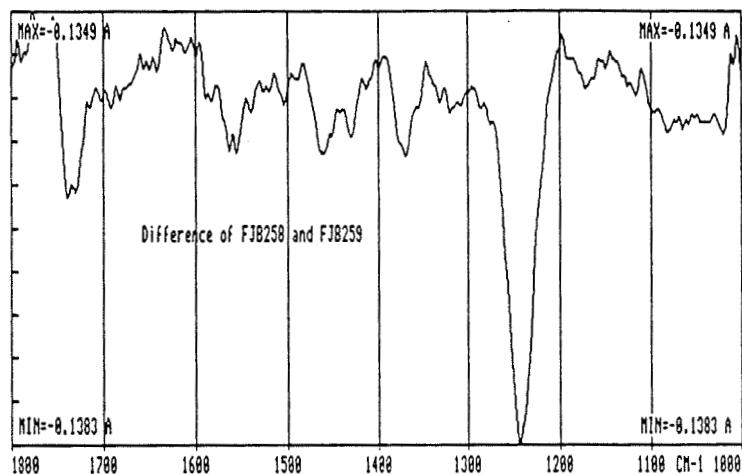
Infrared Spectrum: Silicon Cell Coated with Primer A-11861 and EVA
and then Boiled in Water for 60 min



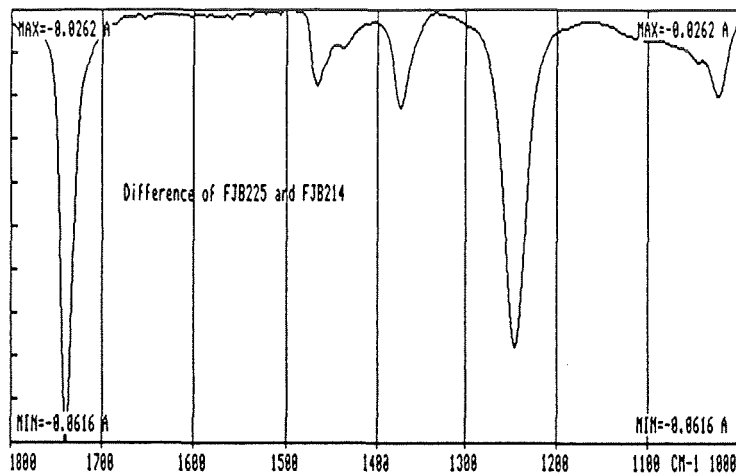
Infrared Spectrum: Silicon Cell Coated with Primer A-11861 and EVA
and then Boiled in Water for 90 min



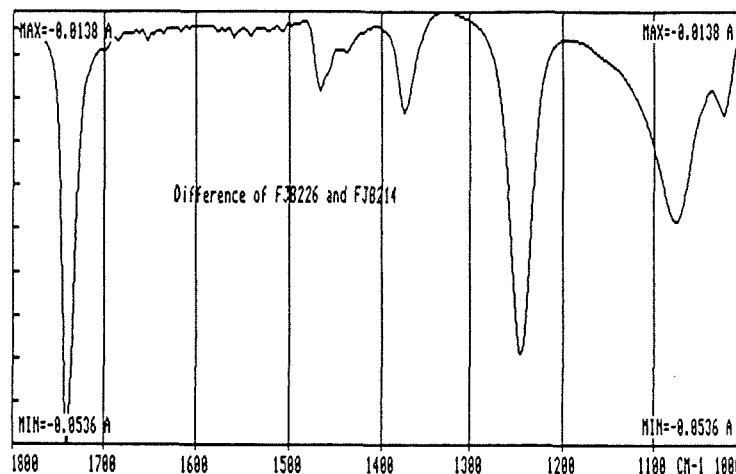
Infrared Spectrum from Aluminized Back Side of Silicon Cell Coated
with Primer A-11861 and EVA and then Boiled in Water for 35 h



Infrared Spectrum from Aluminum Film on Back Side of a Thin Amorphous Silicon Cell After Coating with A-11861 Primer and EVA



Infrared Spectrum from Back Side of a Thin Amorphous Silicon Cell Coated with A-11861 Primer and then Immersed in Boiling Water for 30 min



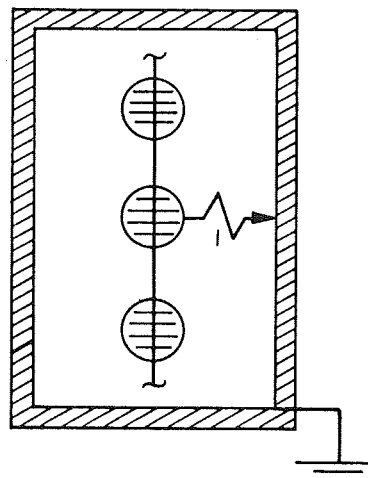
ELECTROCHEMICAL AGING EFFECTS IN PHOTOVOLTAIC MODULES

JET PROPULSION LABORATORY

G. R. Mon

Electrochemical Corrosion of Photovoltaic Modules: A Review

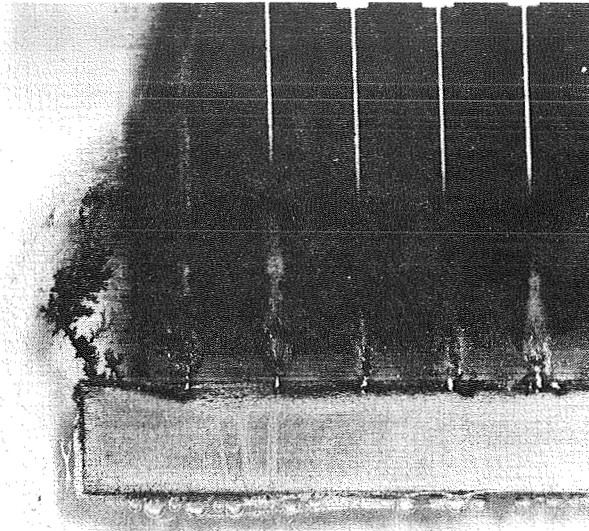
- Cause of corrosion
 - Spurious ionic currents ("leakage currents") between cells and frame
- Corrosion damage
 - Crystalline Silicon
 - Dissolution and migration of metallization
 - Metallization delamination
 - Dendritic growths
 - Encloachment of encapsulation
 - Amorphous silicon
 - Worming and pinholing of metallization and amorphous silicon layers



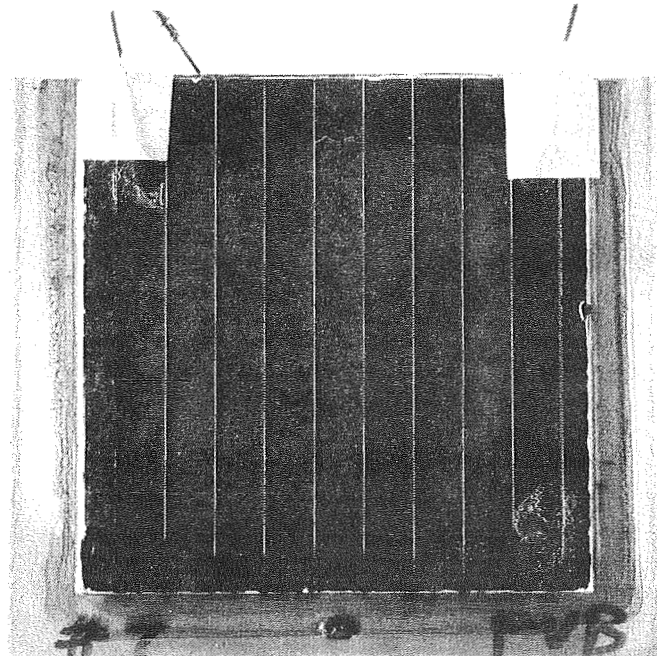
PRECEDING PAGE BLANK NOT FILMED

Typical Electrochemical Damage in Crystalline Silicon Modules

ORIGINAL PAGE IS
OF POOR QUALITY



Typical Electrochemical Damage in Amorphous Silicon Modules



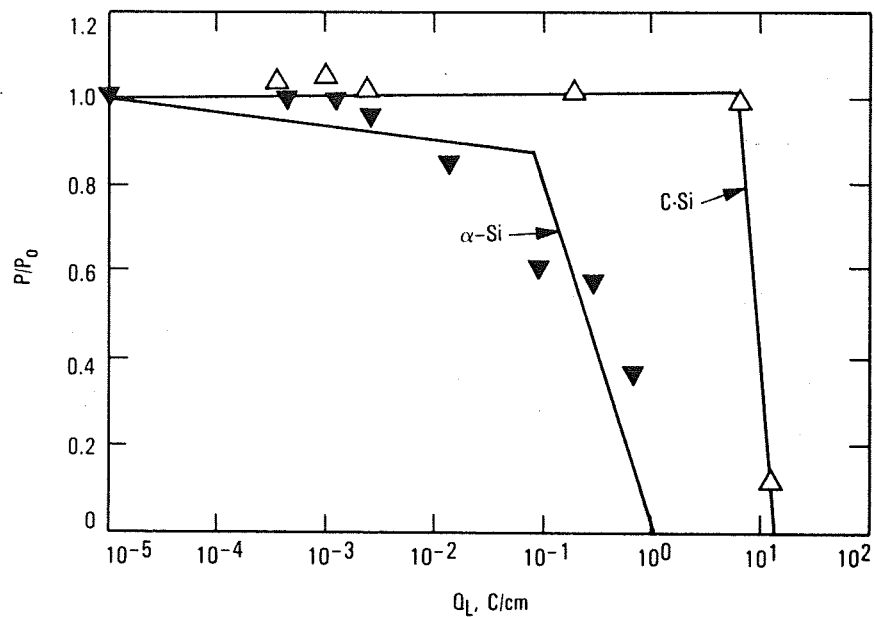
Quantifying Electrochemical Corrosion

- Experimentally, it has been determined that 50% cell failures (>25% reduction in cell power output) occur after the passage between cell and frame of:

- C-Si: 1.0 - 10.0 C/cm of cell-frame edge

- A-Si: 0.1 - 1.0 C/cm of cell-frame edge

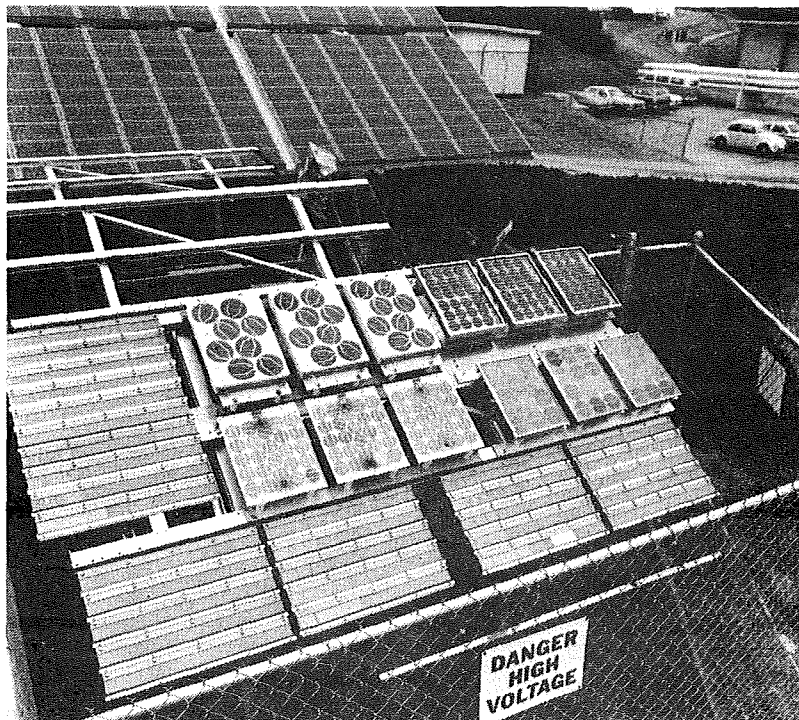
Comparison of Amorphous and Crystalline Silicon Cells for Power Output Versus Accumulated Unit Charge Transfer



Electrochemical Corrosion of Photovoltaic Modules: Present Research Focus

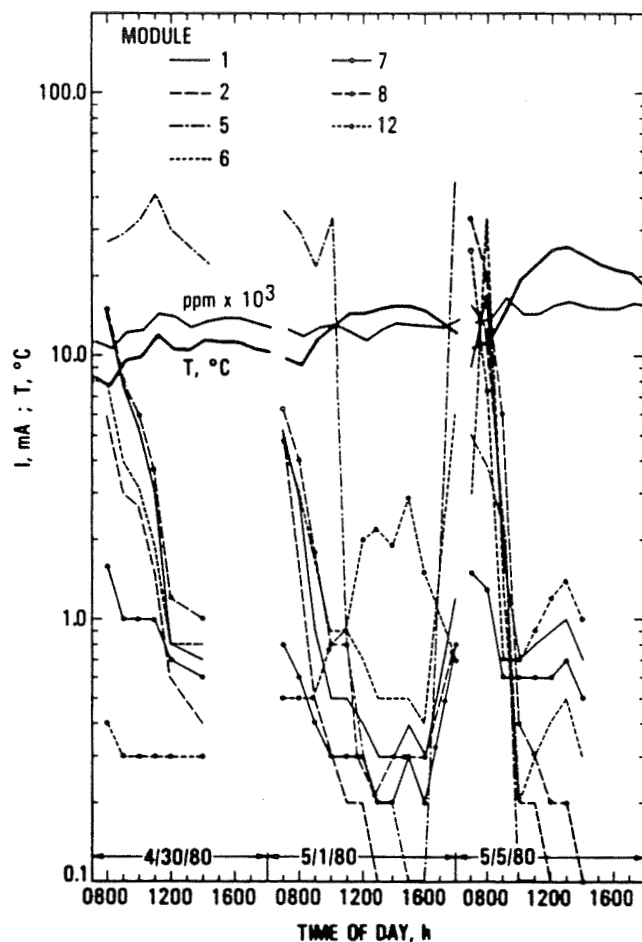
- Quantify factors that determine module leakage current levels
- Determine dominant conduction paths in PV modules
- Create realistic analytical PV module conduction models
- Establish methods to:
 - Predict module life
 - Develop correlations between module behavior in controlled laboratory environments and field environments (acceleration factors)

PVB-Encapsulated Modules Arranged on Outdoor Test Stand



ORIGINAL PAGE IS
OF POOR QUALITY

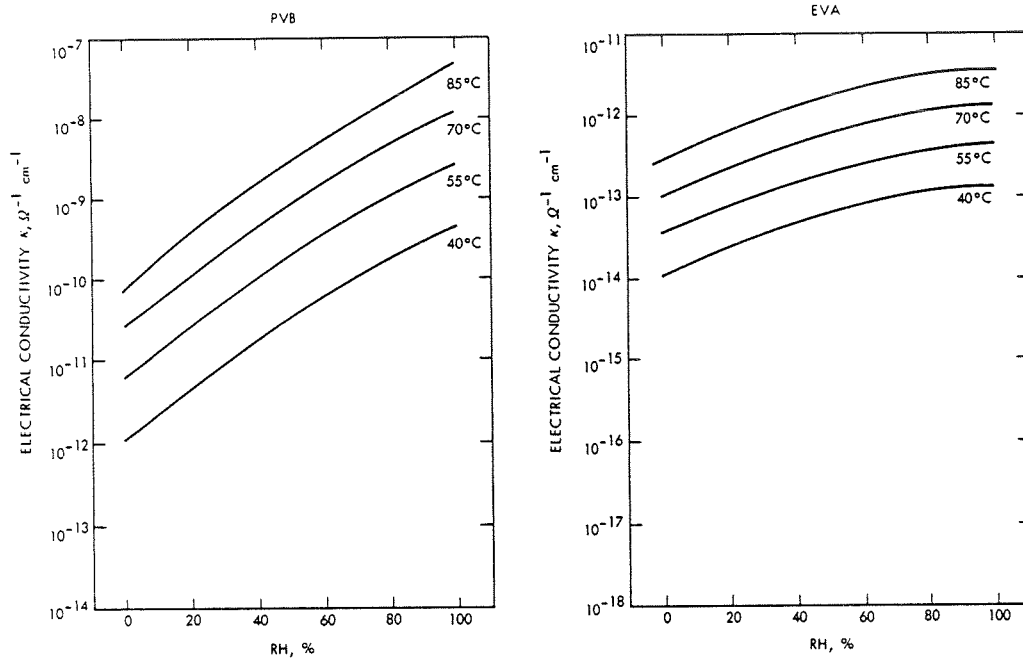
Outdoor Test Stand Data (Minimodules)



Observations on Outdoor Test Stand PVB-Minimodules

- Very high leakage current levels observed during periods of dew and precipitation
- Large current reductions observed as the modules "dried out"
- Sensitivities
 - Temperature: modest
 - Moisture: very large

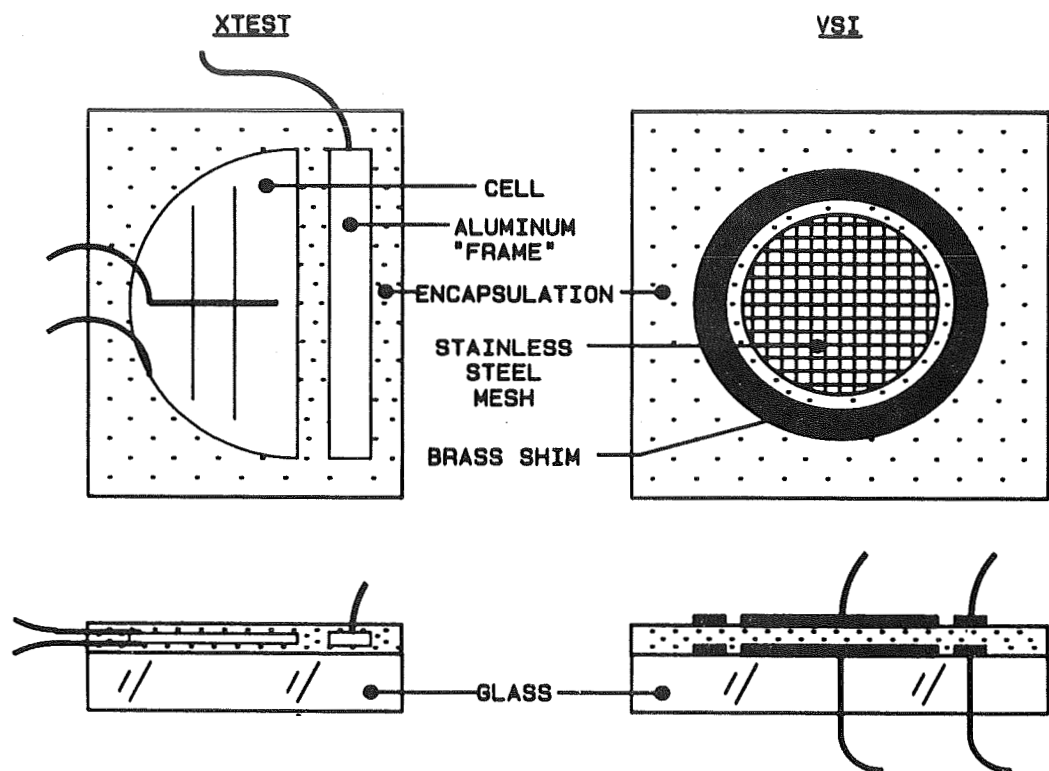
Bulk Conductivity of PVB and EVA



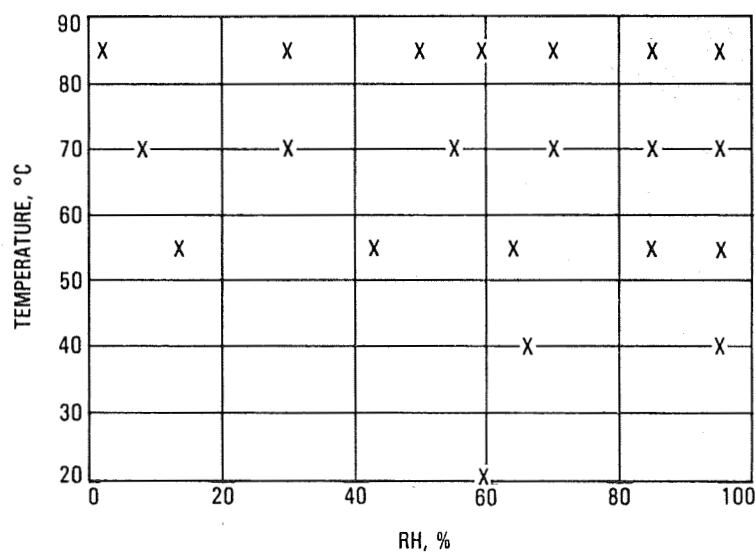
Experimental Program

- Controlled environment tests (equilibrium leakage current measurements over a broad range of constant T/RH-values)
 - VSI (encapsulated symmetric-electrode coupons)
 - Measure fundamental volume, surface, and interfacial electrical conductivities
 - XTEST (encapsulated cell-frame coupons)
 - Establish overall module leakage current levels
 - Determine charge transfer required to induce failure
- Field tests
 - Measure leakage current of VSI and XTEST samples previously characterized in T/RH chambers

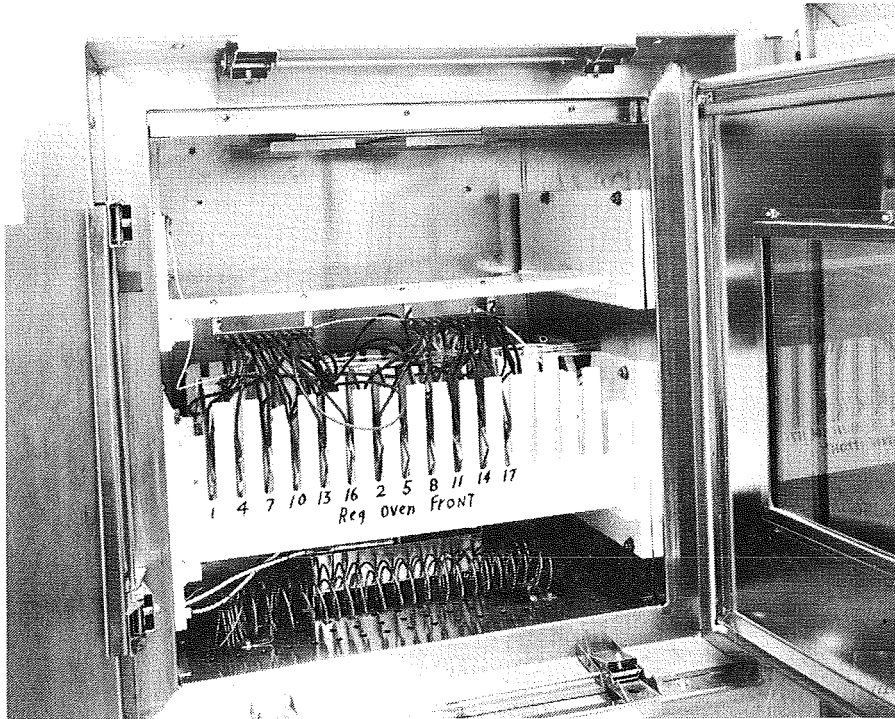
Sample Configurations in Leakage-Current Test



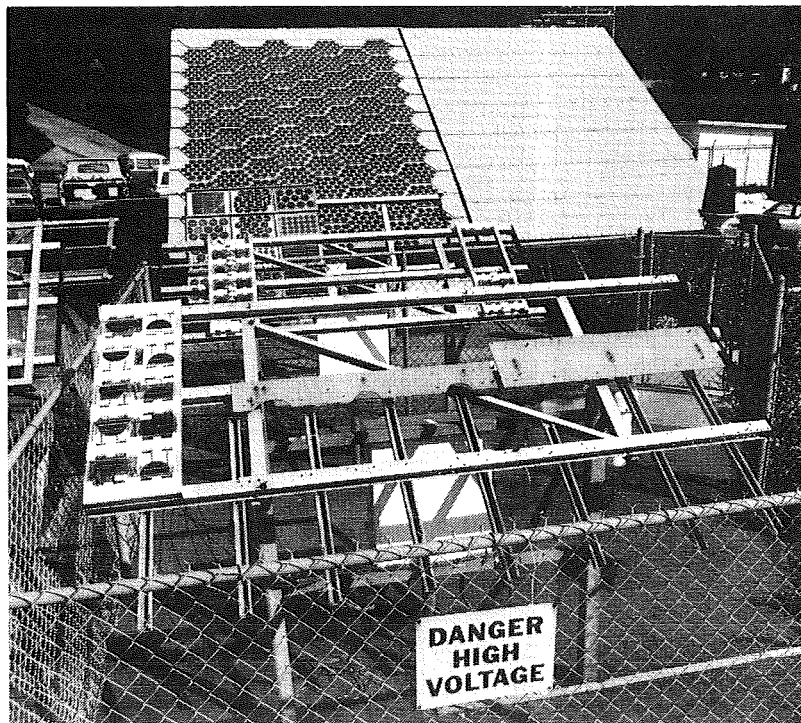
Temperature/Humidity Chamber Test Matrix



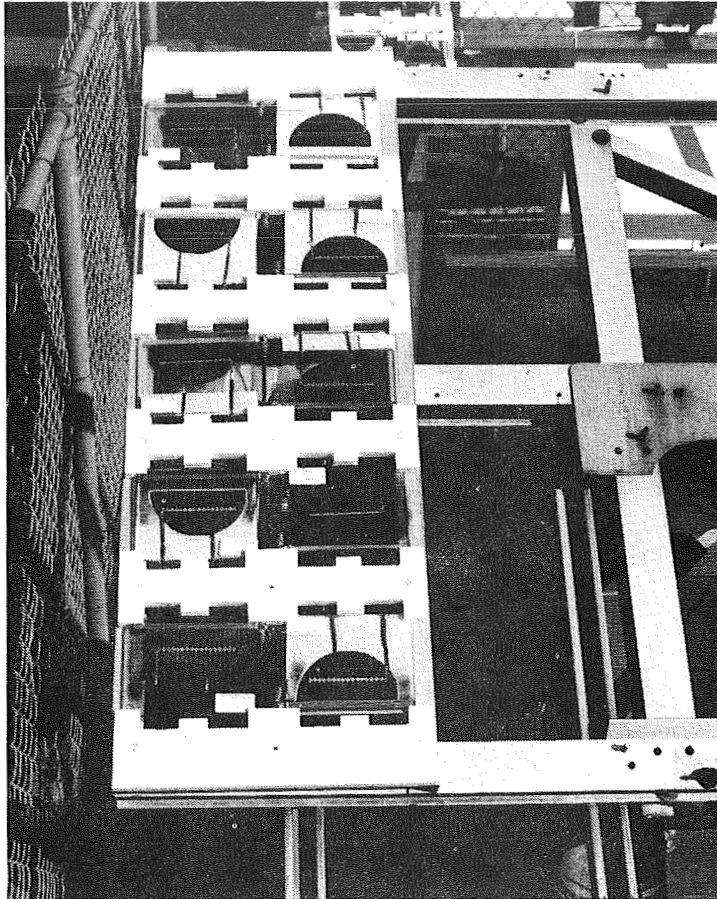
Samples Mounted in Laboratory Environmental Chamber



Overview of Outdoor High Voltage Test Stand

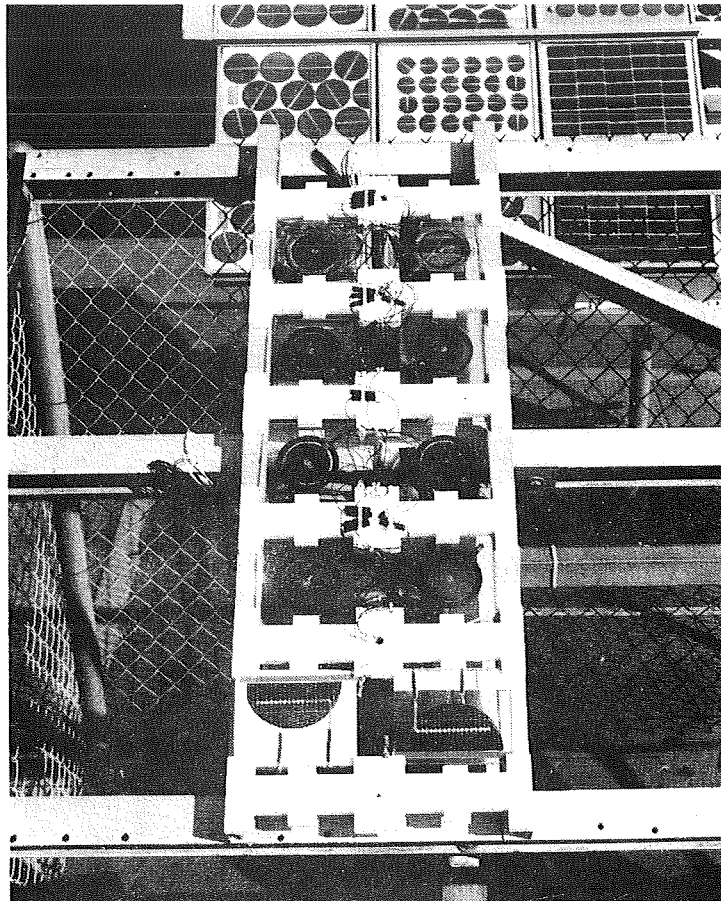


XTEST Samples Mounted on Outdoor High Voltage Test Stand



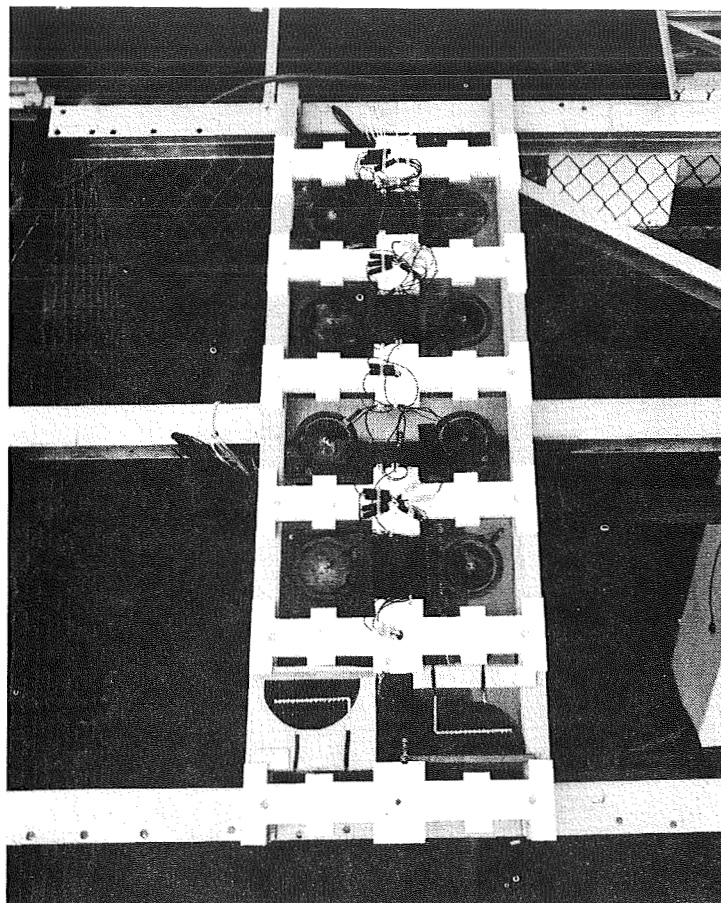
ORIGINAL PAGE IS
OF POOR QUALITY

VSI Samples Mounted on Outdoor High Voltage Test Stand

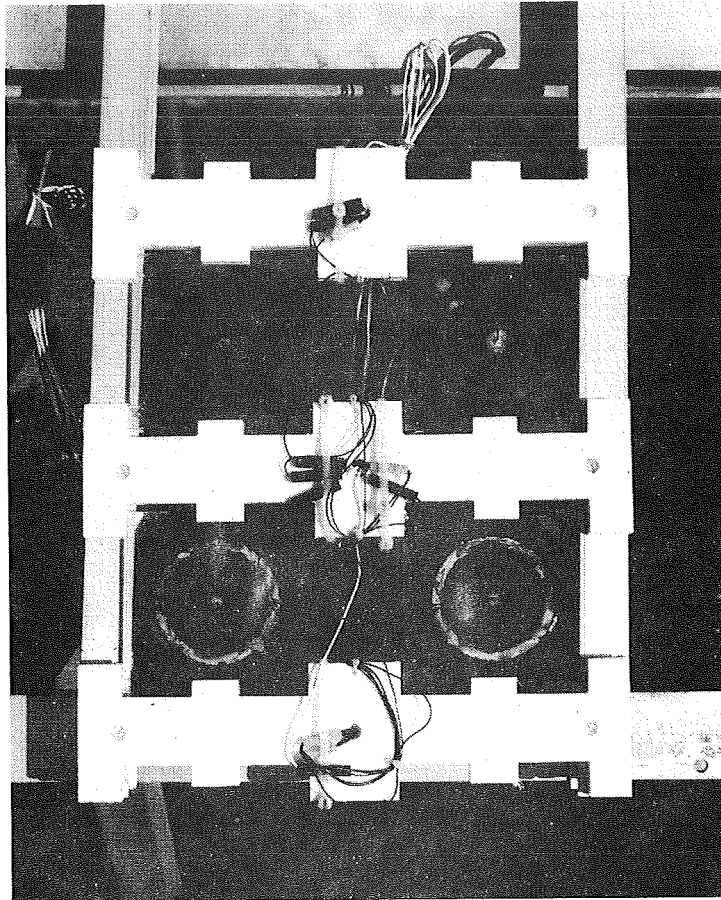


ORIGINAL PAGE IS
OF POOR QUALITY

VSI Samples Mounted on Outdoor High Voltage Test Stand
(Note Delamination)

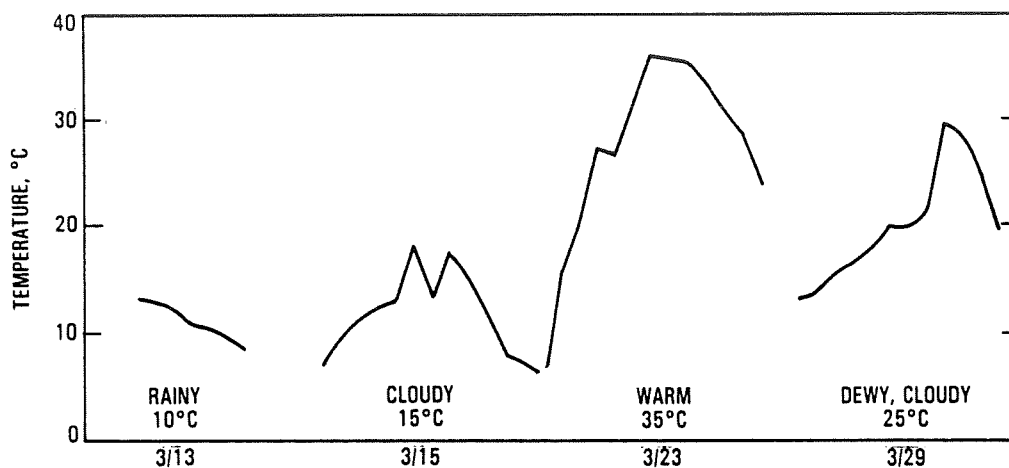


VSI Samples Mounted on Outdoor High Voltage Test Stand

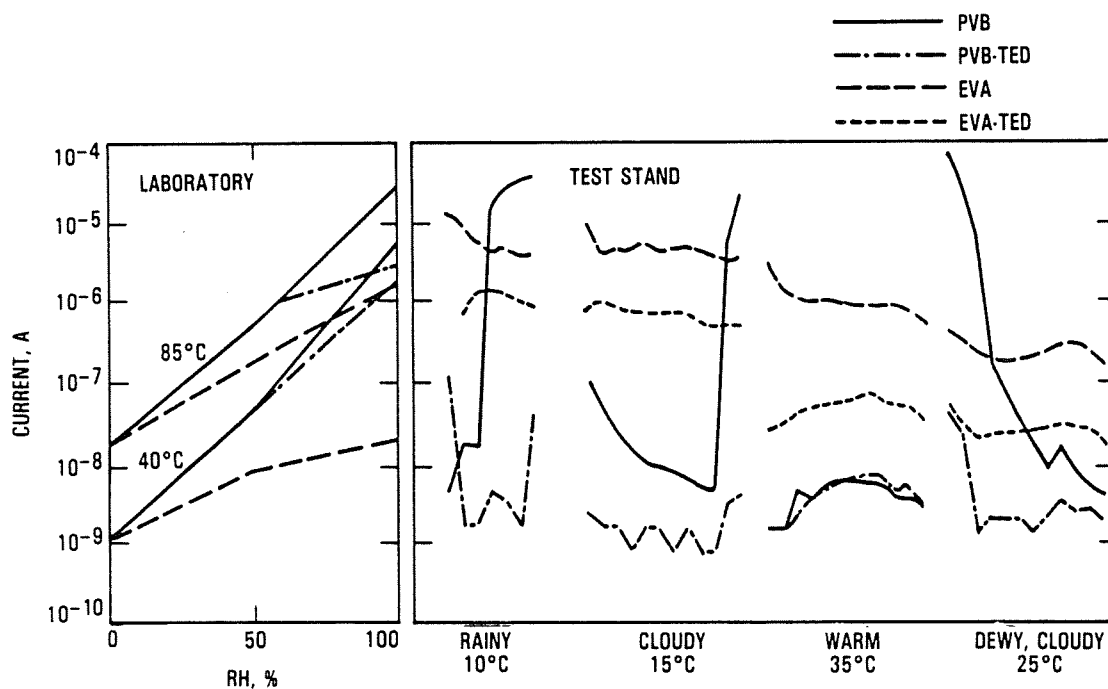


ORIGINAL PAGE IS
OF POOR QUALITY

Test Stand Module Temperatures



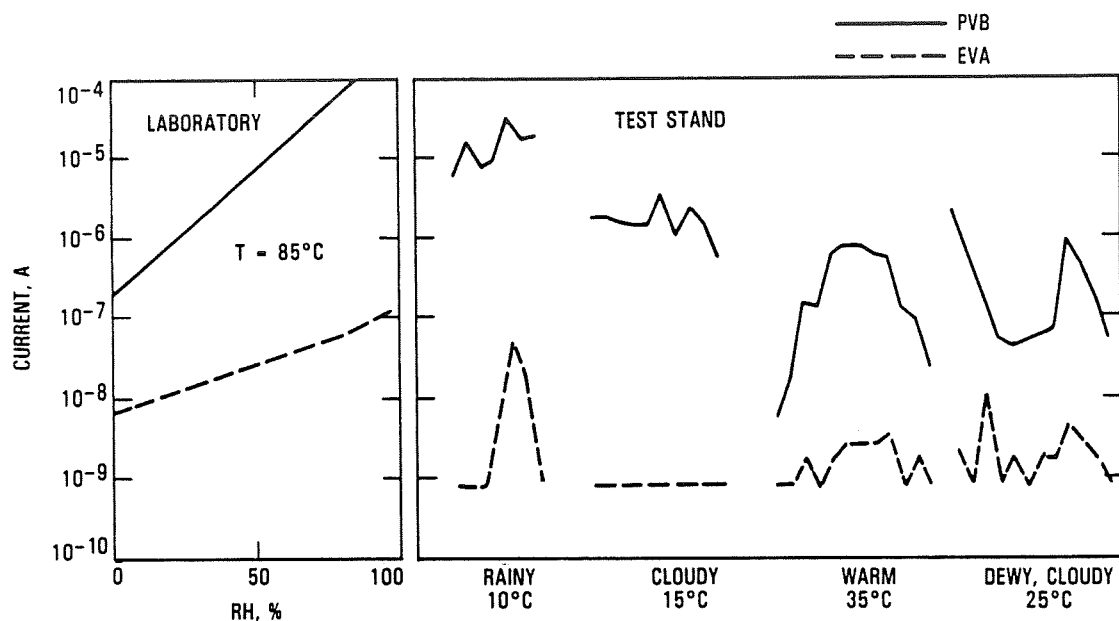
Module Leakage-Current Levels (XTEST Data)



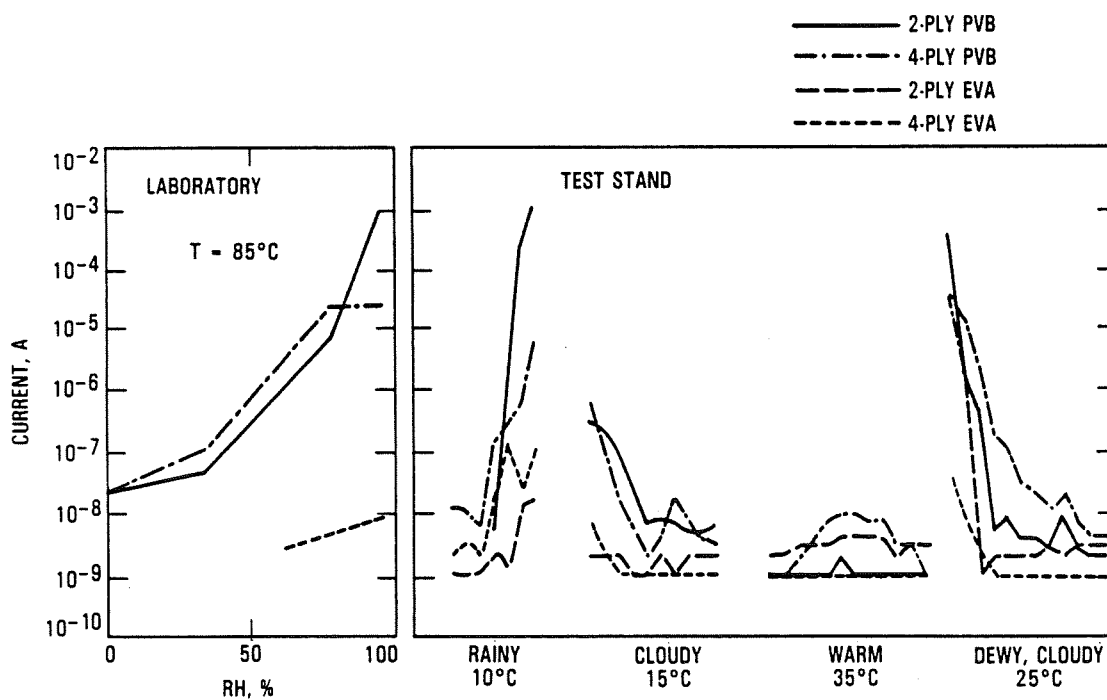
XTEST Observations

- **Laboratory**
 - PVB sensitivity to temperature variations decreases as relative humidity increases
 - EVA sensitivity to temperature variations increases as relative humidity increases
 - At high relative humidities, Tedlar reduces leakage currents in PVB coupons, but not in EVA coupons
 - For PVB coupons, total leakage current sensitivity to temperature variations is considerably less than that of bulk PVB, although sensitivity to humidity variations is somewhat greater than that of bulk PVB
 - For EVA coupons, total leakage current sensitivity to temperature and humidity variations is about the same as that of bulk EVA
- **Test stand**
 - For PVB (but not EVA) coupons, large current excursions were observed during periods of rain and dew, just as had been observed for PVB minimodules
 - Higher leakage current levels were observed in EVA coupons than in PVB coupons
- **Laboratory versus test stand**
 - For both PVB and EVA coupons, sensitivity to temperature variations was about the same at the test stand as in the laboratory
 - For PVB coupons, sensitivity to moisture variations in the field was greater than sensitivity to relative humidity variations in the test chambers

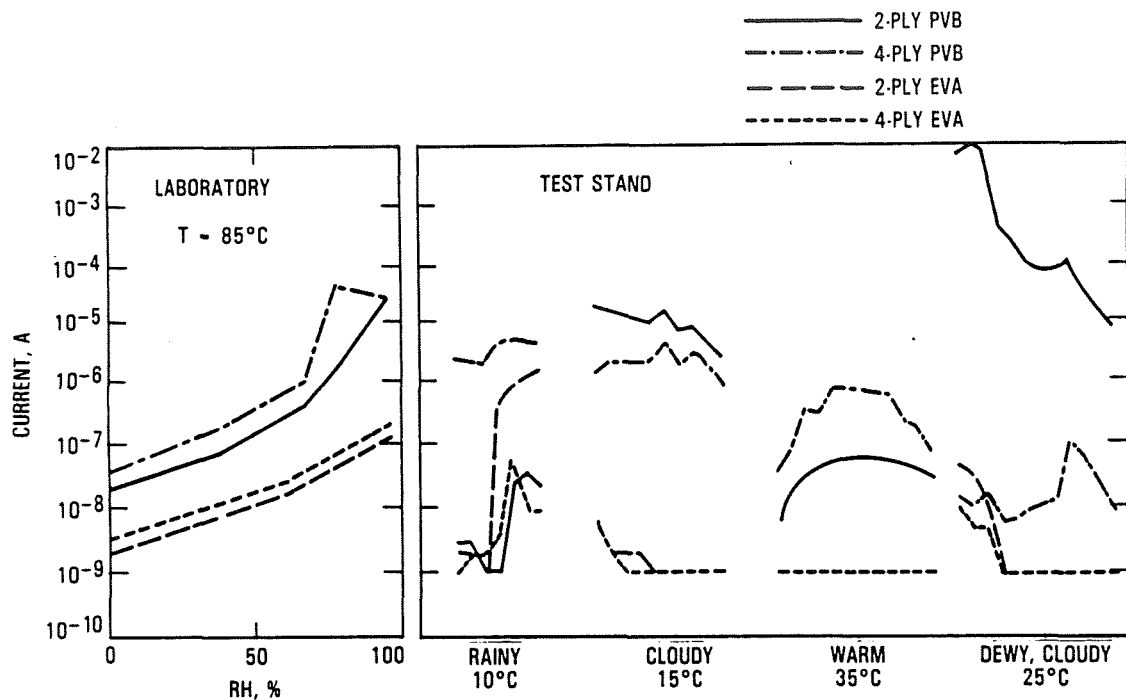
Bulk Leakage-Current Levels (VSI Data)



Surface Leakage-Current Levels (VSI Data)



Interface Leakage-Current Levels (VSI Data)



VSI Observations

- **Laboratory**
 - For PVB, surface and interface currents were observed to be about equal
 - For EVA, interface currents were greater than surface currents
 - Leakage currents in PVB always exceeded those in EVA
- **Test Stand**
 - For PVB, large surface and interface current excursions were observed during periods of dew and rain. Relatively smaller volume current excursions were noted
 - Interface currents generally exceeded surface currents
 - In dry conditions, PVB and EVA surface currents were both very low
 - Currents in PVB generally exceeded currents in EVA
 - Moisture pockets were observed at sample interfaces after extended periods of rain

Inferences

- For PVB, the largest electrochemical corrosion currents occur during periods of dew and after periods of precipitation
- In EVA modules, leakage current is dominated by bulk conduction effects
- In PVB modules, leakage current is governed by bulk conduction effects at high relative humidities and by surface/interface conduction effects at low relative humidities
- Conditions can exist in the field that don't exist in equilibrium T/RH-chambers (liquid water, moisture pockets, environmental transients, etc.). Field leakage currents can even exceed those in 85°C/85% RH laboratory environments. Such tests are inadequate for modeling field conditions
- Water, clustering at module interfaces, can vaporize resulting in blistering and delaminations

Conclusions

- Realistic life prediction and/or lab-field correlations (acceleration factors) require:
 - Consideration of short- and long-term environmental transients
 - Understanding of the relative contributions of volume, surface, and interfacial conduction to overall module conduction
 - Understanding of the roles of temperature, water vapor (RH), and liquid water in establishing module leakage current levels

LEAKAGE-CURRENT PROPERTIES OF ENCAPSULANTS

JET PROPULSION LABORATORY

L. C. Wen

Study Objectives

- Establish reliability assessment methodology associated with module leakage current
 - Leakage current conduction model
 - Dynamic simulation of charge transfer in field conditions
 - Module design considerations
 - Accelerated chamber testing
- Establish leakage-current properties of encapsulant materials
 - Characteristics of ionic conductivity
 - Material property degradation
 - Recommendations for future investigations

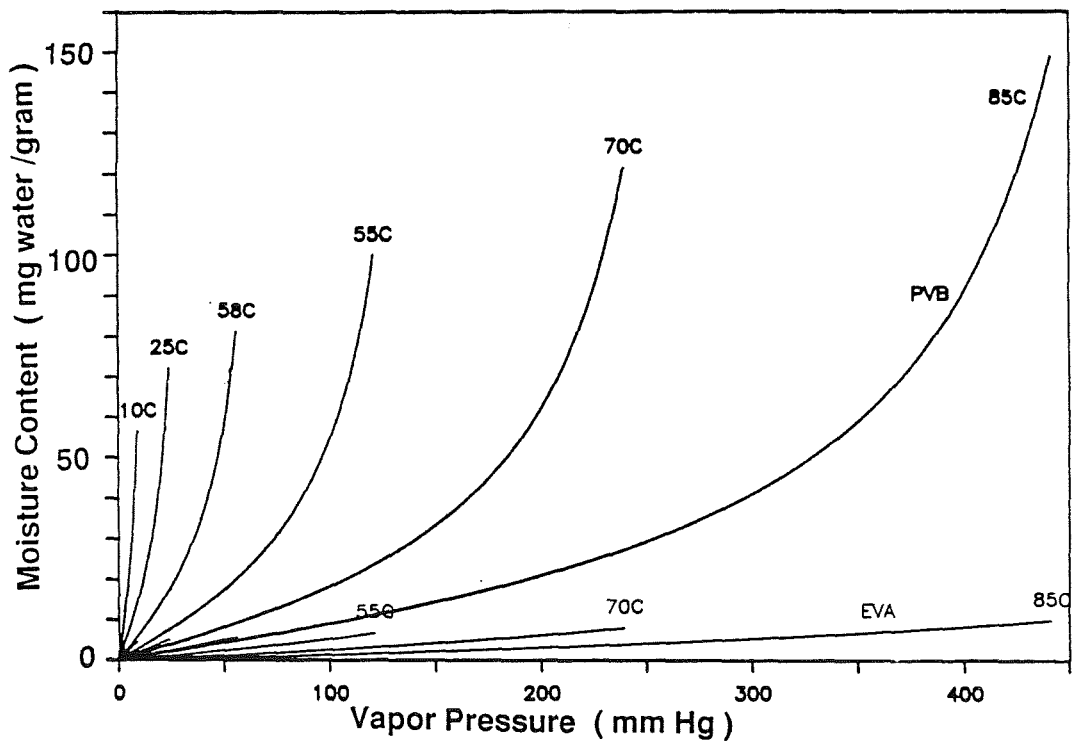
Approach

- Quantify basic encapsulant properties associated with module leakage currents
 - Sorption isotherms
 - Ionic conductivities
- Develop generic models of module conduction including:
 - Bulk conduction
 - Surface conduction
 - Interface conduction
- Conduct sensitivity studies of relevant parameters
- Perform simulation analyses of leakage currents and charge transfer in field environments

Water Vapor Sorption

- Sorption isotherms for pristine materials
 - Temperature/humidity
 - Manufacturing process
 - Lamination/curing process
- Thermal degradation
 - Severe plasticizer loss for PVB
 - Negligible effect on EVA
- Hydrolysis
 - Significant increase in water sorption capacity of EVA and PVB after exposure in high temperature, high humidity environments

Water Sorption Isotherms



Bulk Conductivity: Theory

- Sensitive to both temperature and humidity level

$$K_V = M_V \text{Exp} [(-E_0/RT)(Z_p/Z_w)^C]$$

E_0 = Activation energy

Z_p, Z_w = permittivity of polymer and water

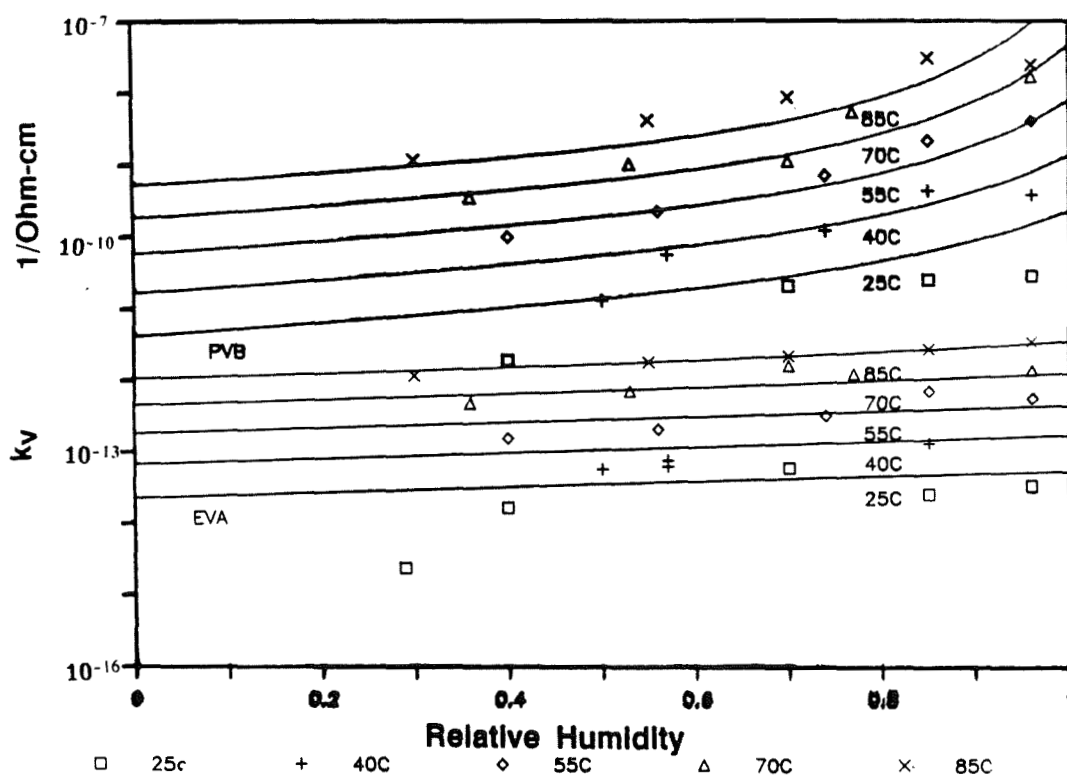
R = Gas constant

T = Temperature (in absolute scale)

C = Moisture concentration

M_V = property constant

Bulk Conductivity: Measurements



Surface and Interface Conductivities: Theory

- Polymer surfaces

$$K_S = M_S \text{ Exp } [(-E_S/RT)(1 - RH\{1 - (Z_p/Z_w)\})]$$

- Glass surfaces

$$K_S = M_S \text{ Exp } [(-E_S/RT)(1 - y RH\{1 - (Z_g/Z_w)\})]$$

RH = Relative humidity

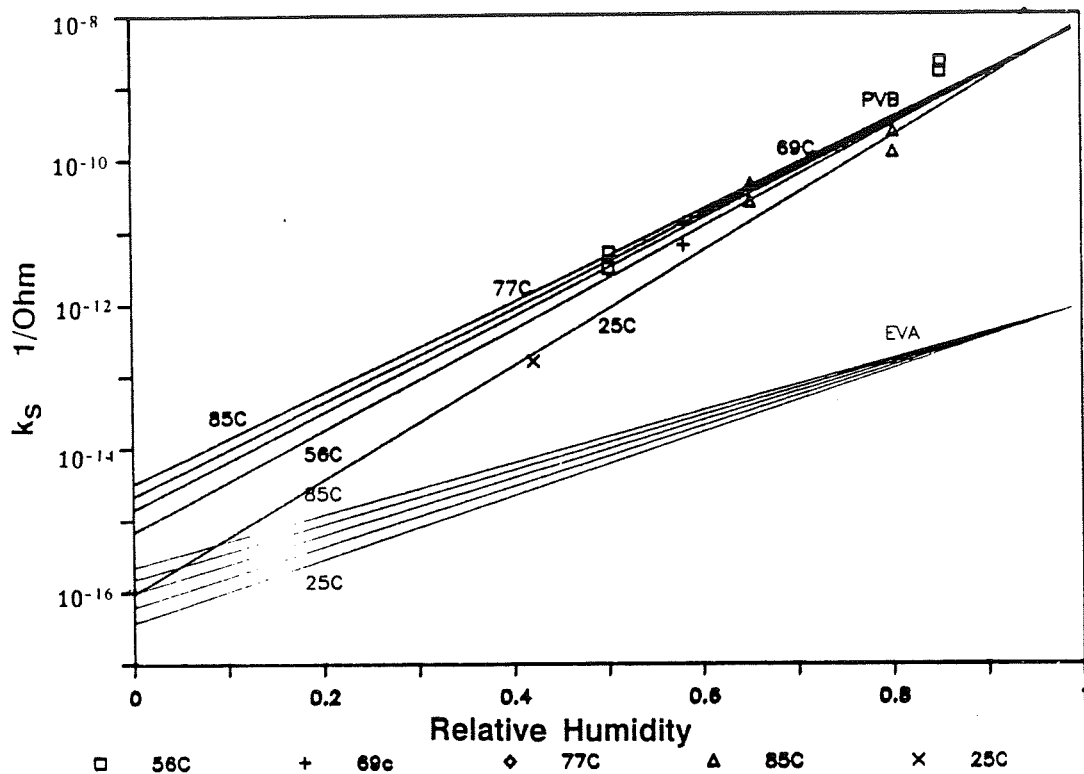
y = SURFACE MOISTURE factor

Z_g = permittivity of glass

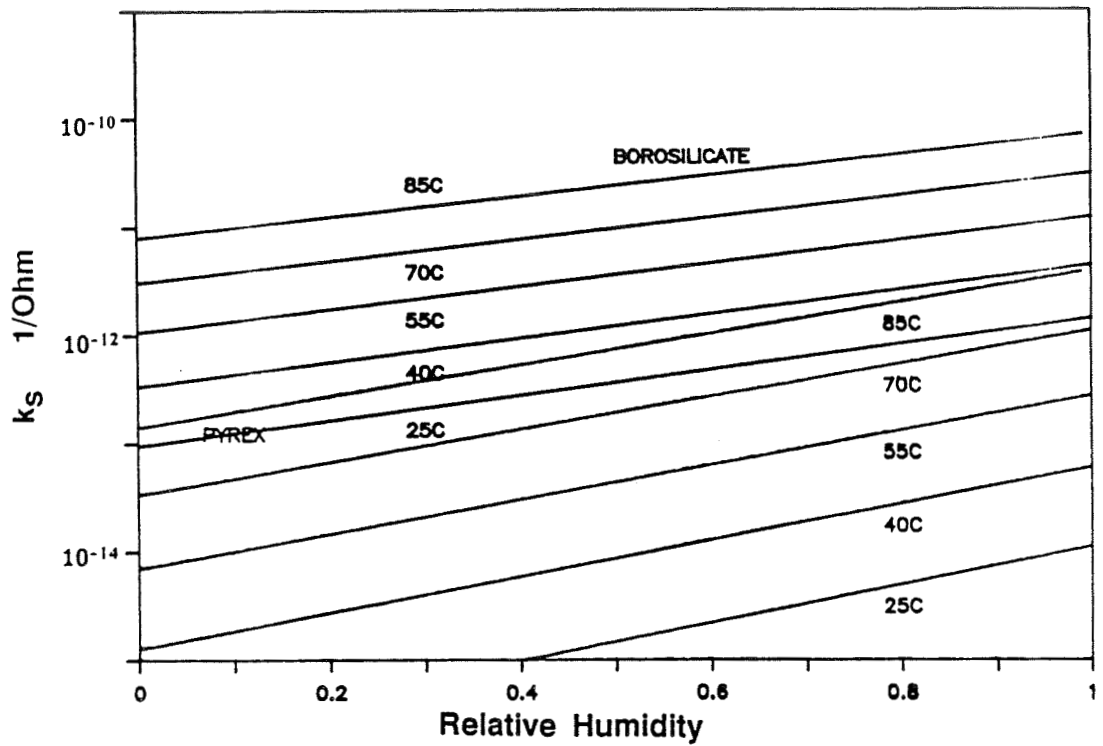
- Interfaces

$$K_i = K_{S1} + K_{S2}$$

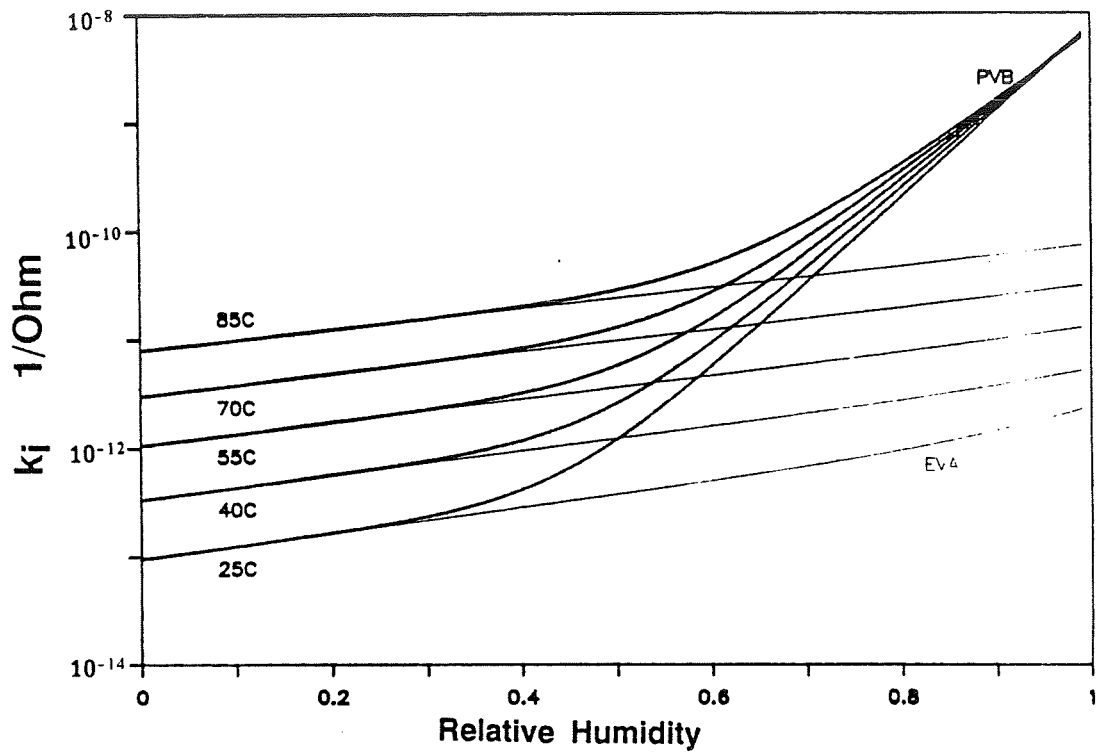
Surface Conductivity: PVB and EVA at Various Relative Humidities and Temperatures



Surface Conductivity: Borosilicate and Pyrex Glasses at Various Relative Humidities and Temperatures



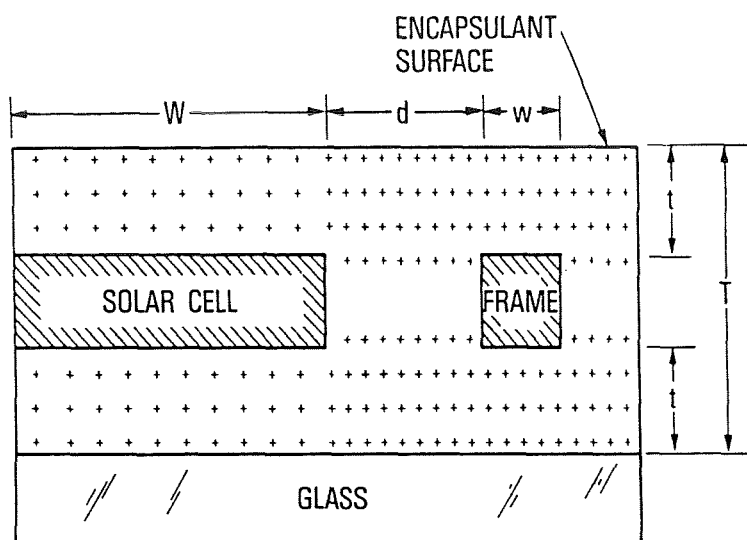
Interface Conductivity: Measurements of PVB and EVA



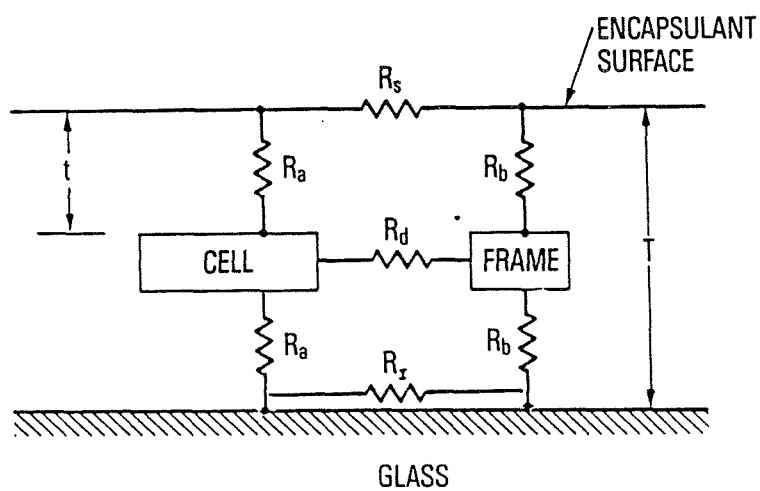
Leakage-Current Simulation

- 2-dimensional ionic conduction model
- Composite conductive paths
- Parametric study of the interplay of bulk, surface and interface conductivities
- Comparison with experimental results

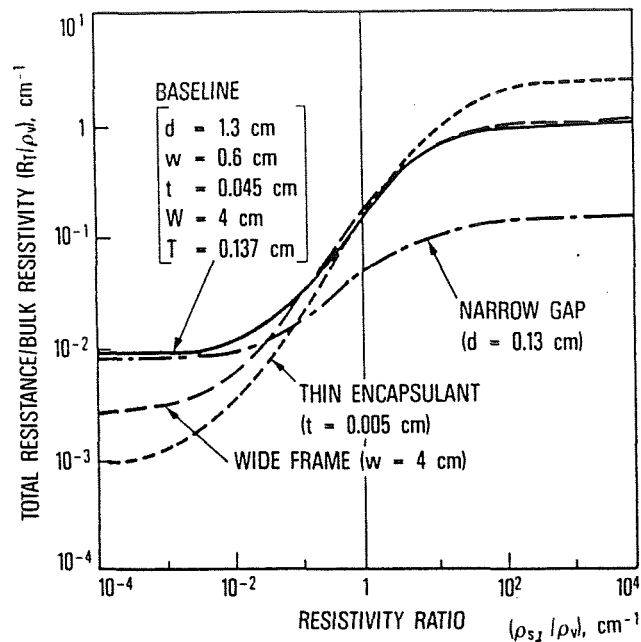
Cross-Sectional View of Test Coupons



Network Conduction Model



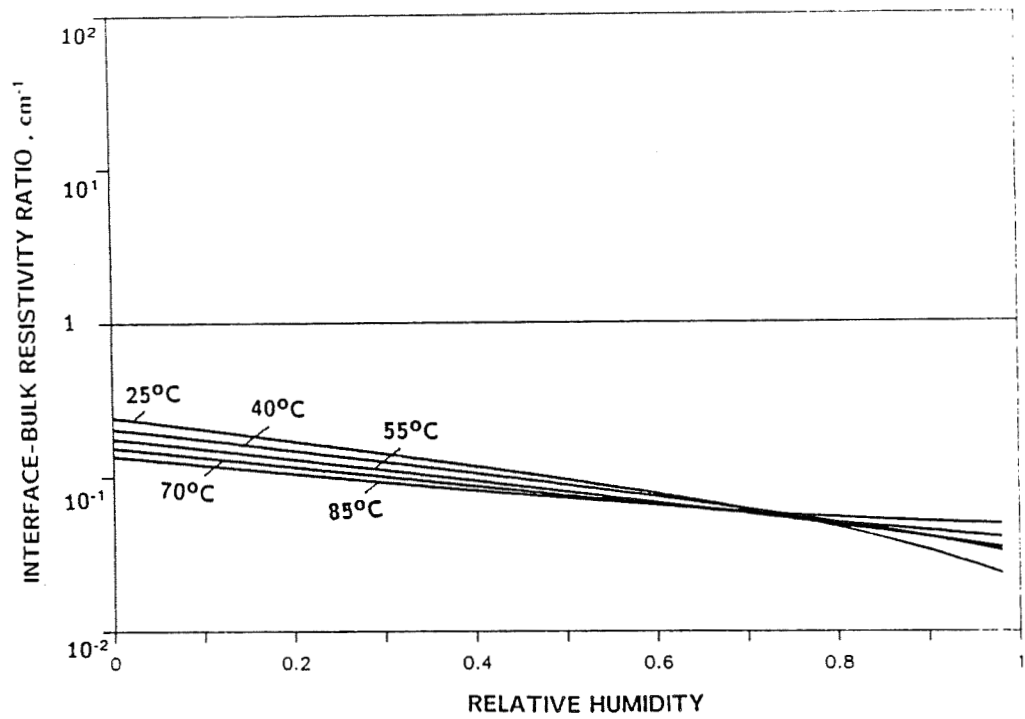
Ionic Conduction Characteristics



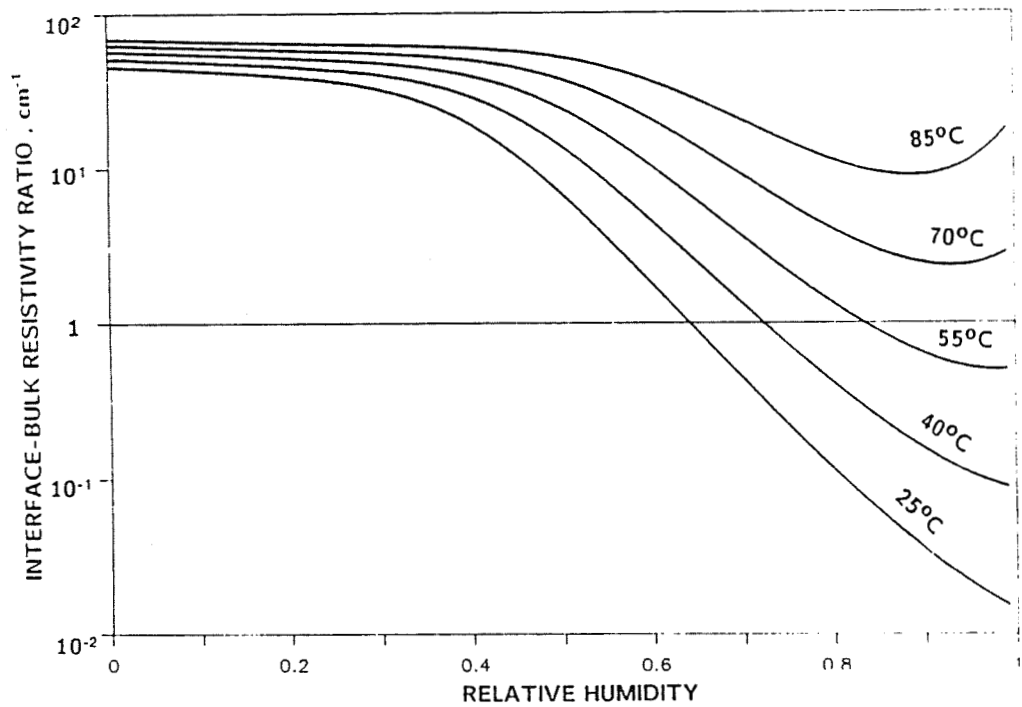
Ionic Conductivities and Their Temperature-Humidity Sensitivities

	Magnitude	Temperature sensitivity	Humidity sensitivity
• Bulk encapsulants			
• PVB	High	High	High
• EVA	Low	Modest	Low
• Encapsulant free surface			
• PVB	High	Very low	High
• EVA	Very low	Low	Modest
• Encapsulant-glass interface			
• PVB	High	Low	High
• EVA	Modest	Modest	Modest

EVA Resistivity Ratio



PVB Resistivity Ratio



Leakage-Current Sensitivity

- Exposed low-conductivity encapsulant (EVA)
 - Key contributor to module leakage-resistance is bulk resistivity of encapsulant between cell and interface
 - High temperature sensitivity
 - Low humidity sensitivity
- Exposed high-conductivity encapsulant (PVB)
 - Key contributors to module leakage resistance are resistivity of interfaces and free surfaces
 - Low temperature sensitivity
 - high humidity sensitivity
- Foil-protected encapsulant
 - Key contributor to module leakage-resistance is bulk resistivity of encapsulant between cell and foil
 - High temperature sensitivity
 - Humidity sensitivity depends on edge seal

Summary

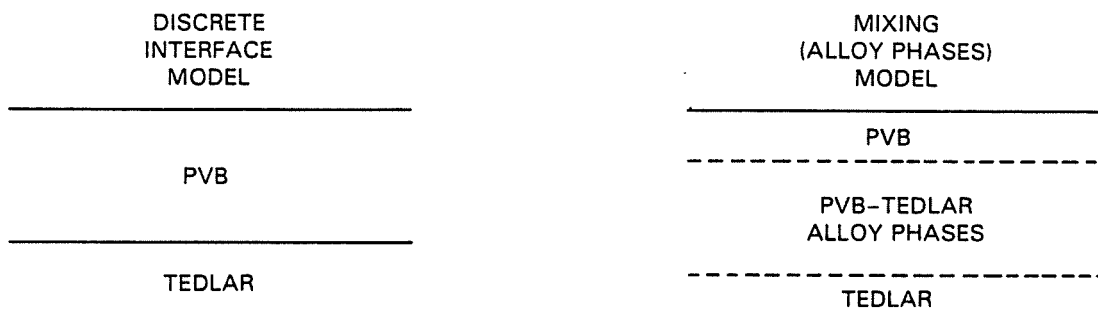
- Have achieved fairly good fundamental understanding of leakage-current paths internal to module and their temperature-humidity sensitivities
- Evaluation of the acceleration factor between test chamber and field condition is a very complex process
- Research areas
 - Effect of liquid water versus water vapor
 - Effect of polymer aging on encapsulant sorption-conductivity properties
 - Non-isothermal and non-equilibrium conditions
 - Transient permeation of moisture
 - Non-equilibrium moisture states

WATER PERMEATION AND ELECTRICAL PROPERTIES OF POTTANTS, BACKINGS, AND POTTANT/BACKING COMPOSITES

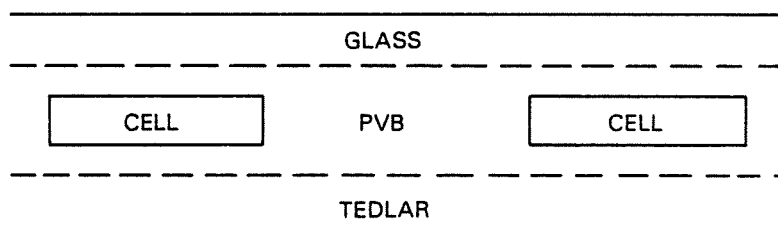
WILKES COLLEGE

J. Orehtsky

Laminates



FOR PATH OF LEAST RESISTANCE IN



Electrical Properties

- Pottants (PVB, EMA, EVA)
- Backing (Tedlar, Mylar)
- Composites (PVB/T, EMA/T, EVA/T)

Object

To Examine Interfacial Effects
by
Evaluating

- DC Dielectric Constant (K)
- AC Dielectric Constant (K)
- Leakage Resistance (R)

of

Pottants (PVB, EMA, EVA)

Backing (Tedlar, Mylar)

Composites (PVB/T, EMA/T, EVA/T)

Theory

Discrete Interface Model

$$K_{p/b} = \frac{K_p K_b [t_p + t_b]}{K_p t_b + K_b t_p}$$

$$R_{p/b} = \frac{\rho_p t_p + \rho_b t_b}{A}$$

DC Dielectric Constant by Charge Measurements Before and After Dipole Alignment

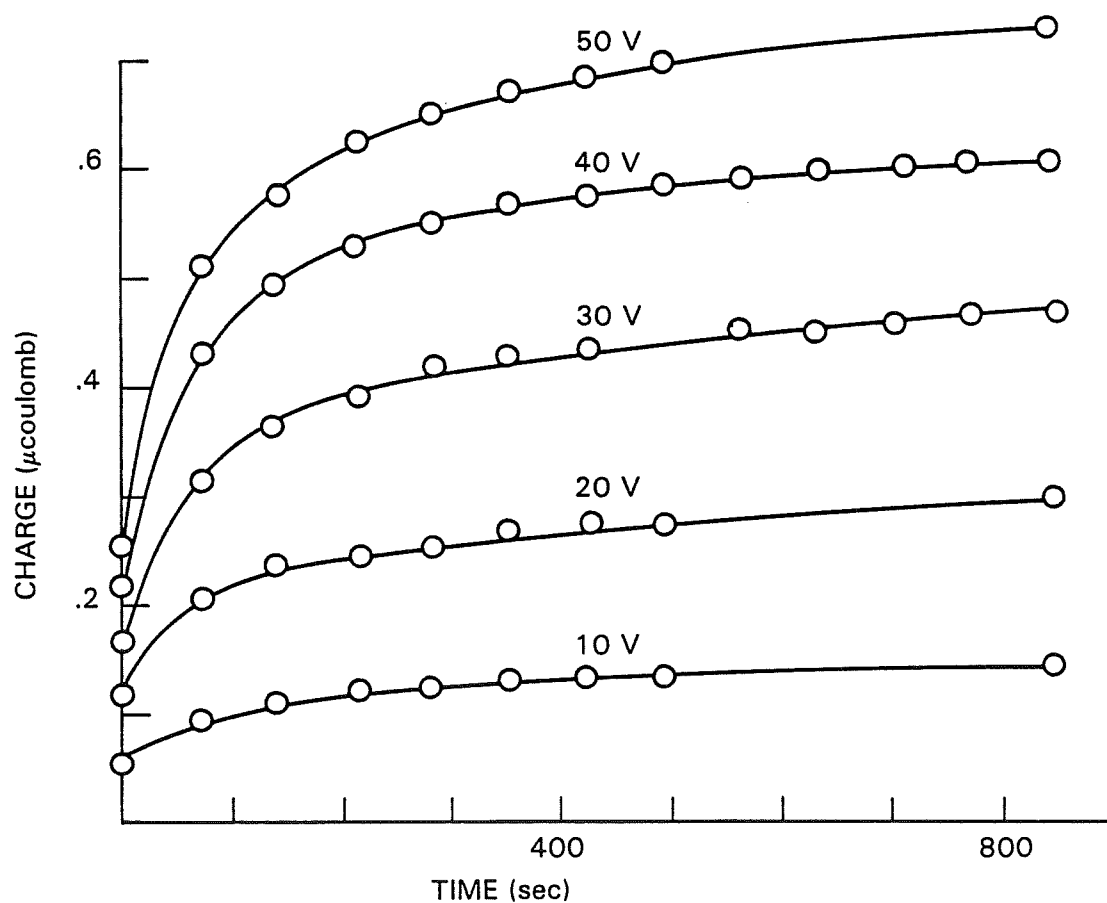
Before:

$$K_i = \frac{[dQ_i/dV_A]t}{\epsilon_0 A}$$

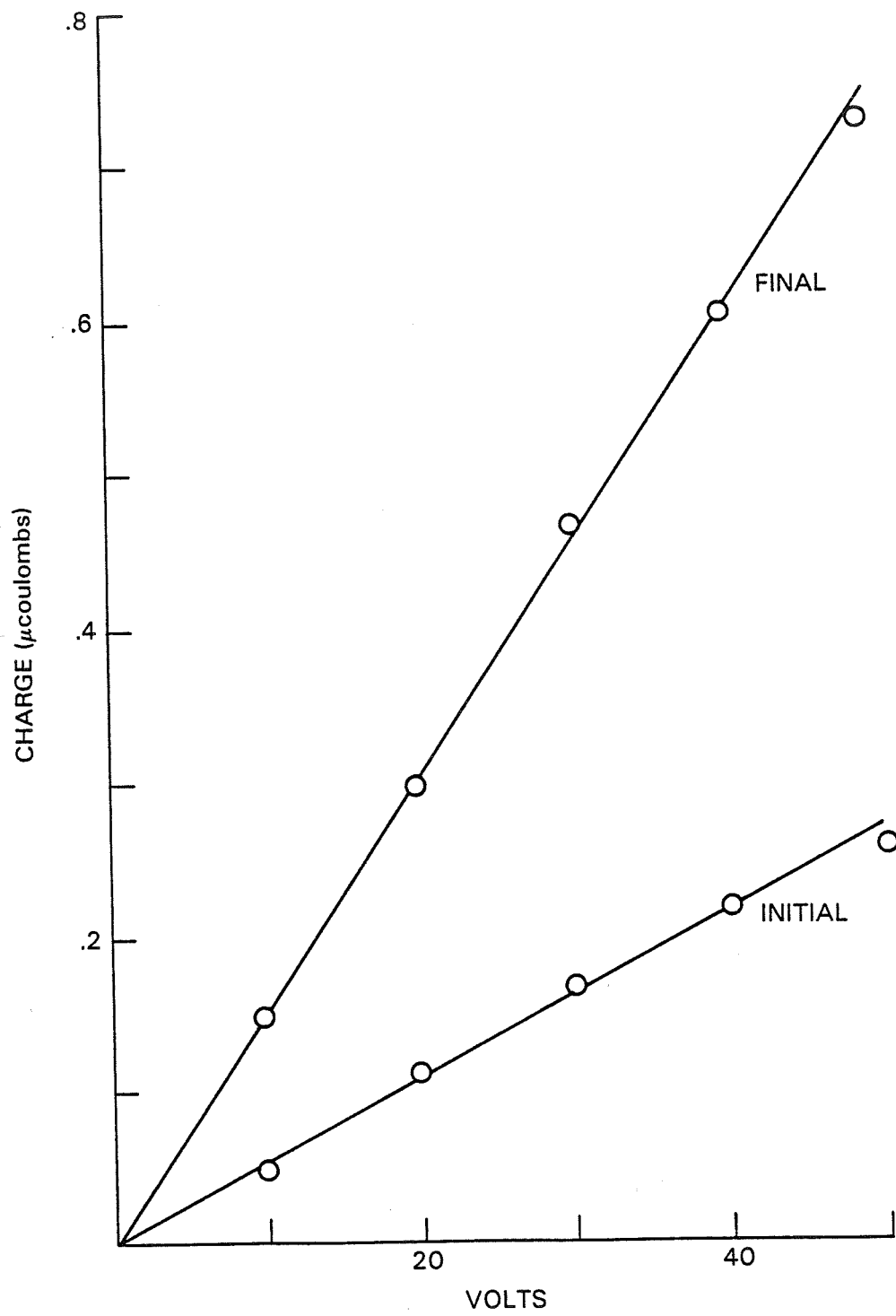
After:

$$K_f = \frac{[dQ_f/dV_A]t}{\epsilon_0 A}$$

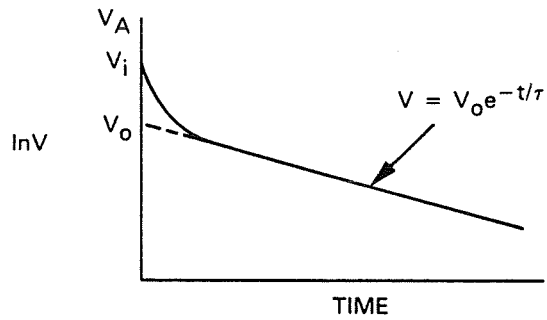
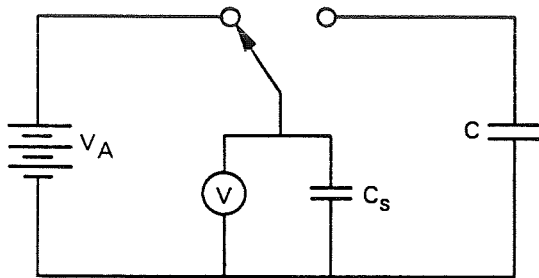
TEDLAR



TEDLAR

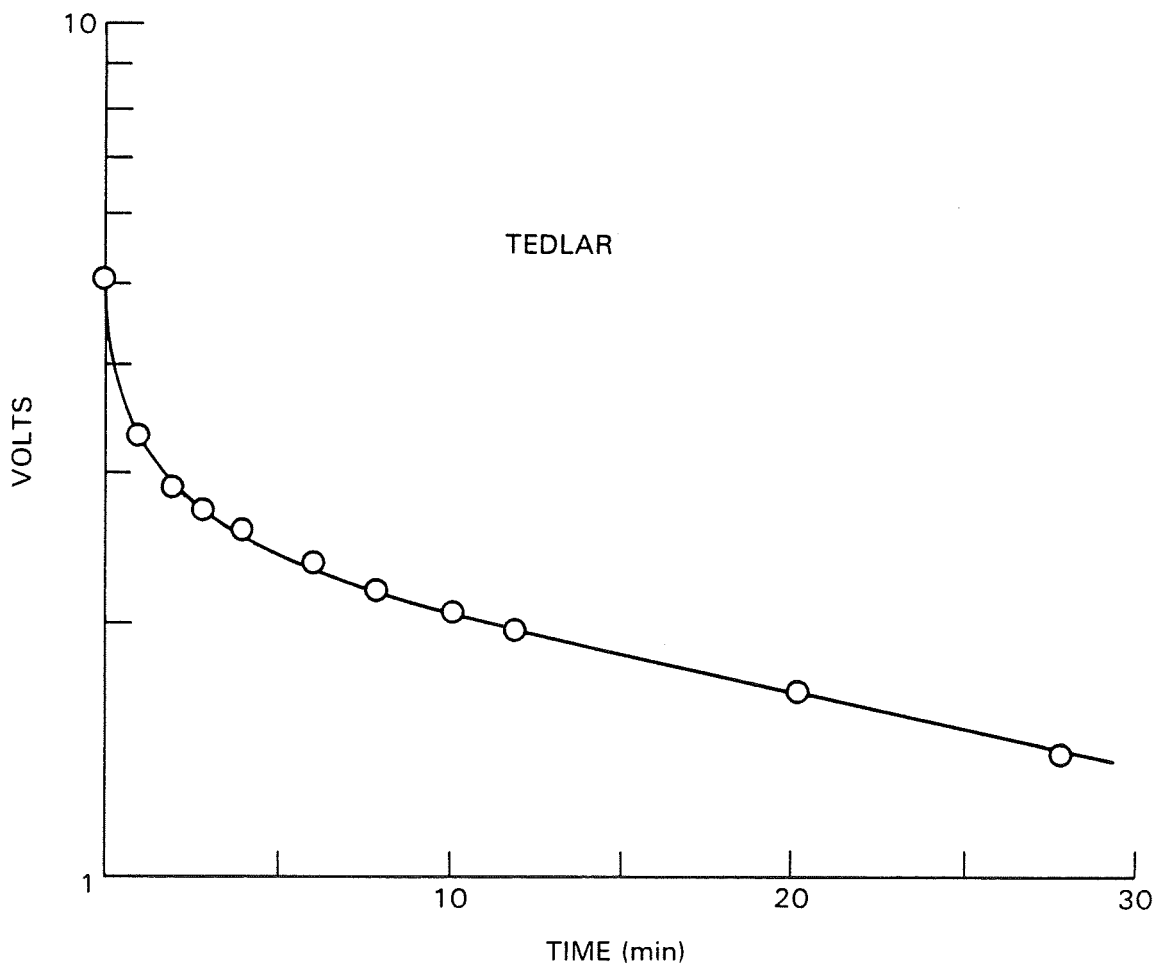


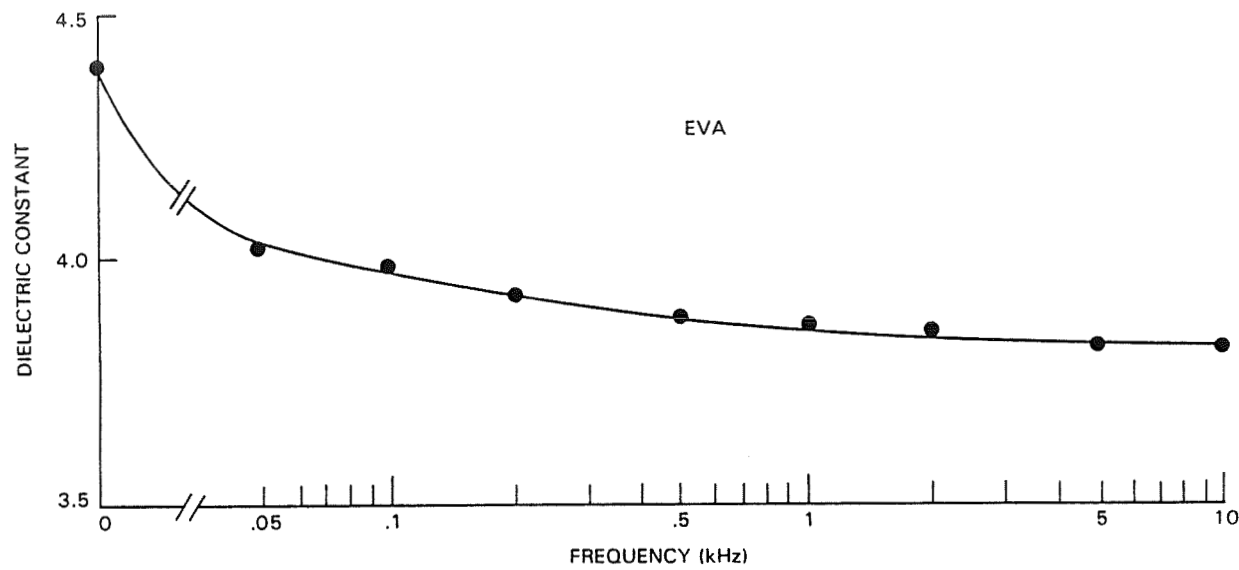
DC Dielectric Constant by Voltage Measurements Using Charge Transfer from Standard Capacitor (C_S)



$$K_i = \frac{C_s t}{\epsilon_0 A} \left[\frac{V_A - V_i}{V_i} \right]$$

$$K_f = \frac{\tau}{\epsilon_0 A} \left[\frac{\tau}{R} - C_s \right]$$





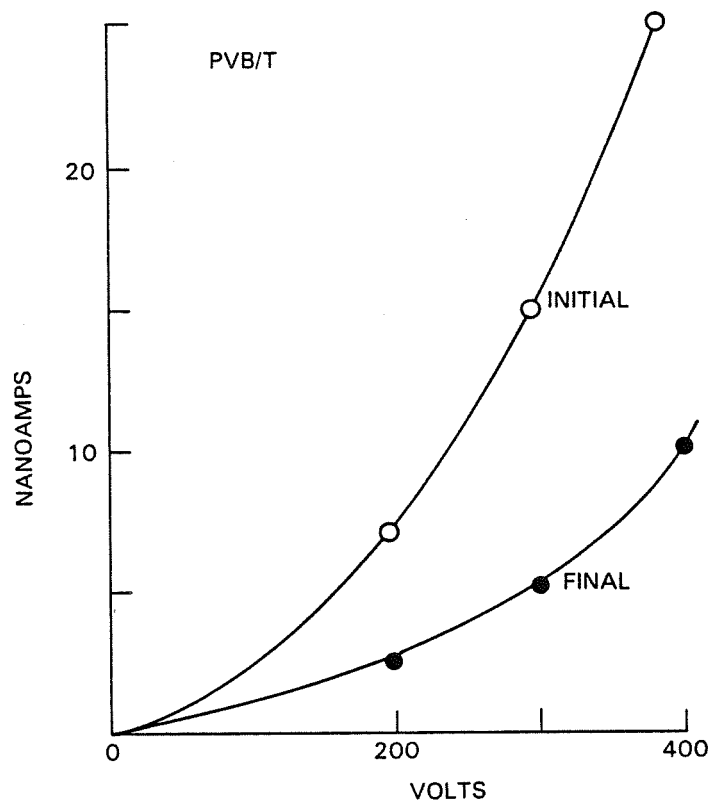
Results

Dielectric Constant

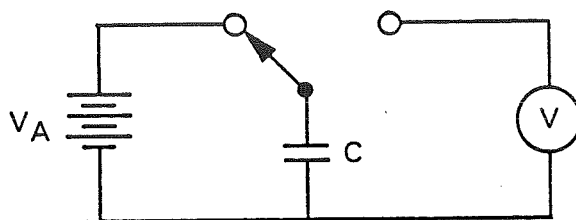
	DC						AC	
	Before			After			1 kHz	Calc.
	<u>Q</u>	<u>V</u>	<u>Calc.</u>	<u>Q</u>	<u>V</u>	<u>Calc.</u>		
PVB	—	6.0		—	8.0		8.7	
EMA	4.3	4.7		4.3	7.1		3.1	
EVA	5.2	4.3		9.4	10.0		3.9	
Tedlar	4.5	4.3		12.7	12.0		3.7	
Mylar	1.3	1.4		—	—		—	
PVB/T	9.1	8.2	5.7	—	—	8.4	4.8	7.3
EMA/T	4.0	3.2	4.3	—	4.7	4.7	3.1	3.1
EVA/T	4.4	4.7	4.7	—	—	9.9	3.7	3.9

Leakage Resistance by Current-Voltage Measurements and Ohm's Law

$$R = dV_A/JI$$

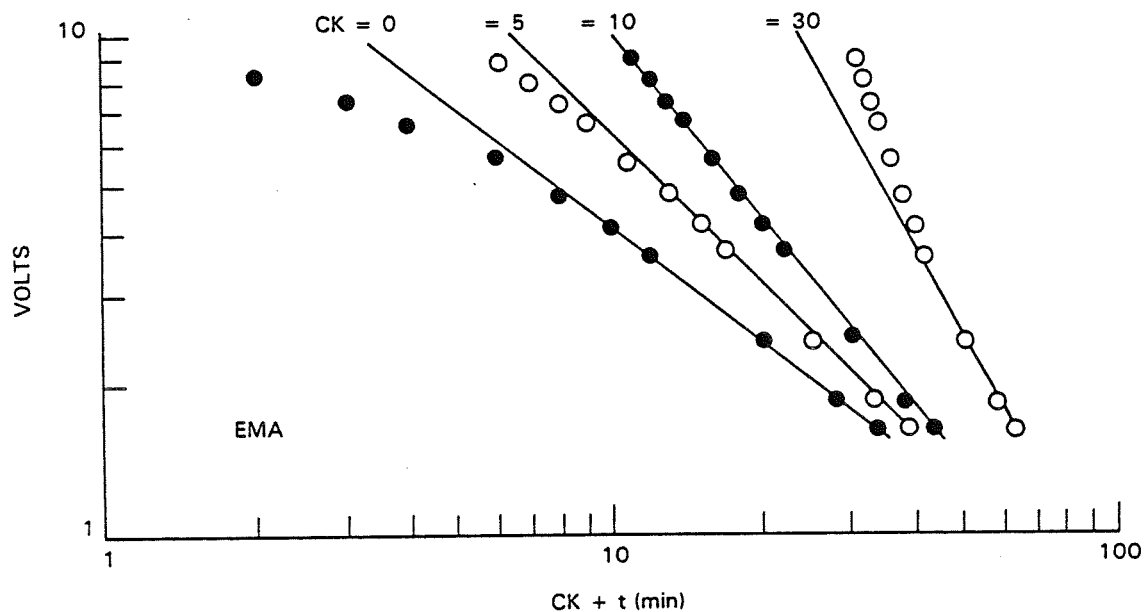


Leakage Resistance by Voltage Decay of a Capacitor



THEORY:

$$V = V_0 CK^{K/R} [CK + t]^{-K/R}$$

Results: Leakage Resistance (Ω)

	<u>Ohm's Law</u>	<u>Voltage Decay</u>	<u>Calc.</u>
PVB	$1.0(10^7)$	$0.4(10^7)$	
EMA	$1.0(10^{12})$	$0.9(10^{12})$	
EVA	$0.4(10^{11})$	$4.6(10^{11})$	
Tedlar	$3.5(10^{11})$	$2.0(10^{11})$	
Mylar	—	$1.4(10^{13})$	
PVB/T	$0.2(10^{12})$	$6.8(10^9)$	$3.4(10^{12})$
EMA/T	$0.3(10^{13})$	$2.3(10^{13})$	$0.1(10^{13})$
EVA/T	$0.3(10^{12})$	$0.8(10^{12})$	$3.4(10^{12})$

Results: Leakage Resistivities ($\Omega\cdot m$)

PVB	$3(10^7)$
EVA	$5(10^{11})$
EMA	$1(10^{13})$
Tedlar	$4(10^{14})$
Mylar	$2(10^{15})$

Results: Are They Consistent with Discrete Interface Model?

Test	Composite Material		
	<u>EVA/T</u>	<u>EMA/T</u>	<u>PVB/T</u>
DC diel.	Yes	Yes	No
AC diel.	Yes	Yes	No
Resis.	No	Yes	No

Summary

- EMA/T Obeys Discrete Interface Model
- PVB/T Does Not Obey Discrete Interface Model
- Order of Increasing Leakage is Mylar, Tedlar, EMA, EVA, PVB
- Charged Capacitor-Voltage Decay Kinetics Obey Theoretically Predicted Relationship:

$$V = V_0 CK^{K/R} [CK + t]^{-K/R}$$

Water Permeation

- Pottants (PVB, EMA, EVA)
- Backing (Tedlar, Mylar)
- Composites (PVB/T, EMA/T, EVA/T)

Object

Theoretically and Experimentally Evaluate

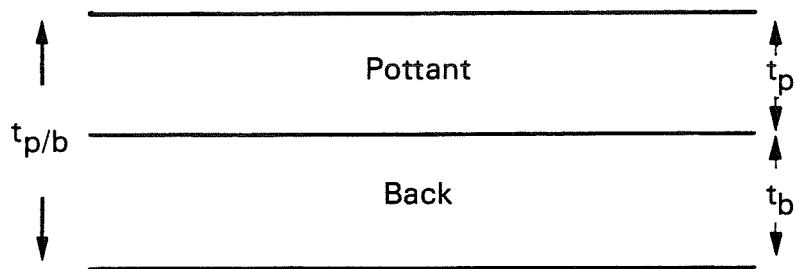
- Temperature Dependence of
 J (water flux)
 and
 P (water permeability)
 in
 Pottants (p) and Backing (b)
- $P_{p/b}$ of p/b Composite in terms of
 P_p and P_b

Theory: Condensation — Self Diffusion — Evaporation Model for Pottants and Backing

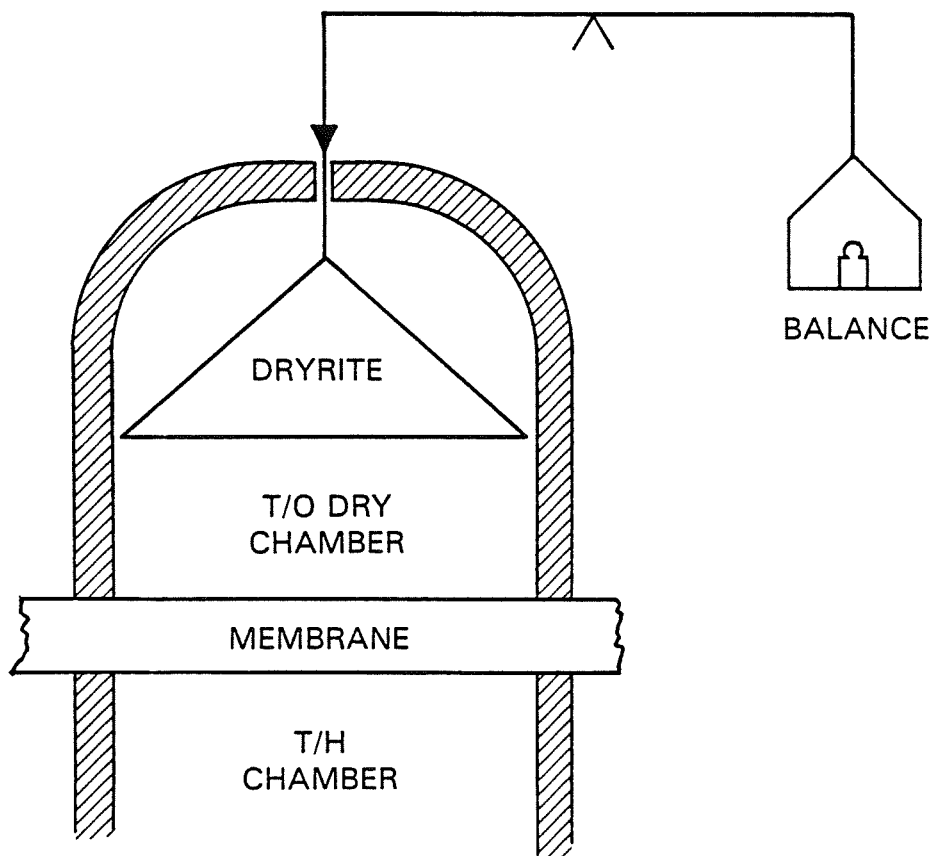
- $P_T = P_0 \exp(-Q_p/RT)$
 $Q_p = 4.6 \text{ Kcal/mole}$ (water self-diffusion activation energy)
- $J T^{6.5} = J_0 \exp(-Q_J/RT)$
 $Q_J = 4.6 + 9.8 = 14.4 \text{ Kcal/mole}$
 $\left(\begin{array}{cc} \text{water} & \text{water heat} \\ \text{self-} & \text{of} \\ \text{diffusion} & \text{vaporization} \end{array} \right)$
 $J_0 \sim S$ (water solubility parameter)

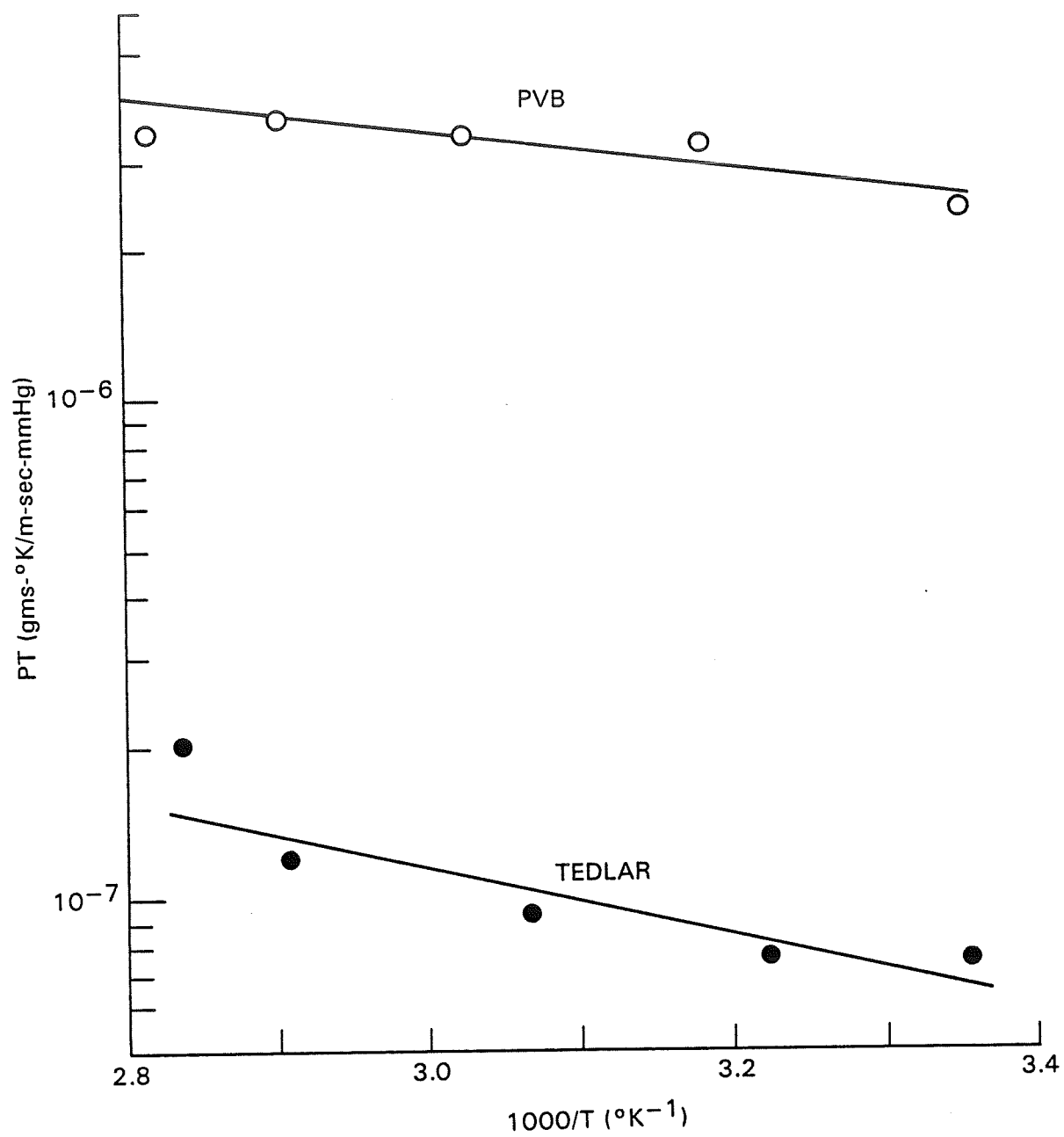
Theory: Discrete Interface Model for Composites (p/b)

$$P_{p/b} = \frac{t_{p/b} P_p P_b}{P_p t_b + P_b t_p}$$

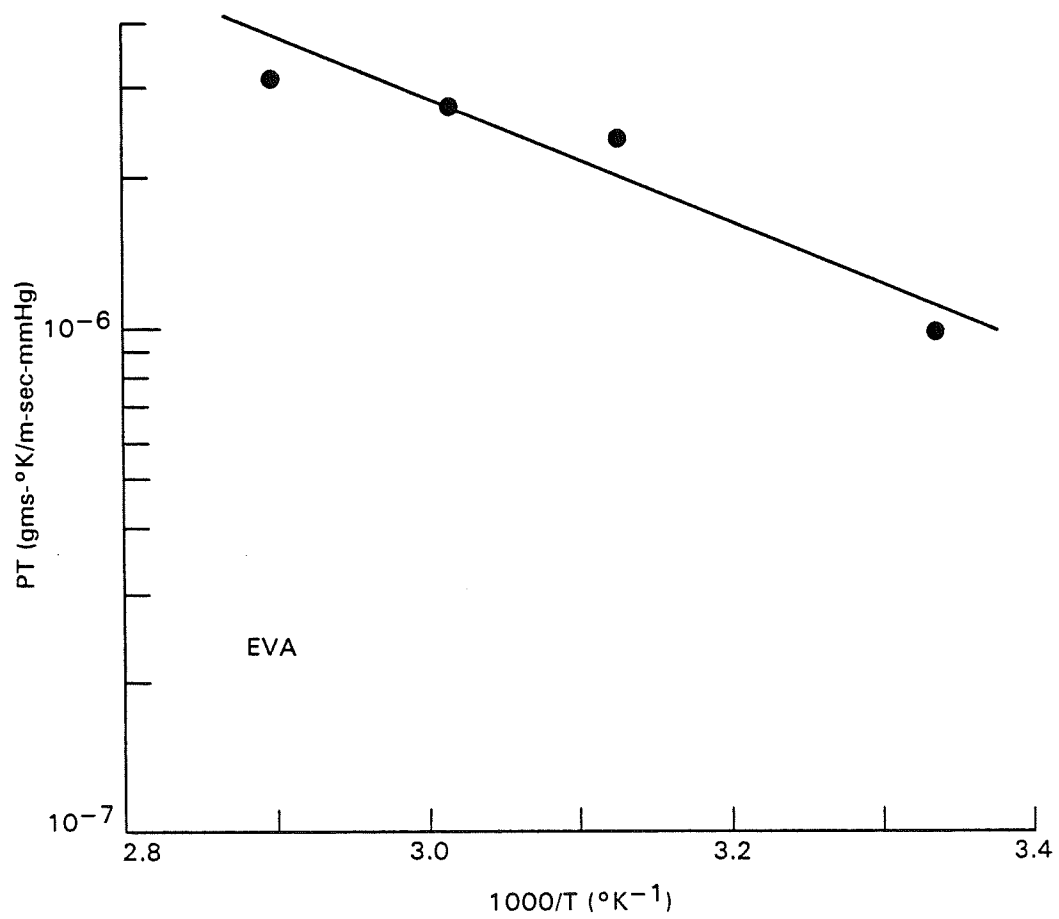
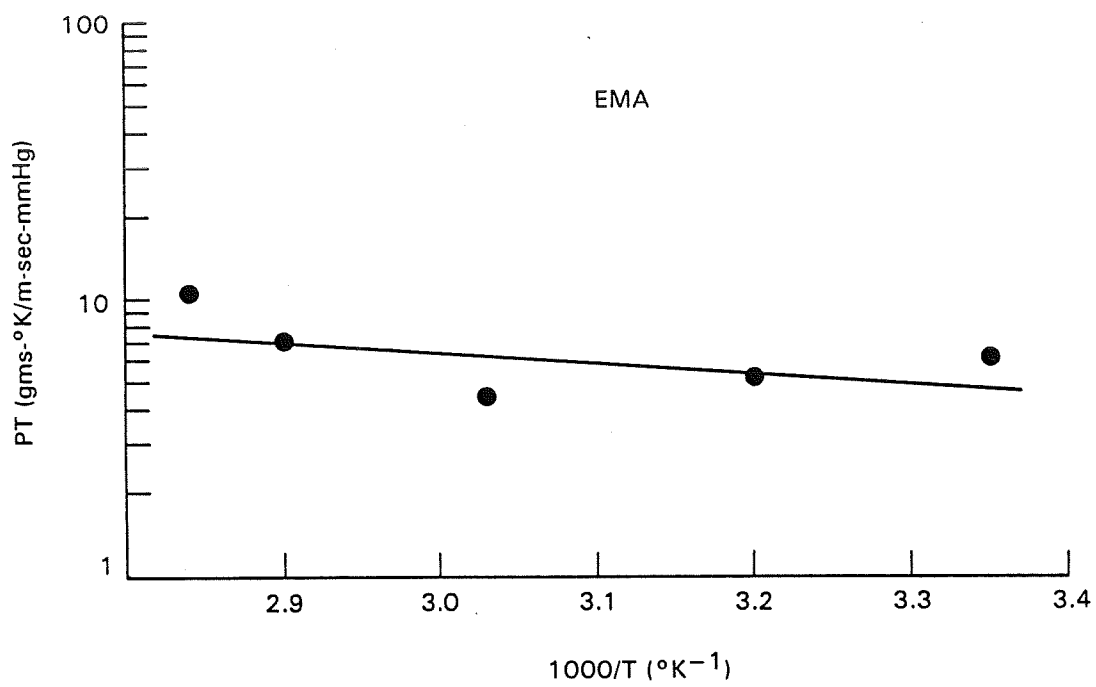


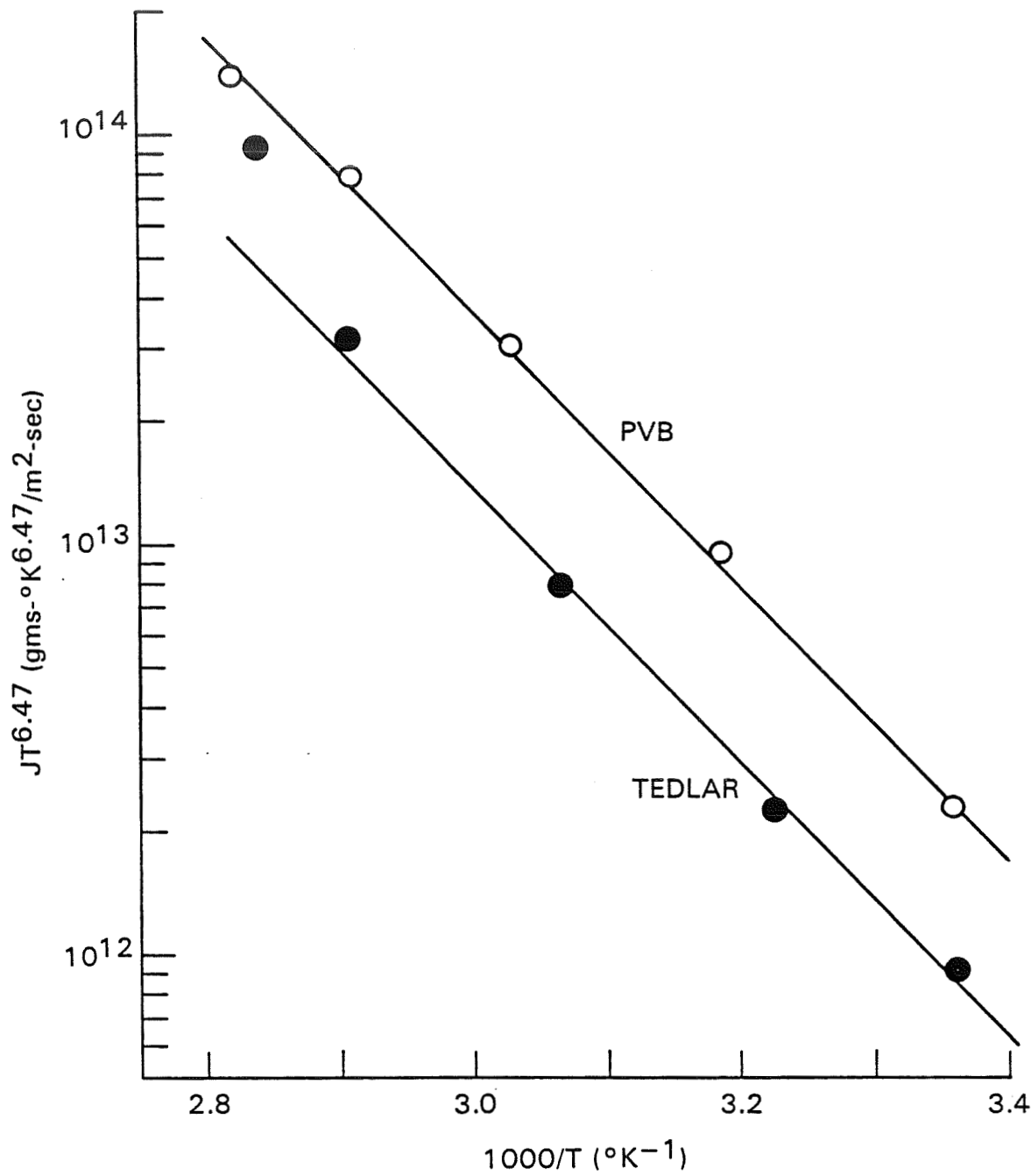
Experimental Arrangement

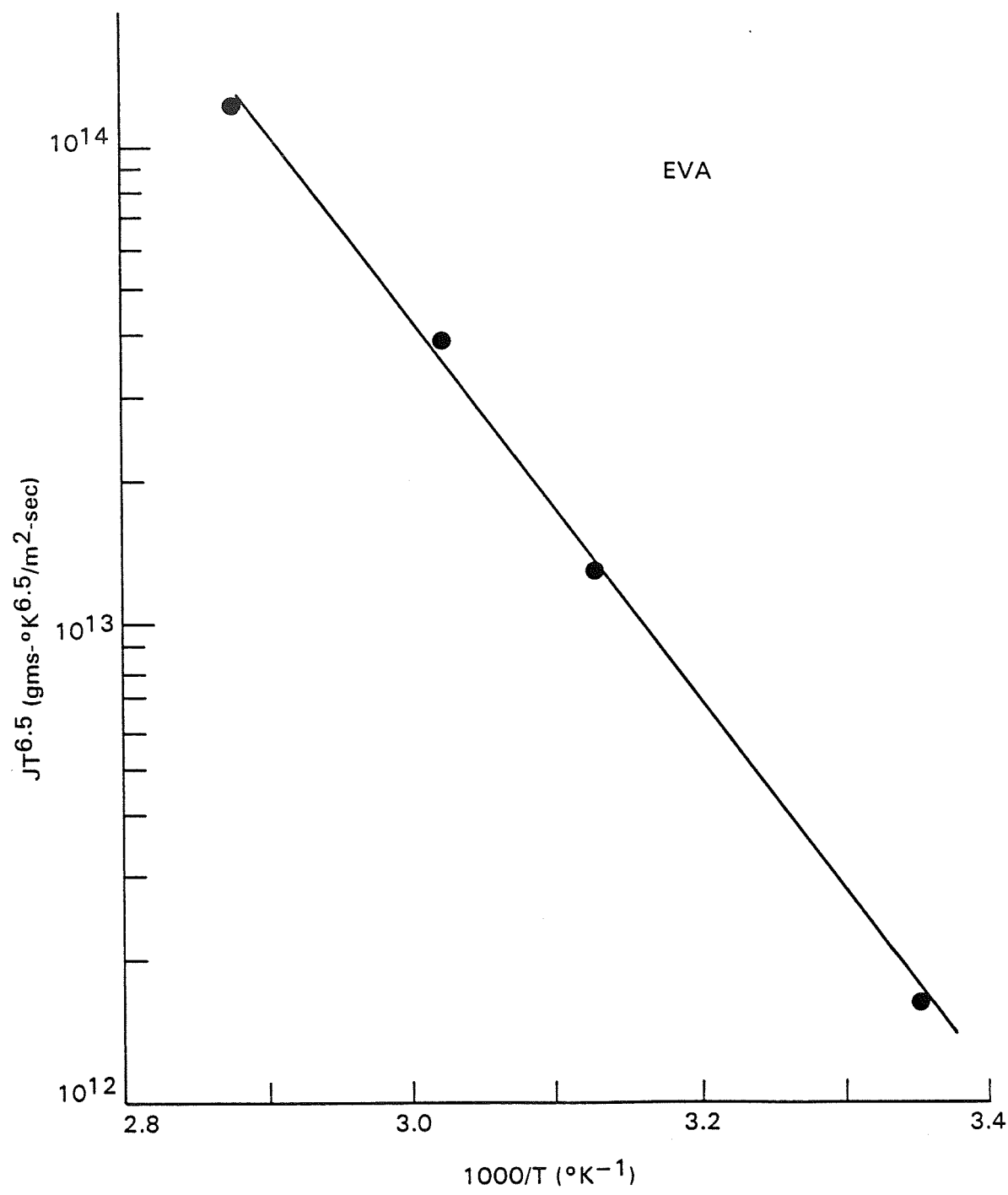


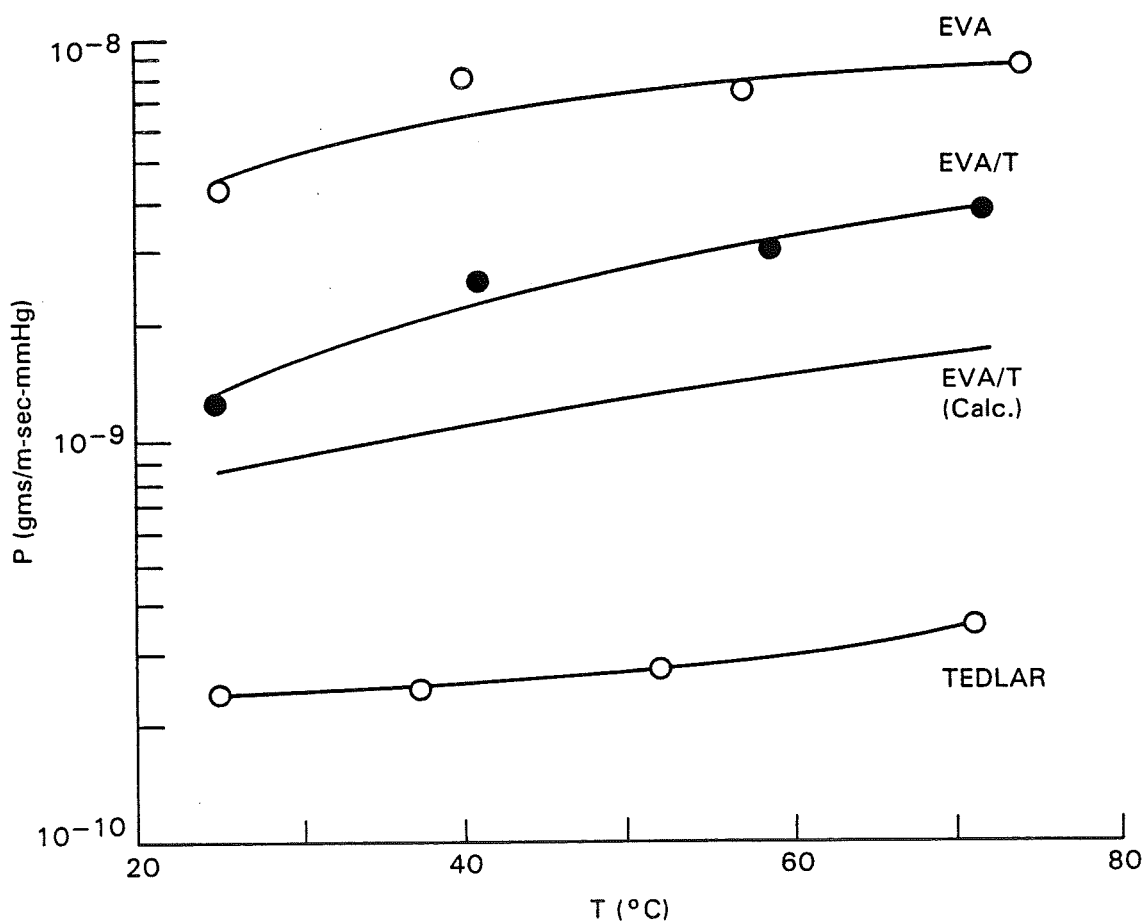
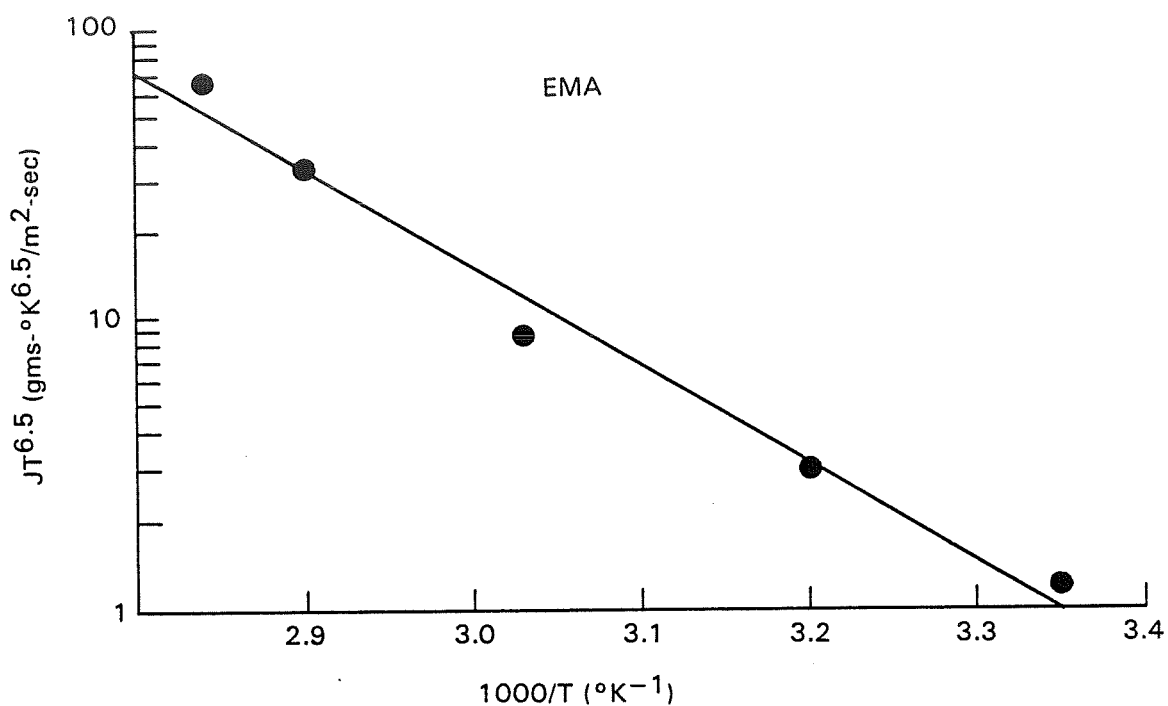


RELIABILITY PHYSICS









Results

	Activation Energy (Kcal./mole)		Solubility Parameter
	<u>Q_P</u>	<u>Q_J</u>	<u>S</u>
Tedlar	~ 2.9	15	.614
EMA	~ 3.1	15	5.2
PVB	~ 1.4	15	175
EVA	~ 2.8	18	730
Theoretical	4.6	14.4	—

Results

	Permeability $P \times 10^9$ <u>(gms/m-sec-mmHg)</u>	Thickness $d \times 10^6$ <u>(m)</u>	Resistance $R \times 10^5$ <u>(m²-sec-mmHg/gm)</u>
Tedlar	0.2	63	3.1
EMA	2.0	480	2.4
EVA	4.0	470	1.2
PVB	8.0	803	1.0

Results

Composites at 25°C

Permeability $P \times 10^9$
(gms/m-sec-mmHg)

	<u>Experimental</u>	<u>Calculated</u>
PVB/T	1.6	1.5
EMA/T	2.0	1.0
EVA/T	1.1	0.8

Conclusions

- $P_T < P_{EMA} < P_{EVA} < P_{PVB}$
- Temperature dependence of J and P for PVB, EMA, and T is consistent with evaporation–self diffusion–condensation model
- P of PVB/T composite is consistent with discrete interface model
- Water solubility: greatest in PVB, least in Tedlar

SILICON MATERIALS

Ralph Lutwack, Chairman

The session on Silicon Materials consisted of two presentations.

JPL reviewed the FSA-sponsored Workshop on Low-Cost Polysilicon for Terrestrial Photovoltaic Solar Cell Applications which was held in Las Vegas, Nevada, October 28-30, 1985.

Union Carbide Corp. (UCC) reported on their development of fluidized-bed reactor technology for producing silicon by the pyrolysis of silane. The technical effort on this program was completed.

REVIEW OF THE WORKSHOP ON LOW-COST POLYSILICON FOR TERRESTRIAL PHOTOVOLTAIC SOLAR CELL APPLICATIONS

JET PROPULSION LABORATORY

R. Lutwack

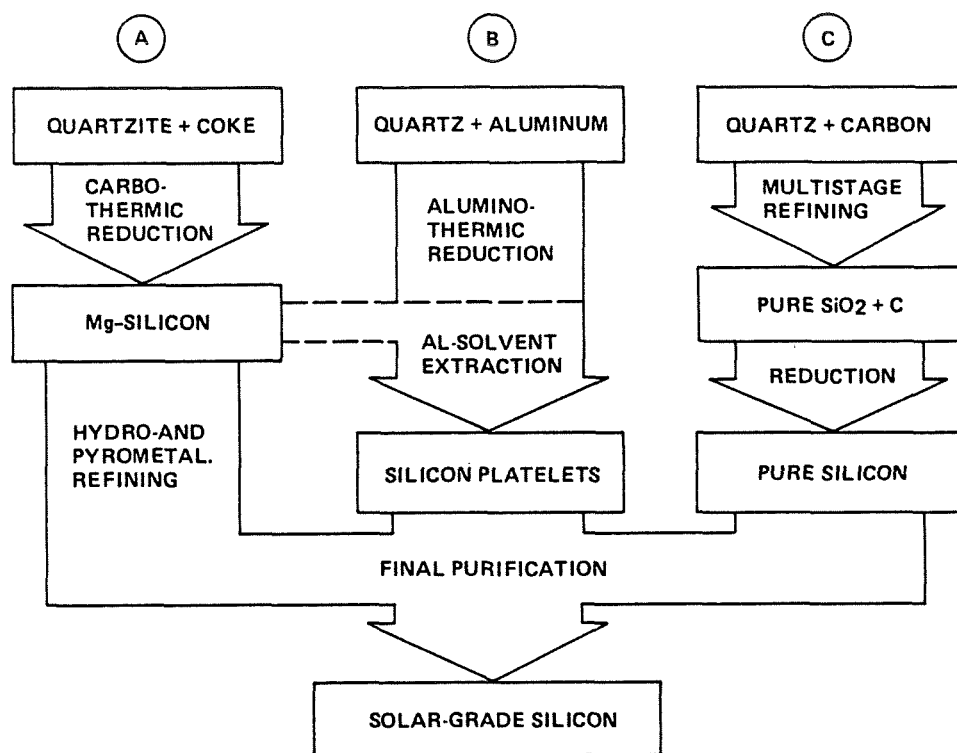
- SILICON MATERIAL TASK OF THE DOE/FSA PROJECT
R. LUTWACK, CHAIRMAN (JET PROPULSION LABORATORY)
- SESSION I: POLYSILICON MATERIAL REQUIREMENTS
CHAIRMAN: J. McCORMICK (HEMLOCK SEMICONDUCTOR CORP.)
 - EFFECTS OF IMPURITIES ON SILICON SOLAR CELL PERFORMANCE
R. HOPKINS (WESTINGHOUSE R&D CENTER)
 - REQUIREMENTS FOR HIGH-EFFICIENCY SOLAR CELLS
C.T. SAH (UNIVERSITY OF ILLINOIS)
- SESSION II: ECONOMICS
CHAIRMAN: R. PELLIN (CONSULTANT)
 - ECONOMICS OF THE POLYSILICON PROCESS: A VIEW FROM JAPAN
Y. SHIMIZU (OSAKA TITANIUM CO., LTD.)
 - ECONOMICS OF POLYSILICON PROCESSES
C. YAWS (LAMAR UNIVERSITY)
 - SENSITIVITY ANALYSIS FOR SOLAR PANELS
R. ASTER (JET PROPULSION LABORATORY)
- SESSION III: PROCESS DEVELOPMENTS IN THE USA
CHAIRMAN: P. MAYCOCK (PV ENERGY SYSTEMS)
 - DEVELOPMENT OF THE SILANE PROCESS FOR THE PRODUCTION OF
LOW-COST POLYSILICON
S. IYA (UNION CARBIDE CORP.)
 - FLUIDIZED-BED DEVELOPMENT AT JET PROPULSION LABORATORY
G. HSU (JET PROPULSION LABORATORY)
 - FLUIDIZED-BED REACTOR MODELING FOR PRODUCTION OF SILICON
BY SILANE PYROLYSIS
M. DUDUKOVIC (WASHINGTON UNIVERSITY AT ST. LOUIS)
 - SILICON PRODUCTION IN AN AEROSOL REACTOR
R. FLAGAN (CALIFORNIA INSTITUTE OF TECHNOLOGY)

PRECEDING PAGE BLANK NOT FILMED

SILICON MATERIALS

- SESSION IV: PROCESS DEVELOPMENTS, INTERNATIONAL
CHAIRMAN: R. LUTWACK (JET PROPULSION LABORATORY)
 - PROCESSES AND PROCESS DEVELOPMENTS IN JAPAN
T. NODA (OSAKA TITANIUM CO., LTD.)
 - PROCESSES AND PROCESS DEVELOPMENTS IN TAIWAN
H-L. HWANG (NATIONAL TSING HUA UNIVERSITY)
 - REFINING OF METALLURGICAL-GRADE SILICON
J. DIETL (HELIOTRONICS GmbH)
 - SOLAR-GRADE SILICON PREPARED BY CARBOTHERMIC REDUCTION OF SILICA
H. AULICH (SIEMENS AG)
 - A METALLURGICAL ROUTE TO SOLAR-GRADE SILICON
A. SCHEI (ELKEM A/S, R&D CENTER)
 - SOLAR SILICON FROM DIRECTIONAL SOLIDIFICATION OF MG SILICON PRODUCED VIA THE SILICON CARBIDE ROUTE
M. RUSTIONI (ENICHIMICA)
- SESSION V: CHAIRMAN: A. BRIGLIO (JET PROPULSION LABORATORY)
 - CHARACTERIZATION OF SOLAR-GRADE SILICON PRODUCED BY THE SiF_4 -Na PROCESS
A. SANJURJO (SRI INTERNATIONAL)
 - A SILANE-BASED POLYSILICON PROCESS
P. GRAYSON (EAGLE-PICHER INDUSTRIES, INC.)
 - SILICON PURIFICATION USING A Cu-Si ALLOY SOURCE
R. POWELL (SOLAR ENERGY RESEARCH INSTITUTE)
 - FORUM: POLYSILICON PROCESS TECHNOLOGY
CHAIRMAN: H. AULICH (SIEMENS AG)

Different Approaches to Large-Scale Production of Solar-Grade Silicon



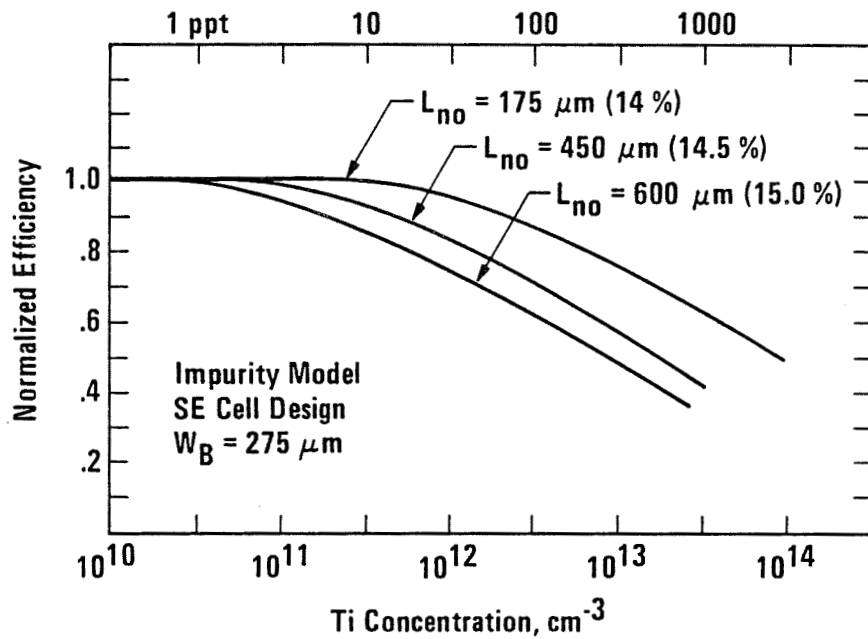
(J. DIETL, WACKER HELIOTRONIC)

- SESSION VI: POLYSILICON MARKET AND FORECASTS
CHAIRMAN: M. PRINCE (U. S. DEPARTMENT OF ENERGY)
- SEMICONDUCTOR MARKET
R. PELLIN (CONSULTANT)
- SILICON REQUIREMENTS OF THE PHOTOVOLTAIC SOLAR CELL MARKET
P. MAYCOCK (PV ENERGY SYSTEMS)
- FORUM: POLYSILICON MARKETS
CHAIRMAN: J. LORENZ (CONSULTANT)

Key Discussion Topics During Forums

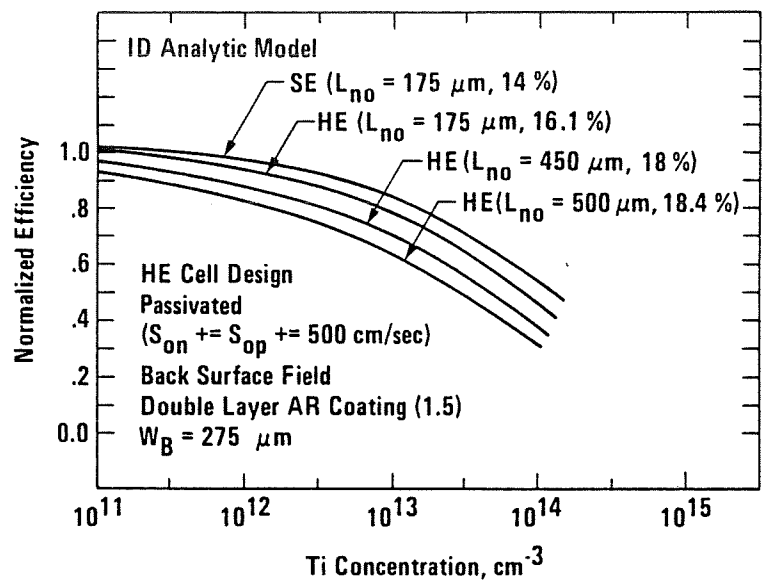
- PRIMARY OBJECTIVE - LOW COST Si vs HIGH CELL EFFICIENCY
- PROCESS DEVELOPMENT OBJECTIVE - CVD Si vs SOLAR GRADE Si
- COMPETITION FROM AMORPHOUS Si
- Si SOURCE - SCRAP Si vs LOW COST Si

Cell Efficiency Variation with Titanium Concentration for Various Initial Base Diffusion Lengths



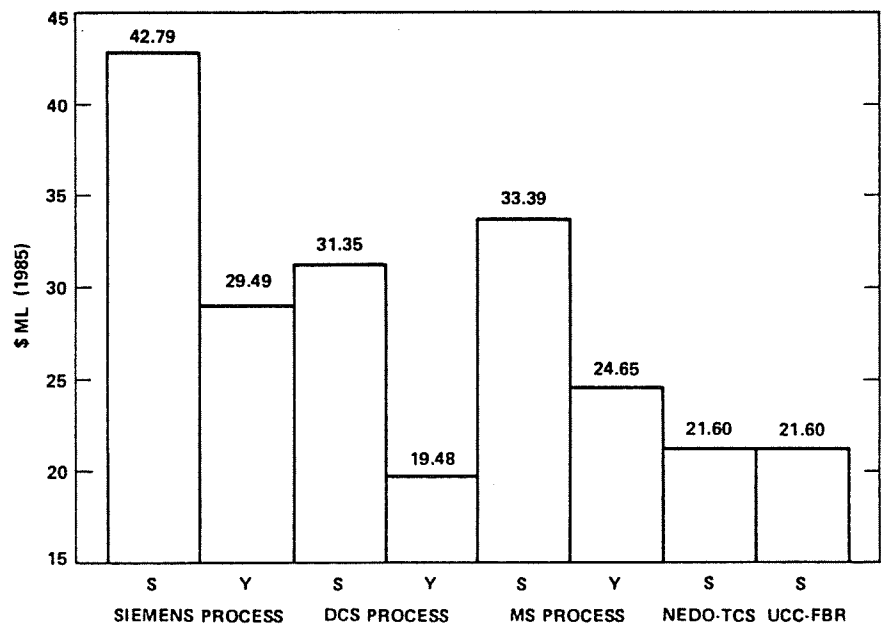
(R. HOPKINS, WESTINGHOUSE RESEARCH CENTER)

Variation in Cell Performance with Titanium Concentration:
High-Efficiency Cell Design



(R. HOPKINS, WESTINGHOUSE RESEARCH CENTER)

Product Costs of Polysilicon Processes



(Y. SHIMIZU, OSAKA TITANIUM CO., LTD.)
(C. YAWS, LAMAR UNIVERSITY)

Comparisons of Analyses

	SiH ₄ -CVD			SiH ₂ Cl ₂ -CVD		
	Y	S	Δ	Y	S	Δ
UTILITIES*	3.87	7.60	3.73	4.86	10.20	5.34
LABOR	1.90	1.80	-.1	1.37	1.80	.43
RAW MATERIALS	2.91	3.94	1.03	3.34	4.52	1.18
OVERHEAD	1.81	3.20	1.39	1.20	2.98	1.78
GENERAL	3.21	4.36	1.15	2.54	4.09	1.55
	Σ Δ		7.21			10.28
PRODUCT COST	24.65	33.39	8.74	19.48	31.35	11.87
* SHIMIZU (S)	6¢/kwh					
YAWS (Y)	5¢/kwh					

Silicon Granule Manufacturing Results (1984)

ITEMS		TARGETS	RESULTS	
			OVERALL *	BEST **
TOTAL REACTION TIME	(hr)	--	4,377	632
MANUFACTURED Si	(kg)	--	8,349	1,504.7
TCS CONCENTRATION	(%)	--	36.5	42.3
POWER CONSUMPTION	(kwh/kg. Si)	30	28.32	21.30
TCS CONSUMPTION	(kg/kg. Si)	20	18.72	18.94
Si YIELD	(%)	20	18.3	21.5

* YEARLY PERFORMANCE

** BEST PERFORMANCE

(T. NODA, OSAKA TITANIUM CO., LTD.)

SILICON MATERIALS

Worldwide Module Sales (Factory Prices - 1985\$)

	<u>1983</u>	<u>1984</u>	<u>1985</u>	<u>1986</u>	<u>1988</u>	<u>1990</u>	<u>1995</u>	<u>MT</u>	<u>Si</u>
MWp	22	22	26	60 (1) 35 (2)	150 50	300 * 107 *	975 * 310 *	(5850 MT)	(1116 MT)
\$/Wp	8	7	6.50	5 (1) 6 (2)	4 5	3 4.50	2 3		
\$(M)	176	155	170	300 (1) 210 (2)	600 250	900 480	1950 930		

(1) U. S. TAX CREDITS EXTENDED TO 1989

(2) U. S. TAX CREDITS EXPIRE AFTER 1985

* INCLUDES JAPANESE GRID-CONNECTED PV POWERED HOUSES

(P. MAYCOCK, CONSULTANT)

A Free World Forecast for Silicon Material

<u>YEAR</u>	<u>SILICON DEVICE USAGE \$</u>	<u>SINGLE CRYSTAL METRIC TONS</u>	<u>POLYSILICON USAGE METRIC TONS</u>	<u>POLYSILICON CAPACITY METRIC TONS</u>
1974	5,750	522	871	
1975	5,170	533	921	
1976	6,545	702	1,170	
1977	8,610	796	1,326	2,395
1978	9,905	1,001	1,668	2,445
1979	11,900	1,289	2,148	2,740
1980	14,120	1,387	2,312	3,760
1981	15,100	1,515	2,568	4,410
1982	16,460	1,793	3,092	5,270
1983	20,822	2,718	4,853	5,650
1984	30,124	3,090	5,617	6,060
1985	25,000	3,039	5,525	6,470
1986	29,000	3,781	6,875	8,540
1987	38,000	4,957	9,013	9,320
1988	50,000	5,647	10,457	12,520
1989	65,000	7,860	14,292	15,120
1990	80,300	9,936	18,067	16,820

(R. PELLIN, CONSULTANT)

POLYCRYSTALLINE SILICON RESEARCH AND
DEVELOPMENT

UNION CARBIDE CORPORATION

S. Iya

<u>TECHNOLOGY</u> POLYCRYSTALLINE SILICON R&D	<u>REPORT DATE</u> APRIL 30, 1986
<u>APPROACH</u> SILANE DECOMPOSITION IN A FLUIDIZED BED REACTOR <u>CONTRACTOR</u> UNION CARBIDE CORPORATION	<u>STATUS</u> <ul style="list-style-type: none">• SHORTER FLUID BED REACTOR WAS INSTALLED & OPERATED• LONG DURATION TEST RUNS WERE CONDUCTED USING QUARTZ & POLYSILICON LINERS• PRODUCT SAMPLES WERE ANALYZED & ALSO DELIVERED TO JPL• FINAL REPORT IS NEARING COMPLETION
<u>GOALS</u> <ul style="list-style-type: none">• DEMONSTRATE PROCESS FEASIBILITY• DETERMINE OPERATING WINDOW• CONDUCT LONG-DURATION TESTS• DEMONSTRATE SILICON PURITY	

PRECEDING PAGE BLANK NOT FILMED

Overview of Recent FBR Test Runs

RUN NO.	DURATION, HOURS	SILANE CONCENTRATION	LINER
J-01	54	20%	QUARTZ
J-02	58	10 - 20%	QUARTZ
J-03	72	15%	QUARTZ
K-01	48	30 - 60%	POLYSILICON

SILICON MATERIALS

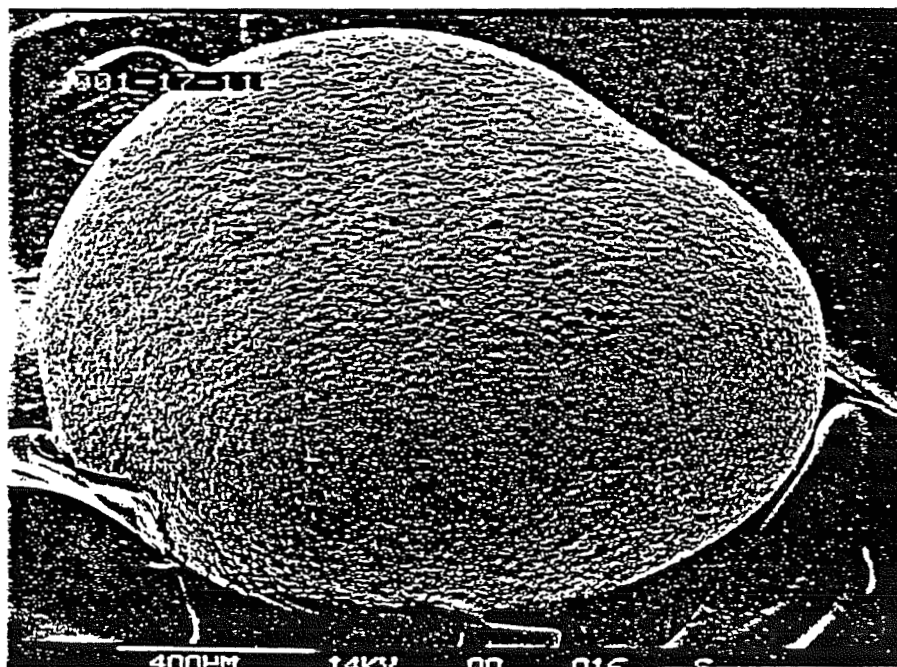
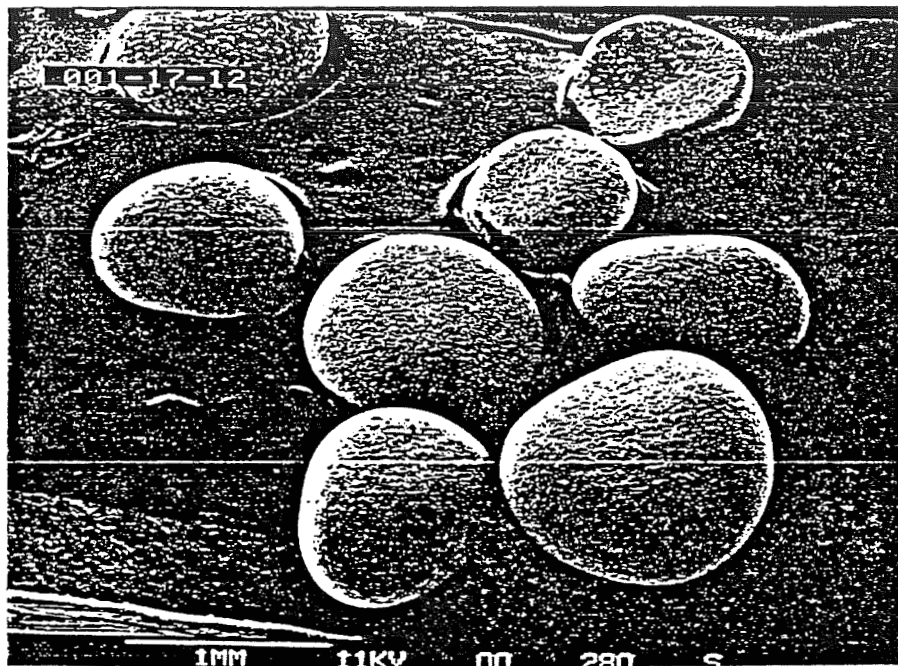
FBR Test Run J-02 Run Summary

- QUARTZ LINER
- 58 HOURS DURATION
- 325 μm SEED GROWN TO 950 μm PRODUCT
- SILANE FEED RATE 2.1 KG/HR
- BED TEMPERATURE 640 - 700°C
- U/U_{MF} 3.0 - 3.5
- COMPLETE SILANE CONVERSION
- 111 KG. PRODUCT WITHDRAWN
- POWDER 9%

FBR Test Run J-02 Mass Balance

INITIAL BED WEIGHT	=	15.7 KG.
SILICON IN	=	109.0 KG.
		<hr/>
TOTAL	=	124.7 KG.
PRODUCT WITHDRAWN	=	111.2 KG.
POWDER IN FILTERS	=	11.3 KG.
		<hr/>
TOTAL	=	122.5 KG.
ERROR IN MASS BALANCE	=	1.8 %

SEM Pictures of Product from Run J-02



ORIGINAL PAGE IS
OF POOR QUALITY

SILICON MATERIALS

Seed and Product Analysis for Heavy Metals Run J-02

ELEMENT	SEED, PPMA	PRODUCT, PPMA	
	NAA	NAA	SSMS
FE	1.6	0.69	1.0
CR	0.35	0.18	0.05
NI	0.11	0.08	<0.05

Summary of Typical FBR Product Characteristics

PARTICLE PROPERTIES

- 1000 μm DIAMETER
- 100 LB/C FT. BULK DENSITY
- SMOOTH ROUND SURFACE
- FREE FLOWING

PARTICLE MORPHOLOGY

- DENSE DEPOSITION LAYER
- LAYERED RING-LIKE GROWTH STRUCTURE
- GROWTH LAYER THICKNESS 350 μm

PARTICLE PURITY

- LOW PPB LEVELS OF BORON & PHOSPHORUS IN SINGLE CRYSTAL
- EXCELLENT POTENTIAL FOR PRODUCING SEMICONDUCTOR GRADE PURITY

Summary of FBR Research and Development

- 6" DIAMETER FBR WAS OPERATED WITH QUARTZ & POLYSILICON LINERS.
- MANY LONG DURATION TEST RUNS WERE CONDUCTED. LONGEST CONTINUOUS RUN DURATION WAS 72 HOURS.
- FEASIBILITY OF GROWING 1000 MICRON PARTICLES BY EFFICIENT SILANE DECOMPOSITION WAS DEMONSTRATED.
- OPERATING PARAMETERS FOR STEADY STATE CONDITIONS WERE DETERMINED.
- FEASIBILITY OF MELTING FBR PRODUCT AND GROWING A HIGH RESISTIVITY DISLOCATION-FREE SINGLE CRYSTAL WAS DEMONSTRATED.
- FURTHER WORK IS REQUIRED IN THE AREA OF HIGH-PURITY SEED PREPARATION.
- FLUID BED PROCESS IS AN ESSENTIAL ROUTE FOR MEETING FSA COST GOALS.

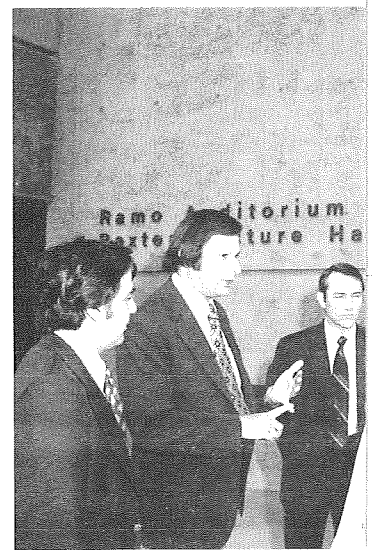
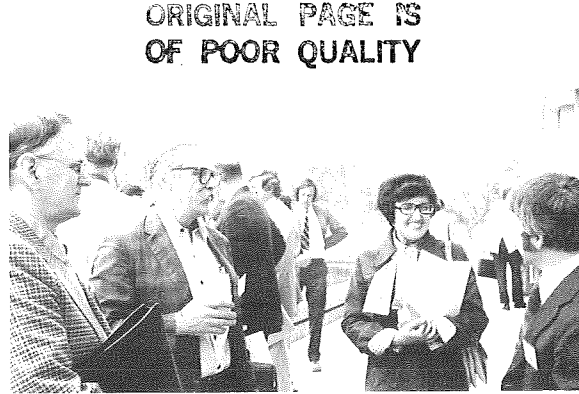
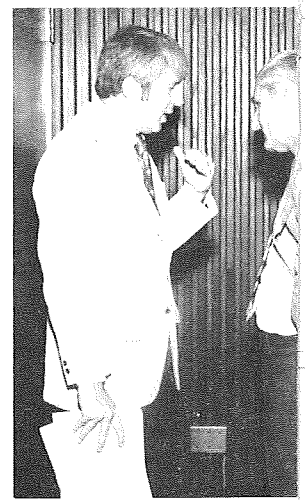
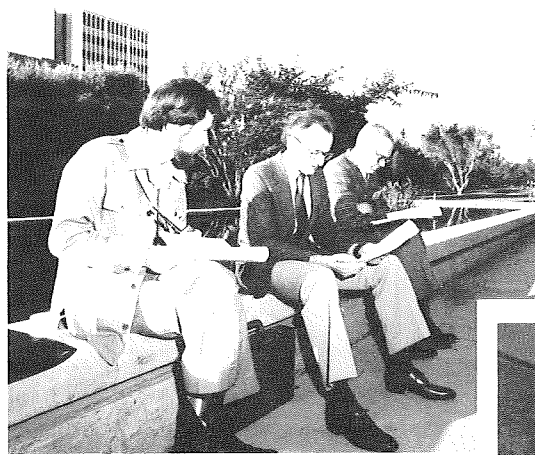
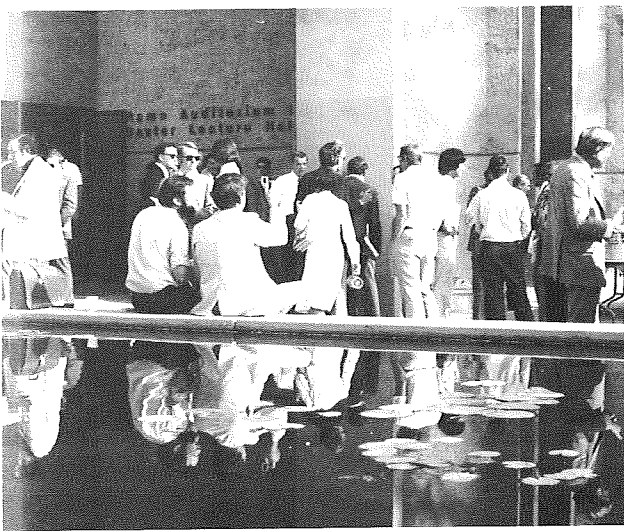
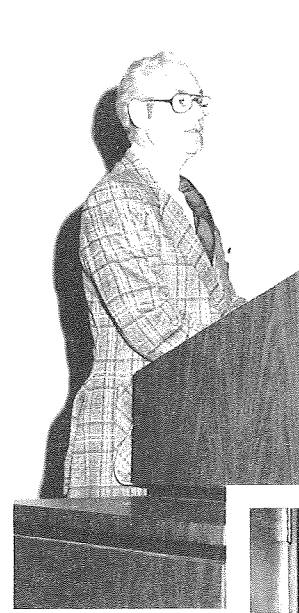
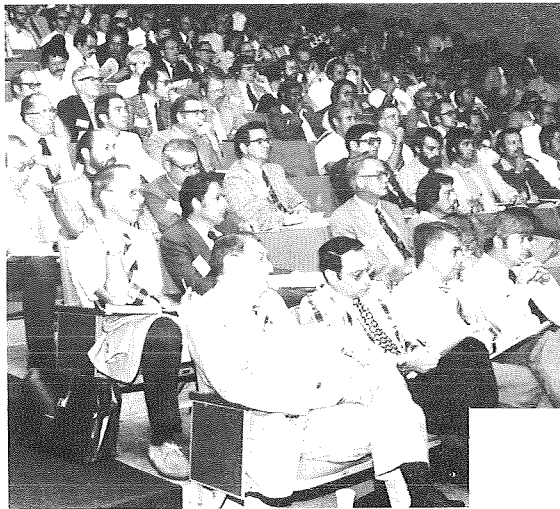
UCC Silane to Silicon Process Major Accomplishments

- DEVELOPMENT OF AN INTEGRATED PROCESS FOR THE PRODUCTION OF HIGH-PURITY SILANE
 - 100 MTY EPSDU
- SUCCESSFUL COMMERCIALIZATION OF UCC SILANE TECHNOLOGY
 - 1200 MTY PLANT
- DEVELOPMENT OF SILANE FLUID BED PROCESS FOR THE PRODUCTION OF LOW COST POLYSILICON
 - 6" DIA. PDU

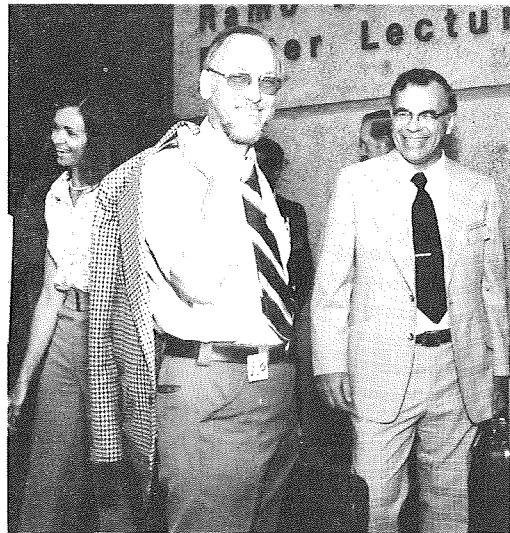
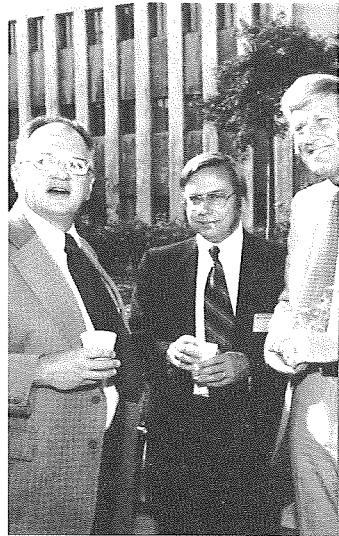
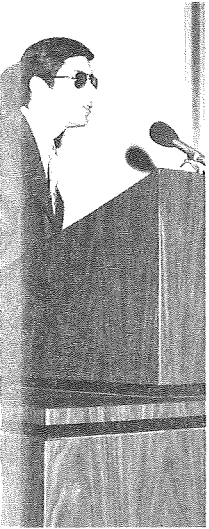
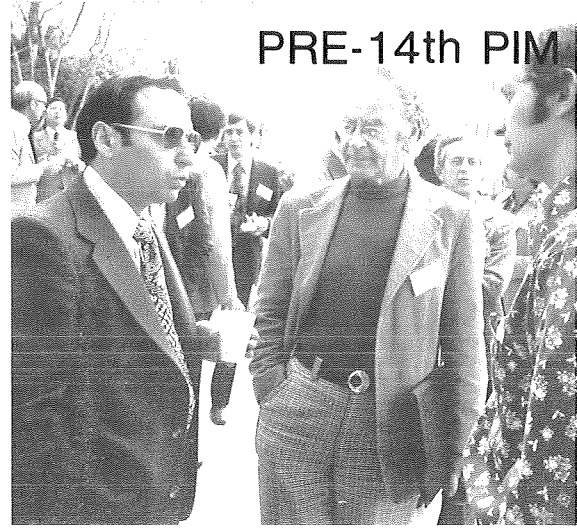
UCC-JPL Contract 954334 Acknowledgments

- SEVERAL UCC CONTRIBUTORS
- JPL CONTRACT MANAGERS
- DOE FINANCIAL SUPPORT

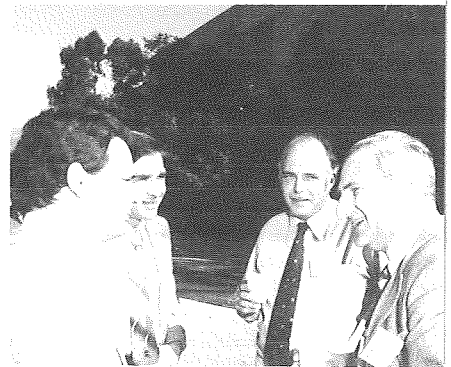
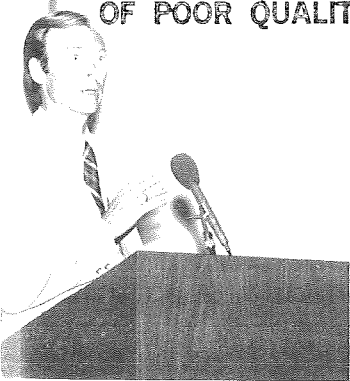
PHOTOGRAPHS OF PREVIOUS
PROJECT INTEGRATION MEETINGS



ORIGINAL PAGE IS
OF POOR QUALITY

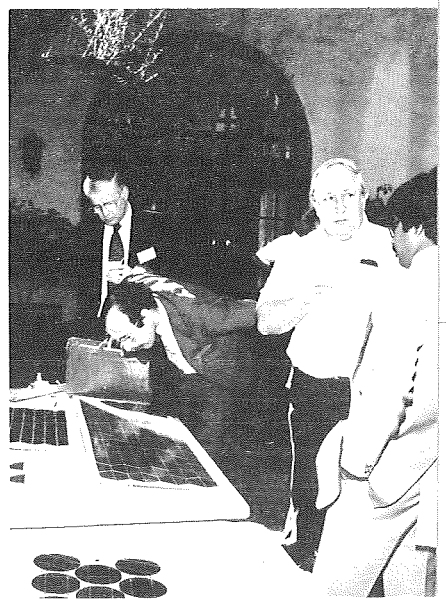


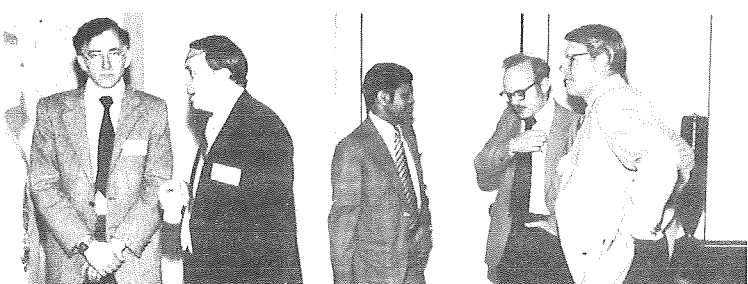
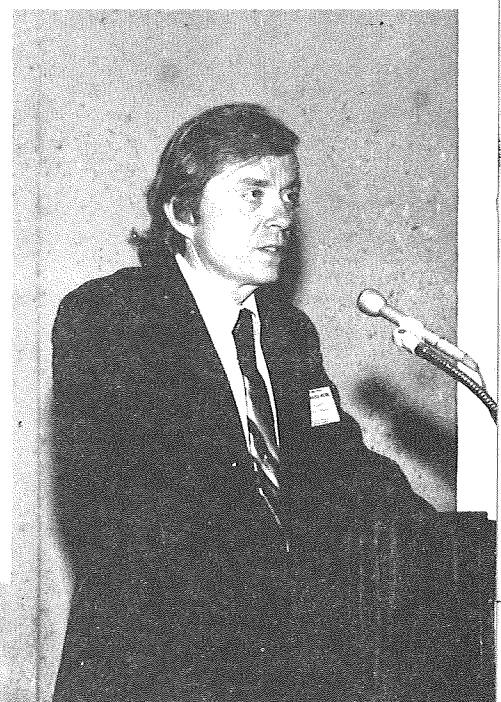
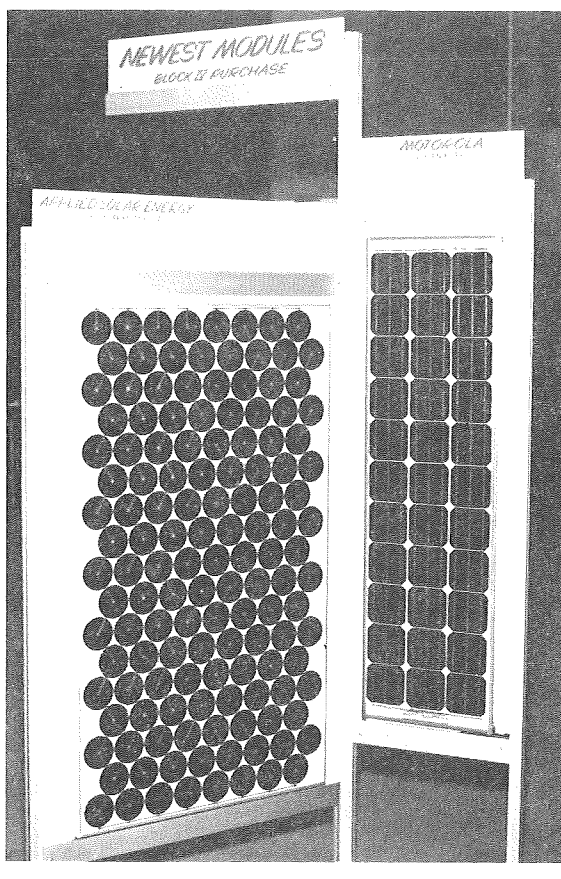
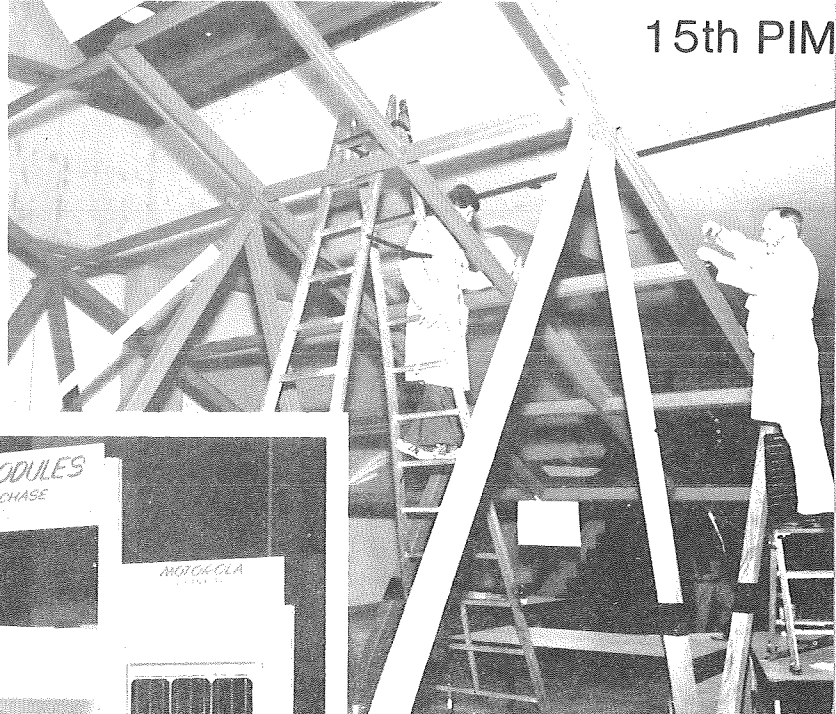
ORIGINAL PAGE IS
OF POOR QUALITY

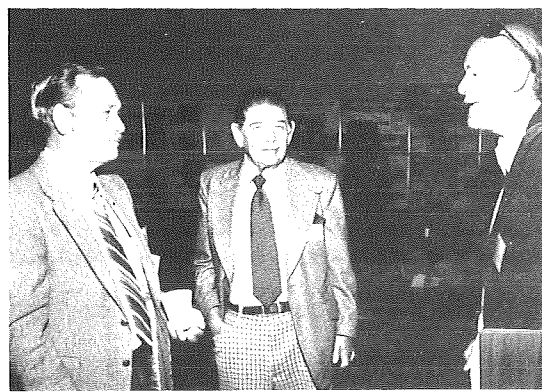
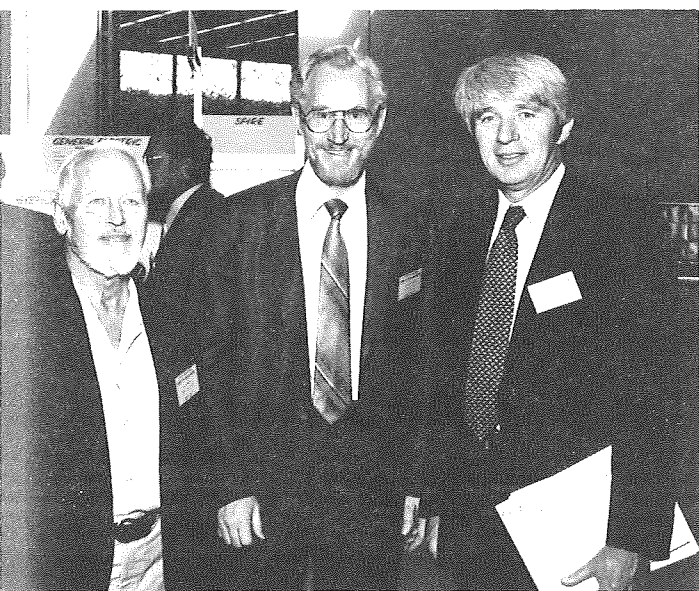
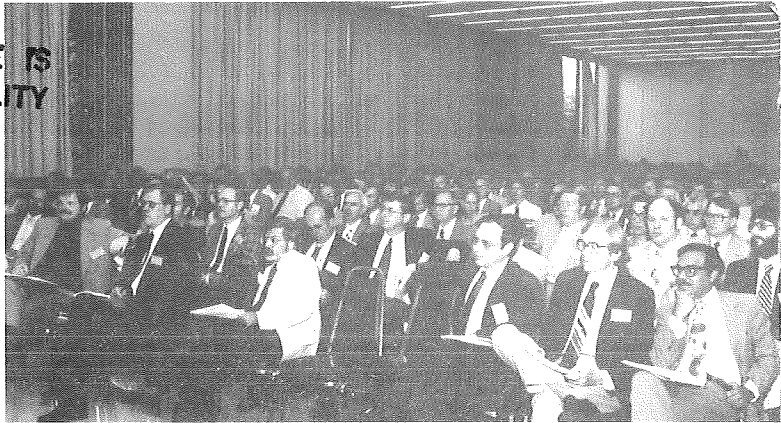
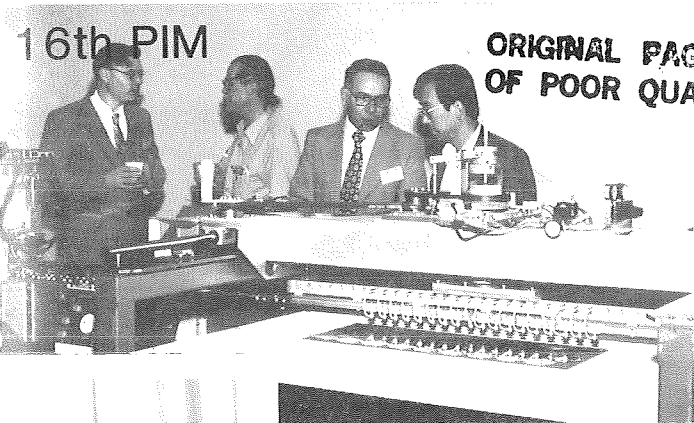


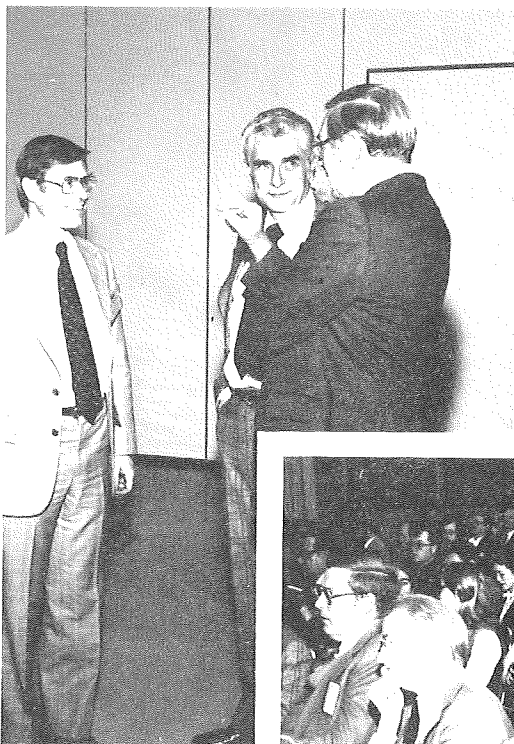
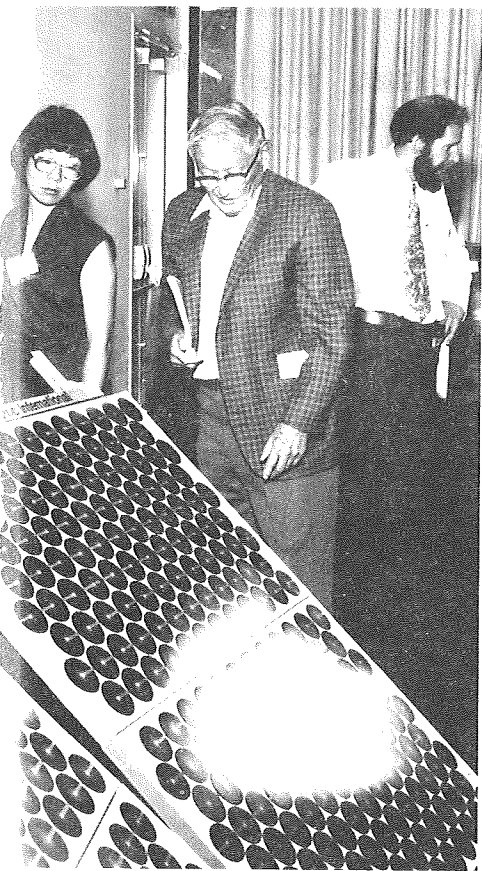
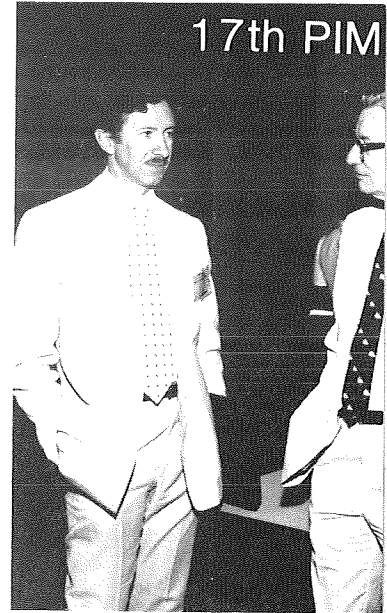


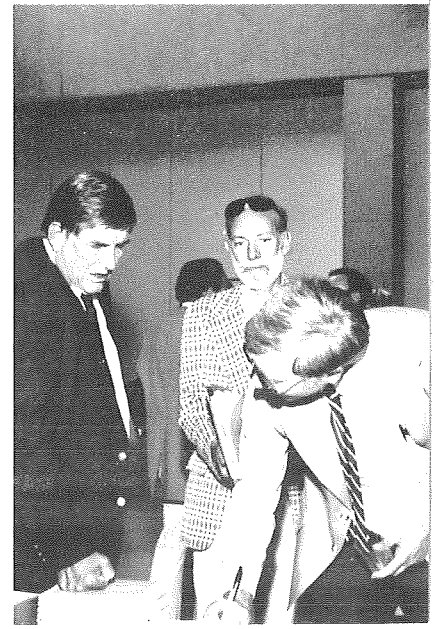
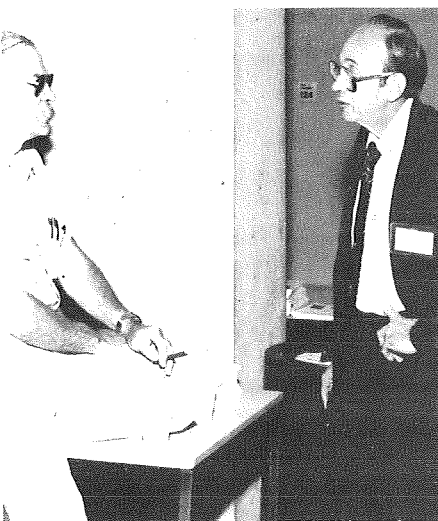
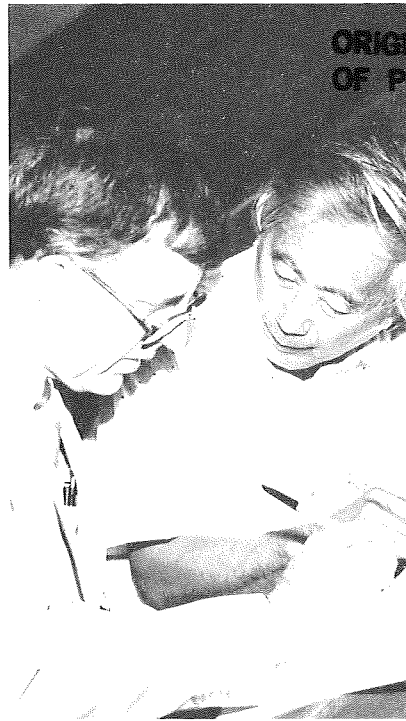
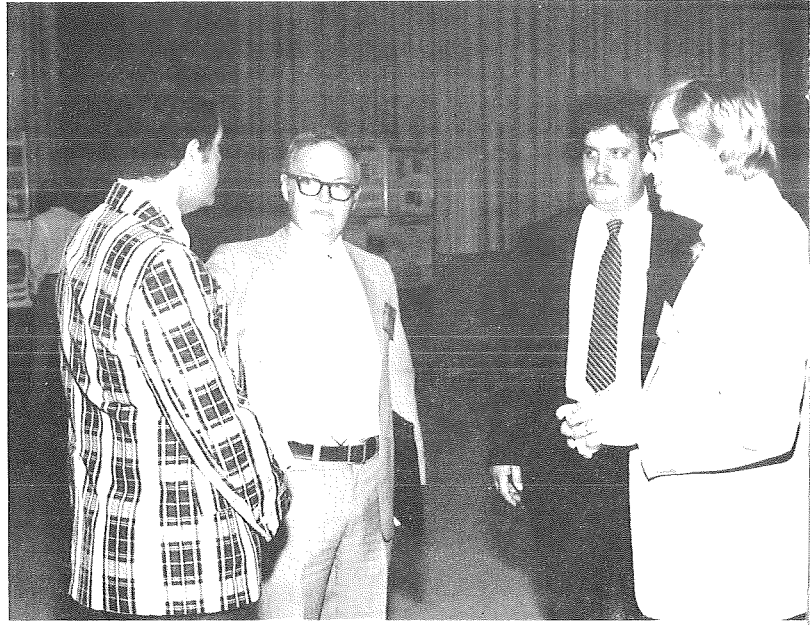
ORIGINAL PAGE IS
OF POOR QUALITY





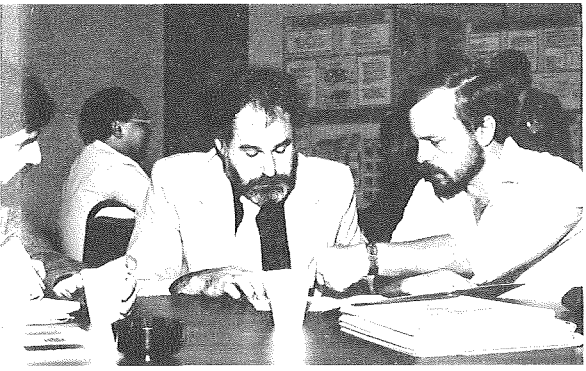
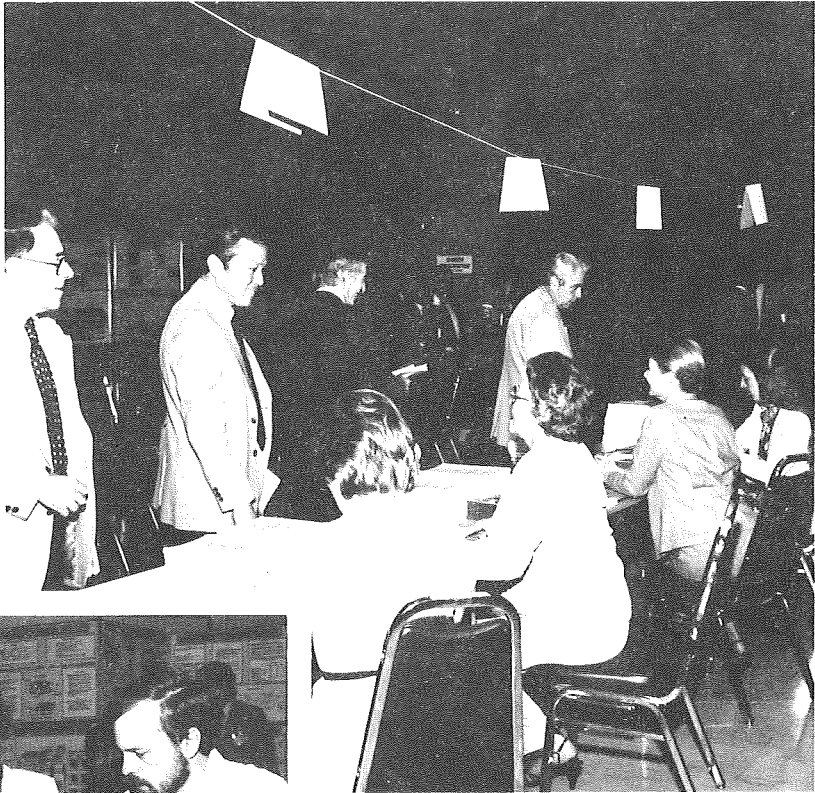
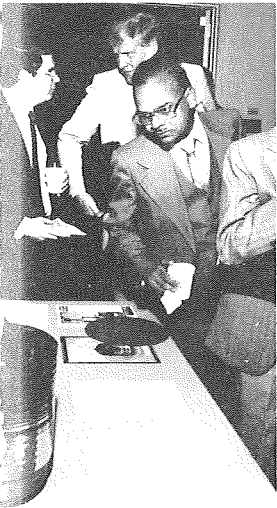
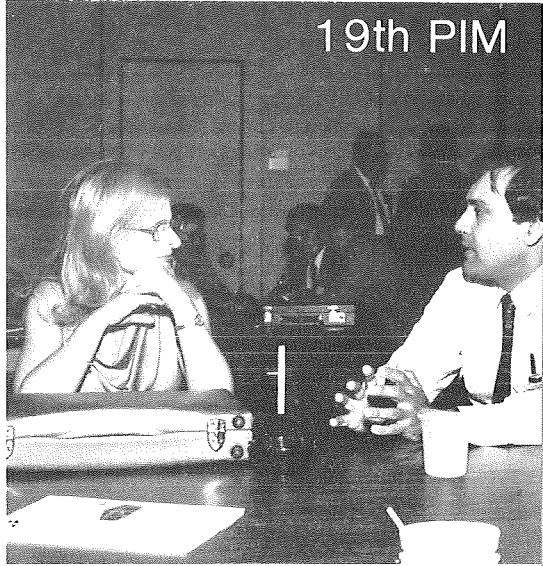


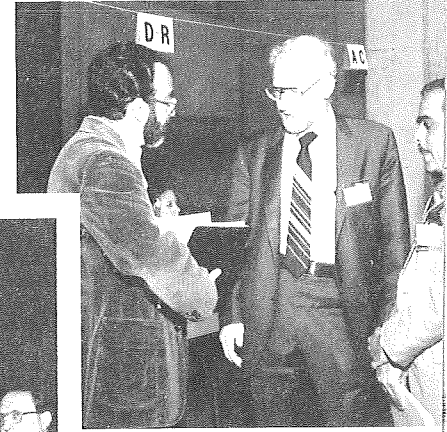
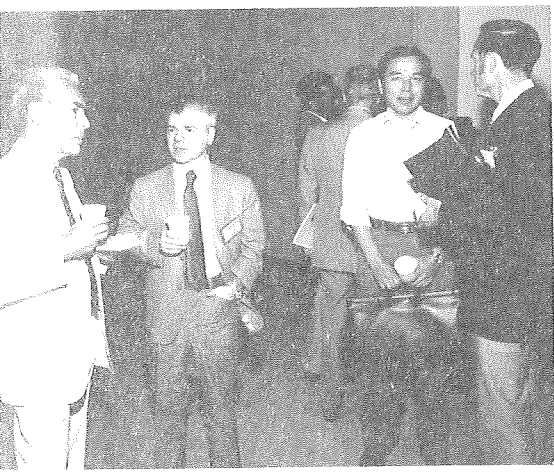
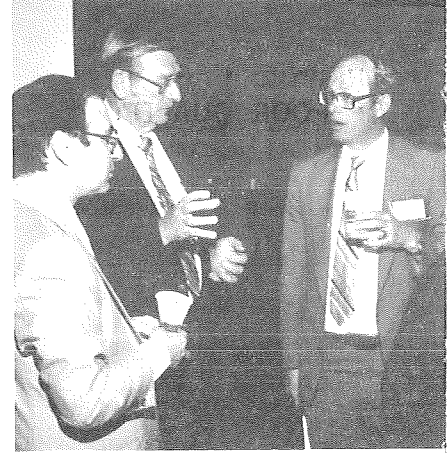
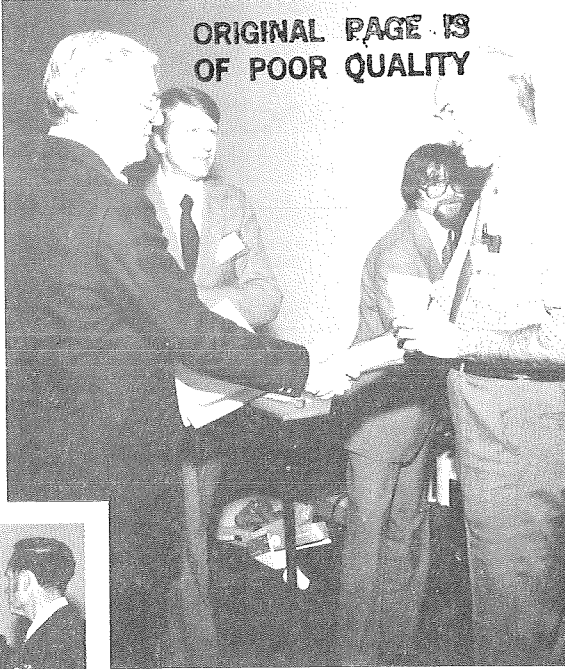


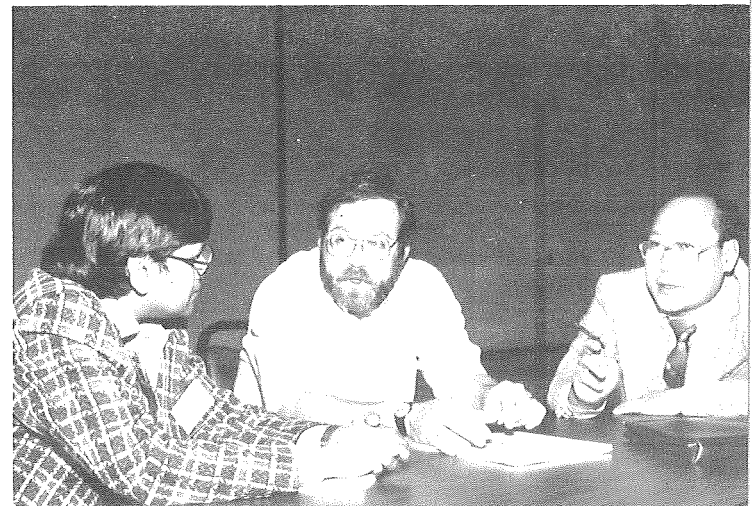
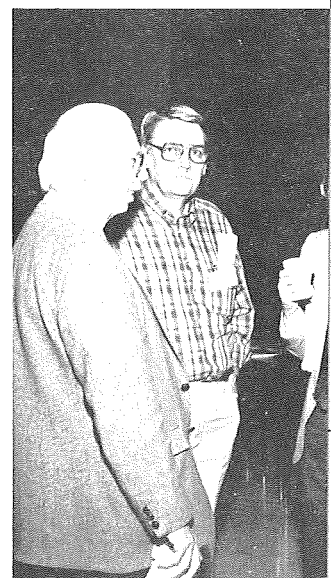
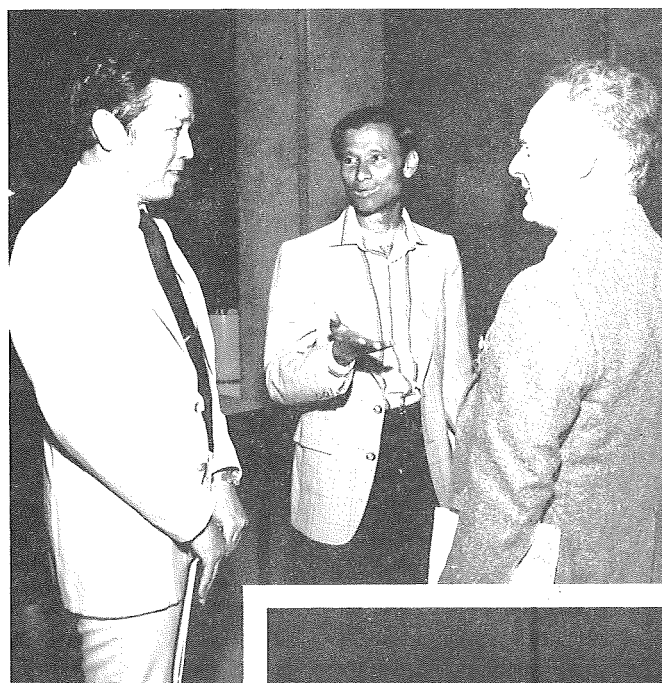
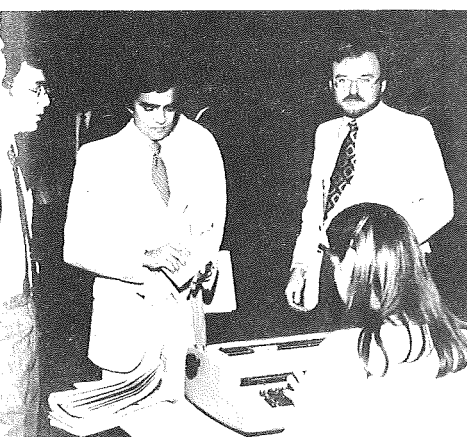


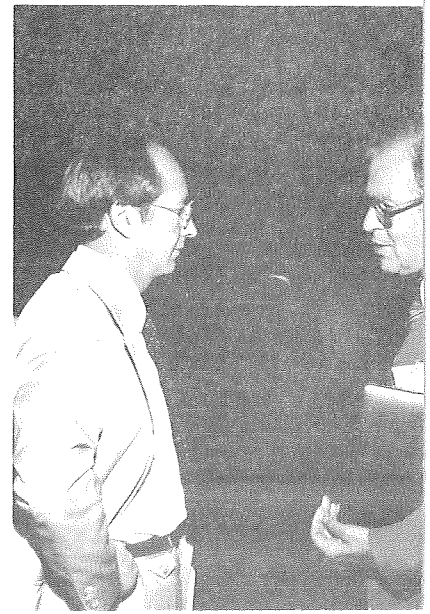
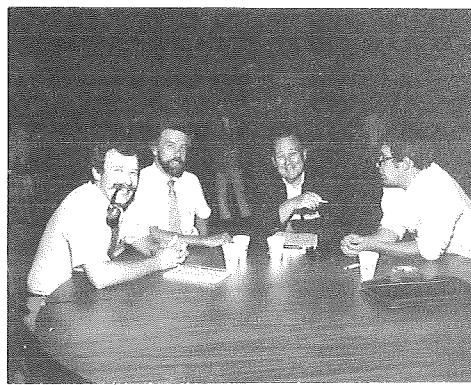
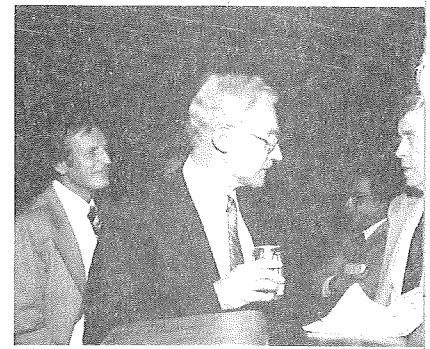
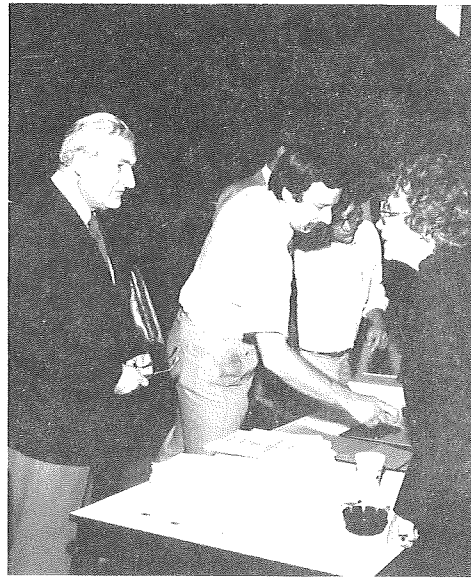
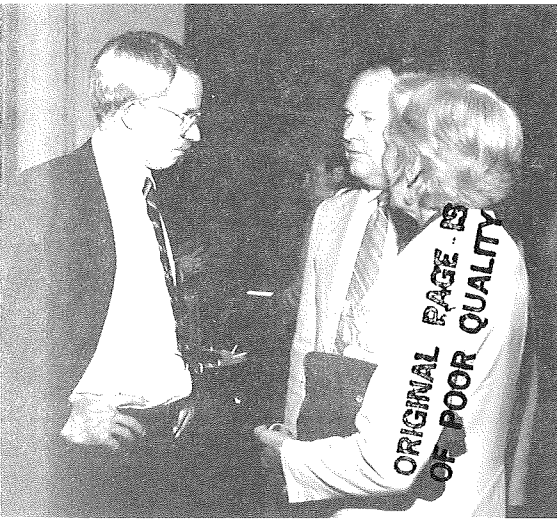
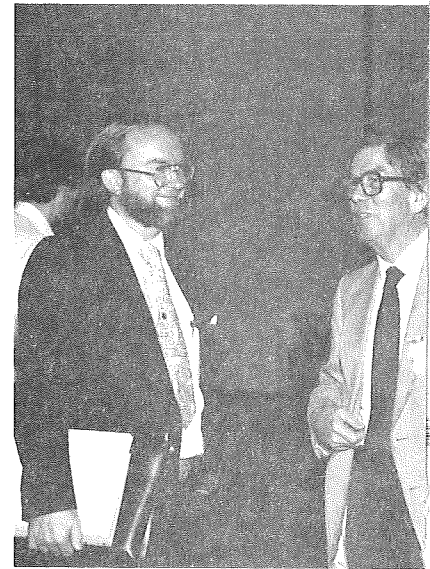
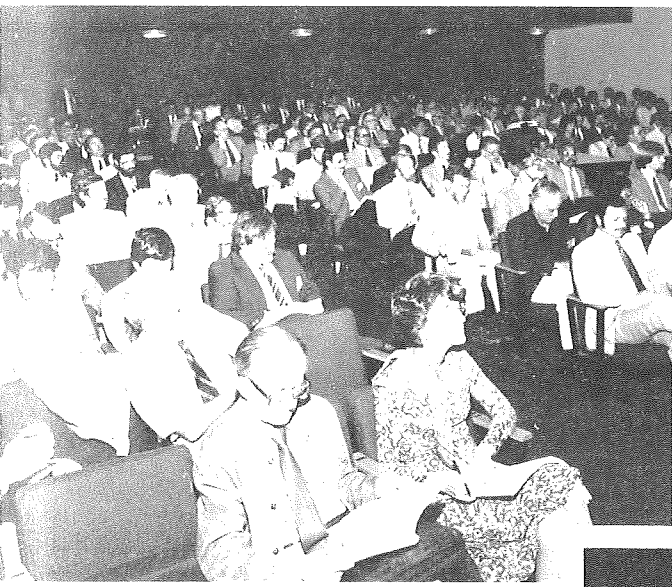
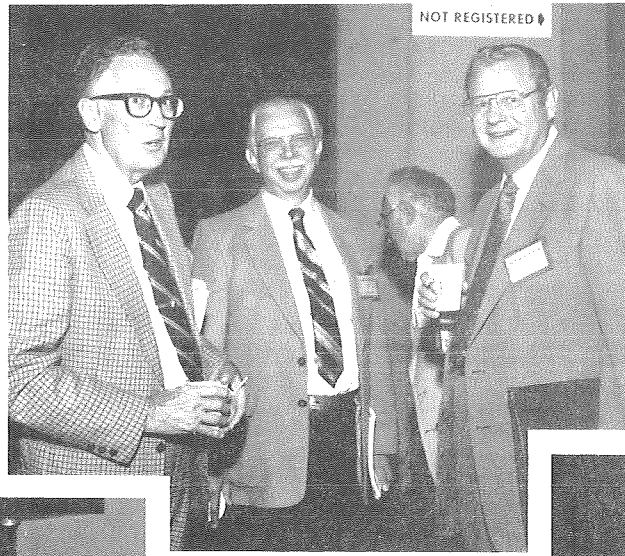
ORIGINAL PAGE IS
OF POOR QUALITY

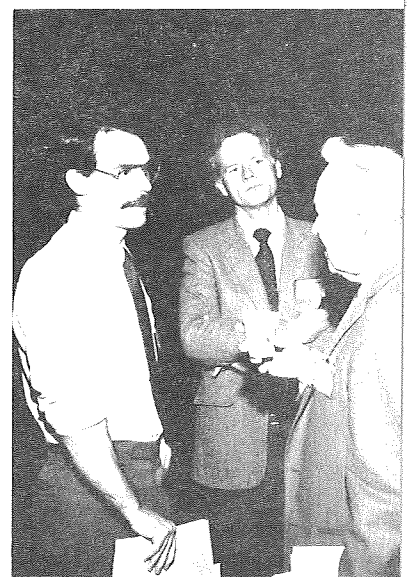
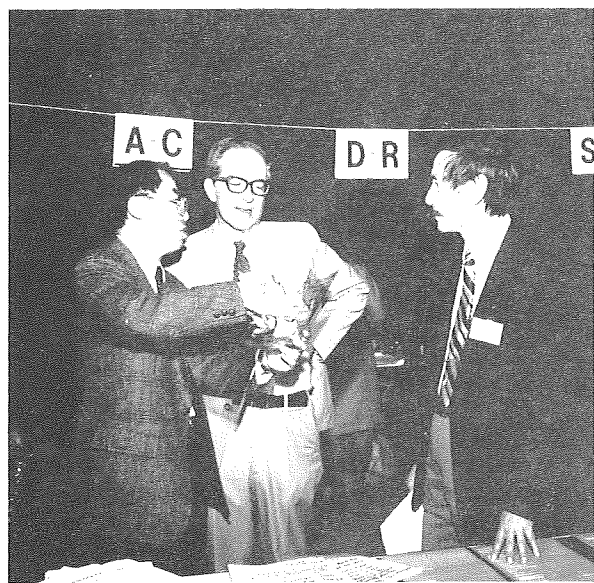
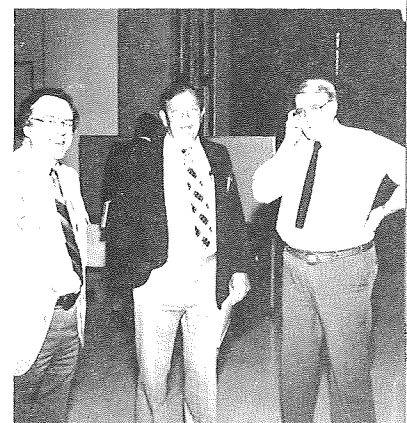
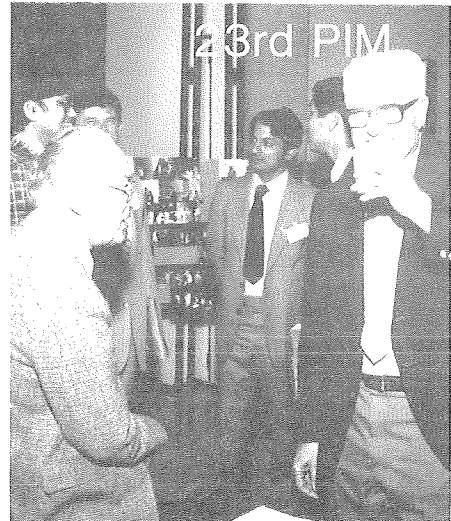
19th PIM











25th PIM

